

Injury Criteria for the THOR 50th Male ATD

Matthew Craig, Daniel Parent, Ellen Lee, Rodney Rudd, Erik Takhounts

Human Injury Research Division
National Highway Traffic Safety Administration

Vikas Hasija

Bowhead Logistics Solutions

September 2020

TABLE OF CONTENTS

TABLE OF CONTENTS.....	2
SUMMARY.....	5
1 INTRODUCTION.....	11
1.1 Real-world Data.....	11
1.2 Scope.....	16
1.3 THOR-50M Technical Documentation.....	16
1.4 Intended Application.....	17
2 METHODOLOGY.....	18
2.1 Statistical Assessment / Creation of Risk Functions.....	18
2.2 Injury Severity and Risk Curve Expansion.....	19
2.3 Field Data.....	19
2.4 Fleet Data: THOR-50M.....	20
2.5 Age Considerations – Injury Risk Functions.....	20
3 HEAD.....	22
3.1 Field and Historical Fleet Data.....	22
3.2 Instrumentation.....	26
3.3 Biofidelity.....	27
3.4 Brain Injuries.....	29
3.5 Skull / Facial Injuries.....	52
3.6 Fleet Test Data: THOR-50M.....	53
4 NECK.....	56
4.1 Field and Historical Fleet Data.....	56
4.2 Literature Review.....	58
4.3 Design.....	59
4.4 Instrumentation.....	59
4.5 Biofidelity.....	60
4.6 Experimental Data.....	61
4.7 Data Analysis.....	64
4.8 Critical Intercepts for Combined Loading Criterion.....	69
4.9 Injury Risk Function Formulation.....	70
4.10 Application of Risk Functions to THOR-50M.....	76
4.11 Fleet Test Data: THOR-50M.....	76
4.12 Limitations.....	78
5 CHEST.....	80
5.1 Field and Historical Fleet Data.....	80

5.2	Literature Review	82
5.3	Design	84
5.4	Instrumentation	84
5.5	Biofidelity	86
5.6	Data	86
5.7	Predictor Variable.....	90
5.8	Covariates.....	92
5.9	Dependent Variable	93
5.10	Injury Risk Function Formulation	93
5.11	Fleet Test Data: THOR-50M.....	101
5.12	Limitations.....	101
6	ABDOMEN.....	109
6.1	Field and Historical Fleet Data	109
6.2	Literature Review	110
6.3	Design	111
6.4	Instrumentation	112
6.5	Biofidelity	113
6.6	Data	113
6.7	Predictor Variable.....	115
6.8	Dependent Variable	115
6.9	Injury Risk Function Formulation	115
6.10	Application of Risk Function to THOR-50M	118
6.11	Fleet Test Data: THOR-50M.....	119
6.12	Limitations.....	119
7	KNEE, THIGH AND HIP.....	125
7.1	Field and Historical Fleet Data	125
7.2	Literature Review	127
7.3	Design	128
7.4	Instrumentation	129
7.5	Biofidelity	129
7.6	Knee/Femur Injury	129
7.7	Hip Injury	145
7.8	Fleet Test Data: THOR-50M.....	167
7.9	Limitations.....	168
8	LOWER EXTREMITY	170
8.1	Field Data and Historical Fleet Data.....	170
8.2	Design	174
8.3	Instrumentation	174

8.4	Biofidelity	175
8.5	Upper Tibia Axial Force	176
8.6	Lower Tibia Axial Force	178
8.7	Tibia Bending.....	182
8.8	Ankle Dorsiflexion	185
8.9	Ankle Inversion/Eversion	187
8.10	Application of Risk Functions to THOR-50M	190
8.11	Fleet Test Data: THOR-50M.....	191
8.12	Limitations.....	195
9	COMPARING FLEET AND FIELD ESTIMATED INJURY RISK.....	197
9.1	Introduction.....	197
9.2	Methods	197
9.3	Results	201
9.4	Discussion and Limitations.....	211
10	REFERENCES.....	213
APPENDIX A.	VEHICLE TEST DATA – BRIC CORRELATION STUDIES.....	223
APPENDIX B.	ALGORITHM FOR COMPUTING TIME DURATION OF ANGULAR VELOCITY PULSE 227	
APPENDIX C.	BRIC DESIGN OF EXPERIMENTS AND OPTIMIZATION	229
APPENDIX D.	FLEET DATA.....	260
APPENDIX E.	THORACIC INJURY CRITERIA SOURCE DATA.....	261
APPENDIX F.	NECK INJURY CRITERIA SOURCE DATA.....	262
APPENDIX G.	LOWER EXTREMITY INJURY CRITERIA SOURCE DATA	266
APPENDIX H.	FIELD DATA CHARTS	270
APPENDIX I.	KNEE/FEMUR CRITERIA SOURCE DATA	275
APPENDIX J.	THOR-50M POST-PROCESSING FOR INJURY CRITERIA CALCULATION	278

SUMMARY

OVERVIEW – This report presents the development of injury criteria for the Test Device for Human Occupant Restraint (THOR) 50th percentile male (or THOR-50M) anthropomorphic test device (ATD). The THOR-50M ATD is intended for use in frontal impact crashworthiness testing.

HEAD – This report presents two head injury criteria. The first, the Head Injury Criterion or HIC_{15} , is a metric currently used with other ATDs for assessing head injury risk in frontal crashes. It is included in FMVSS No. 208 and frontal New Car Assessment Program (NCAP) tests (Eppinger et al., 1999; NHTSA, 2008). The HIC_{15} injury risk curve used in frontal NCAP testing estimates a risk of Abbreviated Injury Scale (AIS) 3+ injury (NHTSA, 2008). However, while HIC_{15} injury assessment values and associated injury risks in frontal NCAP testing have continued to decrease over time as have the field incidence of skull and facial fractures, the incidence of traumatic brain injury in frontal crashes has not decreased at a similar rate (Takhounts et al., 2013). This may be because the HIC_{15} criterion only measures linear acceleration of the head, which does not completely describe the motion of and subsequent injury risk to the brain. To assess the risk of brain injury due to rotation of the head, Takhounts et al. (2013) developed a kinematically-based brain injury criterion (BrIC). BrIC is calculated by combining the angular velocities of the head about its three local axes compared to directionally dependent critical values. BrIC was one of many brain injury correlates that were considered and was found to have the highest correlation to two strain metrics measured in the brain. These metrics, cumulative strain and maximum principal strain, are the mechanical measures that have been shown to be directly associated with brain injury potential (Takhounts et al., 2003; Takhounts, 2015).

$$\begin{array}{l} \text{Injury Criterion:} \\ HIC_{15} \end{array} \quad p(\text{AIS } 2+) = \Phi \left[\frac{\ln HIC_{15} - 6.96362}{0.84687} \right] \quad (1)$$

$$p(\text{AIS } 3+) = \Phi \left[\frac{\ln HIC_{15} - 7.45231}{0.73998} \right] \quad (2)$$

where:

$$HIC_{15} = \left| (t_2 - t_1) \left[\frac{1}{t_2 - t_1} \int_{t_1}^{t_2} a(t) dt \right] \right|_{\max}^{2.5} \quad (3)$$

for $t_2 - t_1 \leq 15$ milliseconds

$$\begin{array}{l} \text{Injury Criterion:} \\ BrIC \end{array} \quad P(\text{AIS } 3+) = 1 - e^{-\left(\frac{BrIC - 0.523}{0.531}\right)^{1.8}} \quad (4)$$

$$P(\text{AIS } 4+) = 1 - e^{-\left(\frac{BrIC - 0.523}{0.647}\right)^{1.8}} \quad (5)$$

where:

$$BrIC = \sqrt{\left(\frac{\omega_x}{\omega_{x_c}}\right)^2 + \left(\frac{\omega_y}{\omega_{y_c}}\right)^2 + \left(\frac{\omega_z}{\omega_{z_c}}\right)^2} \quad (6)$$

$$\omega_{x_c} = 66.25 \text{ rad/s}, \omega_{y_c} = 56.45 \text{ rad/s}, \omega_{z_c} = 42.87 \text{ rad/s}$$

NECK – This report describes a THOR-50M-specific version of the neck injury criterion (N_{ij}) as a metric for assessing neck injury in frontal crashes. The formulation of N_{ij} will be retained, but the critical values have been updated to specifically represent the THOR-50M ATD. Based on a comprehensive review of available experimental data, the current effort is proposing a post-mortem human subject (PMHS)-

based set of critical intercepts that have been adjusted based on the enhanced biofidelity of the THOR-50M ATD. These critical values are based on measurements from the upper neck load cell alone: 4200 N in tension, 4520 N in compression, 60.0 Nm in flexion, and 79.2 Nm in extension. As the PMHS-based values represent a “relaxed” human, this is a conservative estimate of injury risk because it does not account for additional resistance to tension provided by neck musculature (Dibb et al., 2006).

$$\begin{array}{l} \text{Injury Criterion:} \\ N_{ij} \end{array} \quad p(\text{AIS } 2+) = \frac{1}{1 + e^{(5.819 - 5.681N_{ij})}} \quad (7)$$

$$p(\text{AIS } 3+) = \frac{1}{1 + e^{(6.047 - 5.44N_{ij})}} \quad (8)$$

CHEST – This report presents the derivation of a multi-point thoracic injury criterion to predict chest injury with the THOR-50M ATD. A relationship was sought between the measurements available in the thorax of the THOR and PMHS-observed injury through a series of matched-pair sled tests conducted in 14 conditions. Incidence of injury was quantified as AIS 3+ skeletal thoracic injury to the PMHS, which represents three or more fractured ribs based on the 2005 (update 2008) version of AIS. The matched set of PMHS tests included 18 non-injury observations and 30 injury observations. Of the available thoracic measurements, the peak resultant deflection, calculated using the maximum of the peak resultant chest deflections from the four measurement locations on the THOR rib cage, was selected as the most reasonable predictor. Age was determined to be a significant covariate in the prediction of injury, but not mass, stature, or sex. The resulting risk function, assuming an age of 40 to represent the mean age of exposed male drivers in frontal crashes, is shown in Equation (9).

$$\begin{array}{l} \text{Injury Criterion:} \\ \text{Peak Resultant Chest Deflection} \end{array} \quad p(\text{AIS } 3+) = 1 - e^{-\left(\frac{R_{max}}{58.183}\right)^{2.977}} \quad (9)$$

ABDOMEN – This report describes the development of an abdominal injury criterion for the THOR-50M ATD based on peak abdominal deflection as measured by the abdomen deflection instrumentation. This injury criterion is based on testing of porcine surrogates by Kent et al. (2008), who found percent compression to be the best injury discriminator out of the considered metrics. A risk function was developed to relate the peak compression of the THOR-50M ATD abdomen, measured using bi-lateral 3D deflection instrumentation in the lower abdomen, to the risk of AIS 3+ abdomen injury, as shown in Equation (10).

$$\begin{array}{l} \text{Injury Criterion:} \\ \text{Peak Abdomen Compression} \end{array} \quad p(\text{AIS } 3+) = 1 - e^{-\left(\frac{\delta_{max}}{106.222}\right)^{4.3127}} \quad (10)$$

PELVIS – This report describes the development of an acetabulum load criterion to assess the potential for pelvis injuries with the THOR-50M ATD. Rupp et al. (2009a) developed a PMHS injury risk function to relate the force transmitted to the hip, the stature of the occupant, the hip flexion angle, and the hip abduction angle to the risk of a hip fracture. The data used to develop this risk function were re-evaluated herein, and it was confirmed that stature (or sex, which is highly correlated with stature) had a significant contribution to the risk function, and while hip flexion angle is confirmed as a significant covariate, abduction angle was not. The relationship between the force transmitted to the hip of the PMHS and the acetabulum force measured in the THOR-50M ATD is developed based on the ratio of applied force at the knee to measured force at the femur load cell and the ratio of measured force at

the femur load cell and the resultant force measured at the acetabulum load cell. The risk function considers both stature and flexion angle as covariates, and relates the peak resultant acetabulum force measured while the femur is in compression with the THOR-50M ATD to the risk of hip fracture. The resulting risk function is shown in Equation (11), assuming stature of 175.1 centimeters to represent a 50th percentile male and a flexion angle of 15 degrees to represent the nominal flexion angle in a belted frontal crash for both PMHS and THOR.

Injury Criterion:
Peak Resultant Acetabulum Force

$$p(\text{Hip Fracture}) = \Phi \left[\frac{\ln 1.429F_{AR} - 1.5751}{0.2339} \right] \quad (11)$$

KNEE/FEMUR – This report describes the development of a peak femur axial force criterion that can be used as a metric for assessing knee/femur injury risk in frontal crashes. The data from Rupp et al. (2009b) were re-evaluated to consider covariates including sex, stature, age, and mass, using both logistic regression and survival analysis. For all formulations, sex as a covariate had a significant effect on the prediction. As currently applied in FMVSS No. 208 and frontal NCAP, the femur force injury risk function does not account for the difference between the applied force at the knee of the PMHS used to develop the risk function and the peak axial compression force measured at the femur load cell of the ATD. Here, a correction factor was developed to relate the force measured at the THOR-50M femur load cell to the applied force at the knee. The resulting in the risk function relates the force measured at the peak axial force measured at the THOR-50M femur load cell to the probability of AIS 2+ knee and knee/femur injury, as shown in Equation (12).

Injury Criterion:
Peak Axial Femur Force

$$p(\text{AIS 2+}) = \Phi \left[\frac{\ln(1.299F_{LC}) - 2.62}{0.3014} \right] \quad (12)$$

LEG – This report presents injury risk curves developed for the human lower extremity and applied to the lower extremity hardware of the THOR-50M ATD. NHTSA developed injury risk curves for the prediction of tibia plateau fractures using the axial force measured by the upper tibia load cell; tibia/fibula shaft fractures using the resultant moment calculated using measurements from the upper and lower tibia load cells; and distal tibia, calcaneus, talus, ankle, and midfoot fractures using the axial force measured by the lower tibia load cell. Additionally, a risk function for the combined stress approach represented by the Revised Tibia Index was developed.

The upper tibia axial force risk function is:

Injury Criterion:
Upper Tibia Axial Force

$$p(\text{AIS 2+}) = \frac{1}{1 + e^{(5.7415 - 0.8189F_{\text{upper tibia}})}} \quad (13)$$

Where $F_{\text{upper tibia}}$ is the largest compressive z-axis force, in kN, measured in the left and right upper tibia of the THOR-50M ATD.

The lower tibia axial force risk function is:

Injury Criterion:
Lower Tibia Axial Force

$$p(\text{AIS 2+}) = \frac{1}{1 + e^{(3.7544 - 0.4683F_{\text{lower tibia}})}} \quad (14)$$

Where $F_{lower\ tibia}$ is the largest compressive z-axis force, in kN, measured in the left and right lower tibia of the THOR-50M ATD.

The tibia bending moment risk function is:

$$\begin{array}{l} \text{Injury Criterion:} \\ \text{Tibia Bending Moment} \end{array} \quad p(\text{AIS } 2+) = 1 - e^{-e^{\left(\frac{\ln M_{res} - 5.8704}{0.2947}\right)}} \quad (15)$$

Where M_{res} is the largest resultant moment, in Nm, calculated from the x-axis and y-axis moments measured in the left and right upper and lower tibia of the THOR-50M ATD.

The Revised Tibia Index risk function is:

$$\begin{array}{l} \text{Injury Criterion:} \\ \text{Revised Tibia Index} \end{array} \quad p(\text{AIS } 2+) = 1 - e^{-e^{\left(\frac{\ln RTI - 0.3376}{0.3213}\right)}} \quad (16)$$

Where RTI is the largest Revised Tibia Index value, calculated instantaneously using the axial compressive force and the resultant of the x-axis and y-axis moments measured at the left and right upper and lower tibia load cells of the THOR-50M ATD.

Table S1. Summary of THOR-50M injury measures and values at 10, 25 and 50% injury risk.

Injury Measure	AIS Severity			
	Level	10% Risk	25% Risk	50% Risk
BrIC	2	0.62	0.69	0.79
	3	0.68	0.79	0.96
	4	0.71	0.85	1.05
HIC ₁₅	2	357	597	1,057
	3	668	1,046	1,724
Nij	2	0.64	0.83	1.02
	3	0.71	0.91	1.11
Chest Deflection (mm)*	3	27.3	38.3	51.4
Abdomen Deflection (mm)	3	63.0	79.6	97.6
Acetabulum Force (N)	2	2,505	2,887	3,381
Femur Force (N)	2	7,188	8,631	10,577
Upper Tibia Force (N)	2	4,328	5,670	7,011
Lower Tibia Force (N)*	2	3,325	5,671	8,017
Tibia Moment (Nm)	2	183	246	318
Revised Tibia Index	2	0.82	1.01	1.23

*Age set to 40 per GES/CDS analysis of front row occupant age trends

Table S2. Summary of THOR-50M injury criteria, calculations and risk functions.

Criterion	Calculation	Risk Function
HIC_{15}	$HIC_{15} = \left[(t_2 - t_1) \left[\frac{1}{(t_2 - t_1)} \int_{t_1}^{t_2} a(t) dt \right] \right]_{max}^{2.5}$ <p> t_1 Beginning of time window in s t_2 End of time window in s $a(t)$ Head CG resultant acceleration in g; x, y, z components filtered at CFC1000 </p>	$p(\text{AIS } 2+) = \Phi \left[\frac{\ln HIC_{15} - 6.96362}{0.84687} \right]$ $p(\text{AIS } 3+) = \Phi \left[\frac{\ln(HIC_{15}) - 7.45231}{0.73998} \right]$
$BrIC$	$BrIC = \sqrt{\left(\frac{\max(\omega_x)}{66.25 \text{ rad/s}} \right)^2 + \left(\frac{\max(\omega_y)}{56.45 \text{ rad/s}} \right)^2 + \left(\frac{\max(\omega_z)}{42.87 \text{ rad/s}} \right)^2}$ <p> $\omega_{[x,y,z]}$ Angular velocity of the head about the local [x, y, or z] axis, in rad/s, filtered at CFC60 $\omega_{[x,y,z]C}$ Critical angular velocities in rad/s </p>	$p(\text{AIS } 3+) = 1 - e^{-\left(\frac{BrIC - 0.523}{0.531}\right)^{1.8}}$ $p(\text{AIS } 4+) = 1 - e^{-\left(\frac{BrIC - 0.523}{0.647}\right)^{1.8}}$
N_{ij}	$N_{ij} = \left \frac{F_z(t)}{F_{zc}} + \frac{M_y(t)}{M_{yc}} \right _{max}$ <p> F_z Z-axis force measured at upper neck load cell in N, filtered at CFC600 F_{zc} Critical force (tension or compression) in N [4200/-4520] M_y Y-axis moment measured at upper neck load cell Nm, filtered at CFC600 M_{yc} Critical moment (flexion or extension) in Nm [60/-79.2] </p>	$p(\text{AIS } 2+) = \frac{1}{1 + e^{(5.819 - 5.681N_{ij})}}$ $p(\text{AIS } 3+) = \frac{1}{1 + e^{(6.047 - 5.44N_{ij})}}$
Multi-point Thoracic Injury Criterion – Peak Resultant Deflection	$R_{max} = \max(UL_{max}, UR_{max}, LL_{max}, LR_{max});$ $[U/L R/L]_{max} = \max \left(\sqrt{[L/R]X_{[U/L]S}^2 + [L/R]Y_{[U/L]S}^2 + [L/R]Z_{[U/L]S}^2} \right)$ <p> R_{max} Overall peak resultant deflection in mm $[U/L R/L]_{max}$ Peak resultant deflection of the [upper/lower left/right] quadrant in mm $[L/R] [X/Y/Z]_{[U/L]S}^2$ Time-history of the [left/right] chest deflection along the [X/Y/Z] axis relative to the [upper/lower] spine segment in mm, filtered at CFC180 </p>	$p(\text{AIS } 3+) = 1 - e^{-\left(\frac{R_{max}}{58.183}\right)^{2.977}}$
Abdomen Compression	δ_{max} Maximum peak X-axis deflection of the left or right abdomen in mm , filtered at CFC180	$p(\text{AIS } 3+) = 1 - e^{-\left(\frac{\delta_{max}}{106.222}\right)^{4.3127}}$

Criterion	Calculation	Risk Function
Peak Resultant Acetabulum Force	$F_{AR} = \left \sqrt{F_x(t)^2 + F_y(t)^2 + F_z(t)^2} \right _{max}; F_{AR}(t) = 0 \text{ for } F_{FemurZ}(t) > 0$ F_{AR} Peak resultant acetabulum force in <i>kN</i> , x, y, z, components filtered at CFC600	$p(\text{Hip fracture}) = \Phi \left[\frac{\ln 1.429 F_{AR} - 1.5751}{0.2339} \right]$
Femur Axial Load	F_{LC} peak compressive Z-axis force, in <i>kN</i> , measured in the left and right femur, filtered at CFC600	$p(\text{AIS 2+}) = \Phi \left[\frac{\ln(1.299 F_{LC}) - 2.62}{0.3014} \right]$
Proximal (Upper) Tibia Axial Force	$F_{uppertibia}$ largest compressive z-axis force, in <i>kN</i> , measured in the left and right upper tibia, filtered at CFC600	$p(\text{AIS 2+}) = \frac{1}{1 + e^{(5.7415 - 0.8189 F_{uppertibia})}}$
Distal (Lower) Tibia Axial Force	$F_{lowertibia}$ largest compressive z-axis force, in <i>kN</i> , measured in the left and right lower tibia, filtered at CFC600	$p(\text{AIS 2+}) = \frac{1}{1 + e^{(3.7544 - 0.4683 F_{lowertibia})}}$
Tibia Bending Moment	M_{res} largest resultant moment, in <i>Nm</i> , calculated from the x-axis and y-axis moments measured in the left and right upper and lower tibia, filtered at CFC600	$p(\text{AIS 2+}) = 1 - e^{-e^{\left(\frac{\ln M_{res} - 5.8704}{0.2947}\right)}}$
Revised Tibia Index	$RTI = \left \frac{F_z(t)}{12,000} + \frac{M_{res}(t)}{240} \right _{max}$ F_z axial compressive Z-axis force time-history, in <i>N</i> , measured in the left and right upper and lower tibia, filtered at CFC600 M_{res} resultant moment time-history, in <i>Nm</i> , calculated from the x-axis and y-axis moments measured in the left and right upper and lower tibia, filtered at CFC600	$p(\text{AIS 2+}) = 1 - e^{-e^{\left(\frac{\ln RTI - 0.3376}{0.3213}\right)}}$

1 INTRODUCTION

This report describes in detail the methods and results for deriving injury measures and associated injury risk functions or injury criteria to interpret measurements collected using the *Test* device for *Human Occupant Restraint* (THOR) 50th percentile male anthropomorphic test device (ATD), here forward referred to as THOR-50M. The THOR-50M is intended for use in frontal crashworthiness testing.

1.1 Real-world Data

Vehicle crashworthiness or safety performance assessment and associated predictions for injury and fatality risk are influenced by three main areas: (1) the condition or evaluation protocol the vehicle is tested in; (2) the quality of the tools (e.g. test dummies) used in the testing and how well they represent humans; and (3) the injury measures used to estimate the risk of different injuries as applied together with (1) and (2). Item (3) is the focus of this report as it relates to the THOR-50M.

Despite prior/current efforts (standardized tests, test devices or ATDs, injury measures), significant societal harm remains in frontal crashes. Figure 1.1 shows the last 15 years of fatality data sourced from NHTSA’s Fatal Analysis Reporting System (FARS). FARS provides an annual nationwide census of fatalities resulting from motor vehicle crashes on public roadways.

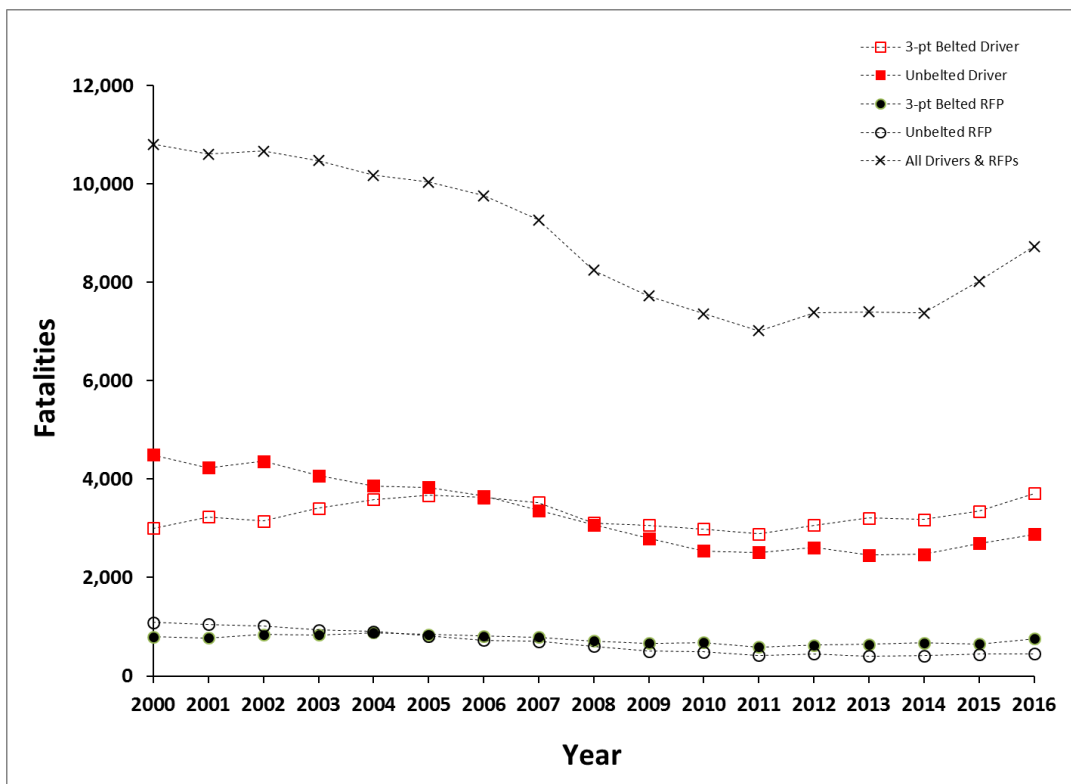


Figure 1.1. Frontal crash fatalities - belted and unbelted drivers and right front passengers (*belted cases coded as wearing lap and shoulder belt; unbelted includes cases coded as no belt, shoulder or lap belt only, incorrect use and unknown use*); FARS 2000-2016.

The National Automotive Sampling System – Crashworthiness Data System (NASS-CDS) was queried for case years 2000 to 2015 in summarizing the total number of injuries by body region at the maximum Abbreviated Injury Scale (MAIS) 2+ and 3+ severity level for AIS version 1990 (1998 update) (AAAM, 1998) by occupant (Table 1.1). Each occupant is only counted once per body region as appropriate and can be counted more than once if multiple body regions are injured at the 2+ and/or 3+ severity level. The results are presented for all occupants and then separately by driver and right front passenger (RFP). Driver and right front passenger is further broken down by belted and unbelted occupants. Table 1.2 presents the same type of data but shows total injury counts for each body region. In this case, occupants could have multiple injuries represented at the 2+ and 3+ severity level for a body region/injury grouping. Both tables are showing the total number of cases over the sixteen years and are not showing annual estimates. The point estimate and 95% upper and lower confidence intervals around the estimates are shown.

Table 1.1. NASS-CDS 2000 to 2015 frontal crashes – weighted MAIS totals by body region.

		Body Region MAIS Counts - Frontal Crashes - NASS 2000-2015 ¹								
Severity	Body Region	All Occupants ²			Belted Drivers/RFPs ³			Unbelted Drivers/RFPs		
		Pt	Lwr	Upr	Pt	Lwr	Upr	Pt	Lwr	Upr
AIS 2+	Total	1,022,168	722,773	1,321,562	729,060	555,953	902,166	293,108	151,997	434,219
	Head/Face	308,576	187,925	429,227	164,624	114,819	214,428	143,952	64,924	222,980
	Brain	270,883	155,510	386,257	150,013	103,207	196,820	120,870	45,316	196,424
	Skull/Facial Fracture	53,720	40,174	67,265	19,922	15,764	24,079	33,798	23,292	44,304
	Neck	51,553	31,832	71,274	30,799	14,599	46,999	20,754	5,892	35,616
	Spinal Cord	5,275	2,721	7,828	2,292	1,099	3,486	2,982	724	5,241
	Osteoligamentous	43,120	21,992	64,248	25,686	8,405	42,966	17,434	4,689	30,180
	Fracture-only	37,917	18,277	57,556	22,657	6,372	38,942	15,260	4,134	26,385
	Thorax	223,644	149,929	297,358	164,456	114,754	214,158	59,188	30,962	87,413
	Rib cage/Sternum	186,404	127,595	245,214	140,153	99,176	181,130	46,251	23,110	69,393
	Lungs	59,102	32,139	86,066	34,119	17,688	50,551	24,983	13,473	36,493
	Heart	6,805	4,298	9,313	2,328	1,014	3,642	4,478	2,838	6,117
	Abdomen	70,223	50,673	89,773	38,753	29,867	47,639	31,470	18,223	44,717
	Vessels/Nerves	2,539	443	4,634	1,215	387	2,044	1,323	0	3,033
	Skin/Tissue/Muscle	193	0	394	172	0	350	21	0	68
	Organs	69,980	50,607	89,354	38,544	29,904	47,185	31,436	18,194	44,678
	Solid	59,582	42,621	76,543	30,081	23,947	36,216	29,501	16,377	42,625
	Hollow	10,054	4,943	15,165	7,045	2,900	11,191	3,009	932	5,085
	Other	10,899	7,714	14,084	7,677	5,236	10,118	3,222	2,091	4,353
	Lower Ext	423,538	282,924	564,153	306,795	187,119	426,470	116,744	81,712	151,776
Knee/Thigh/Hip	198,047	165,567	230,527	123,918	89,931	157,904	74,129	55,142	93,116	
Tibia/Fibula	149,998	120,231	179,765	109,149	90,977	127,322	40,849	22,619	59,078	
Foot/Ankle	175,073	31,027	319,119	146,672	9,603	283,740	28,401	15,304	41,498	
Upper Ext	267,121	173,576	360,666	200,813	120,596	281,029	66,308	37,561	95,055	
AIS 3+	Total	308,617	207,902	409,332	176,007	136,587	215,426	132,610	61,550	203,670
	Head/Face	73,682	26,911	120,454	28,071	17,519	38,623	45,611	3,543	87,679
	Brain	63,402	19,866	106,938	23,948	13,809	34,087	39,454	0	79,383
	Skull/Facial Fracture	16,815	12,061	21,569	6,118	3,998	8,239	10,696	7,347	14,046
	Neck	18,879	9,068	28,690	10,243	4,985	15,500	8,636	913	16,359
	Spinal Cord	5,275	2,721	7,828	2,292	1,099	3,486	2,982	724	5,241
	Osteoligamentous	11,990	3,433	20,547	7,094	839	13,348	4,896	0	9,832
	Fracture-only	11,646	2,892	20,399	6,918	615	13,221	4,728	0	9,676
	Thorax	118,109	77,146	159,073	71,740	48,427	95,052	46,370	24,357	68,383
	Rib cage/Sternum	70,168	45,696	94,640	41,697	23,506	59,887	28,472	14,321	42,622
	Lungs	58,708	31,677	85,738	34,000	17,546	50,455	24,707	13,139	36,276
	Heart	5,588	2,758	8,417	2,132	842	3,423	3,455	1,013	5,897
	Abdomen	24,504	13,427	35,582	14,242	8,533	19,951	10,263	3,487	17,038
	Vessels/Nerves	2,539	443	4,634	1,215	387	2,044	1,323	0	3,033
	Skin/Tissue/Muscle	12	0	37	12	0	37	0	0	0
	Organs	23,630	12,979	34,281	13,643	8,105	19,181	9,987	3,355	16,620
	Solid	18,958	11,003	26,913	10,015	6,976	13,054	8,943	2,235	15,651
	Hollow	3,951	1,374	6,529	2,378	739	4,016	1,574	0	3,440
	Other	2,668	1,072	4,263	1,988	374	3,603	679	177	1,182
	Lower Ext	110,571	91,580	129,562	61,776	52,331	71,222	48,794	35,843	61,746
Knee/Thigh/Hip	75,709	58,459	92,960	38,266	30,707	45,825	37,443	25,217	49,669	
Tibia/Fibula	44,650	36,374	52,927	29,454	22,740	36,168	15,196	10,801	19,592	
Foot/Ankle	-	-	-	-	-	-	-	-	-	
Upper Ext	53,284	31,525	75,043	35,533	21,558	49,509	17,751	3,299	32,202	

1. Unadjusted data, no correction for missing data (e.g. older model year vehicles in 2009-2015 case years) - Frontal/Small Overlap Crashes
2. All occupants - any seating position, no rollovers
3. All frontal/small overlap crashes, no rollover, age 13+ driver/right front passenger

Table 1.2. NASS-CDS 2000 to 2015 frontal crashes – total weighted injury counts.

		Total Injury Counts - Frontal Crashes - NASS 2000-2015 ¹								
Severity	Body Region	All Occupants ²			Belted Drivers/RFPs ³			Unbelted Drivers/RFPs		
		Pt	Lwr	Upr	Pt	Lwr	Upr	Pt	Lwr	Upr
AIS 2+	Total	2,135,757	1,585,223	2,686,291	1,398,864	1,130,473	1,667,256	736,893	423,195	1,050,591
	Head/Face	411,437	269,509	553,365	212,077	157,984	266,171	199,360	102,506	296,214
	Brain	318,849	194,755	442,944	174,867	125,178	224,556	143,982	62,288	225,676
	Skull/Facial Fracture	79,525	59,823	99,226	31,394	26,646	36,142	48,130	31,652	64,609
	Neck	71,770	42,452	101,087	42,239	18,462	66,016	29,531	11,076	47,986
	Spinal Cord	5,275	2,721	7,828	2,292	1,099	3,486	2,982	724	5,241
	Osteoligamentous	61,276	31,234	91,318	36,129	10,919	61,339	25,147	9,412	40,882
	Fracture-only	55,040	27,124	82,956	32,445	8,700	56,190	22,595	8,675	36,516
	Thorax	310,275	220,475	400,075	209,435	151,049	267,822	100,839	62,297	139,382
	Rib cage/Sternum	202,797	142,333	263,261	151,796	109,455	194,136	51,001	26,527	75,475
	Lungs	73,028	43,362	102,693	38,945	21,873	56,018	34,082	20,061	48,104
	Heart	9,956	5,663	14,250	3,285	1,221	5,349	6,671	3,370	9,973
	Abdomen	110,452	76,748	144,156	61,230	44,780	77,680	49,222	28,080	70,364
	Vessels/Nerves	2,723	510	4,936	1,347	389	2,304	1,377	0	3,103
	Skin/Tissue/Muscle	193	0	394	172	0	350	21	0	68
	Organs	107,536	75,025	140,046	59,712	44,163	75,261	47,824	27,364	68,284
	Solid	82,543	56,717	108,369	42,012	32,382	51,642	40,531	21,643	59,420
	Hollow	12,022	6,442	17,602	8,640	4,126	13,154	3,382	1,248	5,516
	Other	12,970	9,067	16,873	9,060	5,780	12,340	3,910	2,508	5,312
	Lower Ext	701,032	492,237	909,826	493,662	334,409	652,914	207,370	137,908	276,832
Knee/Thigh/Hip	263,397	215,929	310,864	158,354	120,649	196,059	105,042	73,505	136,580	
Tibia/Fibula	221,579	175,542	267,616	158,579	130,426	186,731	63,000	35,366	90,634	
Foot/Ankle	216,056	76,007	356,105	176,729	48,741	304,716	39,327	21,815	56,840	
Upper Ext	366,932	253,213	480,651	273,865	178,196	369,534	93,066	49,294	136,838	
AIS 3+	Total	619,595	431,032	808,157	337,869	253,836	421,902	281,726	159,915	403,537
	Head/Face	133,217	83,083	183,351	56,588	41,732	71,444	76,629	33,249	120,009
	Brain	109,869	61,334	158,404	47,756	33,752	61,759	62,113	18,974	105,253
	Skull/Facial Fracture	22,159	16,866	27,452	7,949	5,807	10,091	14,209	10,311	18,108
	Neck	26,033	10,252	41,814	14,295	2,430	26,159	11,738	1,591	21,885
	Spinal Cord	5,275	2,721	7,828	2,292	1,099	3,486	2,982	724	5,241
	Osteoligamentous	18,916	3,987	33,845	11,085	0	23,832	7,831	384	15,278
	Fracture-only	18,557	3,489	33,626	10,906	0	23,677	7,651	226	15,077
	Thorax	172,021	116,719	227,323	98,030	66,620	129,439	73,992	45,093	102,890
	Rib cage/Sternum	70,446	46,013	94,879	41,933	23,786	60,080	28,513	14,359	42,667
	Lungs	71,169	41,608	100,730	38,477	21,373	55,581	32,692	18,837	46,547
	Heart	5,924	2,952	8,895	2,221	914	3,528	3,702	1,159	6,246
	Abdomen	31,018	17,511	44,524	17,391	10,281	24,501	13,626	5,081	22,172
	Vessels/Nerves	2,723	510	4,936	1,347	389	2,304	1,377	0	3,103
	Skin/Tissue/Muscle	12	0	37	12	0	37	0	0	0
	Organs	28,282	16,065	40,499	16,033	9,493	22,573	12,250	4,526	19,974
	Solid	21,244	12,584	29,904	11,312	7,632	14,992	9,932	2,830	17,034
	Hollow	4,327	1,509	7,145	2,732	778	4,687	1,595	0	3,471
	Other	2,711	1,104	4,318	1,988	374	3,603	723	195	1,251
	Lower Ext	144,259	113,727	174,790	81,514	66,915	96,114	62,745	42,636	82,854
Knee/Thigh/Hip	94,362	68,993	119,730	48,103	37,483	58,723	46,259	29,165	63,352	
Tibia/Fibula	49,897	40,129	59,666	33,411	25,934	40,888	16,486	11,189	21,784	
Foot/Ankle	-	-	-	-	-	-	-	-	-	
Upper Ext	72,725	40,686	104,764	49,565	28,322	70,807	23,160	4,404	41,916	

1. Unadjusted data, no correction for missing data (e.g. older model year vehicles in 2009-2015 case years) -

Frontal/Small Overlap Crashes

2. All occupants - any seating position, no rollovers

3. All frontal/small overlap crashes, no rollover, age 13+ driver/right front passenger

Eigen and Martin (2005) presented an approach to quantify the cost of injury for different body regions and injuries relative to other body regions. This attributable cost approach was recreated using updated cost data from Blincoe et al. (2015). Blincoe provided data that broke down the cost of injury associated with motor vehicle crashes into body region and injury severity. Table 1.3 presents the sum of medical, wage, and household costs as well as the cost associated with quality-adjusted life years (QALYs) lost. All values are with a 3% discount rate applied. The total cost in these four areas amounts to over 95% of comprehensive cost for AIS 2 through fatal injury severities.

Table 1.3. QALY and economic costs by body region / injury severity.

Total - QALY ¹ and Economic Costs (Medical Costs ² , Lost Wages ³ , Household Productivity ⁴)													
Severity	Head		Face		Neck		Chest		Abdomen	Lower Extremities		Upper Extremities	
	No Fracture	Fracture	No Fracture	Fracture	No Fracture	Fracture ⁵	No Fracture	Fracture		No Fracture	Fracture	No Fracture	Fracture
AIS 1	\$100,296	\$12,879	\$25,613	\$594,740	\$462,557	-	\$70,194	\$175,330	\$240,252	\$19,643	\$15,962	\$23,546	\$29,860
AIS 2	\$567,415	\$1,524,384	\$979,884	\$321,571	\$1,183,981	\$378,790	\$152,895	\$343,522	\$170,656	\$96,741	\$369,278	\$194,013	\$154,930
AIS 3	\$1,361,799	\$1,941,020	\$936,645	\$969,900	\$2,373,527	\$941,343	\$297,169	\$527,705	\$439,262	\$711,098	\$847,624	\$952,755	\$992,888
AIS 4	\$3,626,768	\$2,121,003	-	-	\$6,428,249	-	\$520,457	\$703,772	\$626,271	\$1,546,776	\$1,680,853	-	-
AIS 5	\$5,939,398	-	-	-	\$7,897,643	-	\$960,200	\$1,063,954	\$652,962	-	\$1,755,062	-	-

1. Table B-2 (Blincoe et al. 2015)

2. Table 2-4 (Blincoe et al. 2015)

3. Table 2-5 (Blincoe et al. 2015)

4. Table 2-6 (Blincoe et al. 2015)

5. AIS 1 and 2 are QALY only costs; AIS 3-5 are spinal cord cases

6. Fracture cases assigned cost from Table 4-2 (Blincoe et al. 2015)

In essence, the attributable cost approach looks at the most costly injury sustained by a given occupant and subtracts the cost associated with the next most costly injury. The cost data from Table 1.3 is used for the respective injuries. The difference between the two costs or attributable cost is recorded for that occupant and associated with the most costly body region. This approach can be applied across a target population of interest. In Figure 1.2 this approach has been applied to belted and unbelted drivers and right front passengers involved in frontal crashes for NASS-CDS case years of 2010 to 2015 with the body region data organized to match body regions that map to those of THOR-50M. This is done for all maximum Abbreviated Injury Scale (MAIS) 2+ occupants and associated AIS 2+ injuries. The version of AIS used was AIS 1995/1998 (AAAM, 1998) given the injury coding used in Blincoe et al. (2015) used that version of AIS. The costs shown represent a total for the case years included.

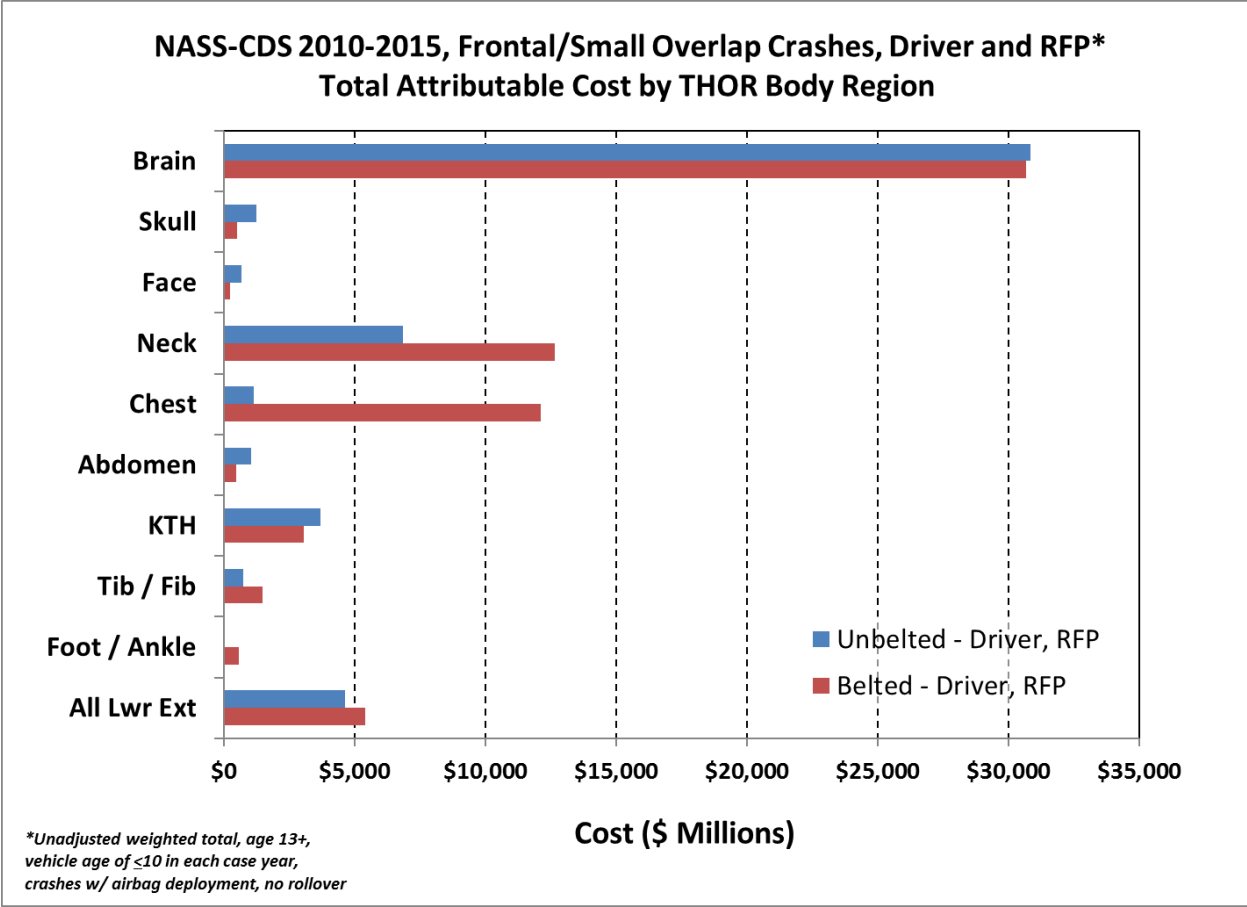


Figure 1.2. Attributable cost by THOR-50M body region for drivers and right front passengers involved in frontal crashes for NASS-CDS 2010-2015 case years.

1.2 Scope

This report describes injury criteria and associated risk function development where both the THOR-50M has available instrumentation and experimental/mathematical injury data exist.

1.3 THOR-50M Technical Documentation

Throughout this document, references to the THOR-50M refer to an ATD described in the August 2018 THOR-50M drawing package (NHTSA, 2020a), for which qualification specifications are defined in the September 2018 THOR-50M Qualification Procedures Manual (NHTSA, 2020b). Additionally, the THOR-50M Procedures for Assembly, Disassembly, and Inspection (NHTSA, 2020c) includes relevant information regarding instrumentation polarity and post-processing.

The THOR-50M is a physical model of a 50th percentile male motor vehicle occupant. The anthropometry of the THOR-50M was developed to meet the requirements of the Anthropometry of Motor Vehicle Occupants (AMVO) study (Robbins, 1983), which defines an average male as 168.8 pounds (76.57 kg) in weight and 175.1 cm in stature. The resulting physical THOR-50M has a mass of 76.11 kg, as

documented in the August 2018 drawing package (NHTSA, 2020a; 472-0000, Sheet 5 of 6). The stature of the physical THOR-50M ATD cannot be measured since the pelvis does not allow a full standing posture; however, since the THOR-50M was developed using the AMVO body segment geometry and seated anthropometry which represents a 175.1 cm occupant, it is assumed that the stature of the THOR-50M is also 175.1 cm.

The kinematic and dynamic biomechanical performance requirements of the THOR-50M were developed based on post-mortem human subject (PMHS) and volunteer response data, described in more detail in Parent et al. (2017).

1.4 Intended Application

The THOR-50M is intended for use in the development/evaluation of vehicle safety countermeasures (e.g. occupant restraint systems such as seat belts and airbags) and vehicle safety performance in frontal crashworthiness testing. NHTSA has traditionally used 50th male crash test dummies or ATDs in a variety of frontal crash conditions for rulemaking/enforcement, consumer metric and/or research purposes in evaluating the performance of passenger cars, light trucks and vans. These conditions include full frontal and small to moderate overlap crashes with those tests being run with various impact angles (collinear and oblique). In these conditions, the dummies are often tested in both belted and unbelted conditions.

2 METHODOLOGY

The following section of the report describes the methods used for collecting and analyzing experimental, real-world crash, and fleet data from crash tests/simulation for the purpose of creating, evaluating and selecting injury criteria and associated risk functions for the THOR-50M ATD.

2.1 Statistical Assessment / Creation of Risk Functions

The following section describes the steps and statistical measures used to describe the respective injury risk functions for the THOR-50M.

2.1.1 Methods for developing risk functions

Hasija et al. (2011) presented a process by which to differentiate between non-correlated and well-correlated datasets when considering the development of injury risk functions. They recommended the use of both logistic regression and survival analysis when using left censored injury data and right censored non-injury data. For a well-correlated dataset with overlapping left and right censored injury and non-injury data, both logistic regression and survival analysis (with Weibull, log-logistic or log-normal) produce nearly identical risk functions. The advantage of survival analysis as compared to logistic regression is that it produces a risk function that presents zero risk with zero stimulus.

For logistic regression-based analyses to be possible, two conditions need to be met. First, the data must include both injury and non-injury data points for the dependent outcome of interest. Second, this dataset must have overlapping injury and non-injury data. As will be described later in this report, it was necessary to consider some datasets that presented only injury data. In these cases, where the experimental protocol allowed for the measurement/estimation of load/stimulus magnitude at failure (possibly different than peak stimulus or left censored data where exact failure stimulus is not known), risk functions are presented using survival analysis.

Throughout this report, three main measures of model fit/predictability were used: area under the receiver operating characteristic (ROC) curve, log likelihood and Hosmer and Lemeshow's (Hosmer and Lemeshow, 2000) goodness of fit test.

Area under the ROC curve: The ROC curve is a plot of true positive versus false positive rates. The area under the ROC curve or AUROC can range from 0.5 (no model discrimination) up to 1.0.

Per Hosmer and Lemeshow (2000), AUROC can be interpreted as follows:

- If AUROC=0.5 this suggests no discrimination
- If $0.7 \leq \text{ROC} < 0.8$ this is considered acceptable discrimination
- If $0.8 \leq \text{AUROC} < 0.9$ this is considered excellent discrimination
- If AUROC ≥ 0.9 this is considered outstanding discrimination

Hosmer and Lemeshow note that "in practice it is extremely unusual to observe areas under the ROC Curve greater than 0.9. In fact, when there is complete separation it is impossible to estimate the

coefficients of a logistic regression model, yet nearly complete separation would be required for the area under the ROC Curve to be >90%.”

Log-likelihood (-2 log L or Max Log-likelihood in SAS 9.3, SAS Institute Inc.): Log-likelihood is minimized (or targeted to be as close to zero as possible) in fitting a model to the associated dataset when optimizing for the model coefficients. It is dependent on the sample (content, sample size) and thus should only be used for comparing models (e.g. AIS 2+ or AIS 3+) derived from the same dataset and not across different datasets.

Goodness of Fit: Hosmer and Lemeshow (2000) described a goodness of fit test that can be used to assess the predictability of the model. Hosmer and Lemeshow’s goodness of fit statistic groups model observations/probabilities (usually near ten groups) for the purpose of comparing predicted versus observed frequencies. The goodness of fit statistic obtained by calculating the Pearson chi-square statistic Gx2 (G equals number of groups) table of observed versus estimated expected frequencies. If the p value (Pr>ChiSq) is high (> 0.1) then one cannot reject the null hypothesis that the model fits (i.e. is correct).

2.2 Injury Severity and Risk Curve Expansion

This report uses the 1990 version (1998 Update) of the Abbreviated Injury Scale (AAAM, 1998) when considering real-world crash data and experimental data used to develop injury risk functions. As needed, further analysis and/or descriptions are provided when considering some datasets and applications that are based on the 2005 (2008 Update) version of AIS (AAAM, 2008). In these cases, the version of AIS used will be specifically noted. Otherwise all listings of AIS severity (e.g. AIS 2+ or AIS 3+ injured occupants or body regions) will be in AIS 1990 (1998 Update) coding.

Where possible, the risk functions for the respective body regions will be presented for more than one AIS severity level. In some cases, (see brain injury) this was simply done through referencing prior expanded curves. In other cases, and as the experimental data allows, risk functions are presented for different levels of injury as derived directly from the experimental data (e.g. see neck).

2.3 Field Data

This report utilizes various sources of real world or field crash data in analyzing trends of field versus fleet data as well as to present case study results of injury mechanisms.

The following is a brief description of each database:

- **National Automotive Sampling System – Crashworthiness Data System (NASS-CDS):** NHTSA’s NASS-CDS database is a nationally representative sample of crashes on public roadways where at least one vehicle was towed from the crash. NASS-CDS contains detailed, crash investigator collected data related to the crash (scene, vehicle) and occupant/injury (demographics, injury coding, injury sources).
- **Crash Injury Research and Engineering Network (CIREN):** NHTSA’s CIREN program dataset is a purposive sample of seriously injured occupants who were admitted to a Level I trauma center.

Vehicle crash data is collected similar to NASS-CDS. CIREN collects additional hospital and medical imaging data and conducts medical/engineering expert team review in assigning sources, causes, and mechanisms of injury.

- **National Automotive Sampling System – General Estimates System (NASS-GES):** NASS-CDS is a nationally representative sample of police reported crashes on a public roadway. NASS-GES collects a larger sample of data as compared to NASS-CDS in an effort to get an overall bigger picture of crashes, but does not have crash investigator collected vehicle crash data or occupant injury data.
- **Fatality Analysis Reporting System (FARS):** NHTSA’s FARS dataset contains a nationwide census of fatal crashes. Like NASS-GES it does not have detailed crash or occupant injury data, but does provide high-level demographic, restraint use and crash type information.
- **Multiple Cause of Death (MCoD):** MCoD is a CDC dataset of national mortality and population data based on death certificates in the U.S. The underlying cause of death (e.g. motor vehicle crash) and associated injury types are documented.

Methods and associated results for comparing rates of injury in field data versus predicted injury risk from use of the THOR-50M in crash tests of fleet vehicles are presented in section 9.

2.4 Fleet Data: THOR-50M

Each injury criterion presented herein is calculated for a set of vehicles which were tested in the frontal rigid barrier (0 degrees, full overlap, 56 km/h) (Keon, 2016) and/or Oblique Moving Deformable Barrier (15 degrees, 35% overlap, 90 km/h barrier speed) (Saunders et al., 2015) crash test procedures. Vehicle selection was limited to those which received a “Good” or “Acceptable” rating in the Insurance Institute for Highway Safety (IIHS) Small Overlap Impact (SOI) crash test and also had side curtain airbags meeting the requirements of Federal Motor Vehicle Safety Standard (FMVSS) No. 226, “Ejection mitigation.” See APPENDIX D for a list of crash tests included in this evaluation. Data, reports, photos, and videos from these crash tests are located in the NHTSA Vehicle Crash Test Database (<https://www.nhtsa.gov/research-data/databases-and-software>).

Fleet data from NHTSA New Car Assessment Program (NCAP) testing is also presented for the purpose of comparing trends in fleet testing versus trends in field data.

2.5 Age Considerations – Injury Risk Functions

The National Automotive Sampling System – General Estimates System (NASS-GES) was queried for case years 2006 to 2015 to present the mean age of male drivers involved in frontal crashes. The 10-year trend is seen in Figure 2.1. Extrapolate forward to 2020 and the estimated mean age for male drivers in frontal crashes is 40-years old. For risk functions presented later in this report that use age as a covariate, 40 will be used as the age as it represents the mean age of exposed male drivers in frontal crashes.

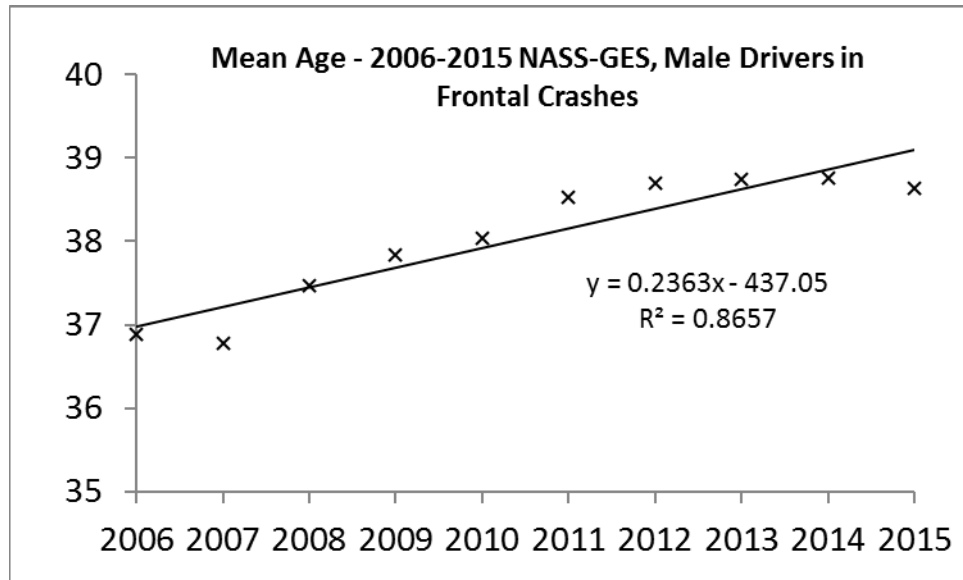


Figure 2.1. NASS-GES mean age for male drivers in frontal crashes, case years 2006-2015.

3 HEAD

3.1 Field and Historical Fleet Data

It can be seen in Table 1.1 that the brain is the most frequently injured body region at the AIS 2+ severity level for all occupants in frontal crashes with knee/thigh/hip, rib cage injuries being the 2nd and 3rd most frequently injured for body regions associated with the THOR-50M. Brain injuries remain prominent when looking at belted and unbelted drivers and right front passengers. Brain injuries are also the most costly injury type per the attributable costs presented in Figure 1.2.

Figure 3.1 shows how the rate of brain injury and skull and facial fractures (both at the AIS 2+ level) have changed in recent model years for belted drivers in frontal crashes where an airbag deployed (no delta-V or damage extent filter). The case years included for NASS-CDS were 1993 to 2015. The rate represents a running 3-year average of the percent injured (i.e. injured cases divided by total number of cases; e.g. model year 1992 includes the total weighted count of 2+ injuries from 1990, 1991 and 1992, divided by the total number of cases for those years). The 1990 model year is the first with over 100 raw count cases that fit the inclusion criteria. Prior model years had very few cases of belted drivers with deployed airbags. This is why 1992 is the first model year considered in the presented 3-year average. It appears that while the rate of facial/skull fracture has not changed given belted, airbag restrained drivers in frontal crashes, the rate of brain injury at the AIS 2+ level has increased. In contrast, Figure 3.2 shows a decreasing trend of HIC₁₅ values/risk of vehicles tested in the 35-mph full frontal test condition (NCAP, FMVSS No. 208) from model year 1990 to 2019. These tests were with the Hybrid III 50th percentile male frontal dummy or H3-50M.

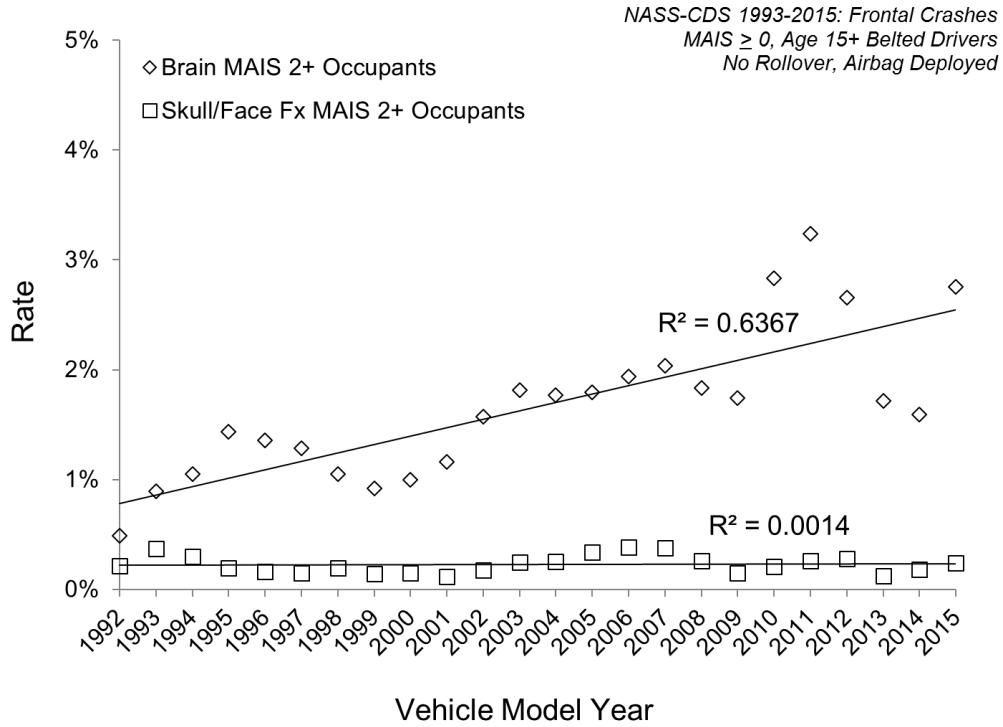


Figure 3.1. Skull/facial fracture MAIS 2+ and brain injury 2+ rate versus model year (1992 to 2015) from NASS-CDS 1993 to 2015.

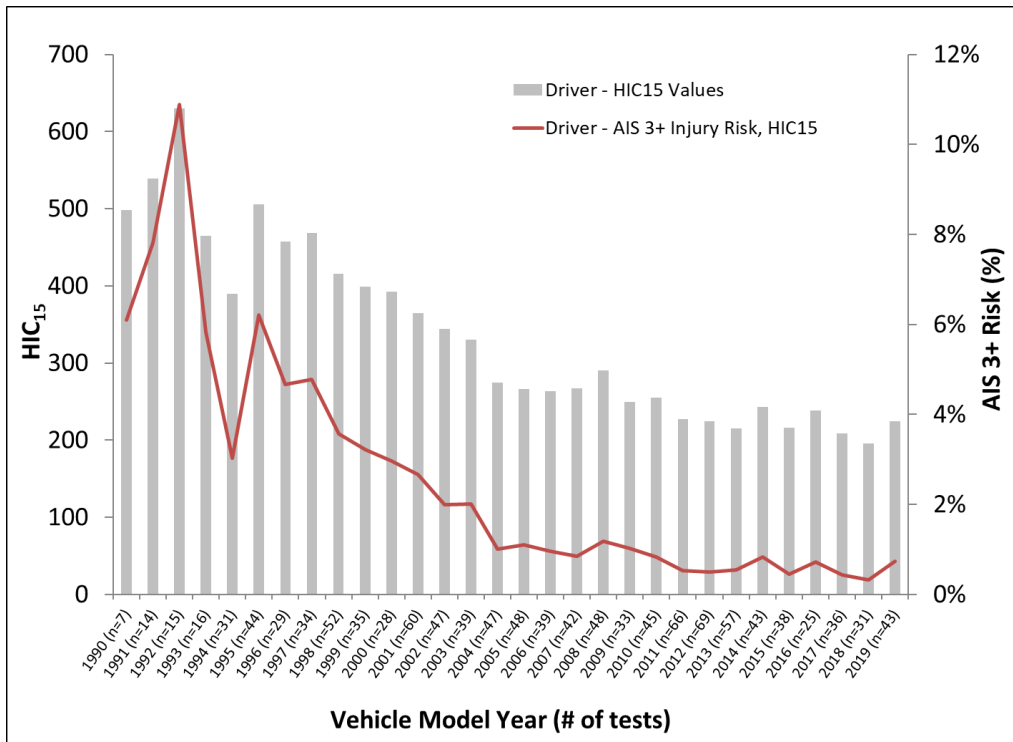


Figure 3.2. H3-50M driver HIC₁₅ values and predicted AIS 3+ risk from model year 1990 to 2019 in 35-mph frontal NCAP tests.

Table 3.1 shows the relative occupant counts of brain injury versus skull/facial fracture for belted drivers in frontal crashes for NASS-CDS case years 2000-2015 where there was a deployed frontal airbag. It can be noted that the majority of occupants with an AIS 2+ or 3+ brain injury sustained those injuries in the absence of skull or facial fractures.

Table 3.1. Brain injury versus skull/facial fracture for belted, airbag restrained drivers in frontal crashes (NASS-CDS 2000-2015).

		Skull/Facial Fracture		Skull/Facial Fracture	
		AIS 2+		AIS 3+	
		0	1	0	1
Brain AIS 2+	0	5,365,132 (13,699)	7,083 (87)	5,370,023 (13,761)	2,192 (25)
	1	82,135 (634)	4,864 (99)	84,758 (679)	2,241 (54)
Brain AIS 3+	0	5,435,570 (14,161)	8,496 (111)	5,441,535 (14,240)	2,531 (32)
	1	11,697 (172)	3,451 (75)	13,246 (200)	1,902 (47)

Figure 3.3 shows trends for traumatic brain injury (TBI) related fatalities due to motor vehicle crashes (MVC) from the Multiple Cause of Death (MCoD) dataset maintained by the Centers for Disease Control and Prevention (<http://wonder.cdc.gov/mcd.html>). Also shown are FARS totals for the same years. It can be seen that TBI-related and total fatality counts follow similar trends.

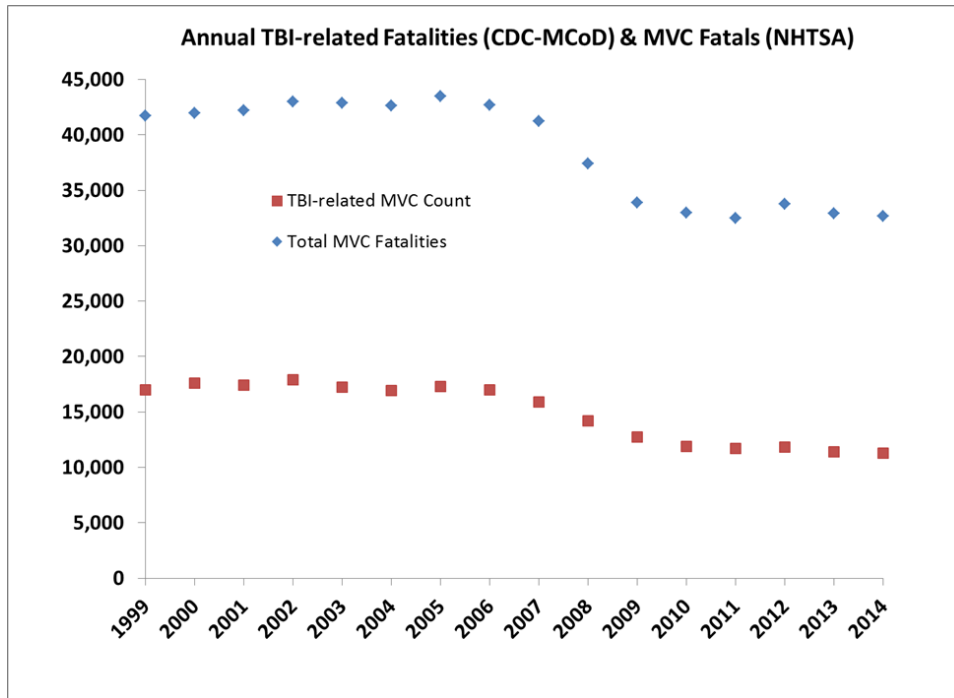


Figure 3.3. TBI-related brain injuries in motor vehicle crashes from MCoD dataset.

The CIREN database includes regional injury mechanisms assigned by biomechanical engineers during the case review process. A query of restrained first row occupants sustaining AIS 2+ head and face injuries in frontal crashes was performed to determine the dominant injury-producing mechanisms. Frontal crashes were broadly defined for this query, and include crashes with principal directions of force within 30 degrees of 12 o'clock and any amount of frontal overlap. Only crashes occurring after June 1, 2010 were included in this query. Of 488 occupants in qualifying frontal crashes, 93 sustained an AIS 2+ injury to the head or face, and the mechanisms of the individual injuries by type are shown in Figure 3.4. Fractures were most often coded as the result of compression. Anatomical brain injuries and loss of consciousness (LOC) were assigned regional mechanisms of rotational motion, linear acceleration, and compression. These recorded mechanisms are inferred from the available data and may have been limited to available researcher/published biomechanical knowledge at the time each case was reviewed. Additionally, in brain/LOC injury cases, when the regional mechanism is assigned as "compression" it is generally referring to the type of loading (i.e. contact to a relatively hard component such as the steering wheel or A-pillar) and not an injury that is physically due to compression of the skull or brain tissue. In most of these cases rotational/translational acceleration/velocity was assigned as the secondary regional mechanism.

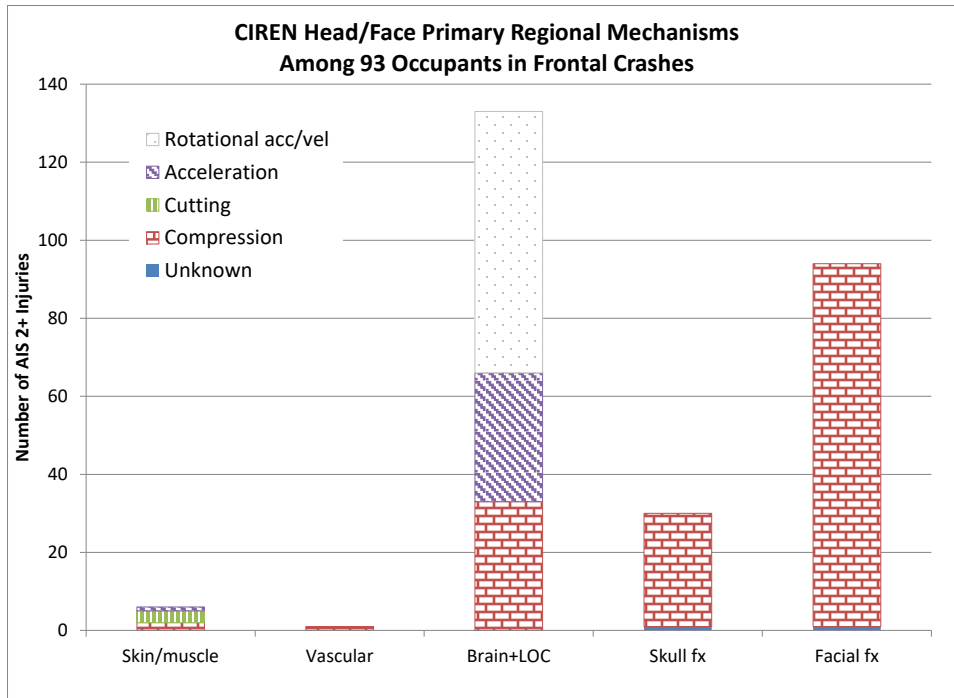


Figure 3.4. Recorded mechanisms of head and face injuries for belted front row occupants involved in frontal crashes from the CIREN database.

3.2 Instrumentation

For measurement of head center of gravity (CG) translational acceleration and angular velocity the THOR-50M is equipped with three uniaxial accelerometers and three angular rate sensors, respectively (Figure 3.5). Five uniaxial face load cells can be installed, though these load cells have not been installed in any vehicle crash tests with THOR-50M ATDs in the NHTSA Vehicle Database. The head also includes a biaxial tilt sensor which measures the quasi-static orientation of the head for pre-test positioning purposes.

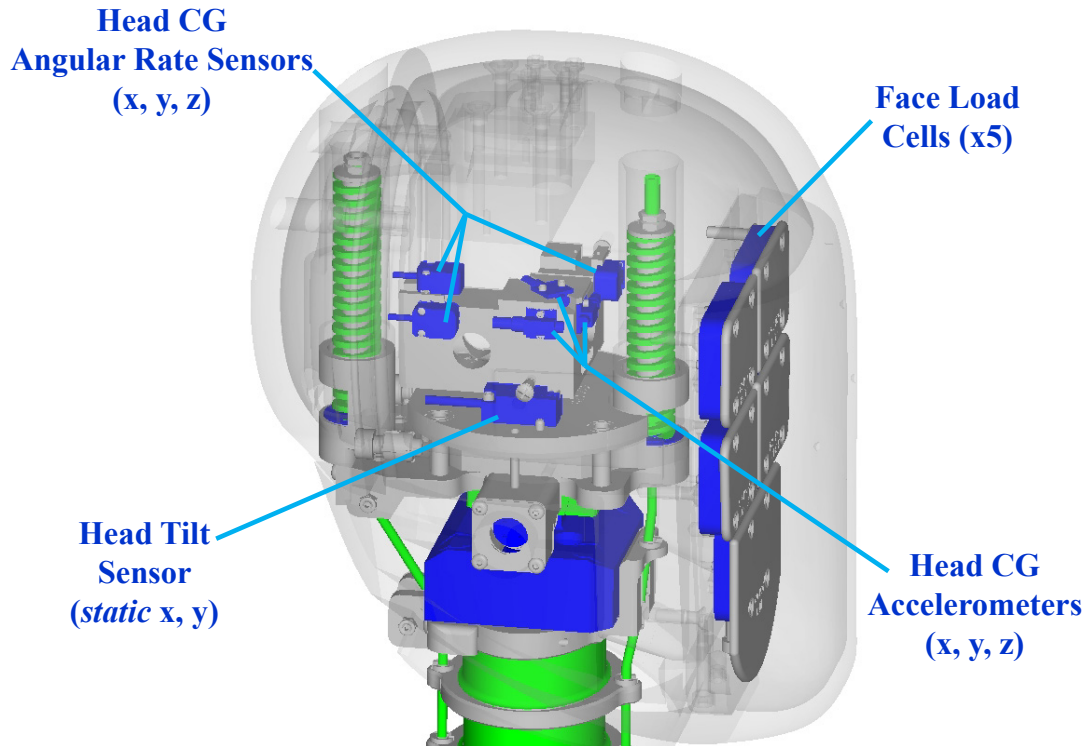


Figure 3.5. THOR-50M head instrumentation.

3.3 Biofidelity

The biofidelity of the THOR-50M is described in Parent et al. (2017). For translational motion the response of the THOR-50M headform was evaluated in head drop, whole-body head impact, face rigid bar, and face rigid disk impact conditions. The classified biofidelity performance was excellent for the head drop, whole-body head impact, and face rigid disk impact conditions. The THOR-50M biofidelity performance in the face rigid bar impact condition was marginal, while the H3-50M has poor biofidelity in both face rigid bar and face rigid disk impact conditions.

The angular velocity response of the THOR-50M head can be observed in a few experimental conditions. First, head and neck response is measured in a frontal flexion condition. In this condition, biofidelity for the head/neck measures (angle, displacement, resultant acceleration) ranges from good to poor. However, a qualitative comparison of head angular rate time-history data of the THOR-50M versus the referenced biofidelity data shows that the peak value and timing is similar. The THOR-50M was also tested in full-body sled test conditions. Four conditions were evaluated: (1) 40 kph, zero degree with standard/non-force limited three-point seat belts; (2) 30 kph, zero degree with force-limited three-point seat belts; (3) similar to 2nd condition, but with the sled buck rotated 30 degrees to represent a near side condition for the occupant; and (4) far-side oblique condition in vehicle buck with production restraints (seat belts, passenger airbag) tested in a condition meaning to duplicate the full-scale angle/severity of NHTSA's left oblique crash test procedure.

For condition (1), the angular rate biofidelity ranged from excellent to marginal. Excellent biofidelity was found for y-axis rotation (dominant axis of rotation in a zero-degree frontal sled). For condition (2), angular rate biofidelity ranged from good to excellent for the respective axes of rotation. Biofidelity for x- and y-axis rotations in condition (3) were either excellent or good. Biofidelity for z-axis rotation was poor. As was noted by Parent et al. (2017), the post-mortem human subjects (PMHS) lacked any resistance to z-axis rotation as compared to the THOR-50M and H3-50M. Additionally, it is noted that this particular oblique condition does not include any head restraint (airbags) and thus does not represent the interactions we see in full-scale fleet testing. Out of all of the conditions, condition (4) is most relevant to the type of airbag loading/restraint we expect for front row seated occupants in frontal/oblique crashes. For the THOR-50M seated in a similar configuration to the three PMHS (“Position C”), the head angular velocity about the x- and y-axes both had good biofidelity while the z-axis angular velocity biofidelity was excellent. In oblique, far-side seated conditions, it is z-axis rotation that contributes most to the angular velocity-based criterion (BrIC) described later in this chapter. BrIC values were also calculated for the respective post-mortem human subjects (PMHS) and paired THOR-50M and H3-50M (Figure 3.6) in the four sled test conditions. The THOR-50M compares well to PMHS in all conditions other than condition (3) (see prior discussion). In looking closer at condition (4), the single THOR-50M test where the lower spine adjustment was changed to allow for the THOR-50M to sit in a more slouched position similar to the three PMHS resulted in a BrIC value of 1.2, which is closer to the average of 1.1 for the three PMHS.

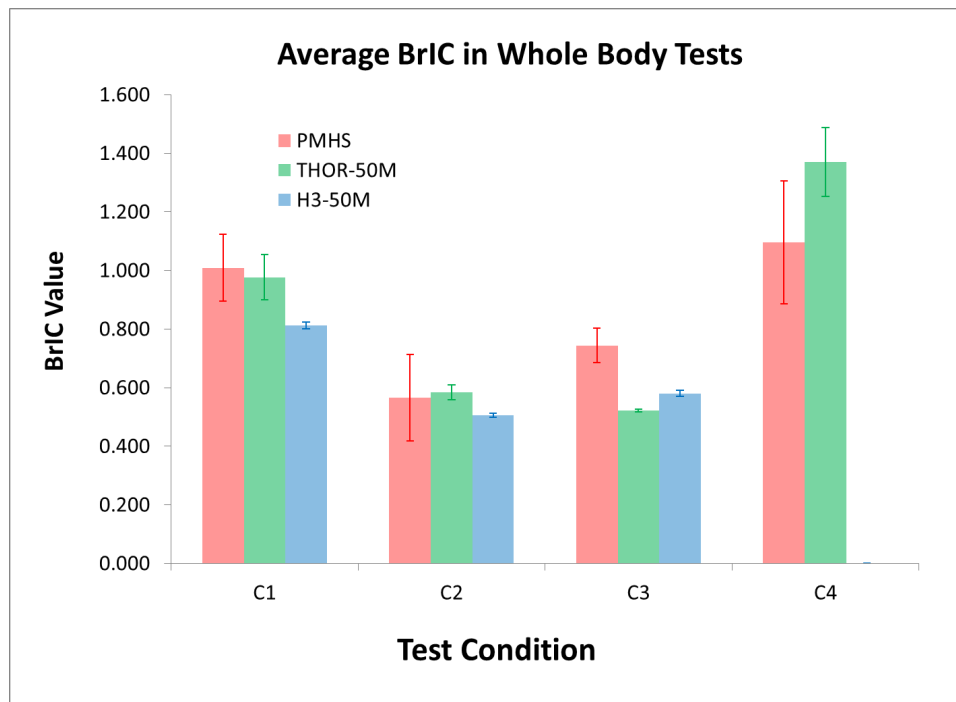


Figure 3.6. Average BrIC values in sled tests of PMHS, THOR-50M and H3-50M.

3.4 Brain Injuries

3.4.1 Introduction

Rotational motion of the head as a mechanism for brain injury was suspected as early as 1865 (Alquié, 1865), mentioned by Goggio (1941), clearly explained by Holbourn (1943), and first observed on live monkeys by Pudenz and Shelden (1946). Since then several research studies by various institutions were conducted to confirm/reject this hypothesis (thorough reviews of these studies can be found, for example, in Gurdjian (1972), Hess et al. (1980), Ommaya (1984), Gennarelli et al. (1985), Melvin et al. (1993), Hardy et al. (1994), McLean and Anderson (1997), Goldsmith (2001), Shaw (2002), Goldsmith and Monson et al. (2005), Monson et al. (2005), Meaney et al. (2014)). Most of the studies were conducted on animals and concluded that rotational kinematics experienced by the animal's head may cause axonal deformations large enough to induce their functional deficit (Ommaya, 1984). Other studies utilized physical and mathematical models of human and animal heads to derive brain injury criteria based on deformation/pressure histories computed from their models (Gennarelli et al., 1971, 1972, 1985; Margulies and Thibault, 1992; Nusholtz et al., 1984; Zhang et al., 2001; Takhounts et al., 2003, 2008).

All of these previous studies together with established scaling techniques were utilized in the development of the Brain Injury Criterion or BrIC. First, loading histories of the available animal head kinematics data were digitized and scaled to the size of the human head. These loading histories were then applied to two different detailed mathematical models of the human head, each validated against various human brain response datasets. Next, physical injury criteria (based on maximum principal strain, or MPS, and cumulative strain damage measure, or CSDM) were established for the human brain based on the injury information obtained from the animal dataset. Since the animal injury data were predominantly for diffuse axonal injury (DAI) type injuries (including severe concussion, subdural hematoma, DAI), which are AIS 4+ in severity, CSDM and MPS risk curves were derived for AIS 4+ injuries. The associated DAI or severe concussion injuries are considered AIS 4+ injuries when looking at both the AIS 1990 (1998 Update) and 2005 (2008 Update) versions of AIS (AAAM, 1998; AAAM, 2008). The AIS 1+, 2+, 3+, and 5+ risk curves for CSDM and MPS were then computed using the ratios between corresponding risk curves for head injury criterion (HIC) at a 50% risk. The risk curves for BrIC were then obtained from CSDM and MPS risk curves using the linear relationship between CSDM - BrIC and MPS - BrIC respectively. The AIS 2+ brain injury risk curve was subsequently verified using angular velocities calculated at a 50% probability of concussion in college football players instrumented with 5 degrees of freedom (DOF) helmet systems. Finally, Anthropomorphic Test Device (ATD) (Hybrid III 50th Male, Hybrid III 5th Female, THOR 50th Male, ES-2re 50th Male, SID-IIs 5th Female, WorldSID 50th Male, and WorldSID 5th Female) test data (NCAP, linear impact, and frontal oblique tests) were used to establish BrIC for all ATDs. A detailed description of the derivation of BrIC is given in Takhounts et al. (2013 and 2011).

BrIC is a function of the max angular velocities (ω_x , ω_y , and ω_z) computed (at any time) about x-, y-, and z-axes respectively along with the corresponding critical angular velocities ω_{xC} , ω_{yC} , and ω_{zC} :

$$BrIC = \sqrt{\left(\frac{\omega_x}{\omega_{xC}}\right)^2 + \left(\frac{\omega_y}{\omega_{yC}}\right)^2 + \left(\frac{\omega_z}{\omega_{zC}}\right)^2}, \quad [3.1]$$

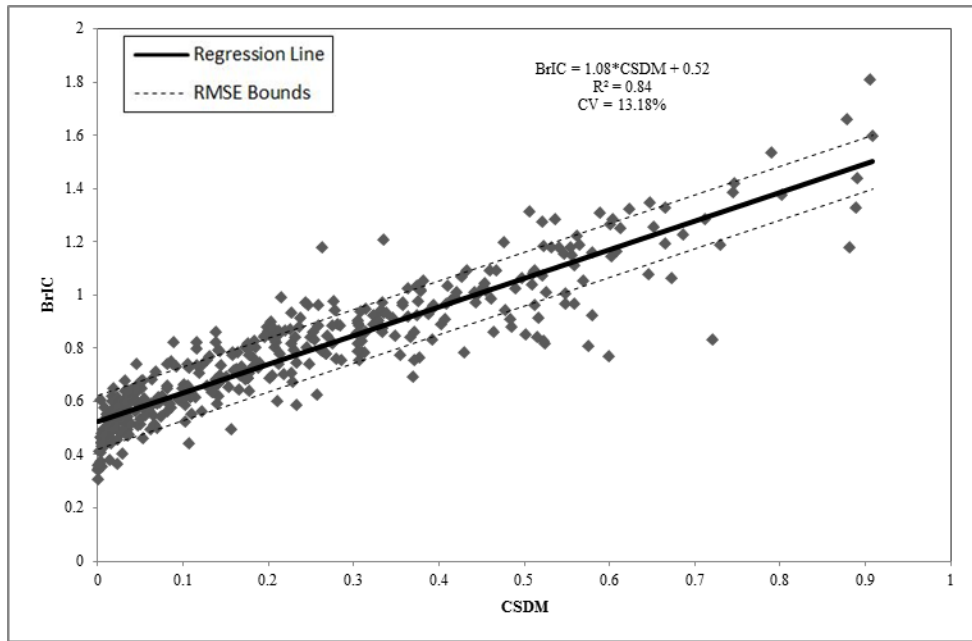
where ω_{xC} , ω_{yC} , and ω_{zC} are given in Table 3.2 below.

Table 3.2. Critical max angular velocities in each direction.

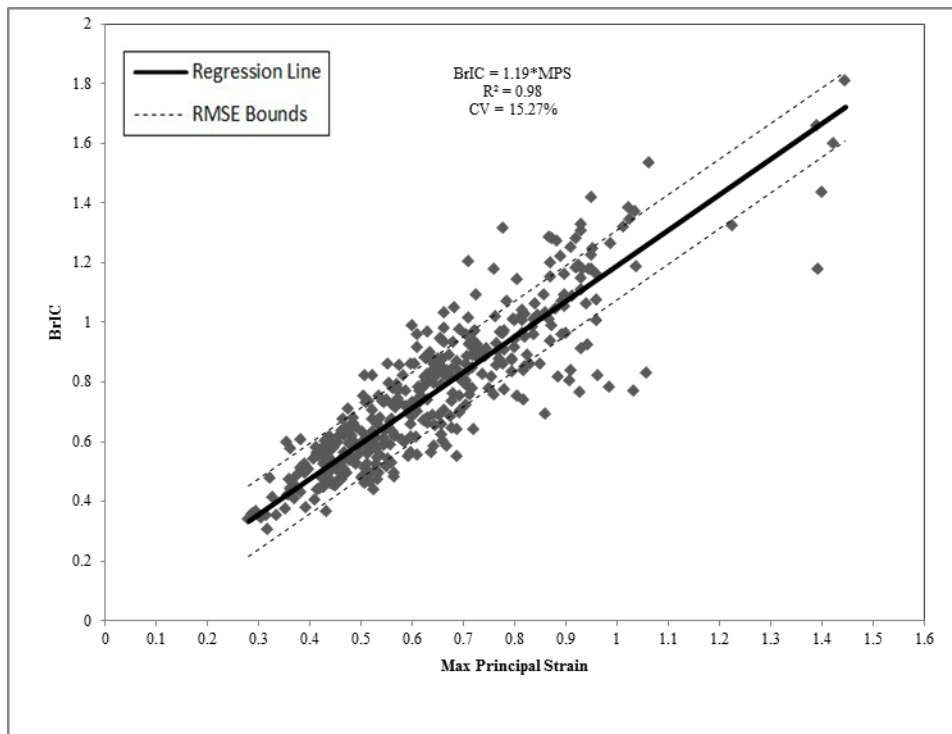
Critical Max Angular Velocity	Rad/s
ω_x	66.25
ω_y	56.45
ω_z	42.87

Besides angular velocities, other head kinematic parameters, such as angular acceleration (see, for example, Takhounts et al., 2011), the time duration of angular velocity components (see below), and other combinations of kinematic parameters were considered in the development of the brain injury criterion, but a simple combination of the max angular velocity components (equation 3.1) was sufficient to correlate to the strain-based measures CSDM and MPS.

Figure 3.7 (a) shows the correlation between BrIC and CSDM for all ATDs, while Figure 3.7 (b) shows the correlation between BrIC and MPS – both correlations were based on the 413 data points available at the time of publication (Takhounts et al., 2013). Note that the maximum angular velocity in each direction was calculated irrespective of the time it had occurred, as the second approach (maximum angular velocities at a fixed time of the maximum of any component) did not improve the correlation between BrIC and CSDM (and MPS). This makes physical sense, because after the head rotates about one axis and accumulates a certain volume of damaged brain cells (elements in the model exceeding 25% MPS – see definition of CSDM in Takhounts et al., 2003, 2008, 2013), any additional accumulation of damaged brain cells due to a second rotation (e.g. about a different axis of rotation) will be added to the previously damaged brain cells (in reality this addition is not simple, but quite complicated – see section below on time duration). This addition is reflected in the formulation of BrIC (equation 1) as a simple addition of the magnitudes of components of angular velocity. The effect of time difference between the peaks of angular velocity components on CSDM was also investigated for up to 150 ms and no significant differences in CSDM were observed.



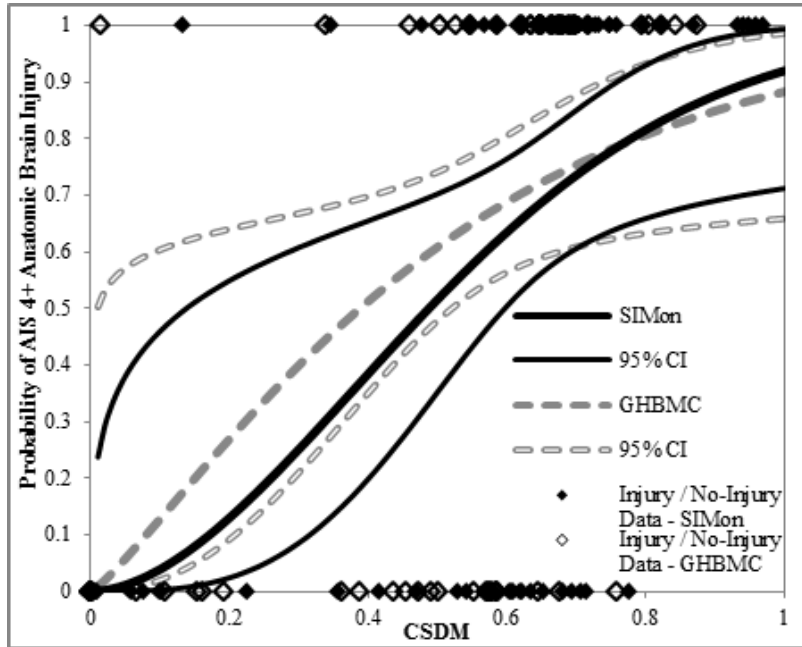
(a)



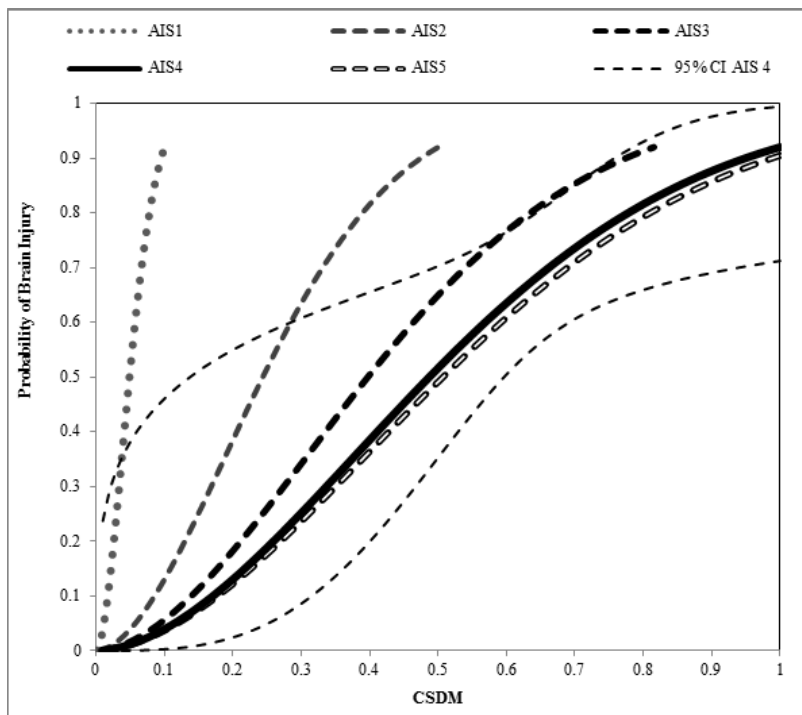
(b)

Figure 3.7. Correlation between (a) BrIC and CSDM and (b) BrIC and MPS for all ATDs in available tests (413 data points); adapted from Takhounts et al. (2013).

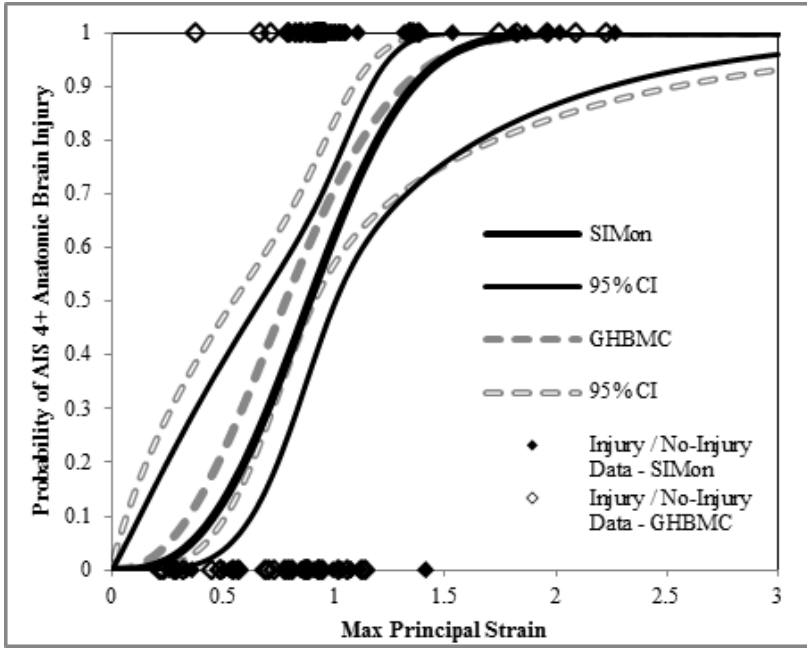
The risk curves for CSDM and MPS are given below in Figure 3.8, where AIS 1+, 2+, 3+, and 5+ risk curves were obtained by scaling the AIS 4+ risk curve at a level of 50% probability of injury using coefficients given in Takhounts et al. (2013), while Table 3.3 and Table 3.4 list equations for each of these curves.



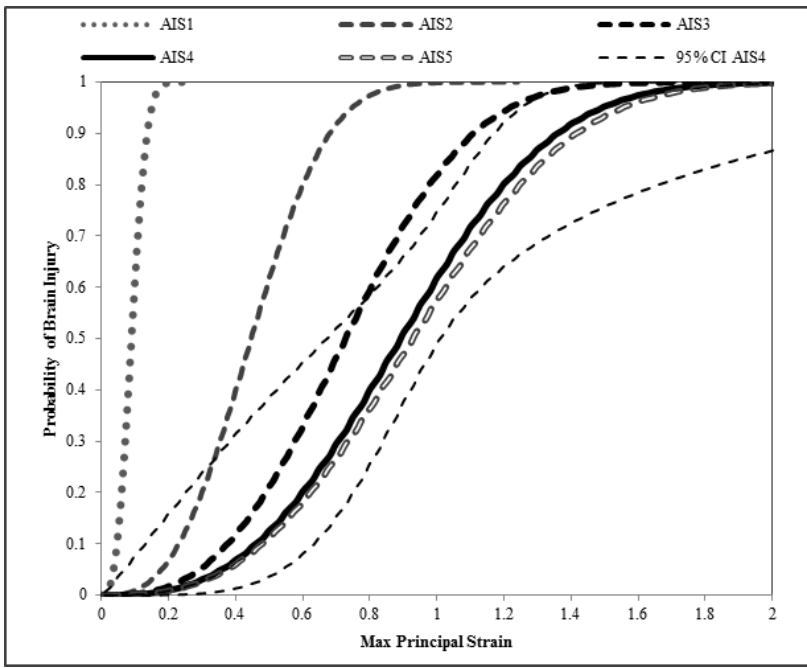
(a)



(b)



(c)



(d)

Figure 3.8. Risk of AIS 4+ anatomic brain injury in scaled animal tests using CSDM (a) and MPS (c) along with the scaled risk curves for various severities based on CSDM (b) and MPS (d) – adapted from Takhounts et al. (2013). Note that the areas under the receiver operator characteristic (AUROC) for the AIS 4+ risk curves are 0.83 for CSDM and 0.78 for MPS, respectively.

Table 3.3. Risk curve equations for CSDM – adapted from Takhounts et al. (2013).

$$P(AIS\ 1\ +) = 1 - e^{-\left(\frac{CSDM}{0.060}\right)^{1.8}}$$

$$P(AIS\ 2\ +) = 1 - e^{-\left(\frac{CSDM}{0.300}\right)^{1.8}}$$

$$P(AIS\ 3\ +) = 1 - e^{-\left(\frac{CSDM}{0.490}\right)^{1.8}}$$

$$P(AIS\ 4\ +) = 1 - e^{-\left(\frac{CSDM}{0.600}\right)^{1.8}}$$

$$P(AIS\ 5\ +) = 1 - e^{-\left(\frac{CSDM}{0.624}\right)^{1.8}}$$

Table 3.4. Risk curve equations for MPS – adapted from Takhounts et al. (2013).

$$P(AIS\ 1\ +) = 1 - e^{-\left(\frac{MPS}{0.101}\right)^{2.84}}$$

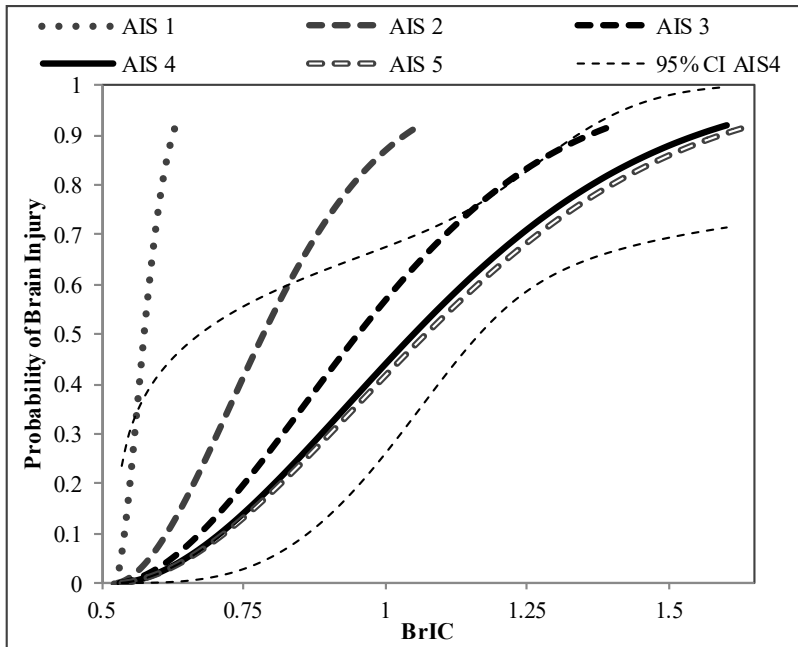
$$P(AIS\ 2\ +) = 1 - e^{-\left(\frac{MPS}{0.505}\right)^{2.84}}$$

$$P(AIS\ 3\ +) = 1 - e^{-\left(\frac{MPS}{0.828}\right)^{2.84}}$$

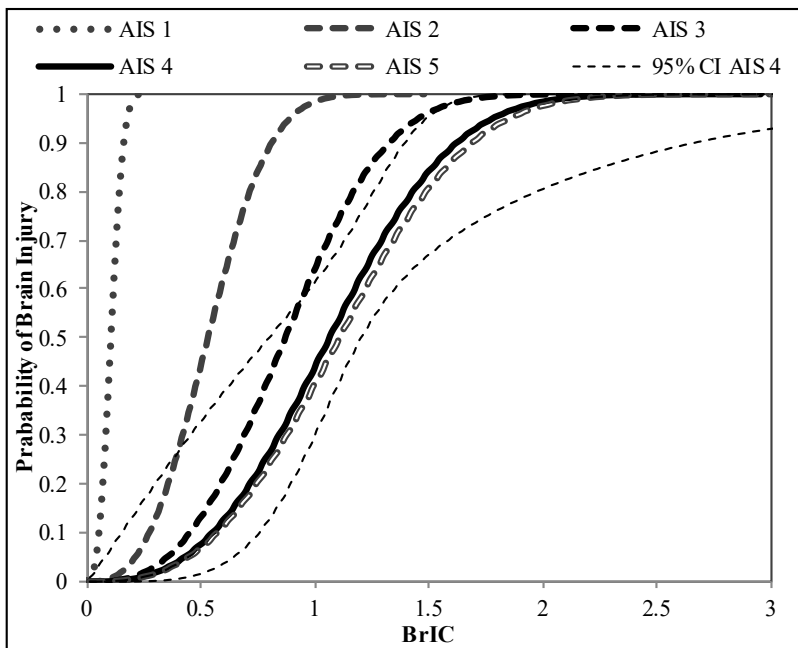
$$P(AIS\ 4\ +) = 1 - e^{-\left(\frac{MPS}{1.010}\right)^{2.84}}$$

$$P(AIS\ 5\ +) = 1 - e^{-\left(\frac{MPS}{1.050}\right)^{2.84}}$$

The risk curves for BrIC were then obtained based on the linear relationship between BrIC and CSDM (MPS) as shown in Figure 3.9. Table 3.5 and Table 3.6 list equations for each of these risk curves.



(a)



(b)

Figure 3.9. BrIC based on CSDM (a) and MPS (b) obtained from equation 1 with critical angular velocities given in Table 3.2 – adapted from Takhounts et al. (2013).

Table 3.5. Risk curves for BrIC based on CSDM – adapted from Takhounts et al. (2013).

$$P(AIS\ 1\ +) = 1 - e^{-\left(\frac{BrIC-0.523}{0.065}\right)^{1.8}}$$

$$P(AIS\ 2\ +) = 1 - e^{-\left(\frac{BrIC-0.523}{0.324}\right)^{1.8}}$$

$$P(AIS\ 3\ +) = 1 - e^{-\left(\frac{BrIC-0.523}{0.531}\right)^{1.8}}$$

$$P(AIS\ 4\ +) = 1 - e^{-\left(\frac{BrIC-0.523}{0.647}\right)^{1.8}}$$

$$P(AIS\ 5\ +) = 1 - e^{-\left(\frac{BrIC-0.523}{0.673}\right)^{1.8}}$$

Table 3.6. Risk curves for BrIC based on MPS – adapted from Takhounts et al. (2013).

$$P(AIS\ 1\ +) = 1 - e^{-\left(\frac{BrIC}{0.120}\right)^{2.84}}$$

$$P(AIS\ 2\ +) = 1 - e^{-\left(\frac{BrIC}{0.602}\right)^{2.84}}$$

$$P(AIS\ 3\ +) = 1 - e^{-\left(\frac{BrIC}{0.987}\right)^{2.84}}$$

$$P(AIS\ 4\ +) = 1 - e^{-\left(\frac{BrIC}{1.204}\right)^{2.84}}$$

$$P(AIS\ 5\ +) = 1 - e^{-\left(\frac{BrIC}{1.252}\right)^{2.84}}$$

3.4.2 New Data

Since the publication of original risk curves for BrIC (Takhounts et al., 2013), more data has become available to test the correlation between BrIC and CSDM/MPS. These include NHTSA oblique tests with the THOR-50M (full frontal, right and left oblique), frontal NCAP tests with the H3-50M and H3-05F, and side moving deformable barrier (MDB) and vehicle to pole conditions with the ES-2re 50th male and SID-IIs 5th female. NHTSA has also run side MDB and side pole tests with the World-SID 50th male. Also, additional Insurance Institute for Highway Safety (IIHS) small and moderate overlap test data with the H3-50M has been added. Finally, NHTSA conducted isolated head-to-airbag tests where several ATDs were driven into the frontal and side airbags at various initial velocities and angles to simulate many possible interactions between the ATDs heads and the restraint systems. For each of these tests, the Simulated Injury Monitor or SIMon finite element head model (Takhounts et al., 2003, 2008) was exercised using the kinematic time-history data from the ATD to obtain CSDM and MPS, while the BrIC metric was calculated directly from the kinematic time-history data.

In total, the updated test dataset is comprised of 749 tests (versus the original 413) – see Appendix A for the publicly available test numbers. Figure 3.10 illustrates the correlation of BrIC with CSDM for all 749 tests. Neither the correlation coefficient nor the trend line have changed appreciably (compare with Figure 3.7a) indicating that new “out-of-sample” data with new test conditions did not affect much the relationship between CSDM and BrIC, thus making this relationship further validated.

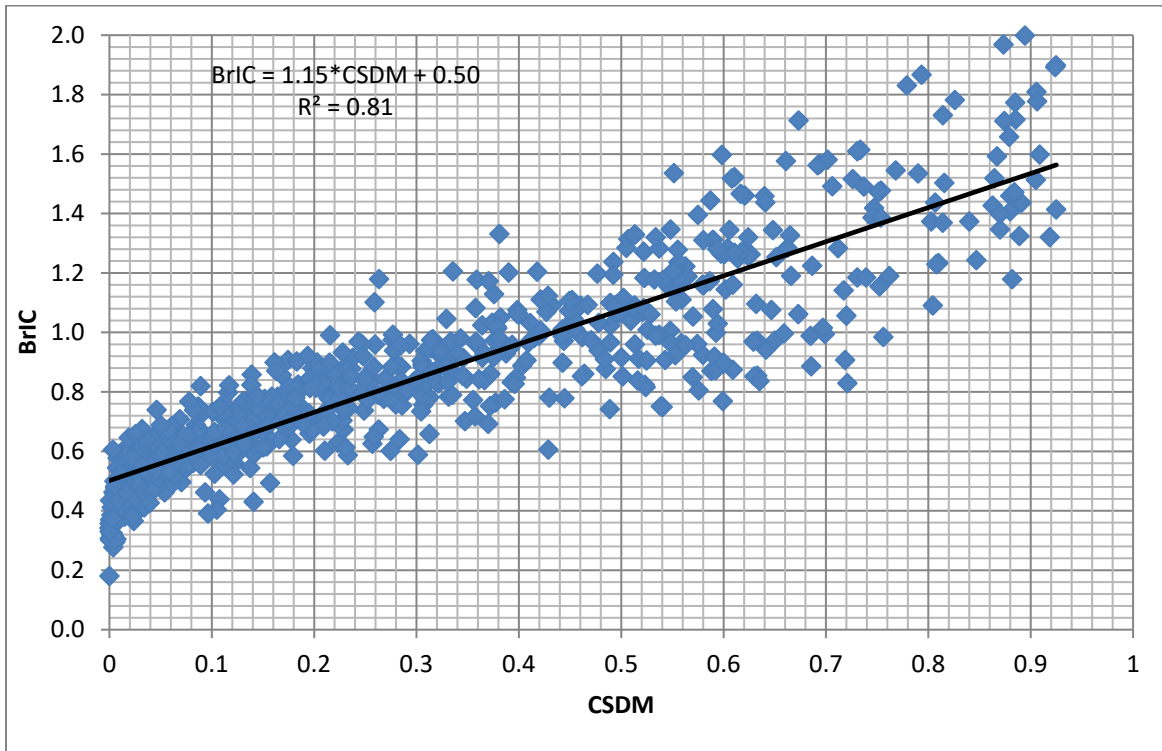
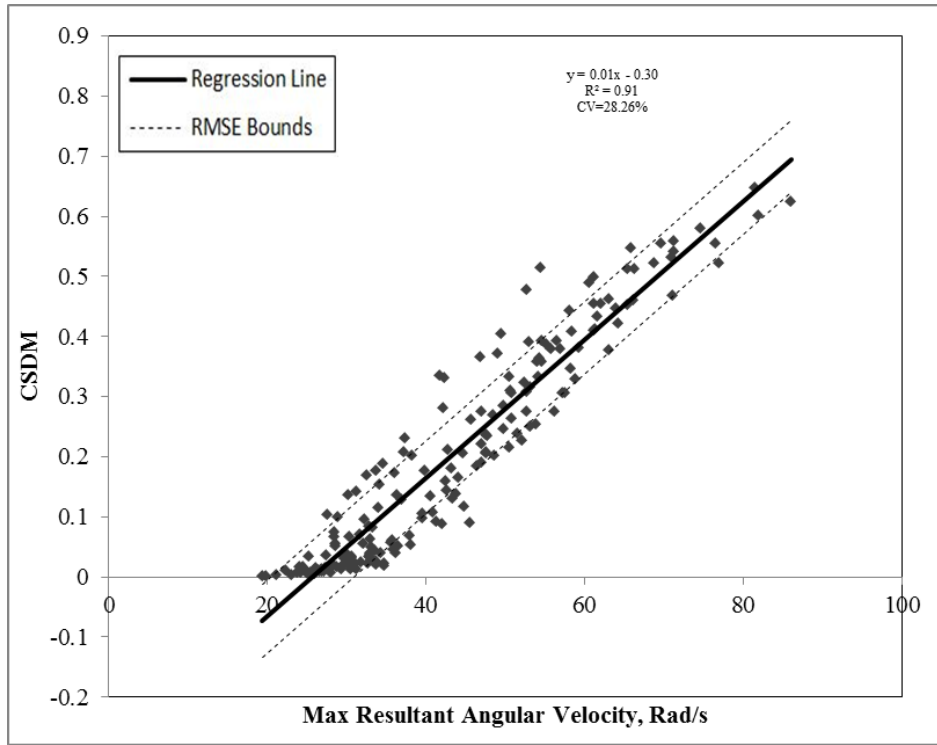


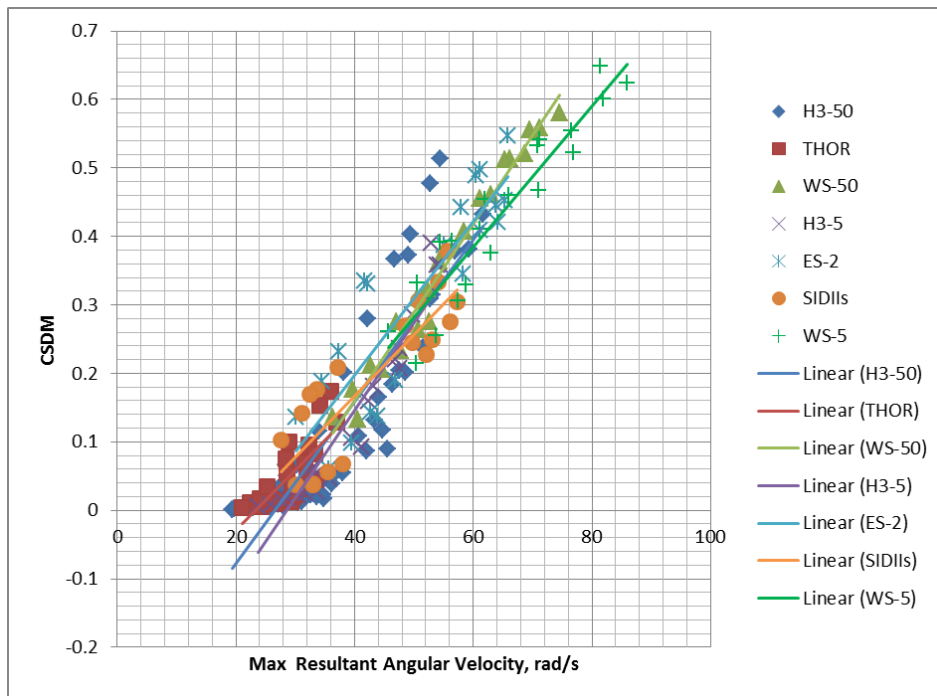
Figure 3.10. Correlation between BrIC and CSDM for all ATDs for all currently available tests (n=749).

3.4.3 Relationships for All ATDs vs Individual ATDs

The correlations between BrIC and CSDM given in Figure 3.7a and Figure 3.10 are given for all ATDs. Although it is apparent from the high R^2 that such relationships for individual ATDs cannot be statistically different from that given for all ATDs, Figure 3.11a replicates Figure I.8 from Takhounts et al. (2013) of the relationship between CSDM and max angular velocity for all ATDs tested, while Figure 3.11b separates the same data for each individual ATD. No significant differences are observed between individual ATD linear regression lines and that of the combined dataset. It should be noted that the data in Figure 3.11 is from the well-controlled linear impactor tests described in Takhounts et al. (2013), where each ATD was impacted in the direction of the primary use (frontal ATDs were impacted at 0° angle, side ATDs at 90° to the SAE x-axis) as well as at the “oblique” angle of 30° from the direction of primary use. Thus, the correlations in Figure 3.11 already incorporate out of plane head rotation (combined y- and z-axes rotation for frontal ATDs; and x- and z-axes rotation for side ATDs), consequently reflecting current neck properties (stiffness) of each ATD (including torsional or z-axis stiffness) in the relationship between BrIC and CSDM.



a)



b)

Figure 3.11. CSDM versus max resultant angular velocity for all ATDs (a) and for each individual ATD (b).

3.4.4 Dependence on Time Duration

It has been hypothesized by Holbourn (1943) that “for blows of long duration the shear strains in the brain are proportional to the force, hence the injury is proportional to the acceleration, or the rate of change of velocity of the head... For very short blows the injury is proportional to the force multiplied by the time for which it acts, hence the injury is proportional to the change of velocity of the head...” The switchover occurs somewhere between 2 and 200 ms. Glaister (1975) presented the following chart (Figure 3.12) that was introduced in H.E. von Gierke (1964) demonstrating that the human body response (injury response) when loaded with acceleration pulses of various magnitudes and time durations depends on the velocity change for the first 200 – 300 ms, then on the pulse length (pulse time duration) for up to 2 – 10 s, then for even longer time durations it depends on the peak acceleration. Note that when referring to the signal/pulse time duration, both Holbourn and Glaister (or von Gierke) implied the time duration of the (angular) acceleration pulse (Figure 3.12), and when angular acceleration and time duration are considered together it represents angular velocity upon which BrIC is based. Here, however, the dependence of BrIC on the angular velocity time duration was analyzed.

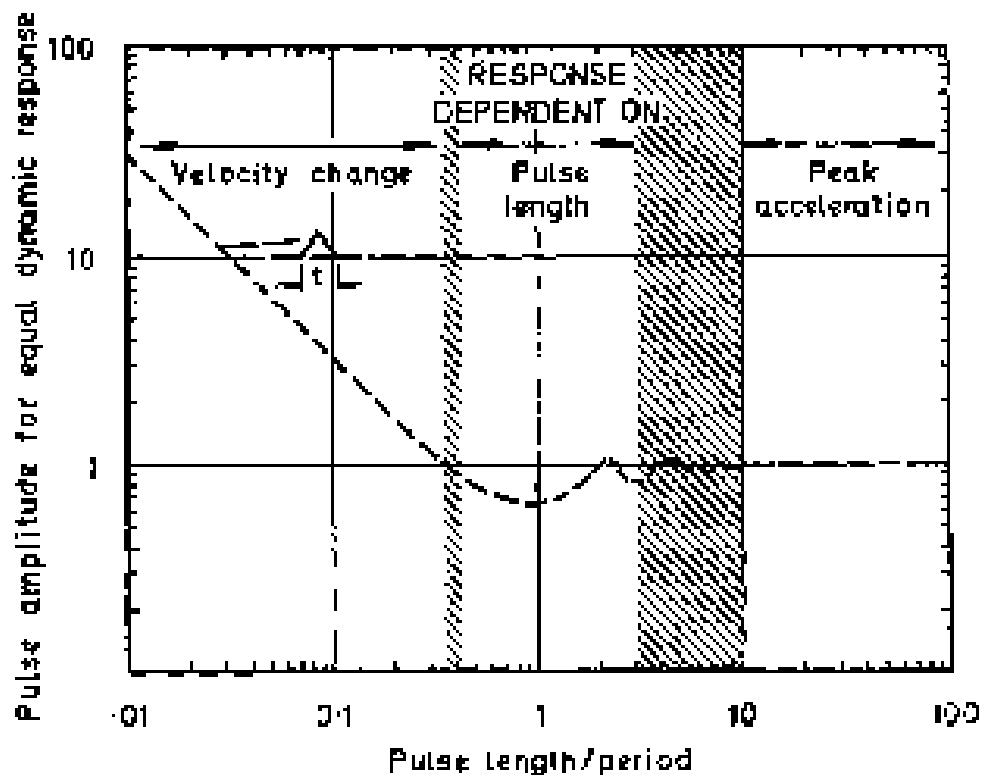


Figure 3.12. Response of human body (injury response) to the applied acceleration pulse of various magnitudes and time durations (copied from Glaister, 1975).

To investigate the potential dependence of BrIC on the angular velocity signal time duration, the haversine type angular velocity time histories shown in Figure 3.13 were applied to the SIMon head model. The magnitude of the max angular velocity about each rotational axis was varied from 20 to 120 rad/s at 10 rad/s intervals, while the time duration ranged from 5 to 200 ms with 15 ms time intervals. It

can be observed from Figure 3.13 that the slopes of the applied angular velocity signals (or max angular acceleration) are decreasing with increased time duration. Hence, this study of the time duration effect on BrIC/CSDM may also be considered a study of the angular acceleration effect. The values of CSDM for each loading case were calculated and the curves of constant CSDM were plotted as functions of the angular velocity signal time duration. Figure 3.14 illustrates such dependence of CSDM on the signal time duration for rotations about the x-axis (coronal plane rotation). It indicates that up to approximately 30 ms, CSDM is increasing with increased time duration for each magnitude of the max applied angular velocity, and begins to monotonically decrease up until approximately 100 ms, after which it doesn't change. The critical values for angular velocity about the x-axis (x-direction) as functions of the signal time duration can be plotted using two values from the CSDM-based risk curve (Figure 3.15): 0.49 and 0.3, representing 50% and 25% risk of AIS 4+ brain injury, respectively. These critical angular velocity values decrease for up to approximately 30 ms time duration, after which they begin to increase until approximately 100-120 ms, after which they become relatively constant (independent of the time duration). The current critical value for the x-direction is 66.25 rad/s (Table 3.2), corresponding to approximately 45-ms time duration.

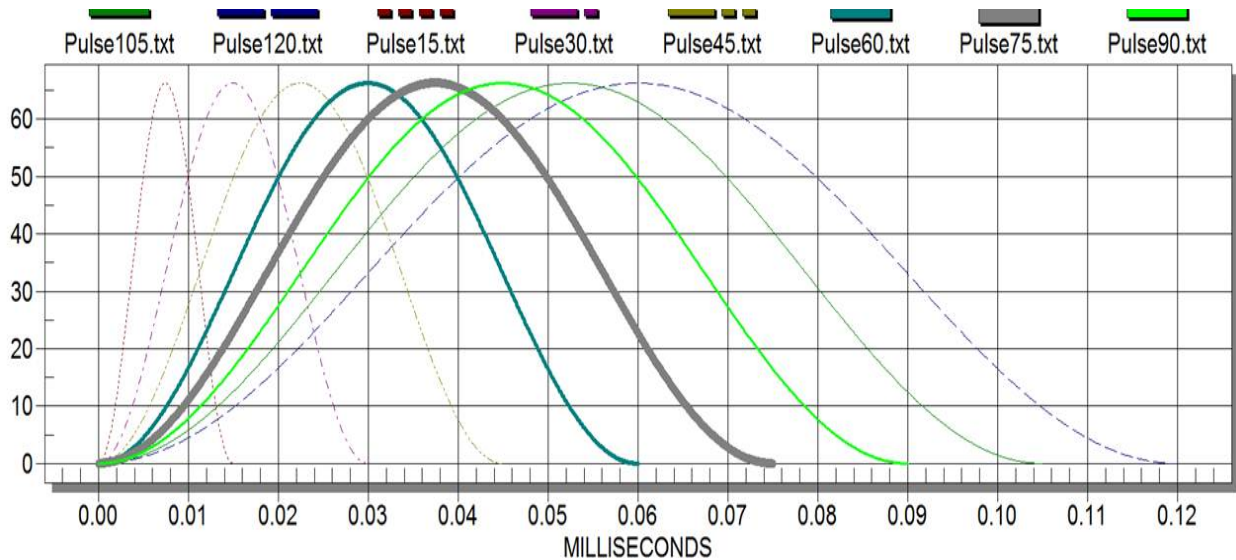


Figure 3.13. Haversine type angular velocity time histories applied to the SIMon head model.

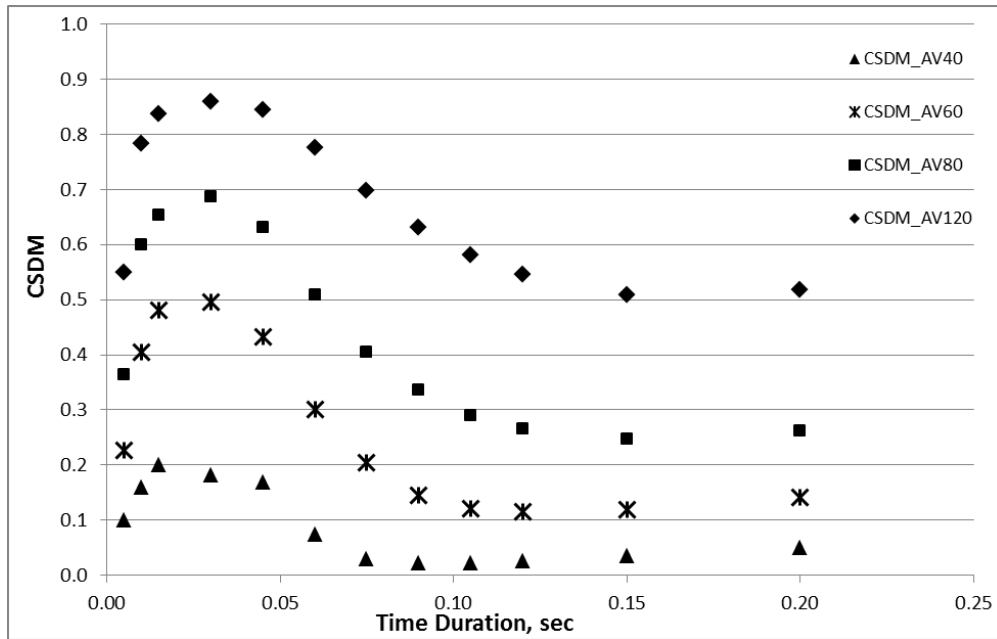


Figure 3.14. CSDM versus x-axis angular velocity signal time duration for four values of the max angular velocity: 40, 60, 80, and 120 rad/s.

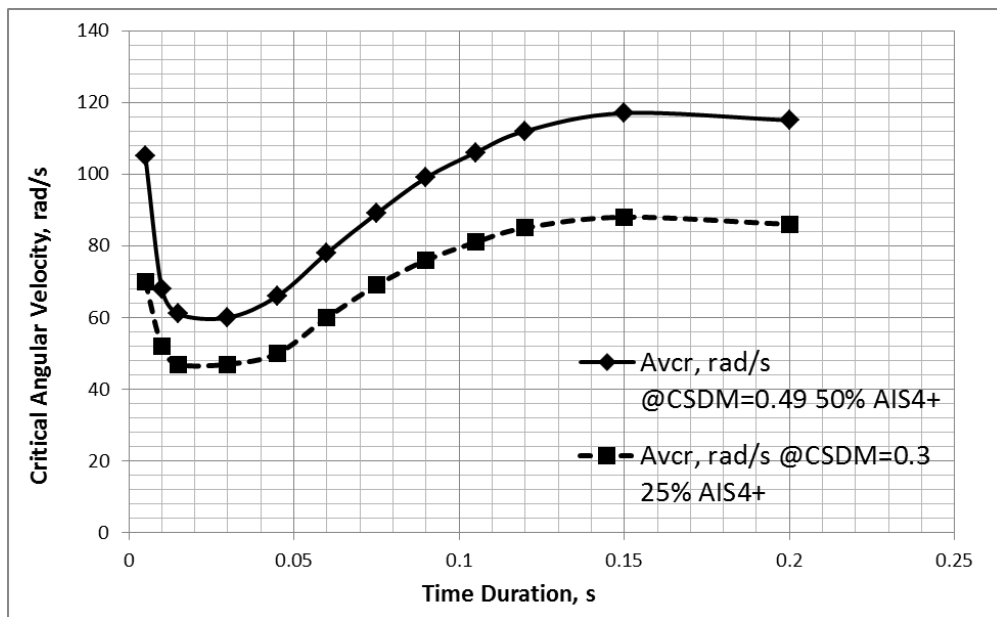


Figure 3.15. Critical angular velocities in x-direction for 50% and 25% risk of AIS 4+ brain injury as functions of signal time duration.

Similar figures for the other two rotational directions (y- and z- directions) were also obtained and their critical values of angular velocity as a function of the signal time duration were plotted and subsequently tabulated (Table 3.7). Table 3.7 can be viewed as a look up table for finding critical angular velocity

when the signal time duration is known. The question now becomes: how to find time duration for an arbitrary angular velocity signal time history?

Table 3.7. Critical angular velocities for each time duration and each rotational direction.

Time, s	X-direction		Y-direction		Z-direction	
	Avcr, rad/s @CSDM=0.49 50% AIS 4+	Avcr, rad/s @CSDM=0.30 25% AIS 4+	Avcr, rad/s @CSDM=0.49 50% AIS 4+	Avcr, rad/s @CSDM=0.30 25% AIS 4+	Avcr, rad/s @CSDM=0.49 50% AIS 4+	Avcr, rad/s @CSDM=0.30 25% AIS 4+
0.005	105	70	92	65	99	57
0.010	68	52	66	52	60	39
0.015	61	47	59	49	46	34
0.030	60	47	58	48	42	32
0.045	66	50	54	46	39	31
0.060	78	60	59	51	50	38
0.075	89	69	68	57	64	49
0.090	99	76	74	62	73	57
0.105	106	81	80	65	81	63
0.120	112	85	84	68	87	68
0.150	117	88	89	70	95	74
0.200	115	86	93	70	100	78

Three methods of estimating time duration for arbitrary signals were devised and the values of BrIC with time adjusted critical values of angular velocities recalculated using Table 3.7 (called “New BrIC”). Only one of the three methods (Appendix B) resulted in an improved R^2 (Figure 3.16) when compared with the “Original BrIC” given in Figure 3.10.

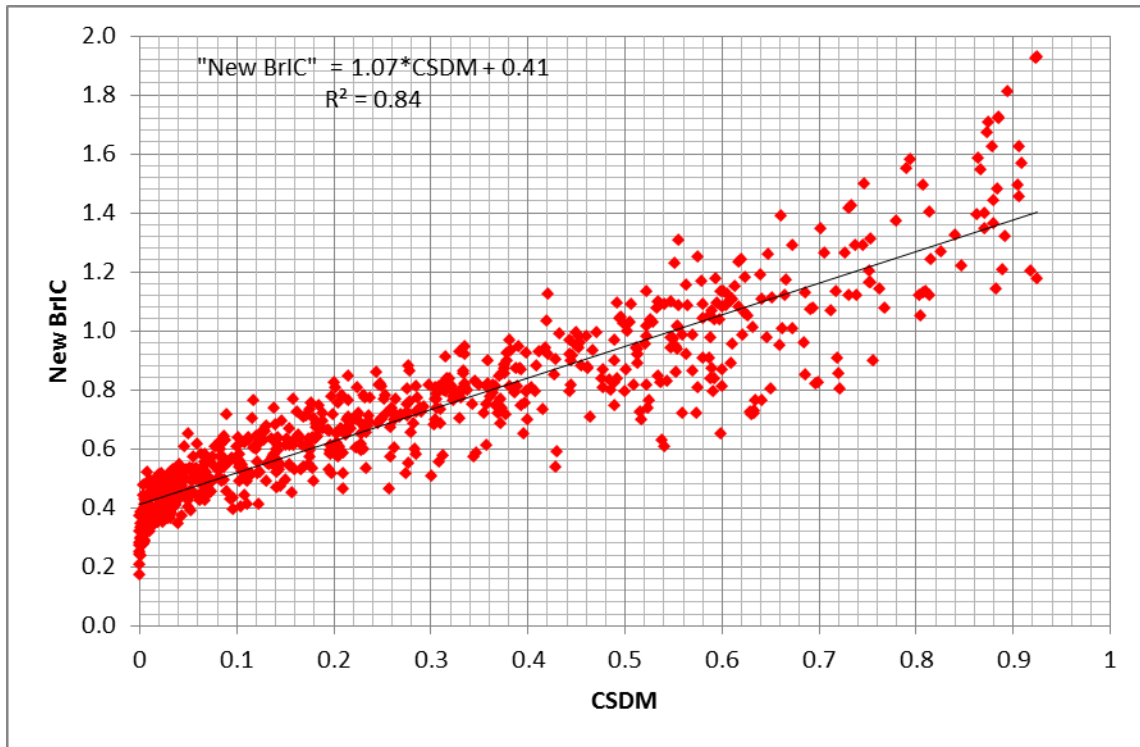
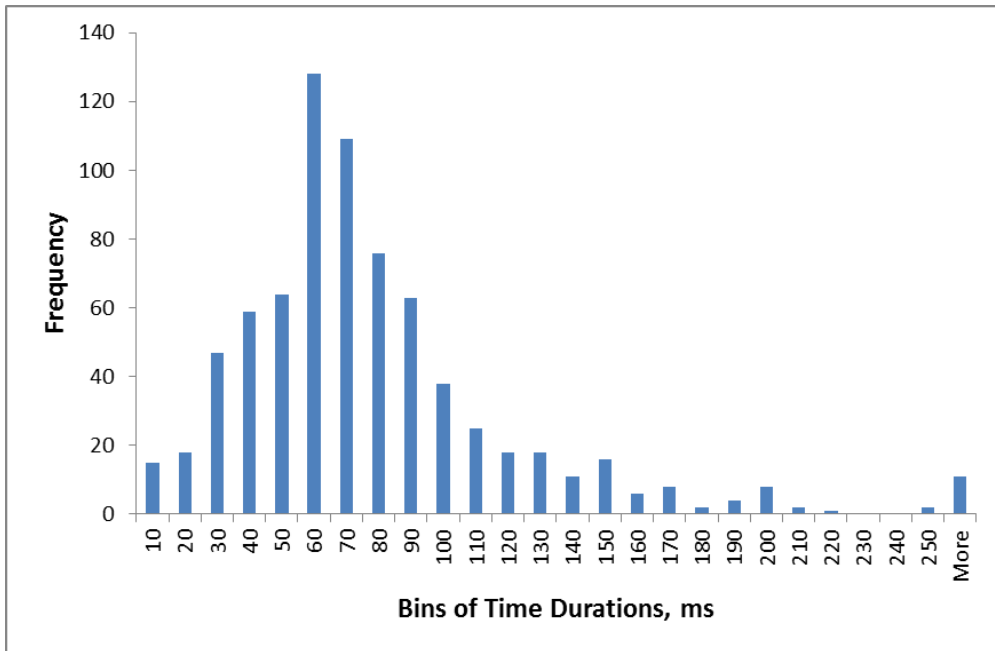


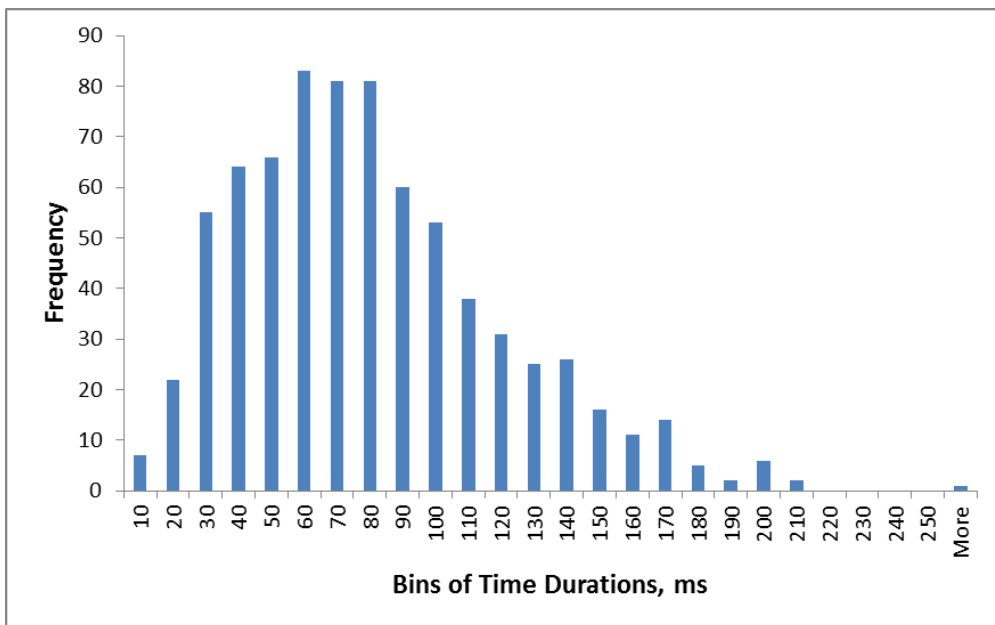
Figure 3.16. Correlation between the “New BrIC” (or time adjusted BrIC) and CSDM.

The R^2 for the “New BrIC” increased to 0.84 from 0.81 for the “Original BrIC,” or by 3.7%. The slope and the intercept of the linear regression line are reduced, thus reducing the value of the “New BrIC” corresponding to the 50% risk of AIS 4+ brain injury. From the regression given in Figure 3.10, it can be calculated that a 50% risk of AIS 4+ brain injury (CSDM = 0.49) corresponds to an “Original BrIC” value of 1.06. Out of 749 data points, 160 exceed a BrIC value of 1.06, corresponding to a failure rate of 21.4% for the “Original BrIC.” For the “New BrIC,” or time adjusted BrIC, the 50% risk of AIS 4+ brain injury at CSDM of 0.49 equals 0.93 as calculated from the regression line given in Figure 3.16. Out of 749 data points, 159 exceed a BrIC value of 0.93, corresponding to a failure rate of 21.2% for the “New BrIC”, which is slightly lower than that of the “Original BrIC.” The number of cases equal or exceeding the value of CSDM of 0.49 is 189, corresponding to a failure rate of 25.2%. Thus, the failure rate for the “Original BrIC” is closer to that of CSDM.

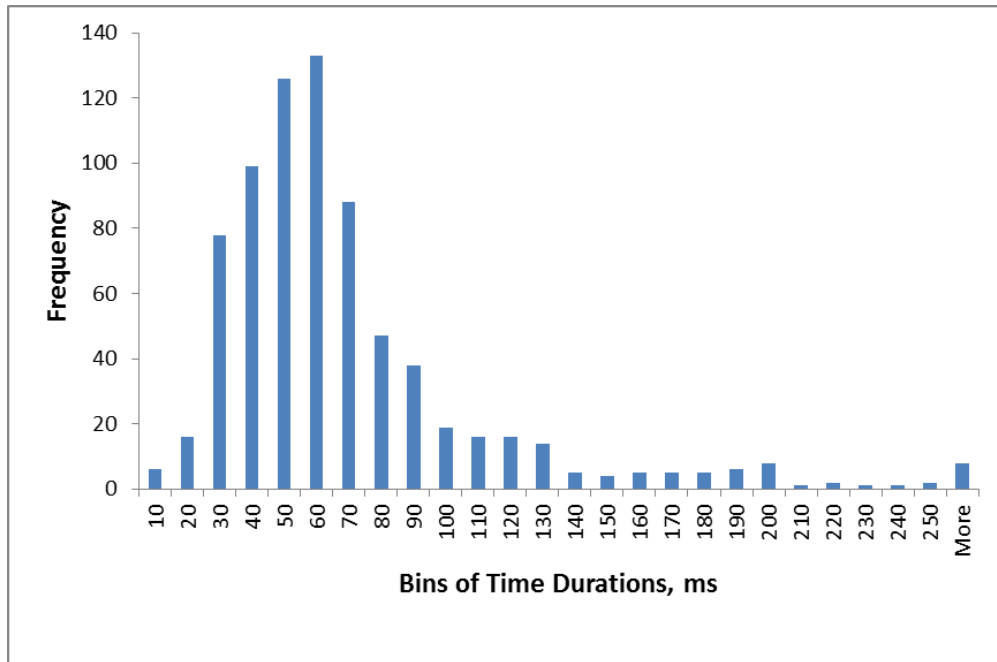
Figure 3.17 shows histograms of time durations of the head angular velocity for all 749 tests in each direction, calculated using the algorithm given in APPENDIX B. The most frequent time duration in all three rotational directions is 60 ms. From Table 3.7 (for CSDM = 0.49), new critical values for BrIC can be selected to represent the most frequently occurring time duration (Table 3.8).



a)



b)



c)

Figure 3.17. Histograms of the angular velocity signal time durations in x-direction (a), y-direction (b) and z-direction (c).

Table 3.8. Critical max angular velocities at the most frequent time durations for each direction.

Critical Max Angular Velocity	Rad/s (Original)	Rad/s (Liberal)
ω_x	66.25	78 @ 60 ms
ω_y	56.45	59 @ 60 ms
ω_z	42.87	50 @ 60 ms

Re-computing BrIC with the critical values of angular velocity shown in the third column of Table 3.8 with higher than original critical values, and replotting another version of the BrIC versus CSDM relationship, gives another version of BrIC, let's call it "Liberal BrIC" (Figure 3.18) due to higher critical values.

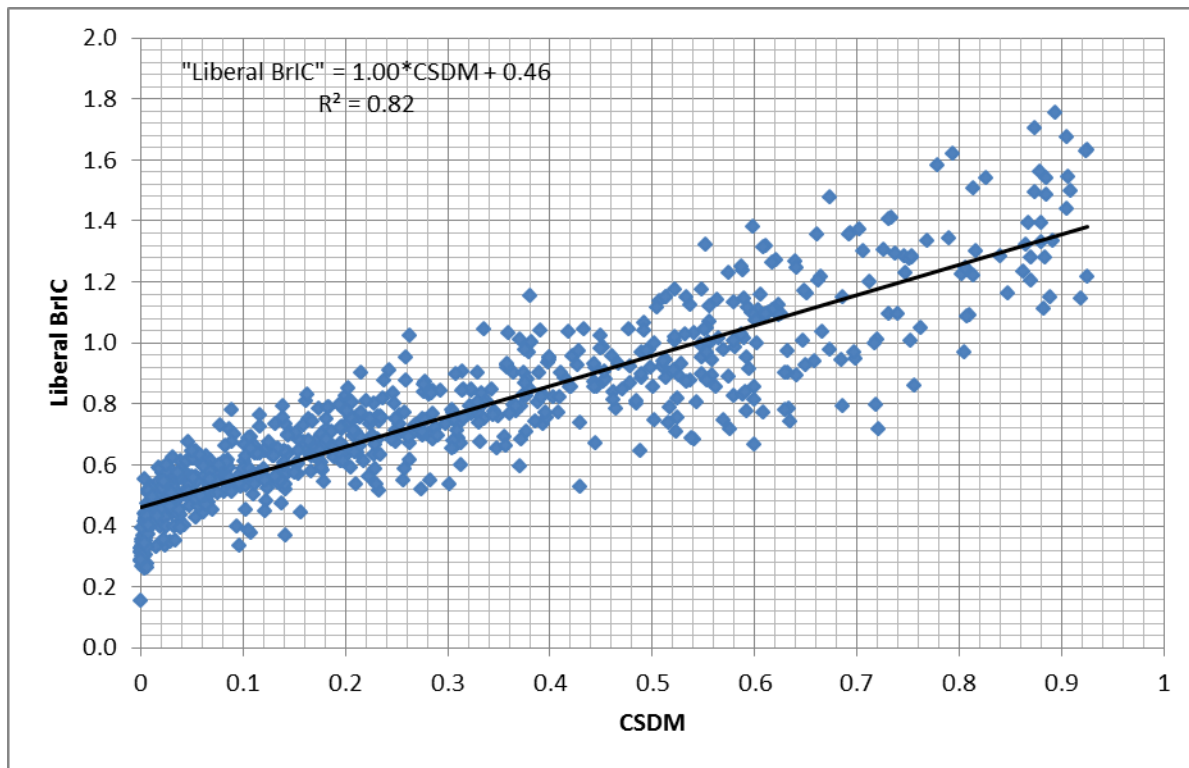


Figure 3.18. BrIC vs CSDM with higher critical values of angular velocities - “Liberal BrIC.”

Now, the 50% risk of AIS 4+ brain injury corresponding to CSDM = 0.49 for “Liberal BrIC” equals 0.95 as calculated from the regression equation (Figure 3.18). Little has changed compared to the “Original BrIC” given in Figure 3.10; the R^2 values are about the same, but the correlation line moved down by 0.04 with the slight change in slope, giving a lower “Liberal BrIC” number for the same value of CSDM (as compared to the “Original BrIC”). Hence, increasing critical values of angular velocities in the BrIC formulation doesn’t accomplish anything but shifting the correlation line down with slight decrease in the slope. The “Liberal BrIC” at higher critical values of angular velocity components fails just two fewer cases than the “Original BrIC.” Note that CSDM fails the highest number of cases and the number of cases failed by the “Original BrIC” is closer to that of CSDM than the “New BrIC” or “Liberal BrIC.”

Figure 3.19 demonstrates the number of true positives (TP), true negatives (TN), false negatives (FN), and false positives (FP) for the “Original BrIC” with the failure level at 1.06 (in blue), “New BrIC” with the failure at 0.93 (in red), and the “Liberal BrIC” with the failure at 0.95 (in green). Overall, the “New BrIC” increases true predictions (based on CSDM = 0.49) from 672 out of 749 for the “Original BrIC” (89.7% of correct predictions, with the area under the receiver-operator curve AUROC of 0.95 – Figure 3.20) to 677 out of 749 (90.4% of correct predictions with AUROC = 0.96), or improvement by 0.8% (improvement in AUROC is ~ 1.05%).

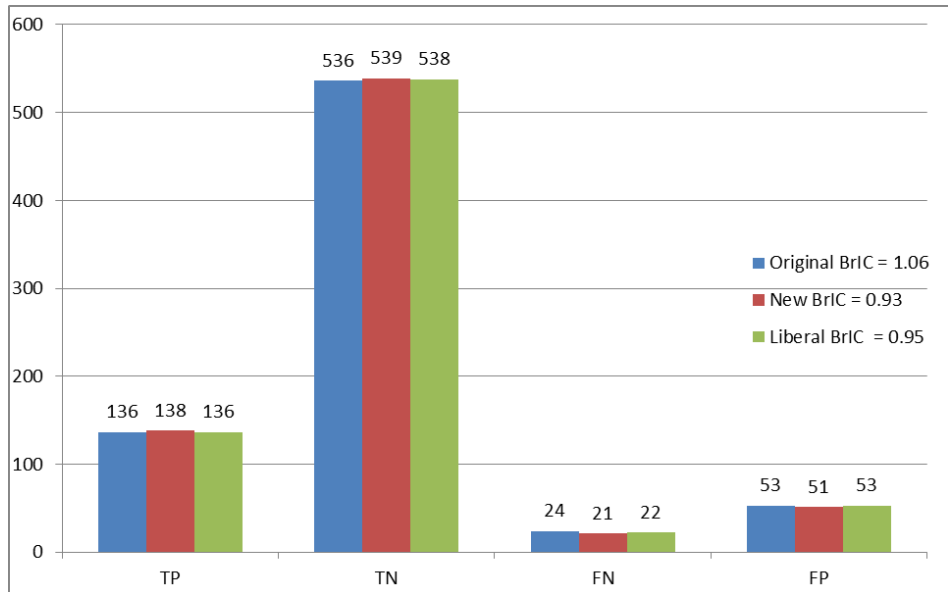


Figure 3.19. Number of true positives (TP), true negatives (TN), false negatives (FN), and false positives (FP) for the “Original BrIC” with the failure at 1.06 (in blue), “New BrIC” with the failure at 0.93 (in red), and the “Liberal BrIC” with the failure at 0.95 (in green).

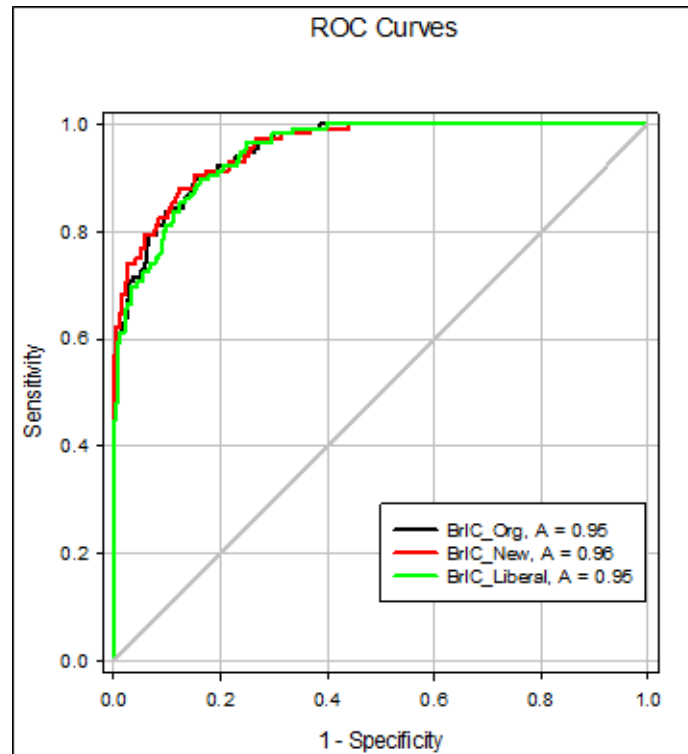


Figure 3.20. Receiver-operator curve (ROC) and the area under the ROC (shown as A) for the “Original BrIC” with the failure at 1.06 (in black), “New BrIC” with the failure at 0.93 (in red), and the “Liberal BrIC” with the failure at 0.95 (in green).

In conclusion, neither adjusting BrIC for the signal time duration nor increasing its critical values offer a clear advantage over the “Original BrIC” when applied for car occupants. A similar conclusion was reached by Gabler et al. (2016). For other loading conditions, such as those seen perhaps in volunteer tests (or twirling figure skaters) or pedestrians where the time durations are presumably higher than those given in Figure 3.17, the time adjusted BrIC may be used.

Another study related to the time duration/interval was conducted in which the time “distance” between the peaks of angular velocity components were altered from 0 to 150 ms, and then applied to the SIMon model to calculate CSDM. This study was carried out for three different total time durations of the angular velocity signals (35, 50 and 70 ms). No significant changes in CSDM were observed. In addition, the correlation between BrIC and CSDM was tested for the “instant BrIC,” in which angular velocity components were taken at the time of the maximum component of BrIC (the highest ratio of a peak angular velocity component over its critical value). The R^2 for the “instant BrIC” dropped to 0.75. Then, the time window for calculating the max of the other two angular velocity components was expanded to ± 25 ms of the time of peak of the angular velocity component contributing most to the value of BrIC, and the correlation between this “clipped-25 BrIC” and CSDM was tested giving the R^2 value slightly lower than that of the original BrIC. The same process was repeated with a ± 50 ms time window with similar results: the original BrIC had higher R^2 value, although the difference was decreasing with increased time window (note that the original BrIC has an unlimited time window).

3.4.5 Human Volunteer Data: CSDM or MPS?

Human volunteer head rotational data (angular velocities) about the x-axis (Ewing et al., 1976) and y-axis (Ewing et al., 1977) were digitized and applied to the SIMon FE head model. CSDM and MPS were monitored. The values of CSDM ranged between 0.000 and 0.009 for rotations about the x-axis (coronal plane rotation for a total of three volunteers) and 0.000 – 0.025 for rotations about the y-axis (sagittal plane rotation for a total of nine volunteers), while MPS ranged from 0.29 – 0.41 and 0.15 – 0.59 respectively. The lower values of CSDM are not surprising due to the much longer signal time duration seen in volunteer tests when compared to those measured in the ATDs and FE models (see DOE and Optimization studies below) for occupants in the vehicle crash environment. Using risk curves for CSDM and MPS (Figure 3.8), the risk of sustaining AIS 4+ brain injury under the loading conditions measured in volunteer tests is 0.003% for the max CSDM of 0.025 and 19.3% for the max MPS of 0.59. Given the fact that none of the volunteers sustained any brain injury, it would appear that CSDM is a more appropriate measure of the brain injury risk than MPS. In addition, MPS may be susceptible to potential numerical inaccuracy of a single finite element in the model, while CSDM is an “integral” measure with much smoother response due to the way it is calculated (see Takhounts et al., 2003 for details of calculating CSDM). Given an almost equal number of pros and cons for CSDM and MPS described in Takhounts et al. (2013), in which MPS-based risk curves for BrIC were suggested, this additional volunteer data makes the case for CSDM-based risk curves for BrIC more appealing. For this reason, all of the prior analysis on the signal time duration was given for CSDM only.

It should be noted, however, that the referenced human volunteer data was for healthy young adults. The risk of injury in those young adults may be different than for the average driving population. For

example, would the risk of brain injury for 80-90-year-olds (who are still driving cars and getting in crashes) exposed to the same loading conditions as the healthy young volunteers have remained as low as was computed by CSDM? Until such data exists or the strains in the “older” brains are compared to those of the “younger” brains under identical loading conditions using computational models, the answer to the question above remains unknown.

3.4.6 Design of Experiments and Optimization Studies

Computational simulations were conducted to investigate the parameters affecting BrIC and to investigate the expected interaction of BrIC with other injury metrics during restraint optimization. The simulations involved design of experiment (DOE) and optimization studies using the Global Human Body Models Consortium (GHBMC) 50th male simplified occupant model (version M50_OS_v1.8, Global Human Body Models Consortium, LLC) in a modified sled model of a Toyota Yaris (Reichert et al., 2014). A summary of the findings from these studies is included in this section, while more detail can be found in APPENDIX C.

3.4.6.1 DOE Study #1

To investigate parameters affecting BrIC, limited DOE studies were conducted. The DOE was limited to the same vehicle dimensions, steering wheel parameters, frontal airbag size, seat position, and occupant parameters including the size, stature, sex, and initial position. When delta-V and PDOF were included into the parameters list the following conclusions were reached:

1. Out of nine parameters varied in this study (see Table C.1 for the list of parameters, their nominal values and the varied range), delta-V influences values of BrIC the most (33.3 % influence), followed by PDOF (28.0 % influence).
2. Increasing PDOF increases the range of values of BrIC, yet it is possible to find a set of parameters with smaller values of BrIC.
3. When investigating relationships between various parameters, such as BrIC and delta-V, metamodels are more useful than just a scatter plot of the two parameters because various other parameters (for example, when looking at the fleet tests of various vehicles with various sets of restraint parameters) contaminate the relationship (contrast Figures C.8 and C.9) leading to erroneous conclusions about the “true” relationship.
4. Correlation between the values of BrIC and delta-V and PDOF is the strongest (higher correlation coefficients) and positive (with increased delta-V and PDOF the values of BrIC also increase).

3.4.6.2 DOE Study #2

When delta-V was fixed to 35 mph and PDOF was fixed at 0^o (representing full frontal crash mode), -20^o (representing near side driver oblique crash mode), and +20^o (representing far side driver oblique crash mode) the following parameters were found to affect BrIC the most (Table C.9): frontal airbag mass flow rate, load limiter, frontal airbag friction, side airbag friction (for the near side driver oblique crash mode), and frontal airbag firing time (for the far side driver oblique crash mode).

Together, the two DOE studies indicated that it was possible to select many combinations of the investigated parameters yielding values of BrIC corresponding to zero to small risk of brain injury depending on the crash mode.

3.4.6.3 Optimization Study #1

Optimization studies were conducted using a genetic algorithm for the global minimum search, in which BrIC was the objective function subject to constraints in HIC_{15} (constrained to 700), central chest (sternal) deflection (constrained to 63 mm), left and right femur force (both constrained to 10 kN). First, parameters identified as important in the DOE studies (Table C.9) were varied and optimal solution for BrIC was searched for each crash mode separately. It was shown that:

1. It was possible to obtain low values of BrIC for each crash mode with the highest optimized BrIC in the far side driver oblique crash mode (just under 0.6), and under 0.5 for the full frontal and near side driver oblique crash modes.
2. Decreasing HIC_{15} and/or sternal deflection caused BrIC to increase (and vice versa) indicating that optimizing for just one injury parameter without the knowledge of others may lead to so called “unintended consequences;” for example, currently both HIC_{15} and sternal deflections are used as injury criteria (but not BrIC), minimization of which without the knowledge of its effects on BrIC may lead to increased risk of brain injuries – the observation that was also confirmed with the field data analysis.

When one set of optimization parameters was chosen and ran at various PDOFs (or crash modes), the following observations were made (Table C.12):

1. The values of BrIC (not optimized) can be kept in a relatively low range for the near side driver oblique runs up until -25° PDOF; when the PDOF angle was furthered to -30° , BrIC significantly increased due to the head almost missing the frontal airbag.
2. The value of BrIC for the far side driver oblique run at PDOF of $+20^{\circ}$ was relatively high compared to that when optimized for just this test condition (BrIC was equal to 0.59 – see last column of Table C.10).
3. HIC_{15} values were relatively low with the highest value of 362 in a full frontal run – this is the crash mode in which BrIC was the lowest.
4. Similar to HIC_{15} , the highest value of the sternal deflection of 53 mm was in a full frontal condition, while the lowest was at -30° , the condition in which BrIC was the highest (0.93).

3.4.6.4 Optimization Study #2

To investigate the effect of greater airbag coverage, the frontal airbag volume was scaled up from 50 liters (used in all previous studies) to 98 liters and optimization similar to that described above was run for PDOF = -20° only (near side driver oblique crash mode). Then a parameter set was identified (not at a minimal BrIC) to investigate if BrIC can be further reduced for all PDOFs (Table C.16) when compared to that given in Table C.12 (for a smaller size airbag). Significant reduction in the values of BrIC was observed demonstrating conceptually that just increasing the frontal airbag size will reduce the values of BrIC while keeping other injury criteria values below their respective limits.

3.4.7 Summary - BrIC

The equation for BrIC as a function of max angular velocity components (equation 3.1) - along with its correlation to CSDM - originally developed in Takhounts et al. (2013) was tested extensively. These tests included:

1. Additional data was added (various NHTSA tests, IIHS tests, and laboratory airbag tests, etc.) to investigate if the correlation between BrIC and CSDM from the originally published 413 data points (shown in Figure 3.7a) would change with the addition of 336 data points (Figure 3.10). Neither slope nor the intercept have changed significantly (compare Figure 3.7a) and Figure 3.10). The change in R^2 was also insignificant (changed from 0.84 to 0.81). This indicates the “stability” of the BrIC versus CSDM relationship irrespective of the ATD and the test mode.
2. Developing BrIC for individual ATDs is futile as is demonstrated in Figure 3.11.
3. Dependence of critical angular velocities for BrIC (in equation 3.1) on the signal time duration (and/or dependence of CSDM on the signal time duration) was thoroughly investigated and found that such dependence is significant. However, when applied to the occupants of vehicles in various crash conditions, this dependence on signal time duration becomes insignificant as is assessed by the change in R^2 and AUROC. The “New BrIC” (time duration dependent BrIC) improved performance (AUROC) of the “Original BrIC” by approximately 1%, which was concluded to be insignificant based on the Pareto principle.
4. For demonstration purposes, the critical values of the angular velocity components in the BrIC formulation (equations 3.1) were increased significantly (called it “Liberal BrIC”) to investigate how such increase will affect the assessment of the brain injury risk. It was demonstrated that such increase in critical values of angular velocity components only shifts the correlation between BrIC (“Liberal BrIC”) and CSDM down (reduces the intercept and the value of BrIC corresponding to CSDM = 0.49 - 50% risk of AIS 4+ brain injury) with no significant changes in R^2 or AUROC (Figure 3.20).
5. Another time duration/interval study was conducted in which the time interval between the peaks of angular velocity components was altered and the effect of such alteration on CSDM was studied. The effect was found to be insignificant. In addition, “instant BrIC” (all angular velocity components values are taken at the same time of the highest component of BrIC), clipped to ± 25 ms, and ± 50 ms were looked at and found that R^2 value decreases with the decreased clipping time with the lowest value for the “instant BrIC.”
6. Human volunteer data (Ewing et al., 1976, 1977) was used to compute the risk of injury (or non-injury since none have reportedly sustained any brain injury). It was found that CSDM (showing low risk of brain injury) was more representative of the injury outcome from these volunteer tests. Based on these volunteer tests, the CSDM based risk curves for BrIC were recommended (Figure 3.9a and Table 3.3).

3.5 Skull / Facial Injuries

3.5.1 Injury Criteria

The Head Injury Criterion or HIC is a criterion that has been used by NHTSA and many other safety agencies in regulatory and consumer metric crash testing for decades. The risk function for HIC with 15 ms duration (or HIC_{15}) as applied in the current NCAP rating scheme (NHTSA, 2008) is based on short duration (10 ms and under) linear skull fracture experimental data. Prasad and Mertz (1985) tabulated skull fracture experimental data from other experimental sources showing HIC versus the presence or absence of skull fracture (primarily linear fractures). Hertz (1993) performed regression studies on the fracture data from Prasad and Mertz (1985) to produce the AIS 2+ risk function for HIC_{15} that is presented in Eppinger et al. (1999). NHTSA (NHTSA, 2000) created an expanded set of curves producing the current AIS 3+ risk function used in NHTSA's New Car Assessment Program (NHTSA, 2008). The formulation for HIC_{15} and associated risk functions are presented below.

	$p(\text{AIS } 2+) = \Phi \left[\frac{\ln HIC_{15} - 6.96362}{0.84687} \right]$
	$p(\text{AIS } 3+) = \Phi \left[\frac{\ln HIC_{15} - 7.45231}{0.73998} \right]$
where:	
Φ	= Cumulative normal distribution function
HIC_{15}	= $\left[(t_2 - t_1) \left[\frac{1}{t_2 - t_1} \int_{t_1}^{t_2} a(t) dt \right] \right]^{2.5} \Big _{max}$
	$t_2 - t_1 \leq 15 \text{ milliseconds}$
t_1, t_2	= beginning and end of calculation time window (in seconds)
$a(t)$	= Head CG resultant acceleration time-history (in g)

Attempts have been made to relate HIC to concussion/brain injury, but are not supported theoretically based on studies of brain injury mechanisms (Takhounts et al., 2013; Takhounts 2015) nor by observed trends in fleet and field data (see Figure 3.1, Figure 3.2 and Table 3.1). For example, Takhounts et al. (2013) showed how HIC has poor correlation to the strain-based measures that are associated with brain injury (Figure 3.21). Takhounts (2015) presented the results of investigations related to two physical brain injury mechanisms were investigated: strain and pressure. It was demonstrated that based on the mechanical properties of the brain and skull, and the experimental data, pressure doesn't cause brain injuries, while strain does. It was also shown that head translational accelerations (upon which HIC is based) correlate to pressure while causing small strains in the brain compared to those caused by the rotational head motion.

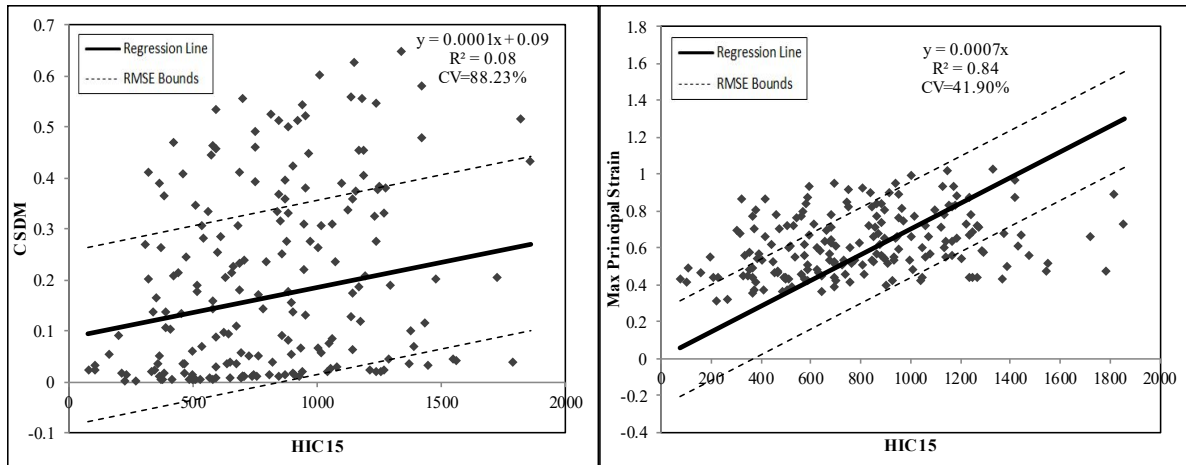


Figure 3.21. CSDM and MPS vs. HIC₁₅ (from Takhounts et al., 2013).

The previously mentioned DOE study (APPENDIX C) also found in some cases a negative correlation between BrIC and HIC meaning that optimizing to reduce one measure may result in an increase in the other.

Based on the findings from fleet and field data, the findings from the DOE studies and the fact that the current functions are based on linear skull fractures produced from short duration head impacts to rigid surfaces, both HIC and BrIC should be considered for use with the THOR-50M. BrIC can be applied for the purpose of mitigating brain injuries while HIC can be applied to mitigate against the types of hard contacts that can cause skull and/or facial fractures.

3.6 Fleet Test Data: THOR-50M

The recommended head injury risk functions were applied to THOR-50M measurements collected in frontal rigid barrier and frontal Oblique fleet testing. Figure 3.22 and Figure 3.23 show the risk of AIS 3+ and AIS 4+ injury, respectively, as a function of BrIC, with observations representing the injury risk predicted from each occupant response grouped by occupant position and test mode. Based on BrIC, the predicted injury risks to the Oblique right front passengers are generally higher than those predicted for the Oblique drivers, which in turn are higher than those predicted for the drivers in the frontal rigid barrier test mode.

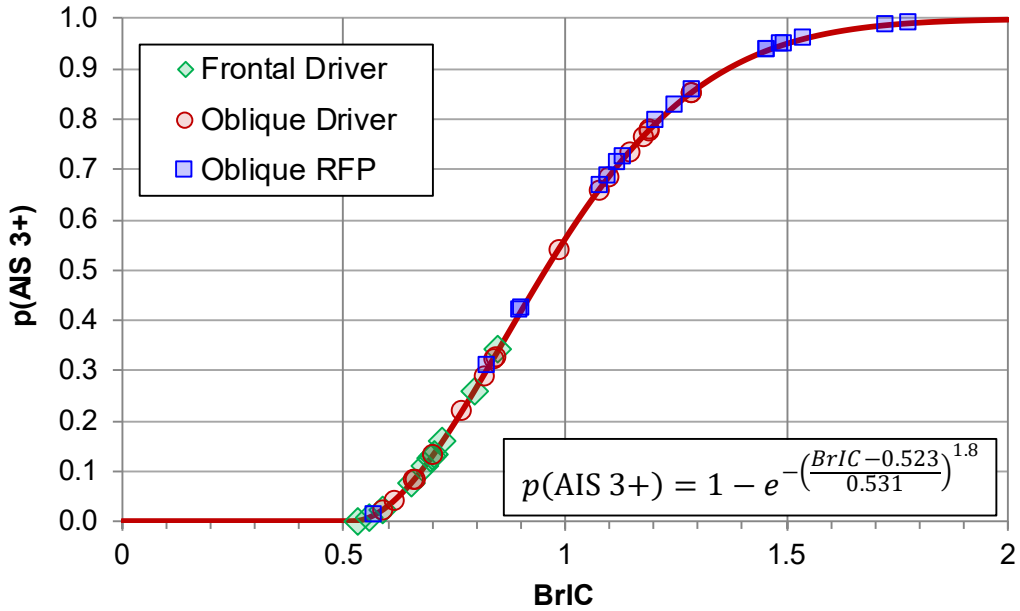


Figure 3.22. Probability of AIS 3+ brain injury predicted using BrIC measured from fleet test results for the driver in the frontal rigid barrier test mode and both the driver and right front passenger in the Oblique MDB test mode.

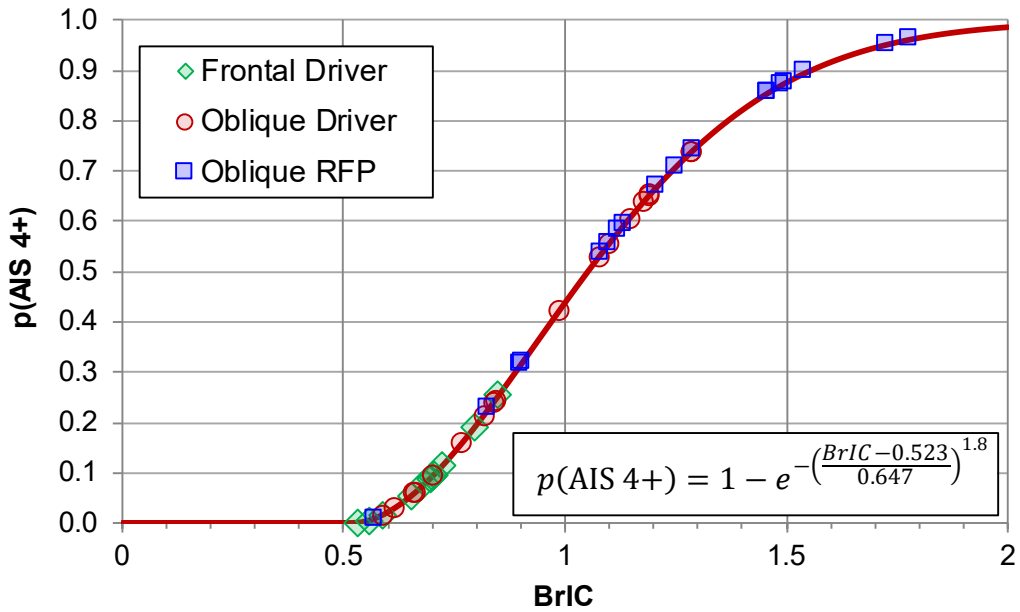


Figure 3.23. Probability of AIS 4+ brain injury predicted using BrIC measured from fleet test results for the driver in the frontal rigid barrier test mode and both the driver and right front passenger in the Oblique MDB test mode.

Figure 3.24 and Figure 3.25 show the risk of AIS 2+ and AIS 3+ injury, respectively, based on HIC₁₅. Skull/facial Injury risk is generally low except for three Oblique right front passenger observations where the head contacted the center instrument panel.

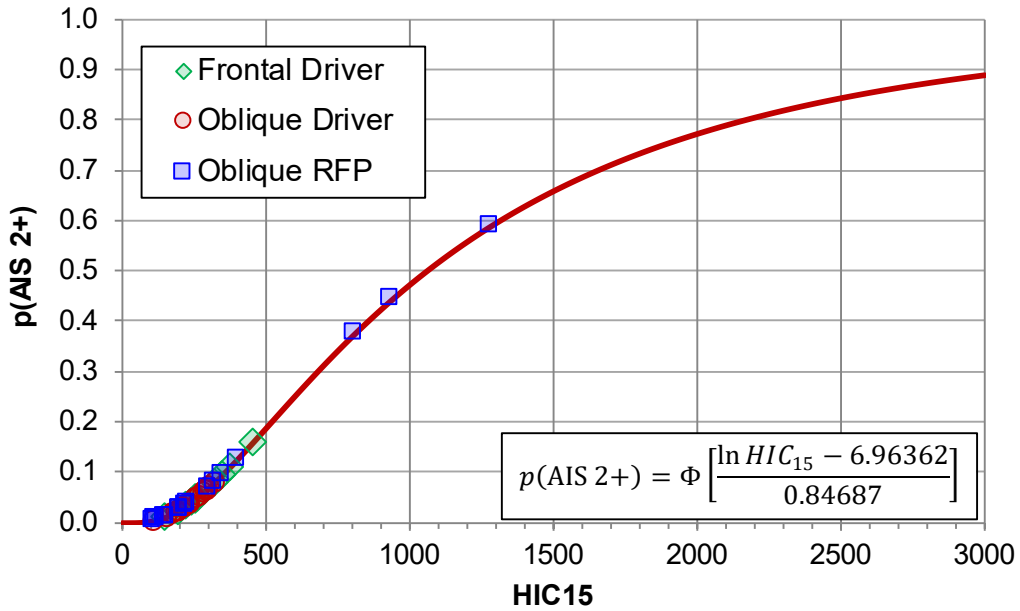


Figure 3.24. Probability of AIS 2+ skull/facial injury predicted using HIC₁₅ measured from fleet test results for the driver in the frontal rigid barrier test mode and both the driver and right front passenger in the Oblique MDB test mode.

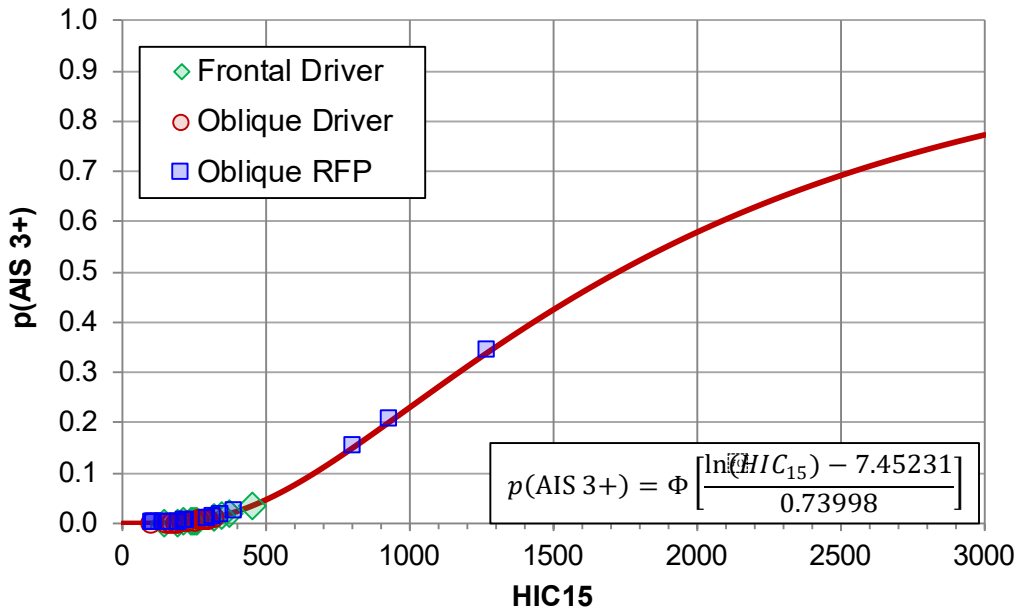


Figure 3.25. Probability of AIS 3+ skull/facial injury predicted using HIC₁₅ measured from fleet test results for the driver in the frontal rigid barrier test mode and both the driver and right front passenger in the Oblique MDB test mode.

4 NECK

4.1 Field and Historical Fleet Data

Figure 4.1 presents the regional mechanisms of injury assigned to neck and cervical spine injuries in CIREN front-row belted occupants involved in frontal crashes. While these recorded mechanisms are inferred from the available data and may have been limited to available researcher/published biomechanical knowledge at the time, it can still be concluded from these CIREN cases that neck injuries result from a variety of combinations of loading. It is important to note that the mechanisms shown are regional mechanisms, not local mechanisms at the specific vertebral level. That is, the chosen mechanism represents the type of loading/motion experienced by the entire neck structure.

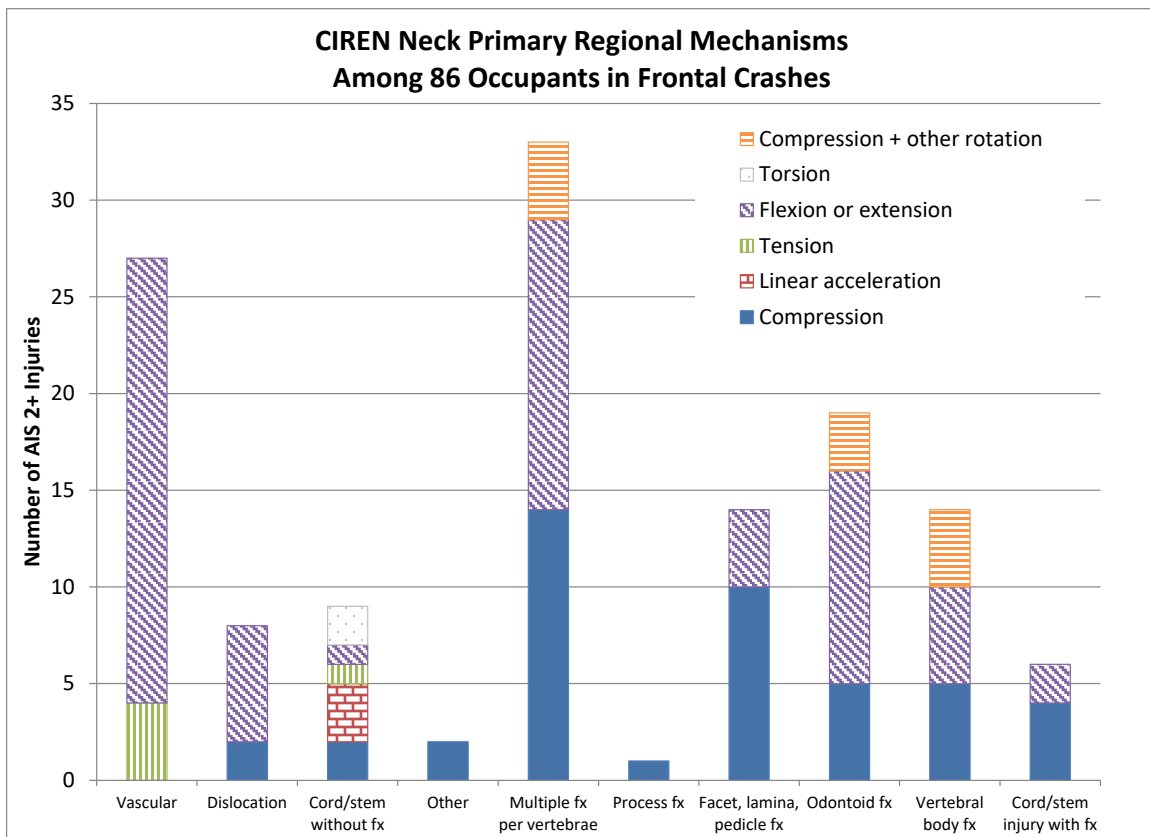


Figure 4.1. Recorded mechanisms of neck and cervical spine injuries for belted front row occupants involved in frontal crashes from the CIREN database.

Figure 4.2 presents the vehicle model year-based trend for AIS 3+ neck injuries for belted drivers in frontal crashes. The injury rate represents a running three-year average of the percent of injury cases (injury cases divided by total number of cases; e.g. model year 1992 includes the total weighted count of AIS 3+ injuries from model years 1990, 1991 and 1992, divided by the total number of cases for those model years). While there appears to be an increasing trend, the percent risk is 0.2% or less for all model years.

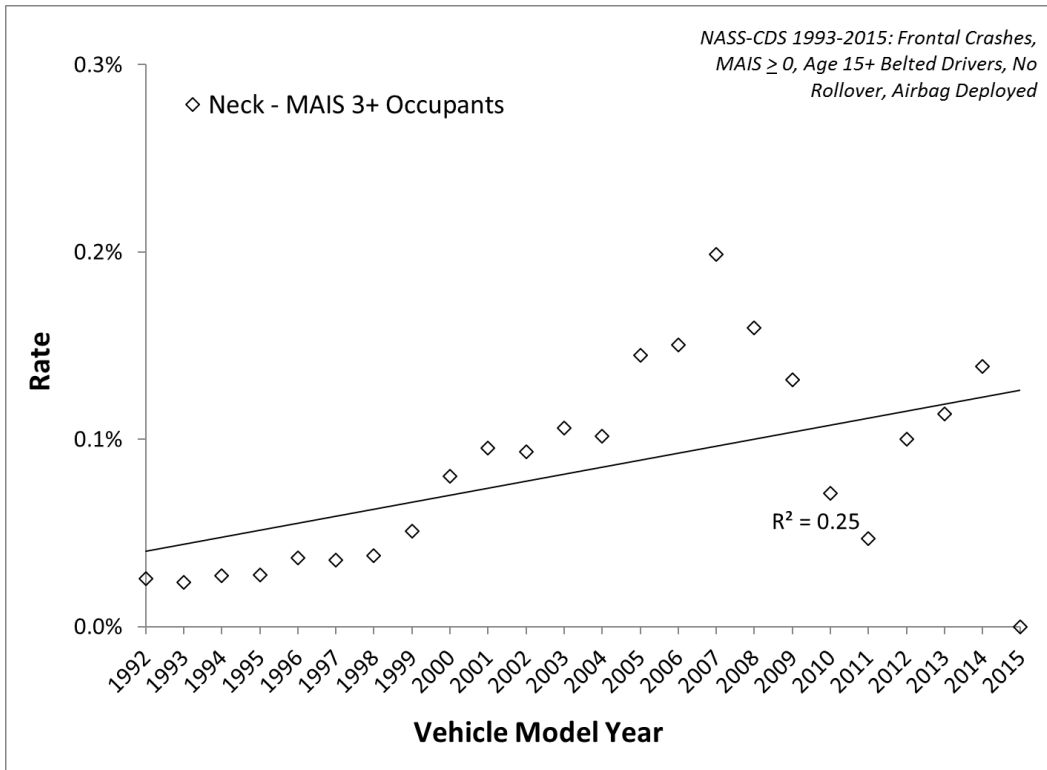


Figure 4.2. Neck injury rate by model year (1992 to 2015) for frontal crashes in NASS-CDS 1993 to 2015.

The trend for Hybrid III 50th male (H3-50m) Nij values in 35-mph full frontal tests can be seen in Figure 4.3. Two versions of risk are presented. The first is based on the Nij risk curve that is used in the current NCAP program (NHTSA, 2008). The second uses updated data presented in Mertz and Prasad (2000) and a Weibull curve-based risk function developed using survival analysis.

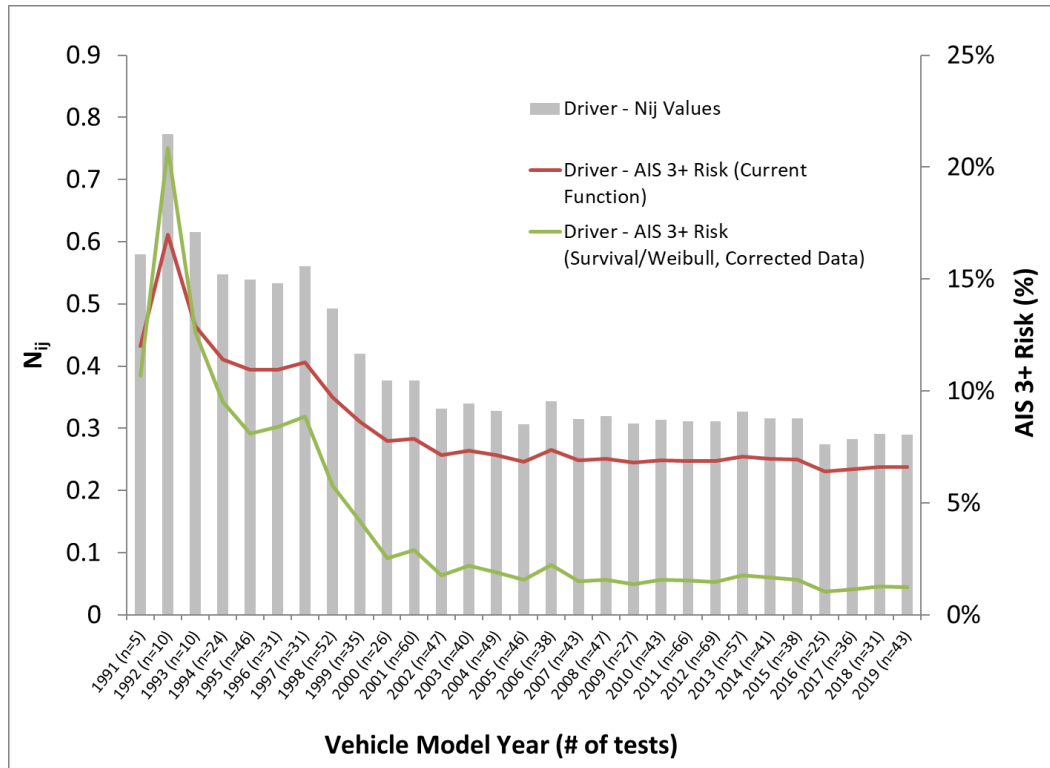


Figure 4.3. H3-50M driver Nij values and predicted AIS 3+ risk (both current NCAP risk function and revised version based on corrected data and Survival-Weibull function) from model year 1991 to 2019 in 35-mph frontal NCAP tests.

4.2 Literature Review

The risk of neck (i.e. cervical spine, including spinal cord) injury in motor vehicle crashes is important to consider because cervical spine injuries in motor vehicle crashes continue to result in significant morbidity (Wang et al., 2009) and have high attributable cost relative to other body regions (Figure 1.2). In belted front row adults, cervical spine injuries are caused by a variety of mechanisms, including all four primary modes (flexion, extension, tension, compression) as well as combined loading (Figure 4.1). In addition, for the CIREN population shown in Figure 4.1, the most common involved physical components were the belt (flexion/extension of the neck due to restraint of the torso by the belt), A-pillar (head contact), airbag (head/torso restraint by the airbag) and steering rim (head contact). The wide variety of injury causation mechanisms and involved physical components demonstrate the need for either a number of separate injury risk functions, or an inclusive injury measure such as the Nij neck injury criterion.

The Nij neck injury criterion used in Federal Motor Vehicle Safety Standards (FMVSS) No. 208 (Eppinger et al., 1999; Klinich et al., 1996) was originally developed to target out-of-position occupants. The Nij criterion was formulated based on paired tests conducted with anesthetized piglets and baboons, and an instrumented 3-year old anthropomorphic tests devices (ATDs) built by General Motors (Mertz et al., 1982) and Ford (Prasad and Daniel, 1984), in typical out-of-position configurations (i.e. with the occupant close to deploying airbags). The injuries sustained suggested a primary mechanism of high

tensile loads in the neck. Based on the paired tests, Prasad and Daniel (1984) proposed that combined tension and bending moments was a better predictor of injury than tensile forces alone. Critical intercepts for the Hybrid III family of dummies were derived from these animal tests, scaled up to adult human level. Other data used in forming the intercepts were from Mertz et al. (1978), where a H3-50M ATD was subjected to impacts using a spring-loaded tackling dummy, Nyquist et al. (1980) wherein a H3-50M ATD was used to reconstruct field crashes (of which only five were injured, and those at the AIS 1 level), and Mertz et al. (1971), wherein flexion and extension bending moment tolerances were described based on volunteers tested up to pain tolerance and post-mortem human subject (PMHS) tests that were non-injurious. Given a reliance on the H3-50M to develop these intercepts, and the inherent differences in the neck design between the H3-50M and the THOR-50M, they would not be appropriate for use with the THOR-50M dummy.

Since the original formulation of Nij, newer experimental data has been conducted (e.g. Nightingale et al., 2007; Dibb et al., 2009) that expands the knowledge of human tolerances without relying upon scaled animal or dummy data. These data will be described in more depth in upcoming sections. In addition, computational human models have been developed (Chancey et al., 2003) and validated under a wide variety of conditions including pure bending, tension-bending, compressive impact, and volunteer frontal flexion (Dibb et al., 2011). Human models allow estimation of the contribution of muscles to neck response whereas PMHS do not. The THOR-50M separates muscle and osteoligamentous contributions to neck loads due to its design involving anterior and posterior neck cables, making comparisons to both PMHS and computational models feasible (Luck et al., 2014). The availability of new experimental data and the human-like design of the THOR neck allow for improved ability to develop a PMHS-based set of neck injury measures for THOR-50M. In contrast to previous efforts that focused heavily on protecting out-of-position occupants who were seated close to a deploying airbag, current injury measures are being developed for normally seated or in-position front row occupants, due to both THOR's intended use applications as well as the current understanding of neck injury causation in the field, as described above.

4.3 Design

The THOR-50M neck assembly consists of a series of aluminum disks and rubber pucks which are molded together using an epoxy resin system. The elliptical rubber pucks provide the desired frontal, lateral, and torsional bending responses for the neck assembly. Compression springs are located in the fore and aft regions of the skull. A center safety cable provides durability, while a neoprene spacer at the attachment of the lower neck load cell provides compliance in axial tension. In addition, rubber soft stops at the base of the neck aid in achieving the desired bending characteristics in both front and rear motion.

4.4 Instrumentation

The instrumentation for the neck assembly includes a pair of skull spring load cells, which measure the compression at the front and rear spring locations; six-axis load cells at the top and base of the neck to

measure the forces and moments developed at these locations; and a rotary potentiometer at the occipital condyle pin to measure the relative rotation between the head and top of the neck (Figure 4.4).

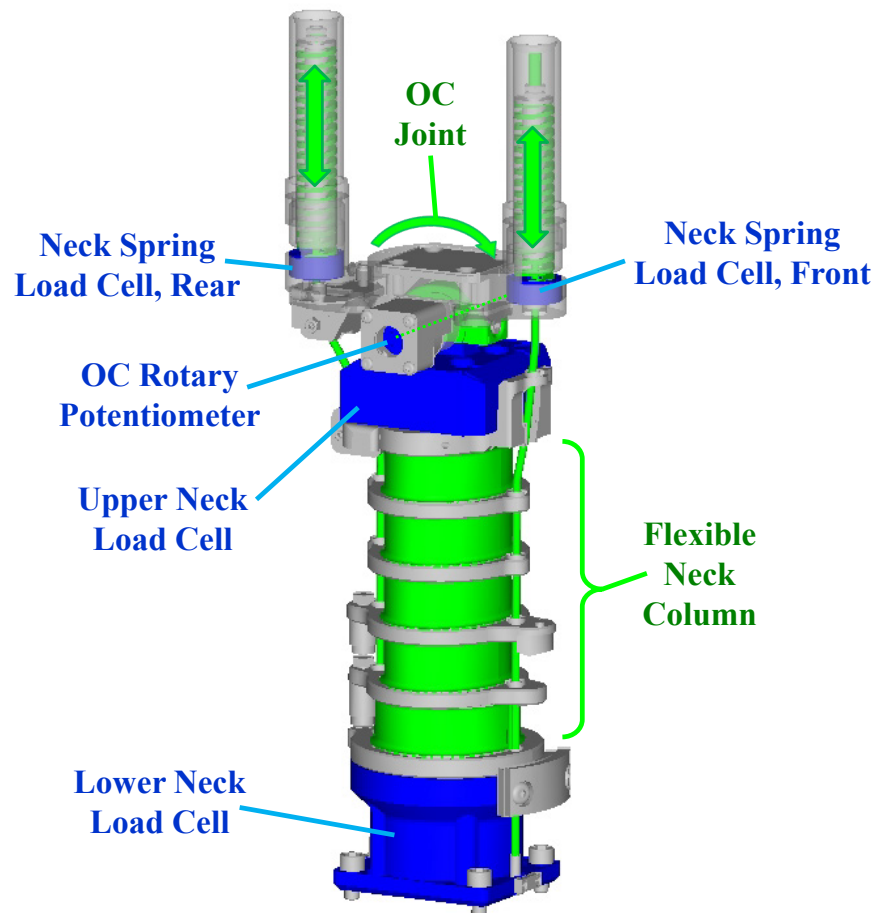


Figure 4.4. THOR-50M neck instrumentation.

4.5 Biofidelity

Biofidelity of the THOR-50M neck was assessed in three conditions (Parent et al., 2017): frontal flexion, lateral flexion and torsion. In the frontal and lateral flexion conditions, from which the response was based on volunteer testing conducted by the Naval Biodynamics Laboratory (known as the “NBDL” condition), the THOR-50M demonstrated overall good biofidelity, as defined by Parent et al. (2017). In torsion, the THOR-50M response qualitatively showed a similar loading slope to the PMHS response corridor, but did not exhibit the low-moment toe region over the first 50 to 75 degrees of rotation in the human response. The overall neck internal and external BioRank scores were 2.155 and 1.677, respectively. The THOR-50M was quantitatively more biofidelic than the H3-50M (overall BioRank scores of 2.185 and 4.318, respectively).

4.6 Experimental Data

As noted above, the data used in the development of the Nij neck injury criterion for use in Federal Motor Vehicle Safety Standards (FMVSS) No. 208 as presented by Eppinger et al. (1999) were not considered to be appropriate for use with the THOR-50M dummy. Instead, PMHS-based data sources, mostly published since Eppinger et al. described the current Nij formulation and risk functions used with the Hybrid III family of dummies, were identified that could be used to develop risk functions in combined loading (Nij). These data sources are described in more detail in the subsection corresponding to each particular loading mode (tension, flexion, extension, compression, and combined loading) and are tabulated in Appendix F (Tables F.1 and F.2).

4.6.1 Tension

In tension, testing on osteoligamentous neck structures and motion segments was evaluated first. Dobbins et al. (2009) conducted tensile tests on upper cervical spine motion segments (OC-C2) both in “pure” tension (loading through the OC) and combined tension-extension (loading through the head center of gravity). All specimens were male and all were loaded to failure. The specimens were tested with a free cranial end condition (fixed at C2). Ultimate failure was defined as the maximum tensile load each spinal segment could withstand, and the injuries sustained included complete joint disruption, Type III dens fracture, occipital condyle fracture and posterior ligament disruption. Before testing to failure, each specimen was subjected to cyclical pre-conditioning and multiple non-injurious tests with peak loads of about 300 N.

Next, data on whole neck structures was evaluated. Assuming that under tension, the neck acts as a set of springs in series, the tensile tolerance for motion segments is not expected to differ significantly from that of the entire neck. Yliniemi et al. (2009) conducted high rate tensile testing to failure using intact PMHS head and torso specimens. Specimens were intact head-neck-torso (including skin and other soft tissues surrounding the skeletal structures). Tension was applied with a military helmet with an integrated chin-nape strap. To ensure tension as the primary mode of loading, the top of the helmet was allowed free rotation about all three axes. The caudal end was fixed at T8-T11, with additional straps over the shoulders to secure the torso. Actuator displacement rates ranged from 0.52 to 0.74 m/s, which resulted in tensile loading rates between 35,000 and 60,000 N/s in a Hybrid III ATD neck. The tensile loading rates for the PMHS were not given. There were four females and eight males, and all specimens were tested to failure. Failure was defined by a constant or decreasing slope in the load-displacement curve. Injuries sustained included atlanto-occipital dislocation, Type II dens fracture, as well as endplate fractures at various spinal levels.

4.6.2 Flexion-Extension

For flexion and extension, Nightingale et al. (2007) conducted pure bending tests of male upper cervical spine motion segments (OC-C3) at a loading rate of approximately 90 Nm/s. The cranial end of the segment was secured using halo fixation, and both C2 and C3 were cast. Each specimen was used for low load (10-15% of failure load) flexibility testing prior to failure testing. Two of the eight specimens tested in flexion sustained AIS 3+ injury (C1-C2 dislocation, Type III dens fracture), and one sustained AIS

2 injury (C1 facet fracture). In extension, five specimens tested sustained injury (Type III dens fracture, OC-C1 dislocation). Three additional extension specimens sustained fractures at the fixation; therefore, these were excluded from the analysis.

4.6.3 Compression

For compression, studies have been conducted on both motion segments and whole neck structures. Panjabi et al. (1991) conducted compression testing on upper cervical spine motion segments (OC-C3) using a falling mass impact configuration. Specimens were fixed at the lower end and free at the upper end. Motion of the falling mass was constrained to a single axis, resulting in compression of the motion segment. Age and sex of individual specimens was not reported, so all specimens were assumed to be male and 61 years (i.e. equal to the mean age). Three specimens sustained no injury to C1, and the results from those specimens were not reported. The remaining eight specimens sustained various types of C1 injuries, four of which were at the AIS 3+ level.

Carter et al. (2002a) conducted pure compression of lower cervical spine motion segments (C3-C5, C4-C6, C5-C7, and C6-T1) using a high-rate materials testing fixture. Soft tissues were removed from the specimens, though osteoligamentous structures surrounding the vertebrae were left intact. Both ends of the specimen were potted, resulting in fixed boundary conditions. Four males and four females were tested to failure. The specific injuries sustained were not detailed in the paper but the structures injured were identified in Carter et al. (2002b). All specimens sustained bony injuries consistent with AIS 2+ severity, but lack of detail was available to determine whether the injuries could be described as AIS 3+. Several specimens were noted to have canal occlusion consistent with potential for neurologic injury, however this was not taken as sufficient evidence to assign a severity of AIS 3. Although an upper cervical spine injury criterion is being targeted, the failure loads in the lower cervical spine motion segments were not significantly different from the upper cervical segments tested by Panjabi ($p > 0.05$). Thus, they were considered for this analysis.

A number of studies involving compression of whole neck structures were evaluated for inclusion in this study. These included Pintar et al. (1995), Maiman et al. (1983), Nightingale et al. (1997) and Saari et al. (2013). These studies used a variety of experimental test conditions, including drop tests and impact loading to an upright, straightened spine. For the whole neck in compression, there are influential factors that contribute to failure, such as buckling behavior, cervical alignment, and confounding bending moments that were not measured in any of these studies, but nonetheless would have contributed to overall failure. Even anatomic considerations (e.g. disc integrity) can have a great effect on injury tolerance but were not reported in these studies. Due to these confounding factors, these whole neck compression studies were deemed unacceptable for inclusion in the present study.

4.6.4 Combined Loading

Pintar et al. (2005) conducted high rate tension-extension testing of intact PMHS, using a strap under the chin. The specimens used were both males and females and were intact (muscles, ligamentum nuchae, and skin included) from head to torso. The torso was strapped to the frame using a harness. The mandible was removed and a load cell was fixed to the hard palate, where the external load was

applied. Initial non-injurious tests were performed at low speed, followed by high-speed failure tests. The input load rate for the high-speed tests was between 520 and 3954 kN/s, while the tension load rate experienced by the neck (defined as the slope of the positive portion of the neck force time-history between 15% and 85% of the peak tension force) ranged from approximately 465 to 1,600 kN/s (mean 852 kN/s). Injuries produced were predominantly C1-C2 separations or partial separations.

Carter et al. (2002a), in addition to testing pure axial compression, also conducted tests in compression-flexion and compression-extension. The methods were similar to that described above, with the modification that the load was applied with eccentricity, allowing concomitant bending moments to develop. Eight specimens were tested in compression-flexion (six females and two males), and eight specimens were tested in compression-extension (five females and three males). In the compression-flexion group, the structural damage was primarily associated with soft tissue failure, while in the compression-extension group, structural damage occurred primarily in the posterior elements (spinous process, lamina) and anterior elements (disc and vertebral body). Where only soft tissue (ligament, facet capsule) injuries were sustained, severity level was considered AIS 1. Where disc and/or bony injuries were sustained, these were considered to be consistent with AIS 2+ severity, but lack of detail was available to determine whether the injuries could be described as AIS 3+. As noted above, several specimens were noted to have canal occlusion consistent with potential for neurologic injury, however this was not taken as sufficient evidence to assign a severity of AIS 3.

An additional data source for combined loading is a recent matrix of PMHS sled tests collected by the University of Virginia, consisting of frontal impact sled tests in 14 different velocity or restraint conditions with a total of 48 PMHS observations. In each of these test conditions, at least two THOR-50M tests were conducted (Table F.2). Of the 48 PMHS tested, 3 sustained AIS score of 3 or greater (AIS 3+), based on the AIS 2005 Update 2008 (AAAM, 2008), cervical spine injury. A limitation to this test series is that PMHS neck loads were not directly measured. Due to this limitation, the matched pair tests are used herein to relate PMHS outcome to THOR measurements in the same test condition.

Another data source consists of the volunteers and PMHS run in the NBDL 15 g frontal sled condition. In that condition, there were five volunteers who sustained no injury, and nine PMHS specimens, only one of which sustained an AIS 2 injury (Thunnissen et al., 1995; Wismans et al., 1987). The volunteers were young, healthy males who were instructed to pre-tense their muscles during the test. Volunteers had instrumentation (mass 0.5 kg) added to their head. Matched pair tests were conducted with THOR-50M in the equivalent condition. As with the UVA sled test series, volunteer and PMHS neck loads were not directly measured. Due to this limitation, the matched pair test is used herein to relate PMHS outcome to THOR measurements in the same test condition (Table F.2).

Finally, Parr et al. (2013) conducted volunteer tests in a frontal sled condition at 8 g and 6 g. Twenty-seven subjects (11 females and 16 males) wore either a 1.6 kg or 2 kg flight helmet and were instructed to brace during the test. Subjects participated in up to three different experimental test conditions (8 g with a 2 kg helmet, 8 g with a 1.6 kg helmet, and 6 g with a 2 kg helmet), though only the most severe test condition for each subject was included in the current analysis. Upper neck loads (tension and flexion) were calculated based upon subject anthropometry, helmet inertial properties, and head

acceleration recorded at a bite bar. No subject sustained neck injury. The volunteer neck load time histories were obtained from the authors and N_{ij} was calculated using the critical intercepts developed for the current study.

4.7 Data Analysis

For purposes of developing critical intercepts for an N_{ij} injury metric, most of the experimental data previously discussed was used directly, while some required additional analysis.

4.7.1 Applicability to THOR-50M

For inclusion of the matched pair tests with THOR-50M, and to allow direct comparison of the THOR-50M response to the human-based risk function, transfer functions were developed for each loading mode, and then applied to the THOR-50M data prior to N_{ij} injury risk function development. Because PMHS neck stiffness underestimates neck stiffness, it may not be an ideal surrogate for tension neck loading (Dibb et al., 2006). This limitation can be addressed by using a computational model that includes the effects of musculature. Thus, for this analysis, the load-displacement response in each loading mode of the THOR-50M was compared to the response of the Duke Adult Head and Neck Model (DAHNM), which is a hybrid multibody and finite element model that consists of an osteoligamentous cervical spine and head, as well as 22 pairs of cervical muscles (Chancey et al., 2003). Validation of the DAHNM in axial tension and tension-bending was done by simulating whole spine PMHS tests from Dibb et al. (2009), using the osteoligamentous model only (Dibb, 2011). In these tests, force was applied at 50 N/s up to a maximum of 300 N. Model validation in pure bending was conducted by simulating quasi-static whole spine bending tests from Wheeldon et al. (2006), up to rotation angles of approximately 40 degrees (and moment of 2 N-m) (Dibb, 2011). Again, this validation used the osteoligamentous spine model only (no muscles). For the purposes of the current analysis, modeling was performed using a relaxed muscle configuration, meaning that muscles were included and exhibited relaxed muscle activation levels. The THOR-50M was tested in matched configuration both with and without the cables attached. The relaxed model condition most closely relates to a condition in the THOR-50M wherein muscle cables are not included.

In tension, both the DAHNM (Dibb et al., 2006) and the THOR-50M neck (with and without cables) were exercised in “pure” tension with the tensile line of action aligned over the occipital condyles, at a loading rate of 50 N/s and up to a peak force of 1000 N (Luck et al., 2014). Three tests were averaged to generate the THOR-50M response. In this condition, the THOR-50M neck was two times stiffer than the human model, exhibiting 3.3 mm of displacement at 1000 N of applied axial load, compared with 6.6 mm in the model (Figure 4.5).

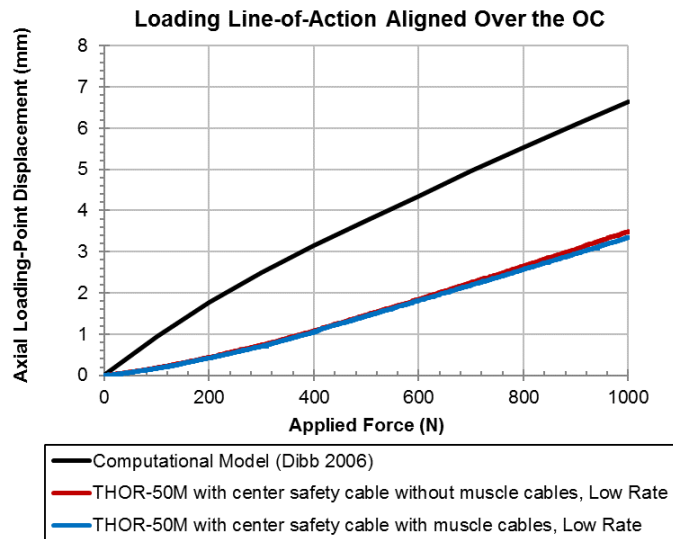


Figure 4.5. THOR-50M response in tension, with and without muscle cables, compared with the computational model. The tensile line of action was aligned over the occipital condyles and the loading rate was 50 N/s.

In compression, there was no matched THOR-50M data available to develop a transformation. The assumption is therefore made that the compression stiffness ratio is equal to the tension stiffness ratio.

In dynamic flexion and extension, Luck et al. (2014) compared applied moment to the resulting head angular displacement and upper neck load cell moment, in both the THOR-50M neck (without cables) and the human model (DAHNM) with relaxed musculature, at a loading rate of approximately 90 Nm/s. Six THOR-50M tests were averaged. The response of the THOR-50M was nonlinear, particularly in the head angular displacement range of approximately -20 to 20 degrees, where applied moment was small. Thus, the current stiffness comparison focuses on the approximately linear stiffness region involving head displacement between approximately 25 and 60 degrees in flexion and extension. The difference in rotational stiffness (i.e. the slope of upper neck load cell moment and angular displacement, $\Delta M\gamma/\Delta\theta$) was evaluated for both flexion and extension (Figure 4.6). The rotational stiffness of the THOR-50M response was about 1.14 and 1.21 times that of the model in flexion and extension, respectively.

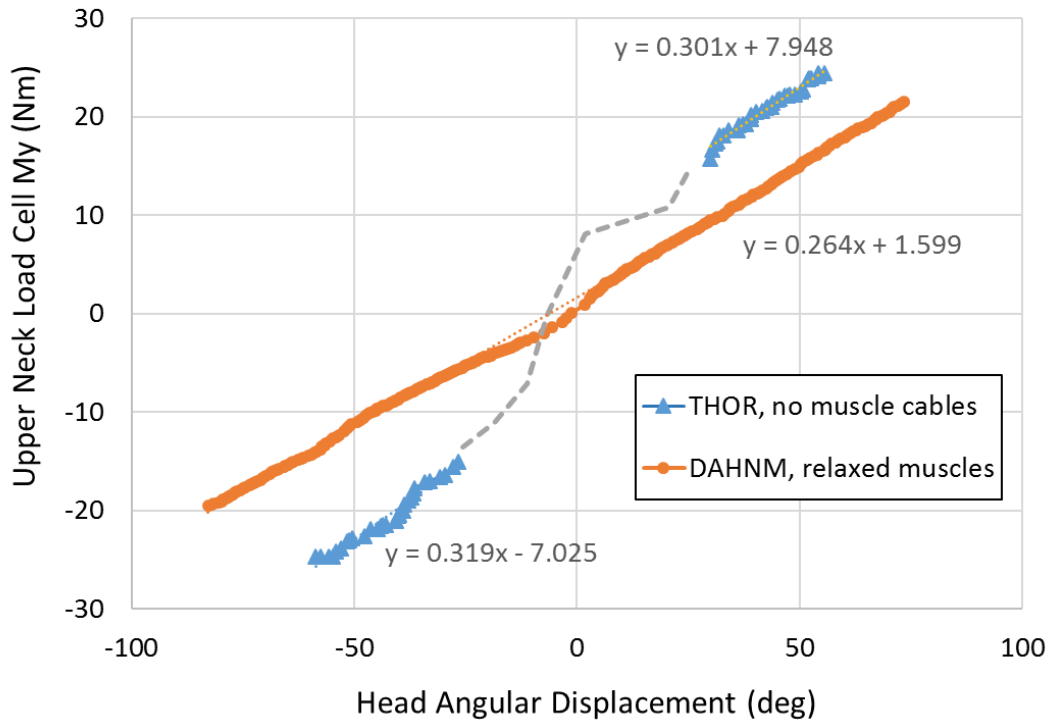


Figure 4.6. Rotational stiffness ($\Delta My/\Delta\theta$) of THOR-50M (average of six tests) and human model response, adapted from Luck et al. (2014). The stiffness comparison focuses on the approximately linear stiffness region involving head displacement between approximately 25 and 60 degrees in flexion and extension. The non-linear portion in the head angular displacement range of approximately -20 to 20 degrees is shown in dashed gray.

For tension, flexion and extension, the THOR-50M neck was stiffer than human. To develop a transfer function, scaling was applied using an equal work approach. In other words, it was assumed that the work to failure is the same for human and THOR-50M. Assuming the neck behaves as a linear spring, the force (Eq. 4.1) and work to failure (Eq. 4.2) can be combined to yield a transfer function for failure force as a function of stiffness ratio (Eq. 4.3). These transfer functions (Table 4.1) were applied to all THOR-50M data used in development of the Nij risk function.

$$F = kx \quad [4.1]$$

$$W = \frac{1}{2}kx^2 \quad [4.2]$$

$$F_{THOR} = \sqrt{\frac{k_{THOR}}{k_{model}}} F_{Human} \quad [4.3]$$

Table 4.1. Transfer functions to equate forces/moments measured in THOR-50M to human-equivalent forces, assuming equal work to failure.

Loading Mode	$\frac{k_{THOR}}{k_{model}}$	$\frac{F_{THOR}}{F_{Human}}$
Tension	2	1.4
Compression*	2	1.4
Flexion	1.14	1.1
Extension	1.20	1.1

*Compression transfer function assumed to be equal to tension

4.7.2 Load Rate Scaling

Tensile failure load is known to increase with loading rate (Nuckley et al., 2005). It was desired to have the data used to develop the risk curve be representative of loading rates experienced in the crash environment. To define the loading rate of the crash environment, fleet tests with THOR-50M were identified (Table F.3) and the loading rate was calculated as the slope of the positive portion of the upper neck load cell Z-axis force time-history between 15% and 85% of the peak tension force.

Nuckley et al. (2005) developed scaling ratios for baboon spine segments for loading rates between 0.5 mm/s (80 N/s) and 5000 mm/s (1,757,000 N/s) (Table 4.2). For PMHS data conducted in tension (where load rates were known), a ratio was determined using the baboon failure load at both the original PMHS loading rate and the target load rate (i.e. the mean THOR-50M loading rate from fleet tests). The original failure data was then scaled by this load rate ratio.

$$F_{PMHS(THOR\ load\ rate)} = F_{PMHS(original\ load\ rate)} \frac{F_{baboon(THOR\ load\ rate)}}{F_{baboon(PMHS\ load\ rate)}} \quad [4.4]$$

Table 4.2. Failure loads based on loading rate, from Nuckley et al. (2005).

Displacement rate (mm/s)	Mean stiffness (N/mm)	Loading rate (N/s)	Baboon mean failure load (N)
0.5	161.4	80.7	468.3
5	193.1	965.5	626.9
50	207.9	10,395	809.3
500	262.6	131,300	1135.3
5000	351.4	1,757,000	2189.5

Flexion and extension are expected to exhibit similar load rate dependence to that in tension, due to dependence on the same ligaments. For the data described above, if tensile load rate was unknown but flexion/extension rate was known, the flexion and extension loading rate can be converted into the equivalent tensile loading rate experienced by the spinal ligaments by dividing by the moment arm. To determine the moment arm, one needs to know the distance from the center of rotation (COR) in

flexion and extension to the relevant ligaments. While these distances were not known for each specimen tested, representative distances were established for mid-sized males using the 50th Percentile Male GHBM (M50-O v.4.3 Occupant Model, Global Human Body Models Consortium, LLC). According to Chancey et al. (2007), the combined center of rotation of OC-C2 is approximately located at the centroid of the OC. The distances from the COR to the anterior and posterior ligaments at C2 were measured on the GHBM (Figure 4.7). Because ligaments are located at varying locations and orientations across the neck, and cervical ligaments have differing failure strains and failure forces (Mattucci et al., 2012), the total neck moment has a distribution across the entire distance and does not just act at the extreme limits of the geometry. Although the exact moment distribution is unknown, for the purposes of this analysis, the combined moment arm is assumed to be located at approximately two thirds of the total distance. Moment arms of 20.2 mm (two thirds of 30.3 mm) and 13.6 mm (two thirds of 20.4 mm) were used for flexion and extension, respectively. The equivalent tensile loading rate was determined by the original moment load rate divided by the respective moment arm. Once the equivalent tensile loading rate was calculated, a load rate ratio was established from the baboon data using the same procedure described above.

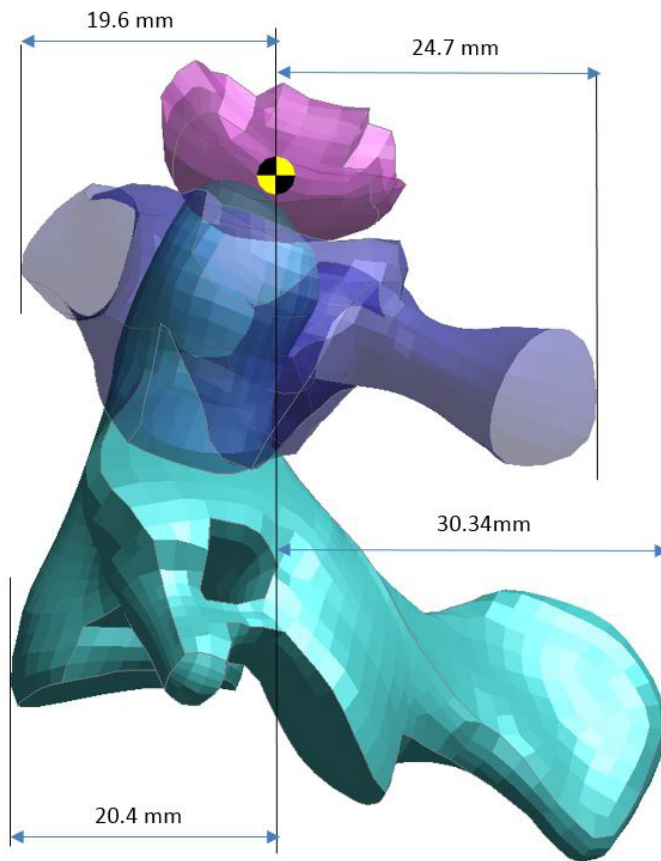


Figure 4.7. Distances from the center of rotation (COR) to the anterior and posterior ligaments at C1 and C2, measured on the GHBM M50-O in the normal driving posture.

The mean THOR-50M tensile loading rate in fleet testing was approximately $54,000 \pm 29,000$ N/s (Table F.3). Given the THOR-50M transfer functions described above, this equates to approximately 38,200 N/s for PMHS (i.e. $54,000/1.4$). By interpolation, the baboon failure load at 38,200 N/s is approximately 885 N. Tensile loading rates were known for the Dibb et al. (2009) study and the Pintar et al. (2005) study. The baboon failure load at each respective loading rate was compared to 885 N (the failure load at the target load rate), resulting in the load rate ratios shown in Table 4.3.

Table 4.3. Load rate ratios applied for tension.

Study	Loading rate (N/s)	Load rate ratio
Dibb et al. (2009)	1000	1.4
Pintar et al. (2005)	mean 852,000	0.55

For flexion and extension (Nightingale et al., 2007), using the assumed moment arms, the resulting tensile loading rates were approximately 4400 and 6600 N/s. Using the Nuckley et al. (2005) scaling ratios, the failure load at an equivalent load rate of 38,200 N/s is approximately 1.3 and 1.2 times the failure load at 4400 and 6600 N/s, respectively (Table 4.4)

Table 4.4. Load rate ratios for flexion and extension (Nightingale et al., 2007).

Loading type	Approximate loading rate (Nm/s)	Distance to extreme limits of C2 geometry (mm)	Assumed moment arm for ligaments (mm)	Tensile loading rate (N/s)	Load rate ratio
Flexion	90	30.4	20.2	4400	1.3
Extension	90	20.4	13.6	6600	1.2

4.8 Critical Intercepts for Combined Loading Criterion

To develop critical intercepts, data (with load rate scaling where applicable) from each loading mode was analyzed separately. The mean AIS 3+ injury value was used as the critical intercept in each mode. THOR-specific critical intercepts were obtained using the previously described transfer functions for each loading mode (Table 4.5). These intercepts assume a relaxed muscle state.

While several methods have been proposed in the literature for development of critical intercepts for combined loading criteria, there is no “gold standard.” Previous combined injury metrics such as BrIC (Takhounts et al., 2013) and Combined Thoracic Index (Eppinger et al., 1999) have targeted 50% risk levels for each critical intercept. Critical intercepts for the earlier published Nij criterion (Eppinger et al., 1999) were based on differing methods such as minimum injury levels (Prasad and Daniel, 1984) and age-force linear regression (Pintar et al., 1998). Others have used mean injury values (Revised Tibia Index, Kuppa et al., 2001). Mean injury values tend to represent a higher level of risk than 50%, while minimum values would represent a lower level of risk.

Table 4.5. Summary of proposed Nij critical intercepts based on mean AIS 3+ injury values.

Loading Mode	Studies used	PMHS intercept	THOR-50M transfer function	THOR-50M intercept
Tension (N)	Dibb et al., (2009), Yliniemi et al., (2009)	3000	1.4	4200
Compression (N)	Panjabi et al., (1991), Carter et al., (2002)	3230	1.4	4520
Flexion (Nm)	Nightingale et al., (2007)	54.5	1.1	60.0
Extension (Nm)	Nightingale et al., (2007)	72.0	1.1	79.2

The intercepts presented here differ from those in use with the H3-50M (Table 4.6), with flexion being the most different. Because of the construction of the THOR-50M neck, which allows load sharing between the neck cables and neck structure during neck flexion/extension, it makes sense that moments measured at the THOR-50M upper neck load cell would be less than those measured at the H3-50M upper neck, given a similar input condition.

Table 4.6. Comparison of THOR-50M intercepts to historical H3-50M intercepts.

Loading Mode	THOR-50M intercept	H3-50M intercept
Tension (N)	4200	6806
Compression (N)	4520	6160
Flexion (Nm)	60.0	310
Extension (Nm)	79.2	125

4.9 Injury Risk Function Formulation

Once critical intercepts were developed for the THOR-specific version of the neck injury criterion (Nij) as a metric for assessing neck injury in frontal crashes, the combined loading criterion was evaluated. For each specimen, Nij was calculated using instantaneous axial force and y-axis moment data, using the standard formulation and new intercepts. For tests conducted with the THOR-50M ATD, loads and moments were obtained directly from the upper neck load cell. This was more comparable to experimental flexion and extension data conducted on motion segments (Nightingale et al., 2007), from which the flexion and extension critical intercepts were developed, than calculated OC moment.

The dependent variable used in the development of the neck injury criterion was the presence of an AIS score of 2 or greater (AIS 2+) or 3 or greater (AIS 3+), based on the AIS 2005 Update 2008 (AAAM, 2008). Using Nij as the predictor variable, stepwise multiple regression was carried out to assess the sensitivity of occupant-based covariates (age and sex). The criteria for covariates to enter and stay in the model was $p < 0.1$. Model significance and goodness of fit were evaluated.

4.9.1 AIS 2+ model

For the dependent variable of AIS 2+ injury, results of the stepwise logistic regression indicated that the model was significant ($p < 0.05$), and age met the significance standard for inclusion in the model. Sex did not enter the model. Model fit statistics are shown in Table 4.7.

The final AIS 2+ model parameters (Figure 4.8) are given by Table 4.9. An age of 40 years was used for calculation of 95% confidence intervals. The age of 40 represents an approximation of the mean age of male drivers in frontal crashes, based on the National Automotive Sampling System – General Estimates System.

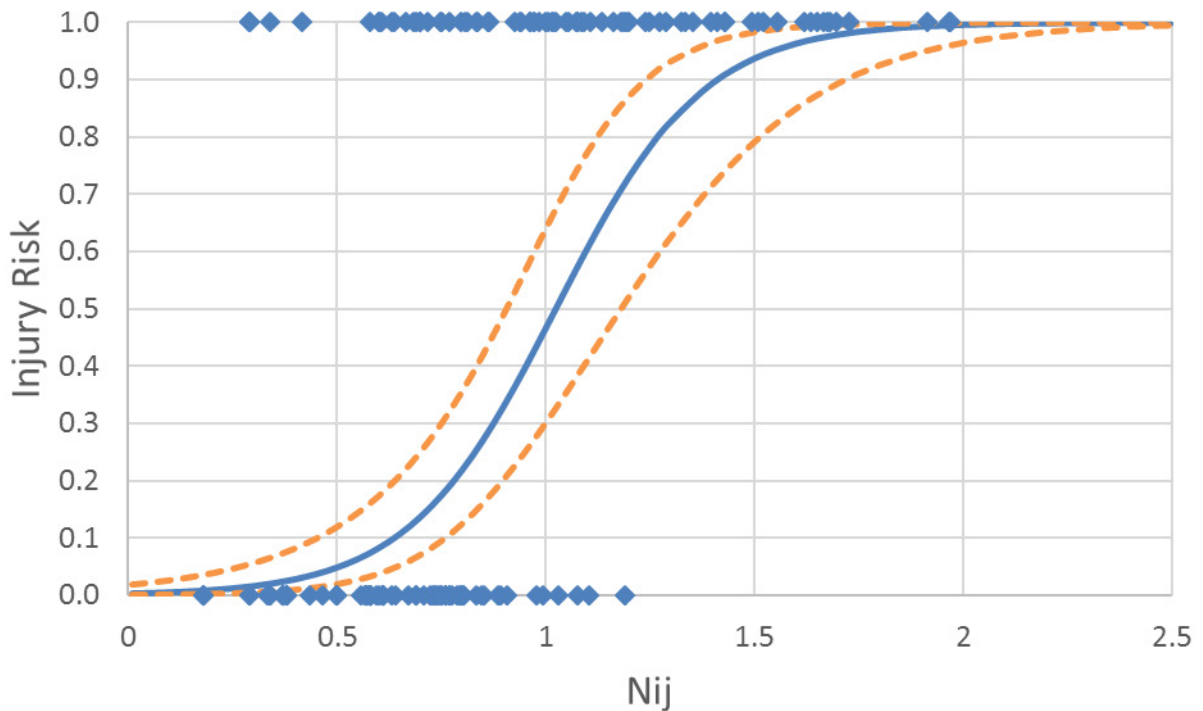


Figure 4.8. AIS 2+ injury risk curve (mean and 95% confidence intervals), using an age of 40 years. Experimental data also shown.

4.9.2 AIS 3+ model

For the dependent variable of AIS 3+ injury, results of the stepwise logistic regression indicated that the model was significant ($p < 0.05$), and age met the significance standard for inclusion in the model. Sex did not enter the model. Model fit statistics are shown in Table 4.7. The final AIS 3+ model parameters (Figure 4.9) are given in Table 4.9.

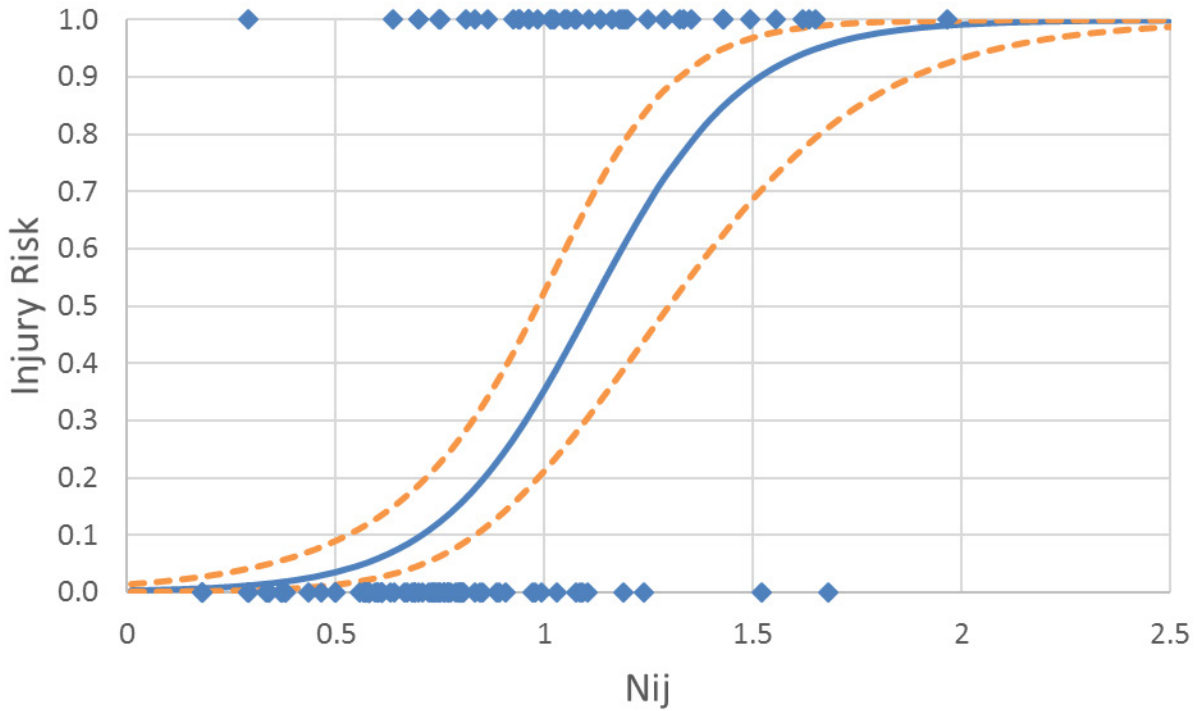


Figure 4.9. AIS 3+ injury risk curve (mean and 95% confidence intervals), using an age of 40 years.

Table 4.7. Model fit statistics for AIS 2+ and AIS 3+ risk functions.

Model	Covariates	Wald Pr>ChiSq	AUROC	Hosmer-Lemeshow Pr>ChiSq	-2 Log L
AIS 2+	Age	<0.0001	0.907	0.978	130.9
AIS 3+	Age	<0.0001	0.898	0.0278	115.6

4.9.3 Sensitivity Analysis

For the AIS 3+ risk function, there were three observations that were overly influential, which were identified by the DFBETAS diagnostic. Two of the observations were specimens from Pintar et al. (2005) that sustained injury at the AIS 2 level but not the AIS 3 level, yet had high N_{ij} values (greater than 1.5). The other influential observation was a 67-year-old specimen in the whole-body sled test performed by University of Virginia, in which a bilateral facet dislocation was sustained (note that the other four PMHS specimens tested in the identical condition did not sustain AIS 3+ injury). The matched pair test with THOR-50M recorded peak tension of only 685 N and peak N_{ij} of only 0.29. With one or all of these three observations removed, the model fit improved (Table 4.8), although the resulting risk functions were still captured within the upper and lower confidence bounds of the original risk function with all data included (Figure 4.10). Because there is no physical reason for exclusion of these specimens, it is therefore recommended to retain the original risk function using all available data.

Table 4.8. Model fit statistics for AIS 3+ risk functions with influential observations removed.

Model	Covariates	Wald Pr>ChiSq	AUROC	Hosmer-Lemeshow Pr>ChiSq
AIS 3+ original	Age	<0.0001	0.898	0.0278
UVA specimen removed	Age	<0.0001	0.914	0.1054
Pintar et al., (2005) specimens removed	Age	<0.0001	0.914	0.3686
Three influential observations removed	Age	<0.0001	0.93	0.4583

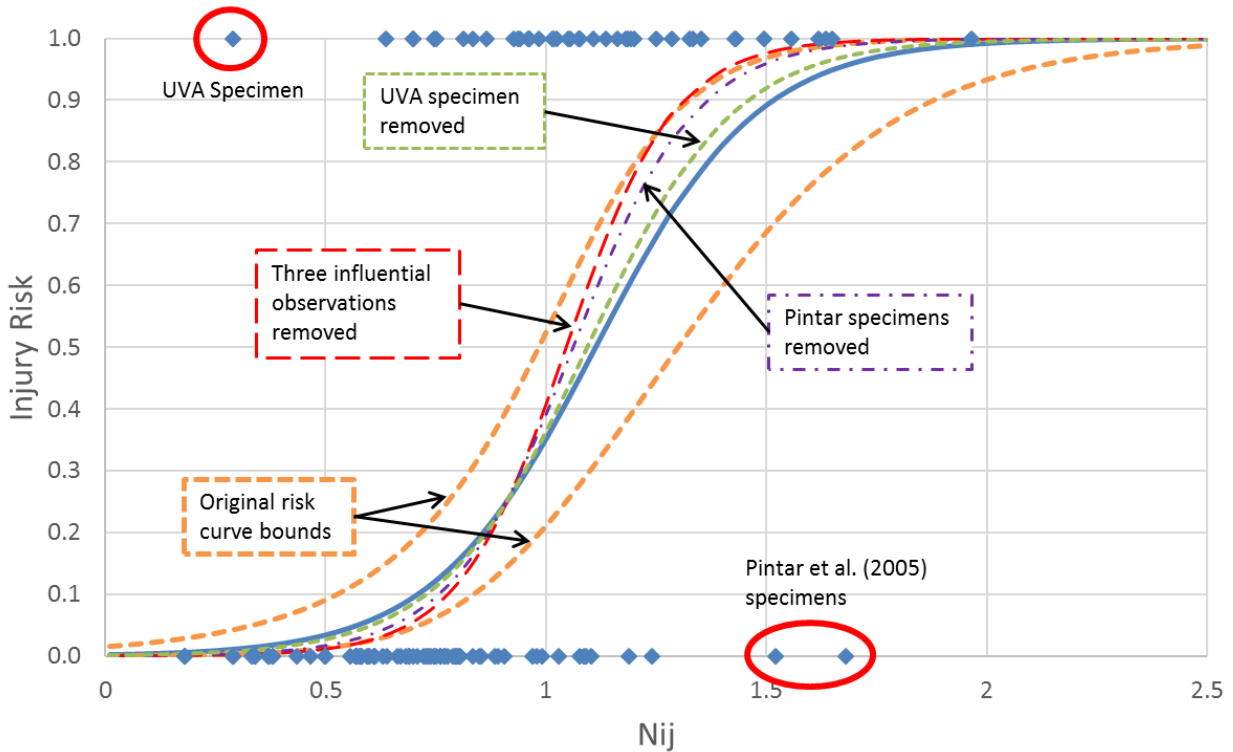


Figure 4.10. For the AIS 3+ risk function, three observations (circled in red) were overlay influential. Removal of these observations improved model fit but the resulting risk functions were still captured within the confidence bounds of the original risk function.

4.9.4 Final logistic regression model

Using all available data, the resulting logistic regression takes the form:

$$p(\text{AIS } 2+/3+) = \frac{1}{1+e^{(-\beta_0-\beta_1x-\beta_2age)}}$$

where:

- β_0 = Intercept
- β_1 = Independent parameter coefficient
- β_2 = Age coefficient
- x = Nij (calculated using upper load cell values)

Table 4.9. Model parameter estimates for Nij.

Model	β_0 (Int.)	β_1 (Nij)	β_2 (Age)
AIS 2+	-9.031	5.681	0.0803
AIS 3+	-7.447	5.440	0.0350

Table 4.10. Resulting Nij injury assessment reference values.

Model	10%	25%	50%
AIS 2+	0.64	0.83	1.02
AIS 3+	0.71	0.91	1.11

4.9.5 Survival model

Once logistic regression was used to determine model goodness of fit, an additional form of the risk function was developed using left/right censored survival analysis. All failure data were considered to be left censored and all non-failure data were right-censored. The survival analysis risk function, which assumes a Weibull distribution, takes the form:

$$p(AIS \geq 3) = 1 - \exp\left(\exp\left(\frac{\ln(x) - \beta_0 - \beta_1 \text{age}}{\alpha}\right)\right)$$

where:

- β_0 = Intercept
- β_1 = Age parameter
- x = Nij (calculated from upper neck load cell values)
- α = scale

Table 4.11. Model parameter estimates and goodness-of-fit.

Model	β_0 (Int.)	β_1 (Age)	α (Scale)	-2 Log L
AIS 2+	0.8842	-0.0175	0.3603	138.7
AIS 3+	0.5307	-0.0064	0.3281	120.1

The AIS 2+ and AIS 3+ risk functions presented here demonstrated differences between the logistic regression and survival curves, particularly when the age of 40 was considered. This was unexpected considering that the data was generally well correlated. The closest match between the logistic regression and survival curve was for an age of 60 years in the AIS 2+ curve. An age of 60 years more closely represents the actual specimens used in the risk function development (average age of the

injured specimens was 62 years, with range 30 to 94 years). Given the lower log likelihood values for the logistic model (compared with the survival model), the logistic regression curves are recommended.

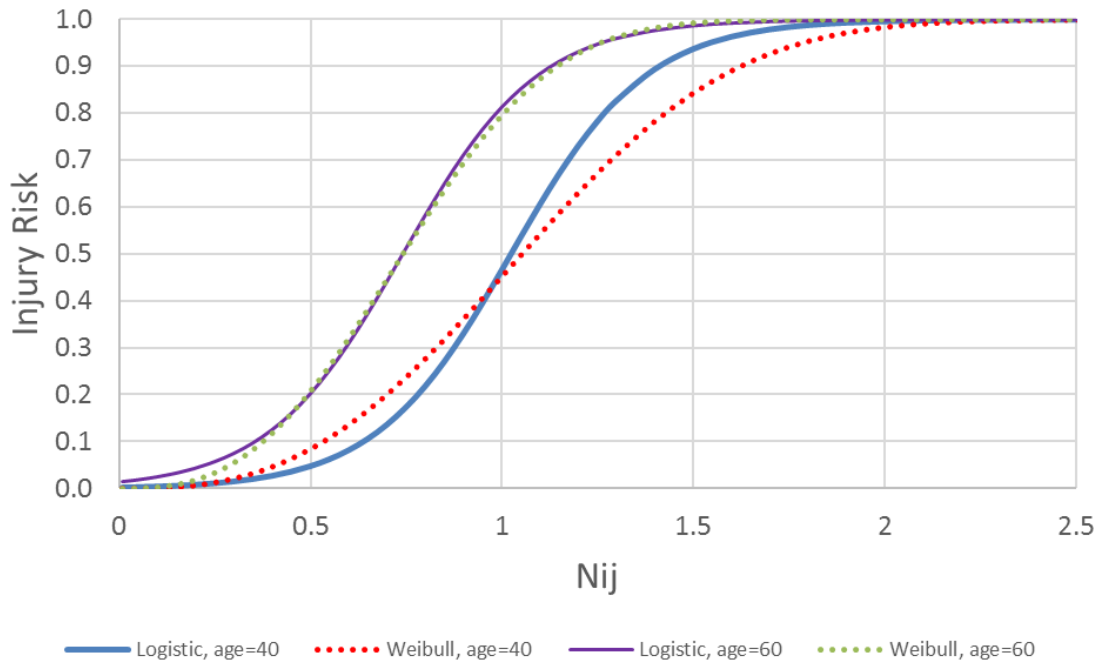


Figure 4.11. Comparison of logistic regression and survival analysis for AIS 2+ injury risk. For an age of 60, the logistic regression and survival curves closely match. For an age of 40 years, the curves diverge at higher risk levels.

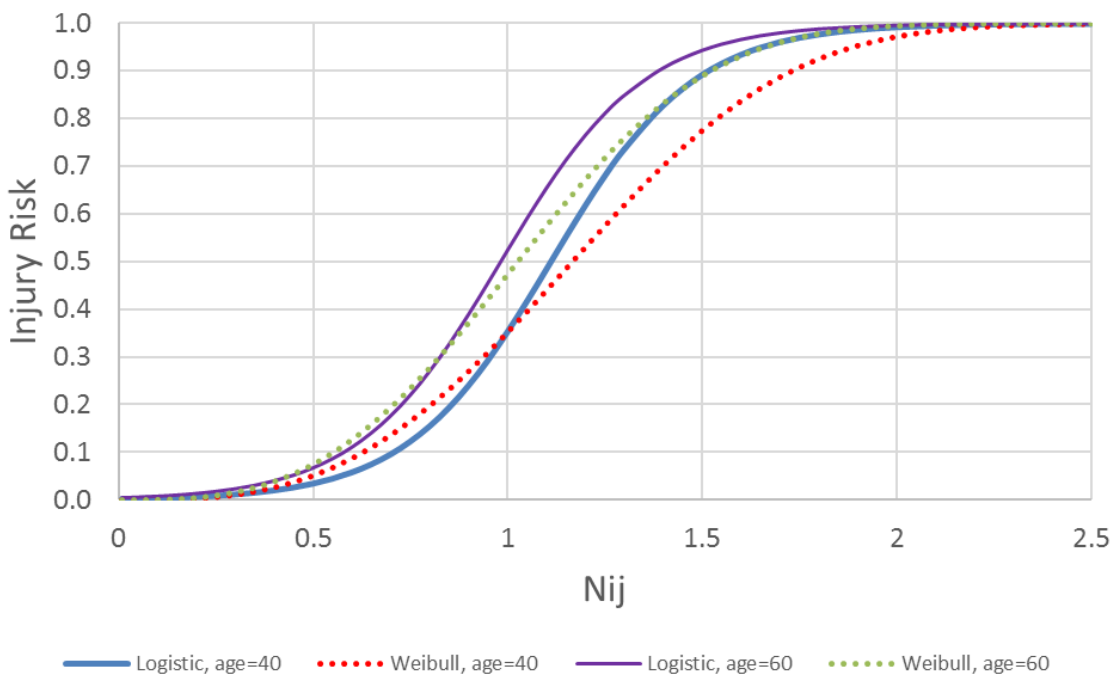


Figure 4.12. Comparison of logistic regression and survival analysis for AIS 3+ injury risk. For both age 40 and age 60, the logistic regression and survival curves diverge at higher risk levels.

4.10 Application of Risk Functions to THOR-50M

As the development of the N_{ij} risk function considered application to the THOR-50M in the development of critical intercepts (Section 4.8), no additional modification is necessary. The measurements from the THOR-50M upper neck load cell used to calculate the risk of AIS 2+ or AIS 3+ neck injury as follows:

$$p(\text{AIS } 2+) = \frac{1}{1 + e^{(5.819 - 5.681N_{ij})}}$$

$$p(\text{AIS } 3+) = \frac{1}{1 + e^{(6.047 - 5.44N_{ij})}}$$

$$N_{ij} = \left| \frac{F_z(t)}{F_{zc}} + \frac{M_y(t)}{M_{yc}} \right|_{max}$$

where:

$F_z(t)$ = Force time-history measured by the z-axis of the THOR upper neck load cell (in N)

$M_y(t)$ = Moment time-history measured by the y-axis of the THOR upper neck load cell (in Nm)

F_{zc} = Critical intercept for force:

$$F_{zc} = \begin{cases} 4200 & \text{for } F_z(t) > 0 \\ -4520 & \text{for } F_z(t) < 0 \end{cases}$$

M_{yc} = Critical intercept for moment:

$$M_{yc} = \begin{cases} 60 & \text{for } M_y(t) > 0 \\ -79.2 & \text{for } M_y(t) < 0 \end{cases}$$

4.11 Fleet Test Data: THOR-50M

The recommended neck injury risk functions were applied to THOR-50M measurements collected in frontal rigid barrier and frontal Oblique fleet testing. Figure 4.13 and Figure 4.14 show the risk of AIS 2+ and AIS 3+ injury, respectively, as a function of N_{ij} , with observations representing the injury risk predicted from each occupant response grouped by occupant position and test mode. Risk of AIS 2+ neck injury was below 15 percent for all observations, while risk of AIS 3+ neck injury was below 10 percent for all observations.

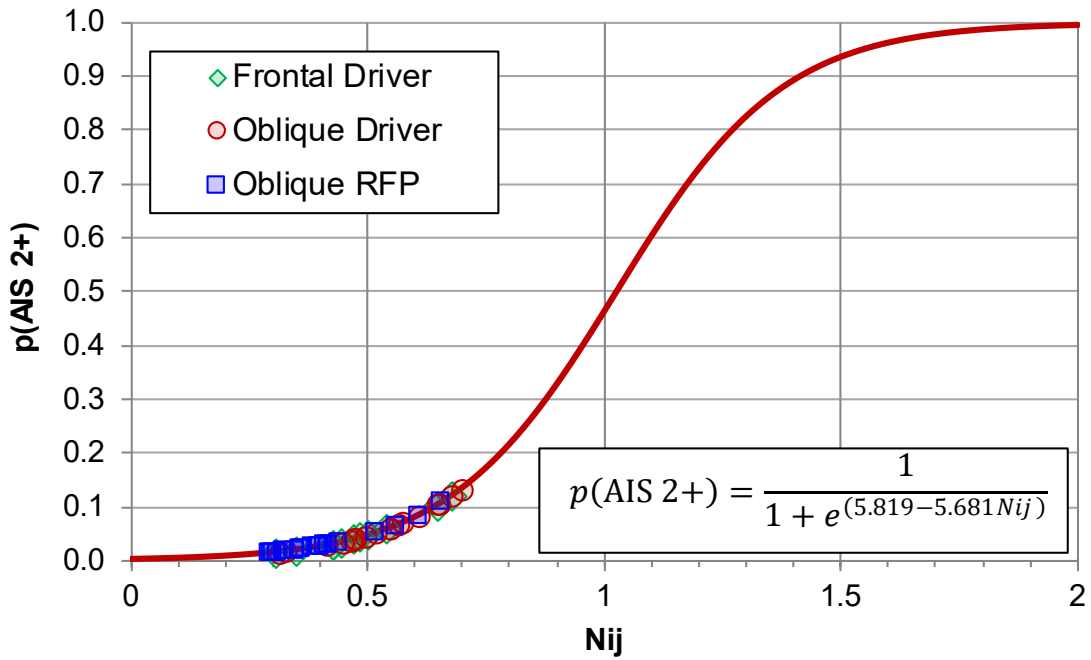


Figure 4.13. Probability of AIS 2+ neck injury predicted using N_{ij} measured from fleet test results for the driver in the frontal rigid barrier test mode and both the driver and right front passenger in the Oblique MDB test mode.

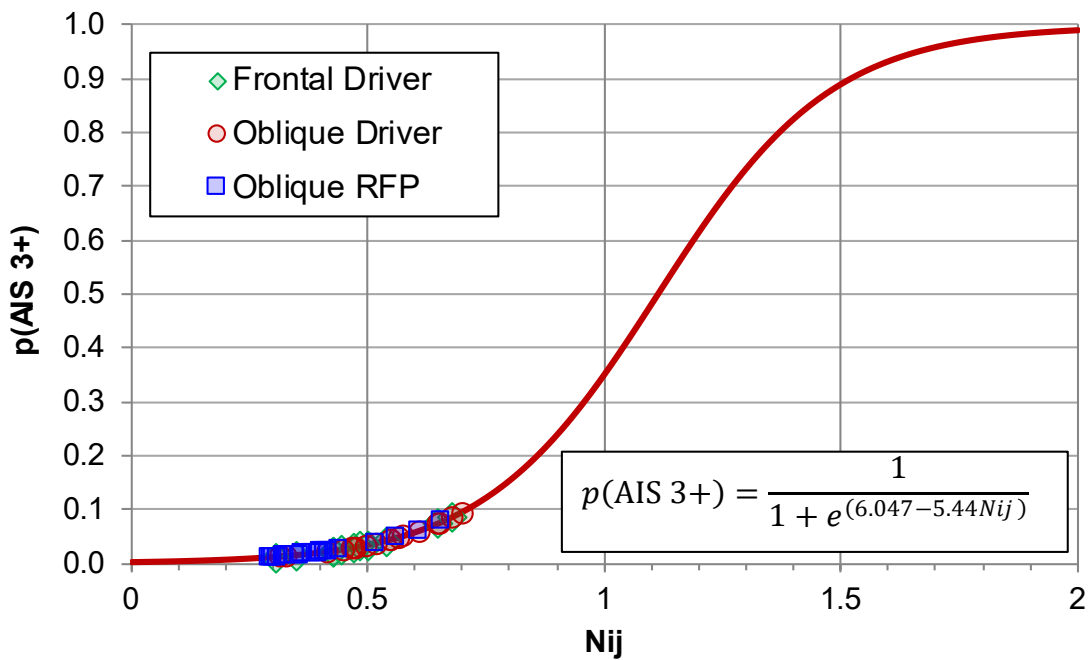


Figure 4.14. Probability of AIS 3+ neck injury predicted using N_{ij} measured from fleet test results for the driver in the frontal rigid barrier test mode and both the driver and right front passenger in the Oblique MDB test mode.

4.12 Limitations

There are many limitations to the current work. The method used here in the development of the Nij risk function was to combine available data, despite differences in test conditions, loading rates, and specimen type (e.g. PMHS vs. volunteer). Some of the studies contained all non-injured specimens (e.g. the volunteer data), while some contained all injured specimens (e.g. the Dibb et al., 2009 and Yliniemi et al., 2009 tension data). Since each study did not contain both injured and non-injured specimens, there may be inherent laboratory bias that cannot be accounted for. This method was employed because there were insufficient studies containing both injury and non-injury to develop a robust injury criterion. A similar method has been used in many previously published risk functions. For example, early work on femur tolerance by Morgan et al. (1989) included sled test data on PMHS that was not conducted for the purpose of creating knee-thigh-hip injury (in fact, its purpose was interaction between driver thorax and steering wheel) (Morgan et al., 1987). There were no knee-thigh-hip injuries sustained and risk of injury in that study were mainly less than 5%, and yet it was included in risk function development. Yoganandan et al. (2015) have published several versions of lower leg risk functions using tests on repeated subjects, in which one low energy test was intended to not produce injury and one high energy test was intended to produce injury. Takhounts et al. (2013) used volunteer data (i.e. college football players) in the development of the Brain Injury Criterion (BrIC). Laituri et al. (2016) used volunteer data in their version of risk curves for BrIC. Poplin et al. (2017) included low-speed sled tests (10 km/hr) in development of a chest injury risk curve, which had very low risk of injury. Despite the limitations of the current approach, inclusion of a wide variety of studies yielded sufficient available injury and non-injury data for risk function development.

While more than 150 specimens were included for the development of the Nij risk function, the sample sizes in each loading mode used for critical intercept values were much smaller. In particular, the number of injured specimens in flexion and extension was only two and five respectively. In addition, subject preparations, such as instrumentation/mounting hardware and/or the use of helmets may have influenced the inertia of the head in these tests. However, because these added masses were accounted for in calculation of upper neck loads, the desired comparison of neck load to injury status should not be significantly affected.

The critical intercepts developed in this effort assume relaxed musculature. Therefore, muscle tensing was not accounted for. As was previously done for the Hybrid III ATD, these intercepts could be adjusted by assuming a level of protection provided by muscle tensing. However, the assumed relaxed state is more conservative, and may be more appropriate considering that 40 to 50% of occupants in frontal crashes exhibit no pre-impact braking (indicative of being unaware of the impending crash) (Craig et al., 2011).

Another limitation has to do with the use of the Duke Adult Head and Neck Model for predicting THOR-50M response in tension, flexion and extension. The transfer functions were developed for motion beyond the range the model was validated for. This could affect the transfer functions developed and the resulting injury risks predicted by the THOR-50M. In addition, transfer functions were based on an assumption of equal work between the human and THOR-50M. Because this method assumes a linear

response, it may not account for the rate effects seen in the PMHS response. Also, there was no matched THOR-50M data with which to develop a transfer function in compression. Thus, the application of the Nij risk curve in compression-flexion and compression-extension should be used with caution. For in-position occupants, the THOR-50M should rarely experience a peak Nij in either compression mode. Only one of the THOR-50M fleet tests examined (Table F.3) had a peak Nij in compression (Nij=0.3), while the remaining tests all had the peak Nij in either tension-flexion (28%) or tension-extension (69%).

Finally, a combined loading criterion was targeted here, which may be desirable due to the many different mechanisms associated with real world injury. Through parametric analysis of the 50th Percentile Male GHBMCM50-O, Hasija et al. (2017) demonstrated that both axial force and moment at the occipital condyles are necessary for prediction of ligamentous neck injuries (rather than axial force alone), suggesting the continued need for a criterion such as the Nij that includes both metrics. Nonetheless, the traditional Nij formulation presented herein has limitations. For example, the Nij formulation is based on the assumption that the neck structure acts as an Euler-Bernoulli beam, with the principle of superposition being used to sum the stress due to the moment and the stress due to the axial force, for a composite total stress in the bone. In fact, the neck exhibits complex dynamic behavior (e.g. multiple mode buckling) that may not be accurately represented by beam theory.

5 CHEST

5.1 Field and Historical Fleet Data

Similar to observations with brain injury, there appears to be an opposite trend in fleet data predicted injury risk from NCAP tests (Figure 5.1) and injury rates from field data (Figure 5.2). The field data injury rate or risk represents a running three-year average of the percent of injury cases (injured case count divided by the total number of cases; e.g. model year 1992 includes the total weighted count of AIS 3+ injuries from model years 1990, 1991 and 1992, divided by the total number of cases for those model years). Injury risk was calculated using the risk function that is currently in use with the H3-50M in frontal NCAP testing (NHTSA, 2008).

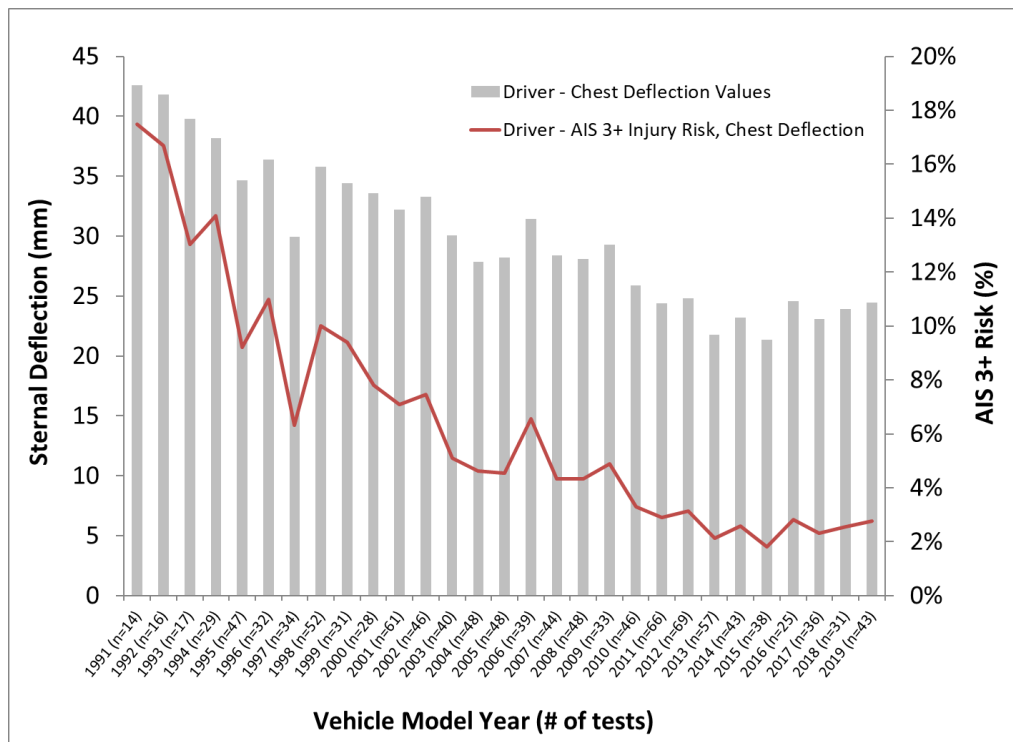


Figure 5.1. H3-50M NCAP driver chest deflections and predicted injury risk (AIS 3+) for tests from model year 1991 to 2019.

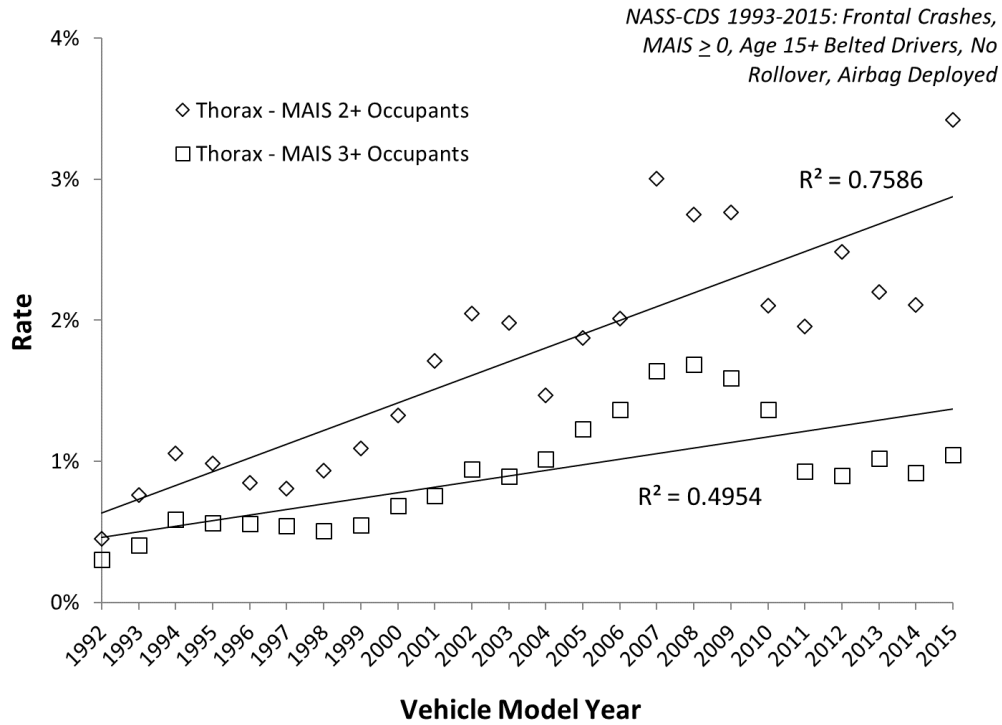


Figure 5.2. Thorax MAIS 2+ and 3+ rate versus model year (1992 to 2015) for belted and airbag restrained drivers in frontal crashes from NASS-CDS 1993 to 2015.

Figure 5.3 shows the regional mechanisms of injury assigned to thoracic injuries in 280 CIREN front-row belted occupants involved in frontal crashes. These mechanisms are inferred from the available data and may have been limited to available researcher/published biomechanical knowledge at the time. It is important to note that the mechanisms shown are regional mechanisms, not organ-specific mechanisms. That is, the chosen mechanism represents the type of loading/motion experienced by the entire thoracic region. Compression is the dominant mechanism for skeletal injuries, while the soft tissues are more frequently injured from a combination of compression and the rate of compression.

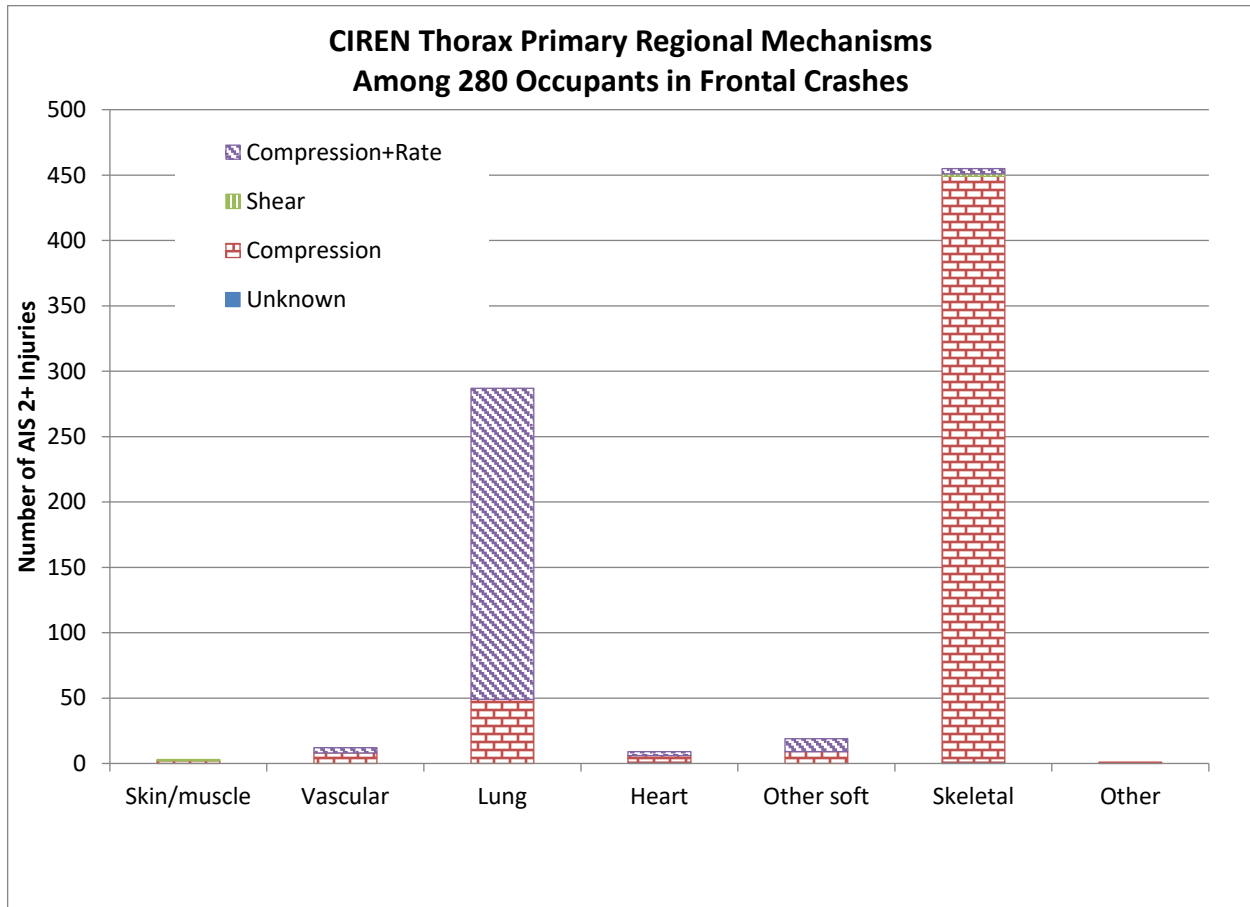


Figure 5.3. Recorded mechanisms of thoracic injuries for belted front row occupants involved in frontal crashes from the CIREN database.

5.2 Literature Review

Eppinger et al. (1999) presented a summary of historical research into the development of thoracic injury criteria, primarily focused on those applicable to the H3-50M for use in Federal Motor Vehicle Safety Standards (FMVSS) No. 208. Based on the historical research, a set of thoracic injury risk predictors were selected and logistic regression models were fit to the results of 71 post-mortem human subject (PMHS) sled tests. The predictor variables investigated were thoracic spine resultant acceleration (A_s), normalized central chest deflection at the measurement location of the H3-50M (dc), normalized deflection at any of five measurement locations on the chest ($dmax$), chest deflection velocity, and viscous criterion. Of these predictors, the best injury predictor was a linear combination of thoracic spine resultant acceleration and the normalized deflection at any of the five measurement locations on the chest. This predictor was defined as the combined thoracic injury criterion, or *CTI*. Injury risk functions were developed for A_s alone, dc alone (as measurement of $dmax$ is not possible for the H3-50M), and *CTI*. These injury risk curves were not directly implemented to develop injury assessment reference values (IARVs) for FMVSS No. 208, as the dc limit was taken to be 63 mm and the A_s limit was

taken to be 60 gs to harmonize with the Canadian Motor Vehicle Safety Standards (CMVSS). The *CTI* was not used for regulatory purposes, but for analysis purposes only.

In the 2008 NCAP Final Decision Notice (NHTSA, 2008), it was noted that the injury risk function developed by Eppinger et al. (1999) did not account for age and was not adequately adjusted to reflect real-world chest injury risk. Instead, the chest injury risk function presented by Laituri et al. (2005), which was developed based on a larger set of published PMHS test data and included more diverse loading conditions, was used. To relate the PMHS-based injury risk function to the H3-50M, a transfer function was developed by Laituri et al. (2005) using a subset of matched pair tests. The resulting chest injury risk function related the peak chest deflection as measured by the H3-50M sternum potentiometer along with the age of the subject to the risk of AIS 3+ thoracic injury, as defined as seven or more rib fractures. For AIS 1990 (1998 update) four fractured ribs or more constituted an AIS 3+ thoracic injury. Laituri et al. added three fractured ribs for the threshold of seven per reference to earlier studies that had found a difference in the number of fractured ribs between dead specimens (e.g. PMHS) and live subjects (Viano et al., 1977; Foret-Bruno et al., 1978). As implemented in Frontal NCAP, an age of 35 years was selected to represent the average age of the driving population.

Both the Eppinger et al. (1999) and Laituri et al. (2005) injury risk functions required corrections or assumptions to account for the limitation of the single-point measurement capability of the H3-50M. NHTSA has previously identified instrumentation opportunities beyond a single-point chest deflection measurement system that may improve the assessment of thoracic loading in a vehicle environment with advanced restraint technology such as airbags and pretensioners (Yoganandan et al., 2009). Thoracic trauma imparted to restrained occupants does not always occur at the same location on the rib cage for all occupants in all frontal crashes (Morgan et al., 1994). Kuppa and Eppinger (1998) found that, in a dataset consisting of 71 human subjects in various restraint systems and crash severities, using the maximum deflection from multiple measurement locations on the chest resulted in improved injury prediction. As such, multi-point deflection instrumentation was prioritized in the development of the THOR ATD (Haffner et al., 2001).

Real-world data also demonstrate the need for a multipoint deflection measurement to better reflect actual fracture/injury patterns and better discriminate between vehicle performances. In a small sample of restrained occupants with rib fractures, Shimamura et al. (2003) found that rib fractures were more common in the lower ribs (6-12) compared with the upper ribs, suggesting that the deployed airbag shared and distributed the load to the upper chest but had less effect near the seat belt buckle where concentrated seat belt loads still occurred. Lee et al. (2015) used the CIREN database to examine the rib fracture patterns of 158 belt- and airbag-restrained front seat occupants and found that 63% of fractures occurred on the inboard (with respect to the vehicle) side of the chest. Notably, only 40% of the occupants sustained sternal fracture (indicative of central loading). Asymmetric fracture patterns (both upper/lower and left/right) suggest that peak deflections typically do not occur centrally and thus are unlikely to correspond to the location of the mid-sternal chest slider in the Hybrid III family of dummies.

5.3 Design

Throughout the development of the THOR-50M ATD, specific attention was given to the human-like response and injury prediction capability of the chest. The rib cage geometry is more realistic because the individual ribs are angled downward to better match the human rib orientation (Kent et al., 2003). Performance requirements were selected to ensure human-like behavior in response to central chest impacts, oblique chest impacts, and steering rim impacts to the rib cage and upper abdomen (NHTSA, 2005a). Better chest anthropometry means that the dummy's interaction with the restraint system (as the seat belt lies over the shoulder and across the chest, for example) is more representative of the interaction humans would experience. The THOR-50M ATD is capable of measuring three-dimensional deflections at four different locations on the rib cage. This instrumentation, coupled with its thoracic biofidelity, provides the THOR-50M ATD with the ability to predict thoracic injuries and to potentially drive realistic restraint system countermeasures.

5.4 Instrumentation

THOR-50M ATD was designed to measure thoracic deformation at multiple points to facilitate the prediction of injury risk. The three-dimensional position time-history is measured for four points on the anterior rib cage relative to the local spine segment of rib origination (Figure 5.4). The anterior attachment points are at the vertical level of the fourth and eighth anatomical ribs, and at the lateral level of the costochondral junction. The upper chest instrumentation anterior attachment points are 40 millimeters from the sagittal centerline of the ATD, while the lower chest instrumentation anterior attachment points are 80 millimeters from the sagittal centerline. The posterior attachment point of the upper thorax instrumentation is on the Upper Thoracic Spinebox, which spans the anatomical landmarks of T4 through T8. The posterior attachment point of the lower thorax instrumentation is on the Thoracic Spine Load Cell Flex Joint Adaptor Plate, which is at the anatomical level of L1. Between the upper and lower thorax instrumentation attachment points is a flexible joint known as the Upper Thoracic Spine Flex Joint, so the reference coordinate system for the upper and lower thorax 3D motion measurements can change dynamically during a loading event. The deflection instrumentation used for the matched-pair testing conducted for this study was the Infrared Telescoping Rod for Assessment of Chest Compression (IR-TRACC).

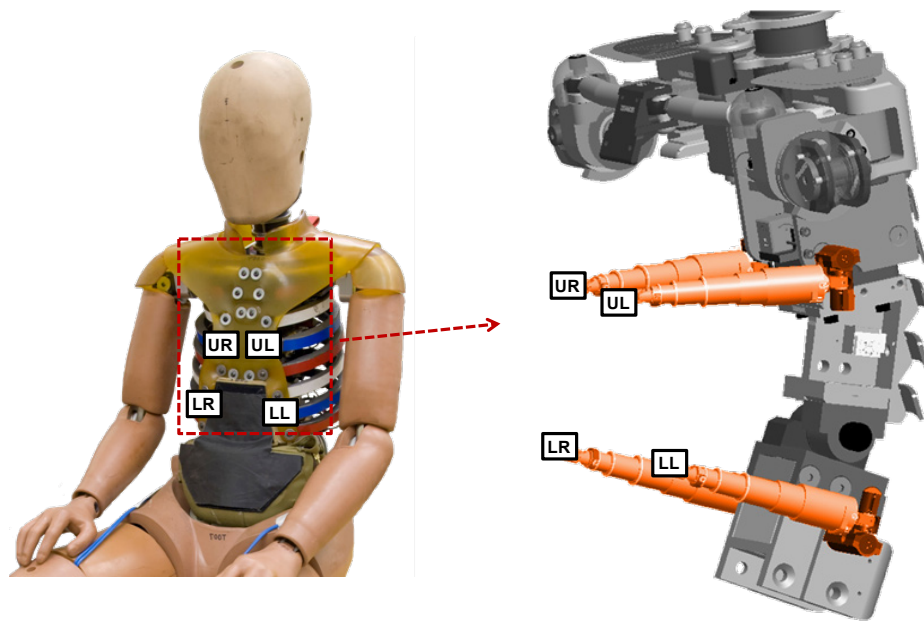


Figure 5.4. (Left) Location of the four measurement points on the thorax of the THOR. (Right) Attachment of the 3D deflection instrumentation assemblies to the spine.

THOR-50M was not designed to measure sternum deflection, in part due to the design of the sternum assembly which was developed to meet the biofidelity requirement in the low-speed blunt thoracic impact condition. The space occupied by the sternum assembly prevents installation of a measurement device to the anterior surface of the sternum. However, since the upper thorax deflection instrumentation attachment points are at the vertical level of the anatomic mid-sternum landmark, sternum deflection can be approximated using the midpoint of the line between the two upper thorax deflection instrumentation assemblies.

In addition to the deflection measurement system, the THOR-50M can also be instrumented with a uniaxial sternum accelerometer, triaxial accelerometers installed along the spine at the level of T1, T6, and T12, and a five-axis (three forces, two moments) load cell installed between the lumbar spine pitch change mechanism and the lumbar spine flex joint at the approximate anatomical level of T12. Clavicle loads cells can also be installed, but are not included in the THOR-50M described in the September 2015 drawing package (NHTSA, 2015a). THOR-50M thoracic instrumentation is summarized in Table 5.1.

Table 5.1. THOR-50M ATD thoracic instrumentation.

Sensor	Measurement Description	Measurement Axes
Upper Left 3D deflection	3D position of left 4 th rib WRT upper thoracic spine	XL, YL, ZL
Upper Right 3D deflection	3D position of right 4 th rib WRT upper thoracic spine	XL, YL, ZL
Lower Left 3D deflection	3D position of left 8 th rib WRT lower thoracic spine	XL, YL, ZL
Lower Right 3D deflection	3D position of right 8 th rib WRT lower thoracic spine	XL, YL, ZL
Sternum accelerometer	Acceleration of sternum	XL
Spine accelerometer(s)	Acceleration of the spine at T1, T6, T12	XL, YL, ZL
Spine load cell	Force and moment at T12	Force: XL, YL, ZL; Moment: XL, YL

5.5 Biofidelity

Parent et al. (2017) evaluated the biofidelity of the THOR-50M chest in two conditions: sternal impact and lower ribcage oblique impact. In the sternal impact condition, THOR-50M demonstrated excellent internal and external biofidelity, with Biofidelity Ranking System (BioRank) scores of 0.815 and 0.732, respectively. In the lower ribcage oblique impact condition, the THOR-50M demonstrated good internal and external biofidelity, with BioRank scores of 1.019 and 1.163, respectively. In all thoracic impact conditions, the THOR-50M was quantitatively more biofidelic than the H3-50M. Additionally, in four whole-body restraint frontal impact sled test conditions, the THOR-50M demonstrated good internal biofidelity, which is primarily a measure of the biofidelity of multi-point rib cage deflection.

5.6 Data

Several datasets were considered in the development of a thoracic injury criterion for the THOR ATD. First, the data presented in the development of the thoracic injury criterion for the H3-50M for use in Federal Motor Vehicle Safety Standards (FMVSS) No. 208 as presented by Eppinger et al. (1999) were reviewed. This set of 71 data points, of which 63 were considered after removing outliers, included PMHS sled tests at velocities of between 23 km/h and 59 km/h in various restraint configurations including belt-only (2-point and 3-point), airbag only, and belt and airbag conditions. In each test, chestbands were used to measure external chest deformation, which was presented at five different locations: left, center, and right at the vertical level of the 4th rib, and left and right at the vertical level of the 8th rib. The relationship between PMHS external deflection and the internal deflection measured by the Hybrid III ATD was accounted for in the development of the Combined Thoracic Injury (CTI) criterion by subtracting 8 millimeters from the deflection component of the deflection vs. acceleration regression line. It is not clear, however, if this 8-millimeter shift was accounted for in the development of the chest deflection risk function. Such a relationship would be necessary to apply the injury criteria developed by Eppinger et al. (1999) to THOR, as the relationship between the measured and calculated PMHS chestband deflection and the multi-point internal deflection measured by THOR is unknown.

One approach to address this limitation would be to conduct identical tests with THOR-50M ATD and relate the measured THOR internal deflection to the measured PMHS external deflection. However, since many of these tests were conducted in the early 1990s, obtaining identical test fixtures and restraint systems would be difficult or impossible. Instead, a more recent matrix of PMHS tests was

collected by the University of Virginia based on the availability of test fixtures and restraints, consisting of frontal impact sled tests in 12 different velocity or restraint conditions with a total of 42 PMHS observations. In each of these 12 test conditions, at least two THOR-50M tests were conducted (summarized in Crandall, 2013; individual test references presented in Table 5.2). Later, two additional matched pair test conditions were conducted using both PMHS and THOR-50M, one set with the occupant in a near-side oblique configuration (Crandall, 2015), the other with the occupant in a far-side oblique configuration (Crandall, 2014). A total of 14 test conditions were considered in this matched-pair study, with a total of 48 PMHS observations (Table 5.2). For tests sponsored by NHTSA, which include a majority of the PMHS tests and all of the THOR-50M tests, NHTSA Biomechanics Test Database test numbers are included in the table. A limitation to this test series is that the measurement of PMHS thoracic deformation was not consistent for all tests, as some used single chestbands, some used multiple chestbands, and others used the VICON system to measure skeletal deformation directly. Due to this limitation, the matched pair tests are used herein to relate PMHS outcome to THOR measurements in the same test condition.

Table 5.2. Source data for PMHS sled tests.

Occupant Position	Environment [Reference]	Restraint	Delta-V (km/h)	Age	Sex	Mass (kg)	Height (cm)	AIS 3+	PMHS BioDB	THOR BioDB
Front Driver	Gold Standard [Lopez-Valdes, 2010]	3-point standard belt	10	59	F	80	167	No		11125
				69	M	84	178	No		11126
				60	M	81	191	No		
Front Driver	Gold Standard [Lopez-Valdes, 2010]	3-point standard belt	40	59	F	80	167	Yes		11123
				69	M	84	178	Yes		11124
				60	M	81	191	Yes		
Front Passenger	1997 Ford Taurus [Forman, 2006a]	3-point force-limited belt plus airbag	48	57	M	70	174	No	8371	11129
				69	F	53	155	Yes	8372	11130
				72	F	59	156	Yes	8373	
				57	M	57	177	No	8374	
Front Passenger	1997 Ford Taurus [Kent, 2001]	Lap belt with airbag	48	40	M	47	150	Yes	8377	11131
				70	M	70	176	No	8378	11132
				46	M	74	175	No	8379	
Front Passenger	1997 Ford Taurus [Forman, 2006a]	3-point standard belt with airbag	48	55	M	85	176	Yes	8382	11127
				69	M	84	176	Yes	8383	11128
				59	F	79	161	Yes	8384	
Front Passenger	1997 Ford Taurus [Forman, 2006a]	3-point standard belt	29	49	M	58	178	No		11133
				44	M	77	172	No		11134
				39	M	79	184	No		
Front Passenger	1997 Ford Taurus [Forman, 2006b]	3-point standard belt	38	44	M	77	172	No		11135
										11136
Front Passenger	Gold Standard 1 [Shaw, 2009]	3-point standard belt	40	76	M	70	178	Yes	9546	11117
				47	M	68	177	Yes	9547	11118
				54	M	79	177	Yes		11119
				49	M	76	184	Yes		
				57	M	64	175	Yes		
				72	M	81	184	Yes	11014	
				40	M	88	179	Yes	11015	
				37	M	78	180	No	11016	
Front Passenger	Gold Standard 2 [Shaw, 2012]	3-point force-limited belt	30	59	M	68	178	No	11468	11120
				66	M	70	179	No	11469	11121
				67	M	68	177	Yes	11509	11122
				67	M	68	173	Yes	11510	
				74	M	70	183	No	11511	
Rear Passenger	2004 Ford Taurus [Forman, 2009]	3-point standard belt	48	51	M	55	175	Yes	9337	11143
				57	F	109	165	Yes	9338	11144
				57	M	59	179	Yes	9339	11145
Rear Passenger	2004 Ford Taurus [Forman, 2009]	3-point force-limited belt with pretensioner	48	67	M	71	175	Yes		11140
				69	M	60	171	No		11141
				72	M	73	175	Yes		11142
Rear Passenger	2004 Ford Taurus [Kent, 2011]	3-point inflatable force-limited belt with pretensioner	48	72	M	88	173	Yes		11137
				69	M	69	175	No		11138
				40	M	83	186	No		11139
Front Passenger	Gold Standard 3 (Near-side Oblique) [Crandall, 2015]	3-point force-limited belt	30	69	M	72	173	Yes	11518	11514
				66	M	76	172	Yes	11519	11515
				67	M	65	177	No	11520	11516
										11517
Front Passenger	Far-side Oblique [Crandall, 2014]	3-point force-limited belt with airbag	59.5	73	M	69	180	Yes	11500	11503
				83	M	85	178	Yes	11501	11504
				63	M	69	187	Yes	11502	11505
									11506	

Given the approach of using matched pair tests to relate PMHS outcome to THOR measurements in the same test condition, the Eppinger et al. (1999) dataset was revisited to consider any test conditions that were similar enough to the test conditions presented in Table 5.2 to be included. Subjects were considered for inclusion if they were unembalmed, could be located in the NHTSA Biomechanics

Database, were tested at a velocity within ± 2 km/h of a matched THOR test, and were tested in the same restraint condition as a matched THOR test. This winnowed the original 71 subjects down to just 5 possibilities: three subjects in a lap belt with airbag condition at 48 km/h, and two subjects in a three-point belt plus airbag condition at 48 km/h (Table 5.3). It is hypothesized that the similarity in restraint is more important than the difference in occupant position (driver vs. right front passenger) and environment (1986 Ford Tempo vs. 1997 Ford Taurus).

Table 5.3. Source data for additional PMHS sled tests.

Occupant Position	Environment	Restraint	Delta-V (km/h)	Age	Sex	Mass (kg)	Height (cm)	AIS 3+	PMHS BioDB	THOR BioDB
Driver	1986 Ford Tempo	Lap belt with airbag	48.3	67	F	50		Yes	2857	
				64	M	70		Yes	2854	11132
				58	M	73		No	2856	
Driver	1986 Ford Tempo	3-point standard belt with airbag	48.3	67	F	57		Yes	2861	11127
				68	M	59		Yes	2878	

Additionally, impactor tests were considered for inclusion in the matched pair dataset, as THOR-50M response data are available for both blunt sternal impact and lower thorax oblique impact conditions. PMHS observations in blunt sternal impact tests at various speeds and masses are presented in Kroell et al. (1971 and 1974). Based on the analysis presented by Neathery et al. (1975), half of the 48 observations presented by Kroell were recommended for elimination based on differences in spine fixation, impactor travel restriction, post-test injury assessment technique, and instrument failure, as well as one subject that was “clearly an outlier.” Of the 24 remaining tests, 17 were considered herein based on similarity in impact velocity (4.3 m/s, 4.8 m/s, and 6.7 m/s) and impact mass (23 kg) to existing THOR-50M test conditions (Table 5.4). Also considered herein are 7 PMHS observations in a lower thorax oblique impact condition presented by Yoganandan et al. (1997).

Table 5.4. Source data for PMHS impactor tests.

Test Condition	Delta-V (km/h)	Age	Sex	Mass (kg)	Height (cm)	AIS 3+	PMHS BioDB	THOR BioDB
Blunt Thoracic Impact Nominal 23kg Impactor @ 6.7 m/s	26.7	81	M	76.2	168	Yes		
	24.8	80	M	53.1	165	Yes		
	24.2	78	M	65.8	176	Yes		
	24.2	19	M	71.2	196	No		
	24.2	29	M	56.7	180	No		
	24.2	72	M	74.8	188	Yes		
	25.9	52	M	74.8	183	Yes		
	26.4	46	M	94.8	178	No		
	24.9	72	M	63.0	163	Yes		
	22.7	60	F	59.0	160	Yes		
	26.1	67	F	62.6	163	Yes		
	26.4	76	F	57.6	156	Yes		
	27.8	58	F	61.2	163	Yes		
	Blunt Thoracic Impact Nominal 23kg Impactor @ 4.8 m/s	17.5	61	M	54.4	183	No	
18.2		64	M	64.0	181	Yes		
18.8		75	M	77.1	174	Yes		
Blunt Thoracic Impact Nominal 23kg Impactor @ 4.3 m/s	15.6	66	M	79.4	180	Yes		
		72	M	82	170	Yes	3085	
Lower Thorax Oblique Impact Nominal 23kg Impactor @ 4.3m/s		81	M	63	175	Yes		
		84	M	68	168	No		
	15.5	86	M	56	170	No		
		62	M	61	174	Yes		
		70	M	91	169	Yes		
		68	M	83	178	Yes		

Different combinations of the datasets presented in Table 5.2, Table 5.3, and Table 5.4 are carried through the analysis and referenced throughout this report as follows:

Table 5.5. Description of dataset combinations evaluated throughout report.

Name	Description
SledOnly	only the observations in Table 5.2
SledExtended	combined observations in Table 5.2 and Table 5.3
Sled+Impactor	combined observations in Table 5.2, Table 5.3, and Table 5.4
ImpactorOnly	only the observations in Table 5.4
SledNoOBL	only the observations from Table 5.2, but without either set of oblique observations
SledNoFSO	only the observations from Table 5.2, but without the Far-side Oblique (FSO) observations

5.7 Predictor Variable

Several variables were considered for use as the predictive parameter in a thoracic injury criterion. As the input dataset includes test data measured using the THOR-50M ATD, measurements from the sensors shown in Table 5.1 and metrics calculated from these sensors can be considered as independent parameters. While sternum and spine acceleration and spine force data are often collected during THOR crash tests, this study focused on deflection-based measurements as previous research has demonstrated a strong relationship between rib deflection and rib strain, which in turn relates to risk of fracture. Several calculations of deflection-based measurements were considered for application as the independent parameter in the THOR thoracic injury criterion (Table 5.6).

Table 5.6. Deflection metrics considered.

Deflection Metric	Description	Calculation
x-axis Deflection	Deflection of the anterior attachment point of the 3D deflection instrumentation along the x-axis of the local spine coordinate system (LCS)	See <i>THOR PADI</i>
Resultant Deflection	Vector resultant deflection of the anterior attachment point of the 3D deflection instrumentation	$\max\left(\sqrt{X_{LCS}^2 + Y_{LCS}^2 + Z_{LCS}^2}\right)$
Change in Chord Length	Change in distance between the anterior and posterior 3D deflection instrumentation attachment points	$\sqrt{r_0^2 + \delta^2} - \max\left(\sqrt{r^2 + \delta^2}\right)$
Peak Deflection	The above three metrics can be calculated at each of the four quadrants; the peak deflection measurement calculates the maximum of a given metric across all four quadrants	$\max(UL, UR, LL, LR)$
PC Score	Result of Principal Component Analysis (PCA)	See Poplin et al. (2017)

While change in chord length was originally considered because it was thought to better correlate with rib strain, it was found to be well-correlated with peak x-axis deflection. This is demonstrated for the SledOnly dataset in Figure 5.5, but held true for all combinations of datasets as well. Thus, chord length was eliminated from consideration as an independent variable for simplicity.

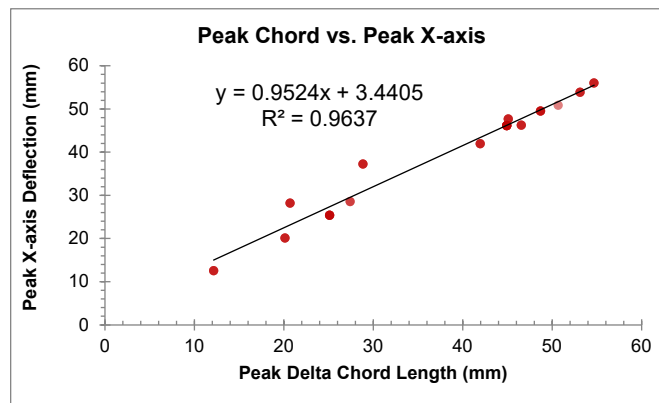


Figure 5.5. Relationship between change in chord length and peak x-axis deflection in the SledOnly dataset.

The remaining deflection terms, x-axis deflection and resultant deflection, can be calculated at each of the four quadrants of the thorax. Due to the physical relationship between the measurement locations, some correlation between these measurement locations is expected, thus including all four individual quadrant deflections in a prediction model is likely to cause overfitting. The upper left and upper right measurement locations are expected to be highly-correlated due to the proximity of the measurement locations to each other and to the shoulder belt, if used. The upper and lower measurement locations on each side are expected to be highly correlated due to connectivity of the ribcage. On the other hand, the lower left and lower right measurement locations are not expected to be highly correlated, as they are the furthest away from each other and from a shoulder belt, if used.

To investigate whether these expected correlations are true in the current sample, a stepwise multiple logistic regression was carried out for both x-axis and resultant deflection metrics. The stepwise regression began with only an intercept and considered four parameters for inclusion – the upper left, upper right, lower left, and lower right quadrant deflections. For both deflection metrics, no more than two parameters were added and retained in the resulting regression model (upper right and lower left for x-axis deflection, lower left and lower right for resultant deflections). This suggests that two deflection terms are necessary to describe the variance in the data set.

Due to the limited size of the data set, two approaches were considered to examine whether the number of parameters necessary to describe the thoracic deflection could be reduced to one: a peak overall deflection term, and principal component analysis.

A single peak deflection term was developed, which considered only the maximum deflection in any of the four individual quadrants. An additional round of stepwise multiple logistic regression was then carried out which included a peak deflection term in addition to the initial four parameters. For both deflection metrics, and for all datasets considered, the resulting model contained only the peak deflection term. Adding any of the individual quadrant deflections in addition to the peak deflection term did not result in a statistically-significant description of the remaining variance for this sample. This is not unexpected, as the peak deflection term is highly correlated to the individual quadrant deflection terms since, in each observation, the peak deflection term is equal to one of the four individual deflection terms. Furthermore, the regression models containing only the peak deflection term demonstrated a better model fit than the corresponding two-parameter models described above. As such, the peak deflection terms (peak x-axis deflection and peak resultant deflection) were considered instead of a combination of individual quadrant deflections for the remainder of this analysis.

An additional approach to variable reduction was principal component analysis (PCA), which was carried out by the University of Virginia (Poplin et al., 2017) and used to develop the PC Score metric. The PC Score is a single parameter calculated from combinations of the four individual quadrant deflections, which was developed to be positive and left/right symmetric. Additional details of the PCA analysis and resulting PC Scores for the SledNoOBL and SledNoFSO datasets can be found in McMurry et al. (2016a and 2016b respectively), which were provided as deliverables under Cooperative Agreement DTNH22-07-H-00247.

5.8 Covariates

A stepwise multiple logistic regression was carried out to assess the sensitivity of several covariates. If addition of a given variable as a covariate in a logistic regression along with the independent variable described above resulted in a statistically-significant ($p < 0.05$) description of variance in the fitted model, the covariate should be included in the injury risk function. Covariates considered were age, mass, stature, and sex, which were available for all subjects in all datasets. For all datasets considered, adding age as a covariate in addition to the peak x-axis deflection or peak resultant deflection resulted in a statistically-significant description of the remaining variance. Mass, stature, and sex were not significant explanatory variables for this sample.

5.9 Dependent Variable

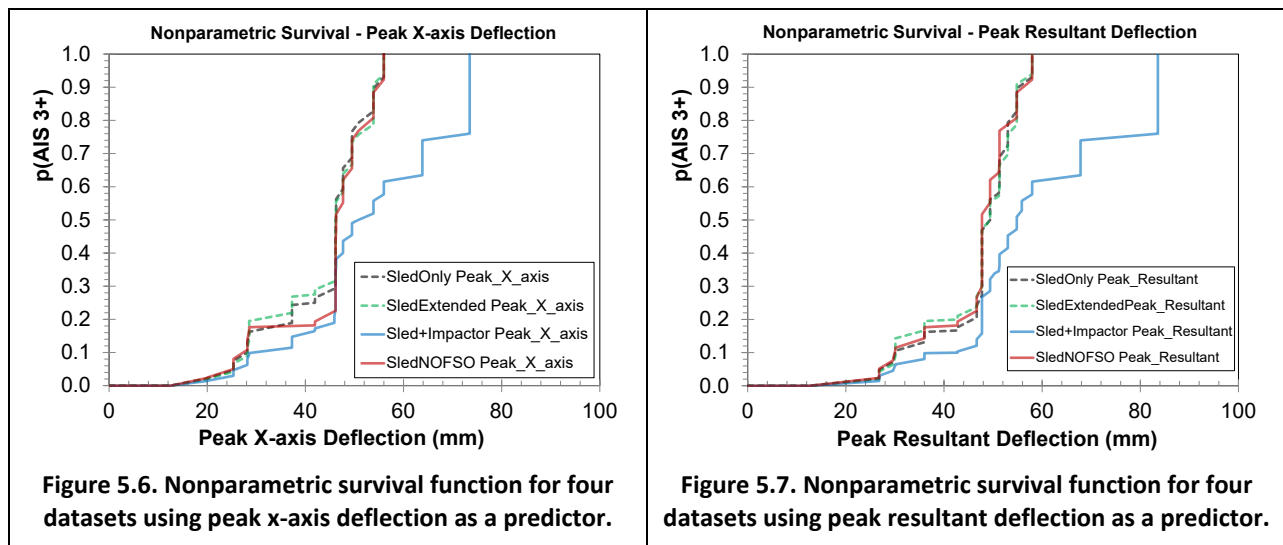
The dependent variable used in the development of a thoracic injury criterion was the presence of an Abbreviated Injury Scale (AIS) score of 3 or greater (AIS 3+). Based on the AIS 2005 Update 2008, an AIS 3 skeletal injury to the thorax is defined by fractures of three or more ribs without flail at any location of either or both sides of the ribcage including costal cartilage (AAAM, 2008). While soft tissue injuries can also result in AIS 3 or greater scores, these injuries are difficult or impossible to diagnose in PMHS, at least per the rules of 2005/2008 AIS (AAAM, 2008). For example, pulmonary contusions result from an inflammatory response and require living tissue for this to occur.

5.10 Injury Risk Function Formulation

Three sets of injury risk functions (nonparametric, logistic, and survival analysis) were formulated for each independent parameter (peak x-axis deflection, peak resultant deflection), for each dataset (SledOnly, Sled+Impactor, SledExtended, SledNoFSO), and both with and without age as a covariate. Goodness-of-fit metrics described in Hasija et al. (2011) were calculated for the logistic and survival analysis risk curves, including the Receiver Operating Characteristic (ROC) Area Under Curve (AUC), maximum log likelihood, and Hosmer-Lemeshow Goodness-of-Fit test.

5.10.1 Nonparametric

Nonparametric survival functions were formulated using the SAS PROC LIFETEST procedure for both peak x-axis deflection (Figure 5.6) and peak resultant deflection (Figure 5.7) metrics. Both metrics indicate only subtle differences between the SledOnly, SledExtended, and SledNOFSO datasets, but marked differences in the Sled+Impactor dataset.



5.10.2 Logistic Regression

Logistic regression was carried out to develop risk functions for both predictors for all four datasets, both with and without age as a covariate using the SAS PROC LOGISTIC procedure. For each

combination, the AUROC, maximum log likelihood, and Hosmer-Lemeshow Goodness-of-Fit test results are reported in Table 5.7. The logistic regression risk functions take one of two forms:

Without Age:	$p(\text{AIS } 3+) = \frac{e^{(\beta_0 + \beta_1 x)}}{1 + e^{(\beta_0 + \beta_1 x)}}$
With Age:	$p(\text{AIS } 3+) = \frac{e^{(\beta_0 + \beta_1 x + \beta_2 a)}}{1 + e^{(\beta_0 + \beta_1 x + \beta_2 a)}}$
where:	
β_0	= Intercept
β_1	= Independent parameter coefficient
x	= Independent parameter value
β_2	= Age coefficient
a	= Subject age, in years

Table 5.7. Fit statistics for logistic regression models.

Dataset	Predictor	Age as Covariate	N	-2 Log L	AUROC	Hosmer and Lemeshow Pr>ChiSq
Sled+Impactor	Peak X	Yes	77	80.450	0.803	0.0007
Sled+Impactor	Peak X	No	77	90.631	0.686	0.5447
ImpactorOnly	Peak X	Yes	24	22.748	0.676	0.0085
ImpactorOnly	Peak X	No	24	26.988	0.519	0.8010
SledExtended	Peak X	Yes	53	52.079	0.832	0.3280
SledExtended	Peak X	No	53	60.111	0.742	0.3553
SledNoFSO	Peak X	Yes	45	50.735	0.823	0.4490
SledNoFSO	Peak X	No	45	57.054	0.757	0.0781
SledOnly	Peak X	Yes	48	48.248	0.833	0.3388
SledOnly	Peak X	No	48	54.979	0.736	0.2850
Sled+Impactor	Peak Resultant	Yes	77	80.545	0.803	0.0287
Sled+Impactor	Peak Resultant	No	77	89.952	0.708	0.2477
ImpactorOnly	Peak Resultant	Yes	24	22.453	0.732	0.0664
ImpactorOnly	Peak Resultant	No	24	26.981	0.519	0.8250
SledExtended	Peak Resultant	Yes	53	50.230	0.856	0.6463
SledExtended	Peak Resultant	No	53	56.911	0.792	0.7974
SledNoFSO	Peak Resultant	Yes	45	45.449	0.830	0.7542
SledNoFSO	Peak Resultant	No	45	50.152	0.772	0.8132
SledOnly	Peak Resultant	Yes	48	45.842	0.851	0.7010
SledOnly	Peak Resultant	No	48	51.265	0.796	0.7322
SledNoOBL	Peak Resultant	Yes	42	41.599	0.845	0.5021
SledNoOBL	Peak Resultant	No	42	45.804	0.788	0.2906
SledNoFSO	PCA	Yes	45	45.642	0.838	0.6925
SledNoFSO	PCA	No	45	50.280	0.758	0.3577
SledNoOBL	PCA	Yes	42	41.856	0.850	0.3565
SledNoOBL	PCA	No	42	46.142	0.772	0.4626

A common thread among the lowest AUROCs was that the associated datasets included observations from impactor tests. In five combinations, the Hosmer and Lemeshow goodness of fit test indicated the possibility of a poor model fit – four of these five also included observations from impactor tests (Sled+Impactor and ImpactorOnly for both peak x-axis and peak resultant in models including age as a covariate). Of the logistic regression models, the highest AUROCs occurred for the models using peak resultant deflection as the predictor, with age as a covariate, and either the SledOnly or SledExtended datasets (Figure 5.8). Parameter estimates for these two models are shown in Table 5.8. As shown in Figure 5.9, presented at an age of 40 years, the logistic risk functions fit to the SledOnly and SledExtended datasets are virtually indistinguishable.

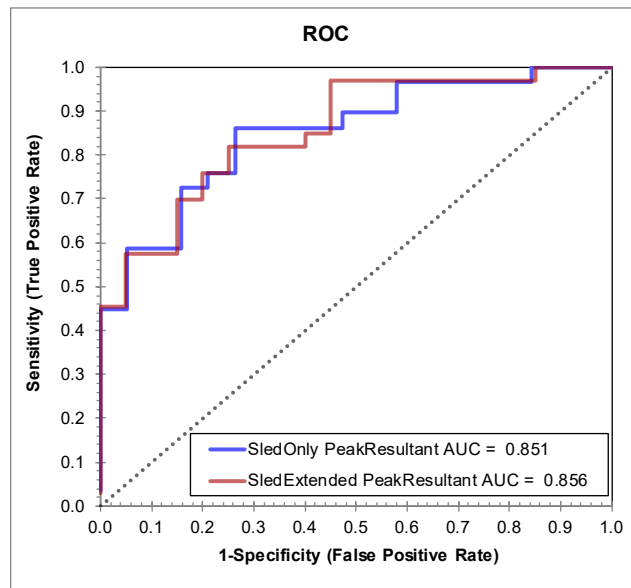


Figure 5.8. Receiver Operating Characteristic (ROC) for the logistic regression models with the highest AUC.

Table 5.8. Model parameter estimates.

Model	β_0	β_1	β_2
SledOnly, Peak Resultant	-8.8086	0.1168	0.0744
SledExtended, Peak Resultant	-8.9322	0.1121	0.0819

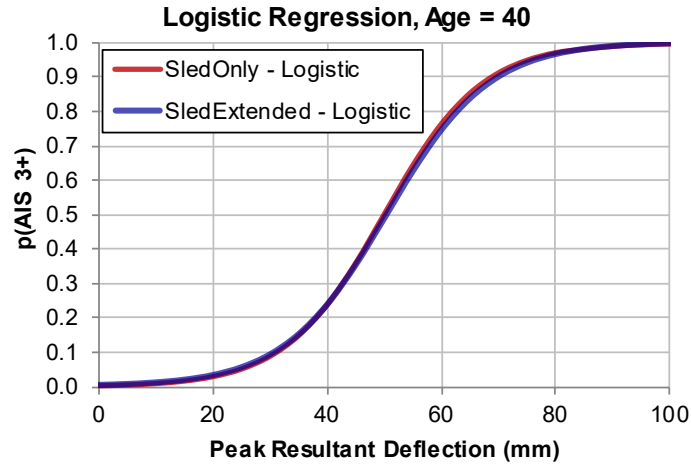


Figure 5.9. Logistic risk functions fit to the SledOnly and SledExtended datasets (Table 5.8).

The risk functions and confidence intervals for the two models with the highest AUROC were calculated at two different values of the age covariate: 40 years old, the mean age of exposed male drivers in frontal crashes, and 61 years old, the mean age of the PMHS subjects in the dataset (Figure 5.10). For both the SledOnly and SledExtended models, the prediction at 61 years of age demonstrates a higher probability of AIS 3+ injury for all values of peak resultant deflection, and the models calculated at 40 years of age show wider confidence intervals compared to those calculated at age 61.

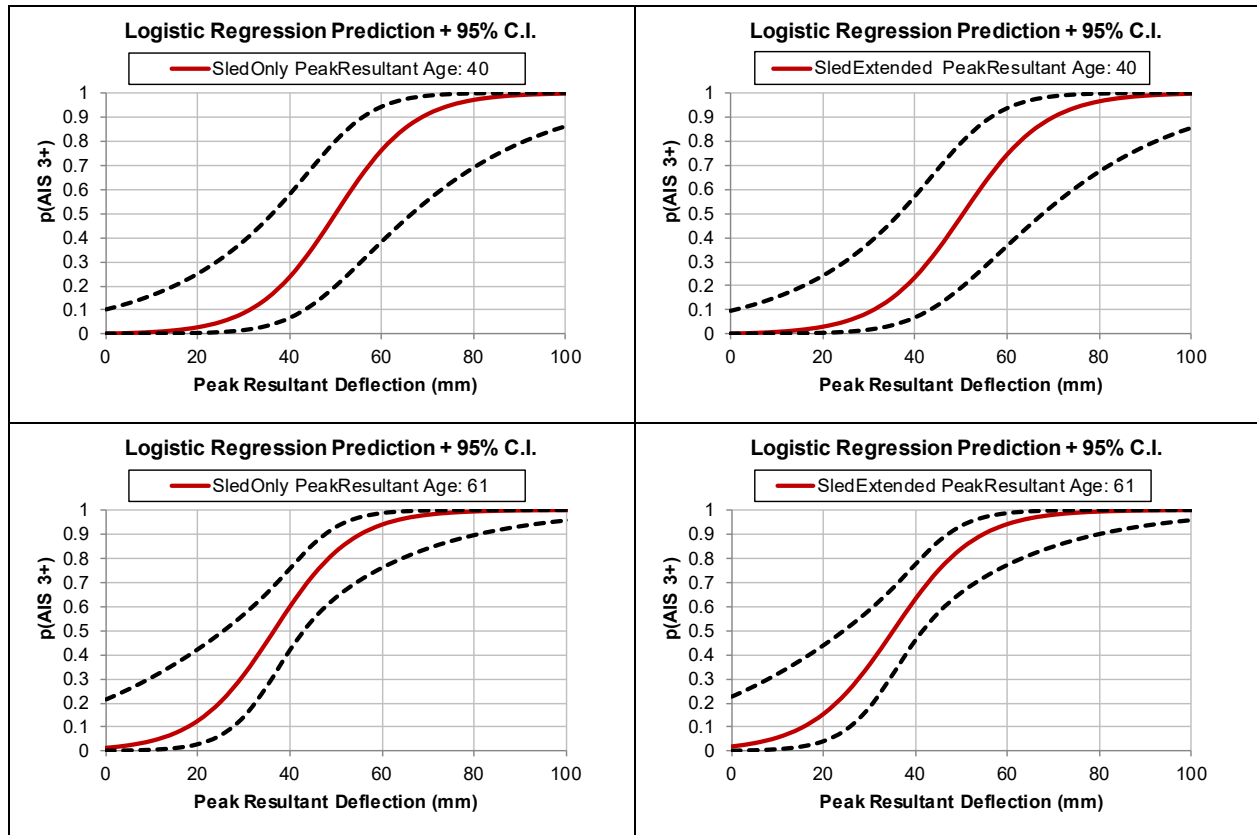


Figure 5.10. Risk function and confidence intervals for logistic models with highest AUROC, shown at different values of the age covariate.

5.10.3 Survival Analysis

Survival analysis was also carried out to develop risk functions using the SAS PROC RELIABILITY procedure. Models were developed for peak resultant deflection, since this parameter provided a similar or better model fit than peak x-axis deflection for all logistic models, and for PCA for the applicable datasets. All survival models also included age as a covariate, as including age resulted in a better model fit for all logistic models. Three of the subjects (Front Driver, as shown in Table 5.2) were tested in both low-speed and high-speed conditions. Since these subjects were all non-injured after the low-speed tests and injured after the high-speed test, these observations were treated as interval censored. For the remaining observations, the non-injury points were treated as right-censored and the injury points were treated as left-censored. For each combination, maximum log likelihood is reported in Table 5.9. The survival analysis risk function assuming a Weibull distribution takes the form:

$$p(\text{AIS } 3+) = 1 - e^{-\left(\frac{x}{e^{(\beta_0 + \beta_1 a)}}\right)^\alpha}$$

where:

- β_0 = Intercept
- x = Independent parameter value
- β_1 = Age coefficient
- a = Subject age, in years
- α = 1/scale

Table 5.9. Parameter estimates and fit statistics for survival analysis models.

Dataset	Predictor	N	β_0	β_1	α	Maximum Log Likelihood
Sled+Impactor	Peak Resultant	74	5.1466	-0.0218	1.2483	-40.8130
ImpactorOnly	Peak Resultant	24	5.2861	-0.0187	1.4873	-11.7869
SledExtended	Peak Resultant	50	4.8535	-0.0191	2.7450	-24.6966
SledOnly	Peak Resultant	45	4.7276	-0.0166	2.9770	-22.4988
SledNoFSO	Peak Resultant	42	4.7262	-0.0165	2.9060	-22.3690
SledNoOBL	Peak Resultant	39	4.6919	-0.0158	2.9560	-20.4446
SledNoFSO	PCA	42	2.8104	-0.0177	2.6761	-22.4464
SledNoOBL	PCA	39	2.8010	-0.0176	2.6789	-20.5598

Survival functions and associated confidence intervals resulting from analysis of the SledOnly, SledExtended, SledNoFSO, and SledNoOBL were similar (Figure 5.11), with minimal differences in the peak resultant deflection values associated with 10%, 25%, and 50% risk of AIS 3+ injury (Table 5.10). The Sled+Impactor and ImpactorOnly survival functions, on the other hand, demonstrate a shape with a less pronounced toe region. Accordingly, the Weibull shape parameters for these two datasets is noticeably lower (α in Table 5.9). The confidence intervals for the ImpactorOnly dataset are divergent, further demonstrating the poor fit suggested by the logistic regression of the same dataset.

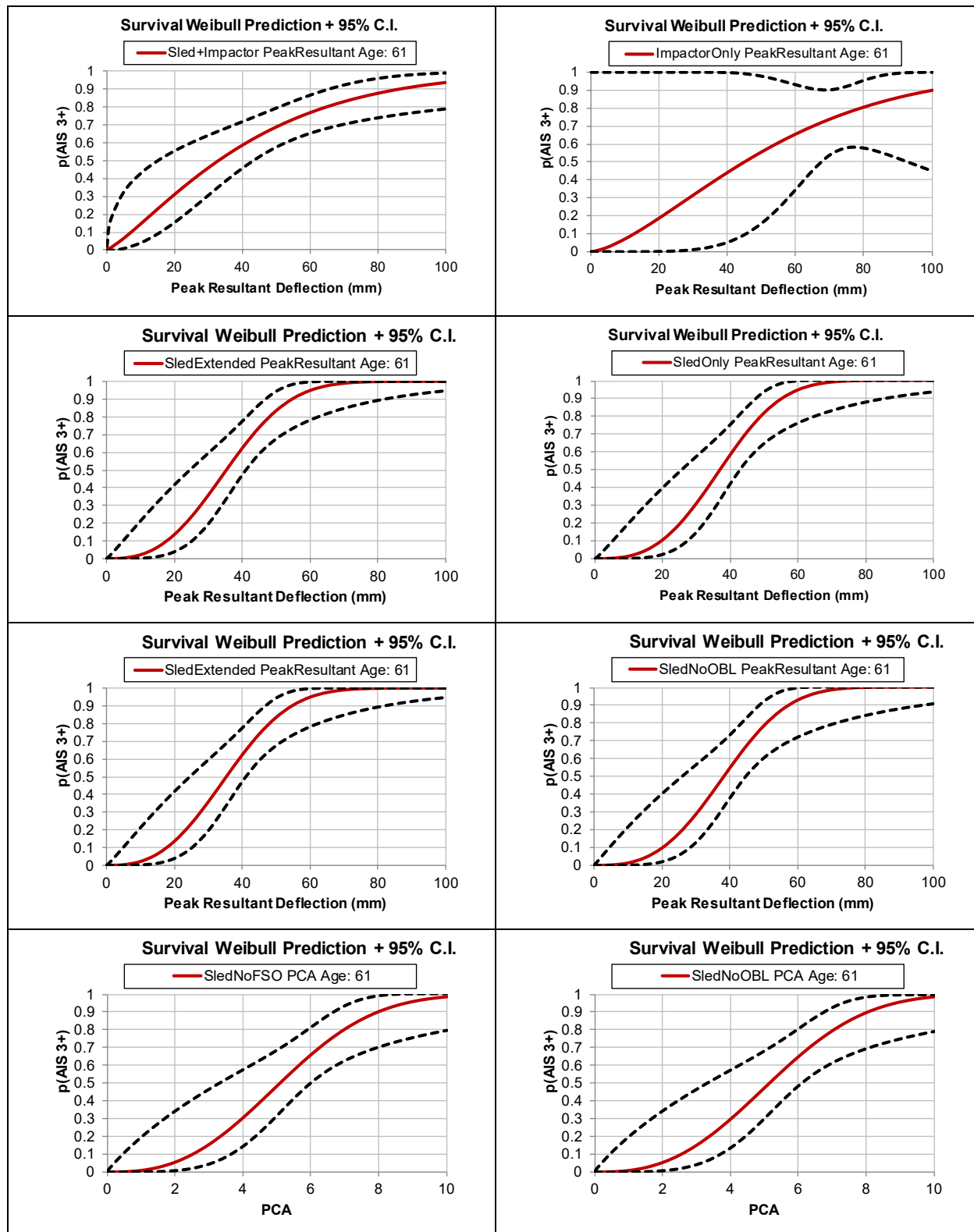


Figure 5.11. Survival Weibull estimates and 95% confidence intervals for models in Table 5.9.

Table 5.10. Peak resultant deflections at 10%, 25%, and 50% risk of AIS 3+ thoracic injury, shown for both age 40 and age 61.

Dataset	Peak Resultant Deflection (mm) Risk of AIS 3+ at Age 40			Peak Resultant Deflection (mm) Risk of AIS 3+ at Age 61		
	10%	25%	50%	10%	25%	50%
SledExtended	26.3	37.9	52.2	17.6	25.4	35.0
SledOnly	27.3	38.3	51.4	19.3	27.0	36.3
SledNoFSO	26.9	38.0	51.4	19.0	26.9	36.4
SledNoOBL	27.1	38.0	51.2	19.4	27.3	36.7
Sled+Impactor	11.8	26.5	53.6	7.5	16.8	33.9
ImpactorOnly	20.6	40.5	73.1	13.9	27.3	49.4

As the SledOnly and SledNoOBL datasets result in nearly identical survival functions (Figure 5.11) and injury assessment reference values (Table 5.10), it is assumed that the influence of the oblique loading on the relationship between chest deflection and AIS 3+ thoracic injury risk is not significant. Therefore, the SledOnly dataset is preferred because it includes more of the available data. Similarly, the SledExtended and SledOnly datasets result in similar survival functions and injury assessment reference values, but since the additional tests included in the SledExtended dataset require more assumptions, the SledOnly dataset is preferred as it is more defensible.

As both PCA and peak resultant deflection appear to show similar predictive ability, peak resultant deflection is preferred for its relative simplicity. Likewise, while there are some discernable differences between the logistic and Survival Weibull models (Figure 5.12), Survival Weibull model is preferred for its representation of zero risk at a zero-stimulus value.

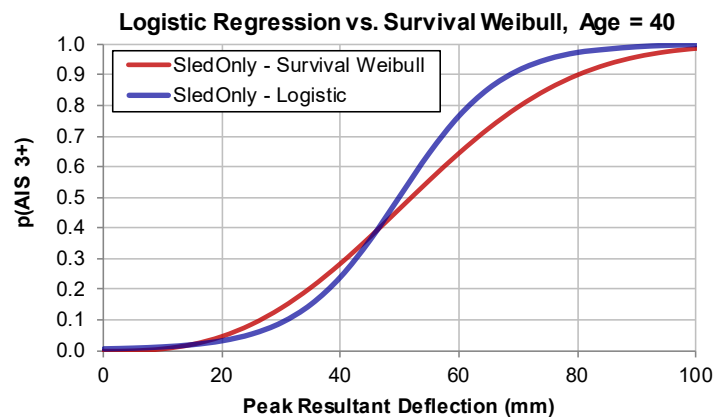


Figure 5.12. The difference between the Survival Weibull and logistic risk functions, both including age as a covariate, presented at an age of 40 years old.

The recommended risk function is:

$$p(\text{AIS } 3+) = 1 - e^{-\left(\frac{R_{max}}{e^{(4.7276-0.0166a)}}\right)^{2.977}}$$

where:

R_{max} = Peak resultant deflection, in millimeters
 a = Age, in years

Simplifying, assuming Age = 40 years (see Section 2.5):

$$p(\text{AIS } 3+) = 1 - e^{-\left(\frac{R_{max}}{58.183}\right)^{2.977}}$$

5.11 Fleet Test Data: THOR-50M

The recommended thoracic injury risk function was applied to THOR-50M measurements collected in frontal rigid barrier and frontal Oblique fleet testing. Figure 5.13 shows the injury risk function with observations representing the injury risk predicted from each occupant response, grouped by occupant position and test mode. Predicted probability of AIS 3+ injury spans from just under 20 percent to just over 70 percent, with lower risk associated with the right front passenger in the Oblique crash test compared to the driver in the Oblique or frontal rigid barrier crash.

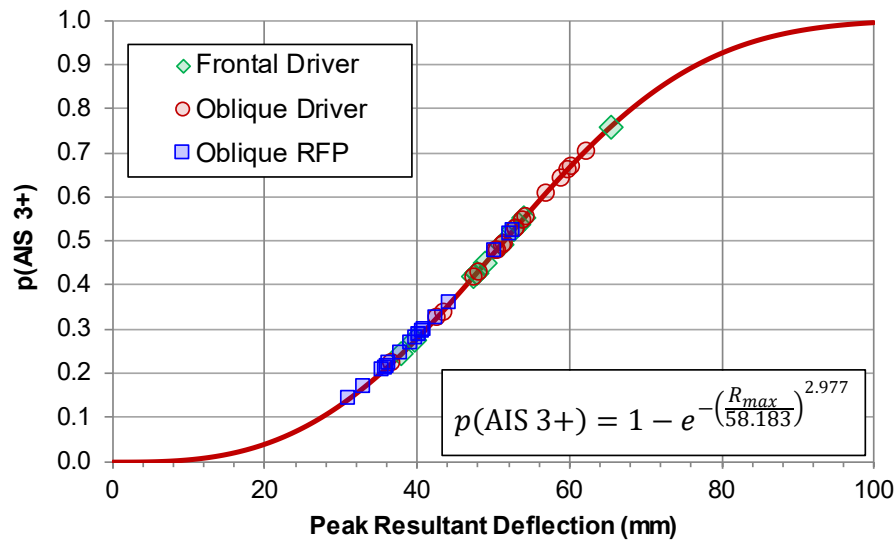


Figure 5.13. Distribution of fleet test results superimposed over Survival Analysis risk function.

5.12 Limitations

The assessment of injury to PMHS is more rigorous than possible on live subjects sustaining injury in car crashes. For example, the PMHS are often autopsied after the research test, and rib fractures are investigated at a level of detail that is not possible through physical external examination and reading of

radiology from live subjects. Because of this, the number of rib fractures recorded from PMHS research tests may be an overestimate of the number of rib fractures that would be clinically diagnosed in a living human. Eppinger et al. (1999) describes how the thoracic injury risk curves were shifted to account for this over-reporting, along with age differences between the PMHS dataset and the average driving population and the increased fragility of PMHS compared to live humans, by shifting the curve to the right along the independent axis such that the 50% risk level for PMHS became the 25% risk level for live humans. While the reasoning for the shift appears to be sound, sufficient information to describe the magnitude of the shift is not provided thus cannot be replicated herein.

To assess the sensitivity of the resulting risk function to the possible overestimation of rib fractures in PMHS, the formulation of the dependent variable was modified to represent a variable number of fractured ribs (NFR). Previous research has demonstrated that post mortem subjects may sustain 2 to 3 more fractured ribs (Viano et al., 1977), or 3 and 5 more rib fractures (Foret-Bruno et al., 1978), than live subjects. Therefore, formulations of the dependent variable were carried out at $NFR \geq 3$, which is consistent with the dependent variable defined in Section 5.9; $NFR \geq 4$, which would be consistent with the description of an AIS 3+ injury according to AIS 1998 (AAAM, 1998); $NFR \geq 5$, to bridge the gap; $NFR \geq 6$, to represent a number of fractured ribs measured in PMHS tests which, once adjusted to represent live subjects based on an adjustment by 3 fractured ribs (to be consistent with both referenced studies), would represent an AIS 3+ skeletal thoracic injury to a live subject according to AIS 2005 (2008 Update) (AAAM, 2008); and $NFR \geq 7$, similar to the $NFR \geq 6$ but to represent an AIS 3+ injury to a live subject according to AIS 1998 (AAAM, 1998). The latter, $NFR \geq 7$, would be consistent with the definition used by Laituri et al. (2005).

Survival Weibull Injury risk functions were fit using the SledOnly dataset and are presented at ages of 40 and 61 years (Figure 5.14, along with the corresponding equations in Table 5.11). Generally, as the number of fractured ribs in the dependent variable definition increases, the risk curve shifts to the right (e.g. higher value of peak resultant definition for the same level of risk). The $NFR \geq 7$ risk function demonstrates a different shape, which is more exaggerated when presented at an age of 40 years. There are only two data points that change between the $NFR \geq 6$ and $NFR \geq 7$ risk functions: a 76-year-old male at 40 km/h and a 67-year-old male at 30 km/h, both toggling from injury to non-injury. These observations were assessed to determine whether they were outliers by examining several influence diagnostics, including Pearson residuals, DFBETAs, and confidence interval displacement diagnostic; however, there was no indication that these observations were overly influential. Instead, this change in shape is more likely an artefact of the relatively small size of the sample, as there are not enough observations to directly predict the number of fractured ribs.

It can be seen that the injury risk functions formulated for 3 and 4 rib fractures as the injury threshold are very comparable, especially up to 50 percent risk of injury when presented at an age of 40 years. Without the aforementioned correction for PMHS versus living specimens, these two curves represent the AIS 2005 (2008 update) and 1990 (1998 update) definitions for AIS 3+ injury, respectively.

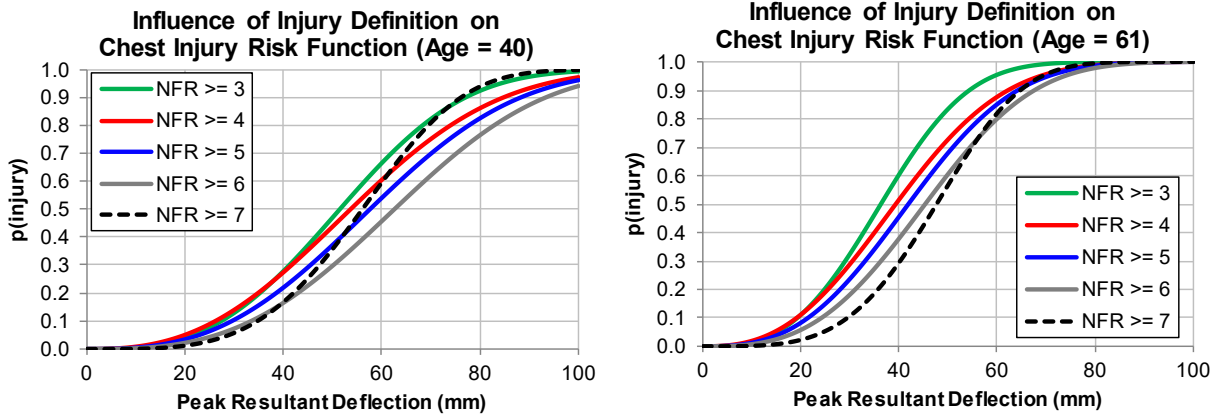


Figure 5.14. Sensitivity of the thoracic injury risk function to the number of fractured ribs selected in the dependent variable definition.

Table 5.11. Injury risk functions shown in Figure 5.14.

Dependent Variable	Risk Function (where a = Age, in years)
$NFR \geq 3$	$p(\text{AIS } 3+) = 1 - e^{-\left(\frac{R_{max}}{e^{(4.7276-0.0166a)}}\right)^{2.977}}$
$NFR \geq 4$	$p(\text{AIS } 3+) = 1 - e^{-\left(\frac{R_{max}}{e^{(4.7151-0.0148a)}}\right)^{2.6172}}$
$NFR \geq 5$	$p(\text{AIS } 3+) = 1 - e^{-\left(\frac{R_{max}}{e^{(4.7870-0.0151a)}}\right)^{2.8129}}$
$NFR \geq 6$	$p(\text{AIS } 3+) = 1 - e^{-\left(\frac{R_{max}}{e^{(4.8697-0.0153a)}}\right)^{3.0018}}$
$NFR \geq 7$	$p(\text{AIS } 3+) = 1 - e^{-\left(\frac{R_{max}}{e^{(4.4272-0.0077a)}}\right)^{3.9245}}$

A Survival Weibull Injury risk function was also fit to evaluate the risk of AIS 2+ injury using the SledOnly dataset. At an AIS 2+ injury level, three observations would change from non-injury to injury: one 37-year-old subject that sustained 2 fractured ribs in the Gold Standard 1 condition, one 40-year-old occupant that sustained 2 fractured ribs in the rear passenger 3-point inflatable force-limited belt with pretensioner condition, and one 69-year-old subject that sustained one fractured rib and a fractured sternum in the rear passenger 3-point force-limited belt with pretensioner condition. The AIS 2+ injury risk function, presented at an age of 40 years (Figure 5.15, along with the corresponding equation in Table 5.12), follows the same shape as the AIS 3+ function ($NFR \geq 3$), but is shifted left an average of 8 millimeters. As this average difference is distributed evenly throughout the risk function, countermeasures intended to reduce the risk of AIS 3+ injuries would proportionately reduce the risk of AIS 2+ injuries.

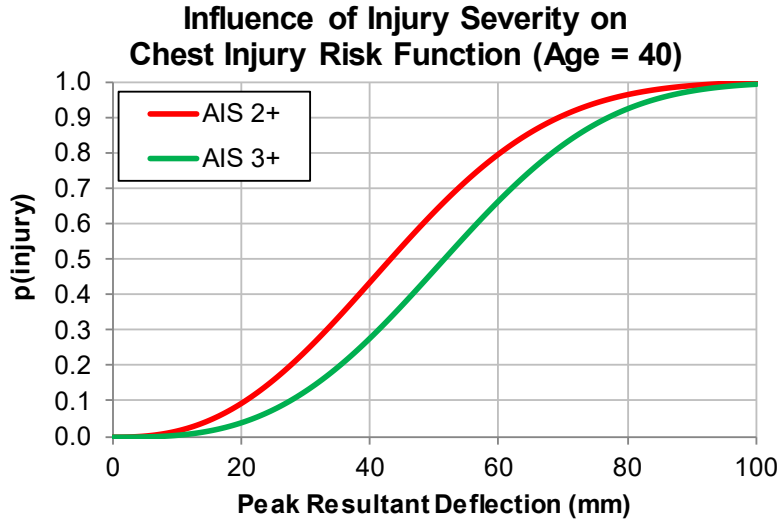


Figure 5.15. Thoracic injury risk function presented at the AIS 2+ and AIS 3+ level.

Table 5.12. Injury risk functions shown in Figure 5.15.

Risk Function
$p(\text{AIS } 2+) = 1 - e^{-\left(\frac{R_{max}}{49.894}\right)^{2.517}}$
$p(\text{AIS } 3+) = 1 - e^{-\left(\frac{R_{max}}{58.183}\right)^{2.977}}$

The ability of PMHS to predict injuries other than rib fractures is also a limitation to the development of thoracic injury criteria. While rib fractures may be overestimated in PMHS research tests, soft tissue injuries such as pneumothorax and lung contusions may be underreported. This limitation arises from the need for clinical diagnosis for classification of these injuries based on the Abbreviated Injury Scale definition. For example, a major hemothorax injury is classified by more than 1000 cc of blood loss on at least one side (AAAM, 2008), which for a PMHS is not possible to measure due to the lack of blood flow. Likewise, other soft tissue injuries such as lung contusions are diagnosed through bruising in live humans, which would not occur in PMHS for the same reason.

One additional limitation to this analysis is the scope of application of the thoracic injury risk functions developed herein. While the intent of this exercise was to arrive at a risk function independent of loading condition, the final dataset did not include all of the available matched pair observations. Specifically, the hub loading conditions were excluded since the ImpactorOnly dataset showed a poor fit when analyzed using logistic regression, and showed divergent confidence intervals when analyzed using survival analysis. There are several possible reasons for this result. One possibility is that the ImpactorOnly data set is relatively small and injury-biased, as it includes 18 injury observations and 6 non-injury observations (75% injured). In contrast, the SledOnly data set includes 29 injury observations and 16 non-injury observations (64% injured). Accordingly, the ImpactorOnly dataset is comparatively more severe; the average peak resultant deflection in THOR-50M matched-pair testing in the ImpactorOnly conditions was 74 millimeters, compared to 44 millimeters in the SledOnly conditions.

Another possibility is that the ImpactorOnly dataset may be demonstrating a different physical relationship than the balance of the test conditions. One way to investigate this is through Principal Component Analysis, as carried out by Poplin et al. (2017). The PCA methodology was used to develop a combined deflection metric, which was formulated to capture both the magnitude and the localization of the chest deflection. After applying the weighting determined by the PCA analysis, the combined deflection metric can be viewed as a description of the chest deflection patterns. Overall, the ImpactorOnly deflection patterns were not consistent with those determined from the SledOnly conditions. The deflection patterns in the SledOnly conditions were evenly distributed between among the four components (sum of upper chest deflection, sum of lower chest deflection, difference between left and right upper chest deflection, and difference between left and right lower chest deflection). In contrast, the localized loading of the ImpactorOnly conditions resulted in disproportionately higher weighting of the sum components compared to the difference components. Thus, the same combined deflection metric could not be used to describe the SledOnly and ImpactorOnly conditions, which implies that the deflection patterns are inherently different.

It is recommended that users applying the injury risk functions developed herein use caution if applying to loading conditions other than two- and three-point restraints with or without airbags. Those investigating injury risk due to hub-like loading, such as an unbelted occupant without an airbag, should investigate adding additional matched-pair observations at lower impact velocities, which would presumably add more non-injury data points to the injury risk function development.

Despite these limitations, the utility of the developed injury risk function beyond the test conditions included in the final dataset was evaluated by calculating injury risk in the excluded tests. Two sets were evaluated: the additional observations in the SledExtended set (Table 5.3), and the ImpactorOnly set (Table 5.4). Injury risk predictions were calculated using the survival function coefficients in Table 5.9 for the SledOnly set, calculated using the matched-pair peak resultant deflection and the age of the subject. Error was calculated using the difference between the predicted injury risk and the actual injury observation (0 for non-injury, 1 for injury). The average error for both the SledExtended (0.32) and ImpactorOnly (0.23) data sets were actually lower than the average error for the SledOnly data set (0.33), though both sets had fewer observations than the SledOnly set.

To further investigate this error, injury predictions were classified by rounding the predicted injury risk to the nearest integer (0 for no injury, 1 for injury) and comparing the predicted outcome to the actual outcome. Table 5.13 shows a breakdown of the accuracy of injury predictions, including a count and percentage of true positives, injury cases accurately predicted to be injury; false negatives, injury observations predicted to be non-injury; false positives, non-injury observations predicted to be injuries; and true negatives, non-injury cases accurately predicted to be non-injury. As a baseline, the injury risk predictions for the SledOnly data set shown. These predictions were accurate 78% of the time, with 24 (53%) being true positives and 11 (25%) being true negatives. Errors were evenly distributed between false negatives and false positives with 5 of each. Predictions made for the SledExtended set were accurate for 60% of observations (2 true positives and 1 true negative), with both errors being false negatives. Predictions made for the ImpactorOnly set were accurate for 75% of observations, with all incorrect predictions being false positives.

Table 5.13. Assessment of injury risk function in other data sets.

Data Set	True Positive		False Negative		False Positive		True Negative		Average Error
	N	%	N	%	N	%	N	%	
SledOnly	24	50	5	10	5	10	14	29	0.31
SledExtended	2	40	2	40	0	0	1	20	0.32
ImpactorOnly	18	75	0	0	6	25	0	0	0.23

To summarize, even though the SledExtended and ImpactorOnly data sets were not used in the development of the injury risk function, injury predictions for observations in those data sets were relatively accurate. For the SledExtended set, the injury risk function generally underpredicted injury, as the only errors were false negatives. For the ImpactorOnly data set, the injury risk function generally overpredicted injury, as the only errors were false positives. However, in both cases, the prediction was accurate for 72% of those observations.

An additional data set was considered for inclusion in the development of a chest injury criteria, but ultimately not included. This data set represents tests conducted by the Laboratory of Accident Analysis, Biomechanics, and Human Behavior (LAB), submitted to ISO TC22 SC36 WG6 in document N1047 (ISO, 2018), and analyzed in document N1083 (ISO, 2019). It contains 35 observations, of which 33 were injured (≥ 7 fractured ribs) and 2 were uninjured (≤ 1 fractured rib). Compared to the SledOnly data set, the mean age was 17 years older (77 ± 10 years), the mean mass was 4 kg lower (69 ± 10 kg), the mean stature was 5 cm shorter (170 ± 6 cm), and the average number of fractured ribs was 9 higher (14 ± 5 NFR). Survival Weibull risk functions using peak resultant deflection as the predictor variable and age as a covariate were developed using this data set alone (LAB) and in combination with the SledOnly data set (SledOnly+LAB). Figure 5.16 shows a comparison of these risk functions with the previously-presented SledOnly data set.

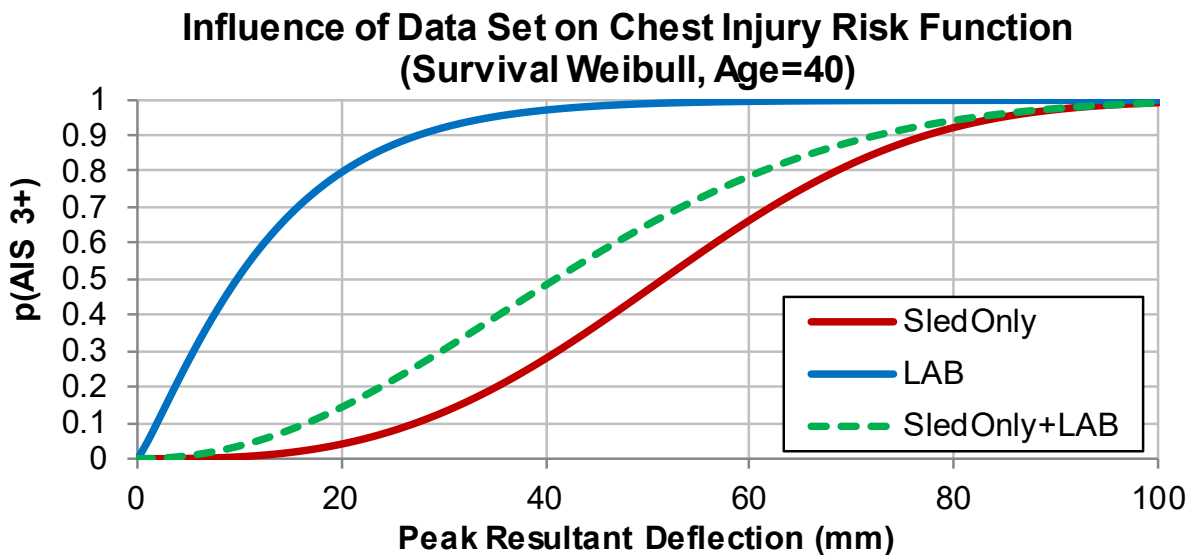


Figure 5.16. Comparison of Survival Weibull risk functions developed using the SledOnly, LAB, and SledOnly+LAB data sets.

As there are only two non-injury observations in the LAB data set, the risk function developed using only the LAB data is nearly asymptotic to the Y-axis. Using this risk function, a 50 percent risk of AIS 3+ injury would occur at a peak resultant deflection of 10 millimeters. When the risk function is formulated using the combined SledOnly+LAB data set, the risk curve shifts to the left by roughly 10 millimeters of peak resultant deflection. The SledOnly+LAB risk function would predict a 50 percent risk of AIS 3+ injury at a peak resultant deflection of 41 millimeters, compared to 51 millimeters using the SledOnly data set. As such, a risk function developed using the SledOnly+LAB data would result in higher predicted injury risks. For example, the average risk of AIS 3+ injury from the fleet data using the SledOnly+LAB risk function would be 58%, compared to 41% using the SledOnly risk function.

To evaluate the effectiveness of the LAB data in the development of chest injury risk functions, the LAB and SledOnly+LAB risk functions were assessed by comparing the predicted outcome to the actual outcome as described above (Table 5.14). The model fit to only the LAB data resulted in the highest average error, and tended to overpredict injury as all but three of the observations were predicted to be injured, and all of the errors were false positives. The model fit to the SledOnly+LAB data showed lower average percent errors, though most of the error classifications were still false positives. The model fit to the SledOnly data resulted in the lowest average error for all data sets, and an even distribution of false positive and false negative errors. The injury classification for the LAB observations is the same for all three injury risk functions, with 33 injured observations correctly predicted to be injured and 2 uninjured observations incorrectly predicted to be injured.

Table 5.14. Assessment of injury risk function in other data sets including LAB data.

Development Data Set	Assessment Data Set	True Positive		False Negative		False Positive		True Negative		Average Error
		N	%	N	%	N	%	N	%	
SledOnly	SledOnly	24	50	5	10	5	10	14	29	0.31
	LAB	33	94	0	0	2	6	0	0	0.065
	SledOnly+LAB	57	69	5	6	7	8	14	17	0.21
LAB	SledOnly	29	60	0	0	16	33	3	6	0.37
	LAB	33	94	0	0	2	6	0	0	0.11
	SledOnly+LAB	62	75	0	0	18	22	3	4	0.26
SledOnly+LAB	SledOnly	25	52	4	8	8	17	11	23	0.33
	LAB	33	94	0	0	2	6	0	0	0.084
	SledOnly+LAB	58	70	4	5	10	12	11	13	0.23

Additional formulations of the chest injury risk function fit to the LAB data were evaluated as well, such as redeveloping Principal Component Analysis terms to fit the extended data set or inclusion of a term to describe the difference between left and right deflections. However, none of these formulations produced lower average errors or more even error distributions than the risk function formulated using peak resultant deflection with age as a covariate and fit to the SledOnly data. The fact that any formulation developed herein predicted the same injury classification for the LAB observations suggests that the LAB data set is biased towards high-severity injured observations and does not provide effective differentiation in the development of an injury risk function. That said, application of the incumbent risk function correctly classifies injury in 94% of the LAB observations.

A final limitation to note is that within the SledOnly dataset, all of the available observations were retained in the development of the final model. To investigate the validity of this approach, an assessment of outliers was carried out through review of several influence diagnostics, including Pearson residuals, DFBETAs, and confidence interval displacement diagnostic. These diagnostics suggested that two observations have a large influence on the regression: a 69-year-old male in the 48 km/h 3-point force-limited belt with pretensioner condition who was uninjured, and a 40-year-old male in the 48 km/h lap belt with airbag condition who was injured. Review of the 69-year-old male observation did not turn up any evidence of improper coding or inconsistent test conditions, thus its inclusion is not thought to be suspect. The 40-year-old male, on the other hand, had a pre-existing physical condition (scleroderma) which may have contributed to the observed injury (Poplin, 2017). However, the effect of scleroderma on injury risk is not explicitly known, and it is possible for this or related pre-existing conditions to exist in the population. For these reasons, along with the desire to retain as many data points in the sample as possible, this observation was not excluded.

Nonetheless, for applications where users deem this 40-year-old observation to be an outlier, the Survival Weibull injury risk function was processed both with and without the 40-year-old observation to examine the magnitude and direction of its influence (Figure 5.17, Table 5.15). If the 40-year-old observation is excluded, the resulting injury risk function is mainly shifted to the right, with 50% risk levels increased by roughly 4 or 1.5 millimeters when evaluated at ages 40 or 61, respectively.

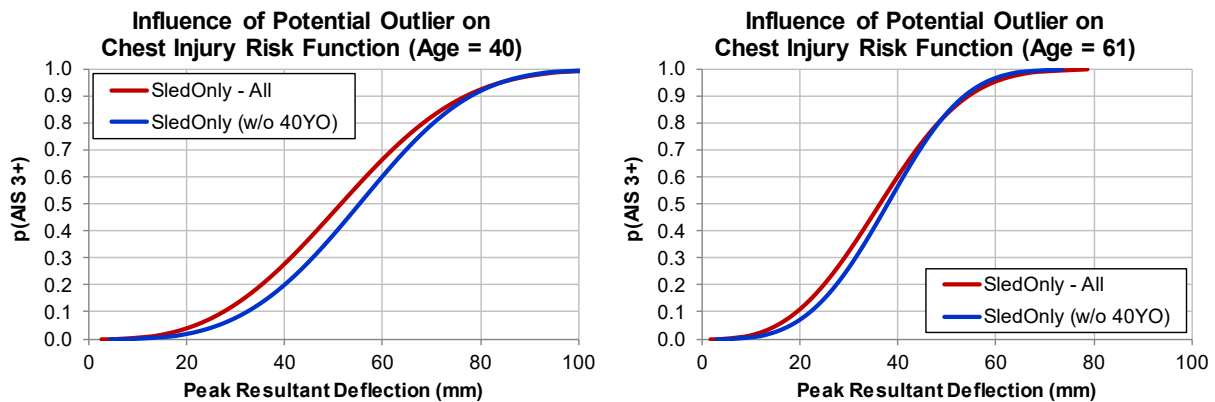


Figure 5.17. The difference between the Survival Weibull risk functions including or excluding the 40-year-old potential outlier observation.

Table 5.15. Injury risk functions shown in Figure 5.17.

Data Set	Risk Function
SledOnly	$p(\text{AIS } 3+) = 1 - e^{-\left(\frac{R_{max}}{e^{(4.7276-0.0166a)}}\right)^{2.977}}$
SledOnly without 40-year-old observation	$p(\text{AIS } 3+) = 1 - e^{-\left(\frac{R_{max}}{e^{(4.8391-0.0180a)}}\right)^{3.474}}$

6 ABDOMEN

6.1 Field and Historical Fleet Data

The current frontal crash test standards and consumer metric programs do not directly measure abdominal injury risk. As such, it is not possible to present any abdominal injury trends from crash testing.

Figure 6.1 shows the trend of AIS 3+ abdominal injury for belted drivers in frontal crashes. The field data injury rate represents a running three-year average of the percent of injured divided by the total number of cases (e.g. model year 1992 includes the total weighted count of AIS 3+ injuries from model years 1990, 1991 and 1992, divided by the total number of cases for those model years). Different than observed in preceding sections, there appears to be no significant increasing or decreasing trend.

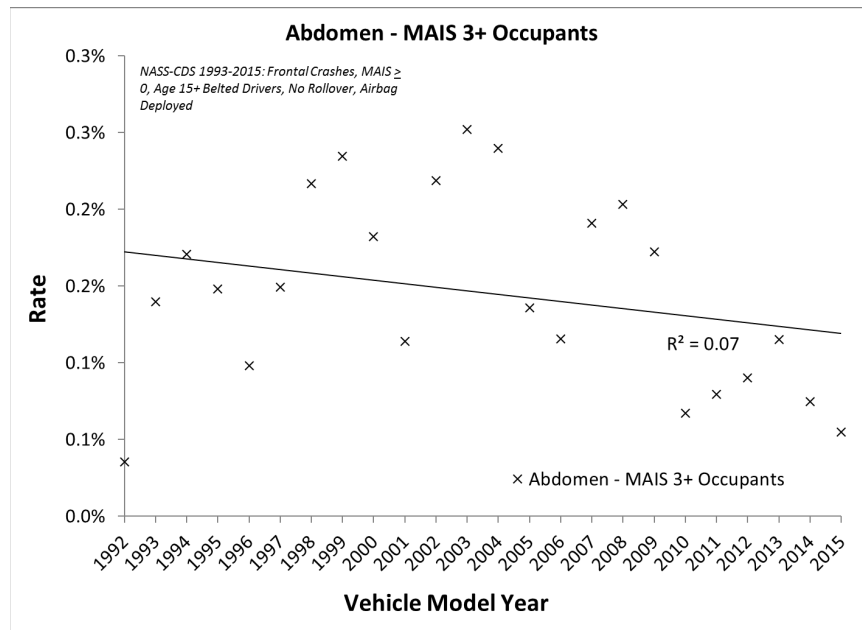


Figure 6.1. AIS 3+ abdominal injury trends by vehicle model year (1992 to 2015) from frontal crashes in NASS-CDS (1993 to 2015).

Table 1.1 and Table 1.2 (presented in Chapter 1) show unadjusted counts of MAIS 2+ and 3+ injured occupants by body regions associated with the THOR-50M as well as total injury counts for those body regions, respectively. Figure 1.2 presents the attributable cost associated with the respective body regions at the AIS 2+ level. For both belted and unbelted front row occupants involved in frontal crashes, the occurrence and attributable cost associated with abdomen injuries is lower than the majority of other body regions. Nonetheless, there remains a need for an abdomen-specific injury criterion to protect against abdominal injuries due to seat belt or steering wheel related compression or other sources of abdominal loading that may be present with different seating positions, restraint geometries, and/or crash types.

Figure 6.2 shows the regional mechanisms of injury assigned to abdominal injuries in 124 CIREN front-row belted occupants involved in frontal crashes. These mechanisms are inferred from the available data and may have been limited to available researcher/published biomechanical knowledge at the time. It is important to note that the mechanisms shown are regional mechanisms, not organ-specific mechanisms. That is, the chosen mechanism represents the type of loading/motion experienced by the entire abdominal region. Abdominal injuries, in general, were attributed to a combination of compression and rate of compression. In this context, rate of compression implies that the injury is not likely to occur from static compression alone, not necessarily that the severity of injury is proportional to the rate of compression.

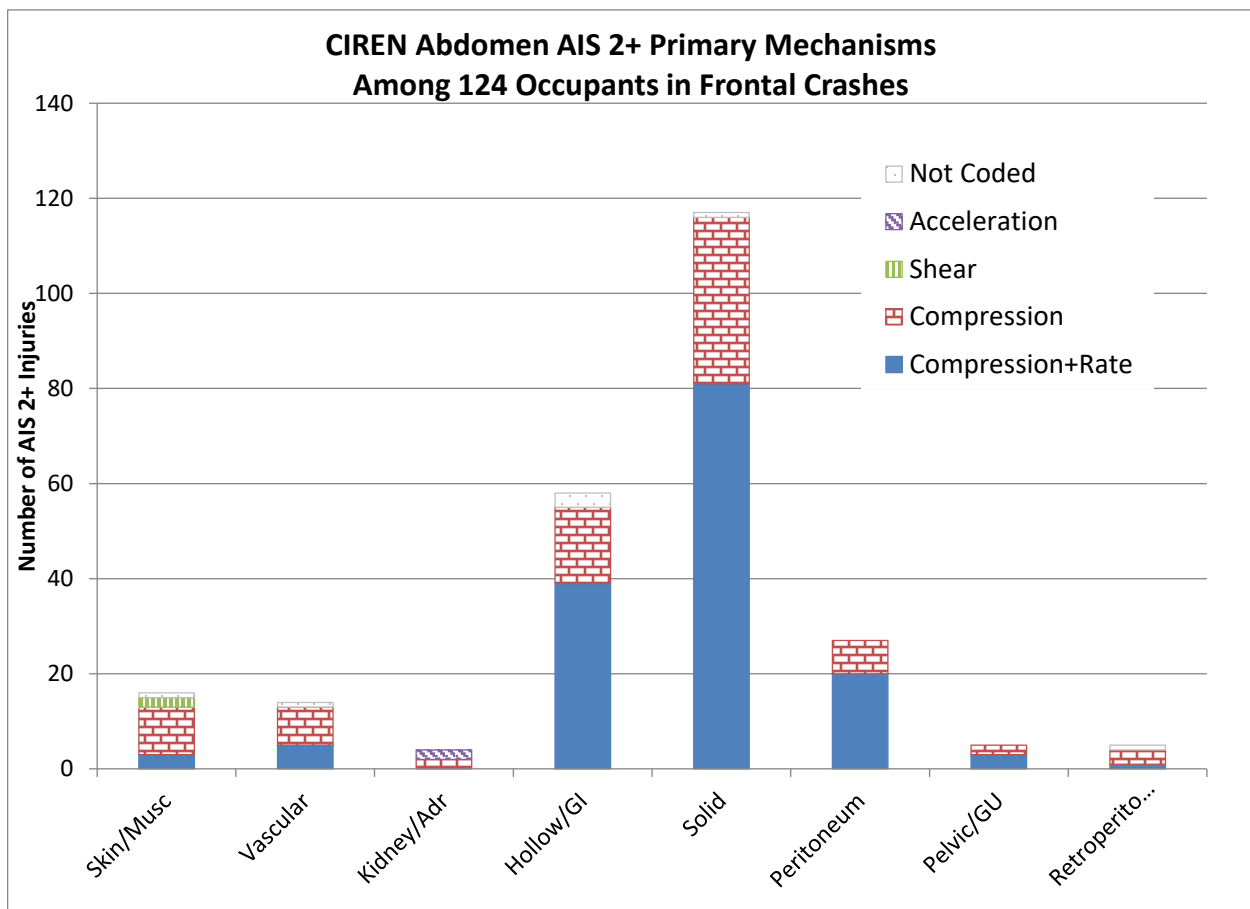


Figure 6.2. Recorded mechanisms of abdominal injuries for belted front row occupants involved in frontal crashes from the CIREN database.

6.2 Literature Review

The risk of abdominal injury in motor vehicle crashes is important to consider because the abdomen is a possible load path of the seat belt, primarily the lap belt portion between the buckle and the belt-to-vehicle anchor. While the intended function of the lap belt is to engage the bony pelvis at the anterior-superior iliac spine (ASIS), this does not always occur due to submarining brought about by occupant posture, initial position, anthropometry, and both vehicle and occupant motion during a crash. Intrusion

of the lap belt into the abdomen can bring about compression of the abdominal organs, including the liver, spleen, and digestive system, which do not necessarily benefit from the protection of the rib cage. Additionally, contact between the steering rim and the abdomen is a potential load path specific to the driver seating position, and has been shown to be the primary object associated with abdominal injuries for drivers.

Klinich et al. (2008) reviewed abdominal injury over the time period of 1998 to 2004, which included vehicles no older than model year 1985. While less common than head, chest, and lower extremity injuries, an estimated 10,000 occupants sustain AIS 2+ abdomen injuries in frontal crashes each year. The liver and spleen are the most frequently injured organs for both drivers and right front passengers in frontal crashes. The odds of a belted driver sustaining an abdominal organ injury are substantially higher when the driver also sustains 2 or more rib fractures compared to 1 or no fractures (16, 30, and 12 times higher for the liver, spleen, and kidney respectively). This study was supplemented with a CIREN dataset, which included 526 cases involving AIS 2+ abdomen injury in vehicles from model year 1985 through 2005. As in the NASS dataset, the liver (50%) and spleen (29%) were the most frequently injured abdominal organs for drivers in frontal crashes.

A study of crash injury data from the United Kingdom's Co-operative Crash Injury Study (CCIS) from 1998 to 2010 showed that rear passengers have a substantially higher rate of AIS 2+ and AIS 3+ abdominal injury compared to front seat passengers and drivers (Frampton et al., 2012). Drivers and front seat passengers most frequently sustained injuries to solid organs (liver and spleen), while rear seat occupants most frequently sustained injuries to the hollow organs (jejunum-ileum, mesentery, and colon). Injury patterns were sensitive to rib fracture, as some organ injuries (kidney, liver, mesentery, pancreas, and spleen) were more likely when two or more rib fractures occurred, while others (colon, duodenum, jejunum-ileum, stomach) were more likely when zero or one rib fractures occurred.

6.3 Design

The abdomen of the THOR-50M consists of two components, the upper abdomen and the lower abdomen. The upper abdomen is the region on the dummy that represents the lower thoracic cavity, which fills the volume that exists between the lowest three ribs, above the lower abdomen and in front of the spine (Figure 6.3). The lower abdomen is defined as the region of the human body between the lower thoracic rib cage and the pelvic girdle.

The upper and lower abdomen components of THOR are represented by structural fabric bags containing foam inserts which define the compression stiffness. Both abdomen inserts are anchored posteriorly to the spine, while the upper abdomen insert is additionally anchored to the lower rib cage through three rib-to-bib attachment bolts on each side. When the lumbar spine pitch change joint is set to the "slouched" position, the abdomen inserts are in contact with one another; when in the "erect" and "neutral" positions, the gap between the abdominal inserts is filled with the lower abdomen neutral/erect position foam. This gap is also spanned by two steel stiffeners on each side that are installed into the torso jacket. The bottom surface of the lower abdomen insert is coincident with the pelvis, which includes bilateral mechanical representations of the anterior-superior iliac spine (ASIS).

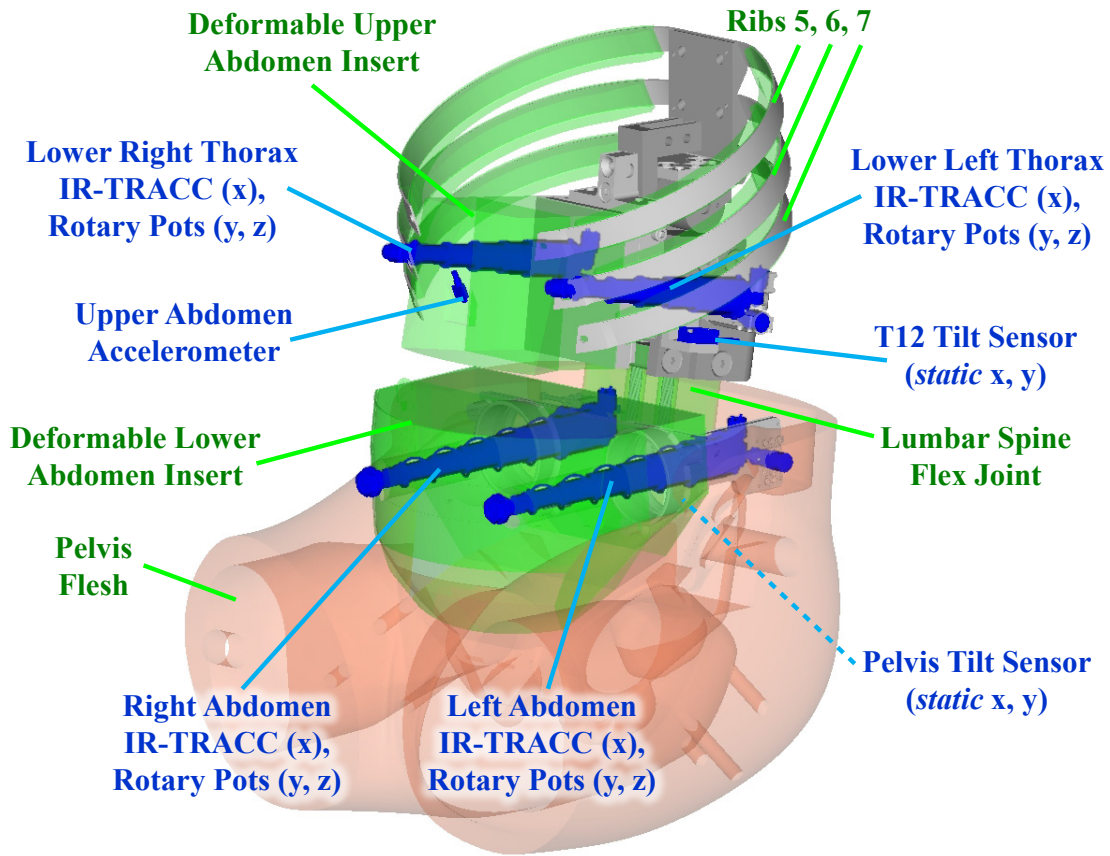


Figure 6.3. Design and instrumentation in the THOR-50M upper and lower abdomen.

6.4 Instrumentation

The upper abdomen is no longer instrumented, as the high-tension string potentiometer in the THOR-NT design resulted in permanent deformation of the foam inserts (Ridella and Parent, 2011) and often underestimated the upper abdominal deflection (Shaw et al., 2004). The upper abdomen deflection instrumentation would be at the same vertical level of the lower thorax 3D deflection measurement locations, should a measure of upper abdomen deflection related to skeletal deformation of the lower rib cage be necessary (Figure 6.3).

The lower abdomen includes bilateral three-dimensional displacement measurement instrumentation located at the vertical center of the lower abdomen insert and laterally offset by roughly 65 millimeters. In the AMVO posture, the anterior attachment location of the 3D deflection instrumentation is nearly coincident with point 25, the maximum abdominal protrusion, in the x-z plane. The anterior attachment point is 24 millimeters inferior of the umbilicus (point 24) along the z-axis and in a similar location along the x-axis. The posterior attachment point is at the vertical level of the iliocristale (point 27).

6.5 Biofidelity

Parent et al. (2017) presented an evaluation of THOR-50M biofidelity in three conditions: steering rim impact to the upper abdomen, rigid bar impact to the lower abdomen, and belt loading to the lower abdomen. Biofidelity was assessed using the Biofidelity Ranking System (BioRank), originally presented by Rhule et al. (2002, 2009) and implemented as described in Parent et al. (2017). Since the upper abdomen loading condition primarily stresses the lower rib cage, it is not relevant to the assessment of lower abdomen biofidelity. In the rigid bar impact condition, the THOR-50M demonstrated good internal biofidelity, but poor external biofidelity as the reaction force was greater than the associated post-mortem human subject (PMHS) response corridor. In the belt loading condition, the THOR-50M demonstrated excellent external biofidelity in comparison to the force-penetration biofidelity corridor, though the maximum deflection measured was lower than that of the mean PMHS response. At the abdomen body region level, the BioRank results for the THOR-50M demonstrate good internal (1.470) and marginal external (2.803) biofidelity. The THOR-50M was quantitatively more biofidelic than the H3-50M, which had abdomen body region BioRank scores of 1.629 and 3.474 respectively.

6.6 Data

Kent et al. (2008) presented the results of 45 tests of porcine specimens subjected to compressive loading of the upper and lower abdomen in both a ramp-and-release (RR) and ramp-and-hold (RH) loading condition (Table 6.1). From this data, several injury risk functions were developed and evaluated, and it was determined that maximum normalized abdominal penetration was the most appropriate predictor of injury resulting from abdomen belt loading. Kent et al. (2008) considered only the RR condition in the development of injury risk functions, as it was thought that the RH condition may have exacerbated the severity of the injuries during the hold phase of the event.

Table 6.1. Source data for PMHS tests.

ID	d_{max}	Condition	Site	MAIS	ID	d_{max}	Condition	Site	MAIS
1.07	0.36	RR	Lower	3	1.32	0.36	RR	Lower	0
1.08	0.37	RR	Upper	4	1.33	0.40	RR	Upper	3
1.09	0.37	RR	Lower	0	1.34	0.45	RR	Upper	3
1.10	0.55	RR	Lower	2	1.35	0.44	RR	Lower	3
1.11	0.32	RR	Lower	0	1.36	0.27	RR	Upper	0
1.12	0.32	RR	Lower	2	1.39	0.46	RR	Upper	3
1.13	0.35	RR	Upper	2	1.41	0.43	RR	Lower	3
1.15	0.40	RR	Lower	2	1.43	0.47	RR	Lower	2
1.16	0.46	RR	Lower	3	1.44	0.56	RR	Lower	3
1.17	0.23	RR	Lower	0	1.45	0.62	RR	Upper	4
1.18	0.26	RR	Upper	2	1.01	0.45	RH	Lower	2
1.20	0.43	RR	Upper	3	1.02	0.54	RH	Lower	4
1.21	0.43	RR	Lower	3	1.03	0.48	RH	Lower	3
1.22	0.39	RR	Lower	3	1.04	0.49	RH	Lower	3
1.23	0.40	RR	Lower	2	1.05	0.50	RH	Upper	4
1.24	0.40	RR	Upper	2	1.06	0.65	RH	Upper	4
1.25	0.42	RR	Lower	4	1.37	0.31	RH	Lower	0
1.26	0.40	RR	Upper	3	1.38	0.48	RH	Upper	3
1.27	0.30	RR	Upper	1	1.40	0.52	RH	Lower	3
1.28	0.42	RR	Lower	3	1.42	0.50	RH	Lower	3
1.29	0.52	RR	Lower	3	1.46	0.64	RH	Upper	3
1.30	0.23	RR	Upper	0	1.47	0.56	RH	Lower	3
1.31	0.37	RR	Upper	3					

Several additional data sets were also considered for inclusion. Miller (1989) subjected 25 anesthetized swine to simulated lap belt loading at velocities between 1.6 and 6.6 meters per second to magnitudes of between 6% and 67% compression in a fixed-back condition, with injuries ranging from AIS 0 to AIS 5. As analyzed in Kent et al. 2008, including these data points resulted in only slight changes to a survival Weibull injury risk function based on maximum normalized penetration. Therefore, this data set was not included in the injury risk function development herein but retained as a validation data set. Hardy et al. (2001) subjected PMHS to rigid bar, seat belt, and airbag loading to the upper, mid, and lower abdomen at nominal velocities between 3 and 9 meters per second. As this study focused on the mechanical response of the abdomen, most the subjects were injured, this data set was not included in the injury criteria development herein to prevent bias. Trosseille et al. (2002) investigated the influence of abdominal loading representative of pyrotechnic pretensioning by subjecting six PMHS to high-speed lap belt tension at velocities between 8.2 and 11.7 meters per second. Similarly, Foster et al. (2006) conducted high-speed lap belt pretensioner loading tests on eight PMHS at loading rates between 4.0 and 13.3 meters per second. Between these two pretensioner-related data sets, only 3 of the 14 PMHS sustained injuries above the AIS 2 level, thus Trosseille and Foster data sets were also not included in the injury criteria development herein but were retained as validation data.

6.7 Predictor Variable

Given the conclusion from Kent et al. (2008) that maximum normalized abdominal penetration is among the best available metrics for injury prediction in abdominal belt loading conditions, and that the THOR-50M is equipped with instrumentation to measure abdominal deflection at two locations, maximum normalized abdominal penetration is used as the predictor variable for the remainder of this analysis.

6.8 Dependent Variable

The dependent variable used in the development of an abdominal injury criterion was the presence of an Abbreviated Injury Scale (AIS) score of 3 or greater (AIS 3+). This injury definition was selected because, compared to AIS 2+ or AIS 4+, using AIS 3+ as the injury definition results in a relatively balanced distribution of injured (28) and non-injured (17) observations from the available data set (Table 6.1).

6.9 Injury Risk Function Formulation

Nonparametric survival analysis was carried out to examine the qualitative influence of two strata on injury outcome: loading condition (RR vs. RH) and loading site (Upper vs. Lower). This analysis is a first step in determining whether to include all available data points in the resulting injury risk function, and whether a covariate is needed to describe the two strata.

There was a notable qualitative increase in survival time of the RH group compared to the RR group (Figure 6.4). Kent et al. (2008) posit that the RH tests could result in more severe injuries than if the belt was not held at the point of peak penetration. While the RH observations were injured more frequently than the RR observations (RH: 83%, RR: 55%), the RH observations also experienced larger maximum normalized abdominal penetrations (RH: 0.51, RR: 0.40), therefore it cannot be concluded that the RH condition was inherently more injurious than the RR condition. While it is understood that the RH condition was not specifically intended for use in injury criteria development, these observations represent valuable data in a relatively small sample, and, although unlikely, it is conceivable that a similar loading scenario could occur in a motor vehicle crash environment. Therefore, two datasets were considered for the development of abdomen injury risk functions: only the RR observations (RR Only), and a combined set of the RR and RH observations (RR+RH). However, the RH condition was not considered independently, as a logistic regression risk function could not be fit to these observations alone due to the lack of overlapping non-injury and injury data points.

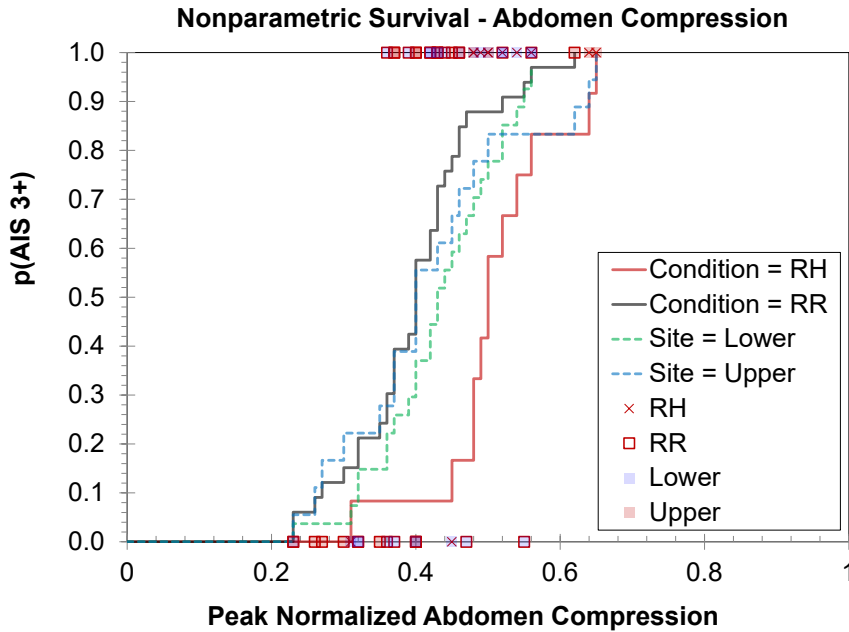


Figure 6.4. Nonparametric survival analysis of abdomen injury risk, stratified by condition and loading site.

Risk functions were developed through both logistic regression and survival analysis for the RR Only and combined RR+RH groups. There was not a significant influence on the shape or magnitude of the risk functions using the RR Only (as in Kent et al., 2008) or the RR+RH datasets (Figure 6.5). The RR+RH dataset was selected for the final abdomen injury risk function model, as it includes a relatively large number of observations, includes a combination of both injured and non-injured observations, has sufficient overlap of these points in the transition region, and does not result in a meaningful difference between the logistic and Survival Weibull risk functions (Figure 6.5). As the difference between the logistic and Survival Weibull risk function is negligible, the Survival Weibull form is preferred for its representation of zero risk at a zero-stimulus value.

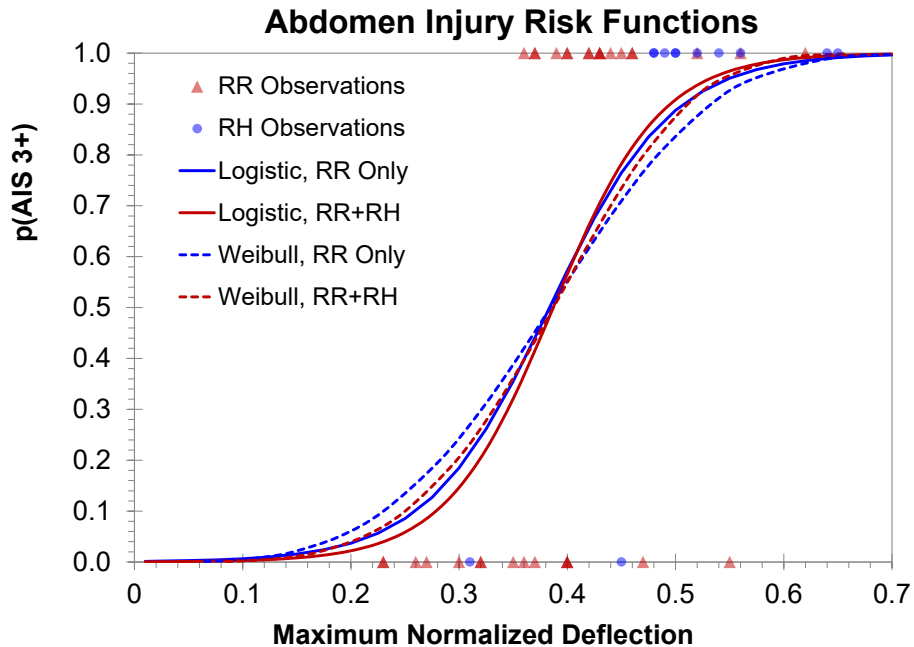


Figure 6.5. Comparison of injury risk functions formed using logistic regression and survival analysis, for both the RR only and the RR and RH groups combined.

The qualitative difference between the Upper and Lower loading site groups was comparatively small (Figure 6.4), which is consistent with the findings of Kent et al. (2008) who found no significant difference between the Upper and Lower groups. To investigate further, injury risk functions were fit using Survival Weibull formulation to the Lower only, Upper only, and combined Upper and Lower observations (Figure 6.6). The risk function for the Upper Only group is steeper than the Lower Only and Combined groups, as there is limited overlap in the non-injury and injury data for the Upper Only group. The Combined group, however, resulted in a similar risk curve to the Lower Only group, suggesting that the influence of the Upper Only group on the combined dataset is relatively small. Therefore, observations from both the Upper and Lower loading site groups were included in this analysis.

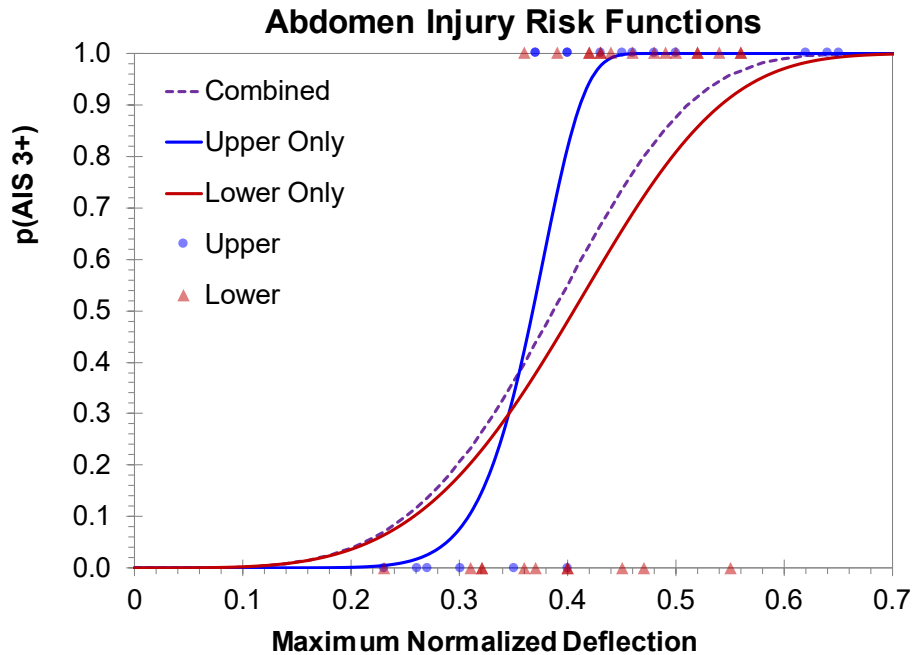


Figure 6.6. Comparison of Survival Weibull injury risk functions for the Lower only, Upper only, and both Lower and Upper groups combined.

6.10 Application of Risk Function to THOR-50M

The THOR-50M ATD is equipped to measure the compression of the abdomen, thus the maximum normalized abdominal penetration can be measured nearly directly using the THOR instrumentation. One limitation is that while the 3D deflection instrumentation is attached to the anterior aspect of the abdomen, there may be some compression of the torso jacket which is not captured in the compression measurements. To calculate maximum normalized abdominal penetration, the peak of the left and right abdominal x-axis deflections is divided by 252 millimeters, the abdominal depth of the THOR-50M ATD at the location of the 3D deflection instrumentation attachment points.

Recommended injury risk function:

$$p(\text{AIS } 3+) = 1 - e^{-\left(2.3724 \frac{\delta_{max}}{d_{THOR}}\right)^{4.3127}}$$

where:

δ_{max} = Maximum of left and right peak abdomen x-axis deflection, in millimeters

d_{THOR} = THOR abdomen depth at location of 3D deflection instrumentation attachment points [252 millimeters]

Simplified:

$$p(\text{AIS } 3+) = 1 - e^{-\left(\frac{\delta_{max}}{106.222}\right)^{4.3127}}$$

6.11 Fleet Test Data: THOR-50M

The recommended abdominal injury risk function was applied to THOR-50M measurements collected in frontal rigid barrier and frontal Oblique fleet testing. Figure 6.7 shows the injury risk function with observations representing the injury risk predicted from each occupant response, grouped by occupant position and test mode. Predicted probability of AIS 3+ injury is below 20 percent for all observations.

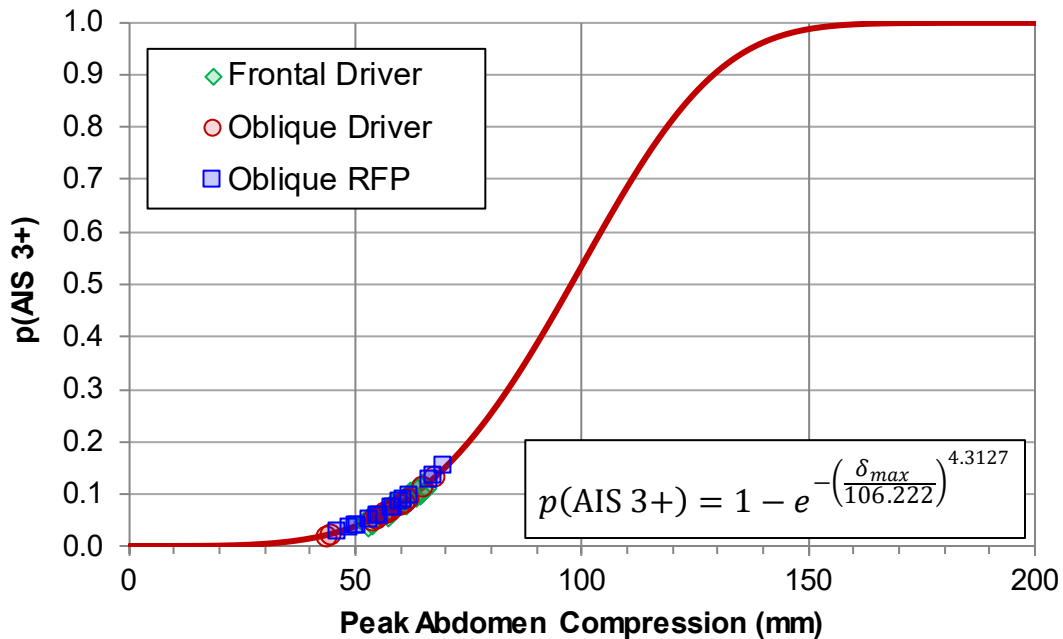


Figure 6.7. Peak abdomen compression from frontal rigid barrier and oblique moving deformable barrier tests using THOR-50M.

6.12 Limitations

While the analysis above used an injury definition of AIS 3+, it would also be possible to construct AIS 2+ and AIS 4+ injury risk functions using the same dataset. Figure 6.8 (further described by Table 6.2) shows injury risk functions calculated using both logistic regression and survival analysis for AIS 2+, 3+, and 4+ injury definitions for both the RR Only and the RR+RH groups. As expected, the AIS 2+ risk functions show an earlier and steeper rise than the AIS 3+ risk functions, indicating a higher risk of injury at lower values of maximum normalized deflection. Likewise, the AIS 4+ risk function shows a later and shallower rise than the AIS 3+ risk function. There are no remarkable differences between the logistic and survival formulations, and the difference between the RR Only and RR+RH groups is only apparent in the AIS 4+ risk function.

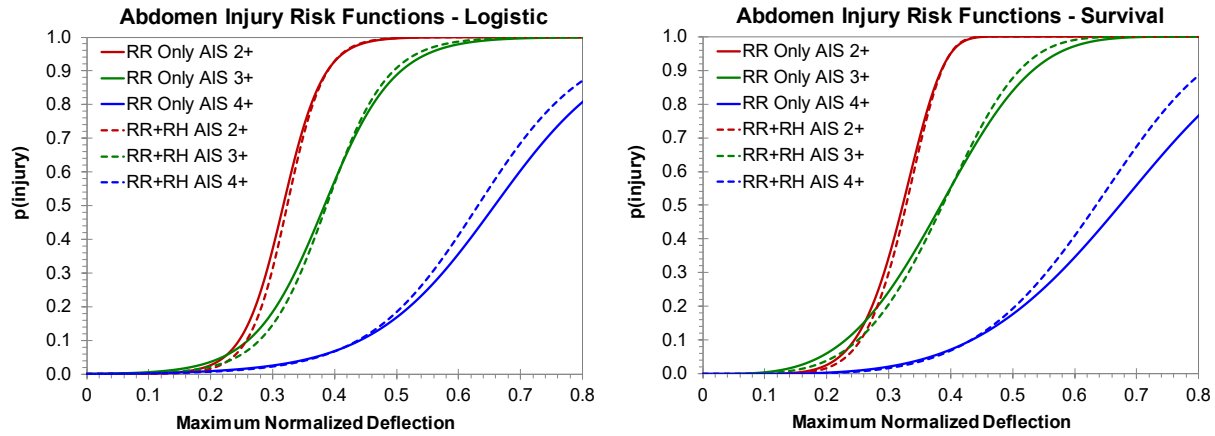


Figure 6.8. Abdomen injury risk functions calculated using AIS 2+, 3+, and 4+ as the injury definition.

Table 6.2. Abdomen injury risk functions shown in Figure 6.8.

Condition	Injury Definition	Logistic			Survival Weibull		
		β_0	β_1	AUC	β_0	α	-2LL
RR Only	AIS 2+	-9.7866	30.8588	0.934	-1.0769	6.7922	-8.68816
RR Only	AIS 3+	-6.8101	17.7572	0.820	-0.8563	3.6719	-17.7432
RR Only	AIS 4+	-6.6325	10.0766	0.661	-0.3103	4.2744	-9.03295
RR+RH	AIS 2+	-10.8588	33.5684	0.956	-1.0646	7.4102	-9.17808
RR+RH	AIS 3+	-7.8489	20.2868	0.857	-0.8639	4.3127	-20.4505
RR+RH	AIS 4+	-7.1525	11.3339	0.752	-0.3797	4.9102	-14.8926
				$p(\text{injury}) = \frac{e^{(\beta_0 + \beta_1 x)}}{1 + e^{(\beta_0 + \beta_1 x)}}$		$p(\text{injury}) = 1 - e^{-\left(\frac{x}{e^{\beta_0}}\right)^\alpha}$	

The risk function presented in Section 6.10 was formulated using observations in both the ramp-and-release (RR) and ramp-and-hold (RH) conditions. As shown in Figure 6.5 and Figure 6.8, including the RH observations results in only a minor change in the resulting risk functions, which likely occurs because the RH observations are primarily injured and have a higher average maximum normalized deflection than the RR observations. Inclusion of the RH observations was done to maximize the number of observations used to develop injury risk functions, though in the end the RH observations were not particularly influential on the resulting risk functions.

An alternate approach to developing the abdomen injury risk functions would be to fit the model to the RR Only observations, and validate the resulting functions against the RH observations for robustness. This exercise was carried out using the AIS 3+ Logistic risk functions shown in Table 6.2. In the process, both the RR Only and the RR+RH AIS 3+ Logistic risk functions were used to evaluate several validation data sets: Miller, 1989; Hardy et al. (2001); Trosseille et al. (2002); Foster et al. (2006); “F+H+T”, a combination of the Foster, Hardy, and Trosseille experiments, which all used PMHS; and “RH+F+M+H+T”, a combination all available validation data along with the Kent RH observations.

For each data set, injury predictions were classified by using the RR Only and RR+RH AIS 3+ Logistic risk functions to calculate a predicted probability of injury, rounding this probability to the nearest integer (0 for no injury, 1 for injury), then comparing the predicted outcome to the actual outcome. Table 6.3 shows the accuracy of the injury predictions, including a count and percentage of: true positives, or injury cases accurately predicted to be injury; false negatives, or injury observations predicted to be non-injury; false positives, or non-injury observations predicted to be injuries; and true negatives, or non-injury cases accurately predicted to be non-injury. Additionally, an average error was calculated for both risk functions using the difference between the predicted injury risk and the actual injury observation (0 for non-injury, 1 for injury) averaged across all of the validation data set observations. Across all of the evaluation data sets, there were no differences in the classification of injury between the RR Only and RR+RH risk functions, thus the confusion matrices for each data set did not differ between the RR Only and RR+RH risk functions. The average error was equal or lower using the RR+RH risk function for all data sets.

Table 6.3. Assessment of abdomen injury risk functions in other data sets.

Data Set	True Positive	False Negative	False Positive	True Negative	Average Error	
	N (%)	N (%)	N (%)	N (%)	SW, RR Only	SW, RR+RH
RR	15 (45%)	3 (9%)	5 (15%)	10 (30%)	0.369	0.356
RH	10 (83%)	0 (0%)	1 (8%)	1 (8%)	0.183	0.157
RR+RH	25 (56%)	3 (7%)	6 (13%)	11 (24%)	0.320	0.303
Miller	6 (24%)	1 (4%)	4 (16%)	14 (56%)	0.211	0.199
Hardy	9 (43%)	7 (33%)	0 (0%)	5 (24%)	0.345	0.345
Trosseille	0 (0%)	1 (17%)	0 (0%)	5 (83%)	0.289	0.264
Foster	2 (22%)	0 (0%)	1 (11%)	6 (67%)	0.296	0.272
F+H+T	11 (31%)	8 (22%)	1 (3%)	16 (44%)	0.324	0.313
RH+F+M+H+T	27 (37%)	9 (12%)	6 (8%)	31 (42%)	0.310	0.298

Across all of the validation data sets, the classification of injury by either the RR Only or RR+RH risk functions was accurate for at least 75% of the observations in all but one of the validation data sets. The RH+F+M+H+T validation data set shows that the injury risk function formulated using either the RR Only or RR+RH observations was accurate in classification of injury in 58 out of 73 (79%) of the observations, resulting in an AUC of 0.869. This demonstrates that the developed injury risk function is able to discriminate between injury and non-injury observations over a wide range of loading conditions and human surrogates.

One exception to the validation data accuracy was in the Hardy data set, where 33% of the observations were classified incorrectly, and all of these errors were false negatives. There are several reasons that this may be occurring. First, several of the subjects in the Hardy data set were impacted multiple times, which may be convoluting the relationship between exposure and injury. Second, many of the injuries were rib fractures, which may have resulted from loading at a higher loading site on the abdomen than would be relevant to measurement by the THOR-50M lower abdomen. Finally, reviewing the Hardy observations, many of the injured observations were among the lowest measured maximum normalized penetrations of the data set. This suggests that additional predictor variables or covariates may be

necessary to capture the variation related to the subjects or loading conditions of the Hardy experiments. However, as the abdomen injury risk functions show good differentiation of injury and non-injury in the remainder of the validation data sets, no additional steps were taken to address this limitation.

The “RH” row of Table 6.3 shows that either risk function (RR Only or RR+RH) would accurately classify the injury outcome for 91% of the observations, with the only miss being a false positive. For both injury risk functions, the average error calculated from the RH observations (0.183 and 0.157) is relatively small compared to the average error in the data sets used to develop the respective models (0.369, 0.303). This, along with the identical injury classifications and small error differences throughout the validation data sets, suggests that the RR Only risk function is sufficiently robust without inclusion of the RH observations during development.

The abdomen injury risk function presented herein uses only maximum normalized abdomen penetration as the independent variable. While it has been suggested that abdomen penetration rate is important to the characterization of abdominal injury, this did not appear to be true in the dataset used to develop the risk function. To check this, Survival Weibull risk functions were developed using either maximum penetration rate alone (v_{max}) or both v_{max} and maximum normalized abdomen penetration (d and v_{max}) as predictor variables (Figure 6.9). The inclusion of v_{max} did not appear to improve the risk function, as both function showed lower AUCs than the risk function which used maximum normalized abdomen penetration alone (d).

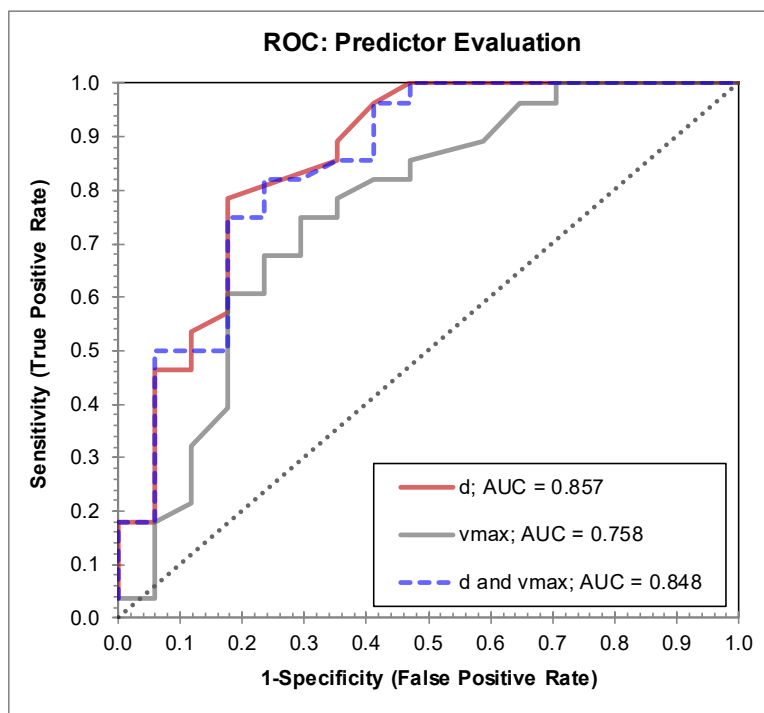


Figure 6.9. Receiver Operating Characteristic (ROC) comparing Survival Weibull risk functions formulated using different predictor variables.

There are several caveats that limit the application of the abdomen injury risk function to the prediction of abdomen injury using the THOR-50M ATD. First, the injury risk function was developed using juvenile porcine specimens as human surrogates. The benefit of this approach is the ability to diagnose soft tissue injuries which would not be possible with PMHS, though the drawback is that the relationship between live juvenile porcine specimens and live adult humans presents some uncertainty. This uncertainty can be qualified in two ways. One, the relationship between juvenile and adult swine can be investigated by comparing the data from Kent et al. (2008) and Miller (1989), as the latter subjects were adult swine. As noted in Kent et al. (2008), differences between injury risk functions developed using juvenile swine and adult swine were slight. This can be confirmed in the current analysis by reviewing the Miller validation dataset (Table 6.3), as either the RR Only or RR+RH injury risk functions accurately classified injury in 80% of observations, with average errors among the lowest of the validation datasets (0.211, 0.199 respectively). This suggests that the difference in injury risk as calculated using maximum normalized abdomen penetration is not substantially different between juvenile and adult swine.

Similarly, the relationship between porcine subjects and human subjects can be investigated by evaluating the F+H+T validation data set, which consists of only PMHS observations. For these observations, the RR Only or RR+RH injury risk functions correctly classify the occurrence of injury in 75% of the observations, with average errors similar to the baseline error. This suggests that a transfer function to relate between porcine subjects and PMHS is not necessary. The relationship between PMHS and live humans is more nuanced, though it has been shown that tensing of the rectus abdominus muscles was not a significant variable in the prediction of abdominal injury (Kent et al., 2008).

Another caveat to the application of the abdomen injury risk function to the THOR-50M ATD is that the experiments used to develop the abdomen injury risk function were conducted in a fixed-back configuration, which does not consider inertial loading due to acceleration or deceleration of the body and the internal organs of the abdomen which would occur in a belted frontal crash environment. Also, the relationship between PMHS response and THOR-50M response presents a limitation since the THOR-50M demonstrated good internal but marginal external biofidelity. While the THOR-50M abdomen showed excellent external biofidelity in a free-back belt loading configuration, biofidelity performance may not be the same in the fixed-back configuration of the injury criteria development tests. As the biofidelity performance of the THOR-50M was compared PMHS, the relationship between the abdominal response of the THOR-50M and a live human is not directly known.

A final caveat is that there is an apparent disconnect between the distribution of abdominal injuries in real-world motor vehicle crashes and the injuries sustained by the subjects used to develop the abdomen injury risk function. As shown in Figure 6.2, a majority of the abdomen injuries suffered by belted front row occupants in frontal crashes were to solid organs, while a majority of the injuries sustained by the subjects in the RR+RH dataset were to hollow organs. Further, as presented in Kent et al. (2008), injuries to the hollow organs of the abdomen are also common in pediatric occupants in frontal motor vehicle crashes. The difference in injury patterns between front-row adult occupants and presumably rear-row pediatric occupants may relate to both differences in restraint systems between the front and rear seat and biomechanical differences between adults and children. As such, the

abdomen injury risk function developed herein may be more effective in predicting injury to rear-row occupants than front-row occupants in frontal motor vehicle crashes.

7 KNEE, THIGH AND HIP

7.1 Field and Historical Fleet Data

Table 7.1 shows the weighted (unweighted in parenthesis) counts for hip/pelvis and knee/femur AIS 2+ and AIS 3+ injuries for belted and airbag restrained drivers in frontal crashes for NASS-CDS case years 2000 to 2015. Roughly two-thirds of hip/pelvis injuries occur in the absence of femur/knee 2+ or 3+ injuries.

Table 7.1 Hip/pelvis versus femur/knee injuries for belted, airbag restrained drivers in frontal crashes; NASS-CDS 2000-2015.

		Femur/Knee AIS 2+		Femur/Knee AIS 3+	
		0	1	0	1
		Hip/Pelvis AIS 2+	0	5,369,812 (13,6945)	70,378 (591)
1	12,398 (167)		6,626 (116)	13,033 (187)	5,990 (99)
Hip/Pelvis AIS 3+	0	5,377,098 (13,746)	74,340 (650)	5,428,282 (14,013)	23,156 (383)
	1	5,111 (66)	2,664 (57)	5,339 (78)	2,436 (45)

Figure 7.1 shows the trend of AIS 3+ KTH injury for belted drivers in frontal crashes. Similar to that done for other body regions, the trend represents a 3-year average starting with model year 1992. There does not appear to be any significant increasing or decreasing trend with newer model years. In contrast, Figure 7.2 shows a decreasing trend of peak femur forces and associated injury risk (risk function from NHTSA, 2008) with newer model year vehicles as evaluated with the H3-50M in full frontal, 35-mph tests.

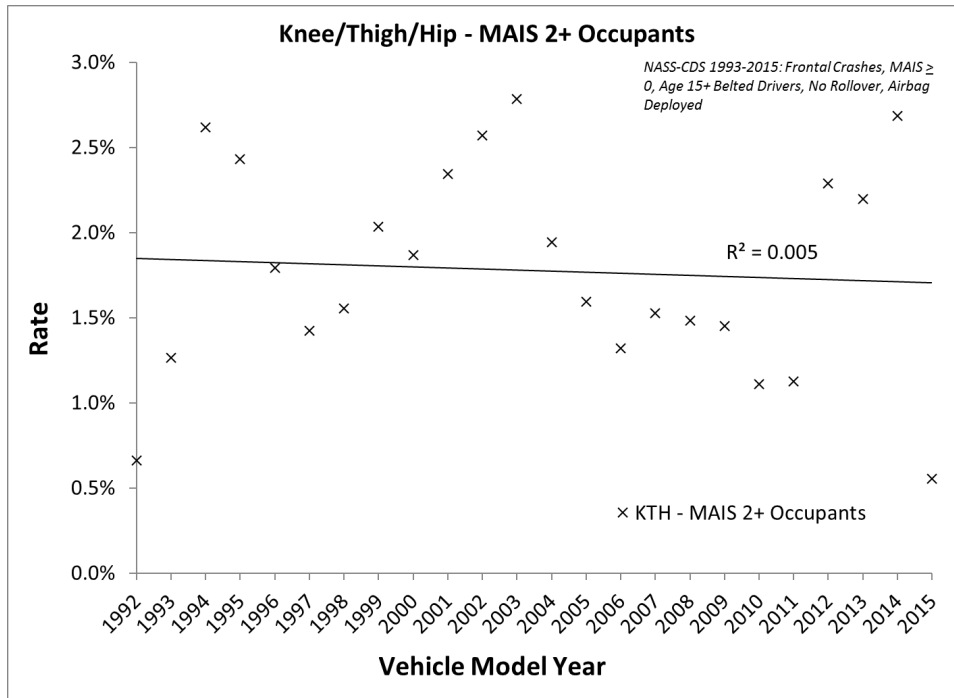


Figure 7.1. AIS 2+ knee/thigh/hip injury trends by vehicle model year (1992 to 2015) from frontal crashes in NASS-CDS (1993 to 2015).

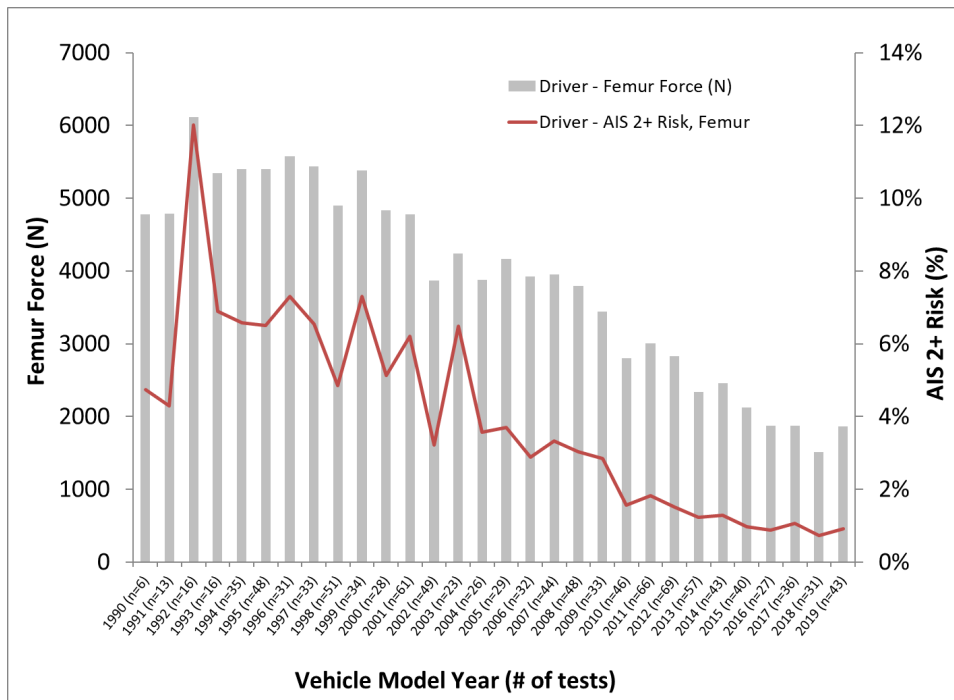


Figure 7.2. H3-50M frontal NCAP average peak femur axial force and injury risk (AIS 2+) for model year 1990 to 2019.

Figure 7.3 shows the regional mechanisms of injury assigned to knee, thigh, hip, and pelvis injuries in 165 CIREN front-row belted occupants involved in frontal crashes. These mechanisms are inferred from the available data and may have been limited to available researcher/published biomechanical knowledge at the time. It is important to note that the mechanisms shown are regional mechanisms, not local mechanisms at the component level. That is, the chosen mechanism represents the type of loading/motion experienced by the entire knee/thigh/hip region. The overwhelming majority of injuries to the knee, thigh, and hip region are due to compression – in most cases directed along the length of the femur.

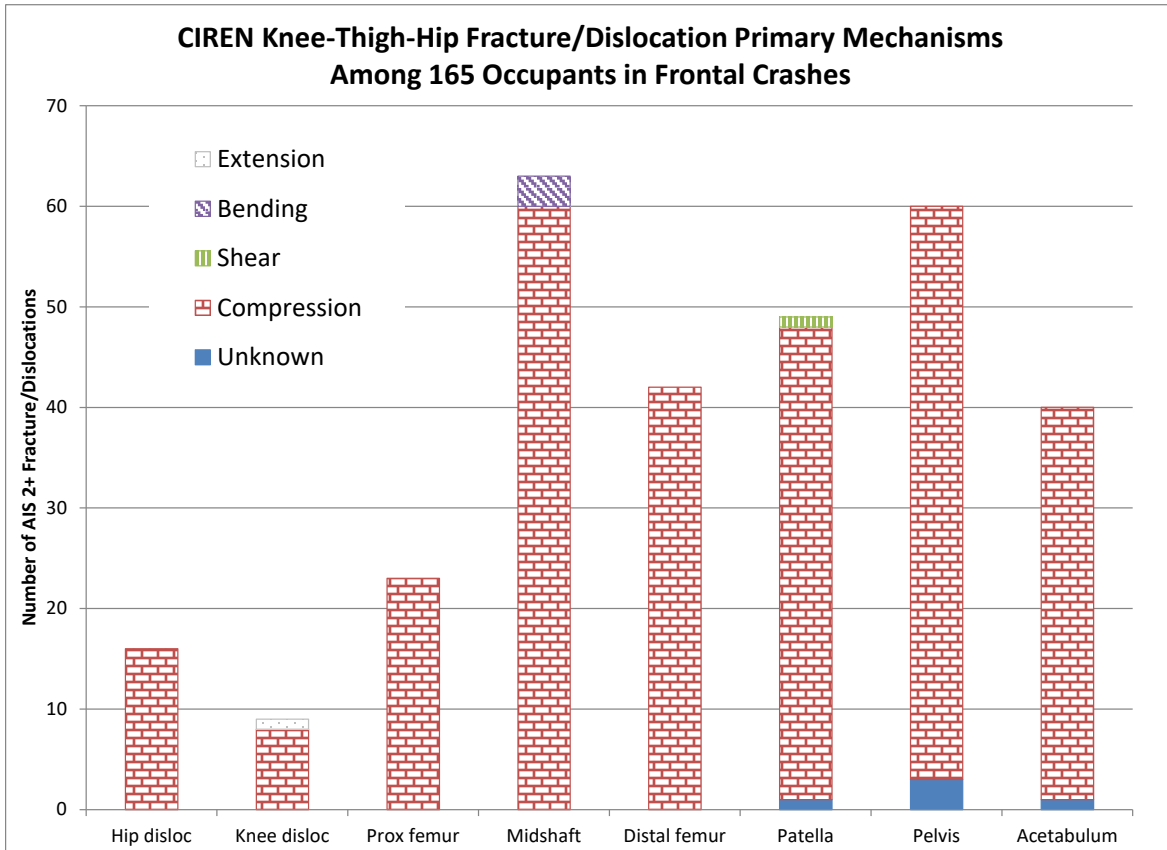


Figure 7.3. Recorded mechanisms of knee, thigh, hip, and pelvis injuries for belted front row occupants involved in frontal crashes from the CIREN database.

7.2 Literature Review

The importance of protection of the knee, thigh, and hip in motor vehicle crashes is highlighted by the research of Rudd et al. (2011), who showed that AIS 3+ KTH injuries were the most commonly-occurring injuries in small overlap and oblique frontal crashes.

In both FMVSS No. 208 and Frontal NCAP, the only KTH injury assessment carried out is an assessment of femur fracture risk based on peak compressive force. As applied in FMVSS No. 208, the IARV for femur compressive force measured by the H3-50M is 10 kN (49 CFR 571.208.S6.5), while the femur force

injury risk function presented by Eppinger et al. (1999) is used in the Frontal NCAP rating system (NHTSA, 2008).

Since the implementation of the injury criteria development study carried out by Eppinger et al. (1999), a large body of work has been conducted and published by the University of Michigan Transportation Research Institute (UMTRI) to understand KTH injury mechanisms and injury prediction in frontal crashes (Rupp et al., 2003; 2005; 2006; 2009a; 2009b). These studies are referenced heavily where appropriate throughout this section.

7.3 Design

The knee/thigh/hip (KTH) region of the THOR-50M is configured to mimic the structure and range of motion of the human. Starting from the knee, a revolute joint at the knee allows flexion and extension of the lower leg with respect to the upper leg. A sliding joint at the interface between the distal femur and the proximal tibia at the knee allows linear translation perpendicular to the tibia that represents both bending of the proximal tibia and extension of the posterior cruciate ligament (PCL). At approximately the mid-shaft of the femur, a translational joint allows compression along the axis of the femur using a guided plunger which compresses a rubber element. This joint was designed to meet the human response to femur compression defined by Rupp et al. (2003). The proximal femur is attached to the pelvis through a spherical joint at the acetabulum, which in turn is attached to the body of the pelvis through a load cell. The pelvis bone is functionally rigid and includes a human-like iliac wing representation, and the entire pelvis is covered with a single-piece flesh component. A diagram of the topology and instrumentation of the THOR-50M KTH is shown in Figure 7.4.

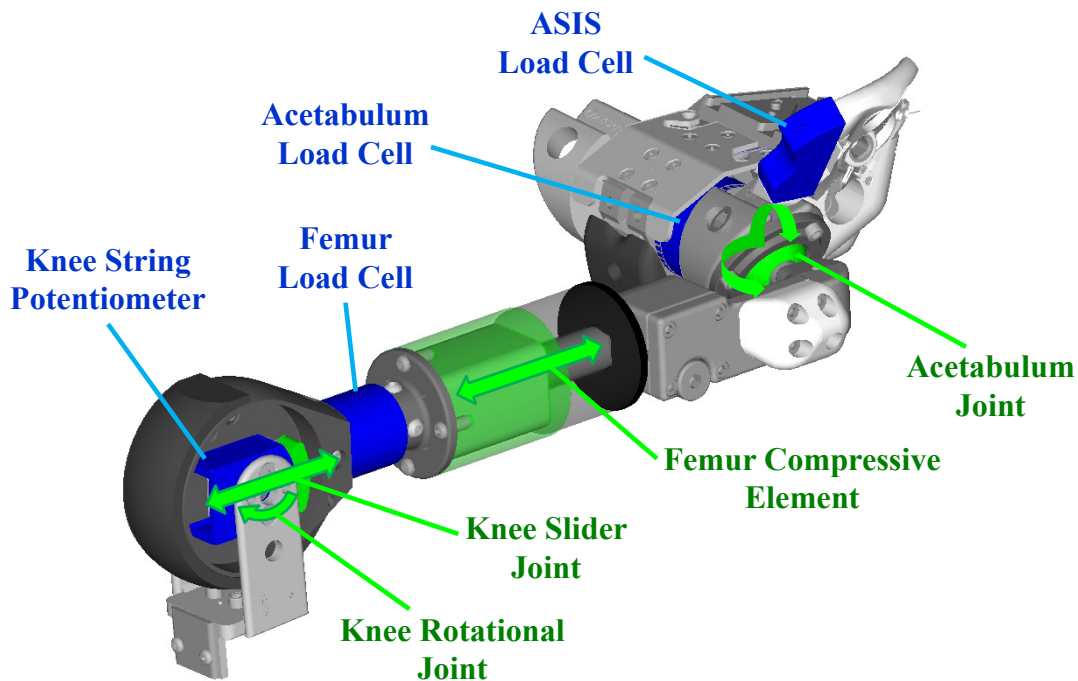


Figure 7.4. Joint and instrumentation configuration of THOR-50M KTH.

7.4 Instrumentation

THOR-50M ATD KTH instrumentation is summarized in Table 7.2.

Table 7.2. THOR-50M ATD thoracic instrumentation.

Sensor	Measurement Description	Measurement Axes
Knee string potentiometer	Translation of proximal tibia with respect to distal femur along an axis perpendicular to tibia	Displacement: XL
Femur load cell	Force and moment between knee and femur	Force: XL, YL, ZL Moment: XL, YL, ZL
Acetabulum load cell	Force between the proximal femur and the pelvis	Force: XL, YL, ZL
ASIS load cell	Force and moment applied to the ASIS, typically through lap belt loading	Force: XL Moment: YL

7.5 Biofidelity

Biofidelity of the THOR-50M KTH was assessed in two conditions (Parent et al., 2017): femur compression and knee shear. In the femur compression condition, the THOR-50M demonstrated good internal and external biofidelity with BioRank scores of 1.400 and 1.180, respectively, while the H3-50M demonstrated poor internal and external biofidelity. In the knee shear condition, for which only external BioRank scores are available, the THOR BioRank score was marginal (2.282), while the H3-50M demonstrated good biofidelity with BioRank score of 1.070.

7.6 Knee/Femur Injury

There are two injury mechanisms for which injury risk functions have been developed for the KTH: knee/femur injury and hip injury. These injury mechanisms are investigated independently and described in this section (knee/femur injury) and the following section (hip injury).

7.6.1 Knee/Femur Injury: Data

Assessment of injury related to knee/femur loading is not unique to THOR-50M, as a femur injury risk function has been developed for human subjects by Kuppa et al. (2001) and is currently being applied in consumer information testing using the Hybrid III family of frontal impact ATDs (NHTSA, 2008). This injury risk function was developed through logistic regression of the results of whole-body post-mortem human subject (PMHS) tests reported by Morgan et al. (1989). The dataset contained 126 tests, of which 14 had no reported data for applied knee force. Since applied knee force is the primary variable of interest, these 14 specimens were excluded. Of the remaining 112 tests (APPENDIX I), 34 sustained AIS 2 or greater injury. Although the injuries were predominantly to the knee (e.g. patella) and distal femur (e.g. femoral condyles), 11 specimens (33%) had thigh injuries (e.g. femoral shaft, femoral neck) and three specimens (9%) sustained hip injury (one of which was isolated and two of which had associated knee/femur injuries). Given the breadth of injuries sustained, the risk function is assumed to apply to all knee/femur injuries.

Rupp et al. (2009b) reanalyzed the same dataset using a Survival Weibull model in order to capture the censoring effects of the injury and non-injury data, though the difference between the resulting risk function and the risk function developed by Kuppa et al. (2001) was negligible (Figure 7.5) aside from the perceived benefit of the Survival Weibull model having exactly zero predicted risk at an applied force level of zero.

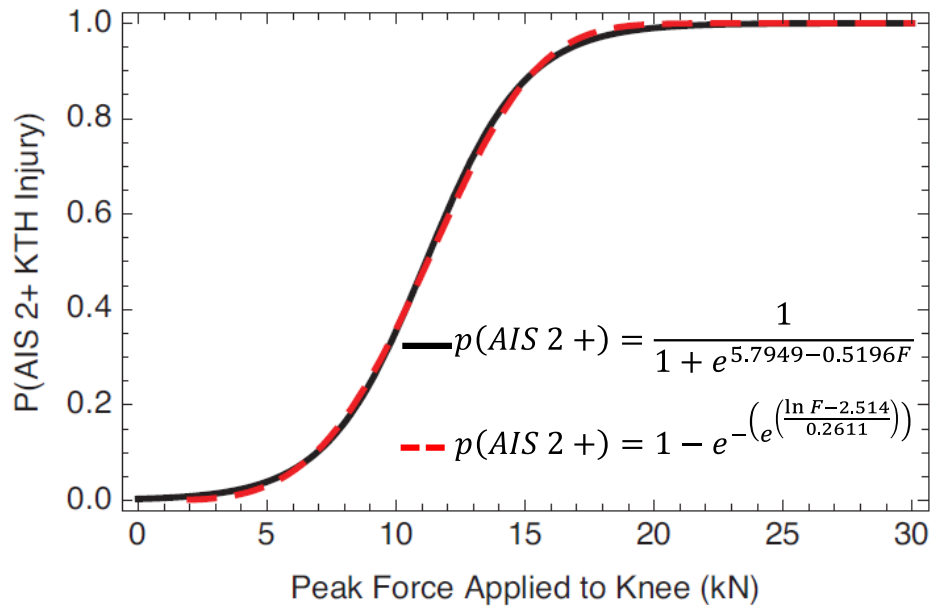


Figure 7.5. Comparison of logistic and Survival Weibull risk curves (modified from Rupp et al., 2009b).

However, neither of these risk functions considered the influence of subject characteristics. Per Rupp 2009b, characteristics such as age, sex, stature, and mass are likely to influence the relationship between peak applied force and injury risk. These characteristics were not investigated previously because their variability in the available data was small (Rupp, 2009b). Despite this statement, an initial review of descriptive statistics suggests some sex differences, as the uninjured female observations have a similar mean applied force to the uninjured male observations (6.2 kN for females compared to 6.92 kN for males) but a noticeably lower mean applied force in injured observations (8.9 kN for females compare to 14.6 kN for males). As such, a more detailed analysis was carried out.

7.6.2 Knee/Femur Injury: Predictor Variable

The peak applied force (as tabulated in APPENDIX I) was the only predictor variable considered for the development of the knee/femur injury risk function, as implanted femur load cell information was only available for a subset of the observations.

7.6.3 Knee/Femur Injury: Covariates

Parametric survival analysis (SAS PROC PHREG) using the stepwise variable selection method was carried out to examine the influence of sex, stature, mass, and age. The maximum significance level for entering

the model was 0.25 and the maximum significance level for staying in the model was 0.10; several other significance levels were tested but provided the same outcome. Using either censored or uncensored observations, none of the covariates demonstrated sufficient significance to enter and remain in the model. This was confirmed by reviewing the Akaike Information Criterion (AIC) value for models using all possible covariate combinations, where in all cases adding additional covariates increased the AIC value compared to a model using only peak applied force.

A similar analysis was carried out using parametric logistic regression (SAS PROC LOGISTIC) using the stepwise variable selection method to examine the influence of sex, stature, mass, and age. The same significance parameters were used as the parametric survival analysis described above. Aside from peak applied force, the covariates of sex and age were found to be a significant component of the model (sex: $\chi^2 = 12.8290, p < 0.0003$; age: $\chi^2 = 5.4897, p = 0.0191$). Mass was added to the model as well ($\chi^2 = 2.0081, p < 0.1565$), but was subsequently removed. Stature was not added to the model, though this may result from a strong correlation between stature and sex in this dataset.

Based on these findings, the covariates included in the remaining model development steps are sex and age.

7.6.4 Knee/Femur Injury: Dependent Variable

The dependent variable used in the development of a knee/femur injury criterion was the presence of an AIS 2+ injury to the femur or knee. In the experimental data described in Section 7.6.1, a majority of the injuries were fractures of the patella and femoral condyles, while a smaller subset of the injuries involved fractures to the femoral shaft, neck, and head, fractures to the proximal tibia, and ligamentous injuries.

7.6.5 Knee/Femur Injury: Injury Risk Function Formulation

7.6.5.1 Nonparametric

A nonparametric survival function was formulated using the SAS PROC LIFETEST procedure, using both the entire dataset (Figure 7.6), stratified by sex (Figure 7.7), and stratified by age group (Figure 7.8).

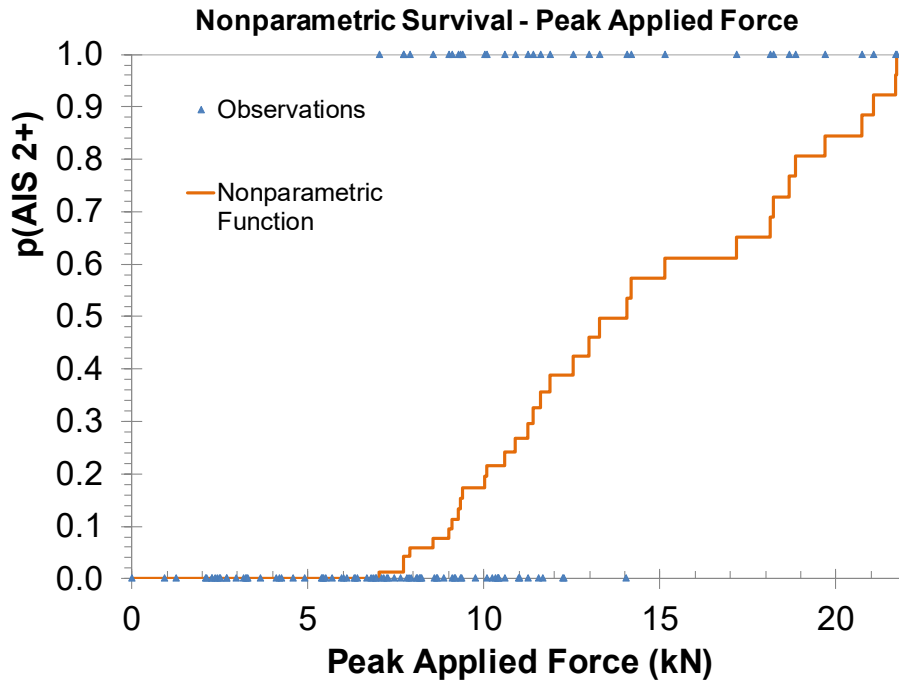


Figure 7.6. Femur/knee injury nonparametric survival function for all observations.

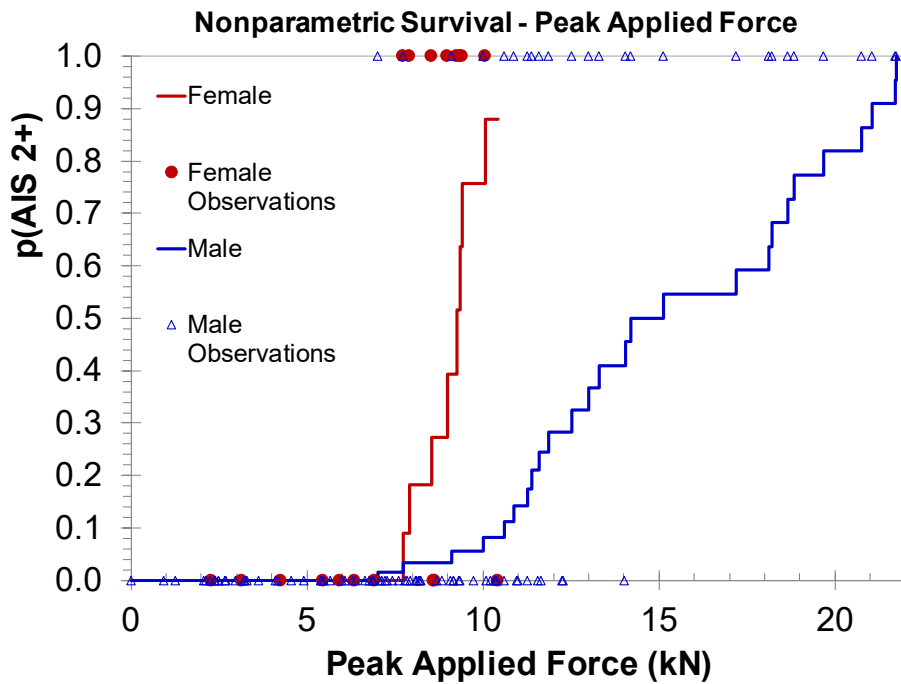


Figure 7.7. Independent femur/knee injury nonparametric survival functions for female (red, red circles) and male (blue, blue triangles) observations.

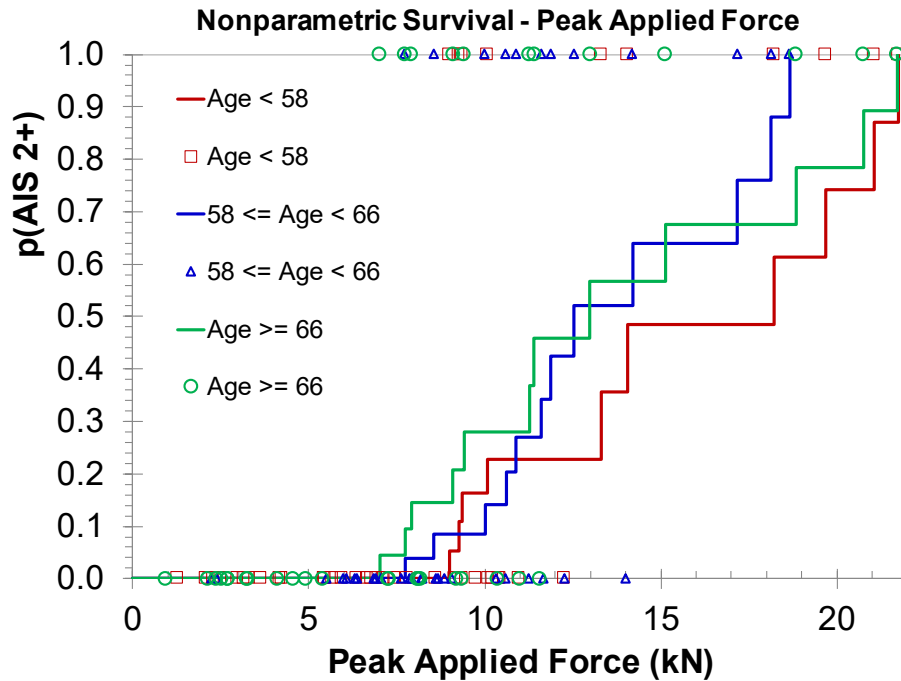


Figure 7.8. Independent femur/knee injury nonparametric survival functions for three evenly-distributed age groups: under 58 years (red, red squares), between 58 and 66 years (blue, blue triangles), and over 66 years (green, green circles).

7.6.5.2 Logistic Regression

Logistic regression was carried out to develop risk functions to relate peak applied force to risk of AIS 2+ femur/knee injury. Functions were developed both with and without the covariates of sex and age using the SAS PROC LOGISTIC procedure. For each combination, the AUROC, maximum log likelihood, and Hosmer-Lemeshow Goodness-of-Fit test results are reported in Table 7.3. The logistic regression risk functions take one of two forms:

Without Covariates:
$$p(\text{AIS } 3+) = \frac{e^{(\beta_0 + \beta_1 x)}}{1 + e^{(\beta_0 + \beta_1 x)}}$$

With Covariates:
$$p(\text{AIS } 3+) = \frac{e^{(\beta_0 + \beta_1 x + \beta_2 a + \beta_3 b)}}{1 + e^{(\beta_0 + \beta_1 x + \beta_2 a + \beta_3 b)}}$$

where:

- β_0 = Intercept
- β_1 = Independent parameter coefficient
- x = Independent parameter value
- β_2 = Age coefficient
- a = Subject age, in years
- β_3 = Sex coefficient
- b = Subject sex (Male = 1, Female = 0)

Table 7.3. Fit statistics for logistic regression models.

Covariates	N	β_0	β_1	β_2	β_3	-2 Log L	AIC	AUROC	Hosmer and Lemeshow Pr>ChiSq
None	112	-5.795	0.5196			83.128	87.128	0.879	0.6682
Age	112	-10.604	0.5373	0.0751		78.317	84.317	0.897	0.5601
Sex	112	-5.4531	0.6727		-2.4308	71.418	77.418	0.919	0.6263
Sex and Age	112	-16.675	0.7658	0.1777	-3.453	61.654	69.654	0.942	0.8632

The logistic regression models demonstrate that including one covariate increases the area under the ROC curve (Figure 7.9), with a larger increase when including sex as compared to age. The model including both age and sex shows the highest AUROC.

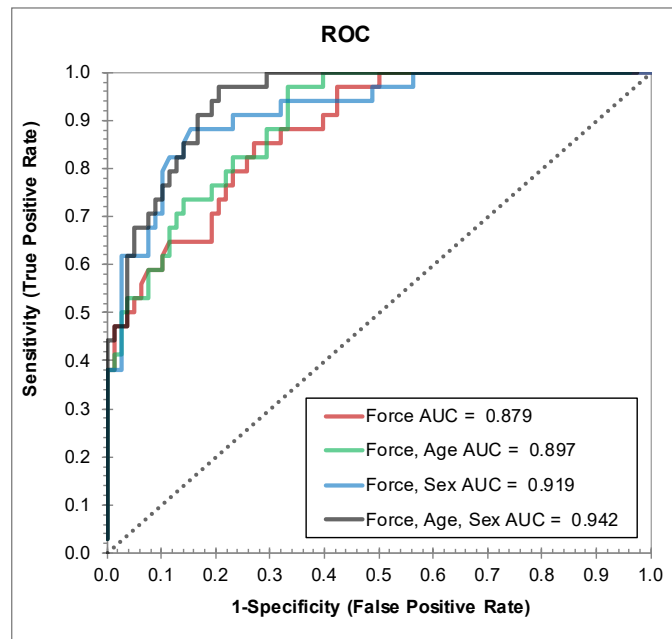


Figure 7.9. Receiver Operating Characteristic (ROC) for the logistic regression models shown in Table 7.3.

The risk function and associated confidence intervals for the model including only peak applied force are shown in Figure 7.10. The risk functions and confidence intervals for the models including covariates were evaluated at two different values for each of the covariates, if included in the model (Figure 7.11). Models including age as a covariate were evaluated at 40 years old, the mean age of exposed male drivers in frontal crashes, and 61 years old, the mean age of the PMHS in the dataset. Models including sex as a covariate were evaluated for both males and females. In general, the models calculated at age 40 show wider confidence intervals compared to those calculated at age 61, which is expected since presenting the model at an age further away from the mean age of the underlying dataset requires more extrapolation. The model prediction for female subjects shows a higher risk for a given peak applied force than the model prediction for males. For example, the model including only sex as a covariate predicts a 50% risk of AIS 2+ injury at a peak applied force of 11.7 kN for males and 8.1 kN for females, which is consistent with the descriptive statistics discussed earlier.

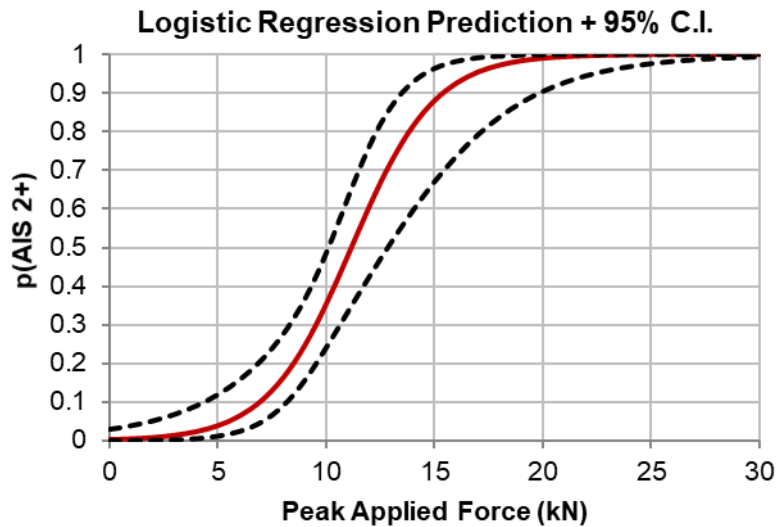


Figure 7.10. Logistic risk function relating peak applied force (without covariates) to AIS 2+ femur/knee injury.

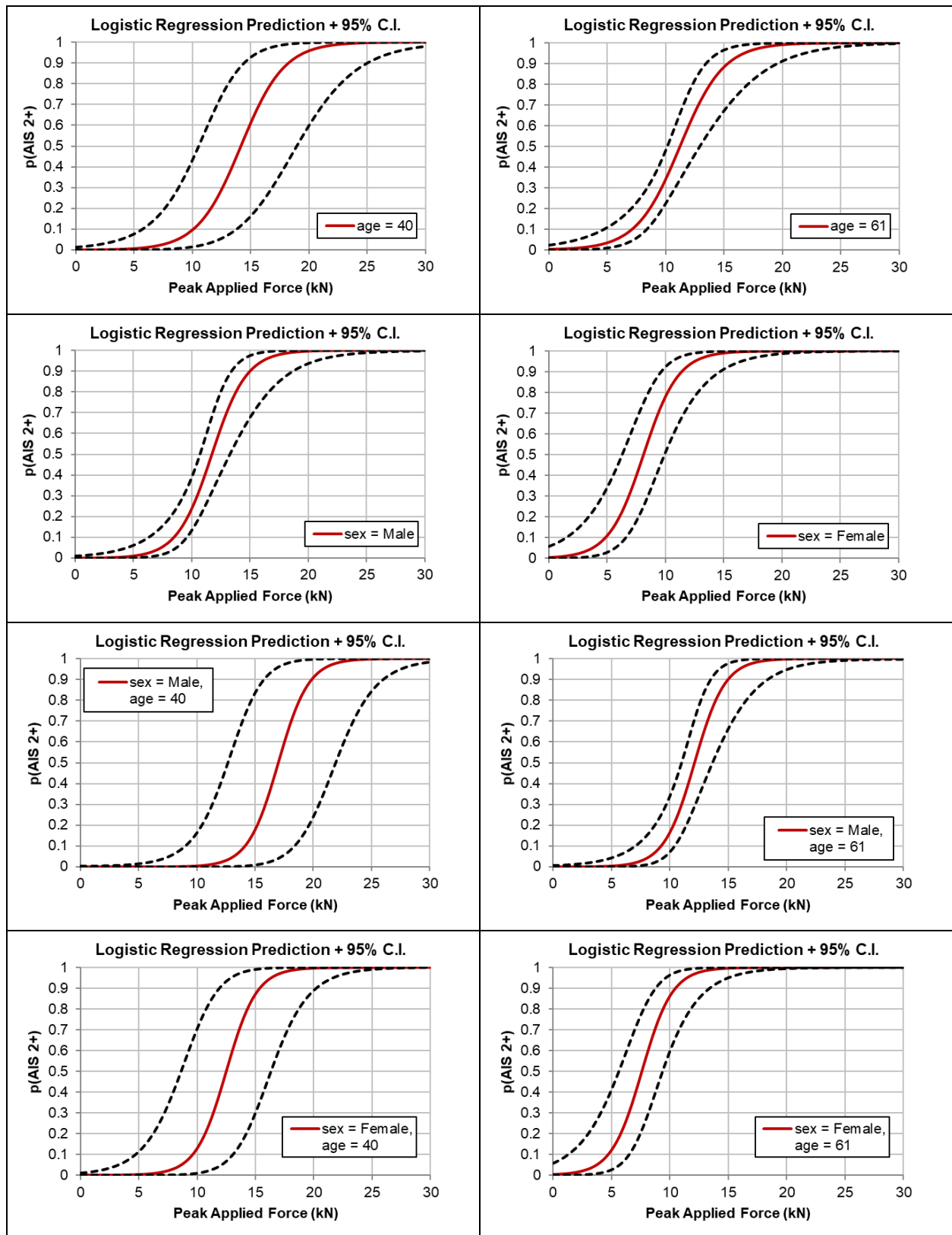


Figure 7.11. Risk function and confidence intervals for logistic models including age (top row), and sex (second row), and both sex and age (bottom two rows) as covariates.

In the model including both sex and age as covariates, the confidence intervals partially overlap when evaluated at 40 years of age (Figure 7.12, left) but only overlap in the tails when evaluating at 61 years of age (Figure 7.12, right). Comparing the male and female predictions, the difference in risk is similar when evaluated at 40 or 61 years, as either way the 50% risk of AIS 2+ injury for females occurs around 4.5 kN of peak applied force lower than for males. However, the confidence intervals are much wider when evaluated at 40 years.

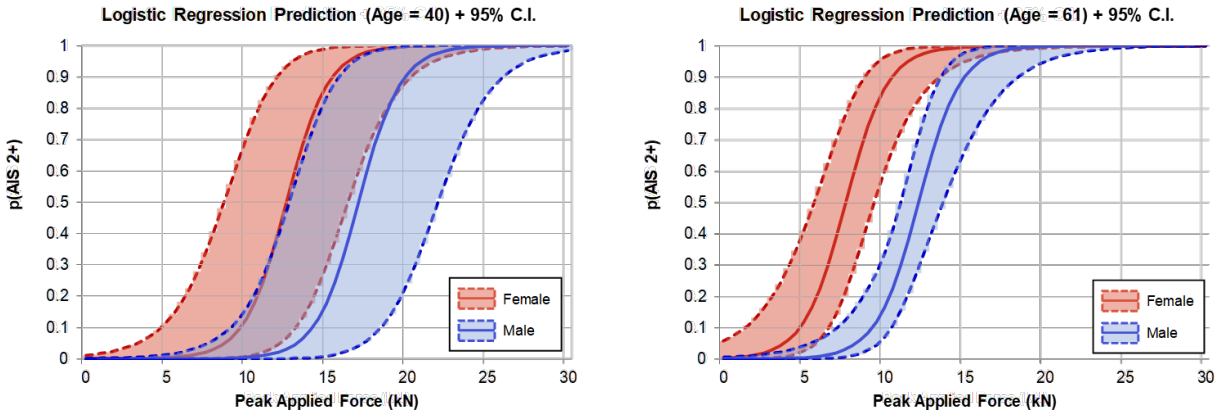


Figure 7.12. Comparison of logistic model confidence intervals between male and female covariate values, presented at ages of 40 years (left) and 61 years (right).

7.6.5.3 Survival Analysis

Survival analysis was also carried out to develop risk functions to relate peak applied force to risk of AIS 2+ femur/knee injury. Functions were developed both with and without the covariates of sex and age using the SAS PROC LIFEREG procedure to estimate model parameters and confidence intervals. Analyses were carried out using three different censoring schemes: uncensored, where non-injury observations are treated as right-censored and injury observations are treated as uncensored; censored, where non-injury observations are treated as right-censored and injury observations are treated as left-censored; and Rupp-censored, where data followed the censoring rationale presented by Rupp at al. (2009b) as documented in APPENDIX I. Models were developed assuming several different probability distributions to determine the best fit to the data. Of these, the two best distributions were Weibull and Lognormal. For each combination of covariates, distribution, and censoring assumptions, model estimates and fit statistics are reported in Table 7.4.

The Survival Weibull model takes the form:

$$p(\text{AIS } 2+) = 1 - e^{-\left(\frac{F_{\text{applied}}}{e^{(\beta_0 + \beta_1 c_1 + \beta_2 c_2)}}\right)^\alpha}$$

where:

F_{applied}	=	Peak force applied to knee (in kN)
β_0	=	Intercept
β_1	=	Age coefficient
c_1	=	Subject age, in years
β_2	=	Sex coefficient
c_2	=	Subject sex (Male = 1, Female = 0)
α	=	1/scale

The Survival Lognormal model takes the form:

$$p(\text{AIS } 2+) = \Phi \left[\frac{\ln F_{\text{applied}} - (\beta_0 + \beta_1 c_1 + \beta_2 c_2)}{\sigma} \right]$$

where:

Φ	=	Cumulative normal distribution function
F_{applied}	=	Peak force applied to knee (in kN)
β_0	=	Intercept
β_1	=	Age coefficient
c_1	=	Subject age, in years
β_2	=	Sex coefficient
c_2	=	Subject sex (Male = 1, Female = 0)
σ	=	Standard deviation or scale

Table 7.4. Parameter estimates and fit statistics for survival analysis models.

Predictor	Covariate(s)*	Distribution	β_0	β_1	β_2	α	-2 LL	AIC
Peak Applied Force at Knee, uncensored	None	Weibull	2.7814			0.2573	42.95	46.95
	Age	Weibull	2.9429	-0.0026		0.2591	42.57	48.57
	Sex	Weibull	2.2871		0.5557	0.2015	21.54	27.54
	Age and Sex	Weibull	2.4817	-0.0033	0.5701	0.2030	20.67	28.67
	None	Lognormal	2.6172			0.3124	38.78	42.78
	Age	Lognormal	3.0087	-0.0062		0.3129	37.37	43.37
	Sex	Lognormal	2.2665		0.4181	0.2630	22.24	28.24
	Age and Sex	Lognormal	2.8461	-0.0097	0.4536	0.2584	18.73	26.73
Peak Applied Force at Knee, censored	None	Weibull	2.5140			0.2611	81.98	85.98
	Age	Weibull	3.3936	-0.0143		0.2561	77.58	83.58
	Sex	Weibull	2.1876		0.3638	0.2049	71.13	77.13
	Age and Sex	Weibull	3.3417	-0.0197	0.4323	0.1830	62.81	70.81
	None	Lognormal	2.3859			0.3297	82.26	86.26
	Age	Lognormal	3.2587	-0.0142		0.3180	76.91	82.91
	Sex	Lognormal	2.0825		0.3646	0.2680	71.79	77.79
	Age and Sex	Lognormal	3.3609	-0.0216	0.4357	0.2247	61.95	69.95
Peak Applied Force at Knee, censored per Rupp 2009b	None	Weibull	2.7342			0.3028	69.54	73.54
	Age	Weibull	2.9965	-0.0041		0.3080	68.80	74.80
	Sex	Weibull	2.2810		0.5124	0.2489	55.37	61.37
	Age and Sex	Weibull	2.5668	-0.0048	0.5359	0.2540	54.12	62.12
	None	Lognormal	2.5543			0.3487	65.78	69.78
	Age	Lognormal	3.0830	-0.0084		0.3510	63.55	69.55
	Sex	Lognormal	2.2240		0.3959	0.3014	54.20	60.20
	Age and Sex	Lognormal	2.9114	-0.0115	0.4423	0.2982	50.03	58.03

*Covariate units: sex represented by male = 1, female = 0; age in years

For most models, the fit statistics of AIC and -2 LL indicate that those assuming a Lognormal distribution provide a better fit than their Weibull counterparts. In all cases, models including both sex and age as covariates show a lower -2 LL than models with either no covariates or only one covariate. However, when considering the AIC, models with two covariates are similar to models with only sex as a covariate, and in two cases (uncensored Weibull, Rupp-censored Weibull) the model with only sex as a covariate demonstrates a better fit.

Comparing models with no covariates, the censored models predict a higher risk for a given peak applied force (Figure 7.13). The Rupp-censored and uncensored models are more similar, with a slightly higher risk predicted by the Rupp-censored models compared to uncensored models. The shape of the Weibull and Lognormal models differ, with the Weibull models predicting lower risk in the middle of the curve and higher risk in the tails.

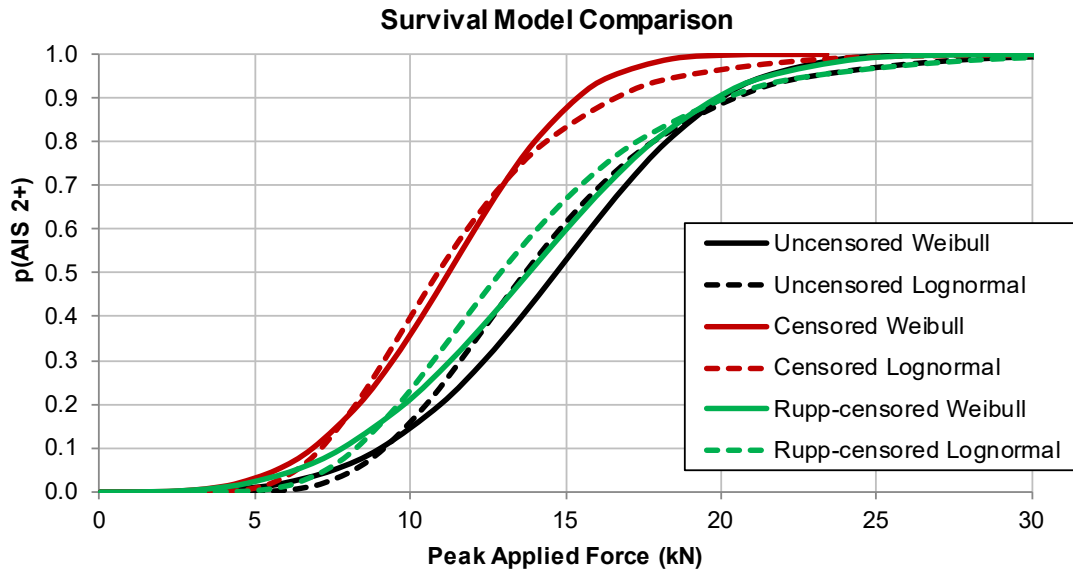


Figure 7.13. Comparison of survival models with no covariates using different censoring schemes, with models assuming a Weibull distribution in solid lines and models assuming a Lognormal distribution in dashed lines.

The censored Weibull model with no covariates is the most similar of the models to the Logistic regression model without covariates (Figure 7.10). This is not surprising, as the parameter values ($\beta_0 = 2.514$, $\alpha = 0.2611$) are identical to those presented in Equation 6.2 from Rupp et al. (2009b). However, this risk function results from treating all observations as censored. When implementing the censoring scheme described in Section 5.2 of Rupp et al. (2009b) and its associated Appendix A, the resulting risk function (Rupp-censored Weibull) appears to be shifted to the right by roughly 3 kN (Figure 7.13).

Comparing models with covariates, similar trends appear. Figure 7.14 shows Survival Lognormal model predictions using the three different censoring schemes, each evaluated at two values of sex. Within each sex, the censored model predicts the highest risk, followed by the Rupp-censored and uncensored models. The difference in risk between male and female models is the lowest for the censored model and progressively higher for the Rupp-censored and then uncensored models. For example, the difference in peak applied force at a 50% risk level is lower for females by 3.5 kN in the censored model, 4.5 kN in the Rupp-censored model, and 5.0 kN in the uncensored model.

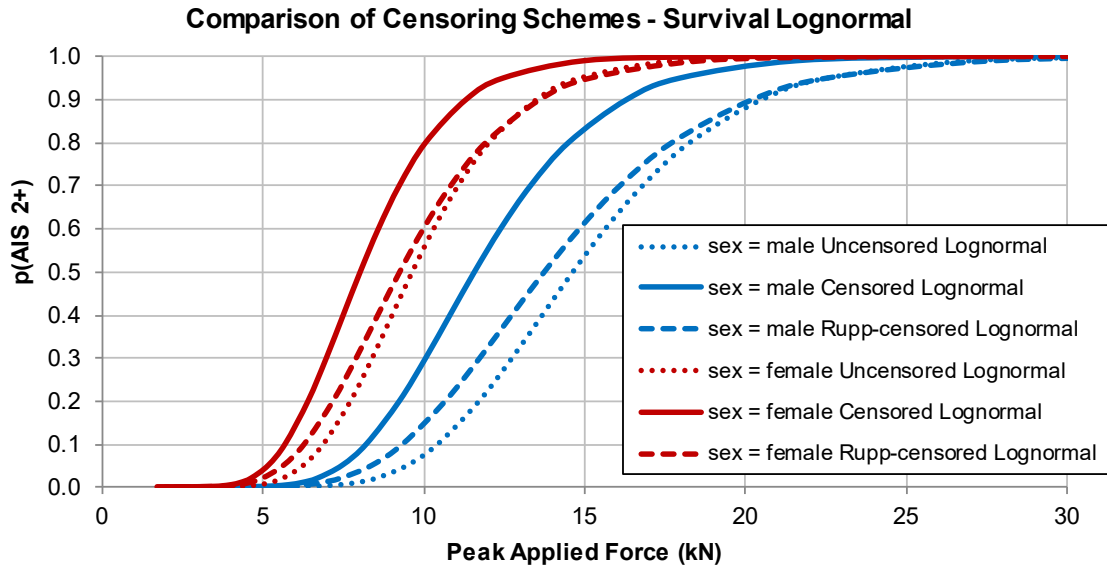


Figure 7.14. Comparison of survival lognormal models with sex as a covariate using different censoring schemes, with uncensored models in dotted lines, censored models in solid lines, and Rupp-censored models in dashed lines. Models evaluated at the covariate values of male and female are shown in blue and red, respectively.

For all censoring schemes, including sex as a covariate had a significant effect on the model prediction, based on Type III Analysis of Effects ($p < 0.01$ in all cases). Including age as a covariate, on the other hand, only showed a significant effect ($p < 0.05$) in the censored models (for both Weibull and Lognormal distributions) when including both age and sex as covariates.

Similar to the logistic regression analysis, confidence intervals for the survival lognormal models with age as a covariate are much larger when evaluating at an age of 40 years, the mean age of exposed male drivers in frontal crashes, compared to 61 years old, the mean age of the PMHS in the dataset. Likewise, in the models that include both sex and age as covariates, the confidence intervals for males and females overlap when evaluated at an age of 40 years (Figure 7.15, left), but only overlap in the tails when evaluated at an age of 61 years (Figure 7.15, right). The overlap of the confidence intervals for the Survival Lognormal prediction, shown here for the censored model, are more pronounced than in the logistic regression model. Also unlike the logistic regression model, the point estimates between the male and female groups are sensitive to age, as difference in peak applied force at the 50% risk level is 6.9 kN lower for females at age 40 and 4.4 kN lower for females at age 61.

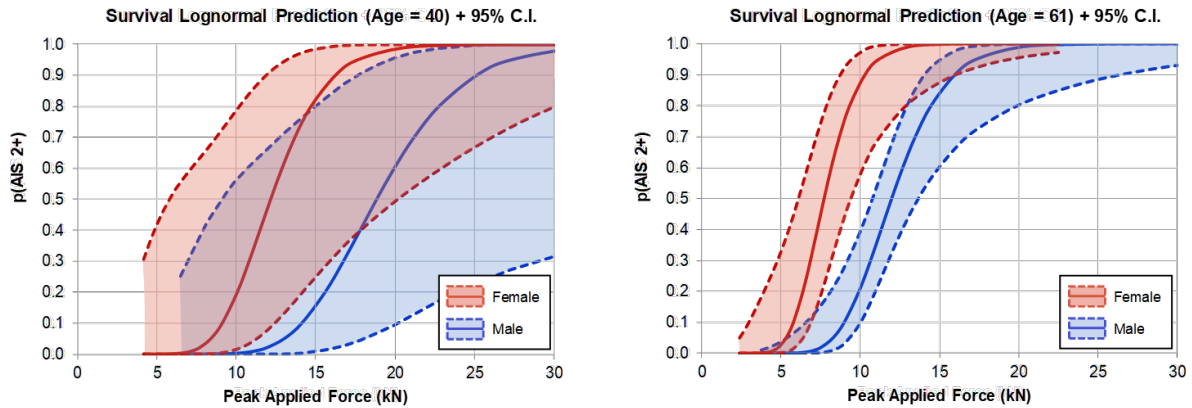


Figure 7.15. Comparison of Survival Lognormal censored model confidence intervals between male and female covariate values, presented at ages of 40 years (left) and 61 years (right).

The three censoring schemes result in noticeably different risk functions and covariate effects. The uncensored scheme assumes that the injured specimens sustained AIS 2+ injuries at exactly the measured peak force applied to the knee, which is unlikely and could only be confirmed using measurement techniques that were not available at the time of these tests. The censored scheme, on the other hand, may overcorrect for this phenomenon in that it assumes no exact injury magnitudes are known, so injuries may have occurred up to (but not greater than) the peak applied force at the knee. However, as described in Rupp et al. (2009b), certain injury types other than femur fractures may still support additional increases in force beyond the point of injury, thus the assumption of peak applied force representing an absolute maximum would not be true. The Rupp-censored scheme treats uninjured observations and specimens sustaining only ligamentous injuries as right-censored, injuries involving the patella as left-censored, and injuries involving femur fracture as exact.

Of the three censoring options, the Rupp-censored scheme requires the fewest assumptions, thus will be used in the remaining analysis of knee/femur injury risk. Within the Rupp-censored models, those assuming a Lognormal distribution result present the best model fit as assessed by $-2 LL$ and AIC. The Lognormal model including both age and sex as covariates presents the lowest AIC, but due to the large confidence intervals when presented at an age of 40 (which, based on Section 2.5, would be used in application to THOR-50M) and the non-significant effect of the age covariate in the model, the model with sex alone as a covariate is preferred.

7.6.6 Knee/Femur Injury: Application to THOR-50M

While the risk curves presented in Section 7.6.5 relate the peak force applied to the knee to the risk of knee and distal femur injury, the injury risk function has been applied for the H3-50M (e.g. as applied in the New Car Assessment Program) using the peak force measured by the femur load cell (NHTSA, 2008). Several studies have demonstrated that the peak force measured in the femur is lower than the peak force applied to the knee for both PMHS and ATDs. Donnelly et al. (1987) conducted pendulum impacts to the unrestrained femur of whole subjects for both PMHS and the H3-50M. The PMHS tests from this study were included in the Morgan et al. (1989) and Kuppa et al. (2001) analyses. In the PMHS tests, an implanted load cell in the shaft of the femur measured force in a similar fashion to the H3-50M femur

load cell. It was found that in the PMHS tests, there was a strong correlation between the force measured at the implanted femur load cell and the force applied to the knee, with the femur load cell measuring 53% of the peak applied force. An even stronger correlation was found in the H3-50M tests, but a higher ratio of the impact force was measured at the femur load cell (68%). A separate estimate of the relationship between H3-50M measured femur load cell forces and applied force to the knee was developed by Rupp et al. (2009a) in a test apparatus developed to represent knee bolster impacts in frontal crash tests. In these tests, the peak force measured at the H3-50M femur load cell was 77% of the applied force independent of knee bolster force-deflection characteristic.

Using the measured H3-50M femur load cell peak force instead of the peak applied force as input to the injury risk function would result in a *lower* estimate of injury risk than intended. For instance, if the H3-50M measured a 10 kN peak femur force, the estimated force applied to the knee of the H3-50M would be either 13.0 kN, assuming the Rupp et al. (2009a) estimate of 77%, or 14.7 kN, assuming the Donnelly et al. (1987) estimate of 68%. Using the measured H3-50M force directly in the Kuppa et al. (2001) injury risk function would predict a 35% risk of AIS 2+ injury, while using the estimated force applied to the knee as the input to the risk function as originally developed would result in a predicted injury risk of 70% to 85%.

Due to the improvements in biofidelity of the THOR-50M compared to the H3-50M, it is assumed that the limitations of the application of the knee/femur injury risk function developed by Kuppa et al. (2001) are only alleviated when applied to THOR-50M compared to H3-50M. However, since the construction of the THOR-50M knee is similar to that of the H3-50M and is likely more coupled than the human knee, the force measured at the femur load cell is still lower than the force applied to the knee. Therefore, correction for this difference between applied force at the knee and peak force measured at the load cell is recommended before calculation of injury risk.

Several approaches were investigated to determine the relationship of the peak applied force at the knee to the peak force measured at the femur load cell of the THOR-50M. One approach would be to assume the same relationship as the H3-50M, for which the distal femur and knee structure is nearly identical. Another approach was to investigate pendulum impacts to the knee of the THOR-50M in a qualification test condition, as described below.

Seated knee impacts to the THOR-50M were conducted at several impact velocities and impact conditions using a 5-kilogram pendulum impactor. In an unrestrained back condition, the knee was impacted at six increasing velocities. The average of the ratios between peak load cell force and peak applied force computed at each velocity is 58%, and a linear fit to the data for each set results in ratio of slopes of 55% (Figure 7.16). However, the ratio of measured force to applied force appears to follow a higher-order polynomial or power relationship, with impacts at lower velocities being closer to an equal ratio. Tests were also conducted in a fixed-back condition at six impact velocities, and the resulting ratios of peak femur load cell force to peak applied force was consistently 55% (Figure 7.17), though this may be due to the smaller range of velocities in the fixed-back condition.

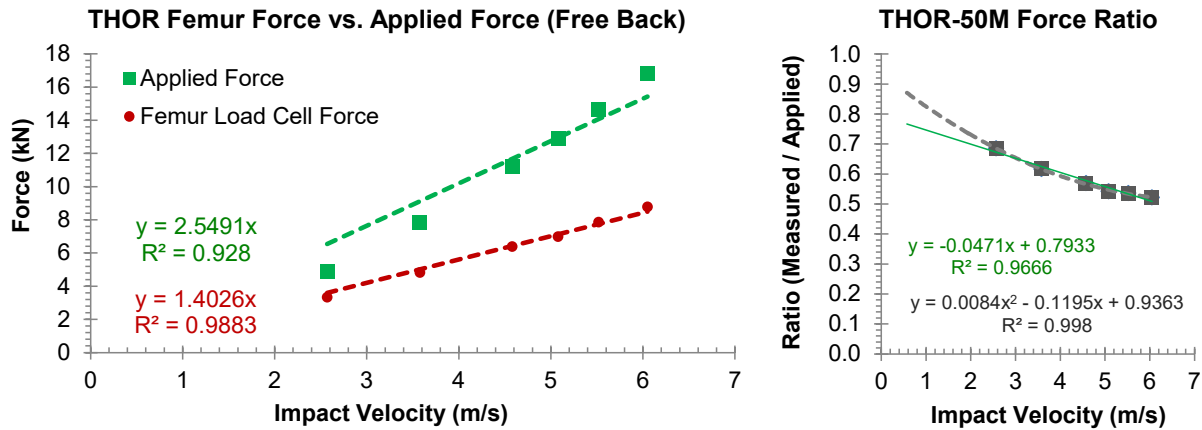


Figure 7.16. Relationship between force applied to the femur and force measured at the femur load cell for free-back tests with THOR-50M.

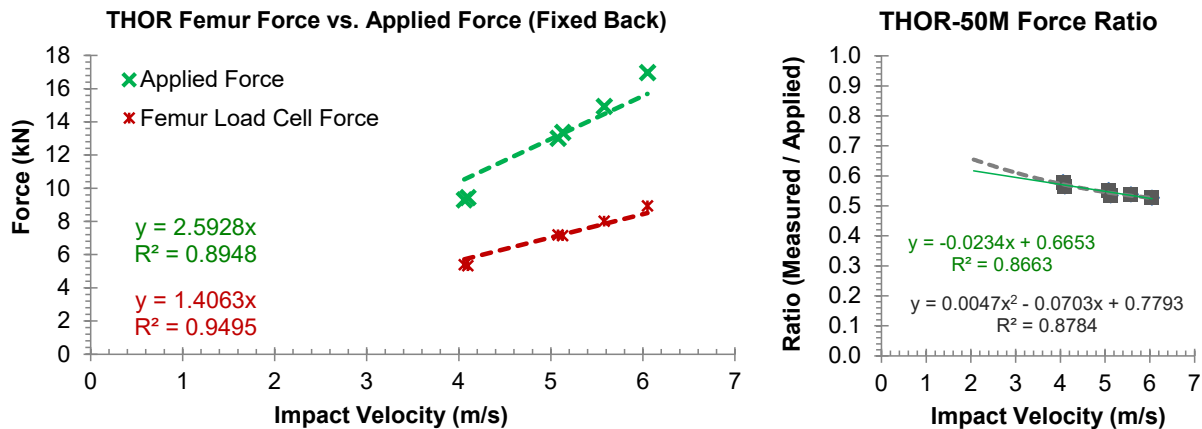


Figure 7.17. Relationship between force applied to the femur and force measured at the femur load cell for fixed-back tests with THOR-50M.

While these results suggest that the relationship of applied femur force to load cell force for THOR is more similar to the PMHS than Hybrid III, it is not clear how significant the difference in impact mass might be, as the tests reported by Donnelly et al. (1987) used a 23-kilogram impactor while the THOR tests reported above used a 5-kilogram impactor. It is also unclear how well either condition relates to the loading condition seen in a motor vehicle crash, where the femurs are restrained by the knee bolster and loaded inertially by the remaining effective mass of the body. In addition, because the relationship between applied force at the knee and measured force at the femur load cell in THOR-50M was shown above to be sensitive to impact velocity in pendulum testing (Figure 7.16 and Figure 7.17), selection of a single transfer function would not be straightforward because the impact velocity could not be measured during a crash test.

For the reasons described above, it is not recommended to use pendulum impacts to the knee of the THOR-50M in a qualification test condition to develop the correction factor for peak applied knee force to the peak measured femur force. Instead, the analysis presented by Rupp et al. (2009a) in testing of

the H3-50M under loading rates occurring in FMVSS No. 208 and US NCAP crash tests is recommended as the knee and distal femur of the THOR-50M and H3-50M are structurally similar. Therefore, a correction factor accounting for the estimated 77% of the applied force at the knee measured by the femur load cell force is recommended for THOR-50M.

In summary, the recommended risk function for application to THOR-50M to predict AIS 2+ knee/femur injury is described below:

$$p(\text{AIS } 2+) = \Phi \left[\frac{\ln(F_{LC} \times r_{KtoF}) - (2.224 + 0.3959\♂)}{0.3014} \right]$$

where:

- Φ = Cumulative normal distribution function
- F_{LC} = Peak compressive force measured by the z-axis for the THOR femur load cell (in kN)
- r_{KtoF} = Ratio of applied force at knee to measured force at femur load cell [1/0.77] (Rupp et al., 2009a)
- $\♂$ = Subject sex (Male = 1, Female = 0)

Simplified:

$$p(\text{AIS } 2+) = \Phi \left[\frac{\ln(1.299F_{LC}) - 2.62}{0.3014} \right]$$

7.7 Hip Injury

Contrary to knee/femur injury, the prediction of pelvis injury related to axial femur loading is a unique capability of THOR-50M due to its biofidelity and instrumentation. As such, further analysis is necessary to determine an appropriate injury risk function to predict injury to the pelvis in motor vehicle crashes.

7.7.1 Hip Injury: Data

Rupp et al. conducted compressive loading tests of 27 PMHS knee-thigh-hip complex specimens using a pneumatic ram (Rupp et al., 2009b). The iliac wing of the specimen was fixed and the knee was loaded along the axis of the femur through a molded knee interface. The target loading rate was 300 N/ms, which was argued to be representative of knee-bolster loading rates seen in unbelted crash tests (Rupp et al. 2003), though individual specimen loading rates varied from 62 N/ms to 566 N/ms. For the dataset presented in Rupp et al. (2009b), the specimens were positioned in a “neutral” posture consistent with standard driving posture as defined by Schneider et al. (1983). Additional tests were conducted with flexion and adduction applied and it was found that there was a statistically-significant decrease in tolerance with increase in both flexion and adduction compared to the standard driving posture (Rupp et al. 2003). For completeness, both the neutral posture dataset presented by Rupp et al. (2009b), referred to here as “Neutral” and including all specimens with flexion and adduction angles of 0°, and the complete set of tests documented in Rupp (2006), referred to here as “Complete,” are considered in this analysis. Subject anthropometry and associated fracture forces are shown in Table 7.5.

Table 7.5. Dataset considered in the development of a hip injury risk function (Rupp 2006).

Test ID	Fracture force (kN)	Sex	Age (yr)	Stature (cm)	Mass (kg)	Adduction (deg)	Flexion (deg)	NHTSA BioDB TSTNO
NB0105L	5.59	F	55	163	113	0	0	5240
NB0105R	5.37	F	55	163	113	0	0	5241
NB0106L	4.85	M	86	173	91	0	0	5419
NB0108L	7.57	M	79	180	82	0	0	5423
NB0108R	7.87	M	79	180	82	0	0	5424
NB0110L	6.6	M	60	178	125	0	0	5427
NB0112L	4.53	M	72	173	81	0	30	5861
NB0112R	6.67	M	72	173	81	0	0	5862
NB0114L	3.06	F	68	165	71	0	30	5864
NB0114R	4.65	F	68	165	71	0	0	5865
NB0216L	3.9	F	71	178	82	0	30	
NB0216R	5.59	F	71	178	82	0	0	
NB0217L	4.79	M	75	175	72	0	0	5924
NB0217R	2.91	M	75	175	72	0	30	5925
NB0218L	5.57	M	72	178	82	0	0	5926
NB0218R	5.35	M	72	178	82	-10	0	5927
NB0222L	8.85	M	41	176	91	0	0	6177
NB0222R	7.87	M	41	176	91	-10	0	6179
NB0224R	3.92	M	60	178	82	0	0	6189
NB0225L	5.65	F	86	168	68	0	0	6213
NB0225R	5.83	F	86	168	68	0	0	6215
NB0226L	6.6	M	62	183	91	0	0	6217
NB0228L	3.08	F	65	163	82	-10	0	6246
NB0228R	4.05	F	65	163	82	0	0	6248
NB0230L	4.71	M	45	185	75	-10	0	6493
NB0230R	6.09	M	45	185	75	0	0	6495
NB0231L	4.48	F	79	165	91	-10	0	6497
NB0231R	5.63	F	79	165	91	0	0	6499
NB0234L	8.17	M	74	175	100	0	0	6532
NB0234R	8.17	M	74	175	100	10	15	6534
NB0337L	5.09	M	58	175	62	10	15	6719
NB0337R	5.09	M	58	175	62	0	0	6722
NB0338LH	3.48	M	86	173	59	-10	0	6725
NB0338RH	4.59	M	86	173	59	0	0	6727
NB0340RH	7.54	M	63	183	66	0	0	
NB0341RH	6.89	M	79	165	68	0	0	6812
NB0342RH	6.26	M	83	189	93	0	0	6987
NB0343RH	9.79	M	79	191	109	0	0	6991
NB0345LH	5.75	M	82	173	75	10	0	6998
NB0345RH	5.11	M	82	173	75	0	0	7001
NB0447LH	7.69	F	49	157	59	10	0	7564
NB0447RH	6.14	F	49	157	59	0	0	7567
NB0448LH	6.1	M	76	178	80	10	0	7570
NB0448RH	6.13	M	76	178	80	0	0	7573
NB0450LH	6.03	M	73	178	86	0	0	7613
NB0450RH	6.12	M	73	178	86	10	0	7616

7.7.2 Hip Injury: Predictor Variable

The peak applied force (as tabulated in Table 7.5) was the only predictor variable considered for the development of the pelvis injury risk function. In line with the rationale presented in Rupp et al. (2009b), since each test resulted in some combination of hip fracture (fracture of the acetabulum, pubic rami,

femoral head/neck, and/or hip dislocation) and there were no evident partial failures prior to the time of peak applied force, it is assumed that the peak applied force is a known point of failure and considered to be uncensored.

7.7.3 Hip Injury: Covariates

To confirm the assumptions of Rupp et al. (2009b), who found only stature to be significant in the model fit to the Neutral dataset, parametric survival analysis (SAS PROC PHREG) using the stepwise variable selection method was carried out. The maximum significance level for entering the model was 0.25 and the maximum significance level for staying in the model was 0.10; several other significance levels were tested but provided the same outcome. As the sex categorical variable resulted in the highest χ^2 score, it was the first parameter added to the model; any other added parameters were subsequently removed. While this appears to contradict previous findings, it may result from the relationship between sex and stature; of the subjects in the considered dataset, the average male stature is 178 cm while the average female stature is 165 cm. To further investigate this discrepancy, both covariates are retained throughout model development.

Flexion and adduction angles were considered as covariates in the Complete model. Flexion was found to be a significant component of the model ($\chi^2 = 8.3948, p < 0.0038$), while adduction angle was not ($\chi^2 = 1.9038, p = 0.1677$). This finding is somewhat consistent with Rupp (2006), who showed that in matched pair tests that an adduction angle of 10 degrees resulted in a significant reduction in tolerance while an abduction angle did not.

Based on these findings, the covariates included in the remaining model development steps are flexion and either sex or stature.

7.7.4 Hip Injury: Dependent Variable

The dependent variable used in the development of a pelvis injury criterion was the presence of a hip fracture, as defined in Rupp et al. (2009b) as a fracture of the acetabulum, pubic rami, femoral head/neck, and/or hip dislocation. Depending on the severity of the fracture, the resulting injury can be coded as either AIS 2 or AIS 3 (Martin and Scarboro, 2011).

7.7.5 Hip Injury: Injury Risk Function Formulation

7.7.5.1 Nonparametric

A nonparametric survival function was formulated using the SAS PROC LIFETEST procedure. This survival function is shown in later comparisons to parametric survival models.

7.7.5.2 Logistic Regression

Logistic regression could not be carried out since there were no non-injury observations; all of the PMHS specimens included in this data sustained a hip fracture.

7.7.5.3 Survival Analysis

Survival analysis was also carried out to develop risk functions for all four datasets using the SAS PROC RELIABILITY procedure to estimate model parameters and confidence intervals. Models were developed to predict failure based on uncensored peak applied force using sex, stature, both sex and stature, both flexion and sex, and both flexion and stature as covariates. Observations generated from the same PMHS, such as NB0112R which was tested in the neutral posture and NB0112L which was tested in 30 degrees flexion, were tested as independent observations. Models developed for the Neutral dataset did not include flexion as a covariate, as this term would be negated by definition. Models were developed assuming several different probability distributions to determine the best fit to the data. Of these, the two best distributions were Weibull and Lognormal.

The Survival Weibull model takes the form:

$$p(\text{Hip Fracture}) = 1 - e^{-\left(\frac{F_{\text{applied}}}{e^{(\beta_0 + \beta_1 c_1 + \beta_2 c_2)}}\right)^\alpha}$$

where:

- F_{applied} = Peak force applied to knee (in kN)
- β_0 = Intercept
- β_1 = 1st covariate coefficient
- c_1 = 1st covariate value
- β_2 = 2nd covariate coefficient (if used)
- c_2 = 2nd covariate value (if used)
- α = 1/scale

For each combination of covariates, model estimates and maximum log likelihood are reported in Table 7.6. The narrowest confidence intervals occurred in the models which include stature as a covariate, while the widest confidence intervals occurred for the models with sex and stature as covariates (Figure 7.18). Individual models presented at relevant covariate levels are shown for the model with sex as a covariate (Figure 7.19), stature as a covariate (Figure 7.20), and both sex and stature as covariates (Figure 7.21) for the Neutral dataset, as well as the models with sex and flexion (Figure 7.22) and stature and flexion (Figure 7.23) as covariates for the Complete dataset.

Table 7.6. Parameter estimates and fit statistics for survival analysis Weibull models.

Predictor	Covariate(s)*	Dataset	β_0	β_1	β_2	α	Maximum Log Likelihood
Peak applied force	Sex	Neutral	1.9639	-0.2563	N/A	5.4396	4.6034
Peak applied force	Stature	Neutral	-0.3564	0.0129	N/A	5.5685	5.5229
Peak applied force	Sex and stature	Neutral	0.3964	-0.1243	0.0087	5.8038	6.2372
Peak applied force	Sex	Complete	1.9036	-0.1988	N/A	4.3397	-3.6318
Peak applied force	Stature	Complete	0.3353	0.0087	N/A	4.2998	-4.0832
Peak applied force	Sex and stature	Complete	1.2439	-0.1381	0.0037	4.3646	-3.3961
Peak applied force	Sex and flexion	Complete	1.9371	-0.2094	-0.0124	4.5527	-0.5221
Peak applied force	Stature and flexion	Complete	0.3333	0.0089	-0.0118	4.4177	-1.4720

*Covariate units: sex represented by male = 0, female = 1; stature in cm; flexion in degrees from neutral posture

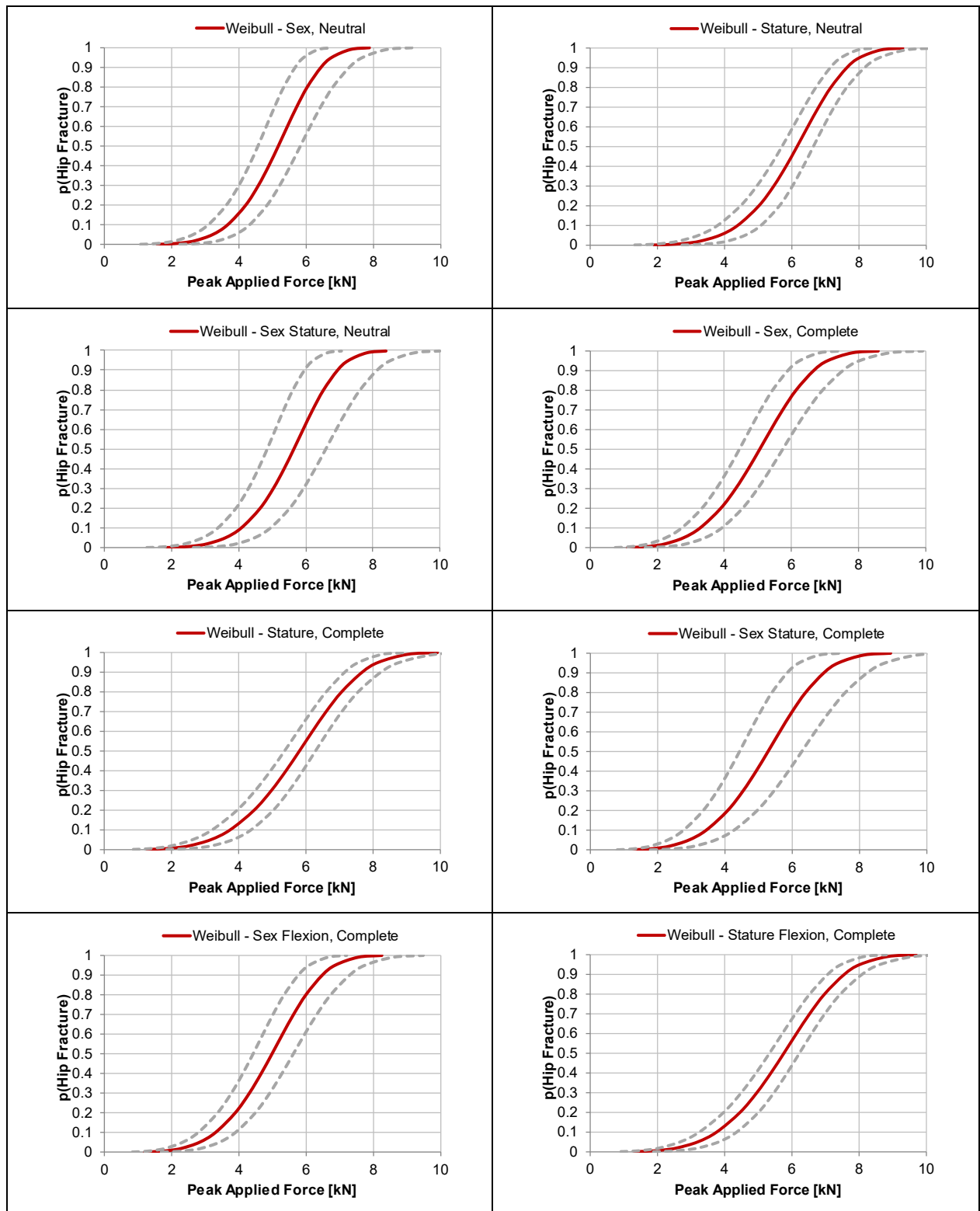


Figure 7.18. Survival Weibull models with 95% confidence intervals.

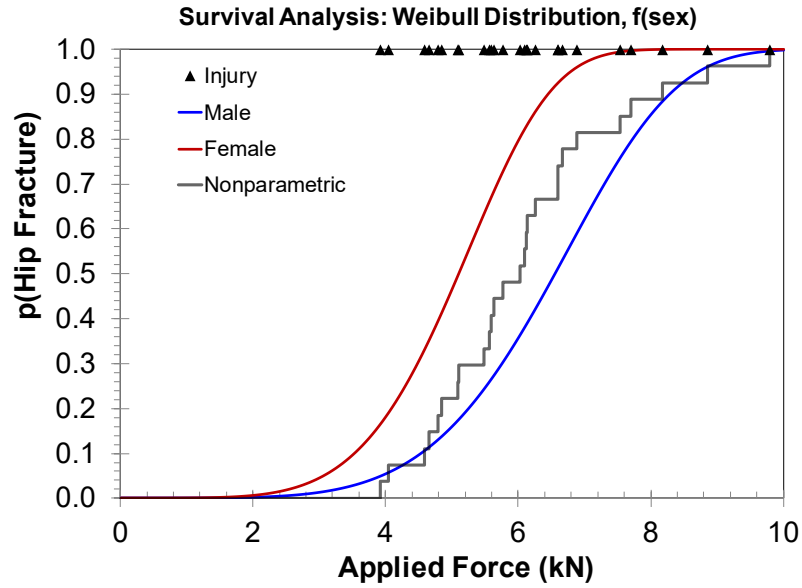


Figure 7.19. Survival Weibull injury risk function for applied force vs. hip fracture, with sex as a covariate.

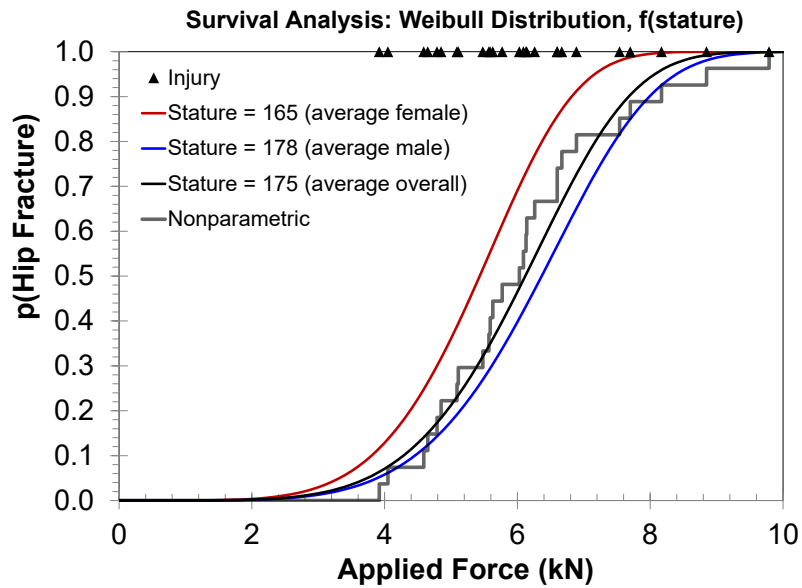


Figure 7.20. Survival Weibull injury risk function for applied force vs. hip fracture, with stature as a covariate, calculated at the average male, average female, and average overall statures from the dataset (Table 7.5).

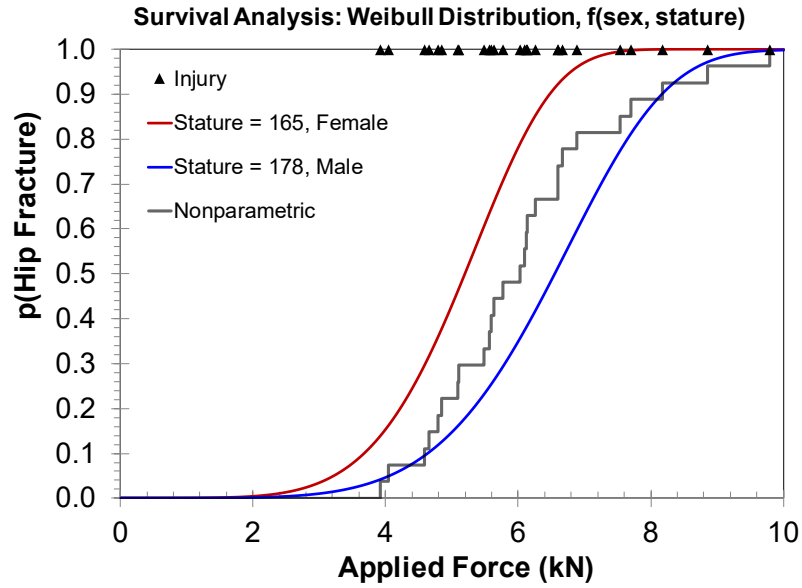


Figure 7.21. Survival Weibull injury risk function for applied force vs. hip fracture, with sex and stature as covariates, calculated at the average stature from the dataset (Table 7.5) for the respective sex.

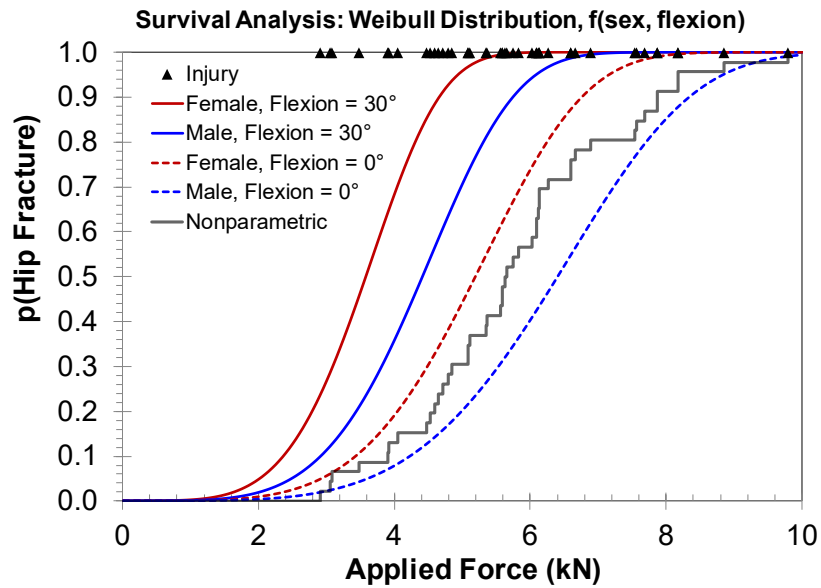


Figure 7.22. Survival Weibull injury risk function for applied force vs. hip fracture, with sex and hip flexion as covariates, presented for males and females and for neutral and 30° flexion covariate levels.

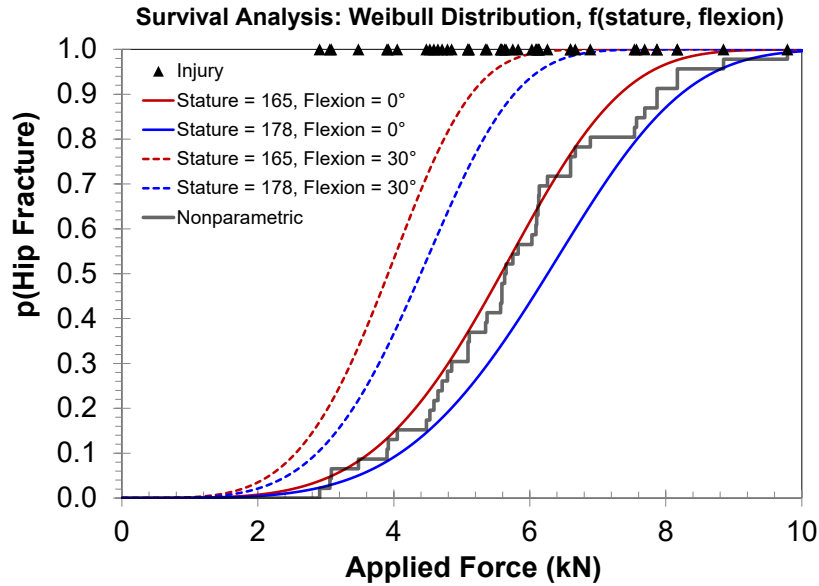


Figure 7.23. Survival Weibull injury risk function for applied force vs. hip fracture, with stature and hip flexion as covariates, presented for the average male and female statures in the dataset (178 cm and 165 cm, respectively) and for neutral and 30° flexion covariate levels.

The Survival Lognormal model takes the form:

$$p(\text{Hip Fracture}) = \Phi \left[\frac{\ln F_{\text{applied}} - \beta_0 + \beta_1 c_1 + \beta_2 c_2}{\sigma} \right]$$

where:

Φ	=	Cumulative normal distribution function
F_{applied}	=	Peak force applied to knee (in kN)
β_0	=	Intercept
β_1	=	1 st covariate coefficient
c_1	=	1 st covariate value
β_2	=	2 nd covariate coefficient (if used)
c_2	=	2 nd covariate value (if used)
σ	=	Standard deviation or scale

For each combination of covariates, model estimates and maximum log likelihood are reported in Table 7.7. As with the Weibull model, the narrowest confidence intervals occurred in the models with stature as a covariate, while the widest confidence intervals occurred for the model with both sex and stature as covariates (Figure 7.24). Individual models presented at relevant covariate levels are shown for the model with sex as a covariate (Figure 7.25), stature as a covariate (Figure 7.26), and both sex and stature as covariates (Figure 7.27) for the Neutral dataset, as well as the models with sex and flexion (Figure 7.28) and stature and flexion (Figure 7.29) as covariates for the Complete dataset.

Table 7.7. Parameter estimates and fit statistics for survival analysis Lognormal models.

Predictor	Covariate(s)*	Dataset	β_0	β_1	β_2	σ	Maximum Log Likelihood
Peak applied force	sex	Neutral	1.8349	-0.1576	N/A	0.2015	5.4913
Peak applied force	stature	Neutral	-0.2441	0.0117	N/A	0.1924	6.8726
Peak applied force	sex and stature	Neutral	-0.0650	-0.0243	0.0107	0.1923	6.8974
Peak applied force	sex	Complete	1.7733	-0.1848	N/A	0.2632	-3.8650
Peak applied force	stature	Complete	-0.2031	0.0110	N/A	0.2633	-3.8789
Peak applied force	sex and stature	Complete	0.6363	-0.1087	0.0064	0.2609	-3.4652
Peak applied force	sex and flexion	Complete	1.8109	-0.1651	-0.0133	0.2357	1.2082
Peak applied force	stature and flexion	Complete	-0.0755	0.0106	-0.0137	0.2339	1.5572

*Covariate units: sex represented by male = 0, female = 1; stature in cm; flexion in degrees from neutral posture

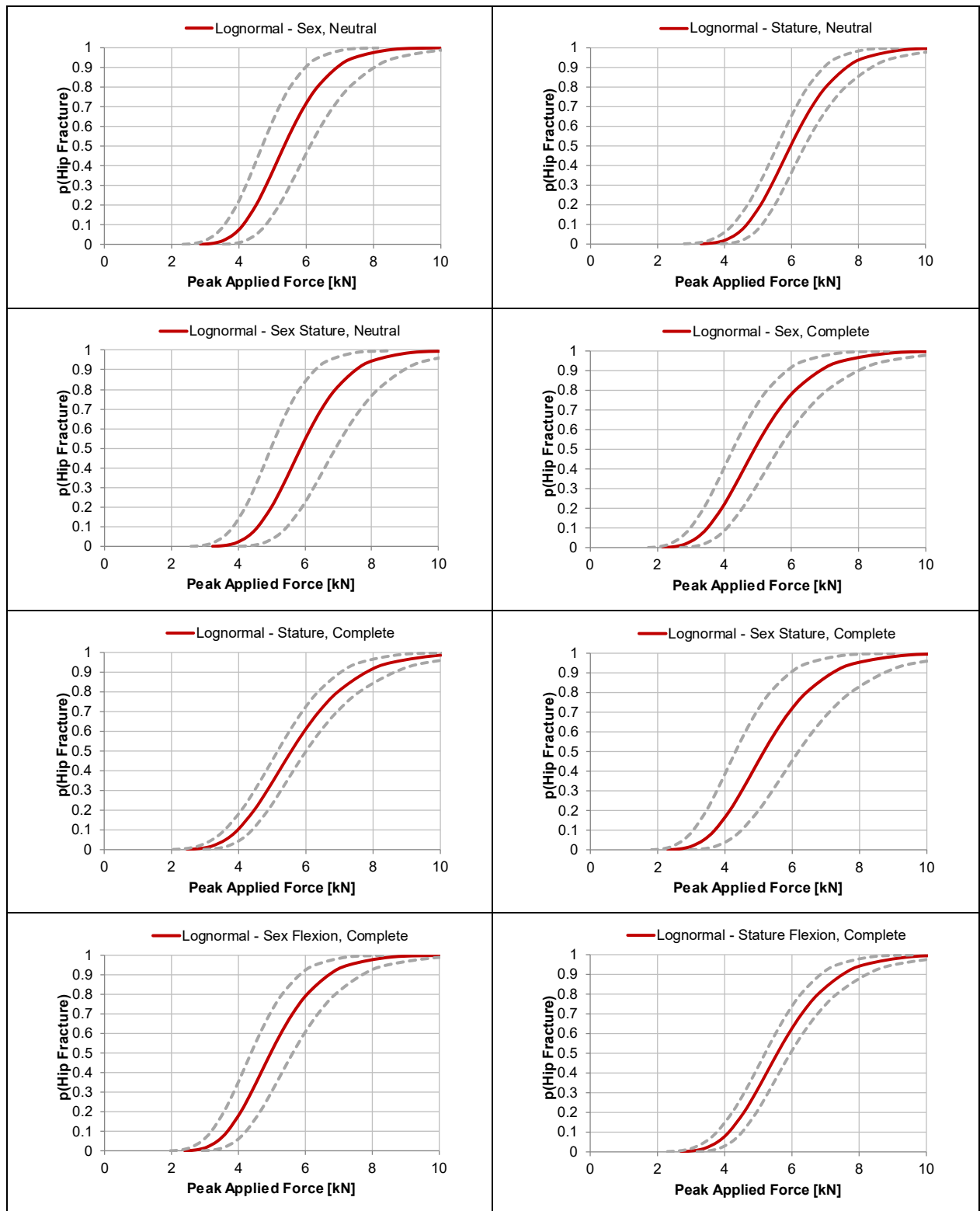


Figure 7.24. Survival Lognormal models with 95% confidence intervals.

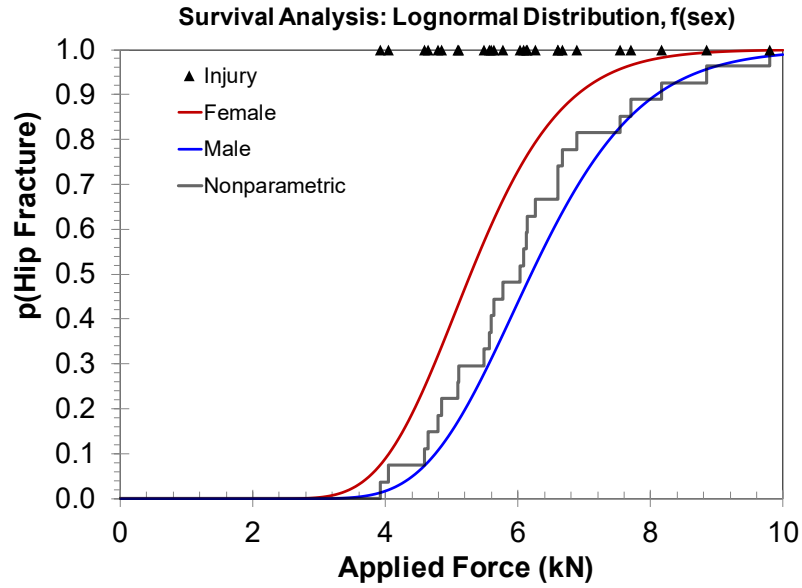


Figure 7.25. Survival Lognormal injury risk function for applied force vs. hip fracture, with sex as a covariate.

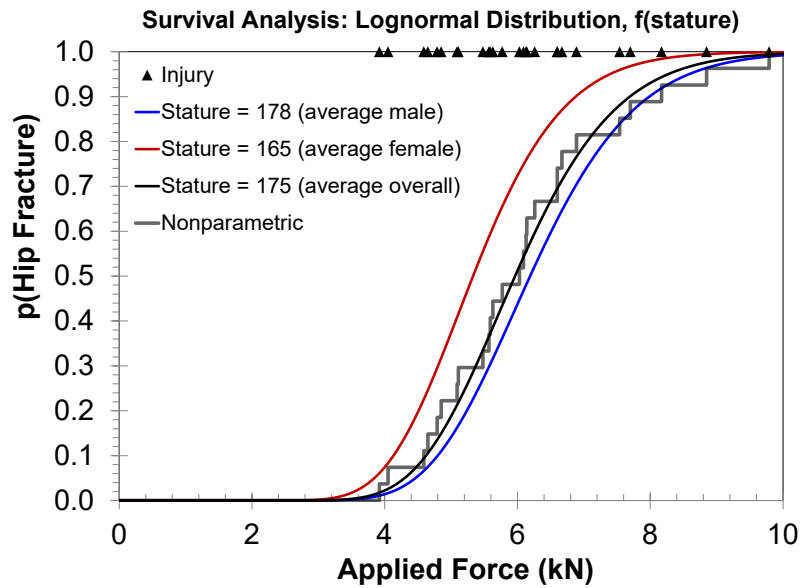


Figure 7.26. Survival Lognormal injury risk function for applied force vs. hip fracture, with stature as a covariate, calculated at the average male, average female, and average overall statures from the dataset (Table 7.5).

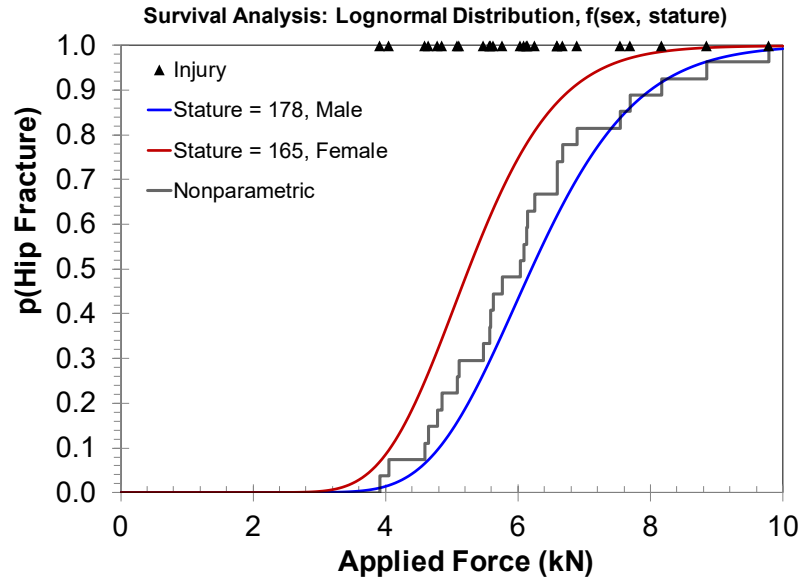


Figure 7.27. Survival Lognormal injury risk function for applied force vs. hip fracture, with sex and stature as covariates, calculated at the average stature from the dataset (Table 7.5) for the respective sex.

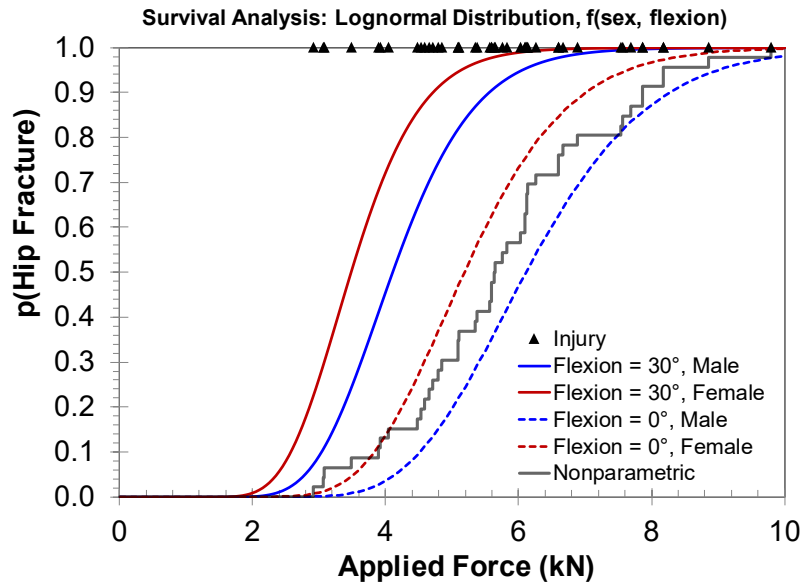


Figure 7.28. Survival Lognormal injury risk function for applied force vs. hip fracture, with sex and hip flexion as covariates, presented for males and females and for neutral and 30° flexion covariate levels.

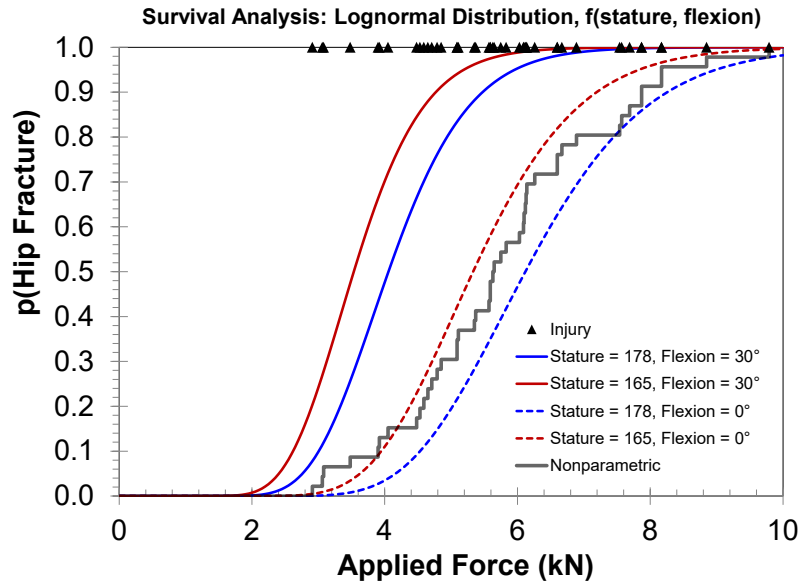


Figure 7.29. Survival Lognormal injury risk function for applied force vs. hip fracture, with stature and hip flexion as covariates, presented for the average male and female statures in the dataset (178 cm and 165 cm, respectively) and for neutral and 30° flexion covariate levels.

7.7.6 Hip Injury: Application to THOR-50M

Since the risk functions described above are based on the response of PMHS specimens, it is necessary to determine a relationship between PMHS response and THOR-50M response to apply the risk function to THOR-50M measurements in vehicle crash tests.

The predictor used to develop the PMHS risk function developed by Rupp et al. (2009b) and recreated here is peak applied force. In the tests used to develop this risk function, the pelvis was fixed and the force was applied to the knee using a pneumatic ram such that inertial effects were minimized and the reaction force at the hip was equal to the force applied at the knee. These forces were measured using load cells, one mounted along the axis of the ram and the other mounted on the hip mounting fixture with its local x-axis parallel to the ram, and as designed the measured forces at both the knee and the hip were similar (Figure 7.30). In tests where the hip posture was different than the neutral automotive seating posture, a bracket was installed between the hip mounting fixture and the hip load cell, so the local x-axis of the hip load cell remained parallel to the ram (Figure 7.31).

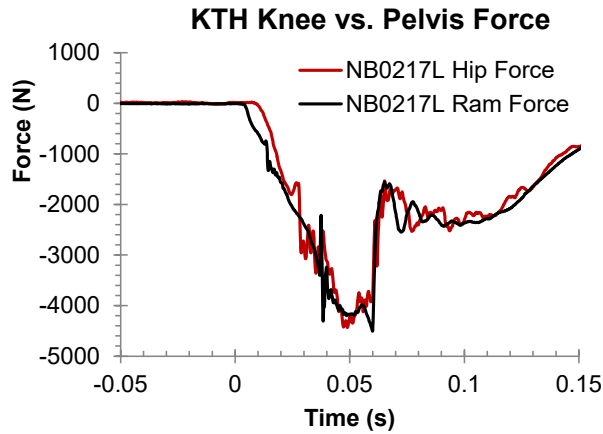


Figure 7.30. Applied force at the knee (ram force) and measured force at the hip (hip force) in test NB0217L (BioDB 5924). Test was conducted in neutral posture.

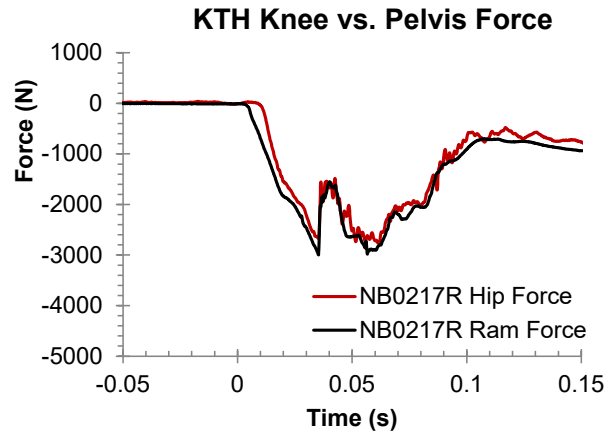


Figure 7.31. Applied force at the knee (ram force) and measured force at the hip in test NB0217R (BioDB 5925). Test was conducted in 30° flexion posture.

Since the THOR-50M femur was shown to be biofidelic in axial compression (Parent et al. 2017), it is assumed that the forces measured at the THOR-50M acetabulum would be equivalent to the forces applied to the PMHS specimens in the KTH injury criteria dataset. However, since the THOR-50M acetabulum measures forces along the x-, y-, and z-axes of the pelvis coordinate system, the nearest approximation of the force at the acetabulum as measured in the PMHS would be the resultant of these three forces.

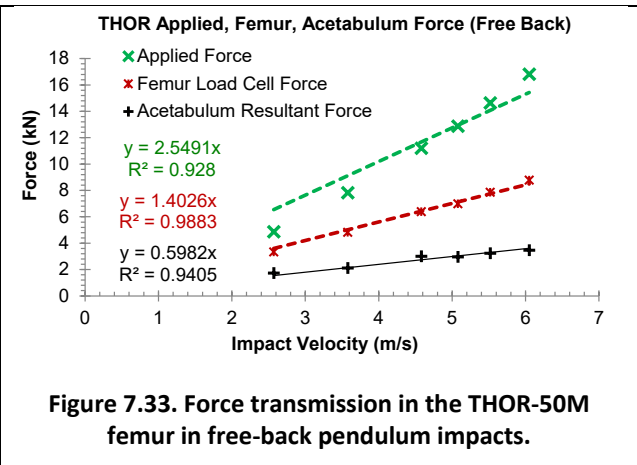
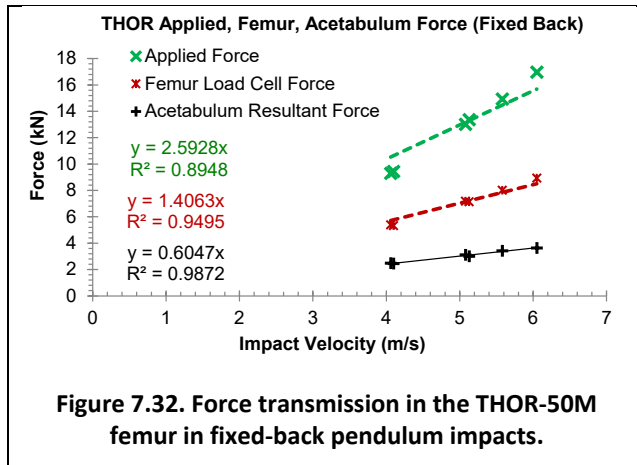
While the THOR-50M demonstrated biofidelity in a laboratory test condition with direct loading along the shaft of the femur, additional correction is necessary to account for the differences in acetabulum forces measured in frontal motor vehicle crash test environments compared to those expected in human occupants. Martin et al. (2011) discussed the relationship between THOR-NT and PMHS regarding force transfer to the hip. In crash tests where there is a well-defined interaction between the femur/knee and the knee bolster, the peak resultant acetabulum force is roughly 50% of the peak axial femur force. Martin et al. (2011) also described a relationship between peak applied force and the peak force measured by the femur load cell of about 80%, presumably rounded from the Rupp et al. (2009a) estimate of 77%, which translates to the acetabulum load cell of THOR-NT measuring 40% of the peak applied force at the knee. For comparable loading to a PMHS, the percentage of peak force applied at the knee that is reacted at the hip is 55% (Rupp et al., 2009a). Combining these arguments, the ratio of the peak force applied to the knee of PMHS to that of the THOR-NT would be $55\% / (80\% \times 50\%)$, or roughly 1.3. In other words, the force measured at the hip of a PMHS would be 1.3 times higher than that measured by the THOR-NT in a comparable condition. This relationship is based on the assumption that the THOR-NT would produce the same force at the knee as a human occupant, which as noted by Martin et al. (2011) is more likely to be true with the modifications to the THOR implemented in the Mod Kit (Ridella and Parent, 2011) to improve KTH biofidelity.

The Mod Kit design updates (Ridella and Parent, 2011) have been incorporated into the THOR-50M design, which includes three changes to the knee-thigh-hip complex that could potentially require adjustments to the aforementioned assumptions made based on the THOR-NT design. First, the knee

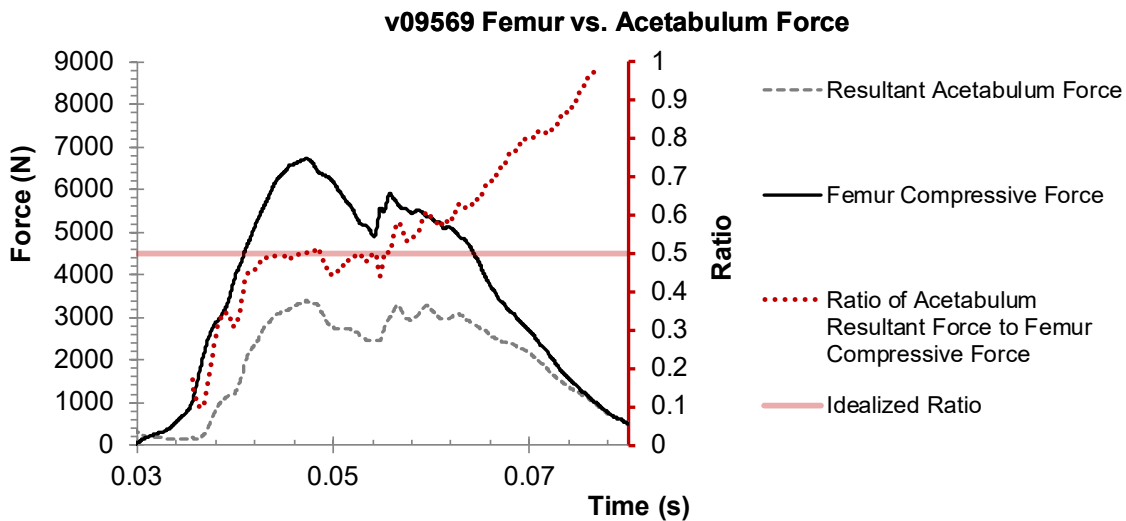
slider force-deflection characteristic was adjusted in an attempt to achieve a more biofidelic response in knee shear. In the case of knee-to-knee-bolster impacts, the knee slider is not directly in the load path. While loading from the tibia can in turn load the femur load cell by way of the knee slider, the injury risk function was not developed with combined knee and tibia loading, thus contributions to the measured femur force through interactions of the tibia with the vehicle interior are not considered. Second, the femur compressive element was redesigned to achieve a more biofidelic response in femur axial compression. Third, the pelvis flesh was redesigned to reduce the coupling with the femur and allow a greater femur range of motion.

The construction of the knee of the THOR-50M is similar to that of the H3-50M, in that the knee cap is effectively rigid and directly mounted to the femur load cell. Therefore, the relationship between applied force at the knee and measured force at the femur presented by Rupp et al. (2009a) is assumed to hold true for the THOR-50M as well. As discussed above, in low-mass pendulum impacts to the femur of the THOR-50M in both free-back and fixed-back conditions, the femur load cell measured roughly 55% of the peak applied force at the knee. However, it is not clear how representative this impact condition is to the knee loading condition seen in a motor vehicle crash, where the femurs are restrained by the knee bolster and loaded inertially by the remaining effective mass of the body. It is also evident that the ratio of impact force to measured femur force is sensitive to impact velocity (Figure 7.16), as lower velocities will result in a larger percentage of the impact force measured by the femur load cell. Given these limitations, and since the analysis carried out by Rupp et al. (2009a) considered loading rates similar to those occurring in FMVSS No. 208 and US NCAP crash tests with the H3-50M, there is insufficient evidence to modify the 77% load transfer ratio of force measured at the femur to force applied to the knee.

Next, to investigate whether the assumption of femur-to-acetabulum force transfer from Martin et al. (2011) holds true for the THOR-50M design, femur and acetabulum forces were analyzed in both pendulum knee impacts (both free- and fixed-back) as well as several frontal rigid barrier crash tests. In both fixed-back (Figure 7.32) and free-back (Figure 7.33) pendulum impacts as described above, the ratio of peak femur load cell compressive force to peak acetabulum resultant force was on average 44% and the ratio of force-vs-velocity slopes was 43% for either condition. Again, such an evaluation is limited by the unknown representativeness of this impact condition to the knee loading condition seen in a motor vehicle crash.



In an exemplar frontal rigid barrier crash test of a 2016 Nissan Rogue (VehDB TSTNO 9569) with a THOR-50M ATD in the driver’s seat, at the time of peak left femur axial compressive force the resultant left acetabulum force measured 50% of the femur force (Figure 7.34). This is consistent with the idealized sled test presented by Martin et al. (2011), which showed the same 50% relationship between peak resultant acetabulum force and peak femur compressive force using the THOR-NT ATD.



Given the uncertainty of the representativeness of low-mass pendulum impacts to knee bolster impacts in motor vehicle crashes, and the similarity of at least one example of femur-to-acetabulum load transfer in a frontal rigid barrier crash test, there is not ample evidence to suggest an alternative to the 77% transfer ratio of impact force to femur force or the 50% transfer ratio of femur force to acetabulum force. Thus, the transfer function to relate peak resultant acetabulum force measured on the THOR-50M to the acetabulum force used in development of the PMHS risk function is recommended as:

$$T_{hip} = \frac{r_{PMHS}}{r_{THOR}} = \frac{r_{PMHS}}{r_{KtoF}r_{FtoA}} = \frac{0.55}{0.77 \times 0.50} = 1.429$$

where:

- T_{hip} = Ratio of estimated PMHS hip force to THOR measured peak acetabulum resultant force
- r_{PMHS} = Ratio of applied force at knee to acetabulum force measured in PMHS (Rupp et al., 2009a)
- r_{THOR} = Ratio of applied force at knee to acetabulum force measured in THOR
- r_{KtoF} = Ratio of applied force at knee to measured force at femur load cell (Rupp et al., 2009a)
- r_{FtoA} = Ratio of measured force at femur to measured resultant force at acetabulum (Martin et al., 2011)

As the injury risk function is sensitive to flexion angle, and the THOR ATD is not equipped to record dynamic flexion angle, estimation of a flexion angle is important for proper application of the hip fracture risk function. In several papers, the hip fracture risk function was presented by assuming a posture of 30 degrees of flexion and 15 degrees of abduction from the hip angles in the standard automotive seating posture, which was argued to be the approximate posture at the time of peak knee force in front-impact sled tests with airbag deployment (Rupp 2006; Rupp et al., 2009b). However, this assumption is based on tests of unbelted occupants with airbag deployment; a more conservative estimate of hip flexion angle in three-point belted occupant environments (as shown in Figure 7.35 for both THOR-50M and PMHS) is 15 degrees. While this results in a shift of the risk curve to the left, it is not as aggressive of a shift as a 30-degree flexion angle would be. Further, injuries occurring at larger flexion angles may be less severe; for example, one of the lowest failure forces in the expanded dataset was a subject in the 30-degree flexion condition. This subject sustained a hip dislocation at a peak applied force of 3.06 kN. In the matched pair test on the opposite aspect of the same PMHS conducted at a flexion angle of zero degrees, a peak applied force of 4.65 kN resulted in a fracture of the femoral neck.

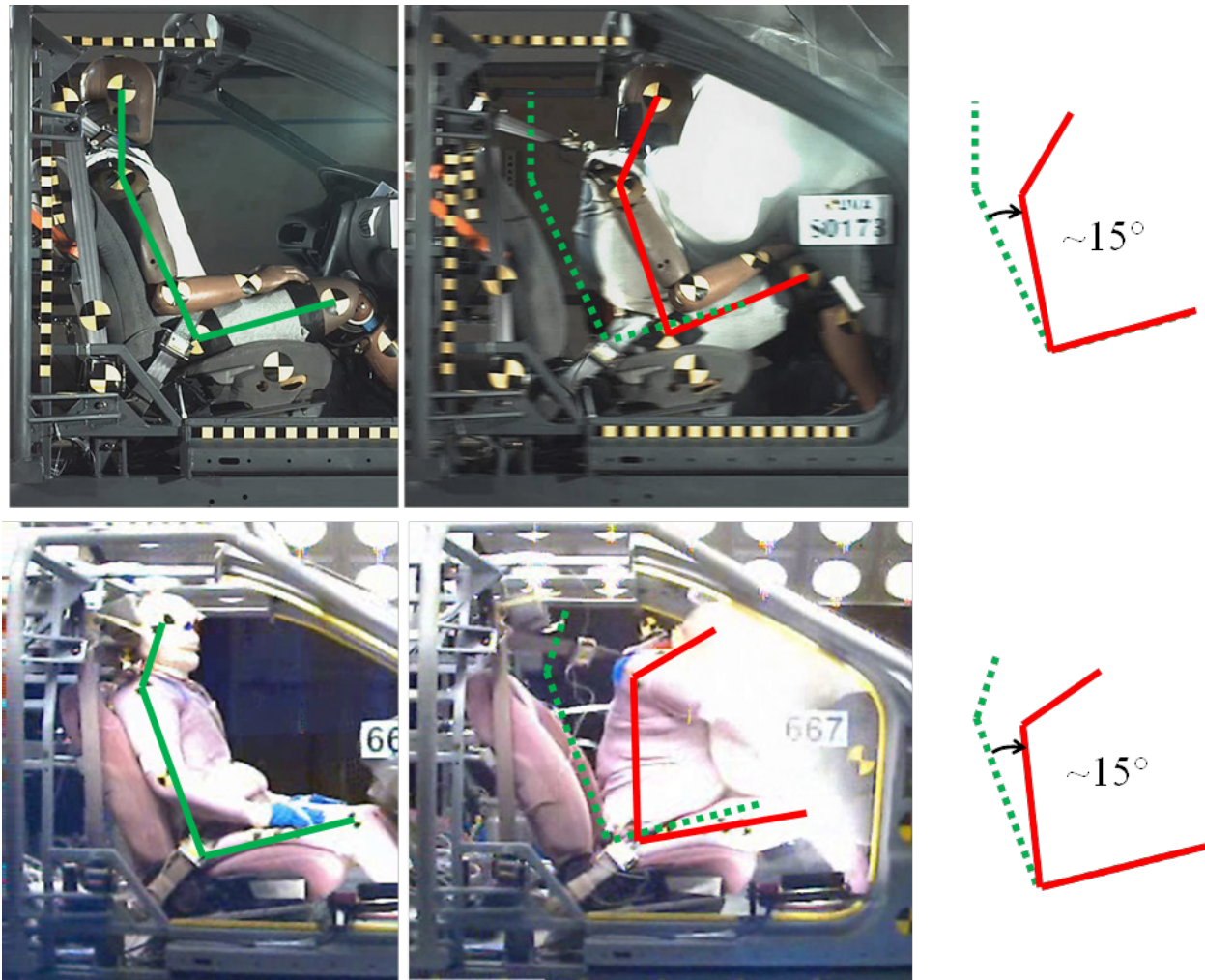


Figure 7.35. Hip flexion angles at time of peak femur load in a frontal sled test condition with three-point belts and airbags. THOR-50M ATD shown at top (BioDB TSTNO 11127) and example PMHS shown at bottom (BioDB TSTNO 8384).

As adduction angle was not found to be significant in the model, estimation of the adduction angle is not necessary to apply the risk function to THOR.

An additional consideration in the assessment of acetabulum injury risk using the THOR-50M ATD is that while the injury risk function was developed considering isolated loading of the acetabulum through compression of the femur, there may be additional load paths which contribute to the force measured at the acetabulum load cell. For example, interaction of the pelvis flesh with the seat structure, including both anti-submarining hardware in the vertical and anterior-posterior direction and seat side bolsters in the lateral direction, may transfer force through the proximal femur and greater trochanter hardware to the acetabulum load cell. Further, in conditions where the knee is not in contact with the knee bolster or knee bolster airbag at the point of maximum pelvis excursion, the femur may be in tension at the time of peak resultant acetabulum load. To minimize the contribution of forces that may not relate to force transferred to the acetabulum through femur compression, it is recommended that the resultant acetabulum force be calculated for a given leg only for time increments where the associated femur is in

compression, indicated by a negative Z-axis force. Simply considering acetabulum X-axis force could be misleading and cumbersome due to the way that the acetabulum polarity is defined, as the left and right polarities are opposite (NHTSA, 2018) and have not been consistently set in past crash test experience.

Of the 32 occupants assessed in the Fleet Test Data set (drivers in the frontal rigid barrier test condition, drivers and right front passengers in the oblique moving deformable barrier test condition), there were five observations for which the overall peak acetabulum force and the peak acetabulum force at the time of femur compression were different (Figure 7.36). Three of these observations resulted in a difference in force of less than 100 N. Two of the observations, both involving the left leg of an occupant in the right front passenger position, demonstrated a more substantial difference. In test number v08789, the right front passenger experienced an overall peak left acetabulum force of 4457 N, while the peak left acetabulum force occurring at a time where the left femur was in compression was 3254 N. In test number v09573, the right front passenger experienced an overall peak left acetabulum force of 3267 N, while the peak left acetabulum force occurring at a time where the left femur was in compression was 1784 N, though the overall peak acetabulum force for this occupant would revert to the right acetabulum force of 2287 N. In both of these instances, the peak resultant acetabulum force occurred later in time than the peak femur force, and resulted primarily from a positive X-axis acetabulum force (Figure 7.37, Figure 7.38). In contrast, test v08488 shows a condition where the overall peak resultant left acetabulum force for the right front passenger occurs at a time when the associated femur is in compression (Figure 7.39). While the response in test v08488 after 100 milliseconds shows a similar behavior to that in tests v08789 and v09573, the relative peak force that occurs during femur compression, or negative femur force, is higher than the peak force that occurs later in the event when the femur is no longer in compression.

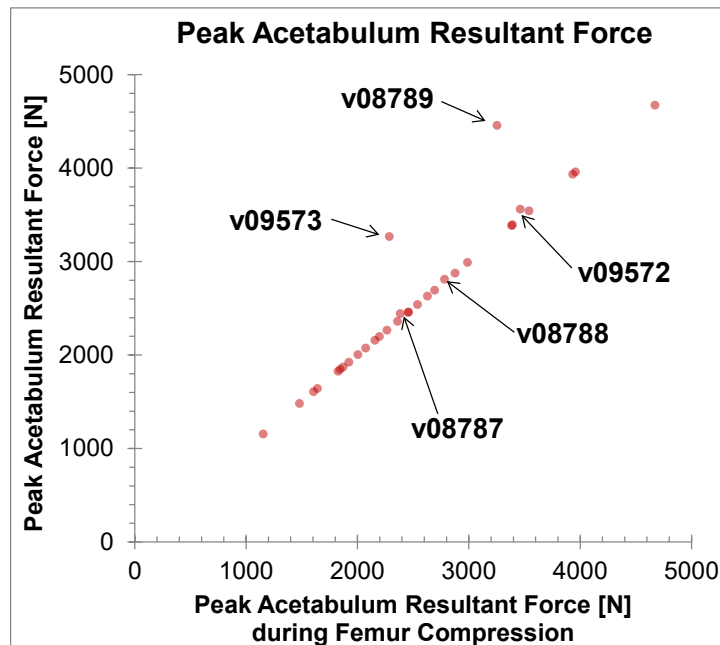
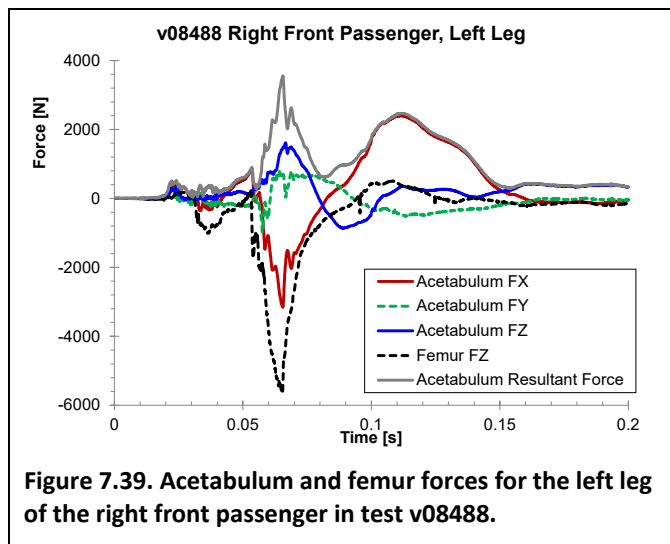
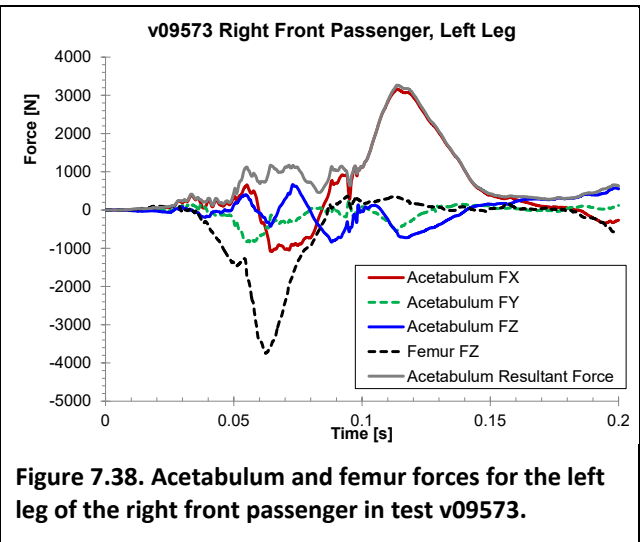
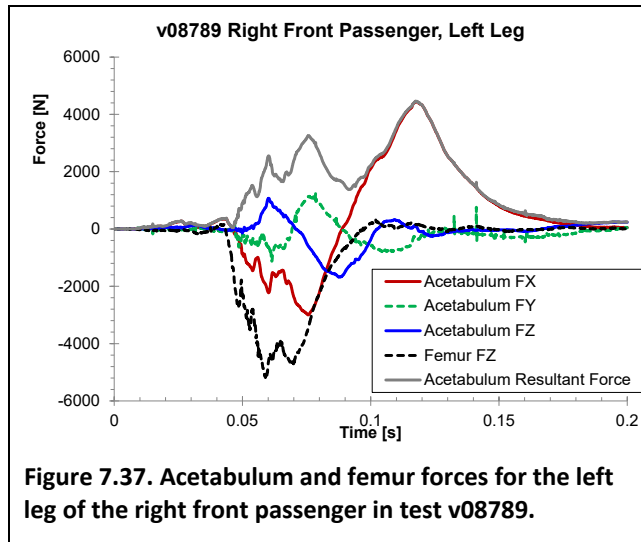


Figure 7.36. Comparison of overall peak resultant acetabulum force to peak resultant acetabulum force measured while the associated femur was in compression.



In summary, given the discussed limitations, the recommended risk function for application to THOR-50M to predict hip injuries is described below and shown in Figure 7.40:

$$p(\text{Hip Fracture}) = \Phi \left[\frac{\ln T_{hip} F_{AR} + 0.0755 - 0.0106s + 0.0137f}{0.2339} \right]$$

where:

- Φ = Cumulative normal distribution function
- T_{hip} = Ratio of estimated PMHS hip force to THOR measured peak acetabulum resultant force [1.429]
- F_{FemurZ} = Femur load cell Z-axis force
- F_{AR} = Peak resultant acetabulum force (in kN); $F_{AR}(t) = 0$ for $F_{FemurZ}(t) > 0$
- s = Stature (in cm) [175.1 cm per Section 1.3]
- f = Flexion angle from neutral automotive posture (in deg) [nominal 15 deg]

Simplified:

$$p(\text{Hip Fracture}) = \Phi \left[\frac{\ln 1.429 F_{AR} - 1.5751}{0.2339} \right]$$

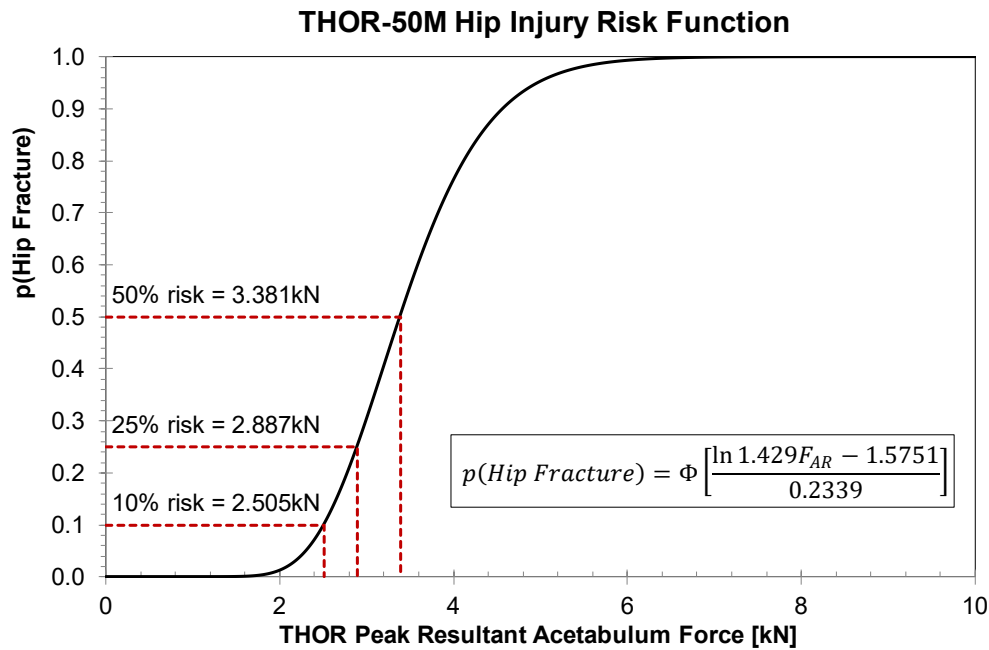


Figure 7.40. Recommended injury risk function for hip fracture with respect to measured peak resultant acetabulum force, including peak measurements for 10%, 25%, and 50% risk of hip fracture.

7.7.7 Hip Injury: Comparison to Literature

The injury risk function developed by Rupp et al. (2009b) is similar to the Survival Lognormal risk function using stature as a covariate. However, Rupp applied an additional correction factor to account for the fact that increases in hip angle, in both flexion and adduction, reduce the human tolerance for

hip fracture (Rupp et al., 2003). This correction factor was appended to the risk function as a mean shift of 1% for each degree of hip abduction and -1% for each degree of hip flexion. This risk function has been presented differently in various publications; the intended application is believed to be:

$$p(\text{Hip Fracture}) = \Phi \left[\frac{\ln F_{\text{applied}} - (0.2141 - 0.0114s) \left(1 - \frac{f - a}{100}\right)}{0.1991} \right]$$

where:

Φ	=	Cumulative normal distribution function
F_{applied}	=	Peak force applied to knee (in kN)
s	=	Stature (in cm)
f	=	Hip flexion angle (in degrees)
a	=	Hip abduction angle (in degrees)

In the equation above, Rupp et al. (2009b) uses covariate values of 178 cm in stature, 30° of flexion, and 15° of abduction. Using these covariates, but updating the stature to 175.1 cm to represent the stature of the THOR-50M (See Section 1.3), the resulting risk function is very similar to the recommended THOR-50M risk function (Lognormal, 15° flexion) (Figure 7.41). However, if evaluated at 15° of flexion and 15° of abduction, the Rupp risk function predicts a lower risk of hip fracture for a given applied force. Not shown is the risk function evaluated at 15° flexion and 0° abduction, which would result in the same risk curve as the 30° flexion/15° abduction condition.

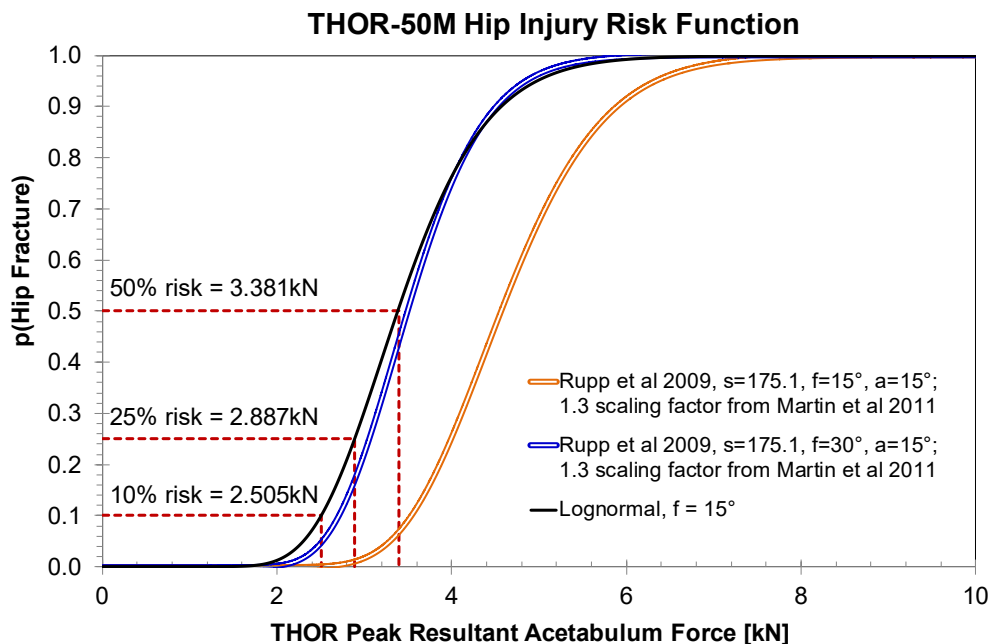


Figure 7.41. Hip fracture risk function compared to Rupp et al. (2009b), evaluated at flexion angles of 15° and 30° and stature of 175.1 cm.

7.8 Fleet Test Data: THOR-50M

The recommended femur compressive force injury risk function was applied to THOR-50M measurements collected in frontal rigid barrier and frontal Oblique fleet testing. Figure 7.42 shows the injury risk function with observations representing the injury risk predicted from each occupant response, grouped by occupant position and test mode. Predicted probability of AIS 2+ injury is generally below 10 percent except for two Oblique driver observations (19 percent and 32 percent).

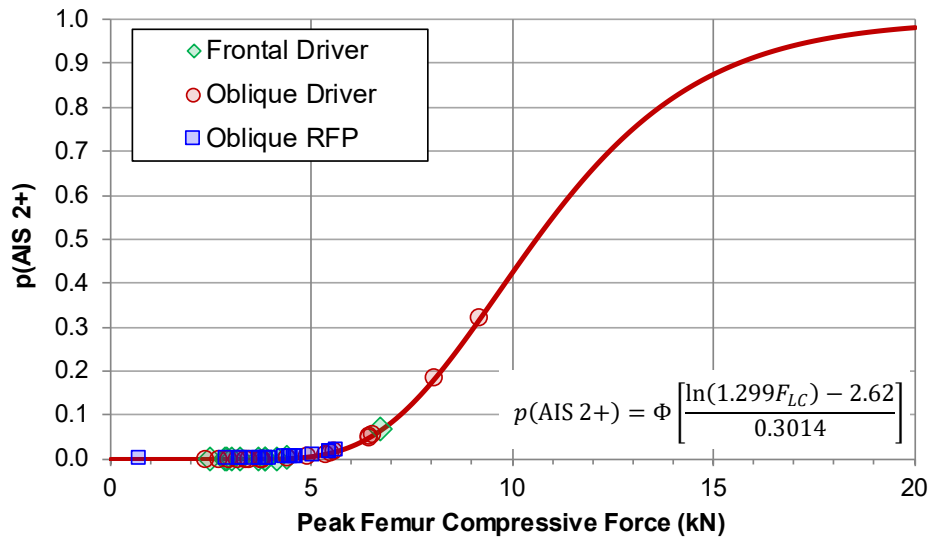


Figure 7.42. Peak femur compressive forces from frontal rigid barrier and oblique moving deformable barrier tests using THOR-50M.

The recommended acetabulum injury risk function was also applied to THOR-50M fleet test data. Higher acetabulum injury risk is predicted for occupants in the Oblique crash mode compared to the frontal rigid barrier crash mode. On average, the risk of hip fracture was higher than the risk of femur fracture, which is consistent with observations from field data suggesting that pelvis and/or hip injury is common in absence of femur shaft fracture (Rudd et al., 2011).

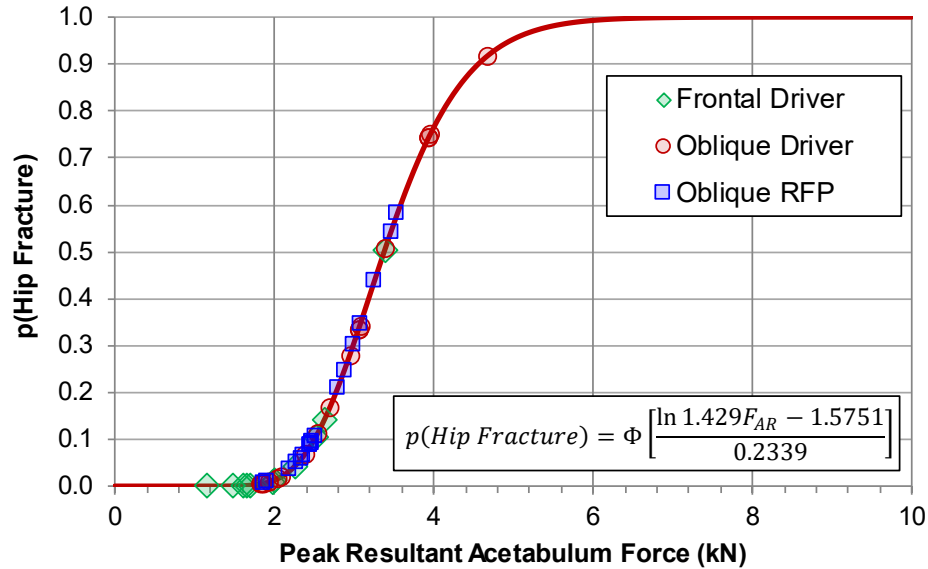


Figure 7.43. Peak acetabulum forces from frontal rigid barrier and oblique moving deformable barrier tests using THOR-50M.

7.9 Limitations

This section presented injury criteria for knee/femur injury and hip injury, both of which are used primarily to predict the occurrence of fracture. One potential injury mode that was not investigated was ligamentous knee injury. While the THOR-50M is instrumented to record the motion of the sliding joint at the interface between the distal femur and the proximal tibia at the knee, its biofidelity in the knee shear loading condition was marginal (Parent et al., 2017). Additionally, the field incidence of knee shear-related injuries is relatively low (Figure 7.3). For these two reasons, an injury criterion for knee shear was not presented for the THOR-50M. The marginal knee shear biofidelity assessment is not believed to influence the knee/femur or hip injury criteria because knee shear is not a primary component of the load path related to compression-induced fracture.

In the development of knee/femur injury risk functions, the Survival analysis considered three censoring schemes. All three censoring schemes included assumptions related to the type and timing of injury occurrence. The censoring scheme described by Rupp et al. (2009b) is believed to be the most appropriate for the available data, though it still assumes that femur fractures occurred at exactly the measured peak applied force at the knee. This assumption is believed to be small relative to the assumptions required by the other censoring options.

The relationship between applied force at the knee and the measurement of peak force at both the femur load cell and the acetabulum load cell has not been specifically validated for the THOR-50M ATD. As has been shown above, this relationship may be dependent on loading scenario, so a simple transfer function does not encapsulate all possible loading rates, stiffnesses, and geometries.

The relationship between applied force at the knee of PMHS and the THOR-50M ATD is not explicitly known. While the femur is quantitatively biofidelic in axial compression, the mass distribution and inertial properties of the knee-thigh-hip complex may differ from that of a PMHS or a live human.

The relationship between PMHS response and live human response is unknown.

8 LOWER EXTREMITY

8.1 Field Data and Historical Fleet Data

Below-knee injuries (leg, foot, and ankle) have been identified as a frequent and costly result of frontal crashes in numerous studies (Rudd et al., 2009; Dischinger et al., 1994; Morgan et al., 1991; Pattimore et al., 1991; Dischinger et al., 2004). Injuries to the leg, foot, and ankle continue to make up a substantial proportion of reported AIS 2+ injuries in frontal crashes, and represent the highest-risk body region for AIS 2+ in frontal crashes regardless of severity (Table 1.1). Considering attributable costs (Figure 1.2), the relative importance of the lower extremity is evident despite being comprised mostly of AIS 2 severity injuries (Table 1.2).

Below-knee injuries in NASS-CDS frontal crashes were separated into sub-regions including the proximal tibia, tibia shaft, distal tibia, fibula, hindfoot, ankle malleoli, midfoot, and forefoot based on individual AIS codes (Figure 8.1). This breakdown demonstrates that the leg, including the tibia and fibula components, sustains the majority of the moderate to severe injuries in frontal crashes. The hindfoot category is made up of the talus, calcaneus, ankle (tibiotalar) joint, and subtalar (talocalcaneal) joint, and is separated from the malleolus injuries due to potential differences in causation.

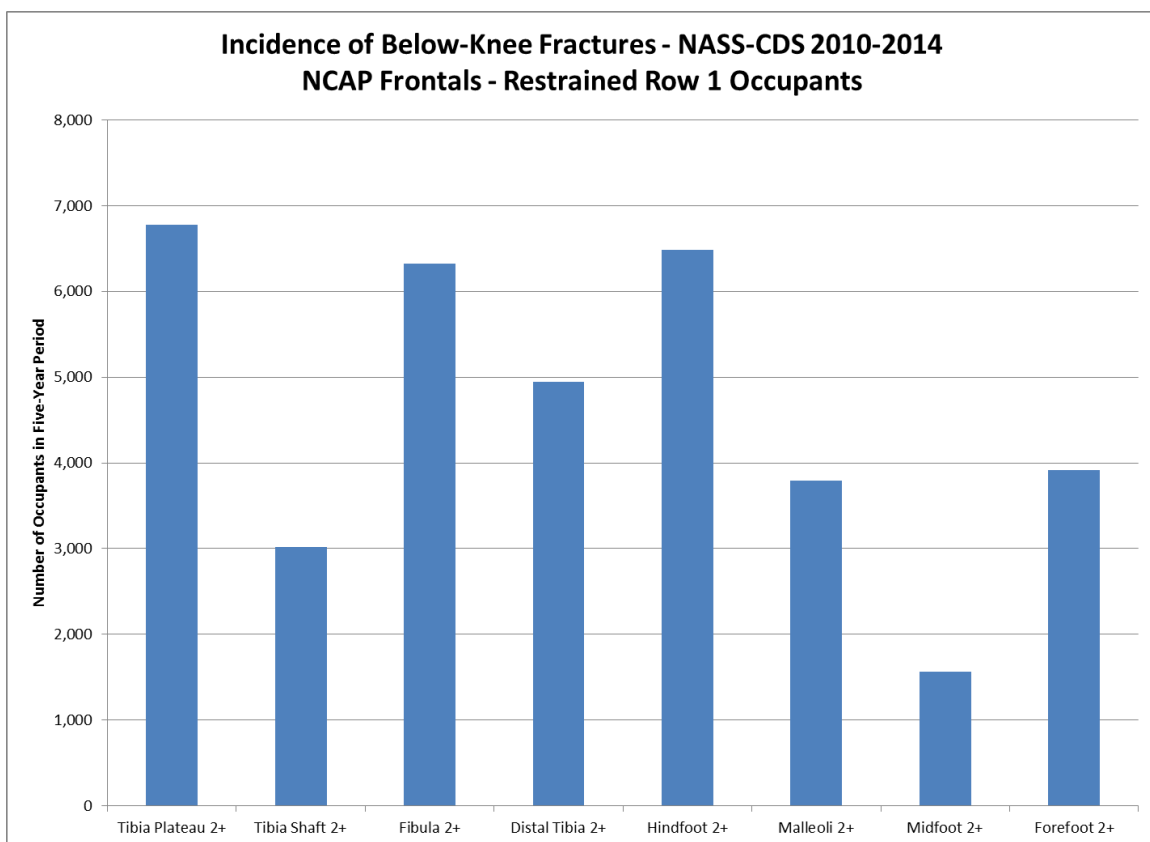


Figure 8.1. Incidence of AIS 2+ fractures and dislocations by below-knee sub-region for NASS-CDS restrained row 1 outboard frontal crash occupants from 2010-2014 data years. Counts represent total weighted numbers of AIS 2+ fractures and dislocations.

A review of frontal crashes with belted first-row occupants from the CIREN database resulted in 770 below-knee AIS 2+ fractures and dislocations among 216 occupants using the same query parameters as for the data in Figure 8.1. Many AIS 2 and all AIS 3+ injuries are assigned primary, and sometimes secondary, regional injury mechanisms in CIREN. Application of the injury breakdown into sub-regions noted above demonstrates the role various injury mechanisms play in producing AIS 2+ fractures and dislocations to the below-knee structures (Figure 8.2). Compression of the leg and hindfoot components is responsible for the large majority of the injuries for which CIREN codes injury mechanisms. Joint rotation is noted as the primary mechanism for some of the ankle injuries (distributed among the fibula, distal tibia, hindfoot, and malleolus groups), but these structures are generally also loaded in compression in frontal crashes. Of the injuries for which a regional injury mechanism is not coded, most of those occur in the foot where compression and twisting due to contact with the toepan or pedals are the most likely mechanisms. Fibula injuries not assigned a mechanism are likely similar to the tibia shaft in causation. Tibia injuries not assigned a mechanism are likely similar to the tibia shaft in causation. Taken in combination with Figure 8.1, the findings in Figure 8.2 suggest that a focus on compression of the tibia and hindfoot would address most of the below-knee injuries, and may also address some midfoot and forefoot injuries.

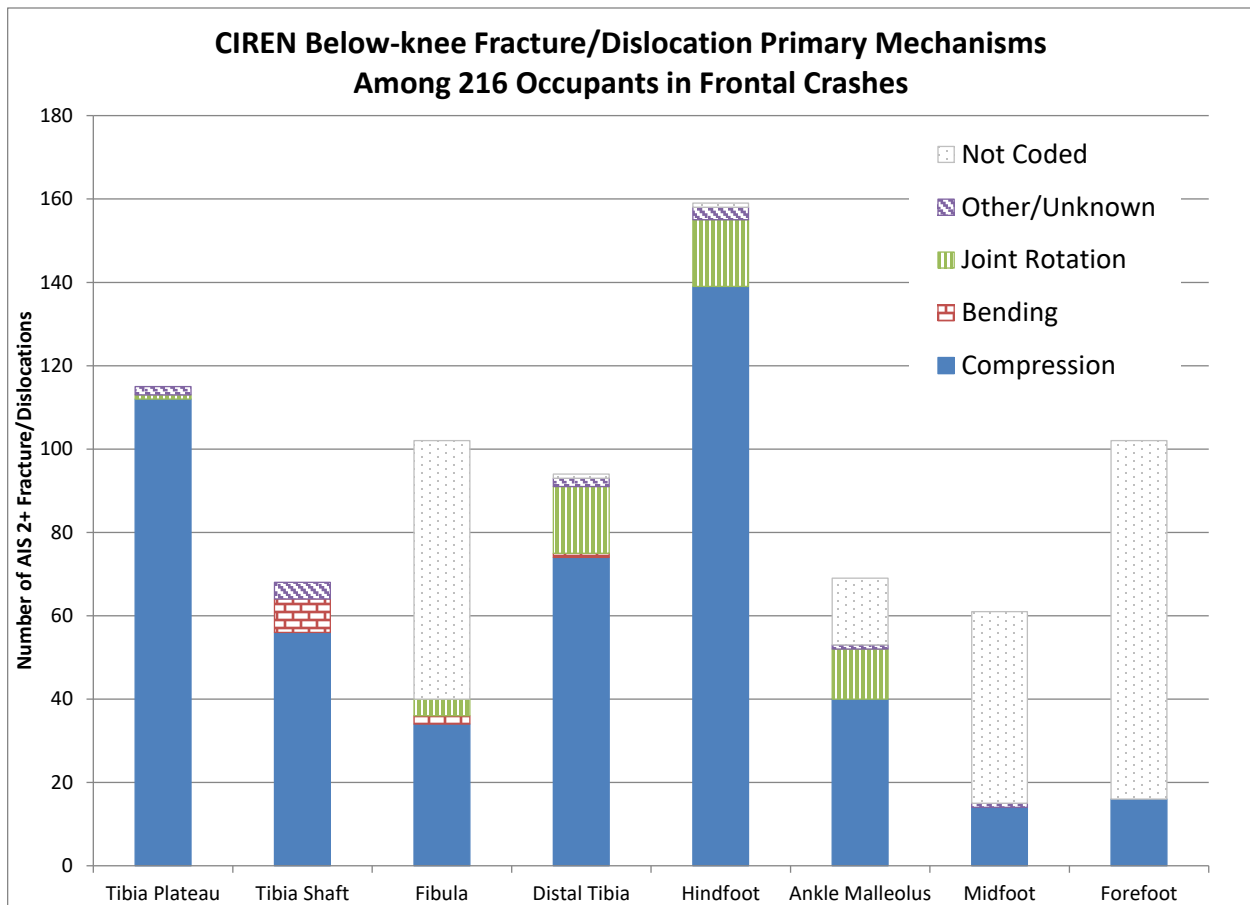


Figure 8.2. Primary regional injury mechanisms for the below-knee sub-regions identified in 216 restrained first row CIREN case occupants involved in frontal crashes.

As presented for other body regions in this report, vehicle model year-based trends for AIS 2+ tibia/fibula and foot/ankle injuries for belted drivers in frontal crashes are shown in Figure 8.3 and Figure 8.4, respectively. The trend for H3-50M Tibia Index and peak tibia force values in 35-mph full frontal tests can be seen in Figure 8.5 and Figure 8.6.

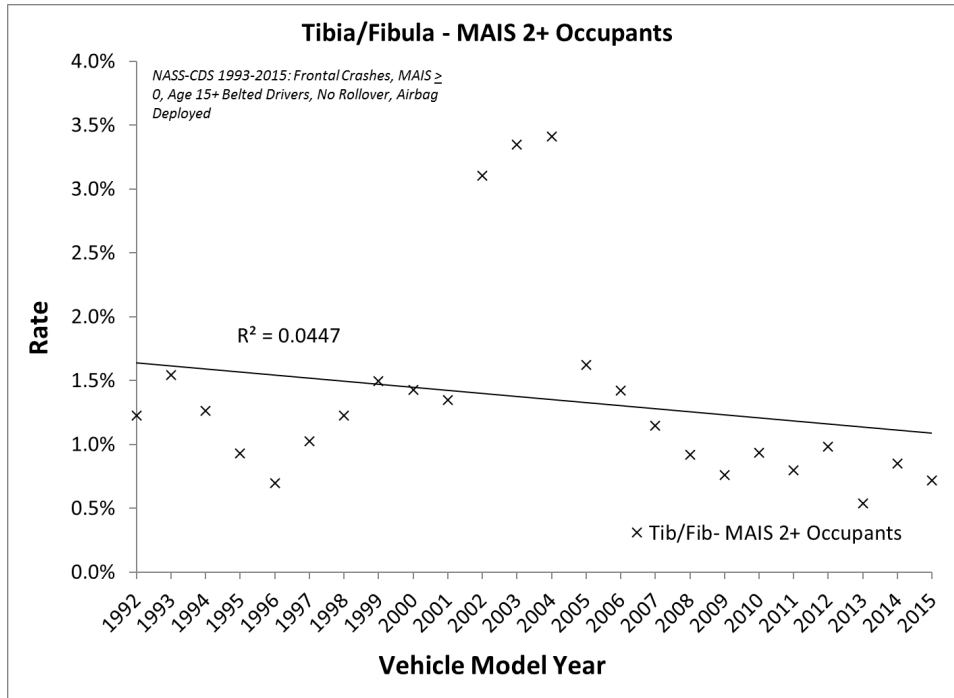


Figure 8.3. AIS 2+ tibia/fibula injury trends by vehicle model year (1992 to 2015) from frontal crashes in NASS-CDS (1993 to 2015).

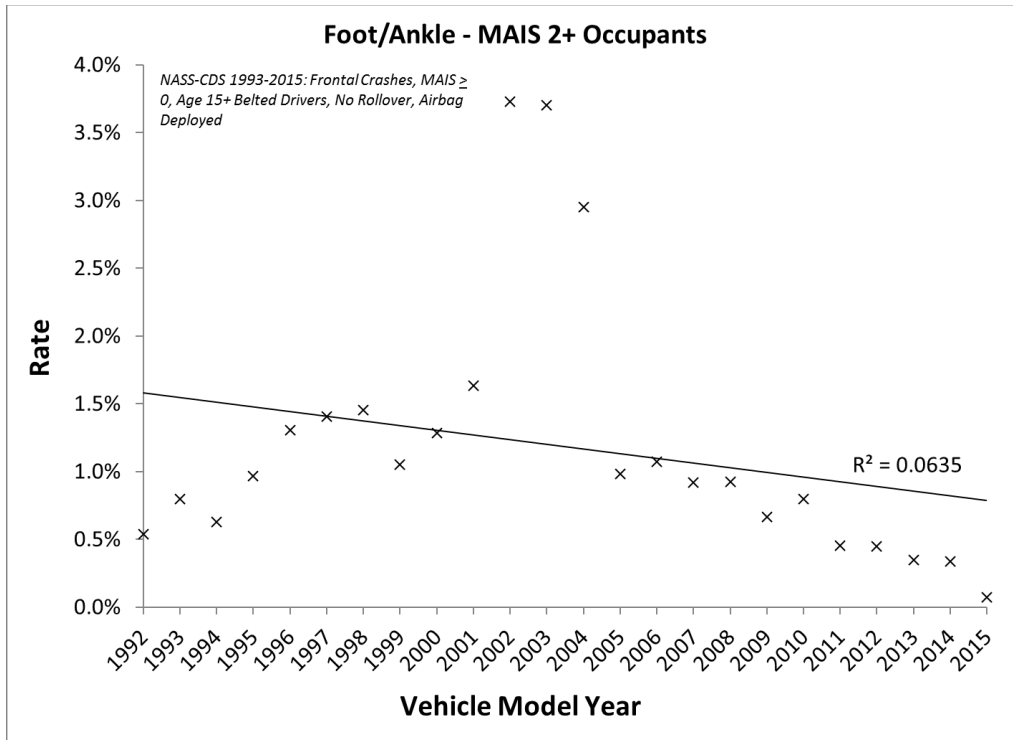


Figure 8.4. AIS 2+ foot/ankle injury trends by vehicle model year (1992 to 2015) from frontal crashes in NASS-CDS (1993 to 2015).

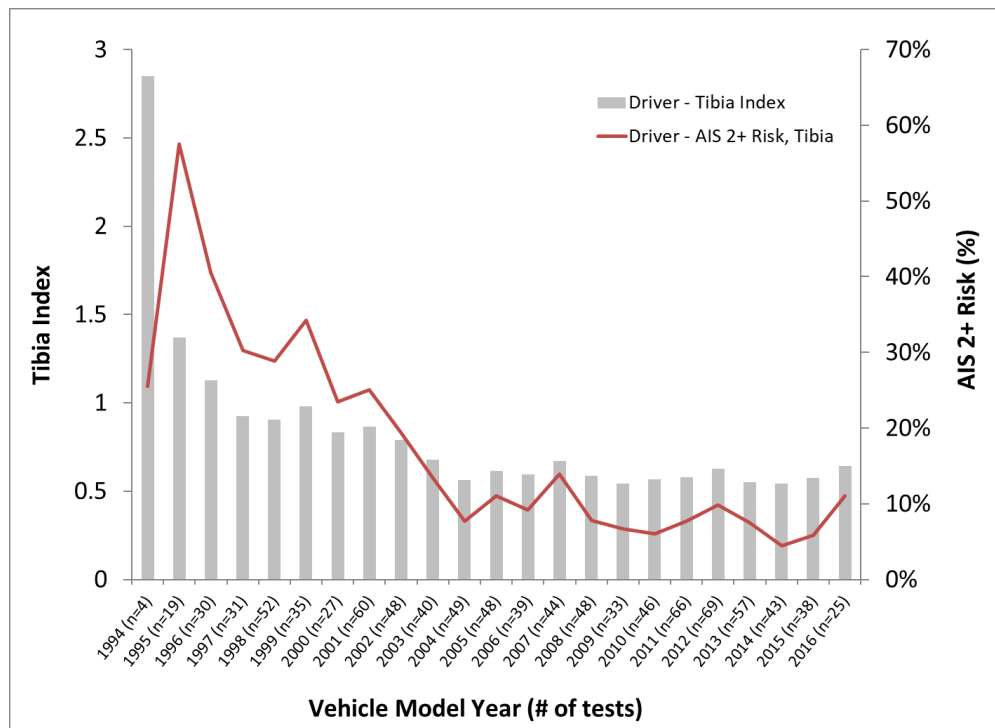


Figure 8.5. H3-50M frontal NCAP average peak Tibia Index for model year 1990 to 2016.

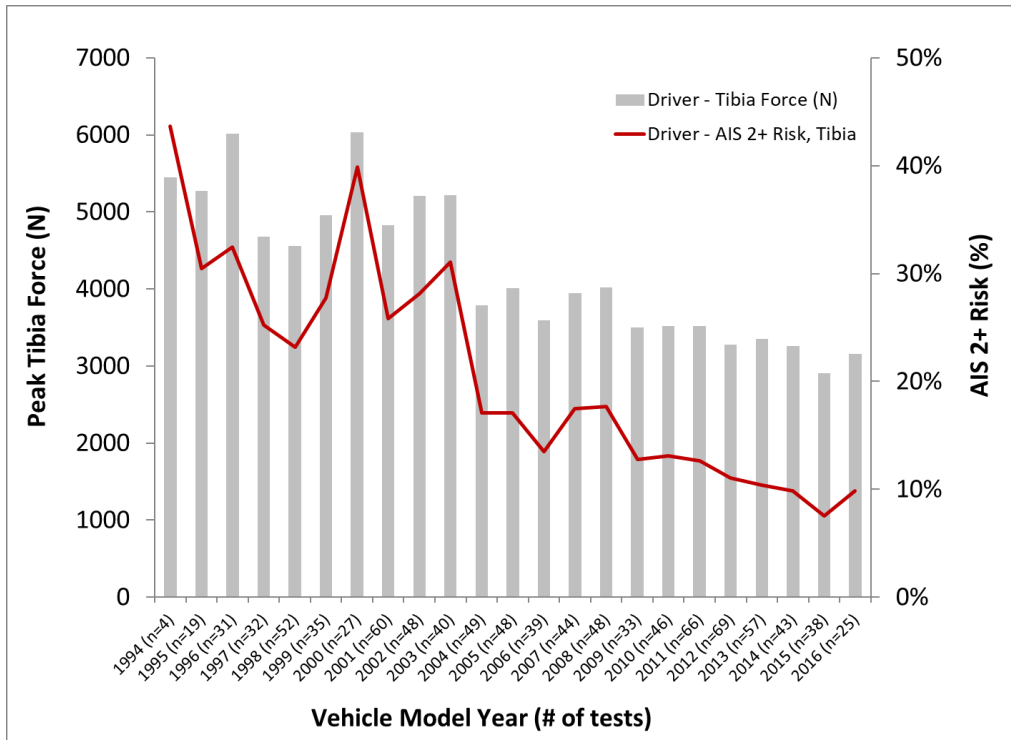


Figure 8.6. H3-50M frontal NCAP average peak tibia force for model year 1990 to 2016.

8.2 Design

The mechanical design of the THOR-50M lower extremity provides several advances over previous lower extremity designs. A compliant section in the tibia shaft, similar to the THOR-50M compliant femur section, provides more biofidelic force transmission from the heel to the knee complex. The spring damper Achilles tendon system aids in producing the desired ankle motion and torque characteristics. The ankle design provides correct range of motion, joint axes placement, and biofidelic torque vs. angle response for the two primary axes (dorsi-/plantar-flexion and inversion/eversion), with soft stop elements defining the stiffness at the extremes of motion. The molded shoe design, which was added to the docketed THOR-50M drawing package in the 2016 drawing package update (NHTSA, 2016b), integrates the foot and shoe into a single part.

8.3 Instrumentation

The lower extremity includes sensors to measure injury parameters (Figure 8.7). Five-channel upper and lower tibia load cells are incorporated into the design to provide force and moment data of the tibia shaft. A uniaxial compression load cell implemented into the Achilles tendon housing provides a direct measurement of the contribution of the Achilles to the overall ankle joint torque. Three rotary potentiometers measure the rotation of the individual ankle joints, thereby providing complete kinematic data. Finally, two uniaxial accelerometers on the tibia and a tri-pack accelerometer assembly on the foot plate allow the transformation of the measured tibia moment to the calculated ankle moment.

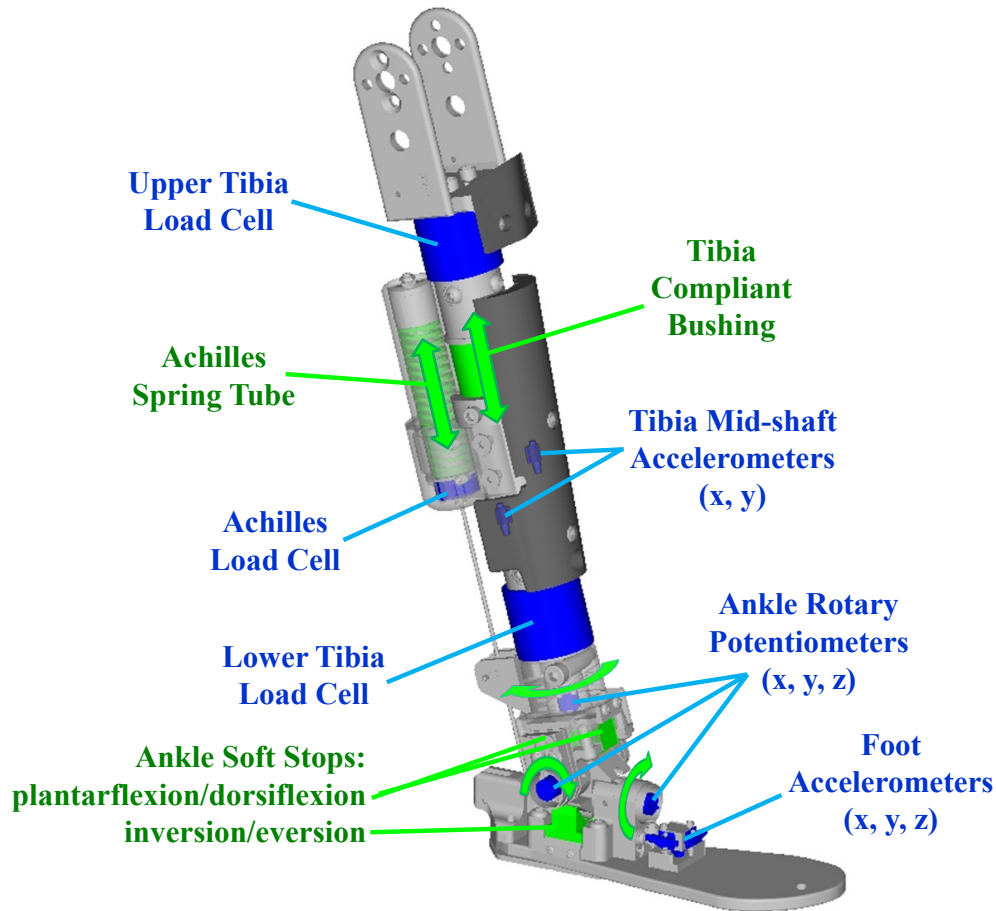


Figure 8.7. THOR-50M lower extremity instrumentation.

8.4 Biofidelity

Parent et al. (2017) evaluated the biofidelity of the THOR-50M leg in three primary conditions: Dynamic Heel Impact, Dynamic Axial Compression, and Dynamic Dorsiflexion. In the Dynamic Heel Impact condition, both the THOR-50M and H3-50M demonstrated either excellent or good biofidelity. The THOR-50M demonstrated marginal internal biofidelity in the Dynamic Axial Compression condition and excellent internal biofidelity in the Dynamic Dorsiflexion condition. The H3-50M was not tested in the Dynamic Axial Compression condition because it lacks a compressible element in the tibia, which would likely have resulted in damage to the test apparatus, and it was not tested in Dynamic Dorsiflexion because it lacks a rotational potentiometer in the ankle necessary to measure dorsiflexion angle. Thus, a biofidelity assessment of the H3-50M in these two test conditions was not possible.

8.5 Upper Tibia Axial Force

8.5.1 Data

Tibial plateau fractures are one of the most prevalent lower extremity injuries in frontal crashes (Figure 8.1). These injuries are typically produced by axial loading of the leg, when the leg is entrapped between the knee bolster and the toepan or pedal. Intrusion of the toepan or knee bolster can intensify the magnitude of the loading. Because forces in the proximal tibia are generated differently from distal tibia (i.e., the entrapment scenario at the knee bolster rather than solely axial load through the foot and ankle), NHTSA believes it is important to retain upper tibia axial force as a separate injury criterion (Figure 8.1). The risk curve proposed by Kuppa et al. (2001) used data from Banglmeier et al. (1999), in which twelve pairs of isolated human tibiofemoral joints were impacted in the superior direction along the axis of the tibia with the joint flexed to 90°. By isolating the knee joint, this test scenario was specifically designed to simulate a knee entrapped at the knee bolster. Newer data considered included Funk et al. (2000), in which axial impacts were applied to the plantar aspect of the foot. In that test series, foot/ankle fractures were produced in 15 tests and tibial plateau fractures were produced in 5 tests, and the average tibial plateau failure load was in agreement with previous studies (Funk et al., 2000). In addition, Funk et al. noted that, “the fact that tibial plateau fractures never occurred independently of foot and ankle injury suggests that an axial loading injury criterion based on the injury tolerance of the foot/ankle complex is sufficiently conservative to protect against tibial plateau fractures in this impact scenario.” Given the differences in injury mechanisms, the original Banglmeier (1999) dataset is retained for injury risk function development (Table 8.1, APPENDIX G). As noted in Kuppa et al. (2001), the group of six impacts conducted at constant energy were excluded due to pressure films being placed in the joint prior to impact.

Table 8.1. Descriptive statistics for upper tibia axial dataset.

n, injured	Mean Failure Force (kN)	Failure Force Range (Min-Max)	n, non-injured	Maximum Non-injury Force (kN)	Non-injury Force Range (Min-Max)
14	7.7 ± 2.0	3.8 to 11.5	16	6.1 ± 1.6	3.7 to 9.4

8.5.2 Injury Risk Function Formulation

Logistic regression was performed on the available data from Banglmeier et al. (1999), using axial load as the predictor variable. Stepwise multiple regression was carried out to assess the sensitivity of occupant-based covariates. Covariates considered were age, sex, stature and mass. For this dataset, mass was a significant covariate, while the others were not. The dependent variable considered was the presence of an AIS 2 or greater (2+) injury.

Goodness-of-fit metrics described in Hasija et al. (2011) were calculated, including the Receiver Operating Characteristic (ROC) Area Under Curve (AUC), maximum log likelihood, and Hosmer-Lemeshow Goodness-of-Fit test. These are reported in Table 8.3. The resulting form of the logistic regression function is the same as proposed by Kuppa et al. (2001). The logistic regression takes the form:

$$p(\text{AIS } 2+) = \frac{1}{1+e^{(-\beta_0-\beta_1x-\beta_2a)}}$$

where:

- β_0 = Intercept
- β_1 = Independent parameter coefficient
- x = Upper Tibia Axial Force (kN)
- β_2 = Mass coefficient
- a = Subject mass, in kg

Table 8.2. Model parameter estimates.

Model	β_0	β_1	β_2
Upper Tibia Axial Force	-0.5204	0.8189	-0.0686

The risk function and 95% confidence intervals were calculated assuming a standard mass of 76.11 kg (per Section 1.3).

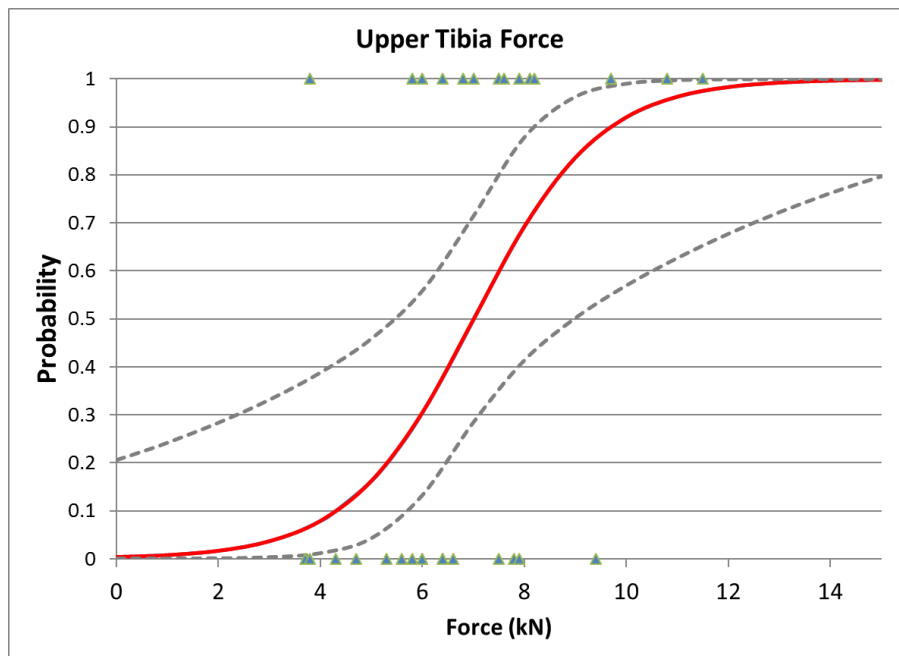


Figure 8.8. Logistic regression of upper tibia axial force data, including mean injury risk function and 95% confidence intervals, assuming mass of 76.11 kg.

Table 8.3. Significance and goodness of fit statistics for upper tibia force logistic regression with mass as a covariate.

Wald Pr>ChiSq	AUROC	Hosmer-Lemeshow Chi-Square	Hosmer-Lemeshow Pr>ChiSq	-2 Log L
0.03	0.83	5.9	0.55	28.4

Logistic regression can clearly differentiate between well-correlated and non-correlated datasets, but has the drawback of resulting in a risk function that has a non-zero risk at zero stimulus level. Thus, an alternate form of the risk function was developed using survival analysis. Survival analysis allows treatment of repeated tests as interval-censored data. For non-repeat tests, the data was treated as right-censored if no injury was sustained and left-censored if a fracture was sustained. The survival analysis risk function assumes a Weibull distribution and takes the form:

$$p(\text{AIS } 2+) = 1 - \exp\left(-\exp\left(\frac{\ln x - \beta_0 - \beta_1 a}{\alpha}\right)\right)$$

where:

- β_0 = Intercept
- x = Upper Tibia Axial Force (kN)
- β_1 = Mass coefficient
- a = Subject mass, in kg
- α = scale

Table 8.4. Model parameter estimates and goodness of fit.

Model	β_0	β_1	α	-2 Log L
Upper Tibia Axial Force	1.2236	0.0103	0.1695	34.96

Although the survival model has the advantage of passing through zero at zero stimulus, given the lower log likelihood values for the logistic model (compared with the survival model), the logistic regression curves are recommended.

8.6 Lower Tibia Axial Force

8.6.1 Data

Distal tibia and hindfoot fractures are common lower extremity injuries sustained in frontal crashes (Figure 8.1). These injuries are most commonly produced by axial loading through the foot and leg (Figure 8.2). Several studies are available wherein axial load was applied to the plantar aspect of the foot (Table 8.5). These studies were evaluated to determine whether they could be combined for risk function development. The risk curve proposed by Kuppa, 2001 used a combined dataset from studies by Yoganandan et al. (1996), Begeman et al. (1996) and Roberts et al. (1993). However, Roberts et al.

(1993) reported only footplate forces, and because peak footplate forces are typically much higher than peak tibial loads, it is inappropriate to combine these datasets. Yoganandan et al. (2015) evaluated these five studies, and combined only Yoganandan et al. (1996), Begeman et al. (1996) and Kitagawa et al. (1998) to develop new injury risk curves. Roberts et al. (1993) was excluded because only footplate force was recorded and Funk et al. (2002) was excluded because mean fracture forces were statistically different from the others. However, there were many small female subjects included in the Funk et al. (2002) study, which had the effect of lowering the overall mean fracture force. When either only male subjects or only “average height” (165-185 cm) subjects are considered, the mean fracture forces in the Funk study are not significantly different from the rest. As such, NHTSA deems it beneficial to include this data into a combined dataset (studies A, B, D and E, Table 8.5 and Table 8.6, APPENDIX G), accounting for age or sex as a covariate in the model (study C remains excluded due to the absence of recorded tibia forces). As demonstrated previously (Funk et al., 2002; Yoganandan et al., 2015), age is also a significant covariate in the model. The benefit to using the combined dataset is that it increases overall sample size and includes an appropriate number of non-injury data (compared with, for example, using the Funk et al., 2002 study alone). Although different boundary conditions and load cell locations exist in the combined dataset, the similarity of the injury-producing forces supports the approach of combining these data.

Table 8.5. Summary of biomechanical studies in which axial load was applied to the plantar aspect of the foot.

Study	Boundary condition	Load-cell location	n, injured	n, non-injured	Specimen data available
A Yoganandan et al. (1996)	Free	Proximal end of tibia	13	13	Age, Sex, Height, Weight
B Begeman et al. (1996)	Fixed	Mid-tibia	5	12	Age, Sex, Weight
C Roberts et al. (1993)	Fixed	Foot plate	9	0	Age, Sex, Height, Weight
D Kitagawa et al. (1998)	Fixed	Proximal tibia	15	1	Age, Sex
E Funk et al. (2002)	Fixed	Implanted in tibial diaphysis	30	4	Age, Sex, Height, Weight

Table 8.6. Descriptive statistics for lower tibia axial dataset.

Study	All specimens		Male specimens only		n, males
	Mean Failure Force (kN)	Failure Force Range (Min-Max)	Mean Failure Force (kN)	Failure Force Range (Min-Max)	
A	7.8 ± 2.4	4.3 to 11.5	8.4 ± 2.1	5.5 to 11.5	11
B	7.8 ± 0.9	6.9 to 8.7	7.0	7.0	1
D	7.6 ± 0.9	5.7 to 9.1	8.0 ± 0.9	7.1 to 8.8	4
E	5.7 ± 2.2	2.6 to 10.8	7.0 ± 2.1	4.5 to 10.8	17
Combined	6.8 ± 2.2	2.6 to 11.5	7.7 ± 2.0	4.5 to 11.5	

8.6.2 Injury Risk Function Formulation

Axial force is the commonly reported predictor variable. The dependent variable considered was the presence of an AIS 2 or greater (2+) injury. Stepwise multiple regression was carried out to assess the sensitivity of occupant-based covariates. Covariates considered were age, sex and height. For this dataset, age and sex were significant covariates, while height was not. Using logistic regression, model significance and goodness of fit were evaluated for four variations of covariates, to determine which model best fit the data (Table 8.7). The model with age and sex performed best (AUROC>0.8).

Table 8.7. Model statistics for lower tibia force logistic regression.

Model Covariates	Studies used	Wald Pr>ChiSq	AUROC	Hosmer-Lemeshow Chi-Square	Hosmer-Lemeshow Pr>ChiSq	-2 Log L
None	A,B,D,E	0.0072	0.67	10.9	0.22	104.2
Age	A,B,D,E	0.0011	0.75	3.9	0.86	93.5
Age+Sex	A,B,D,E	0.0021	0.79	2.6	0.95	88.8
Sex	A,B,D,E	0.002	0.74	15.6	0.049	96.3

The logistic regression takes the form:

$$p(\text{AIS } 2+) = \frac{1}{1 + e^{(-\beta_0 - \beta_1 x - \beta_2 a - \beta_3 b)}}$$

where:

- β_0 = Intercept
- β_1 = Independent parameter coefficient
- x = Lower Tibia Axial Force (kN)
- β_2 = Age coefficient
- a = Subject age, in years
- β_3 = Sex coefficient
- b = Subject sex (Male = 1, Female = 0)

Table 8.8. Model parameter estimates.

Model	β_0	β_1	β_2	β_3
Age+Sex	-5.0755	0.4683	0.0633	-1.2109

For calculation of 95% confidence intervals (Figure 8.9), a baseline age of 40 years and sex equal to 1 (male) were assumed.

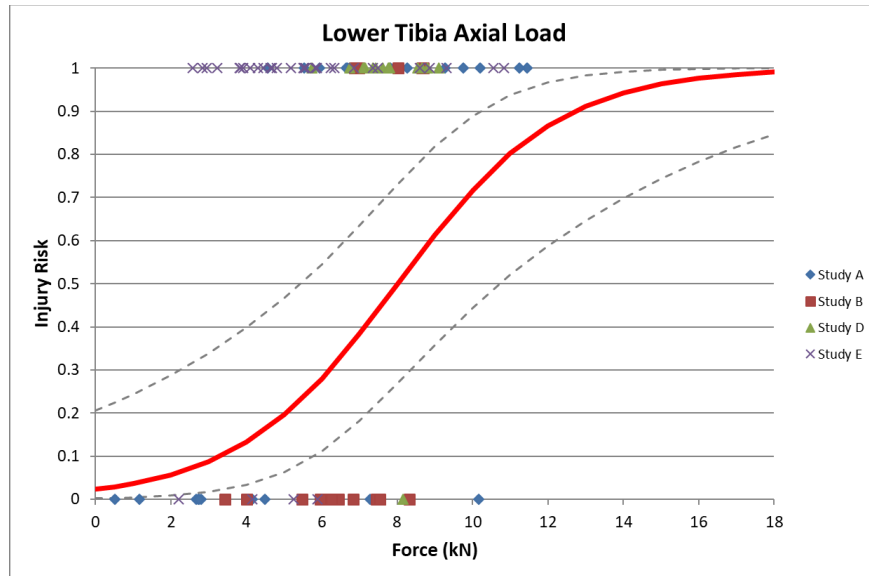


Figure 8.9. Logistic regression of lower tibia axial force data (mean injury risk function and 95% confidence intervals, assuming age of 40 years and male sex).

An alternate form of the risk function was developed using survival analysis. Survival analysis allows treatment of repeated tests as interval-censored data. For non-repeat tests, the data was treated as right-censored if no injury was sustained and left-censored if a fracture was sustained. The survival analysis risk function assumes a Weibull distribution and takes the form:

$$p(\text{AIS } 2+) = 1 - \exp\left(-\exp\left(\frac{\ln x - \beta_0 - \beta_1 a - \beta_2 b}{\alpha}\right)\right)$$

where:

- β_0 = Intercept
- x = Lower Tibia Axial Force (kN)
- β_1 = Age coefficient
- β_2 = Sex coefficient
- a = Subject age, in years
- b = Subject sex (1=male; 0=female)
- α = scale

Table 8.9. Model parameter estimates and goodness of fit.

Model	β_0	β_1	β_2	α	-2 Log L
Lower Tibia Axial Force	2.6935	-0.0198	0.0296	0.5494	104.4

Although the survival model has the advantage of passing through zero at zero stimulus, given the lower log likelihood values for the logistic model (compared with the survival model), the logistic regression curves are recommended.

8.7 Tibia Bending

8.7.1 Data

Compressive axial loading was shown to be the most common mechanism overall for below-knee injuries in Figure 8.2 based on the coded primary mechanism in CIREN cases. The mid-shaft region of the tibia is known to have a higher tolerance to axial loading than the epiphyseal regions, but field data studies suggest bending is a more common mechanism of fracture for the tibia diaphysis (Ivarsson et al., 2008). Tibia and fibula shaft fractures, while mostly attributed to compressive axial loading, also occur in frontal crashes as a result of applied bending from eccentric loads to the foot, ankle rotations, and leg interaction with the knee bolster and surrounding components. In addition to the externally-applied bending, the total bending moment in the mid-shaft is augmented by induced bending due to axial loading given the human tibia's curvature. Unlike a human, the THOR-50M leg is straight and does not experience induced bending from axial load.

The Tibia Index (TI) was developed as an injury criterion for combined bending and axial compressive loads in the mid-shaft of the tibia (Mertz et al., 1993). It was based on classical beam theory, and accounted for the interaction of stresses from bending and axial load. The Revised Tibia Index (RTI) was proposed by Kuppa et al. (2001), which incorporated updated critical values for both force and moment. However, RTI as formulated, may not add value to an independent injury risk function for axial force and resultant moment, given that RTI and resultant moment are highly correlated in THOR-50M tests (Figure 8.10).

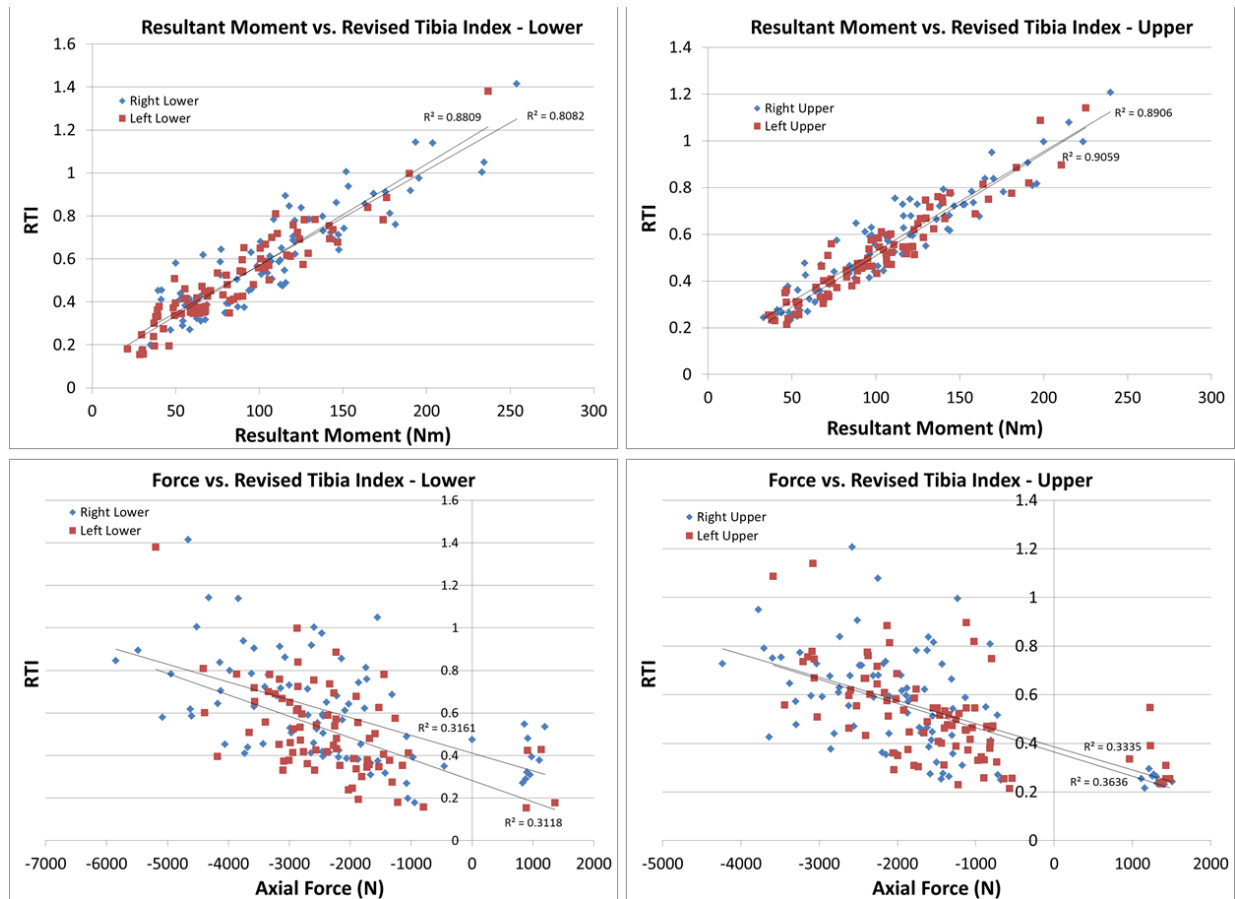


Figure 8.10. Tibia Force and Moment vs. RTI in THOR-50M tests.

A number of studies have examined tibia bending to failure (Table 8.11, APPENDIX G). Studies by Nyquist et al. (1985) and Schreiber et al. (1998) conducted quasi-static and dynamic tests at the mid-tibia, using varying load directions (anterior-posterior, AP, posterior-anterior, PA, and lateral-medial, LM). Only the dynamic results from these two studies were used. Some of Schreiber’s tests included an imposed axial load of 4448 N, which contributed an estimated 65 Nm in induced bending. This was added to the applied moment to determine the total moment for these tests.

Work conducted by Ivarsson et al. (2006) included pure bending, pure compression, and combined compression-bending loading. The impact location for all bending tests was at the distal 1/3 of the tibial shaft. Four levels of varying superimposed axial load were applied for the combined loading tests. For the AP combined loading tests, the total moment, inclusive of the applied moment and induced moment, was calculated and reported in Untaroiu et al. (2008) (Table 8.11). Note that for the Ivarsson et al. (2006) study, tests with injuries noted as being “In Distal Potting” or “Distal Potting Interface Fracture” were excluded.

Table 8.10. Available studies for tibia bending and combined loading.

Study	Impact location	Impact speed	Load direction	n	Loading type
Nyquist et al. (1985)	Mid-tibia	2.4 – 6.9 m/s	AP, LM	19	Pure Bending
Schreiber et al. (1998)	Mid-tibia	5.55 m/s	PA	12	Pure Bending
				9	Combined
Ivarsson et al. (2006)	Distal 1/3 of tibia	1.5 m/s	AP, PA	5	Pure Bending
			AP	16	Combined
			PA	10	Combined
			-	4	Pure Compression

Table 8.11. Summary statistics from bending studies.

Study		Average specimen age	Average applied moment (Nm)	Average total moment (Nm)
Nyquist et al. (1985)		56	300	300
Schreiber et al. (1998)	Pure Bending	68	408	408
	Combined	72	311	376
Ivarsson et al. (2006)	Pure Bending	51	252	252
	Combined, AP	55	149	257 [†]
	Combined, PA	55	147	- [‡]

[†]calculated by Untaroiu et al. (2008)

[‡]data not available to calculate the induced moment

8.7.2 Predictor variable

Because superimposed axial load affects the bending tolerance of the tibia (Schreiber et al., 1998; Untaroiu et al., 2008), two main predictor variables were investigated: Total moment and Revised Tibia Index. Both are presented here for completeness.

Total moment is comprised of the applied bending moment plus induced bending moments due to axial loading. The total moment risk function was developed using pure bending data (for which total moment equals applied moment) and the combined loading data for which total moment was able to be calculated (Ivarsson et al., 2006, Combined AP data).

RTI was also examined as a predictor variable, given previous formulations of a combined axial loading and bending moment metric (Kuppa et al., 2001). All available data (Table 8.11, APPENDIX G) could be used in the RTI-based risk function.

8.7.3 Injury Risk Function Formulation

Logistic regression-based analyses were not possible, because only failure data were available. Thus, risk functions were developed using survival analysis, assuming a Weibull distribution. Fracture moments were treated as uncensored for the survival analysis. Covariates considered were age, mass, sex. Mass and sex were not significant in any of the models and therefore were not considered further. Older

specimens in the sample tended to have higher failure moments (Figure 8.11). This effect may relate to differences between test conditions used in various studies, rather than age itself, since the Schreiber study had both the highest failure moments and highest average specimen age (Table 8.11). Because this effect is contrary to other studies indicating reduced tolerance to bone fracture with age (Yamada et al., 1970), age was not considered further in the model.

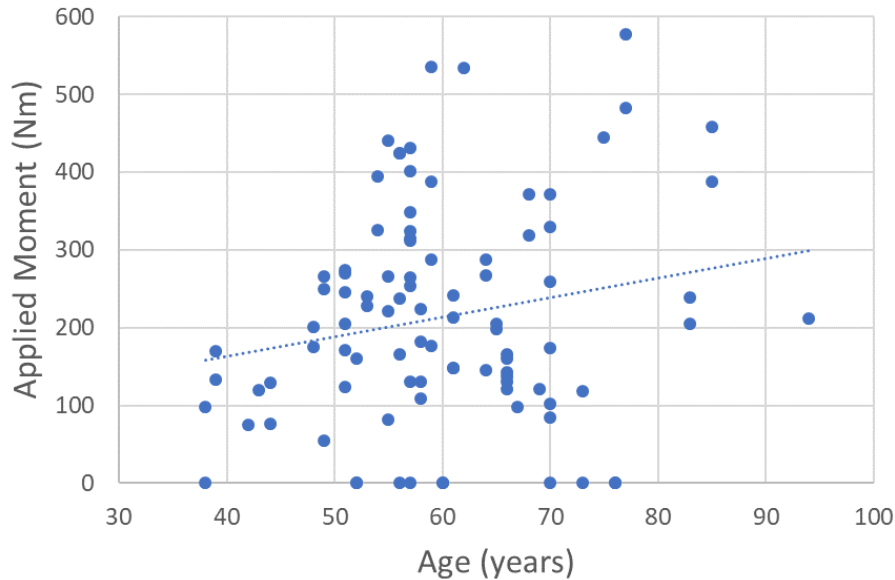


Figure 8.11. Failure moment as a function of age.

The survival analysis risk function takes the form:

$$p(\text{AIS } 2+) = 1 - \exp\left(-\exp\left(\frac{\ln x - \beta_0}{\alpha}\right)\right)$$

where:

- β_0 = Intercept
- x = Predictor variable
- α = scale

Table 8.12. Model parameter estimates for tibia bending.

Predictor	β_0	α
Total moment	5.8704	0.2947
RTI	0.3376	0.3213

8.8 Ankle Dorsiflexion

Ankle malleolar fractures, while frequently associated with compressive axial loading in the CIREN dataset (Figure 8.2), are more commonly associated with rotation of the ankle, i.e. dorsiflexion.

Available data in dorsiflexion includes a study by Portier et al. (1997) and a newer study by Rudd et al. (2004). The risk curve developed by Kuppaa et al. (2001) was based on data from Portier et al. (1997). Rudd combined both datasets to create survival-based injury risk curves based separately on moment and angle.

To evaluate risk function development in dorsiflexion, stepwise multiple regression was carried out to assess model fit using different combinations of datasets and predictor variables. Both ankle moment and angle were evaluated as predictor variables. The dependent variable considered was the presence of an AIS 2 or greater (2+) injury. Logistic regression on the original Portier et al. (1997) demonstrated poor goodness-of fit statistics (Table 8.13) and extremely wide 95% confidence intervals (Figure 8.12). In addition, the combined dataset also did not appear to be well correlated based on moment or angle, and therefore logistic regression did not yield sufficiently robust results (Table 8.13, Figure 8.12). Further work is necessary to understand the experimental data, examine confounding factors, and/or conduct additional tests.

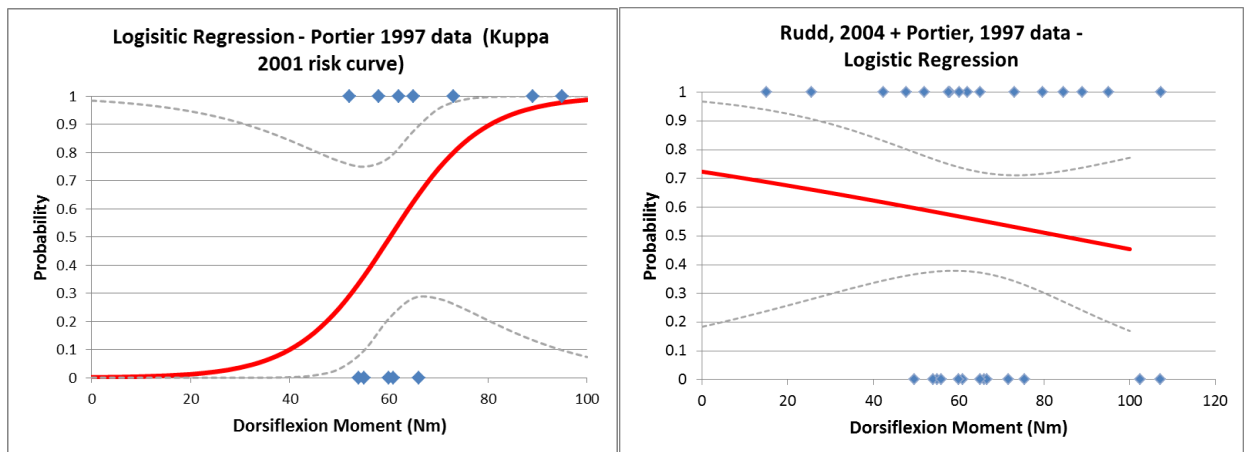


Figure 8.12. Logistic regressions on Portier et al. (1997) data alone and Portier and Rudd combined data demonstrates poor correlation. Dorsiflexion angle (not shown) also had poor correlation.

Table 8.13. Significance and goodness of fit statistics for logistic regression on combined dorsiflexion data.

Studies used	Predictor variable	Wald Pr>ChiSq	AUROC	Hosmer-Lemeshow Chi Square	Hosmer-Lemeshow Pr>ChiSq
Portier	Moment	0.22	0.71	10.5	0.40
Portier and Rudd	Moment	0.52	0.55	9.9	0.27
Portier and Rudd	Angle	0.09	0.73	7.1	0.53

While the lack of correlation in the available dorsiflexion data does not support development of a separate risk function at this time, results from field data analysis demonstrate that a focus on compression of the tibia and hindfoot will address most of the below-knee injuries (Figure 8.2). In addition, ankle dorsiflexion will rarely, if ever, occur in the absence of applied axial load. Thus, it is expected that there will be benefit for these injuries even by assessing injury based on only tibia loads and moments until a more in-depth examination of ankle rotation and the effects of axial loading can be conducted.

8.9 Ankle Inversion/Eversion

Ankle malleolar fractures, while mostly attributed to compressive axial loading in the CIREN dataset (Figure 8.2), also occur in frontal crashes as a result of rotation of the ankle, i.e. inversion/eversion. Several studies have examined inversion and eversion (Table 8.14 and Table 8.15). These studies were evaluated to determine whether they could be combined for risk function development. The risk curve published by Kuppa et al. (2001) was developed using only the mean and standard deviation from a set of quasi-static data conducted by Parenteau et al. (1998), rather than the original data from that paper. Additional inversion/eversion data comes from Begeman et al. (1993), Petit et al. (1996), Jaffredo et al. (2000) and Funk et al. (2002). Of these, the test conditions employed by Parenteau et al., Petit et al., Jaffredo et al., and Funk et al. were designed to impose rotations about a nominal center of rotation. By contrast, the condition used by Begeman et al. applied an off-axis load to the plantar surface of the foot, and did not control for rotation about the center of the ankle joint. Foot plate angles were reported in Begeman et al. as surrogate for ankle rotation, but because of the test setup, these were not equivalent. This is also evidenced by the significantly higher ankle failure angles seen in the Begeman test series, compared with the other studies noted (Table 8.15). For these reasons, Begeman data has not been included in further analysis.

Injury risk curves were developed by Funk et al. (2002) using survival analysis, with covariates of applied Achilles load, sex, and rotation direction (inversion vs. eversion) and neglecting the contribution of the few non-injury data points. The human ankle becomes much stiffer with axial load (either applied or via superimposed Achilles loading), while THOR doesn't demonstrate this behavior. Thus, it is unclear whether these risk curves can be directly applied to THOR. In addition, the Funk analysis used only the injury data and did not include the available non-injury data.

Table 8.14. Studies on inversion/eversion of foot/ankle.

Study	Condition	Rotation	n, injured	n, non- injured	Notes
A Begeman et al. (1993)	Dynamic	Inversion	6	3	
		Eversion	7	2	
B Petit et al. (1996)	Quasi- static	Inversion	5	0	Individual subject responses not reported
		Eversion	5	0	
C Parenteau et al. (1998)	Quasi- static	Inversion	8	0	
		Eversion	8	0	
D Jaffredo et al. (2000)	Dynamic	Inversion	0	6	Individual subject responses not reported
		Eversion	0	6	
E Funk et al. (2002)	Dynamic	Inversion	6	0	No applied Achilles load
		Eversion	7	0	
		Inversion	8	3	Applied Achilles load
		Eversion	10	2	

Table 8.15. Average failure and non-failure moments and angles in inversion and eversion.

Study	Rotation	Mean Failure Moment (N-m)	Non-injury moment range (N-m)	Mean Failure Angle (deg)	Mean Non- injury Angle (deg)
A Begeman et al. (1993)	Inversion	33 ± 7	14 to 70	61 ± 6	51 ± 16
	Eversion	41 ± 14	25 to 120	59 ± 6	45 ± 11
B Petit et al. (1996)	Inversion	40 ± 46	-	34 ± 8	-
	Eversion	35 ± 9	-	32 ± 7	-
C Parenteau et al. (1998)	Inversion	34 ± 15	-	34 ± 8	-
	Eversion	48 ± 12	-	32 ± 7	-
D Jaffredo et al. (2000)	Inversion	-	13 to 40	-	19 ± 5
	Eversion	-	24 to 71	-	13 ± 1
E Funk et al. (2002) (no Achilles load)	Inversion	24 ± 6	-	34 ± 10	-
	Eversion	42 ± 15	-	30 ± 8	-
Funk et al. (2002) (Achilles load)	Inversion	72 ± 26	40 to 115	40 ± 12	33 ± 20
	Eversion	141 ± 65	46 to 76	41 ± 9	30 ± 23

As previously described, it was desired to follow a consistent process by which to differentiate between non-correlated and well-correlated datasets when considering the development of injury risk functions. Thus, to evaluate risk function development in inversion/eversion, stepwise multiple regression was carried out to assess model fit using both ankle moment and angle were evaluated as predictor variables. The dependent variable considered was the presence of an AIS 2 or greater (2+) severity injury.

As Petit et al. and Jaffredo et al. reported only mean injury or non-injury moment/angle values (not individual responses), these data were also excluded from risk function development. Results demonstrated that the combined dataset was not well correlated based on either ankle angle or moment (Wald Pr > 0.05; AUROC < 0.8, Table 8.16) and therefore logistic regression did not yield sufficiently robust results.

Table 8.16. Significance and goodness of fit statistics for logistic regression on xversion data.

Studies Used	Rotation direction	Predictor variable	Wald Pr>ChiSq	AUROC	Hosmer-Lemeshow Chi Square	Hosmer-Lemeshow Pr>ChiSq
C,E	Inversion	Moment	0.11	0.80	3.9	0.69
C,E	Inversion	Angle	0.64	0.44	7.3	0.29
C,E	Eversion	Moment	0.65	0.5	6.6	0.35
C,E	Eversion	Angle	0.42	0.52	20.2	0.0025

Lack of non-injury data affected the logistic regression development. To investigate, the mean non-injury values from Jaffredo et al. (2000) were assigned to each of the 6 subjects in inversion and eversion. When those non-injury data points were included, ankle angle became a significant predictor of injury (Wald Pr < 0.05; AUROC > 0.8, Table 8.17), although goodness of fit statistic (based on Hosmer and Lemeshow test) was highly significant (p<0.0001), indicating that one can reject the null hypothesis that the model is correct. As such, the resulting logistic regressions was not considered further. Ankle moment did not correlate with injury, even with Jaffredo data included (Wald Pr > 0.05; AUROC < 0.8, Table 8.17).

Table 8.17. Significance and goodness of fit statistics for logistic regression on xversion data, including mean non-injury data from Jaffredo et al. (2000).

Studies Used	Rotation direction	Predictor variable	Wald Pr>ChiSq	AUROC	Hosmer-Lemeshow Chi Square	Hosmer-Lemeshow Pr>ChiSq
C,D,E	Inversion	Moment	0.506	0.56	3.5	0.75
C,D,E	Inversion	Angle	0.0150	0.81	30.9	0.0001
C,D,E	Eversion	Moment	0.3775	0.60	5.1	0.65
C,D,E	Eversion	Angle	0.0037	0.88	176.7	<0.0001

8.10 Application of Risk Functions to THOR-50M

Upper Tibia Force

$$p(\text{AIS } 2+) = \frac{1}{1 + e^{(0.5204 - 0.8189F + 0.0686m)}}$$

where:

- F = Peak compressive force measured by the Z-axis for the THOR upper tibia load cell (in kN)
- m = Subject mass (in kg)

Given the THOR-50M mass of 76.11 kg (per Section 1.3), simplifies to::

$$p(\text{AIS } 2+) = \frac{1}{1 + e^{(5.7415 - 0.8189F)}}$$

Lower Tibia Force

$$p(\text{AIS } 2+) = \frac{1}{1 + e^{(5.0755 - 0.4683F - 0.0633a + 1.2109\delta)}}$$

where:

- F = Peak compressive force measured by the z-axis for the THOR lower tibia load cell (in kN)
- a = Subject age (in years)
- δ = Subject sex (Male = 1, Female = 0)

Simplified, assuming a 40-year-old Male:

$$p(\text{AIS } 2+) = \frac{1}{1 + e^{(3.7544 - 0.4683F)}}$$

Tibia Bending Moment

$$p(\text{AIS } 2+) = 1 - e^{-e^{\left(\frac{\ln M_{res} - 5.8704}{0.2947}\right)}}$$

where:

- M_{res} = Peak resultant moment = $\left| \sqrt{M_x(t)^2 + M_y(t)^2} \right|_{max}$
- M_x, M_y = Moments measured at the x- and y-axes of the THOR upper or lower tibia load cell (in Nm)

Revised Tibia Index

$$p(\text{AIS } 2+) = 1 - e^{-e^{\left(\frac{\ln RTI - 0.3376}{0.3213}\right)^2}}$$

where:

$$RTI = \left| \frac{F_z(t)}{12,000} + \frac{M_{res}(t)}{240} \right|_{max}$$

$F_z(t)$ = Axial compressive force time-history measured at the z-axis of the THOR upper or lower tibia load cell (in N)

$M_{res}(t)$ = Resultant moment time-history = $\sqrt{M_x(t)^2 + M_y(t)^2}$

$M_x(t), M_y(t)$ = Moments measured at the x- and y-axes of the THOR upper or lower tibia load cell (in Nm)

8.11 Fleet Test Data: THOR-50M

The recommended lower extremity injury risk functions were applied to THOR-50M measurements collected in frontal rigid barrier and frontal Oblique fleet testing. Figure 8.13 and Figure 8.14 show the risk of AIS 2+ injury as a function of upper and lower tibia compressive force, respectively. Risk of AIS 2+ injury is below 10 percent for all test modes based on upper tibia compressive force, and 20 percent or below for all but one observation (an Oblique driver) based on lower tibia compressive force. Figure 8.15 and Figure 8.16 show the risk of tibia fracture as a function of upper and lower tibia resultant moment, respectively. Risk of tibia fracture is below 20 percent for all but one observation, and generally higher for the Oblique driver observations compared to the Oblique right front passenger and frontal driver. Figure 8.17 and Figure 8.18 show the risk of tibia fracture as a function of upper and lower RTI, respectively. As with tibia resultant moment, Oblique driver observations are generally higher than Oblique right front passenger and frontal driver observations. For the upper tibia, two observations (one Oblique driver and one Oblique right front passenger) showed risks above 20 percent. For the lower tibia, six observations (five Oblique driver and one frontal driver) showed risks above 20 percent. The observation showing the highest risk of AIS 2+ injury based on lower RTI (68%) also shows among the highest risk of AIS 2+ injury in the fleet tests based on both peak lower tibia resultant moment (21%) and peak lower tibia compressive force (18%).

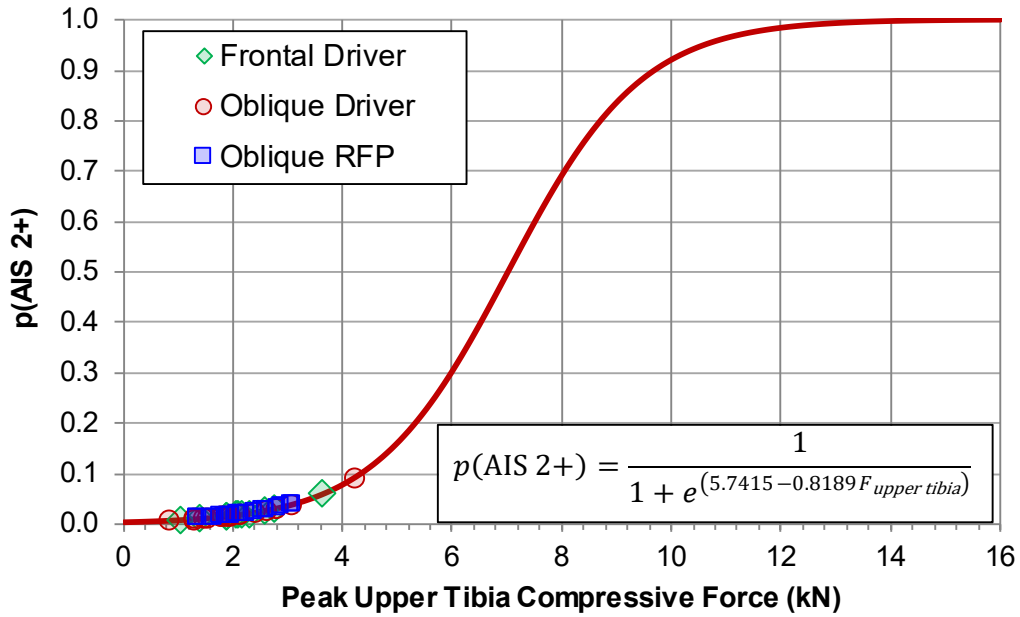


Figure 8.13. Probability of AIS 2+ lower leg injury predicted using peak upper tibia compressive force measured from fleet test results for the driver in the frontal rigid barrier test mode and both the driver and right front passenger in the Oblique MDB test mode.

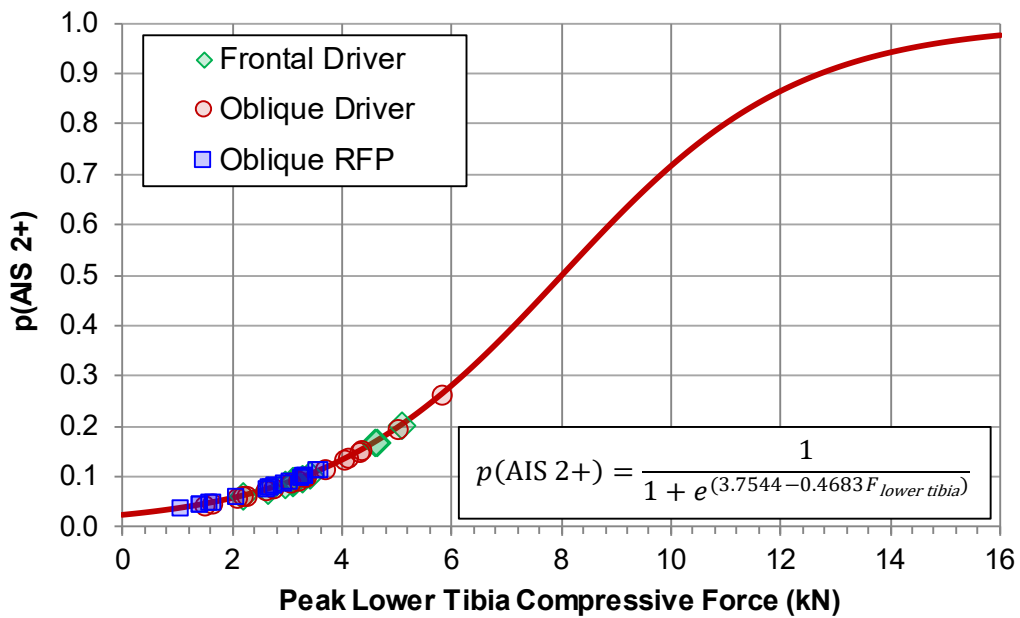


Figure 8.14. Probability of AIS 2+ lower leg injury predicted using peak lower tibia compressive force measured from fleet test results for the driver in the frontal rigid barrier test mode and both the driver and right front passenger in the Oblique MDB test mode.

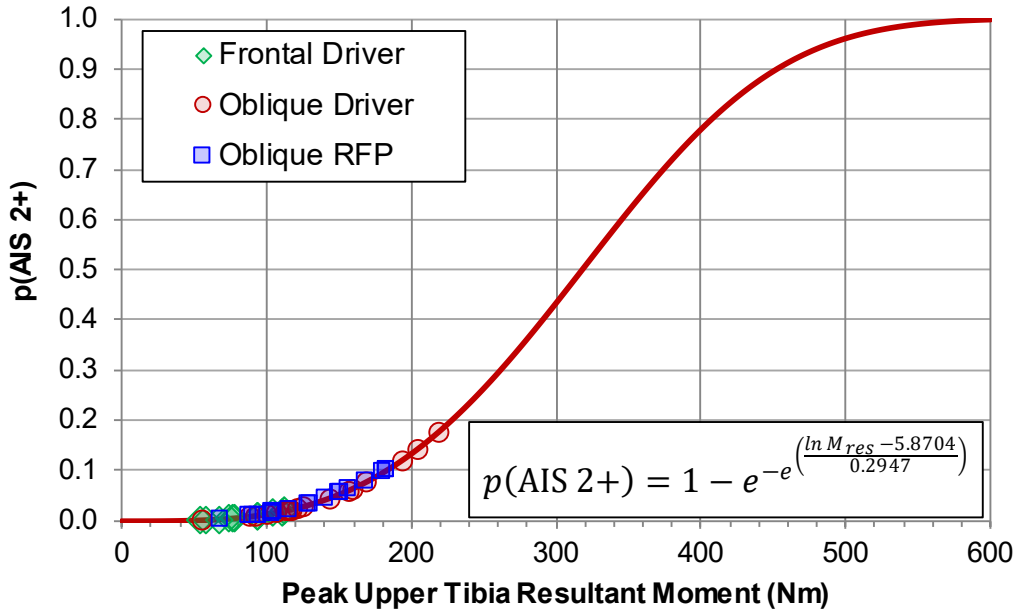


Figure 8.15. Probability of tibia fracture predicted using peak upper tibia resultant moment measured from fleet test results for the driver in the frontal rigid barrier test mode and both the driver and right front passenger in the Oblique MDB test mode.

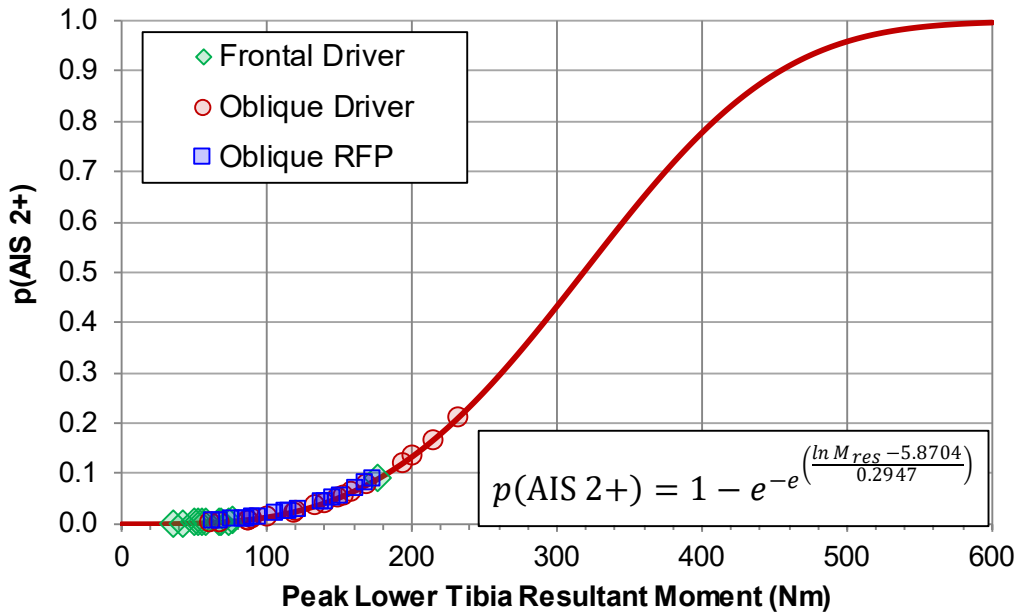


Figure 8.16. Probability of tibia fracture predicted using peak lower tibia resultant moment measured from fleet test results for the driver in the frontal rigid barrier test mode and both the driver and right front passenger in the Oblique MDB test mode.

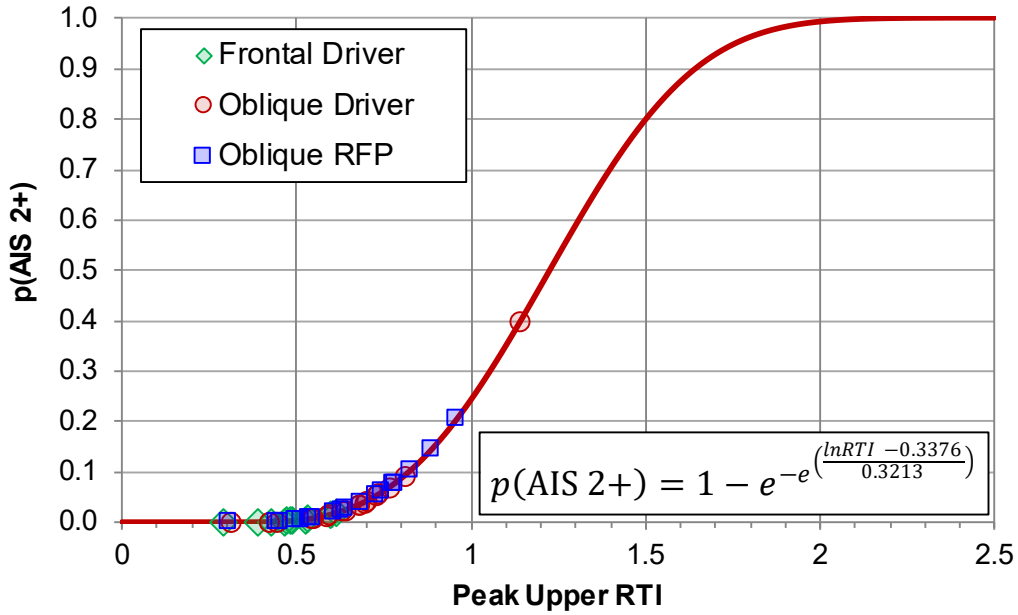


Figure 8.17. Probability of tibia fracture predicted using peak upper Revised Tibia Index measured from fleet test results for the driver in the frontal rigid barrier test mode and both the driver and right front passenger in the Oblique MDB test mode.

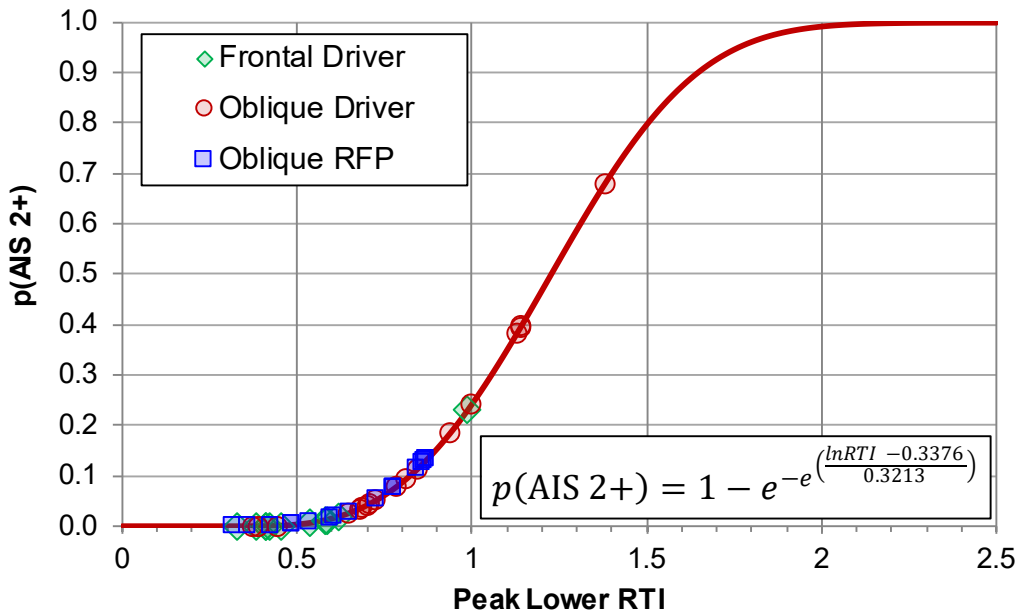


Figure 8.18. Probability of tibia fracture predicted using peak lower Revised Tibia Index measured from fleet test results for the driver in the frontal rigid barrier test mode and both the driver and right front passenger in the Oblique MDB test mode.

8.12 Limitations

Matched pair tests have not been conducted. Therefore, the risk functions presented here assume that THOR-50M responds exactly like a post-mortem human subjects (PMHS). This is a reasonable assumption given THOR-50M's good to excellent biofidelity (Parent et al., 2017).

Age was found to be a significant covariate in the lower tibia axial force risk function, but not in the risk function for upper tibia axial force. The intended age of application of the risk function (40 years old) is notably younger than the average age of the PMHS (73 years for upper tibia force) used to develop these risk functions. For tibia bending moment, as noted previously, older specimens tended to have higher failure moments than younger specimens, which is contrary to other studies indicating reduced tolerance to bone fracture with age. The effect found here may relate to differences between test conditions used in various studies, rather than age itself, since the study with the highest failure moments also had the highest average specimen age.

The injury risk function for lower tibia fracture was developed using datasets with different boundary conditions and load cell locations. While the similarity of the injury-producing forces supports the approach of combining these data, it is nonetheless a possible limitation. In addition, the lower tibia risk function was developed using data from human tibia load cells, without consideration of the load borne by the fibula. The design of the THOR-50M has a tibia that represents the human tibia/fibula. Given that in axial loading, the fibula of a human bears only 6% of the axial load when the ankle is neutrally oriented (Funk et al., 2004), the injury risk formulation may be only slightly improved by separately accounting for fibula load.

Previous experimental studies (Kitagawa et al., 1998; Funk et al., 2002) have examined the influence of Achilles tension on foot/ankle fracture. While Funk et al. (2002) demonstrated that Achilles tension was significant in the prediction of fracture location, Achilles tension was not significant in the prediction of fracture force. Given that the Achilles tension is not known for a given motor vehicle crash occupant, nor is the relationship between the THOR Achilles tension and that of a given motor vehicle crash occupant, the necessary information to include Achilles tension in the risk function is not available. Nonetheless, should this information become available, Achilles tension may prove important in the prediction of fracture risk.

The injury risk functions for tibia bending had several limitations. The risk functions were developed using datasets with differing load directions, impact location, and impact speed. Induced bending moment was unavailable for some of the specimens tested in combined loading, and was estimated for some of the specimens. This resulted in less possible data being used in the total moment-based risk curve, compared with the RTI-based risk curve. In addition, all specimens were tested to failure. Without non-failure data, logistic regression analysis was not possible and therefore the approach used here differed from that of other body regions. Finally, the manner in which the load was applied to the PMHS specimens (i.e. three-point bending) may not be equivalent to the load that would be applied to a THOR-50M tibia in a crash test. In contrast to the mid-tibia loading in the simplified experiments, a modern vehicle interior may present various load paths to the lower extremity, including knee and

upper tibia contact with knee bolsters (with and without airbags), foot and ankle contact with the toepan, footrest, and pedals, and dynamic intrusion of these components.

9 COMPARING FLEET AND FIELD ESTIMATED INJURY RISK

9.1 Introduction

Many studies have attempted to compare the predicted risk of injury as estimated using test dummies and injury criteria in standardized crash tests (Laituri et al., 2009; Prasad et al., 2010; Prasad et al., 2014; Mueller et al., 2015) versus the risk of injury from real-world crash data (i.e. field data). While those studies described “risk” of injury-based point estimates derived from field data and compared them to estimates derived from crash or fleet test data with ATDs, they did not always describe the limitations of the field and/or fleet data (e.g. acknowledge or account for all occupant / crash parameters that affect injury risk) or they did not attempt to describe the error associated with their point or mean estimates of injury risk.

Like the prior studies, the aim of this study was to compare the risk or rates of injury in the real-world crashes versus the predicted risk of injury given frontal crash tests with the THOR-50M and the associated injury measures and risk functions presented earlier in this report.

9.2 Methods

To compare the risk of injury predicted by THOR-50M in crash tests versus the risk of injury in field data it is necessary to describe the severity of the crash test and then attempt to select field cases with equivalent severity.

9.2.1 Crash Tests

For both the left oblique and full frontal conditions, the fleet vehicles chosen for comparison to the field data are vehicles that performed ‘Acceptable’ or better overall in the Insurance Institute for Highway Safety’s (IIHS) small overlap impact (SOI) test condition (IIHS, 2017). The vehicles also had to be equipped with a FMVSS No. 226 compliant side curtain airbag. Both of these prerequisites were intent on evaluating vehicles in the left oblique condition that represent the current state of the art for frontal crash safety. The table with full frontal and oblique driver tests that were used in this analysis can be found in APPENDIX D.

9.2.1.1 Left Oblique

NHTSA has performed over 50 left oblique crash tests. The original aim of the test procedure (Saunders et al., 2011; 2012) was to produce a peak delta-V (or change in velocity) of 56 kph (35 mph) when testing an average size (approximately 1,500 kg) passenger car. The test involves a moving deformable barrier (MDB) striking a stationary vehicle. The overlap between the target vehicle and the MDB is 35% and the angle is 15 degrees. For qualifying vehicle models as described above, the resulting peak delta-V observed in NHTSA left oblique crash tests has ranged from 46 to 67 kph while the estimated principal direction of force (PDOF) has ranged from 336° to 343°. The damage extent, per SAE J224 (SAE, 1980), ranged from 3-6 in these tests.

9.2.1.2 Full Frontal

NHTSA's 0-degree, full overlap rigid barrier test of 56 kph (35 mph) results in a delta-V of approximately 64 kph (40 mph) including rebound velocity. Generally, the damage, per SAE J224, is an extent of 3 for full frontal NCAP tests.

9.2.2 Treatment of NASS-CDS Sample

As mentioned earlier, the aim is to compare field and fleet injury rates/risks and confidence intervals for crash populations of similar severity. In doing so, it is necessary that we restrict the NASS-CDS sample to crash/restraint system/occupant characteristics (delta-V, belt use, crash type, occupant type/age, airbag deployment status) that are similar to the characteristics of the full frontal and oblique crash tests with a belted, airbag restrained THOR-50M.

NASS-CDS is considered a panel survey given that it samples the same data from the same sample or primary sampling units (PSUs) over multiple periods (years). Since the same PSUs are included over multiple case years, the annual estimates can be considered to be positively correlated. In using consecutive years of NASS-CDS data, the dataset needs to be correlated to estimate variance for a pooled, multi-year sample. For the purpose of this analysis, the last 15 years of NASS-CDS (2001 to 2015) are being studied. All of those years with the exception of 2002 to 2007 were limited to the same 24 Primary Sampling Units (PSUs). To maintain a correlated sample, data must be summed from the same 24 PSUs for all years in the sample. Case years 2002 to 2007 had three extra PSUs (42, 47 and 50). These three "extra" PSUs are removed to maintain a correlated sample from 2001 to 2015. PSUs 42, 47, and 50 were in the same stratum as PSUs 9 and 45. The sample weights for PSU 9 (adjusted weight equals $19.66987/7.67598$ times the ratwgt) and 45 (adjusted weight equals $41.43575/16.16911$ times the ratwgt) are adjusted to account for the removal of PSUs 42, 47 and 50. The resulting adjusted weight sample of data from 24 PSUs is the correlated sample used here forward.

Another requirement in maintaining a correlated sample is that we consider the type of data sampled in each year. For NASS-CDS 2001 to 2008, occupant injury and crash data was collected on all vehicles, regardless of vehicle age. Starting in 2009, occupant injury data was only collected and recorded for vehicles that were 10-years-old or newer. For 2009 to 2015 this means that roughly 40% of passenger cars/light trucks/vans did not have injury data recorded. To maintain a correlated sample of injury and non-injury data over the 15 years of NASS-CDS included, all years, including 2001 to 2008, were restricted to analysis of data for vehicles that were 10-years-old or newer in the respective sample years. This results in a range of vehicle model years from 1990 to 2015. While conventional wisdom would have one assume that the newer vehicle would be safer (have a lower injury risk for a given crash type) and that including older vehicles in the sample would present higher injury risk or rates than newer vehicles, the brain (Figure 3.1) and chest injury (Figure 5.2) trends shown earlier in this report suggest that newer vehicles actually have a higher risk of injury for some body regions. Additionally, in looking at the 2001-2015 sample (belted drivers in frontal crashes) with the vehicle model year restriction, there is no significant trend (increase or decrease) in the risk of MAIS 2+ or MAIS 3+ injuries (Figure 9.1). While the relative size of the targeted sample domain as a percent of the total sample does

not change significantly year to year (more on this soon), including more case years allows for a larger raw count sample of cases to be included in the weighted analysis.

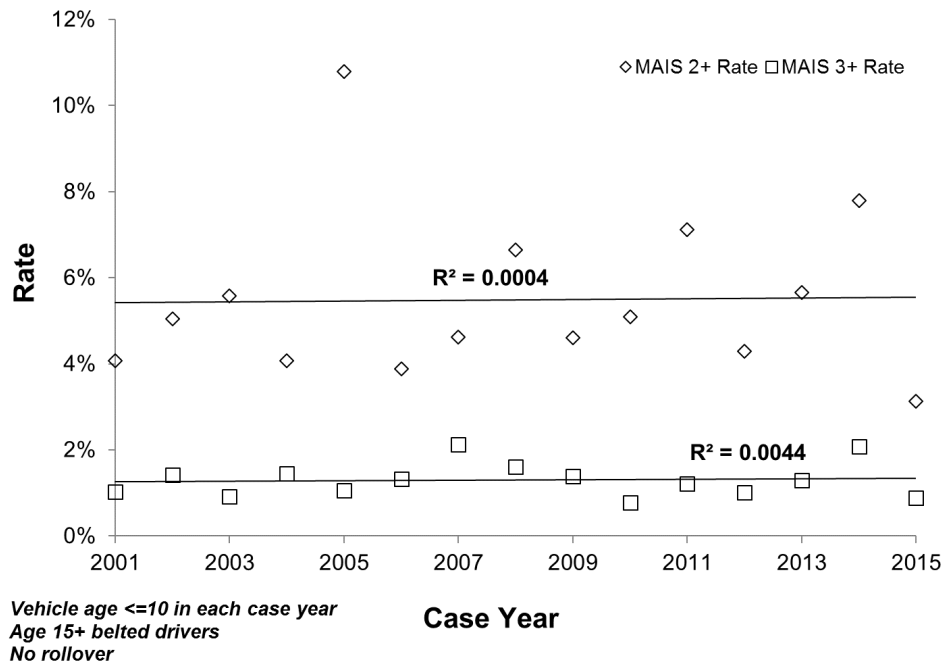


Figure 9.1. MAIS 2+ and 3+ rates for belted drivers in frontal crashes, NASS-CDS 2001 to 2015.

9.2.3 Crash / Occupant / Vehicle Parameters

NASS-CDS records numerous parameters that describe the crash type (type of object contacted, area and type of damage, principal direction of force), severity (damage extent, delta-V, intrusion), occupant type (age, sex, height, weight, seat position, seat track position) and restraint system (belt usage, airbag deployment). The current analysis balances relative domain size concerns (i.e. sample size; details below) and the desire to “match” the full frontal and oblique condition through the selection of crash, occupant and restraint system parameters.

9.2.4 Injury Data

The occupant injury in NASS-CDS is queried for AIS 2+, 3+ and/or 4+ injury severities per AIS 1995/1998 (AAAM, 1998). While AIS 2005/2008 is the latest version (AAAM, 2008), NHTSA did not begin using it until 2010. Prior years used AIS 1995/1998 and 2010 through 2015 has both sets of AIS codes.

For comparing field and fleet data, it is necessary to group the field injury data to match with the intended target population for the corresponding THOR-50M injury measure. Table 9.1 summarizes how the respective injury data and THOR-50M injury measures are being paired for the analysis.

Table 9.1. AIS body regions / injury severity and paired THOR-50M injury measures.

AIS Body Region / Injury - Severity	THOR-50M Injury Measure
Skull or Facial Fracture - 2+	HIC ₁₅
Skull or Facial Fracture - 3+	HIC ₁₅
Brain - 3+	BrIC
Brain - 4+	BrIC
Neck - 2+	Nij
Neck - 3+	Nij
Thorax - 3+	Resultant Chest Deflection (mm)
Abdomen - 3+	Resultant Abdomen Deflection (mm)
Hip/Pelvis - 2+	Resultant Acetabulum Force (N)
Thigh - 2+	Femur Axial Force (N)
Knee - 2+	Femur Axial Force (N)
Proximal Tibia - 2+	Upper Tibia Axial Force (N)
Tibia, Fibula Shaft - 2+	Upper and Lower Resultant Moment (Nm)
Distal Tibia - 2+	Lower Tibia Axial Force (N)

9.2.5 Sample Domain

The size of the target sample relative to the full NASS-CDS sample was considered a constraint in this study. Purcell and Kish (1979) described four classes of relative domain sizes (P_d). Equation (9.1) simply describes what the relative domain size is.

$$P_d = \frac{N_d}{N} \quad [9.1]$$

where N_d is the domain of interest and N is the size of the full sample domain.

For example, N_d is the domain represented by belted drivers in NCAP Frontal crashes over a given delta-V range in NASS-CDS case years 2001-2015 for vehicle ages of less than or equal to 10 years. In this case, N is the total size of the weighted sample for NASS-CDS 2001-2015.

Purcell and Kish (1979) described four classes of P_d .

- Class 1 - Major Domain: $P_d > 1/10$ (or 10%)
- Class 2 - Minor Domain: $1/10 \leq P_d \leq 1/100$ (or 10% to 1%)
- Class 3 - Mini Domain: $1/100 \leq P_d \leq 1/1,000$ (or 1% to 0.1%)
- Class 4 - Rare Type Domain: $1/1,000 \leq P_d \leq 1/10,000$ (or 0.1% to 0.01%)

Purcell and Kish cautioned related to the use of class 3 and class 4 domain sizes. For class 3 they noted that “standard methods of survey estimation break down.” For class 4 or Rare Type, they stated that

“for truly rare items (class 4), sample surveys are usually useless; separate and distinct methods are required.”

For the purposes of the current study, the aim will be to narrow the target population from frontal crashes down to no smaller than a class 3 domain relative to the full NASS-CDS domain. While aiming for a larger (e.g. class 2) relative domain size would be desirable, the reason why this is not achievable will be discussed shortly.

9.2.6 Point Estimates and Confidence Intervals

Mean injury risk, standard deviation and 95% confidence intervals are calculated for the respective combinations of fleet data. The upper and lower limit at the 95% confidence level is calculated using equation 9.2, where 1.96, the Z-score at 95% confidence interval, is multiplied by the standard error of the mean (standard deviation (σ) divided by the square root of the sample size (n)). The resulting product is added and subtracted from the sample mean to establish the upper and lower confidence limits, respectively. It is this mean and the upper and lower 95% confidence limits that can be compared to field data estimates. If the confidence interval of the fleet and field data overlaps, then we cannot reject the hypothesis that the two rates are the same.

$$\text{95\% Confidence Limits} = \text{Sample Mean} \pm 1.96 * \frac{\sigma}{\sqrt{n}} \quad [9.2]$$

For field data estimates, the correlated sample with adjusted weights is used with the PROC SURVEYFREQ procedure in SAS 9.3 (SAS Institute, Inc.) to produce a point estimate for the rate of injury in the NASS-CDS sample as well as the upper and lower 95% confidence intervals.

9.3 Results

9.3.1 Parameter Selection

The previously stated aim was to look at the point estimate and associated 95% confidence interval for injury risk in crashes of similar severity to those that are represented in the frontal oblique and full frontal test conditions. Below are the final selected parameters that were used.

- **Delta-V:** 41 to 67 kph
- **Damage Extent:** 3 to 6
- **Type of Crash:** SOI, Offset, Full frontal with PDOF of 320-40
- **Seatbelt Use:** Yes
- **Airbag Deployment:** Yes
- **Seat Position:** Driver
- **Rollover:** No
- **Occupant Ejection:** No
- **Vehicle Age:** \leq 10 years old to allow for target domain to go from 2001-2015

- **Case Years:** 2001-2015
- **Object Contacted:** Vehicle or large fixed object (medium/large pole, large tree, building, bridge, concrete barrier, building, wall, ditch/culvert)

The range of delta-Vs observed in NHTSA’s frontal oblique fleet testing of vehicles that qualified for this analysis (e.g. “Acceptable” or better structural performance in IIHS testing) was 46 kph to 62 kph. To support the inclusion of more cases the range of delta-Vs used in the current study was extended by 5 kph above and below the fleet range. The delta-V range used in the field versus fleet analysis here was restricted to crashes with delta-V greater than or equal to 41 kph, but less than or equal to 67 mph. In addition to overlapping the range seen in oblique tests, this range also captures the delta-Vs observed in the 35 mph (56.3 kph) full frontal NCAP/FMVSS No.208 test condition. Additionally, given observed crash damage extent severities of 3 to 6, the field data was also restricted to crashes with a damage extent of 3 to 6. Restricting only to extent and not delta-V results in the average crash being much less severe than our standardized test (Table 9.2).

Table 9.2 shows the mean delta-V values for frontal crashes by damage extent. It can be seen that the average delta-V is much higher for MAIS 3+ injury cases than when all cases are included. Further, it can be seen in Table 9.3 how much influence filtering crash severity has on the estimated risk of injury when looking at the final selected crash parameters versus severity filtering only by extent versus no severity filter.

Table 9.2. Delta-V (DV) versus damage extent for all cases versus MAIS 3+ cases (NASS-CDS 2010-15, frontal crashes, belted drivers).

Damage Extent	MAIS 3+ DV (kph)	All MAIS DV (kph)
1	20.6	18.1
2	31.1	24.9
3	41.5	28.5
4	54.5	29.5
5	61.9	24.4
6	54.8	20.1
7	39.4	20.5
8	53.6	18.7
9	31.3	18.1

Attempts were made to look at specific crash types (small overlap left and right, left and right oblique, left and right offset, full frontal) as individual domains, but the domain sizes were always class 4. Therefore, all frontal crashes were grouped together in a single domain with PDOF ranging from 320 to 40 degrees. Given that the majority of field cases are drivers and the fact that we have matched tests in both full frontal and left oblique with THOR-50M, the target population was limited to age 15 and older, belted drivers. Additionally, since all of our fleet tests at these severities result in airbag deployment, the

cases were restricted to those with airbag deployment. Crashes were restricted to vehicle to vehicle crashes and crashes with large fixed objects such as large trees/poles and concrete barriers/walls/buildings, covering almost 90% of frontal crashes that met the other restrictions of target crash population.

Vehicle age was also restricted to vehicles that were 10-years old or newer in their given sample year. This was done due to the fact that for 2009-2015 NASS-CDS injury data was only collected for newer vehicles, while in earlier NASS-CDS case years, injury data was collected for all sampled vehicles. Given this restriction and the requirement to have a correlated sample, 2001 to 2008 NASS-CDS data analysis was also limited to vehicles that were 10-years old and newer.

The relative domain size aim of being class 3 or higher can be achieved by looking at one year of NASS-CDS data. However, the raw count sample size can be very small if restricting to a single year. Similarly, restricting to case years 2010-2015 also presents a relatively small sample of crashes. When looking at only 2010-2015 and restricting to the parameters listed above the raw count sample is limited to only 172 cases (20,701 weighted) with 93 that are MAIS 2+ and 46 that are MAIS 3+. In contrast, when including case years 2001 to 2009 the raw count sample goes up to 602 (72,933 weighted) with 337 MAIS 2+ and 207 MAIS 3+ cases, respectively. Thus, as previously described in the methods section, case years 2001 to 2015 were used.

As noted earlier, while class 3 or higher was the aim, it would be desirable to have a class 2 or higher relative domain size. For belted drivers in 320 to 40-degree PDOF full frontal, offset or small overlap frontal crashes to have a domain size of 2, the delta-V restriction has to be removed. With the delta-V restriction removed (second dataset in Table 9.3), Pd equals 1.19%. This puts the relative domain size for that sample just over the border from class 3 to class 2. However, as discussed earlier, these crashes on average are less severe than NHTSA's full frontal and left oblique crash conditions when restricting to only damage extent as the severity filter.

Table 9.3. Frontal crash severity groupings vs. injury risk estimates.

Injury Risk: All Injuries by Body Region, Age 15+, Belted NCAP Frontal Drivers (2001-2015)¹													
Injury	1. 41-67 KPH and Extent 3-6²				2. Extent 3-6³				3. All⁴				
	Point Estimate	Std Error	CI Lower	CI Upper	Point Estimate	Std Error	CI Lower	CI Upper	Point Estimate	Std Error	CI Lower	CI Upper	
MAIS 2+	52.9%	4.3%	43.4%	62.3%	18.4%	2.6%	12.7%	24.1%	7.9%	0.6%	6.7%	9.1%	
MAIS 3+	27.9%	5.3%	16.4%	39.3%	7.7%	0.9%	5.8%	9.7%	2.4%	0.3%	1.7%	3.0%	
All Head and Face - 2+	9.8%	3.1%	3.1%	16.6%	4.0%	0.5%	3.0%	5.0%	1.6%	0.1%	1.3%	2.0%	
All Head and Face - 3+	5.9%	3.0%	0.0%	12.4%	1.2%	0.4%	0.4%	2.0%	0.4%	0.1%	0.2%	0.5%	
Skull or Facial Fracture - 2+	1.4%	0.7%	0.0%	3.0%	0.6%	0.1%	0.4%	0.7%	0.2%	0.0%	0.2%	0.2%	
Skull or Facial Fracture - 3+	0.2%	0.1%	0.0%	0.4%	0.2%	0.1%	0.1%	0.3%	0.1%	0.0%	0.0%	0.1%	
Brain - 2+	8.8%	2.9%	2.4%	15.2%	3.7%	0.5%	2.7%	4.6%	1.5%	0.1%	1.2%	1.8%	
Brain - 3+	5.9%	3.0%	0.0%	12.4%	1.1%	0.4%	0.4%	1.9%	0.3%	0.1%	0.2%	0.5%	
Brain - 4+	3.0%	1.2%	0.3%	5.6%	0.6%	0.1%	0.3%	0.8%	0.2%	0.0%	0.1%	0.2%	
Neck - 2+	2.5%	0.5%	1.4%	3.7%	0.8%	0.1%	0.6%	1.1%	0.4%	0.1%	0.1%	0.7%	
Neck - 3+	0.6%	0.4%	0.0%	1.4%	0.2%	0.1%	0.1%	0.3%	0.1%	0.0%	0.1%	0.2%	
Thorax - 2+	14.0%	4.0%	5.4%	22.6%	4.6%	0.6%	3.2%	6.0%	1.7%	0.3%	1.1%	2.4%	
Thorax - 3+	11.0%	3.6%	3.2%	18.9%	3.4%	0.6%	2.1%	4.7%	1.0%	0.2%	0.7%	1.3%	
Thorax (skeletal) - 2+	11.1%	3.0%	4.6%	17.7%	3.5%	0.6%	2.2%	4.8%	1.4%	0.3%	0.8%	2.1%	
Thorax (skeletal) - 3+	6.7%	2.3%	1.7%	11.7%	2.0%	0.6%	0.6%	3.3%	0.6%	0.2%	0.3%	1.0%	
Abdomen - 2+	3.6%	1.0%	1.5%	5.7%	1.3%	0.2%	0.8%	1.8%	0.5%	0.1%	0.3%	0.6%	
Abdomen - 3+	1.4%	0.7%	0.0%	3.0%	0.5%	0.1%	0.3%	0.7%	0.2%	0.0%	0.1%	0.3%	
Lower Extremities - 2+	32.7%	4.9%	22.0%	43.3%	9.1%	0.9%	7.2%	11.1%	3.4%	0.2%	2.9%	4.0%	
Lower Extremities - 3+	12.2%	1.7%	8.5%	15.9%	3.3%	0.4%	2.5%	4.1%	0.9%	0.1%	0.7%	1.0%	
Knee, Thigh or Hip - 2+	13.9%	3.8%	5.6%	22.1%	4.4%	0.5%	3.3%	5.6%	1.5%	0.1%	1.2%	1.9%	
Knee, Thigh or Hip - 3+	7.4%	1.6%	4.0%	10.8%	1.9%	0.2%	1.4%	2.5%	0.5%	0.1%	0.4%	0.7%	
Hip/Pelvis - 2+	4.8%	2.1%	0.1%	9.5%	1.3%	0.4%	0.6%	2.1%	0.3%	0.1%	0.1%	0.6%	
Hip/Pelvis - 3+	1.2%	0.5%	0.1%	2.4%	0.5%	0.2%	0.2%	0.8%	0.1%	0.0%	0.0%	0.3%	
Thigh - 2+	8.1%	1.9%	3.9%	12.3%	1.8%	0.3%	1.3%	2.4%	0.5%	0.0%	0.4%	0.6%	
Knee - 2+	4.4%	1.5%	1.2%	7.6%	2.1%	0.4%	1.2%	3.0%	0.9%	0.2%	0.6%	1.3%	
Leg, Foot or Ankle - 2+	24.5%	5.0%	13.6%	35.5%	6.1%	0.6%	4.8%	7.5%	2.2%	0.3%	1.6%	2.9%	
Leg, Foot or Ankle - 3+	6.4%	1.1%	4.0%	8.9%	1.7%	0.3%	1.1%	2.4%	0.4%	0.1%	0.3%	0.6%	
Tibia / Fibula ALL - 2+	16.8%	4.1%	7.8%	25.8%	4.2%	0.6%	3.0%	5.5%	1.6%	0.3%	1.0%	2.2%	
Tibia / Fibula ALL - 3+	6.4%	1.1%	4.0%	8.9%	1.7%	0.3%	1.1%	2.4%	0.4%	0.1%	0.3%	0.6%	
Proximal Tibia - 2+	2.1%	0.9%	0.1%	4.0%	0.8%	0.2%	0.4%	1.2%	0.2%	0.0%	0.1%	0.3%	
Proximal Tibia - 3+	1.3%	0.6%	0.0%	2.6%	0.4%	0.1%	0.2%	0.6%	0.1%	0.0%	0.0%	0.2%	
Tibia, Fibula Shaft - 2+	9.2%	1.3%	6.3%	12.0%	2.2%	0.3%	1.5%	2.9%	0.6%	0.1%	0.5%	0.8%	
Tibia, Fibula Shaft - 3+	3.3%	1.2%	0.6%	6.0%	0.8%	0.2%	0.4%	1.1%	0.2%	0.0%	0.1%	0.3%	
Distal Tibia - 2+	10.6%	5.0%	0.0%	21.5%	2.4%	0.5%	1.4%	3.4%	1.0%	0.2%	0.5%	1.5%	
Distal Tibia - 3+	2.6%	1.0%	0.3%	4.9%	0.7%	0.3%	0.1%	1.3%	0.2%	0.0%	0.0%	0.3%	
Foot/Ankle - 2+	17.9%	5.3%	6.4%	29.4%	4.0%	0.4%	3.1%	4.9%	1.5%	0.3%	0.8%	2.2%	

1. NASS-CDS - Full frontal, offset, SOI; PDOFs of 320 to 40 deg; no center narrow and no unknown PDOF cases

2. Vehicle to vehicle/large fixed object (large tree, medium/large pole, concrete barrier/wall/building/bridge/ditch/culvert); rollover=0; bagdeploy=1; vehage<=10; no ejection (P_d=0.12%)

3. No Delta-V restrictions (P_d=1.19%)

4. No Delta-V or Damage Extent Restrictions (P_d=7.1%)

9.3.2 Fleet Data Injury Values

Table 9.4 and Table 9.5 show the injury value summary for the full frontal and left oblique driver tests with the THOR-50M, respectively. For full frontal there are 11 vehicle tests included while left oblique includes 18 (APPENDIX D).

Table 9.4. Full frontal fleet injury value summary, THOR-50M driver (n=11).

Injury Measure	Avg	SD	95% CI		Min	Max
			Lwr	Upr		
HIC ₁₅	278	88	226	330	149	453
BrIC	0.68	0.10	0.62	0.74	0.53	0.85
Nij	0.48	0.11	0.41	0.54	0.30	0.68
Chest Deflection (mm)	49.7	7.4	45.4	54.1	38.0	65.5
Abdomen Deflection (mm)	60.2	4.2	57.7	62.7	53.1	65.0
Acetabulum Peak F (N)	2032	636	1656	2407	1148	3384
Femur Peak F (N)	3764	1152	3083	4445	2501	6727
Tibia Upper Peak F (N)	2144	688	1737	2551	1035	3627
Tibia Lower Peak F (N)	3459	909	2922	3996	2177	5076
Tibia Moment Peak (Nm)	90	34	70	110	56	177

Table 9.5. Left oblique fleet injury value summary, THOR-50M driver (n=18).

Injury Measure	Avg	SD	95% CI		Min	Max
			Lwr	Upr		
HIC ₁₅	230	61	203	258	104	321
BrIC	0.94	0.24	0.83	1.05	0.59	1.29
Nij	0.52	0.11	0.47	0.58	0.32	0.70
Chest Deflection (mm)	54.0	5.8	51.3	56.7	42.7	62.3
Abdomen Deflection (mm)	57.1	6.2	54.2	59.9	43.8	67.7
Acetabulum Peak F (N)	2849	867	2448	3250	1828	4673
Femur Peak F (N)	4895	1908	4014	5777	2401	9184
Tibia Upper Peak F (N)	2034	778	1675	2394	812	4218
Tibia Lower Peak F (N)	3796	2169	2794	4798	1504	11204
Tibia Moment Peak (Nm)	148	45	127	169	67	232

9.3.3 Injury Risk Point Estimates and Confidence Intervals

Table 9.6 and Table 9.7 show the injury risk summary for the full frontal and left oblique driver tests with the THOR-50M, respectively. The full frontal tests are from 11 vehicles while the left oblique test is from 18 (see APPENDIX D for the make, model and model year of vehicles tested along with the NHTSA test number).

Table 9.6. Fleet injury risk for full frontal tests with THOR-50M seated in driver's seat (n=11).

Injury Measure - Severity	Avg	SD	95% CI		Min	Max
			Lwr	Upr		
Skull/Facial Fx (HIC ₁₅) - 2+	6.2%	4.4%	3.6%	8.8%	1.0%	15.8%
Skull/Facial Fx (HIC ₁₅) - 3+	0.9%	1.0%	0.33%	1.6%	0.0%	3.5%
Brain (BrIC) - 2+	26.1%	19.9%	14.3%	37.8%	0.2%	64.0%
Brain (BrIC) - 3+	12.5%	10.5%	6.3%	18.7%	0.1%	34.3%
Brain (BrIC) - 4+	9.0%	7.8%	4.5%	13.6%	0.1%	25.5%
Neck (Nij) - 2+	5.1%	3.3%	3.1%	7.0%	1.7%	12.1%
Neck (Nij) - 3+	3.6%	2.3%	2.3%	5.0%	1.2%	8.5%
Chest (Deflection) - 3+	46.6%	13.9%	38.3%	54.8%	24.5%	75.9%
Abdomen (Deflection) - 3+	8.5%	2.3%	7.1%	9.8%	4.9%	11.4%
Hip/Pelvis (Acetabulum F) - 2+	7.5%	15.0%	0.0%	16.3%	0.0%	50.2%
Thigh (Femur F) - 2+	5.0%	5.8%	1.6%	8.5%	1.6%	22.2%
Knee (Femur F) - 2+	5.0%	5.8%	1.6%	8.5%	1.6%	22.2%
<i>KTH Peak</i> - 2+	9.3%	14.1%	0.0%	17.6%	1.6%	50.2%
Proximal Tibia (Tibia F Upr) - 2+	2.1%	1.4%	1.3%	2.9%	0.7%	5.9%
Distal Tibia (Tibia F Lwr) - 2+	10.5%	4.1%	8.0%	13.0%	5.4%	18.6%
Tib/Fib Shaft (Tibia M) - 2+	1.7%	2.7%	0.1%	3.3%	0.2%	9.8%
<i>Lower Leg Peak</i> - 2+	10.6%	4.1%	8.2%	13.1%	5.4%	18.6%

Table 9.7. Fleet injury risk for left oblique tests with THOR-50M seated in driver's seat (n=18).

Injury Measure - Threshold	Avg	SD	95% CI		Min	Max
			Lwr	Upr		
Skull/Facial Fx (HIC ₁₅) - 2+	3.9%	2.3%	2.9%	5.0%	0.3%	8.0%
Skull/Facial Fx (HIC ₁₅) - 3+	0.4%	0.4%	0.3%	0.6%	0.0%	1.2%
Brain (BrIC) - 2+	64.8%	35.1%	48.6%	81.1%	5.4%	99.1%
Brain (BrIC) - 3+	45.5%	31.2%	31.1%	59.9%	2.3%	85.4%
Brain (BrIC) - 4+	37.0%	26.9%	24.5%	49.4%	1.6%	74.0%
Neck (Nij) - 2+	6.4%	3.5%	4.8%	8.0%	1.7%	13.5%
Neck (Nij) - 3+	4.5%	2.4%	3.4%	5.6%	1.3%	9.5%
Chest (Deflection) - 3+	54.8%	11.3%	49.6%	60.1%	32.8%	70.7%
Abdomen (Deflection) - 3+	6.3%	3.5%	4.6%	7.9%	0.0%	13.3%
Hip/Pelvis (Acetabulum F) - 2+	29.8%	30.9%	15.5%	44.1%	0.4%	91.7%
Thigh (Femur F) - 2+	4.0%	8.3%	0.1%	7.8%	0.0%	32.0%
Knee (Femur F) - 2+	4.0%	8.3%	0.1%	7.8%	0.0%	32.0%
<i>KTH Peak</i> - 2+	29.8%	30.9%	15.5%	44.1%	0.4%	91.7%
Proximal Tibia (Tibia F Upr) - 2+	2.1%	1.9%	1.2%	3.0%	0.6%	9.2%
Distal Tibia (Tibia F Lwr) - 2+	15.1%	17.5%	7.0%	23.2%	4.5%	81.6%
Tib/Fib Shaft (Tibia M) - 2+	7.2%	6.4%	4.2%	10.1%	0.4%	22.6%
<i>Lower Leg Peak</i> - 2+	16.3%	17.3%	8.3%	24.3%	4.5%	81.6%

Table 9.8 shows the field data injury risks (point estimates and confidence intervals) for the 41-67 kph severity crashes as described earlier. Figure 9.2 and Figure 9.3 show the tabulated results in a bar chart format with bracketed 95% confidence intervals for frontal versus field and oblique versus field, respectively. For both full frontal and oblique, it can be seen that roughly half of the field and fleet confidence intervals are overlapping. Again, this means that we cannot reject the hypothesis that the

two rates are the same when the 95% confidence intervals are overlapping. In some cases, the field and fleet confidence intervals are not overlapping. In the full frontal condition, the fleet predicted risk with THOR-50M is “higher” than the field in some cases (HIC₁₅ 2+, Nij 2+, Nij 3+, Neck Tension 3+, Chest Deflection 3+, Abdomen Deflection 3+) while other fleet confidence intervals are “lower” than the field (Tibia Moment 2+, Tibia/Fibula Peak Risk 2+). In the oblique condition, the fleet and field confidence intervals are overlapping for HIC₁₅ 2+, Tibia/Fibula shaft and Tibia/Fibula combined, while the fleet confidence intervals for BrIC 3+, BrIC 4+ and acetabulum 2+ are higher than the field confidence intervals.

Table 9.8. Field data injury risk estimates for frontal crashes, NASS-CDS 2001-2015.

Injury	Point Estimate	Std Error	95% CI	
			Lwr	Upr
Skull or Facial Fracture - 2+	1.4%	0.7%	0.0%	3.0%
Skull or Facial Fracture - 3+	0.2%	0.1%	0.0%	0.4%
Brain - 2+	8.8%	2.9%	2.4%	15.2%
Brain - 3+	5.9%	3.0%	0.0%	12.4%
Brain - 4+	3.0%	1.2%	0.3%	5.6%
Neck - 2+	2.5%	0.5%	1.4%	3.7%
Neck - 3+	0.6%	0.4%	0.0%	1.4%
Chest - 3+	11.0%	3.6%	3.2%	18.9%
Abdomen - 3+	1.4%	0.7%	0.0%	3.0%
Hip/Pelvis - 2+	4.8%	2.1%	0.1%	9.5%
Thigh - 2+	8.1%	1.9%	3.9%	12.3%
Knee - 2+	4.4%	1.5%	1.2%	7.6%
Knee, Thigh or Hip - 2+	13.9%	3.8%	5.6%	22.1%
Proximal Tibia - 2+	2.1%	0.9%	0.1%	4.0%
Distal Tibia - 2+	10.6%	5.0%	0.0%	21.5%
Tibia, Fibula Shaft - 2+	9.2%	1.3%	6.3%	12.0%
Tibia / Fibula All - 2+	16.8%	4.1%	7.8%	25.8%

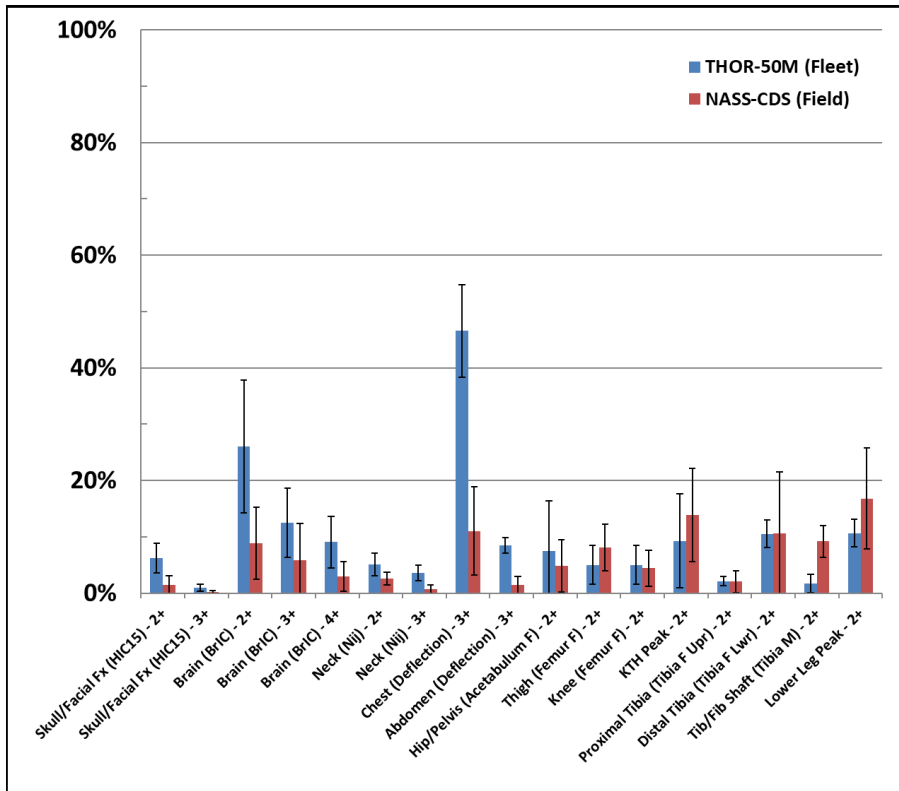


Figure 9.2. Full frontal fleet predicted injury risk with a driver seated THOR-50M versus field estimates and associated 95% confidence intervals.

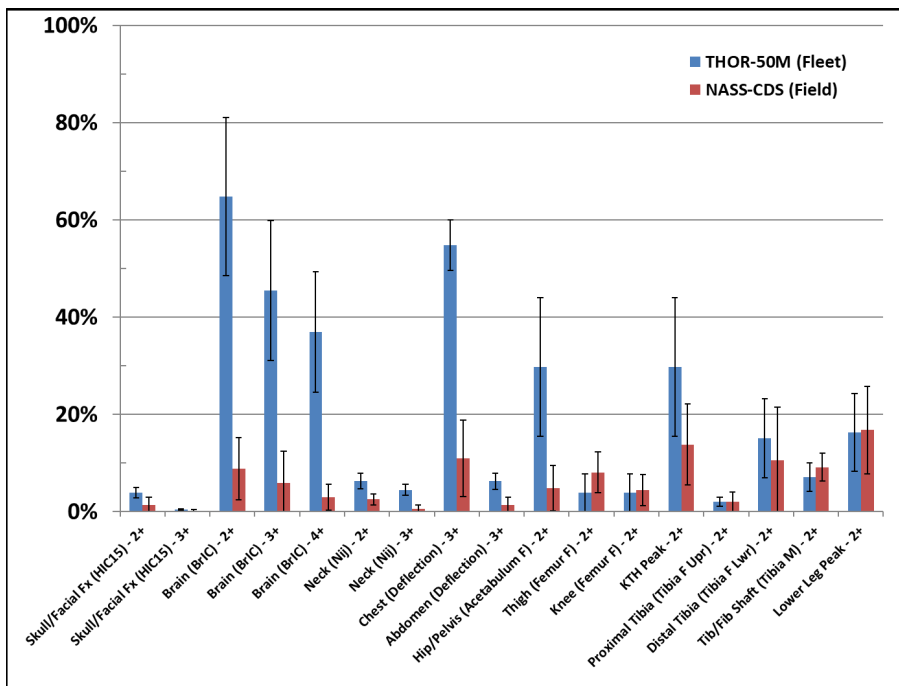


Figure 9.3. Oblique fleet predicted injury risk with a driver seated THOR-50M versus field estimates and associated 95% confidence intervals.

Collinear and frontal conditions can be separated into two separate domains for purposes of comparison. Though, as noted earlier this results in class 4 (“rare type”) relative domain sizes ($P_d < 0.1\%$). Regardless of whether oblique and collinear crashes are separate or together, the oblique fleet data for chest and BrIC does not overlap the field data. However, it can be seen that the risk of AIS 3+ brain injuries (point estimate of 6.9% vs. 4.4%) is higher in oblique than collinear or zero degree frontal crashes. Point estimates for KTH measures are also higher in oblique than collinear frontal field cases. Though, as is the case with all measures in Table 9.9, the confidence intervals between oblique and collinear overlap. Thus, we cannot reject the hypothesis that the point estimates are the same.

Table 9.9. Comparison of oblique vs. collinear injury risk point estimates and confidence intervals.

Injury Risk: All Injuries by Body Region, Age 15+, Belted Drivers in Frontal Crashes (2001-2015)¹						
Injury	Oblique Cases²			Collinear Cases³		
	Point Estimate	CI Lower	CI Upper	Point Estimate	CI Lower	CI Upper
MAIS 2+	52.2%	38.4%	66.1%	53.7%	43.1%	64.3%
MAIS 3+	28.4%	17.0%	39.8%	27.0%	11.6%	42.4%
Skull or Facial Fracture - 2+	1.8%	0.0%	4.0%	0.9%	0.0%	2.1%
Skull or Facial Fracture - 3+	0.2%	0.0%	0.4%	0.2%	0.0%	0.45%
Brain - 2+	10.3%	3.9%	16.7%	6.8%	0.1%	13.5%
Brain - 3+	6.9%	0.0%	14.6%	4.4%	0.0%	9.4%
Brain - 4+	3.1%	0.0%	6.5%	2.7%	0.0%	5.5%
Neck - 2+	3.6%	1.6%	5.7%	1.0%	0.1%	2.0%
Neck - 3+	0.6%	0.0%	1.4%	0.7%	0.0%	1.5%
Thorax - 2+	9.5%	3.8%	15.2%	20.4%	6.3%	34.5%
Thorax - 3+	7.2%	2.8%	11.6%	16.4%	2.4%	30.4%
Abdomen - 3+	1.2%	0.0%	2.7%	1.7%	0.0%	3.7%
Knee, Thigh or Hip - 2+	15.9%	6.2%	25.6%	10.9%	3.7%	18.2%
Hip/Pelvis - 2+	7.1%	0.0%	14.4%	1.5%	0.0%	3.4%
Thigh - 2+	9.4%	4.6%	14.2%	6.3%	2.3%	10.3%
Knee - 2+	4.4%	1.6%	7.2%	4.4%	0.0%	9.2%
Tibia / Fibula ALL - 2+	15.9%	10.6%	21.3%	18.0%	0.0%	39.4%
Proximal Tibia - 2+	2.5%	0.0%	5.7%	1.5%	0.0%	3.1%
Tibia, Fibula Shaft - 2+	13.0%	8.2%	17.8%	3.7%	0.0	4.6%
Distal Tibia - 2+	7.1%	3.2%	11.0%	15.5%	0.0%	36.8%

1. NASS-CDS - Full frontal, offset, SOI; PDOFs of 320 to 40 deg; no center narrow and no unknown PDOF cases; vehicle to vehicle/large fixed object (large tree, medium/large pole, concrete barrier/wall/building/bridge/ditch/culvert); rollover=0; bagdeploy=1; vehage<=10; no ejection; 41-67 kph; extent 3-6

2. Oblique cases - PDOFs include 320 to 350 and 10-40 ($P_d=0.071\%$)

3. Collinear cases - PDOF = 0 ($P_d=0.051\%$)

Figure 9.4 shows mean injury risk and 95% confidence interval for THOR-50M in full frontal and left oblique tests. In this case, the comparison is limited to the eleven vehicles that were tested in both

conditions. Similar to the field data, BrIC (brain) is higher in oblique than full frontal as are KTH measures. In contrast to the field, chest injury risk is higher in left oblique than in the full frontal condition. However, it should be noted that the confidence intervals overlap for all injury risks other than for BrIC and tibia moment.

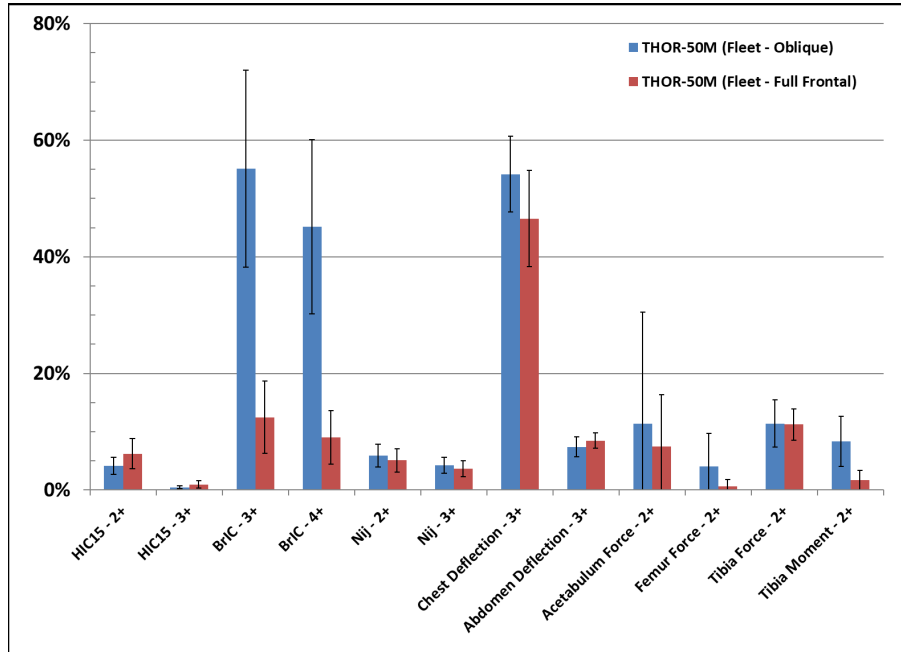


Figure 9.4. THOR-50M injury risk: Left oblique vs. full frontal mean and 95% confidence intervals (n=8).

The design of experiments described in APPENDIX C demonstrates the sensitivity of BrIC to different crash and restraint parameters. Of note, it can be seen in Figure C.8 and Figure C.10 as well as Figure C.11 the positive correlation between BrIC and change in PDOF (i.e. getting further away from zero degrees). For example, it can be seen in Figure C.10 that the range of BrIC at 0-degrees across the various parameters is from under 0.5 to roughly 0.8 while at a PDOF of 340 (20 degrees in the figure, same as the PDOF in NHTSA’s oblique crash test condition) BrIC ranges from just under 0.5 to over 1.5. These DOE-based ranges compare well with the ranges seen in fleet testing with full frontal BrIC values ranging from 0.53 to 0.85 (Table 9.4) and in oblique where BrIC ranged from 0.58 to 1.28 (Table 9.5).

It would be desirable to be able to estimate the risk of injury in crash severities and orientations that match NHTSA’s oblique test (~340-degree PDOF). However, the PDOF of 340 degrees represents roughly 10% of the total cases when looking at the three groupings of frontal crashes described in Table 9.3 (see Figure H.2 in the APPENDIX H). Looking only at 340 degree PDOF cases for the severity range selected results in a very small sample based on very few raw count cases.

9.4 Discussion and Limitations

In attempting to be no smaller than a class 3 or “mini” domain, we could not separate out full frontal and left oblique crashes and maintain severity (delta-V, damage extent), restraint status and vehicle age restrictions. While this gives an overall picture of field injury in frontal crashes, it limits our ability to directly compare NHTSA’s oblique and full-frontal collinear crash test results versus the field.

There are also numerous occupant, crash and vehicle factors parameters (i.e. independent variables) that are not adjusted for due to sample size issues or due to unknown and/or unavailable data. Many of these factors may be positively correlated (such as increased age) or negatively correlated (such as pre-impact braking or bracing) with the respective rates of injury that are estimated in the field data.

Occupant age, sex, seat track position, height, and weight are examples of NASS-CDS coded variables that were not restricted in creating field-based injury risk point estimates and confidence intervals (See APPENDIX H for distributions of these parameters across the frontal crash target population). Other factors such as the occupant’s pre-impact position, pre-impact braking, pre-impact bracing/muscle tone, performance of restraints (such as fit, deployment timing) cannot be accounted for. In particular, pre-impact braking has been shown to be associated with a reduced risk of injury in frontal crashes versus no braking (Craig et al., 2011). Studies have demonstrated the potential for reduced chest displacement and thus chest injury risk with increased levels of bracing or muscle activation (Bose and Crandall, 2008; Iwamoto et al., 2011).

Given the fact that many sensitive parameters are either unknown or left unfiltered and given the small sample size when attempting to limit to crash severities comparable to the NHTSA test conditions, the results of the field data point estimates (Table 9.8, Table 9.9) may not accurately represent the actual risk of injury for an occupant of similar anthropometry, seated similarly to the THOR-50M in mid-seat track position in crashes resulting in the delta-V and PDOF observed in NHTSA’s left oblique and full frontal crash test conditions. Additionally, it is possible that our fleet testing (limited to 11 full frontals and 18 left obliques) may not represent the average vehicle in the current new vehicle fleet or the average vehicle in the field data sample. Of note, the models of vehicles represented in APPENDIX D and used for full frontal and oblique fleet comparisons to the field represent approximately 11% and 20% of total annual vehicle sales, respectively.

While it is desirable to make definitive comparisons and conclusions when contrasting field data- and fleet testing-based injury risks, the limitations described above make these comparisons subject to many limitations. Limiting the field data sample to crashes of similar severity (delta-V, damage extent), restraint system status (belted, airbag deployment) and occupant types (adult drivers) to those in fleet tests, while also removing rollover and ejection cases, results in a relatively small sample size (raw and weighted). Couple this with the limitation described above regarding crash, vehicle, restraint system and occupant variables that could not be accounted for and the limited size of the fleet test sample, and the resulting comparisons of confidence intervals (overlapping or not) need to be used with caution.

Limitations aside, the fleet, field and human body modeling based analyses all show a higher risk of brain injury in oblique crash conditions than in 0-degree or collinear. In an extension of the modeling

work presented in Appendix C, Takhounts et al. (2019) demonstrated, in comparing field- and fleet-based brain injury risk estimates, that it is not sufficient to simply restrict the analysis to ranges of delta-Vs and PDOFs that are comparable between the two data sets. They found that it is also necessary to account for the distributions of PDOF and delta-V. In demonstrating this, Takhounts et al. found that brain injury risks from field and fleet data were comparable when adjusting estimates based on the distribution of delta-V and PDOF in the field data.

The field and fleet data also both suggest a higher risk for knee/thigh/hip injuries in oblique crashes versus collinear crashes. Additionally, lower extremity field and fleet data compared well for both full frontal and oblique where the majority of confidence intervals were overlapping. For both full frontal and oblique, the predicted thoracic injury risk was higher for in fleet testing than predicted by the field. As discussed earlier in the report, the current THOR-50M are post-mortem human subject (PMHS)-based risk functions with no adjustment for living versus post-mortem subjects or clinical versus experimental rib fracture detection. In the current NCAP (NCAP, 2008) the risk function that was applied set the AIS 3+ 1995/1998 based limit at seven fractured ribs instead of four as is described in AIS (AAAM, 1998). If NHTSA entertained changing the chest injury risk function as has previously been done, it would bring the mean risk and associated confidence interval closer to the estimate from the field data. However, the reduction in risk for a given deflection when considering a risk function based on 6 or 7 fractured ribs (Figure 5.14) would not reduce the risk to the level where fleet and field confidence intervals for chest injury risk overlap.

10 REFERENCES

- Alquié, A., 1865. Étude Clinique et Expérimentale de la Commotion Traumatique ou ébranlement de L'encéphale. *Gazette Medical de Paris*, 20, 226–230; 254–256; 314–319; 382–385; 396–398; 463–466; 500–504.
- Association for Advancement of Automatic Medicine, 1998. Abbreviated Injury Scale 1990, Update 1998. AAAM, Des Plaines, IL.
- Association for Advancement of Automatic Medicine, 2008. Abbreviated Injury Scale 2005, Update 2008. AAAM, Barrington, IL.
- Banglmaier, R.F., Dvoracek-Driksna, D., Oniang'o, T.E. and Haut, R.C., 1999. Axial compressive load response of the 90 flexed human tibiofemoral joint. In: *Proceedings of the 43rd Stapp Car Crash Conference* (No. 99SC08), 127-139.
- Begeman, P., Balakrishnan, P., Levine, R. and King, A., 1993. Dynamic human ankle response to inversion and eversion. In: *Proceedings of the 37th Stapp Car Crash Conference* (No. 933115).
- Begeman P.C., Aekbote K., 1996. Axial load strength and some ligament properties of the ankle joint. In: *6th Injury Prevention Through Biomechanics Symposium*. Detroit, MI: Wayne State University, 125–135.
- Blincoe, L. J., Miller, T. R., Zaloshnja, E., and Lawrence, B. A., 2015. The economic and societal impact of motor vehicle crashes, 2010. (Report No. DOT HS 812 013) Washington, DC: National Highway Traffic Safety Administration.
- Bose, D., Crandall, J. R., 2008. Influence of active muscle contribution on the injury response of restrained car occupants. *Ann Adv Automot Med* 52, pp. 61-72.
- Carter, J.W., Ku, G.S., Nuckley, D.J. and Ching, R.P., 2002a. Tolerance of the cervical spine to eccentric axial compression. In: *Proceedings of the 46th Stapp Car Crash Conference* (No. 2002-22-0022).
- Carter, J.W. 2002b. Compressive cervical spine injury: The effect of injury mechanism on structural injury pattern and neurological injury potential. PhD thesis, University of Washington.
- Chancey, V.C., Nightingale, R.W., Van Ee, C.A., Knaub, K.E. and Myers, B.S., 2003. Improved estimation of human neck tensile tolerance: reducing the range of reported tolerance using anthropometrically correct muscles and optimized physiologic initial conditions. *Stapp Car Crash Journal*, 47, 135-153.
- Chancey, V.C., Ottaviano, D., Myers, B.S. and Nightingale, R.W., 2007. A kinematic and anthropometric study of the upper cervical spine and the occipital condyles. *Journal of Biomechanics*, 40(9), 1953-1959.
- Craig, M.J., Scarboro, M. and Ridella, S.A., 2011. Predicting occupant outcomes with EDR data. In: *Proceedings of the 22nd International Technical Conference on the Enhanced Safety of Vehicles*, (No. 11-0326).
- Crandall, J., 2013. Injury criteria development: THOR Metric SD-3 shoulder advanced frontal crash test dummy. NHTSA Biomechanics Database (Report b11117-1).
- Crandall, J., 2014. ATD thoracic response test development, 20 degree far side oblique frontal, front passenger position, Tests UVAS0243-245. NHTSA Biomechanics Database (Report b11500-1).
- Crandall, J., 2015. ATD thoracic response test development, Gold standard buck condition 3: Force limited belt, 30 km/h 30 degree oblique frontal, Tests UVAS0313-315. NHTSA Biomechanics Database (Report b11518-1).
- Dibb, A., Nightingale, R., Chauncey, V., Fronheiser, L., Tran, L., Ottaviano, D., and Myers B., 2006. Comparative structural neck responses of the THOR-NT, Hybrid III, and human in combined tension-bending and pure bending. *Stapp Car Crash Journal*, 50, 567-581.
- Dibb, A.T., Nightingale, R.W., Luck, J.F., Chancey, V.C., Fronheiser, L.E. and Myers, B.S., 2009. Tension and combined tension-extension structural response and tolerance properties of the human male ligamentous cervical spine. *Journal of Biomechanical Engineering*, 131(8), pp 081008-1.
- Dibb, A.T., 2011. Pediatric head and neck dynamic response: A computational study [PhD thesis]. Durham, NC: Duke University.

- Dischinger, P.C., Burgess, A.R., Cushing, B.M., O'Quinn, T.D., Schmidhauser, C.B., Ho, S.M., Juliano, P.J. and Bents, F.D., 1994. Lower extremity trauma in vehicular front-seat occupants: patients admitted to a level 1 trauma center. *Society of Automotive Engineers* (No. 940710).
- Dischinger, P.C., Read, K.M., Kufera, J.A., Kerns, T.J., Burch, C.A., Jawed, N., Ho, S.M. and Burgess, A.R., 2004. Consequences and costs of lower extremity injuries. In: *Proceedings of Association for the Advancement of Automotive Medicine Annual Conference*, 48, 339-353.
- Donnelly, B.R., Roberts, D.P., 1987. Comparison of cadaver and Hybrid III dummy response to axial impacts of the femur. In: *Proceedings of the 31st Stapp Car Crash Conference* (No. 872204), 105-116.
- Eigen, A.M., Martin, P.G., 2005. Identification of real world injury patterns in aid of dummy development. In: *Proceedings of the 19th International Technical Conference on the Enhanced Safety of Vehicles Conference* (No. 05-0219).
- Elhagediab, A., Rouhana, S., 1998. Patterns of abdominal injury in frontal automotive crashes. In: *Proceedings of the 16th International Technical Conference on the Enhanced Safety of Vehicles* (No. 98-S1-W-26).
- Eppinger, R., Sun, E., Bandak, F., Haffner, M., Khaewpong, N., Maltese, M., Kuppa, S., Nguyen, T., Takhounts, E., Tannous, R., Zhang, A., Saul, R., 1999. Development of improved injury criteria for the assessment of advanced automotive restraint systems—II. Washington, DC: National Highway Traffic Safety Administration.
- Ewing C.J., Thomas, D.J., Lustick, L., Muzzy, W.H., Williams, G., Majewski, P.L., 1976. The effect of duration, rate of onset and peak sled acceleration on the dynamic response of human head and neck. In: *Proceedings 20th Stapp Car Crash Conference* (No 760800).
- Ewing C.J., Thomas, D.J., Majewski, P.L., Black, R., Lustick, L., 1977. Measurement of head, T1, and pelvic response to Gx impact acceleration. In: *Proceedings of the 21st Stapp Car Crash Conference* (No 770927).
- Foret-Bruno, J., Hartemann, F., Thomas, C., Fayon, A., Tarrière, C., Got, C., Patel, A., 1978. Correlation between thoracic lesions and force values measured at the shoulder of 92 belted occupants involved in real accidents. In: *Proceedings of the 22nd Stapp Car Crash Conference* (No. 780892), 271-292.
- Forman, J., Lessley, D., Kent, R., Bostrom, O., Pipkorn, B., 2006a. Whole-body kinematic and dynamic response of restrained PMHS in frontal sled tests. *Stapp Car Crash Journal*, 50, 299-336.
- Forman, J., Lessley, D., Shaw, C.G., Evans, J., Kent, R., Rouhana, S.W., Prasad, P., 2006b. Thoracic response of belted PMHS, the Hybrid III, and the THOR-NT mid-sized male surrogates in low speed, frontal crashes. *Stapp Car Crash Journal*, 50, 191-215.
- Forman, J., Lopez-Valdes, F., Lessley, D., Kindig, M., Kent, R., Ridella, S., Bostrom, O., 2009. Rear seat occupant safety: an investigation of a progressive force-limiting, pretensioning 3-point belt system using adult PMHS in frontal sled tests. *Stapp Car Crash Journal*, 53, 49-74.
- Frampton, R., Lenard, J., Compigne, S., 2012. An in-depth study of abdominal injuries sustained by car occupants in frontal crashes. In: *Annals of Advances in Automotive Medicine 56th Annual Conference*, 56, 137-149.
- Funk, J.R., Tourret, L.J. and Crandall, J.R., 2000. Experimentally produced tibial plateau fractures. In: *Proceedings of the 2000 International Conference on the Biomechanics of Impact*, 171-182.
- Funk, J.R., Crandall, J.R., Tourret, L.J., MacMahon, C.B., Bass, C.R., Patrie, J.T., Khaewpong, N. and Eppinger, R.H., 2002. The axial injury tolerance of the human foot/ankle complex and the effect of Achilles tension. *Journal of Biomechanical Engineering*, 124(6), 750-757.
- Funk, J.R., Srinivasan, S.C., Crandall, J.R., Khaewpong, N., Eppinger, R.H., Jaffredo, A.S., Potier, P. and Petit, P.Y., 2002. The effects of axial preload and dorsiflexion on the tolerance of the ankle/subtalar joint to dynamic inversion and eversion. *Stapp Car Crash Journal*, 46, 245-265.
- Funk, J.R., Rudd, R.W., Kerrigan, J.R. and Crandall, J.R., 2004. The effect of tibial curvature and fibular loading on the tibia index. *Traffic Injury Prevention*, 5(2), 164-172.
- Gabler, L.F., Crandall, J.R., Panzer, M.B., 2016. Investigating brain injury tolerance in the sagittal plane using a finite element model of the human head. *International Journal of Automotive Engineering*, 7(1), 37-43.

- Gennarelli, T.A., Ommaya, A.K., Thibault, L.E., 1971. Comparison of linear and rotational accelerations in experimental cerebral concussion. In: *Proceedings of the 15th Stapp Car Crash Conference*, 797-803.
- Gennarelli, T.A., Thibault, L.E., and Ommaya, A.K., 1972. Pathophysiologic responses to rotational and translational accelerations of the head. *Stapp Car Crash Journal*, 16, 296-308.
- Gennarelli, T.A., 1985. The state of the art of head injury biomechanics. In: *Proceedings of the American Association for the Advancement of Automotive Medicine*, 29, 447-463.
- Glaister, D.H., 1975. Human tolerance to impact acceleration, *Injury*, 9, 191-198.
- Goggio, A.F., 1941. The mechanism of contre-coup injury. *Journal of Neurology and Psychiatry*, 4(1), 11-22.
- Goldsmith W. 2001. The state of head injury biomechanics: past, present, and future: Part 1. *Critical reviews in biomedical engineering*, 29, 441-600.
- Goldsmith, W. and Monson, K.L., 2005. The state of head injury biomechanics: past, present, and future, Part 2: Physical experimentation. *Critical Reviews Biomedical Engineering*, 33(2), 105–207.
- Gurdjian, E.S. (1972). Recent advances in the study of the mechanism of impact injury of the head – a summary. *Clin. Neurosurgery*, 19, 1-42.
- Hardy, W., Schneider, L., Rouhana, S., 2001. Abdominal impact response to rigid-bar, seatbelt, and airbag loading. *Stapp Car Crash Journal*, 45, 1-32.
- Haffner, M., Rangarajan, N., Artis, M., Beach, D., Eppinger, R., Shams, T., 2001. Foundations and elements of the NHTSA THOR Alpha ATD design. In: *Proceedings of the 17th International Technical Conference on the Enhanced Safety of Vehicles* (No. 458).
- Hasija, V., Takhounts, E.G. and Ridella, S.A., 2011. Evaluation of statistical methods for generating injury risk curves. In: *Proceedings of the 22nd International Technical Conference on the Enhanced Safety of Vehicles* (No. 11-0331).
- Hasija, V., Takhounts, E., Lee, E., Craig, M. 2017. On the importance of the forces and moments at the occipital condyles in prediction of the ligamentous cervical spine injuries. *Proceedings of the 2017 IRCOBI Conference*.
- Hertz, E., 1993. A note on the head injury criterion (HIC) as a predictor of the risk of skull fracture. In: *Proceedings of the 37th Association for the Advancement of Automotive Medicine Annual Conference*, 303-311.
- Hess, R.L., Weber, K., Melvin, J.W., 1980. Review of literature and regulation relating to head impact, tolerance and injury criteria. (Report no. UM-HSRI-80-52-I) Ann Arbor, MI: University of Michigan Transportation Research Institute.
- Holbourn, A.H.S., 1943. Mechanics of head injuries. *The Lancet*, 242, 438–441.
- Hosmer, D. W., Jr. and Lemeshow, S., 2000. *Applied logistic regression*. 2nd ed. New York: John Wiley & Sons.
- Insurance Institute for Highway Safety, 2017. Small overlap frontal crashworthiness evaluation test protocol (Version VI). https://www.iihs.org/media/ec54a7ea-1a1d-4fb2-8fc3-b2e018db2082/Ztykhw/Ratings/Protocols/current/small_overlap_test_protocol.pdf (accessed Sep 23, 2020)
- International Organization for Standardization (ISO), 2018. ISO/TC22/SC36/WG6 Document N1047.
- International Organization for Standardization (ISO), 2019. THOR Chest Criteria Evaluation: Exploration of Data Set N1047. ISO/TC22/SC36/WG6 Document N1083.
- Ivarsson, J., 2006. Development of a new tibia index. NHTSA Biomechanics Database (Report b12819).
- Ivarsson, B.J., Manaswi, A., Genovese, D., Crandall, J.R., Hurwitz, S.R., Burke, C. and Fakhry, S., 2008. Site, type, and local mechanism of tibial shaft fracture in drivers in frontal automobile crashes. *Forensic Science International*, 175(2), 186-192.
- Iwamoto, M., Nakahira, Y., Sugiyama, T., 2011. Investigation of pre-impact bracing effects for injury outcome using and active human FE model with 3D geometry of muscles. In: *Proceedings of the 22nd International Conference on the Enhanced Safety of Vehicles*, Washington, DC.

- Jaffredo, A., Potier, P., Robin, S., Le Coz, J.Y. and Lassau, J.P., 2000. Cadaver lower limb dynamic response in inversion-eversion. In: *Proceedings of the 2000 International IRCOBI Conference on the Biomechanics of Impact*, 183-194.
- Kent, R.W., Crandall, J.R., Bolton, J., Prasad, P., Nusholtz, G., Mertz, H., 2001. The influence of superficial soft tissues and restraint condition on thoracic skeletal injury prediction. *Stapp Car Crash Journal*, 45, 183-204.
- Kent, R., Shaw, C.G., Lessley, D.J., Crandall, J.R. and Svensson, M.Y., 2003. Comparison of belted Hybrid III, THOR, and cadaver thoracic responses in oblique frontal and full frontal sled tests. In: *Proceedings of Society of Automotive Engineers 2003 World Congress and Exhibition* (No. 2003-01-0160).
- Kent, R., Stacey, S., Kindig, M., Forman, J., Woods, W., Rouhana, S., Higuchi, K., Tanji, H., St. Lawrence, S., Arbogast, K., 2006. Biomechanical response of the pediatric abdomen, Part 1: Development of an experimental model and quantification of structural response to dynamic belt loading. *Stapp Car Crash Journal*, 50, 1-26.
- Kent, R., Stacey, S., Kindig, M., Woods, W., Evans, J., Rouhana, S., Higuchi, K., Tanji, H., St. Lawrence, S., Arbogast, K., 2008. Biomechanical response of the pediatric abdomen, Part 2: Injuries and their correlation with engineering parameters. *Stapp Car Crash Journal*, 52, 135-166.
- Kent, R.W., Lopez-Valdes, F.J., Dennis, N.J., Lessley, D., Forman, J., Higuchi, K., Tanji, H., Ato, T., Kameyoshi, H., Arbogast, K., 2011. Assessment of a three-point restraint system with a pre-tensioned lap belt and an inflatable, force-limited shoulder belt. *Stapp Car Crash Journal*, 55, 141-159.
- Keon, T., 2016. Alternative approaches to occupant response evaluation in frontal impact crash testing. *SAE International Journal of Transportation Safety* (No. 2016-01-1540), 4, 202-217.
- Kitagawa, Y., Ichikawa, H., King, A.I. and Levine, R.S., 1998. A severe ankle and foot injury in frontal crashes and its mechanism. In: *Proceedings of the 42nd Stapp Car Crash Conference* (No. 983145).
- Klinich, K., Saul, R., Auguste, G., Backaitis, S., and Kleinberger, M. 1996. Techniques for developing child dummy protection reference values. National Highway Traffic Safety Administration Report.
- Klinich, K., Flannagan, C., Nicholson, K., Schneider, L., Rupp, J., 2009. Abdominal injury in motor-vehicle crashes. (Report No. UMTRI-2009-40) Ann Arbor, MI: University of Michigan Transportation Research Institute.
- Kroell, C., Schneider, D., and Nahum, A., 1971. Impact tolerance and response of the human thorax. *Society of Automotive Engineers* (No. 710851).
- Kroell, C., Schneider, D., and Nahum, A., 1974. Impact tolerance and response of the human thorax II. *Society of Automotive Engineers* (No. 741187).
- Kuppa, S., Eppinger, R., 1998. Development of an improved thoracic injury criterion. In: *Proceedings of the 42nd Stapp Car Crash Conference* (No. 983153).
- Kuppa, S., Haffner, M., Eppinger, R., and Saunders, J., 2001. Lower extremity response and trauma assessment using the THOR-Lx/HIIIr and the Denton leg in frontal offset vehicle crashes. In: *Proceedings of the 17th International Technical Conference for the Enhanced Safety of Vehicles* (No. 456).
- Kuppa, S., Wang, J., Haffner, M., Eppinger, R., 2001. Lower extremity injuries and associated injury criteria. In: *Proceedings of the 17th International Technical Conference for the Enhanced Safety of Vehicles* (No. 457).
- Laituri, T., Prasad, P., Sullivan, K., Frankstein, M., Thomas, R., 2005. Derivation and evaluation of a provisional, age dependent AIS 3+ thoracic risk curve for belted adults in frontal impacts. In: *Proceedings of Society of Automotive Engineers World Congress and Exhibition* (No. 2005-01-0297).
- Laituri, T.R., Henry, S., Kachnowski, B., Sullivan, K., 2009. Initial assessment of the next-generation USA frontal NCAP: fidelity of various risk curves for estimated field injury rates of belted drivers. In: *Proceedings of Society of Automotive Engineers World Congress and Exhibition* (No. 2009-01-0386).
- Laituri, T.R., Henry, S., Pline, K., Li, G., Frankstein, M. and Weerappuli, P., 2016. New Risk Curves for NHTSA's Brain Injury Criterion (Bric): Derivations and Assessments. *Stapp Car Crash Journal*, 60, 301-362.
- Lebarbé, M., Donnelly, B.R., Petit, P., Moorhouse, K., 2015. A frontal response specification for assessing the biofidelity of an anthropometric test dummy: Part 1 - Upper body. In: *Proceedings of International Conference on the Biomechanics of Impact Conference*, 467-485.

- Lee, E.L., Craig, M. and Scarboro, M., 2015. Real-world rib fracture patterns in frontal crashes in different restraint conditions. *Traffic Injury Prevention*, 16(S2), S115-S123.
- Lopez-Valdes, F.J., Lau, A., Lamp, J., Riley, P., Lessley, D.J., Damon, A., Kindig, M., Kent, R.W., Balasubramanian, S., Seacrist, T., Maltese, M.R., Arbogast, K.B., Higuchi, K., Tanji, H., 2010. Analysis of spinal motion and loads during frontal impacts. Comparison between PMHS and ATD. In: *Annals of Advances in Automotive Medicine 54th Annual Conference*, 54, 61-78.
- Luck, J.F., Cutcliffe, H.C., Kait, J.R., Cox, C.A., Nightingale, R.W., Bass, C.R. (2014) Characterization of the THOR Metric Neck in Tension-Bending, Anterior-Posterior Bending, Lateral Bending, and Torsion; Development of Injury Risk Curves and Critical Values for Injury Assessment. NHTSA Database, (Report b11559).
- Maiman, D.J., Sances Jr, A., Myklebust, J.B., Larson, S.J., Houterman, C., Chilbert, M. and El-Ghatit, A.Z., 1983. Compression injuries of the cervical spine: a biomechanical analysis. *Neurosurgery*, 13(3), 254-260.
- Margulies, S.S. and Thibault, L.E., 1992. A proposed tolerance criterion for future axonal injury in man. *Journal of Biomechanics*, 25(8), 917-923.
- Martin, P. G., Scarboro, M., 2011. THOR-NT: Hip injury potential in narrow overlap and oblique frontal crashes. In: *Proceedings of the 22nd International Technical Conference on the Enhanced Safety of Vehicles* (No. 11-0234).
- Mattucci, S.F., Moulton, J.A., Chandrashekar, N. and Cronin, D.S., 2012. Strain rate dependent properties of younger human cervical spine ligaments. *Journal of the mechanical behavior of biomedical materials*, 10, 216-226.
- McLean, A.J. and Anderson, R.W.G., 1997. Biomechanics of closed head injury. Chapter 2. In: Reilly, P., Bullock, R. (Eds) *Head injury*. London: Chapman & Hall, 25–37.
- McMurry, T., Poplin, G., Forman, J., Ash, J., Shaw, C.G., Crandall, J., “Provisional THOR Chest Injury Risk Function,” NHTSA Biomechanics Database (Report b11117-2), 2016a.
- McMurry, T., Poplin, G., Forman, J., Ash, J., Shaw, C.G., Crandall, J., “Provisional THOR Chest Injury Risk Function with Frontal and Oblique Sled Tests,” NHTSA Biomechanics Database (Report b11514-2), 2016b.
- Meaney, D.F., Morrison, B., Bass, C.D., 2014. The mechanics of traumatic brain injury: a review of what we know and what we need to know for reducing its societal burden. *Journal of Biomechanical Engineering*, 136(2), pp 021008.
- Melvin J.W., Lighthall J.W., Ueno K., 1993. Brain injury biomechanics. In: Nahum, A.M., Melvin, J.W. (Eds) *Accidental Injury*. New York: Springer-Verlag, 269–290.
- Mertz, H.J., Patrick, L.M., 1971. Strength and response of the human neck. *Society of Automotive Engineers* (No. 710855).
- Mertz, H.J., Hodgson, V.R., Thomas, L.M., and Nyquist, G.W., 1978. An assessment of compressive neck loads under injury-producing conditions. *Physician and Sports Medicine*, 6(11), 95-106.
- Mertz, H.J., Weber, D.A., 1982. Interpretations of the impact responses of a 3-year-old child dummy relative to child injury potential. *Society of Automotive Engineers* (No. 826048).
- Mertz, H.J., 1993. Anthropometric test devices. Chapter 4. In: Nahum, A.W., Melvin, J.W. (Eds) *Accidental Injury*. New York: Springer-Verlag.
- Mertz, H.J., Prasad, P., 2000. Improved neck injury risk curves for tension and extension moment measurements of crash dummies. In: *Proceedings of the 44th Stapp Car Crash Conference* (No. 2000-01-SC05), 59-76.
- Miller, M.A., 1989. The biomechanical response of the lower abdomen to belt restraint loading. *Journal of Trauma*, 29(11), 1571-1584.
- Monson K.L, Goldsmith W, Barbaro NM, Manley G.T. 2005. Significance of source and size in the mechanical response of human cerebral blood vessels. *J Biomech*, 38(4):737-44.
- Morgan, R., Schneider, D., Eppinger, R., Nahum, A. et al. 1987. Interaction of Human Cadaver and Hybrid III Subjects with a Steering Assembly. SAE Technical Paper 872202.

- Morgan, R., Eppinger, R.H., Marcus, J., 1989. Human cadaver patella-femur-pelvis injury due to dynamic frontal impact to the patella. In: *Proceedings of the 12th International Conference on Experimental Safety Vehicles*.
- Morgan, R.M., Eppinger, R.H. and Hennessey, B.C., 1991. Ankle joint injury mechanism for adults in frontal automotive impact. In: *Proceedings of the 35th Stapp Car Crash Conference* (No. 912902).
- Morgan, R.M., Eppinger, R.H., Haffner, M.P., Yoganandan, N., Pintar, F.A., Sances, A., Crandall, J.R., Pilkey, W.D., Klopp, G.S., Kallieris, D., Miltner, E., Mattern, R., Kuppa, S.M., and Sharpless, C.L., 1994. Thoracic trauma assessment formulations for restrained drivers in simulated frontal impacts. In: *Proceedings of the 38th Stapp Car Crash Conference* (No. 942206), 15-34.
- Mueller, B., MacAllister, A., Nolan, J., Zuby, D., 2015. Comparison of HIC and BrIC head injury risk in IIHS frontal crash tests to real-world head injuries. In: *Proceedings of the 24th International Technical Conference on the Enhanced Safety of Vehicles* (No. 15-0272).
- Nahum, A., Smith, R., Ward, C., 1977. Intracranial pressure dynamics during head impact. In: *Proceedings of the 21st Stapp Car Crash Conference* (No. 770922), 337–366.
- National Highway Traffic Safety Administration, 2000. Final Economic Assessment: FMVSS No. 208 Advanced Air Bags. www.regulations.gov, NHTSA-2000-7013-0006.
- National Highway Traffic Safety Administration, 2005. Biomechanical response requirements of the THOR NHTSA advanced frontal dummy, Revision 2005.1. (Report No: GESAC-05-03), Washington, DC: U.S. Department of Transportation [http://www.nhtsa.gov/DOT/NHTSA/NVS/Biomechanics%20&%20Trauma/THOR-NT%20Advanced%20Crash%20Test%20Dummy/thorbio05_1.pdf]
- National Highway Traffic Safety Administration, 2008. Consumer Information; New Car Assessment Program; Final Decision Notice. 73 Federal Register 134, pp 40016-40050.
- National Highway Traffic Safety Administration, 2015a. THOR-50M Drawing Package, September 2015 Draft. Docket ID NHTSA-2015-0119-0005.
- National Highway Traffic Safety Administration, 2015b. THOR 50th Percentile Male Qualification Procedures Manual DRAFT 2015-10-16. Docket ID NHTSA-2015-0119-0016.
- National Highway Traffic Safety Administration, 2016a. NCAP. Docket ID NHTSA-2015-0119-0001.
- National Highway Traffic Safety Administration, 2016b. Parts List and Drawings THOR-50M Advanced Frontal Crash Test Dummy THOR-50M Male August 2016. Docket ID NHTSA-2015-0119-0376.
- National Highway Traffic Safety Administration, 2020a. THOR-50M Drawing Package, August 2018. Docket ID NHTSA-2019-0106-0002.
- National Highway Traffic Safety Administration, 2020b. THOR-50M Qualification Procedures Manual, September 2018. Docket ID NHTSA-2019-0106-0001.
- National Highway Traffic Safety Administration, 2020c. THOR-50M Procedures for Assembly, Disassembly, and Inspection, August 2018. Docket ID NHTSA-2019-0106-0007.
- Neathery, R., Kroell, C., Mertz, H., 1975. Prediction of thoracic injury from dummy responses. *Society of Automotive Engineers* (No. 751151).
- Nightingale, R.W., McElhaney, J.H., Camacho, D.L., Kleinberger, M., Winkelstein, B.A. and Myers, B.S., 1997. The dynamic responses of the cervical spine: buckling, end conditions, and tolerance in compressive impacts. In: *Proceedings of the 41st Stapp Car Crash Conference* (No. 973344).
- Nightingale, R.W., Chancey, V.C., Ottaviano, D., Luck, J.F., Tran, L., Prange, M. and Myers, B.S., 2007. Flexion and extension structural properties and strengths for male cervical spine segments. *Journal of Biomechanics*, 40(3), 535-542.
- Nuckley, D.J., Hertsted, S.M., Eck, M.P. and Ching, R.P., 2005. Effect of displacement rate on the tensile mechanics of pediatric cervical functional spinal units. *Journal of Biomechanics*, 38(11), 2266-2275.
- Nusholtz, G.S., Lux, P., Kaiker, P.S., Janicki, M.A., 1984. Head impact response - skull deformation and angular accelerations. In: *Proceedings of the 28th Stapp Car Crash Conference* (No. 841657), 41-74.

- Nusholtz, G.S., Kaiker, P.S., Lehman, R.J., 1988. Steering system abdominal impact trauma. (Report No. UMTRI-88-19) Ann Arbor, MI: University of Michigan Transportation Research Institute.
- Nusholtz, G.S., Kaiker, P.S., 1994. Abdominal response to steering wheel loading. In: *Proceedings of the International Technical Conference on the Enhanced Safety of Vehicles* (No. 94-S1-O-05).
- Nyquist, G.W., Cheng, R., El-Bohy, A.A. and King, A.I., 1985. Tibia bending: strength and response. *Society of Automotive Engineers* (No. 851728).
- Nyquist, G.W., Begeman, P., King, A.I. and Mertz, H.J., 1980. Correlation of field injuries and GM Hybrid III dummy responses for lap-shoulder belt restraint. *Journal of Biomechanical Engineering*, 102(2), 103-109.
- Ommaya, A.K., 1984. Biomechanics of head injury: Experimental aspects. In: Nahum, A., Melvin J.W. (Eds) *The Biomechanics of Trauma*. East Norwalk, CT: Appleton-Century-Crofts, 245-269.
- Panjabi, M.M., Oda, T., Crisco III, J.J., Oxland, T.R., Katz, L., and Nolte, L.P. 1991. Experimental study of atlas injuries I: Biomechanical analysis of their mechanisms and fracture patterns. *Spine*, 16, S460-S465.
- Parent, D., Craig, M., Ridella, S., McFadden, J., 2013. Thoracic biofidelity assessment of the THOR Mod Kit ATD. In: *Proceedings of the 23rd International Technical Conference on the Enhanced Safety of Vehicles* (No. 13-0327).
- Parent, D., Craig, M., Moorhouse, K. 2017. Biofidelity Evaluation of the THOR and Hybrid III 50th Percentile Male Frontal Impact Anthropomorphic Test Devices. *Stapp Car Crash Journal*, 61, 227-276.
- Parenteau, C.S., Viano, D.C. and Petit, P.Y., 1998. Biomechanical properties of human cadaveric ankle-subtalar joints in quasi-static loading. *Journal of Biomechanical Engineering*, 120(1), 105-111.
- Parr J.C., Miller M.E., Pellettiere J.A., Erich R.A. 2013. Neck injury criteria formulation and injury risk curves for the ejection environment: a pilot study. *Aviat Space Environ Med*. 84(12), 1240-8.
- Pattimore, D., Ward, E., Thomas, P. and Bradford, M., 1991. The nature and cause of lower limb injuries in car crashes. In: *Proceedings of the 35th Stapp Car Crash Conference* (No. 912901).
- Petit, P., Portier, L., Foret-Bruno, J.Y., Trosseille, X., Parenteau, C.S., Tarriere, C. and Lassau, J., 1997. Quasistatic characterization of the human foot-ankle joints in a simulated tensed state and updated accidentological data. In: *Proceedings of the International Research Council on the Biomechanics of Injury Conference*, 25, 363-376.
- Pintar, F.A., Yoganandan, N., Voo, L., Cusick, J.F., Maiman, D.J. and Sances, A., 1995. Dynamic characteristics of the human cervical spine. In: *Proceedings of the 39th Stapp Car Crash Conference* (No. 952722).
- Pintar, F.A., Yoganandan, N. and Voo, L., 1998. Effect of age and loading rate on human cervical spine injury threshold. *Spine*, 23(18), 1957-1962.
- Pintar, F.A., Yoganandan, N. and Baisden, J., 2005. Characterizing occipital condyle loads under high-speed head rotation. *Stapp Car Crash Journal*, 49, 33-47.
- Poplin, G.S., McMurry, T.L., Forman, J.L., Ash, J., Parent, D.P., Craig, M.J., Song, E., Kent, R., Shaw, G. and Crandall, J. 2017. Development of thoracic injury risk functions for the THOR ATD. *Accident Analysis & Prevention*, 106, 122-130.
- Portier, L., Petit, P., Domont, A., Trosseille, X., Le Coz, J.Y., Tarrière, C. and Lassau, J.P., 1997. Dynamic biomechanical dorsiflexion responses and tolerances of the ankle joint complex. In: *Proceedings of the 41st Stapp Car Crash Conference* (No. 973330).
- Prasad, P. and Daniel, R.P., 1984. A biomechanical analysis of head, neck, and torso injuries to child surrogates due to sudden torso acceleration. In: *Proceedings of the 28th Stapp Car Crash Conference* (No. 841656).
- Prasad, P., Mertz, H.J., 1985. The position of the United States delegation to the ISO Working Group 6 on the use of HIC in the automotive environment. In: *Society of Automotive Engineers Government/Industry Meeting and Exposition* (No. 851246).
- Prasad, P., Mertz, H.J., Dalmotas, D.J., Augenstein, J.S., Digges, K., 2010. Evaluation of the field relevance of several injury risk functions. In: *Proceedings of the 54th Stapp Car Crash Conference* (No. 2010-22-0004).
- Prasad, P., Dalmotas, D., German, A., 2014. The field relevance of NHTSA's oblique research moving deformable barrier tests. In: *Proceedings of the 58th Stapp Car Crash Conference* (No. 2014-22-0007).

- Purcell, N., Kish, L., 1979. Estimation for small domains. *Biometrics*, 35(2), 365-84.
- Pudenz, R.H. and Shelden, C.H., 1946. The lucite calvarium; a method for direct observation of the brain; cranial trauma and brain movement. *Journal of Neurosurgery*, 3(6), 487-505.
- Reichert, R., Park, C., Morgan, R.M., 2014. Development of integrated vehicle-occupant model for crashworthiness safety analysis. (Report No. DOT HS 812 087) Washington DC: National Highway Traffic Safety Administration.
- Rhule, H., Maltese, M., Donnelly, B., Eppinger, R., Brunner, J., Bolte, J., 2002. Development of a new Biofidelity Ranking System for anthropomorphic test devices. *Stapp Car Crash Journal*, 46, 477-512.
- Rhule, H., Moorhouse, K., Donnelly, B., Stricklin, J., 2009. Comparison of WorldSID and ES-2RE biofidelity using updated Biofidelity Ranking System. In: *Proceedings of the 21st International Technical Conference on the Enhanced Safety of Vehicles* (No. 09-0563).
- Ridella, S., Parent, D., 2011. Modifications to improve the durability, usability, and biofidelity of the THOR-NT dummy. In: *Proceedings of the 22nd International Technical Conference on the Enhanced Safety of Vehicles* (No. 11-0312).
- Robbins, D.H., 1983. Development of anthropometrically based design specifications for an advanced adult anthropomorphic dummy family; Volume 2-Anthropometric specifications for mid-Sized male dummy. (Report No. DOT-HS-806-716) Washington, DC: National Highway Traffic Safety Administration.
- Roberts, D., Donnelly, B., Severin, C., Medige, J., 1993. Injury Mechanisms and Tolerance of the Human Ankle Joint. Atlanta, GA: Centers for Disease Control.
- Rudd, R., Crandall, J., Millington, S., Hurwitz, S. and Heglund, N., 2004. Injury tolerance and response of the ankle joint in dynamic dorsiflexion. *Stapp Car Crash Journal*, 48, 1-26.
- Rudd, R.W., 2009. Updated analysis of lower extremity injury risk in frontal crashes in the United States. In: *Proceedings of the 21st International Technical Conference on the Enhanced Safety of Vehicles* (No. 09-0556).
- Rudd, R., Scarboro, M., Saunders, J., 2011. Injury analysis of real-world small overlap and oblique frontal crashes. In: *Proceedings of the 22nd International Technical Conference on the Enhanced Safety of Vehicles* (No. 11-0384).
- Rupp, J.D., Reed M.P., Jeffrey, T.J., Schneider, L.W., 2003. Effects of hip posture on the frontal impact tolerance of the human hip joint. *Stapp Car Crash Journal*, 47, 21-33.
- Rupp, J.D., Reed, M.P., Madura, N.H., Miller, C.S., Kuppa, S.M., Schneider, L.W., 2005. Comparison of the inertial response of the THOR-NT, Hybrid III, and unembalmed cadaver to simulated knee-to-knee-bolster impacts. In: *Proceedings of the 19th International Technical Conference on the Enhanced Safety of Vehicles* (No. 05-0086).
- Rupp, J.D., 2006. Biomechanics of hip fractures in frontal motor vehicle crashes [Ph.D. Dissertation]. Ann Arbor, MI: University of Michigan.
- Rupp, J.D., Reed, M.P., Miller, C.S., Madura, N.H., Klinich, K.D., Schneider, L.W., Kuppa, S.M., 2009a. Development of new criteria for assessing the risk of knee-thigh-hip injury in frontal impacts using Hybrid III femur force measurements. In: *Proceedings of the 21st International Technical Conference on the Enhanced Safety of Vehicles* (No. 09-0306).
- Rupp, J.D., Flannagan, C.A., Kuppa, S.M., 2009b. Development of new injury risk curves for the knee/distal femur and the hip for use in frontal impact testing. (Report No. UMTRI-2009-08) Ann Arbor, MI: University of Michigan Transportation Research Institute.
- Saari, A., Dennison, C.R., Zhu, Q., Nelson, T.S., Morley, P., Oxland, T.R., Cripton, P.A. and Itshayek, E., 2013. Compressive follower load influences cervical spine kinematics and kinetics during simulated head-first impact in an in vitro model. *Journal of biomechanical engineering*, 135(11), 1-11.
- Saunders, J., Craig, M., Suway, J., 2011. NHTSA's test procedure evaluations for small overlap/oblique crashes. In: *Proceedings of the 22nd International Technical Conference on the Enhanced Safety of Vehicles* (No. 11-0343).
- Saunders, J., Parent, D. P., Craig, M. J., 2012. Moving deformable barrier test procedure for evaluating small overlap/oblique crashes. *SAE International Journal of Commercial Vehicles*, 5, 172-195.

- Saunders, J., Parent, D., Ames, E., 2015. NHTSA oblique crash test results: vehicle performance and occupant injury risk assessment in vehicles with small overlap countermeasures. In: *Proceedings of the 24th International Technical Conference for the Enhanced Safety of Vehicles* (No. 15-0108).
- Schneider, L.W., Robbins, D.H., Pflüg, M.A., Snyder, R.G., 1983. Development of anthropometrically based design specifications for an advanced adult anthropomorphic dummy family, Volume 1. (Report No. DOT-HS-806-715) Washington, DC: National Highway Traffic Safety Administration.
- Schreiber, P., Crandall, J., Hurwitz, S. and Nusholtz, G.S., 1998. Static and dynamic bending strength of the leg. *International Journal of Crashworthiness*, 3(3), 295-308.
- Shaw, N.A., 2002. The neurophysiology of concussion. *Progress in Neurobiology*, 67(4), 281-344.
- Shaw, G., Lessley, D., Bolton, J., Crandall, J., 2004. Assessment of the THOR and Hybrid III crash dummies: steering wheel rim impacts to the upper abdomen. *Society of Automotive Engineers* (No. 2004-01-0310).
- Shaw, C.G., Parent, D., Purtsezov, S., Lessley, D., Crandall, J.R., Kent, R.W., Guillemot, H., Ridella, S., Takhounts, E., Martin, P., 2009. Impact response of restrained PMHS in frontal sled tests: skeletal deformation patterns under seat belt loading. *Stapp Car Crash Journal*, 53, 1-48.
- Shaw, C.G., Lessley, D., Ash, J., Crandall, J., 2012. Development of an alternative frontal impact condition to assess thoracic response using the THOR Mod Kit dummy. In: *Proceedings of Society of Automotive Engineers of Japan* (No. 20125216).
- Shimamura, M., Ohhashi, H., Yamazaki, M., 2003. The effects of occupant age on patterns of rib fractures to belt-restrained drivers and front passengers in frontal crashes in Japan. *Stapp Car Crash Journal*, 47, 349-365.
- Society of Automotive Engineers, 1980. Collision Deformation Classification, Surface Vehicle Standard J224.
- Takhounts, E., Eppinger, R., Campbell, J., Tannous, R., Power, E., and Shook, L., 2003. On the development of the SIMon finite element head model. *Stapp Car Crash Journal*, 47, 107-33.
- Takhounts, E., Ridella, R., Hasija, V., Tannous, R., Campbell, J., Malone, D., Danelson, K., Stitzel, J., Rowson, S., and Duma, S., 2008. Investigation of traumatic brain injuries using the next generation of Simulated Injury Monitor (SIMon) finite element head model. *Stapp Car Crash Journal*, 52, 1-31.
- Takhounts, E.G., Craig, M., Moorhouse, K., McFadden, J., Hasija, V., 2013. Development of Brain Injury Criteria (BrIC). *Stapp Car Crash Journal*, 57, 243-66.
- Takhounts, E.G., 2015. Computational modeling and injury criteria for motor-vehicle crashes. In: *Proceedings of the 59th Stapp Car Crash Conference*, invited lecture.
http://www.nhtsa.gov/DOT/NHTSA/NVS/Biomechanics%20&%20Trauma/Stapp_2015.pdf
- Takhounts, E.G., Hasija, V., Craig, M.J., 2019. BrIC and field brain injury risk. In: *Proceedings of the 26th International Technical Conference for the Enhanced Safety of Vehicles* (No 19-0154).
- Thunnissen, J., Wismans, J., Ewing, C.L. and Thomas, D.J., 1995. Human volunteer head-neck response in frontal flexion: a new analysis. In: *Proceedings of the 39th Stapp Car Crash Conference* (No. 952721).
- Trosseille, X., Le-Coz, J., Potier, P., Lassau, J., 2002. Abdominal response to high-speed seatbelt loading. *Society of Automotive Engineers* (No. 2002-22-0004).
- Untaroiu, C.D., Ivarsson, J., Genovese, D.R., Bose, D. and Crandall, J.R., 2008. Biomechanical injury response of leg subjected to combined axial compressive and bending loading. *Biomedical Sciences Instrumentation*, 44, 141-146.
- Viano, D., Kroell, C., Warner, C., 1997. Comparative thoracic impact response of living and sacrificed porcine siblings. In: *Proceedings of the 21st Stapp Car Crash Conference* (No. 770930).
- Von Gierke, H., 1964. Transient acceleration, vibration and noise problems in space flight. In: Schaefer K.E. (ed.) *Bioastronautics*. New York: Macmillan, 27-75.
- Wang, M.C., Pintar, F., Yoganandan, N. and Maiman, D.J., 2009. The continued burden of spine fractures after motor vehicle crashes. *Journal of Neurosurgery: Spine*, 10(2), 86-92.

- Wheeldon, J.A., Pintar, F.A., Knowles, S. and Yoganandan, N., 2006. Experimental flexion/extension data corridors for validation of finite element models of the young, normal cervical spine. *Journal of biomechanics*, 39(2), 375-380.
- Wismans, J., Philippens, M., Van Oorschot, E., Kallieris, D. and Mattern, R., 1987. Comparison of human volunteer and cadaver head-neck response in frontal flexion. In: *Proceedings of the 31st Stapp Car Crash Conference* (No. 872194).
- Yamada, H. *Strength of Biological Materials*. Baltimore, The Williams & Wilkins Company, 1970.
- Yliniemi, E.M., Pelletiere, J.A., Doczy, E.J., Nuckley, D.J., Perry, C.E. and Ching, R.P., 2009. Dynamic tensile failure mechanics of the musculoskeletal neck using a cadaver model. *Journal of Biomechanical Engineering*, 131(5), pp 051001.
- Yoganandan, N., Pintar, F.A., Boynton, M., Begeman, P., Prasad, P., Kuppa, S.M., Morgan, R.M. and Eppinger, R.H., 1996. Dynamic axial tolerance of the human foot-ankle complex. In: *Proceedings of the 40th Stapp Car Crash Conference* (No. 962426).
- Yoganandan, N., Pintar, F., Kumaresan, S., Haffner, M., Kuppa, S., 1997. Impact biomechanics of the human thorax-abdomen complex. *International Journal of Crashworthiness*, 2(2), 219-228.
- Yoganandan, N., Pintar, F., Rinaldi, J., 2009. Evaluation of the RibEye deflection measurement system in the 50th percentile Hybrid III dummy. (Report No. DOT HS 811 102) Washington DC: National Highway Traffic Safety Administration.
- Yoganandan, N., Arun, M.W., Pintar, F.A. and Banerjee, A., 2015. Lower leg injury reference values and risk curves from survival analysis for male and female dummies: meta-analysis of postmortem human subject tests. *Traffic Injury Prevention*, 16(S1), S100-S107.
- Zhang, L., Yang, K.H., Dwarampudi, R., Omori, K., Li, T., Chang, K., Hardy, W.N., Khalil, T.B., King, A.I., 2001. Recent advances in brain injury research: a new human head model development and validation. *Stapp Car Crash Journal* 45: 369-394.

APPENDIX A. Vehicle Test Data – BrIC Correlation Studies

TEST-OCCLC	DATABASE	TEST-OCCLC	DATABASE	TEST-OCCLC	DATABASE
4303-01	NHTSA	5301-02	NHTSA	7292-01	NHTSA
4242-01	NHTSA	5567-01	NHTSA	7293-01	NHTSA
4205-02	NHTSA	5594-02	NHTSA	7366-01	NHTSA
4273-01	NHTSA	5595-01	NHTSA	7368-01	NHTSA
4198-01	NHTSA	5595-02	NHTSA	7371-01	NHTSA
3897-01	NHTSA	5609-01	NHTSA	7429-01	NHTSA
4266-02	NHTSA	5613-01	NHTSA	7433-01	NHTSA
4247-01	NHTSA	5711-01	NHTSA	7434-01	NHTSA
3916-01	NHTSA	5715-01	NHTSA	7428-01	NHTSA
4264-02	NHTSA	6370-01	NHTSA	7431-01	NHTSA
3901-02	NHTSA	7966-01	NHTSA	7427-01	NHTSA
4250-01	NHTSA	7977-01	NHTSA	7432-01	NHTSA
4251-01	NHTSA	7978-01	NHTSA	7430-01	NHTSA
4215-02	NHTSA	7989-01	NHTSA	7426-01	NHTSA
4237-02	NHTSA	8000-01	NHTSA	7458-01	NHTSA
4080-01	NHTSA	8024-01	NHTSA	7441-01	NHTSA
4090-01	NHTSA	8035-01	NHTSA	7457-01	NHTSA
4264-01	NHTSA	8045-01	NHTSA	7444-01	NHTSA
4090-02	NHTSA	8048-01	NHTSA	7456-01	NHTSA
4223-02	NHTSA	8055-01	NHTSA	7467-01	NHTSA
4267-02	NHTSA	8064-01	NHTSA	7468-01	NHTSA
4215-01	NHTSA	8068-01	NHTSA	7476-01	NHTSA
4242-02	NHTSA	8071-01	NHTSA	7967-01	NHTSA
4259-01	NHTSA	8077-01	NHTSA	7984-01	NHTSA
3987-01	NHTSA	8080-01	NHTSA	7990-01	NHTSA
4255-02	NHTSA	8081-01	NHTSA	7998-01	NHTSA
4235-01	NHTSA	8091-01	NHTSA	8033-01	NHTSA
4235-02	NHTSA	8106-01	NHTSA	8047-01	NHTSA
4265-02	NHTSA	8153-01	NHTSA	8053-01	NHTSA
4249-02	NHTSA	8151-01	NHTSA	8054-01	NHTSA
4240-01	NHTSA	8156-01	NHTSA	8069-01	NHTSA
4237-01	NHTSA	6830-01	NHTSA	8072-01	NHTSA
4259-02	NHTSA	6831-01	NHTSA	8078-01	NHTSA
4198-02	NHTSA	6852-01	NHTSA	8079-01	NHTSA
3915-02	NHTSA	6855-01	NHTSA	8082-01	NHTSA
3901-01	NHTSA	6872-01	NHTSA	8092-01	NHTSA
4241-01	NHTSA	6873-01	NHTSA	8102-01	NHTSA
4252-01	NHTSA	6937-01	NHTSA	8108-01	NHTSA

TEST-OCCLC	DATABASE	TEST-OCCLC	DATABASE	TEST-OCCLC	DATABASE
3952-02	NHTSA	7144-01	NHTSA	8149-01	NHTSA
5287-01	NHTSA	7145-01	NHTSA	8157-01	NHTSA
9089-01	NHTSA	5461-01	NHTSA	7145-04	NHTSA
3800-01	NHTSA	5472-01	NHTSA	7431-04	NHTSA
4551-01	NHTSA	7977-02	NHTSA	7467-04	NHTSA
3875-01	NHTSA	7989-02	NHTSA	7468-04	NHTSA
3899-01	NHTSA	8024-02	NHTSA	7476-04	NHTSA
3818-01	NHTSA	8035-02	NHTSA	8069-04	NHTSA
4547-01	NHTSA	8045-02	NHTSA	8078-04	NHTSA
4380-01	NHTSA	8055-02	NHTSA	8092-04	NHTSA
3845-01	NHTSA	8064-02	NHTSA	7955-01	NHTSA
4497-01	NHTSA	8068-02	NHTSA	7979-01	NHTSA
4547-04	NHTSA	8080-02	NHTSA	7988-01	NHTSA
3898-01	NHTSA	8081-02	NHTSA	7997-01	NHTSA
4551-04	NHTSA	8091-02	NHTSA	8052-01	NHTSA
3799-04	NHTSA	8104-02	NHTSA	9089-04	NHTSA
4380-04	NHTSA	8106-02	NHTSA	7773-01	NHTSA
3820-01	NHTSA	8153-02	NHTSA	7851-01	NHTSA
4456-04	NHTSA	8156-02	NHTSA	7852-01	NHTSA
3819-04	NHTSA	5713-03	NHTSA	7861-01	NHTSA
4456-01	NHTSA	5714-03	NHTSA	7862-01	NHTSA
3799-01	NHTSA	5715-03	NHTSA	7867-01	NHTSA
4378-01	NHTSA	6852-04	NHTSA	8084-01	NHTSA
4292-01	NHTSA	6855-04	NHTSA	8084-02	NHTSA
4498-01	NHTSA	6865-04	NHTSA	8085-01	NHTSA
3803-04	NHTSA	6925-04	NHTSA	8085-02	NHTSA
3802-01	NHTSA	6937-04	NHTSA	8086-01	NHTSA
4292-04	NHTSA	7366-04	NHTSA	8086-02	NHTSA
3803-01	NHTSA	7368-04	NHTSA	8087-01	NHTSA
4482-01	NHTSA	7428-04	NHTSA	8087-02	NHTSA
3800-04	NHTSA	7441-04	NHTSA	8088-01	NHTSA
4471-01	NHTSA	7457-04	NHTSA	8088-02	NHTSA
4313-01	NHTSA	7427-04	NHTSA	8089-01	NHTSA
3819-01	NHTSA	7432-04	NHTSA	8089-02	NHTSA
4859-01	NHTSA	7444-04	NHTSA	8096-01	NHTSA
5296-01	NHTSA	7426-04	NHTSA	8096-02	NHTSA
5317-01	NHTSA	7456-04	NHTSA	8097-01	NHTSA
5405-01	NHTSA	7429-04	NHTSA	8097-02	NHTSA
5406-01	NHTSA	7434-04	NHTSA	8099-01	NHTSA
5407-01	NHTSA	7433-04	NHTSA	8099-02	NHTSA

TEST-OCCLC	DATABASE	TEST-OCCLC	DATABASE	TEST-OCCLC	DATABASE
5408-01	NHTSA	6872-04	NHTSA	8381-01	NHTSA
5416-01	NHTSA	7144-04	NHTSA	8381-02	NHTSA
8475-01	NHTSA	9126-01	NHTSA	9482-02	NHTSA
8476-01	NHTSA	9126-02	NHTSA	9483-01	NHTSA
8477-01	NHTSA	9127-01	NHTSA	9483-02	NHTSA
8478-01	NHTSA	9127-02	NHTSA	9499-01	NHTSA
8478-02	NHTSA	9206-01	NHTSA	9499-02	NHTSA
8488-01	NHTSA	9207-01	NHTSA	9500-01	NHTSA
8488-02	NHTSA	9208-01	NHTSA	9500-02	NHTSA
8510-01	NHTSA	9209-01	NHTSA	9501-01	NHTSA
8512-01	NHTSA	9210-01	NHTSA	9501-02	NHTSA
8591-01	NHTSA	9211-01	NHTSA	9566-01	NHTSA
8787-01	NHTSA	9212-01	NHTSA	9567-01	NHTSA
8787-02	NHTSA	9213-01	NHTSA	9568-01	NHTSA
8788-01	NHTSA	9214-01	NHTSA	9569-01	NHTSA
8788-02	NHTSA	9216-01	NHTSA	9570-01	NHTSA
8789-01	NHTSA	9217-01	NHTSA	9571-01	NHTSA
8789-02	NHTSA	9218-01	NHTSA	9572-01	NHTSA
8875-01	NHTSA	9219-01	NHTSA	9572-02	NHTSA
8875-02	NHTSA	9220-01	NHTSA	9573-01	NHTSA
8881-01	NHTSA	9221-01	NHTSA	9573-02	NHTSA
8881-02	NHTSA	9222-01	NHTSA	9574-01	NHTSA
8882-01	NHTSA	9332-01	NHTSA	9574-02	NHTSA
8882-02	NHTSA	9333-01	NHTSA	9585-01	NHTSA
8998-01	NHTSA	9334-01	NHTSA	9585-02	NHTSA
8998-02	NHTSA	9335-01	NHTSA	9586-01	NHTSA
8999-01	NHTSA	9336-01	NHTSA	9586-02	NHTSA
8999-02	NHTSA	9337-01	NHTSA	9587-01	NHTSA
9042-01	NHTSA	9354-01	NHTSA	9587-02	NHTSA
9042-02	NHTSA	9354-02	NHTSA	9699-01	NHTSA
9043-01	NHTSA	9476-01	NHTSA	9699-02	NHTSA
9110-01	NHTSA	9476-02	NHTSA	9725-01	NHTSA
9110-02	NHTSA	9477-01	NHTSA	9725-02	NHTSA
9121-02	NHTSA	9477-02	NHTSA	9726-01	NHTSA
9122-01	NHTSA	9478-01	NHTSA	9727-01	NHTSA
9122-02	NHTSA	9478-02	NHTSA	9727-02	NHTSA
9123-01	NHTSA	9479-01	NHTSA	9802-01	NHTSA
9123-02	NHTSA	9479-02	NHTSA	9802-02	NHTSA
9124-01	NHTSA	9480-02	NHTSA	9804-01	NHTSA
9124-02	NHTSA	9481-01	NHTSA	9804-02	NHTSA

TEST-OCCLC	DATABASE	TEST-OCCLC	DATABASE	TEST-OCCLC	DATABASE
9125-01	NHTSA	9481-02	NHTSA	CEN1324-01	IIHS
9125-02	NHTSA	9482-01	NHTSA	CEN1326-01	IIHS
9806-01	NHTSA	9151-01	NHTSA	CEN1327-01	IIHS
9807-01	NHTSA	9151-02	NHTSA	CEN1328-01	IIHS
9807-02	NHTSA	9152-01	NHTSA	CEN1335-01	IIHS
9202-04	NHTSA	9152-02	NHTSA	CEN1336-01	IIHS
9204-04	NHTSA	9154-01	NHTSA	CEN1337-01	IIHS
9332-02	NHTSA	9154-02	NHTSA	CEN1338-01	IIHS
9333-02	NHTSA	9155-01	NHTSA	CEN1339-01	IIHS
9334-02	NHTSA	9155-02	NHTSA	CEN1341-01	IIHS
9335-02	NHTSA	9223-01	NHTSA	CEN1344-01	IIHS
9336-02	NHTSA	9223-02	NHTSA	CEN1345-01	IIHS
9337-02	NHTSA	9805-01	NHTSA	CEN1346-01	IIHS
9566-02	NHTSA	9805-02	NHTSA	CEN1347-01	IIHS
9567-02	NHTSA	CEN1219-01	IIHS	CEN1348-01	IIHS
9568-02	NHTSA	CEN1220-01	IIHS	CEN1349-01	IIHS
9569-02	NHTSA	CEN1221-01	IIHS	CEF1206-01	IIHS
9570-02	NHTSA	CEN1223-01	IIHS	CEF1207-01	IIHS
9571-02	NHTSA	CEN1224-01	IIHS	CEF1208-01	IIHS
9135-02	NHTSA	CEN1225-01	IIHS	CEF1301-01	IIHS
9137-01	NHTSA	CEN1227-01	IIHS	CEF1302-01	IIHS
9137-02	NHTSA	CEN1228-01	IIHS	CEF1303-01	IIHS
9138-01	NHTSA	CEN1229-01	IIHS	CEF1304-01	IIHS
9138-02	NHTSA	CEN1230-01	IIHS	CEF1305-01	IIHS
9139-01	NHTSA	CEN1231-01	IIHS	CEF1306-01	IIHS
9139-02	NHTSA	CEN1233-01	IIHS	CEF1307-01	IIHS
9140-01	NHTSA	CEN1234-01	IIHS	CEF1308-01	IIHS
9140-02	NHTSA	CEN1235-01	IIHS	CES1308-01	IIHS
9142-01	NHTSA	CEN1236-01	IIHS	CES1309-01	IIHS
9143-01	NHTSA	CEN1301-01	IIHS	CES1310-01	IIHS
9144-01	NHTSA	CEN1302-01	IIHS	CES1308-04	IIHS
9144-02	NHTSA	CEN1303-01	IIHS	CES1309-04	IIHS
9145-01	NHTSA	CEN1304-01	IIHS	CES1310-04	IIHS
9146-01	NHTSA	CEN1307-01	IIHS	CEN1330-01	IIHS
9146-02	NHTSA	CEN1309-01	IIHS	CEN1333-01	IIHS
9147-02	NHTSA	CEN1313-01	IIHS		
9148-01	NHTSA	CEN1314-01	IIHS		
9148-02	NHTSA	CEN1321-01	IIHS		
9150-01	NHTSA	CEN1322-01	IIHS		
9150-02	NHTSA	CEN1323-01	IIHS		

APPENDIX B. Algorithm for Computing Time Duration of Angular Velocity Pulse

A sample pulse is shown in Figure B.1 to explain the algorithm:

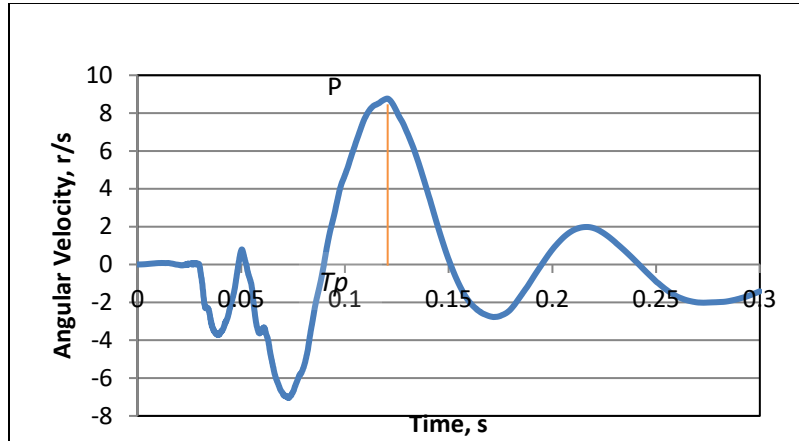


Figure B.1. Peak of the pulse (P) and time of peak (T_p) for an example angular velocity time-history.

1. Time step is determined (dt)
2. The peak of the pulse (P) is computed along with the time of peak (T_p)
3. The area around the peak is then incrementally calculated by moving the time counter (i) on either side as:
 - a. Compute area under the curve A_i from $T_p - i \times dt$ to $T_p + i \times dt$.
 - b. If the peak is too close to either end of the time spectrum, then the counter movement is not symmetrical around the peak i.e.
 - i. if peak is close to time zero then,
 1. compute area from $T_p - i \times dt$ to $T_p + i \times dt$ till $t = 0$ is reached
 2. then compute area from 0 to $T_p + i \times dt$
 - ii. if peak is close to *end time* then,
 1. compute area from $T_p - i \times dt$ to $T_p + i \times dt$ till $t = end$ is reached
 2. then compute area from $T_p - i \times dt$ to *end time*
4. Counter is stopped when the first maximum in area is found in the first 100ms. ΔT is computed at this point, which corresponds to the time duration of the angular velocity pulse
$$\Delta T = (T_p + i \times dt) - (T_p - i \times dt)$$
5. P and ΔT are used in the BrIC formulation.

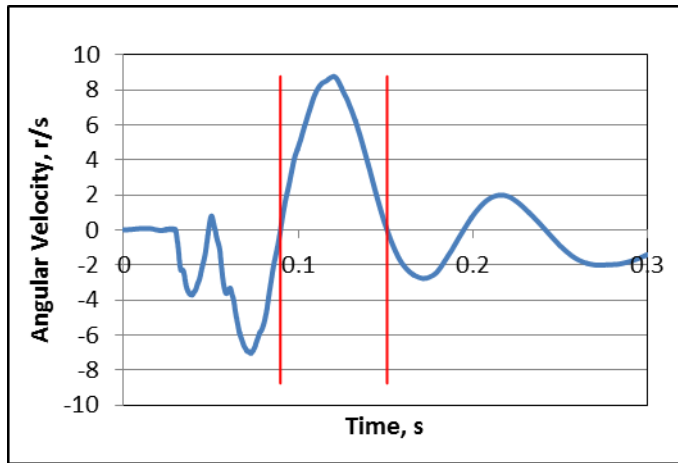


Figure B.2. Delta T for an example angular velocity time-history.

APPENDIX C. BrIC Design of Experiments and Optimization

DESIGN OF EXPERIMENTS

Design of experiments (DOE) is frequently used to investigate the effect of various parameters on the outcome variable. To conduct the DOE study and investigate the effect of various parameters on BrIC, a full finite element (FE) model of a Toyota Yaris (developed by the George Washington University) was modified and simplified in the manner shown below (Figure C.1).

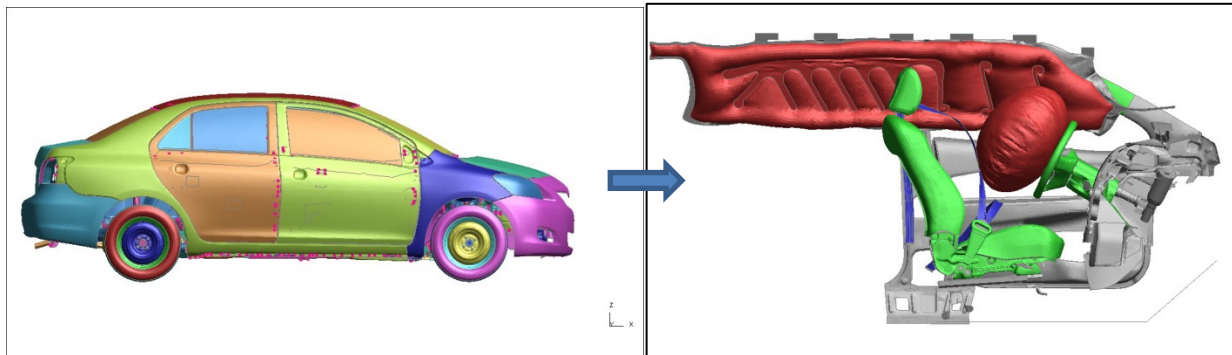


Figure C.1. Full FE model of Toyota Yaris (left) with simplified interior and restraint system components (right).

Following are the simplifications made in the model for the DOE study:

- Roof rails, door, B-pillar on the driver side and floor were deformable in the full FE model, but were made rigid so that no intrusion is considered in this analysis
- Knee bolster, A-pillar were kept deformable
- Driver seat was kept deformable and the Simplified 50th percentile male GHBM model was used and positioned in the seat using pre-simulation
- Steering column assembly was kept deformable including the steering wheel; steering wheel stiffness was increased to represent steering wheel deformation of the majority of mid-size sedans (this stiffness in the original model was too low causing excessive deformations of the steering wheel when compared to those of the majority of the cars)
- The distance to the side door was increased to represent a mid-sized sedan
- A 50-liter frontal airbag was used
- The side curtain airbag was obtained from TRW and used in this analysis
- The belt system with retractor, pre-tensioner and load limiter was used; the belt is fitted to the Simplified GHBM model using Primer 12.0 software package (Oasys Ltd., Solihull, UK)
- The seat was positioned to represent mid-track position of a mid-sized sedan

Several DOE studies were conducted using metamodeling techniques, which allowed for construction of surrogate design models for the purpose of design exploration, such as variable screening. Surrogate design models help save time when compared to running direct simulations. LS-Opt software package (LSTC Inc., Livermore) was used in this analysis, which provided the capability of using five standard types of metamodeling techniques, namely polynomial response surfaces, Neural Networks, Radial Basis Function (RBF) Networks, Kriging and Support Vector Regression. At the core, these techniques differ in the regression methods employed to construct the surrogate models. The polynomial response surface method and the RBF use linear regression, while neural networks use nonlinear regression methods.

Of the metamodeling techniques tested, the Feed Forward Neural Network (FFNN) method provided the best accuracy for the response parameters and is thus used in all DOE studies presented here (example of the fit is given in Figure C.2).

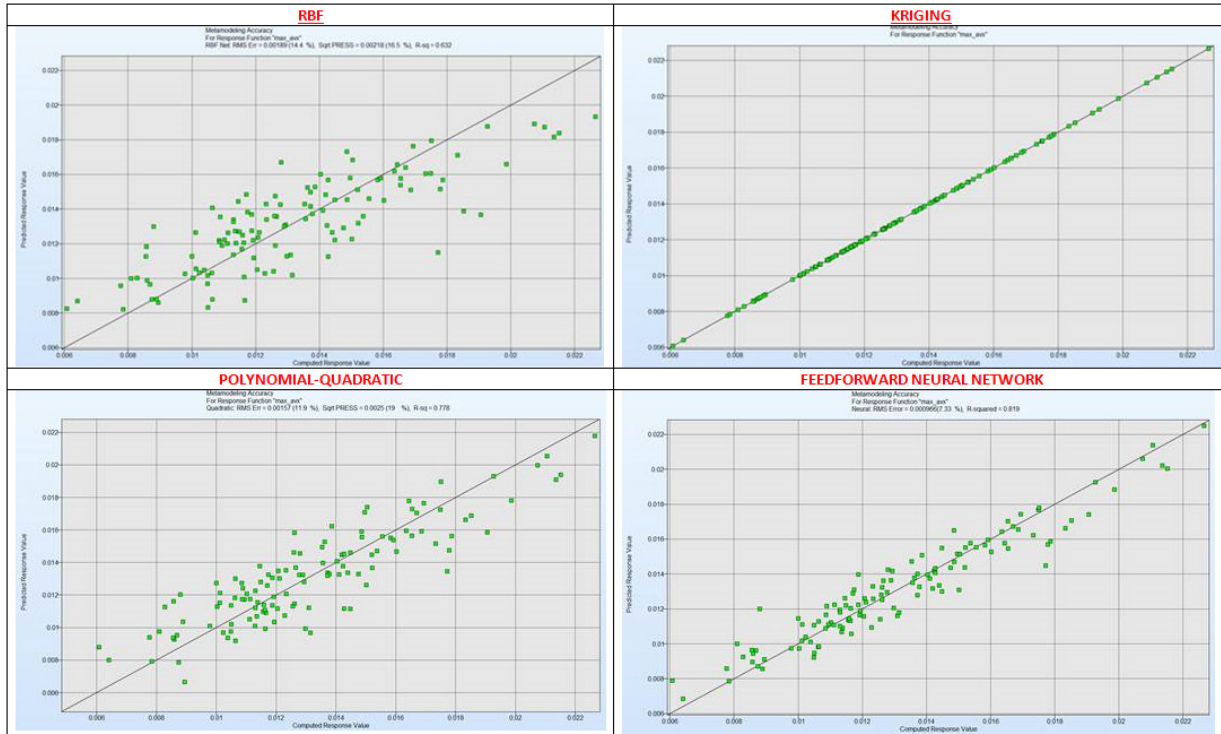


Figure C.2. Fit of various metamodels. Note that Kriging by definition gives a perfect fit and shows zero prediction errors. This prevents the use of standard model selection criteria (such as R^2). Since the metamodel fit using Kriging method is difficult to assess, the next best method (FFNN) was used.

Space-filling sampling scheme guarantees an optimal coverage of the design space and was used in these studies (Figure C.3).

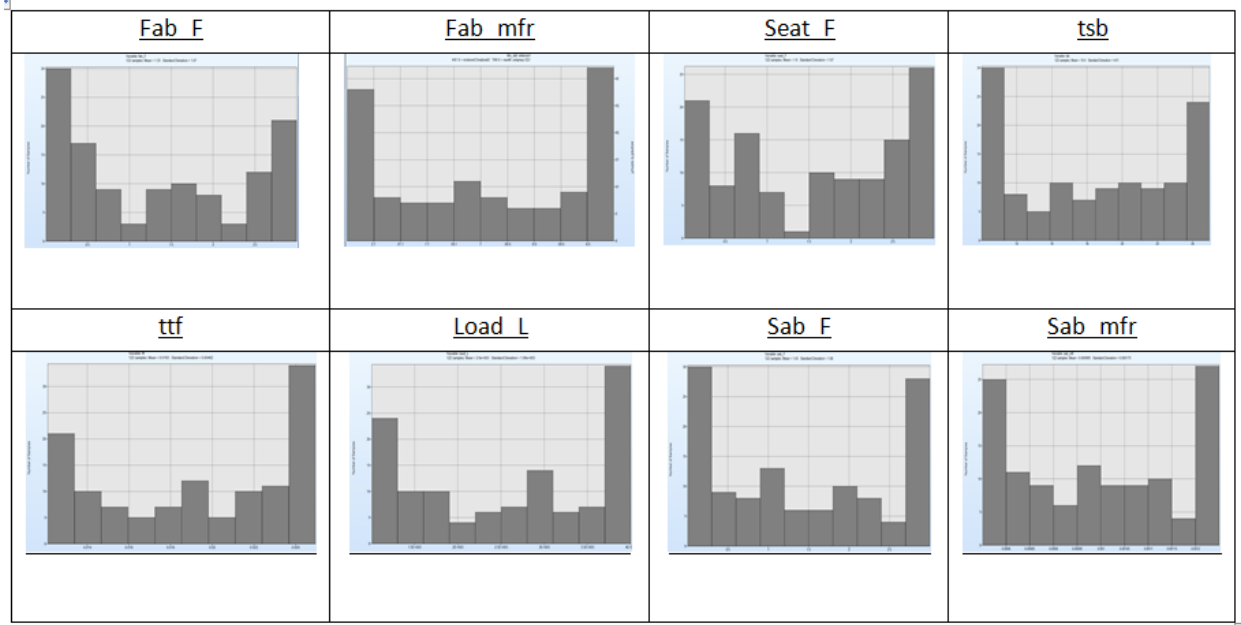


Figure C.3. Space filling sampling method demonstrates sampling for each varied parameter. For example, the full factorial DOE for nine parameters (Table C.1) and 10 values per parameter would require approximately 1,000,000,000 simulations, which will take (at 2.5 hours per simulation) approximately 285,288 years to be completed (instead of approximately one week).

The nominal crash pulse used for these analyses was taken from NHTSA Research and Development test 9224 (the setup is shown in Figure C.4).

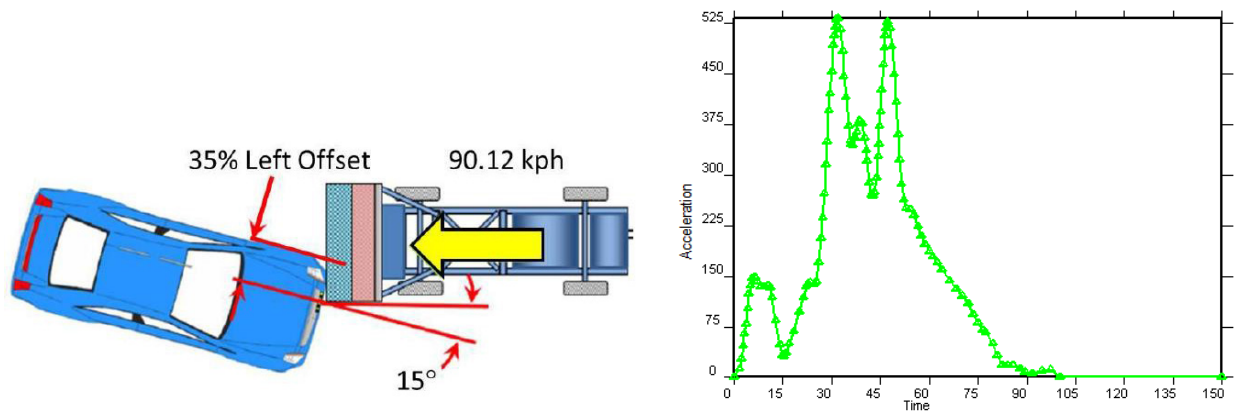


Figure C.4. Test setup for test number 9224 and the corresponding crash pulse that was used in all studies (frontal and oblique impacts). Note that the crash pulse was taken from the oblique test and is more severe than that of a typical NCAP crash pulse.

The simplified human FE model, used in these studies, complements the Global Human Body Models Consortium (GHBMC) detailed 50th percentile male occupant (M50-O) by providing kinematic and kinetic data with a significantly reduced run time using the same body habitus. The simplified occupant model (M50-OS) was developed using the same source geometry as the M50-O. Though some meshed components were preserved, the total element count was reduced by remeshing, homogenizing, or in some cases omitting structures that are explicitly contained in the M50-O. Bones are included as rigid

bodies, with the exception of the ribs, which are deformable but were remeshed to a coarser element density than the M50-O. Material models for all deformable components were drawn from the biomechanics literature. Kinematic joints were implemented at major articulations (shoulder, elbow, wrist, hip, knee, and ankle) with moment vs. angle relationships from the literature. The M50-OS simplified model has 354,000 elements; in contrast, the M50-O detailed model has 2.2 million elements. The model can be repositioned without requiring simulation. The M50-OS model ran a 150-ms event on 40 processors in 2.5 hours compared to 25 hours for M50-O detailed model. M50-OS model (Figure C.5) exhibited a significant reduction in run time and thus was used for DOE and optimization studies.

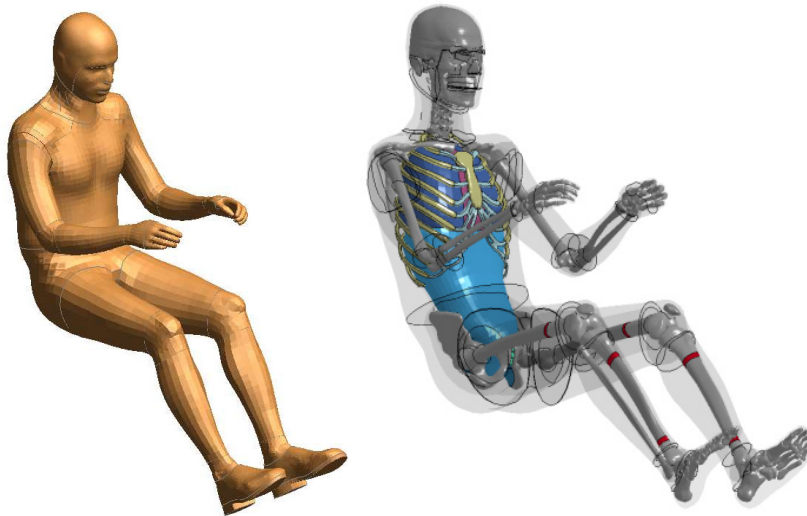


Figure C.5. Simplified GHBM human 50th percentile male occupant model (M50-OS) was used in all DOE and optimization studies.

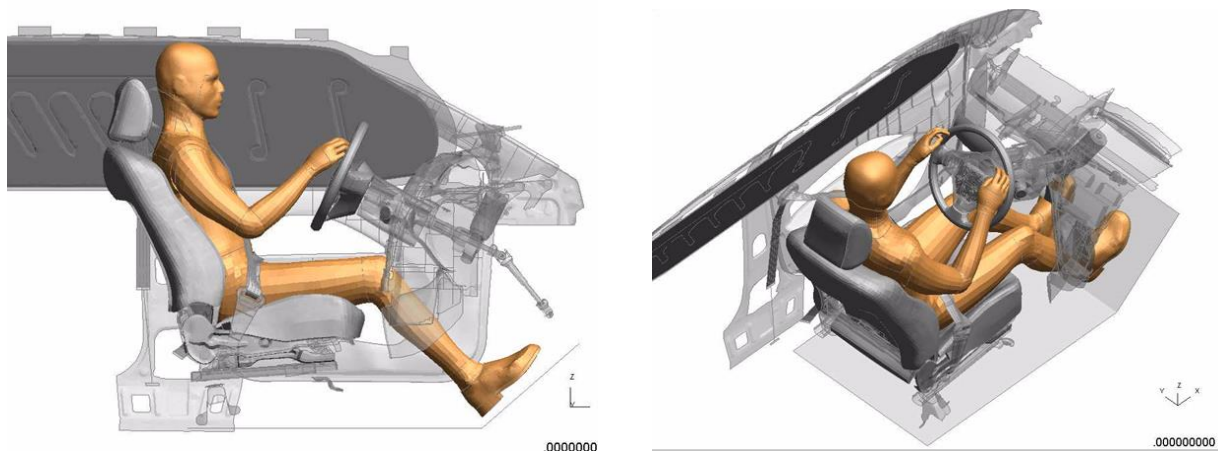
DOE Study #1 (include Delta-V and PDOF)

The first DOE study included changes in delta-V and the principal direction of force (PDOF) in the analysis. The range of delta-V was obtained by scaling the magnitude of the pulse shown in Figure C.4 while keeping the time unchanged. Table C.1 lists all the parameters varied in the DOE study #1, including their nominal values and the range.

Table C.1. Parameters varied in the DOE study #1.

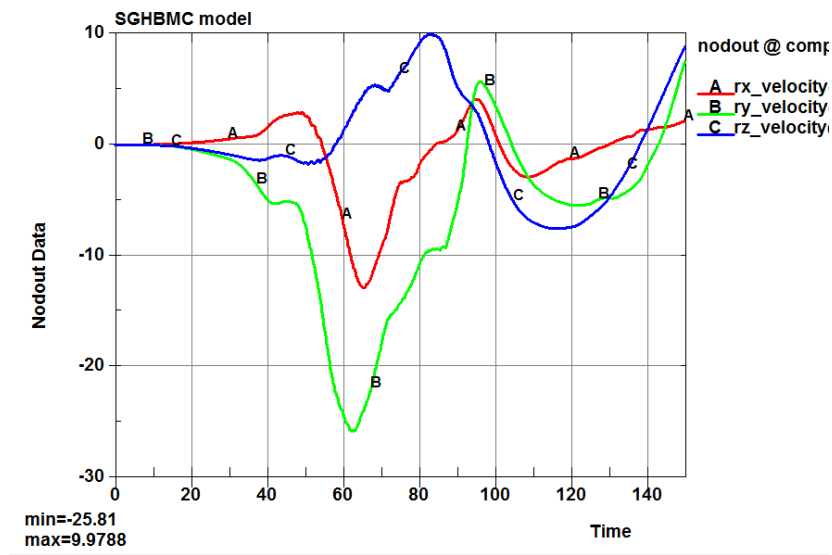
<u>Parameters</u>	<u>Nominal</u>	<u>Range</u>
Crash Pulse, cpulse	0.94 (35mph)	0.65 (25mph) – 1.25 (47mph)
PDOF	0°	0° - 30°
Front Airbag Friction, fab_F	0.5	0 – 3
Frontal Airbag Mass Flow Rate, fab_mfr	1	0.75 – 1.25
Load Limiter, load_L	3000 N	1000- 4000
Side Airbag Friction, sab_F	0.3	0 - 3
Frontal Airbag (firing) Time, ttf	18 ms	12- 25
Side Airbag (firing) Time, tsb	18 ms	12 - 25
Side Airbag Mass Flow Rate, sab_mfr	1	0.75 – 1.25

Figure C.6 demonstrates the setup and results for the nominal values of parameters given in Table C.1 and Table C.2 relists the nominal values and the value of BrIC.



(a)

(b)



(c)

Figure C.6. Initial position setup for the run with nominal values given in Table C.2; right view (a), top oblique view (b), and the FE model output for the head angular velocity components time histories (c).

Table C.2. Results of the run with the nominal parameters.

Crash Pulse	Fab_F	Fab_MFR	Load_L	Sab_F	tff	tsb	Sab_mfr	BrIC
35 mph	0.5	1.0	3000	0.3	18	18	1.0	0.55

The value of BrIC for the nominal run (somewhat representing NCAP tests with more aggressive pulse) was 0.55, representing rather low risk of brain injury.

Figure C.7 demonstrates the metamodel-based global sensitivity of BrIC for various parameters when varied within the ranges given in Table C.1.

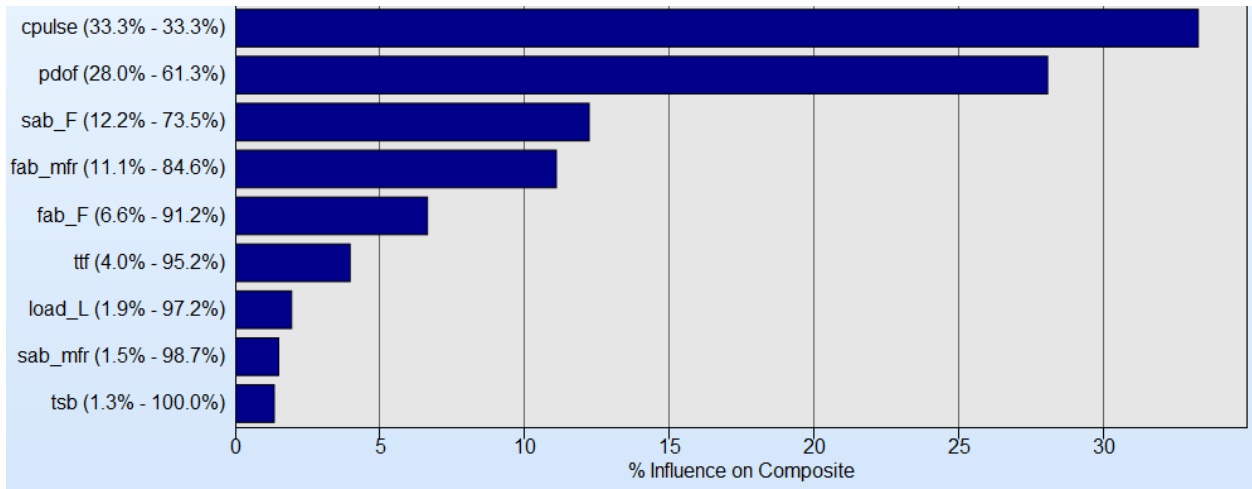


Figure C.7. Influence of all parameters listed in Table C.1 on BrIC.

It is clear that the most influential parameter affecting BrIC is delta-V (cpulse) changing BrIC by a third (33.3%) within the given range. The next most influential parameter affecting BrIC is PDOF (28.0% influence). Cumulatively delta-V and PDOF affect the values of BrIC by 61.3%. Figure C.8 gives a more detailed look of the influence of delta-V and PDOF on the values of BrIC when other parameters are constrained to their nominal values, demonstrating that with the increased PDOF the influence of delta-V on the values of BrIC increases. For example, for a 20° oblique test, the value of BrIC will change from approximately 0.55 at delta-V of 25 mph to 1.2 at delta-V of 47 mph (in Figure C.8 the delta-V of 35 mph corresponds to the value of cpulse of 0.00094). The relationship between delta-V and BrIC is almost linear for any PDOF.

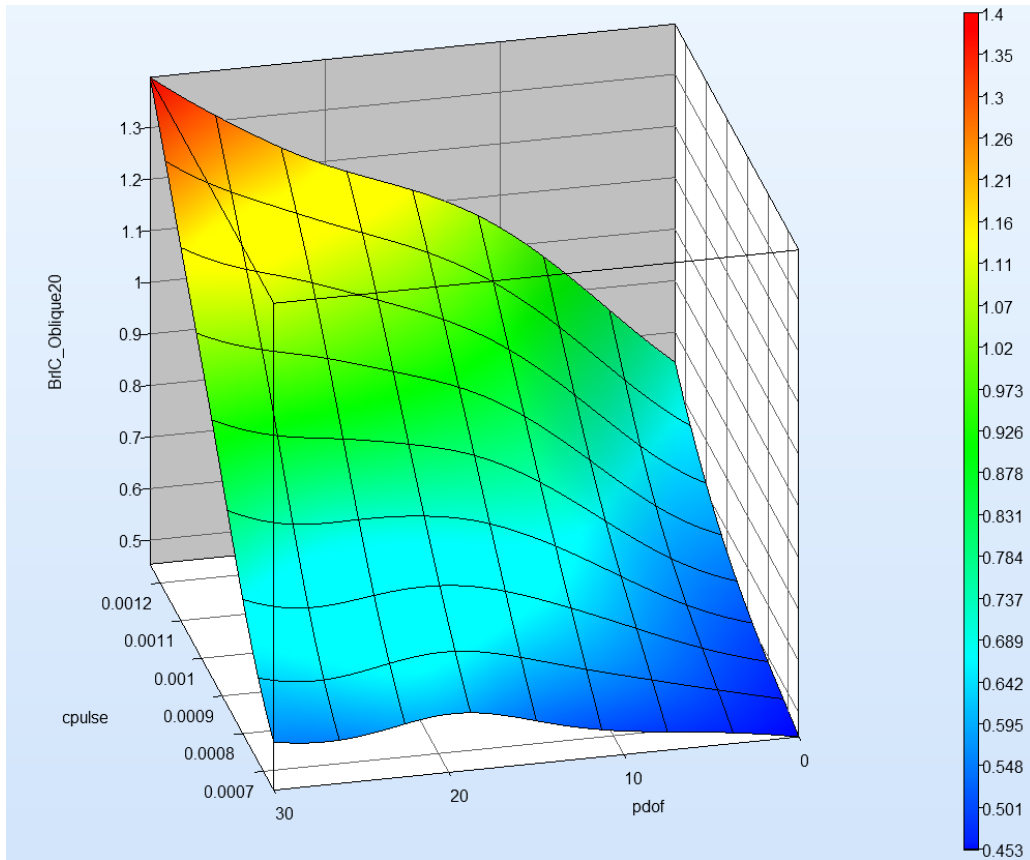


Figure C.8. Relationship between BrIC and Delta-V and PDOF demonstrating strong relationship between all three parameters, and especially that between BrIC and Delta-V.

Without the use of metamodels, however, when a limited number of tests is used to investigate relationships between various parameters, misleading conclusions about their complex inter-relationships may be reached. For example, Figure C.9 demonstrates a scatter plot of BrIC versus delta-V for each run in this DOE study, in which the relationship between the two parameters may appear rather weak especially when the range of other parameters is rather large (representing various vehicles) and when a limited range of delta-Vs is considered. This is the situation where the use of metamodels is very helpful (contrast the scattered plot in Figure C.9 with the actual relationship between the parameters given in Figure C.8).

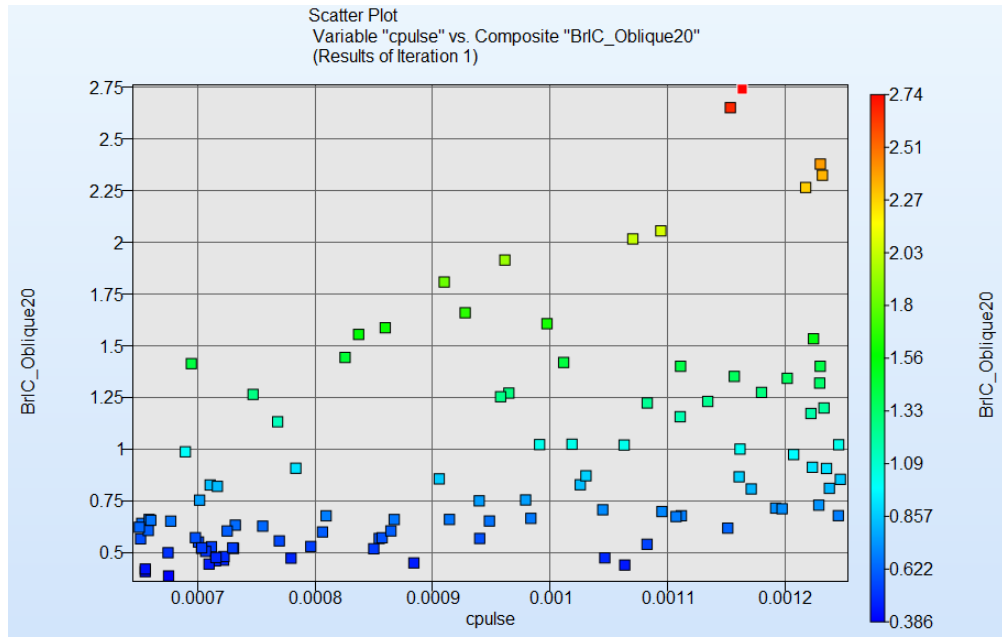


Figure C.9. BrIC versus Delta-V demonstrating a rather large scatter when all other parameters are varied.

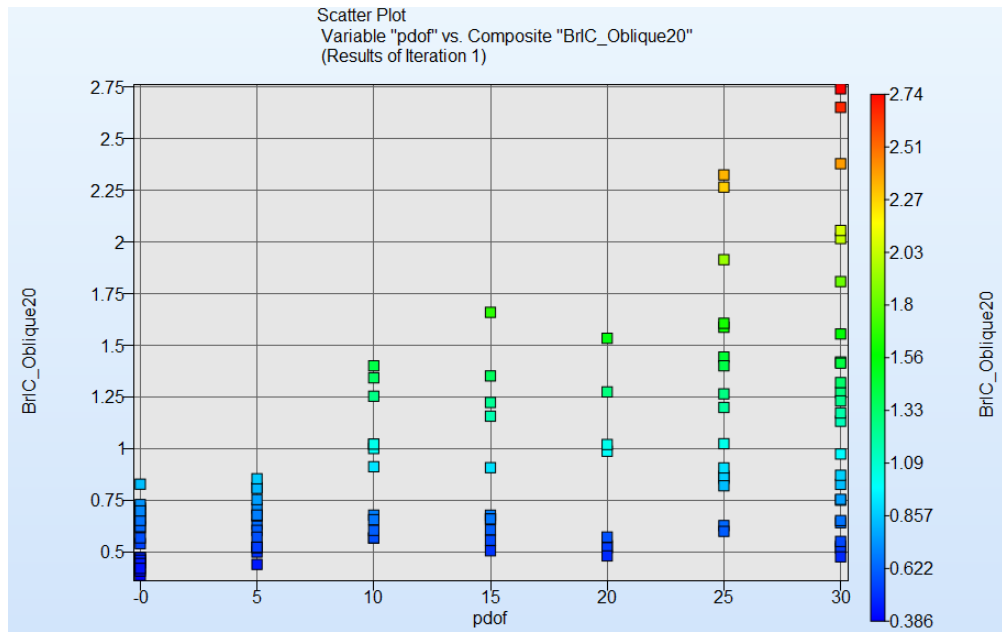


Figure C.10. BrIC versus PDOF demonstrating an increasing range of values of BrIC with increased PDOF.

Figure C.10 shows the relationship between BrIC and PDOF. With increased PDOF angle the range of values of BrIC is increasing. However, it can also be observed that there exists a set of parameters reducing the values of BrIC to under 0.6 for almost all angles of PDOF.

Figure C.11 completes the description of the DOE study #1 with the simulation based correlation matrix demonstrating that the relationships between BrIC and delta-V (cpulse) and PDOF are also the strongest (higher correlation coefficients) and positive (increasing delta-V and PDOF causes BrIC to increase). Note

the correlation coefficient is higher for PDOF than for delta-V in the simulation based correlation matrix, while the percent influence is higher for the delta-V (Figure C.9). This is because Figure C.9 is based on the metamodel results, while the correlations matrix is based on the actual limited number of runs.

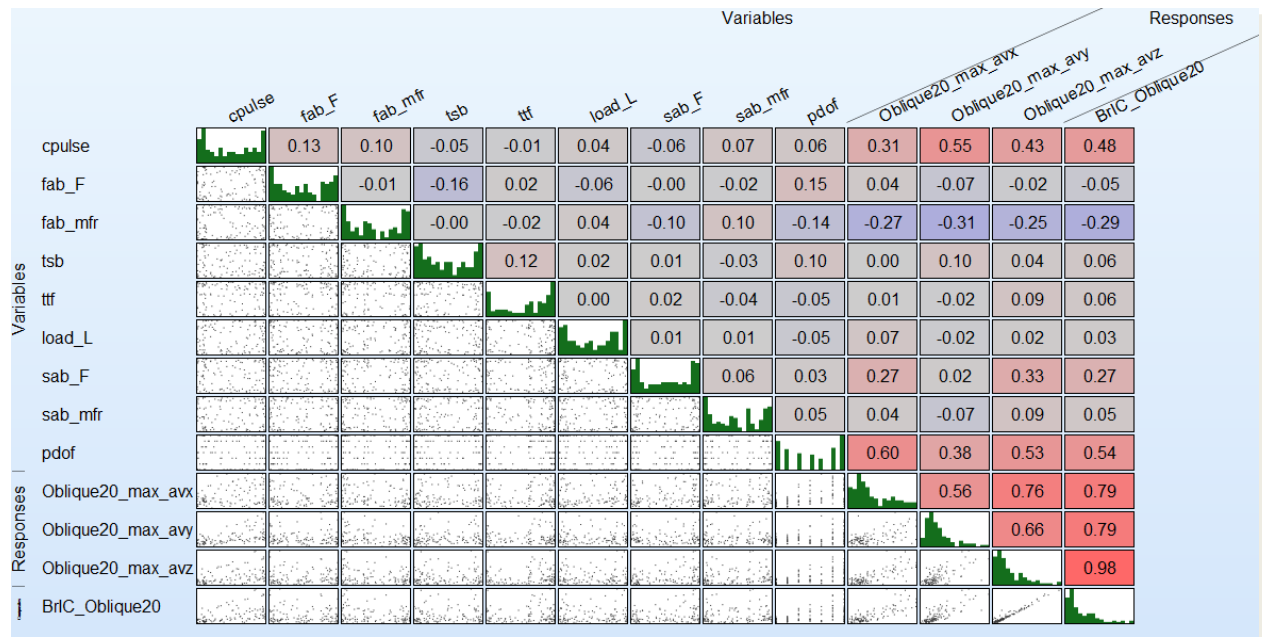


Figure C.11. Correlation matrix for the DOE study #1 showing correlation coefficients between all the variables and responses of the study.

Following are the conclusions from the DOE study #1:

- Out of nine parameters varied in this study (see Table C.2 for the list of parameters, their nominal values and the varied range), Delta-V influences BrIC the most, followed by PDOF.
- Increasing PDOF increases the range of values of BrIC, yet it is possible to find a set of parameters with values of BrIC less than 0.6.
- When investigating relationships between various parameters, such as BrIC and Delta-V, metamodels are more useful than just a scatter plot of the two parameters because various other parameters (for example, when looking at the fleet tests of various vehicles with various sets of restraint parameters) contaminate the relationship (contrast Figures C.8 and C.9) leading to erroneous conclusions about the “true” relationship.
- Correlation between the values of BrIC and Delta-V and PDOF is the strongest (higher correlation coefficients) and positive (with increased Delta-V and PDOF the values of BrIC also increase).

Now that the importance of delta-V and PDOF has been established, the next DOE study will investigate influence of other parameters on BrIC with fixed delta-V at 35 mph and three values of PDOFs (0° representing frontal impact, -20° representing near side driver oblique impact, and +20° representing far side driver oblique impact).

DOE Study #2 (Fixed Delta-V and PDOF)

Table C.3 lists the eight parameters investigated in the DOE study #2 (instead of nine in DOE study #1). Here delta-V and PDOF were removed and Seat Friction added to see if, for example, having a leather or fabric seat makes a difference in BrIC response.

Table C.3. Parameters varied in the DOE study #2.

<u>Parameters</u>	<u>Nominal</u>	<u>Range</u>
Frontal Airbag Friction, fab_F	0.5	0 – 3
Frontal Airbag Mass Flow Rate, fab_mfr	1	0.75 – 1.25
Seat Friction, seat_F	0.5	0 - 3
Load Limiter, load_L	3000 N	1000- 4000
Side Airbag Friction, sab_F	0.3	0 - 3
Frontal Airbag (firing) Time, ttf	18 ms	12- 25
Side Airbag (firing) Time, tsb	18 ms	12 - 25
Side Airbag Mass Flow Rate, sab_mfr	1	0.75 – 1.25

The simulation setup and results for the nominal values of parameters for frontal impact (0° PDOF) are identical to those given in Figure C.6 and Table C.2, where BrIC was equal to 0.55. The time histories of the head angular velocities for the near side driver impact (-20° PDOF) with the nominal values of parameters are shown in Figure C.12, giving BrIC of 0.58 (Table C.4).

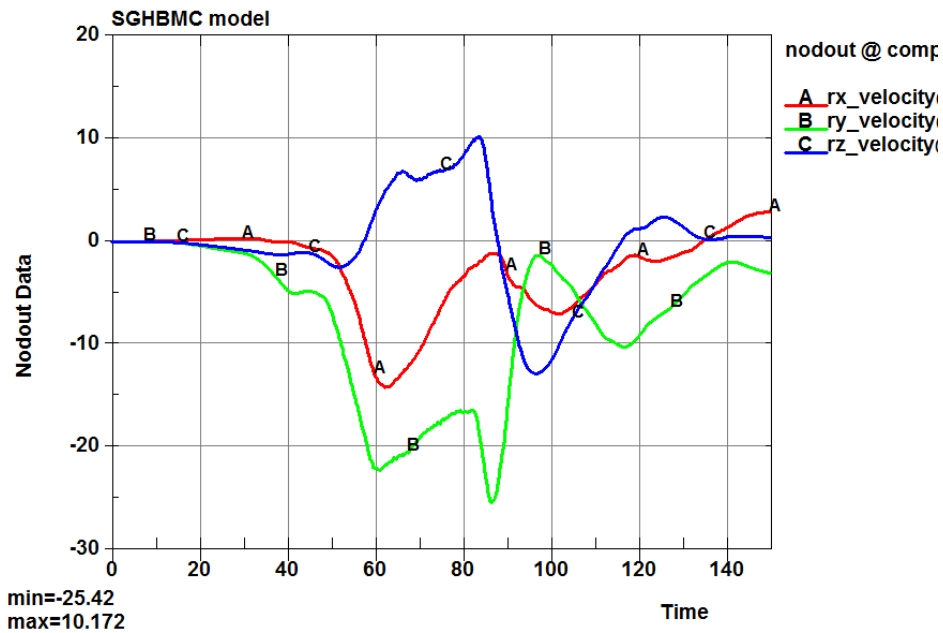


Figure C.12. FE model output for the head angular velocity components time histories for the driver near side oblique run (-20° PDOF) with nominal parameters.

Table C.4. Results of the driver near side oblique run with the nominal parameters.

Fab_F	Fab_MFR	Seat_F	Load_L	Sab_F	ttf	tsb	Sab_mfr	BrIC
0.5	1.0	0.5	3000	0.3	18	18	1.0	0.58

For the driver far side oblique run (20° PDOF) with nominal values of parameters the time histories of the head angular velocities are shown in Figure C.13 and the corresponding BrIC of 1.07 in Table C.5.

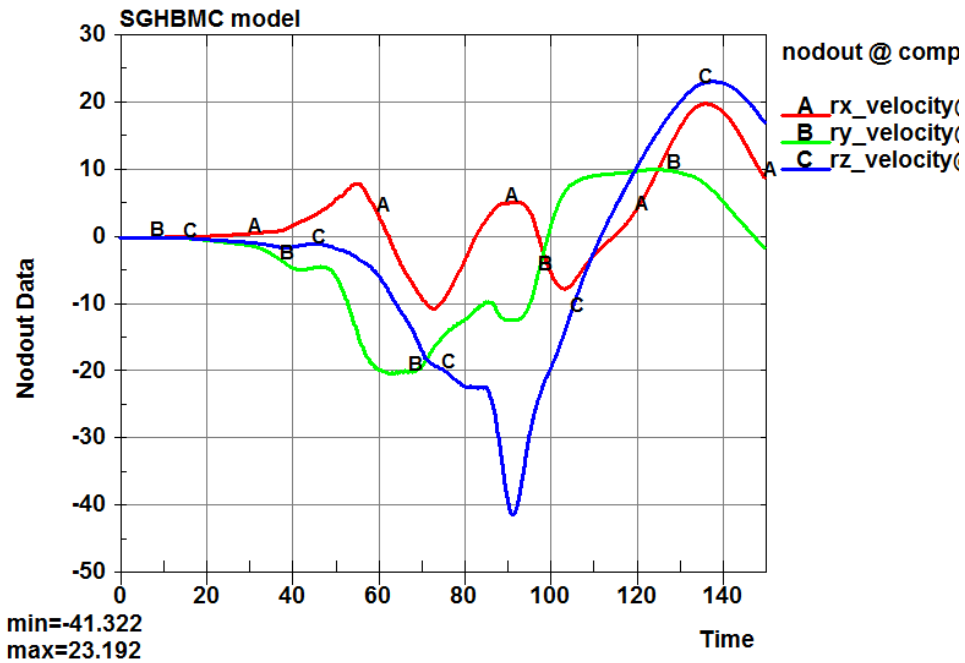


Figure C.13. FE model output for the head angular velocity components time histories for the driver far side oblique run (20° PDOF) with nominal parameters.

Table C.5. Results of the driver far side oblique run with the nominal parameters.

Fab_F	Fab_MFR	Seat_F	Load_L	Sab_F	ttf	tsb	Sab_mfr	BrIC
0.5	1.0	0.5	3000	0.3	18	18	1.0	1.07

While for frontal and near side oblique runs with nominal values of parameters, the highest angular velocity was about the y-axis (green line in Figure C.6c and Figure C.12), for the far side oblique run, the highest angular velocity is about the z-axis (blue line in Figure C.13).

The metamodel-based global sensitivity plot for the frontal impact is shown in Figure C.14 demonstrating that frontal airbag mass flow rate affects the values of BrIC the most (30.2%) in this test condition, followed by the frontal airbag friction (17.2%), then load limiter (14.3%), and frontal airbag firing time (10.4%). Collectively these four parameters can alter the value of BrIC by 72.1%. An example of parameters giving low BrIC (0.38 with zero risk of any brain injury based on CSDM risk curve) and high BrIC (1.01 corresponding to 56% risk of AIS 4+ brain injury based on CSDM risk curve) in frontal impact are given in Table C.6. It should be noted that the values of parameters given in Table C.6 were selected

for demonstration purposes and are just examples that give low and high values of BrIC; also, these are not the parameter values giving the lowest or highest values of BrIC. There are many different combinations of the restraint parameters that influence BrIC. For example, one could fix the values of the frontal and side airbag friction coefficients to those of nominal values and still find a set of parameters giving low and high BrIC values.

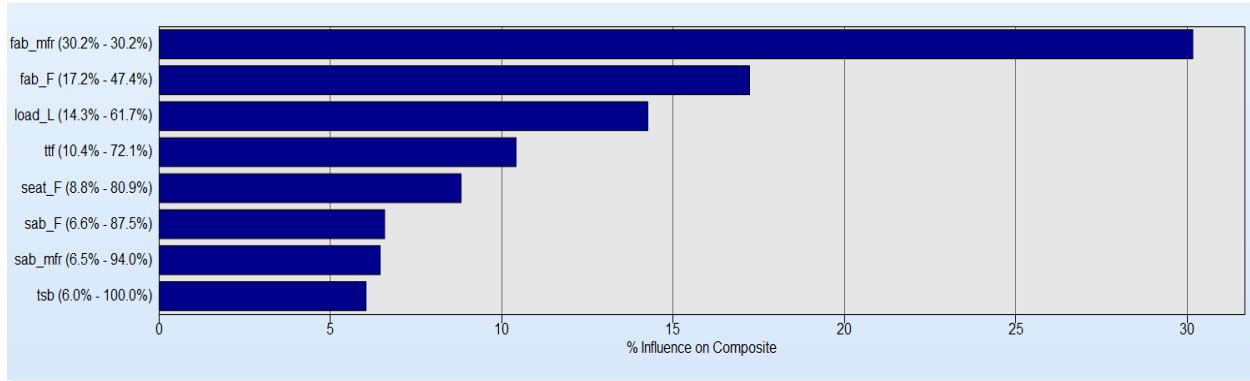


Figure C.14. Influence of all parameters given in Table C.3 on BrIC of driver in frontal impact.

Table C.6. Results of the frontal runs with parameters yielding low (0.38) BrIC and high (1.01) BrIC values.

Fab_F	Fab_MFR	Seat_F	Load_L	Sab_F	ttf	tsb	Sab_mfr	BrIC
1.84	0.85	0.1	2860	0.04	12	20	1.24	0.38
0.06	0.75	2.46	3075	1.58	14	25	0.97	1.01

The metamodel-based global sensitivity plot for the near side driver oblique impact is shown in Figure C.15. Here the most influential (over 10% influence) parameters on BrIC are: side (23.5%) and frontal (23.0%) airbag friction coefficients, followed by the load limiter (17.2%) and the frontal airbag mass flow rate (12.2%), with combined influence on BrIC of 75.9%. The friction coefficients between the airbags and the head appear to be the most influential in this test condition, and may be considered by the restraint system designer as the parameters to work on (reducing friction coefficient of the airbag fabric). However, the frontal airbag mass flow rate may be tuned along with the load limiter to affect the values of BrIC. Table C.7 gives examples of several combinations of parameters making BrIC as small as 0.50 (corresponding to zero risk of any brain injury) and as high as 2.04 (corresponding to 99.1% of AIS 4+ brain injury risk). Again, these are just examples of parameter sets giving extreme values of BrIC.

The designer of a restraint system must understand all the complex interactions between various parameters that influence the values of BrIC (and other injury criteria) in one direction or another to properly select a combination that would minimize overall injury risk (see below the section on optimization of the restraint systems).

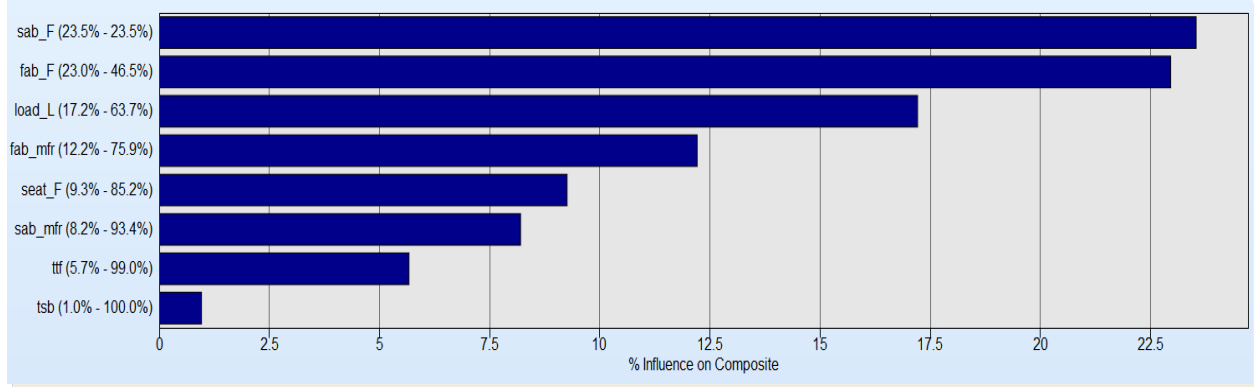


Figure C.15. Influence of all parameters given in Table C.3 on BrIC of driver in near side oblique impact.

Table C.7. Results of the near side oblique with parameters yielding low (0.50) BrIC and high (2.04) BrIC values.

Fab_F	Fab_MFR	Seat_F	Load_L	Sab_F	ttf	tsb	Sab_mfr	BrIC
0.29	1.25	2.51	1822	0.12	13.6	12	0.785	0.50
0.17	0.98	0.98	1050	1.2	24	17.3	1.05	1.34
0.22	0.78	2.94	3040	2.95	13.4	12.8	1.06	2.04

Finally, the metamodel-based global sensitivity plot for the driver far side oblique runs is shown in Figure C.16. In this test condition the most influential parameters affecting BrIC are: frontal airbag friction coefficient (24.5%), frontal airbag firing time (20.2%), frontal airbag mass flow rate (18.4%), and the load limiter (12.1%) collectively affecting values of BrIC by 75.2%. Note that side airbag parameters – the bottom three parameters in Figure C.16 – are not important and should be ignored; the fact they are not equal to zero is the by-product of the DOE analysis, hence only parameters with the influence greater than 10% were considered here. In the far side driver oblique impacts, the frontal airbag firing time becomes very important and the design space may be further expanded with the increased upper limit of this parameter (currently set at 25 ms – Table C.3).

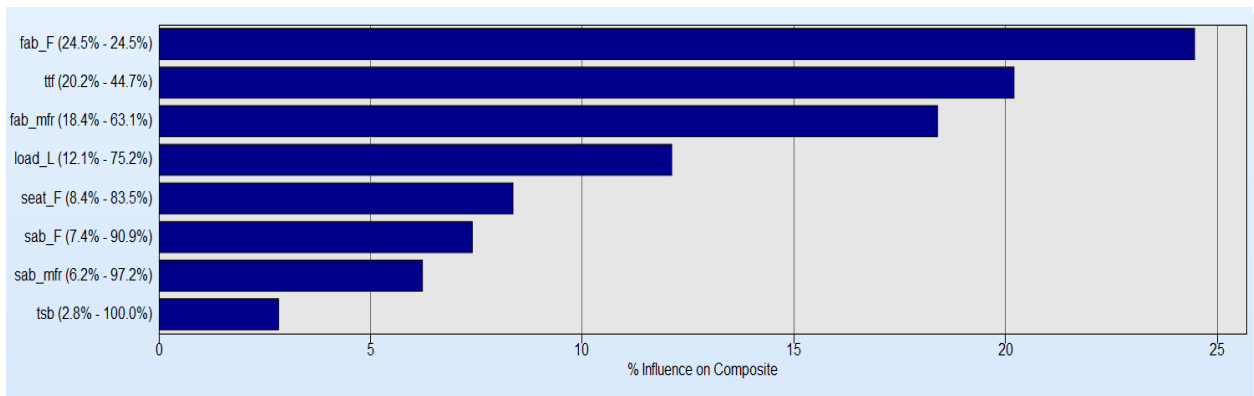


Figure C.16. Influence of all parameters given in Table C.3 on BrIC of driver in far side oblique impact.

Table C.8. Results of the far side oblique with parameters yielding low (0.62) BrIC and high (2.15) BrIC values.

Fab_F	Fab_MFR	Seat_F	Load_L	ttf	BrIC
0.322	1.11	2.92	1040	19	0.62
0.19	0.76	2.38	3950	23	0.62
2.89	0.75	0.13	1894	13	2.15

Despite this limitation, low values of BrIC (0.62) were obtained (these are not the lowest possible but just the values for these example parameter sets), corresponding to approximately 4% of AIS 4+ risk of brain injury (see examples in the first two rows Table C.8). It also appears that reducing the frontal airbag mass flow rate and firing time may cause increase in BrIC values. Table C.9 lists all the parameters affecting BrIC based on this limited DOE study (limited to the vehicle size, frontal and side airbag size, occupant size, posture, seating position, etc.) for each crash mode: frontal, near and far side driver oblique.

Table C.9. Parameters list affecting BrIC the most for each crash mode.

Frontal	Near Side	Far Side
Frontal Airbag MFR	Frontal Airbag MFR	Frontal Airbag MFR
Load Limiter	Load Limiter	Load Limiter
Frontal Airbag Friction	Frontal Airbag Friction	Frontal Airbag Friction
Frontal Airbag Firing Time	Side Airbag friction	Frontal Airbag Firing Time

Again, DOE analysis gives a general picture of the influence of various parameters on BrIC. However, it doesn't answer the question of the exact parameters values that will minimize BrIC for a given geometry of the restraint system (airbag volume), vehicle dimensions, and occupant characteristics (size, seating position, etc.). This question is analyzed in the following section.

OPTIMIZATION STUDIES

After identification of the parameters affecting BrIC with the help of DOE studies (Table C.9), it is important to demonstrate that it is possible to select a set (or a number of sets) of these parameters that minimize BrIC while keeping other injury criteria constrained to their critical values. In these optimization studies, the following constraints on injury criteria were imposed: HIC₁₅ was constrained to be under 700, central chest (sternal) deflection to 63 mm, and femur force (left and right) to 10 kN. The objective function was BrIC itself, i.e. the study minimized BrIC subject to the four constraints listed above.

The vehicle, restraint, and occupant descriptions were given in the DOE section above and remained similar for the optimization studies (except for the optimization study #2 in which the size of the frontal airbag was increased to demonstrate the effect of increased airbag coverage on BrIC).

Instead of metamodels (see DOE section), direct simulation-based optimization was used. Genetic algorithms (GA) were used for optimization. Genetic algorithms are nature inspired search algorithms

that emulate the Darwinian principle of ‘survival of the fittest.’ The differences between genetic algorithms and most conventional optimization methods are:

- GA does not require derivative information to drive the search of optimal points.
- While conventional methods use a single point for each iteration, GA uses a population based approach.
- GA is a global optimizer whereas conventional methods may get stuck in local optima.
- GA is a probabilistic optimization method, that is an inferior solution (that may help evolve the correct design variables structure) may also have a non-zero probability of participating in the search process.
- The computational cost of using GA may be high compared to derivative based methods.

It was also initially assumed in these optimization studies that an intelligent in-crash censoring may identify the crash mode (full frontal, near side driver oblique or far side driver oblique) within the first few milliseconds of the crash, so that separate optimizations were carried out for each crash mode. However, a single parameter set was also identified (as an example) that would work (minimize BrIC) for all crash modes.

Optimization Study #1

In this study the parameters listed in Table C.9 were varied and their range was identical to those given in Table C.3. The frontal airbag volume along with other restraint, vehicle, and occupant parameters were also kept the same as were described in the DOE studies.

The optimization history for the frontal runs is shown in Figure C.17 according to which only eight iterations were necessary to identify a global minimum for BrIC.

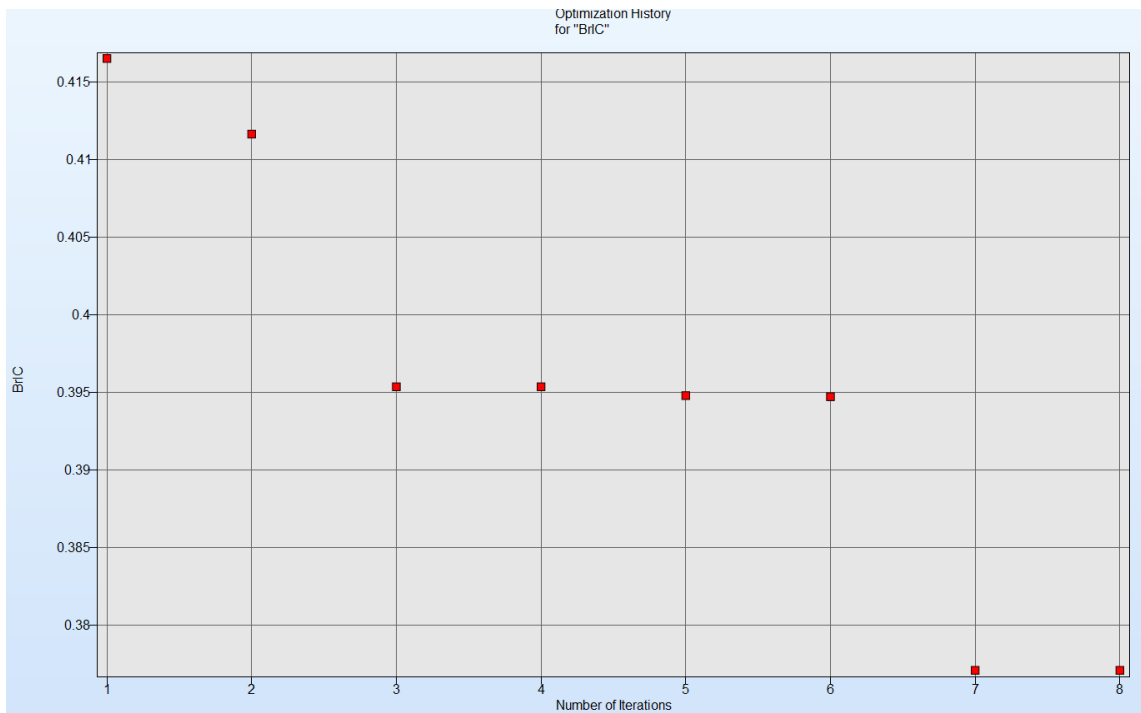


Figure C.17. Optimization history for BrIC for frontal runs.

The parallel coordinate chart for the frontal runs is given in Figure C.18. The vertical lines in Figure C.18 represent the range for each parameter varied. The names of the parameters varied are given at the bottom of the chart – first five parameters from left to right: frontal airbag friction coefficient, frontal airbag mass flow rate, frontal airbag firing time, load limiter, and side airbag friction (should be ignored in these frontal runs). The next four parameters are constraints (from left to right): left femur force, right femur force, max sternum deflection, and HIC₁₅. Finally, the response function is BrIC (rightmost parameter). The red line represents the constraint envelope, while the purple line shows the optimized value of each parameter (given in yellow rectangles). Each gray line represents the result of a single run.

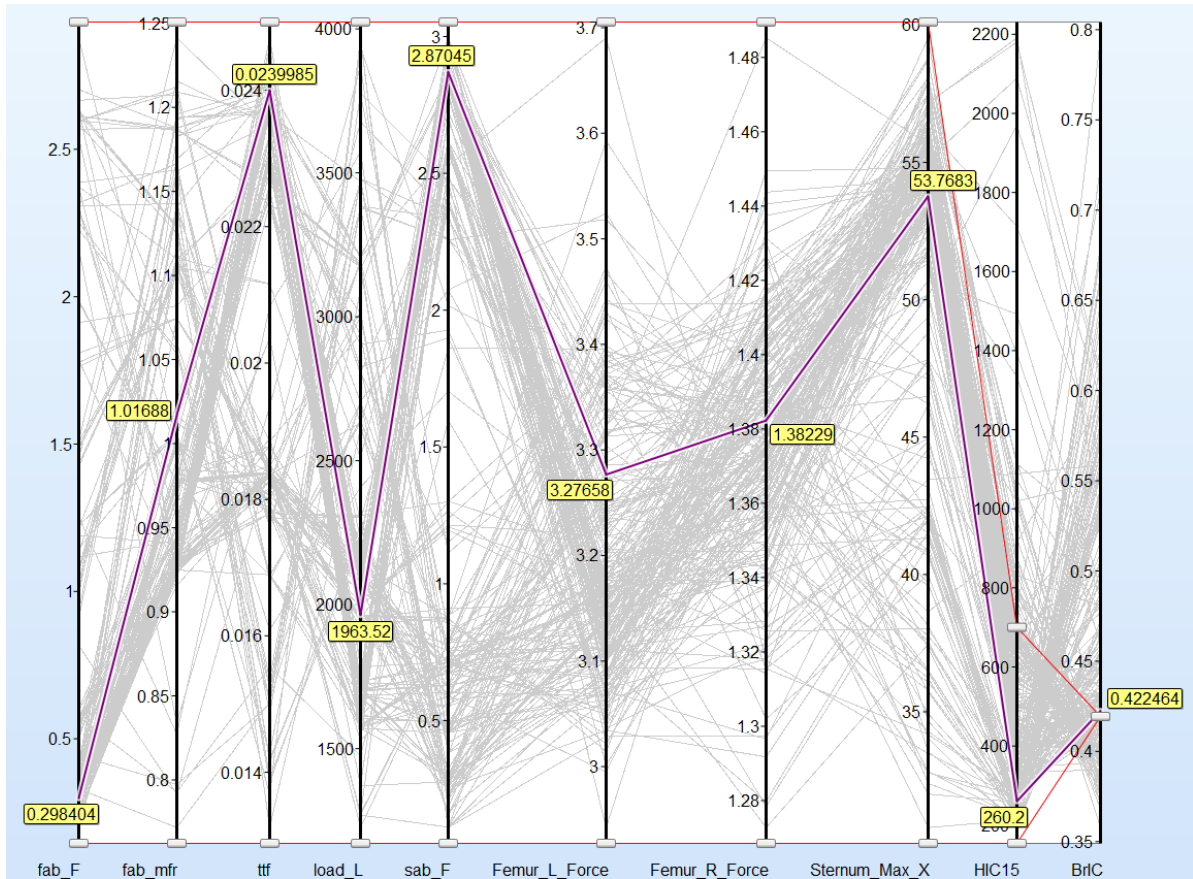


Figure C.18. Parallel coordinate chart for frontal runs.

It should be noted here that the values of constraints could be further reduced to search, for example, for the parameter sets with smaller sternal deflection and smaller BrIC. Also, the actual values here represent those measured by the simplified GHMBC model and are not directly translated to any ATD, i.e. if the optimized sternal deflection is about 54 mm for the frontal crash mode, it doesn't mean that if a model of an ATD was used instead of the GHMBC, this value would've been the same. The purpose of this exercise was to demonstrate the possibility/feasibility of reducing BrIC, while keeping other injury criteria within their constrained values. In addition, the objective function could've been redefined in a way that would minimize all the injury criteria simultaneously.

To investigate the relationships between various parameters in the frontal impact configuration, a simulation-based correlation matrix was plotted (Figure C.19), in which the first five columns (counted

from the left) and first five rows (counted from the top) are the correlation coefficients for the investigated parameters/variables, the next seven are those of responses – four constraints and three max angular velocities, and the last column/row gives correlation coefficients for the objective function (called composite response here as it is comprised of the max angular velocities) – BrIC. The positive values in the cells at the intersection of each row and column represent positive correlation between the two parameters of interest (with increased value of one parameter, the other one increases as well). The greater the value of a correlation coefficient the more pronounced (significant) the relationship. For example, the load limiter (fourth row) and BrIC have a correlation coefficient of 0.65 indicating that increasing load limiter value will increase the value of BrIC. Another example is the correlation coefficient between BrIC and sternal deflection (-0.73), indicating that reducing sternal deflection will increase BrIC and vice-versa. In other words, if a designer of a restraint system selects a parameter set that would reduce sternal deflection without the knowledge of the effect on BrIC, this could lead to increased risk of brain injuries. The opposite is true as well. Similarly, there is a negative correlation between BrIC and HIC₁₅, although not as strong as that between BrIC and sternal deflection, suggesting that reducing HIC₁₅ (risk of skull fractures) will increase BrIC (risk of brain injuries). In general, the human body is a complex mechanical system and minimizing one parameter, while ignoring others, may lead to the so-called “unintended consequences” or “side effects” of such optimization. It is extremely important (as demonstrated by this example) to be aware of all the parameters affecting injury risks for various body regions. This knowledge gives a designer of restraint system the tools necessary to achieve the objective – minimize the risk of all injuries as well as the risk of “unintended consequences”.

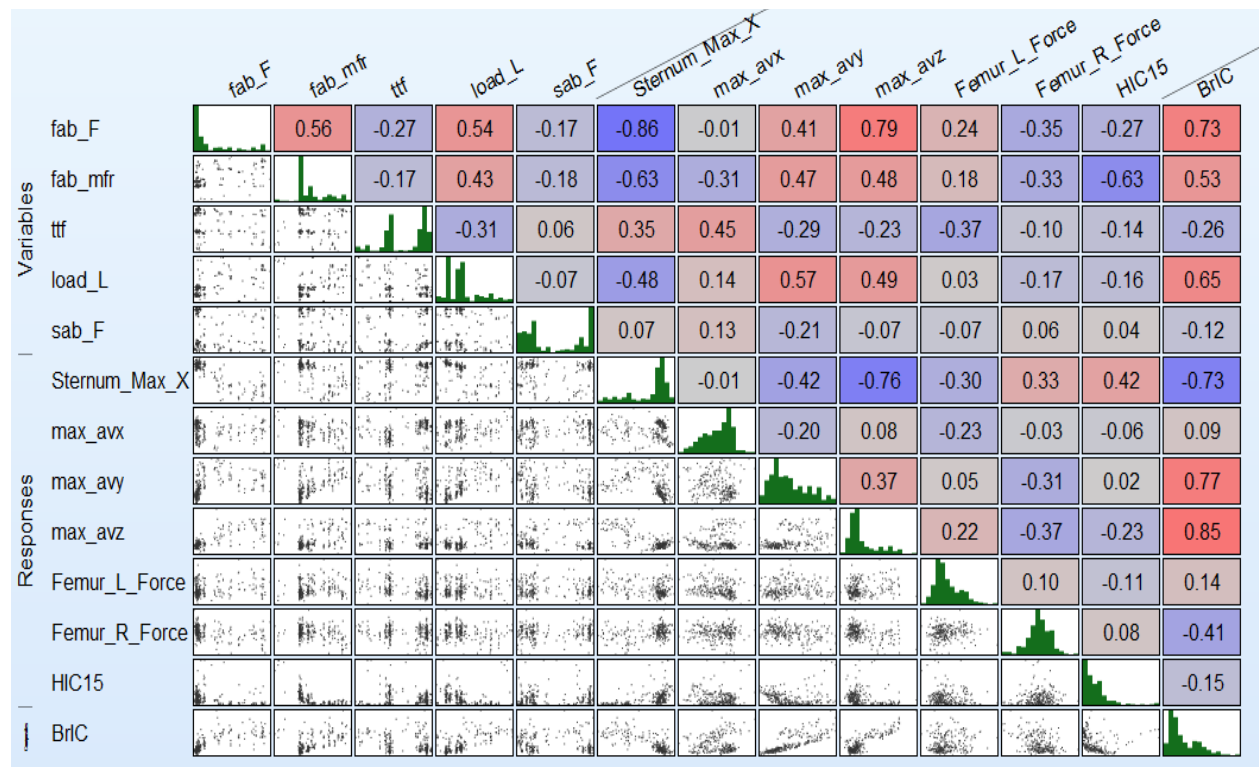


Figure C.19. Correlation matrix for frontal runs.

The relationship between HIC₁₅ and BrIC (and max sternal deflection) is plotted in Figure C.20, where the inverse nature of the relationship is very clear. However, the plot also indicates that it is possible to

select many different solutions with low values of both HIC_{15} and $BrIC$ (lower left corner of the plot) and at the same time to keep max sternal deflection to less than 40 mm (blue colored squares) in frontal crash mode as measured by the simplified GHBM model. Exploring additional restraint design parameters in the optimization, such as steering wheel rim stiffness, etc. may offer further reduction in the values of different injury metrics.

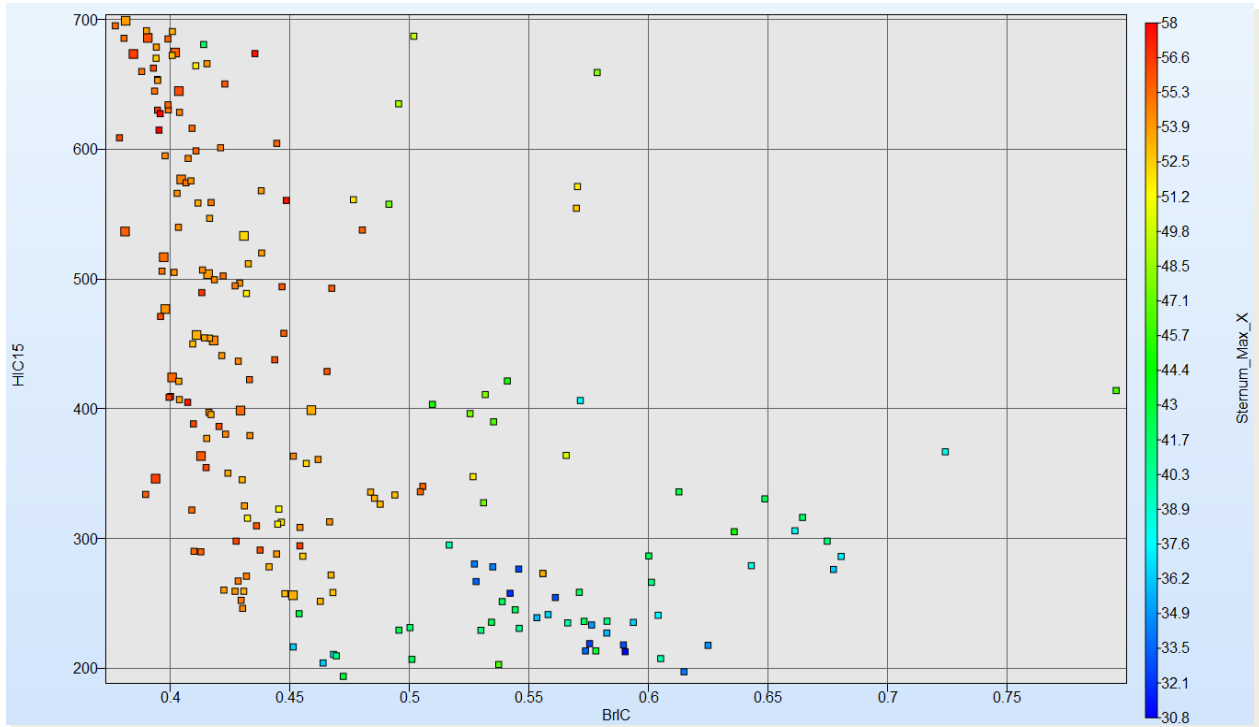


Figure C.20. Relationship between HIC_{15} , $BrIC$, and max sternal deflection in frontal runs (only feasible designs are shown).

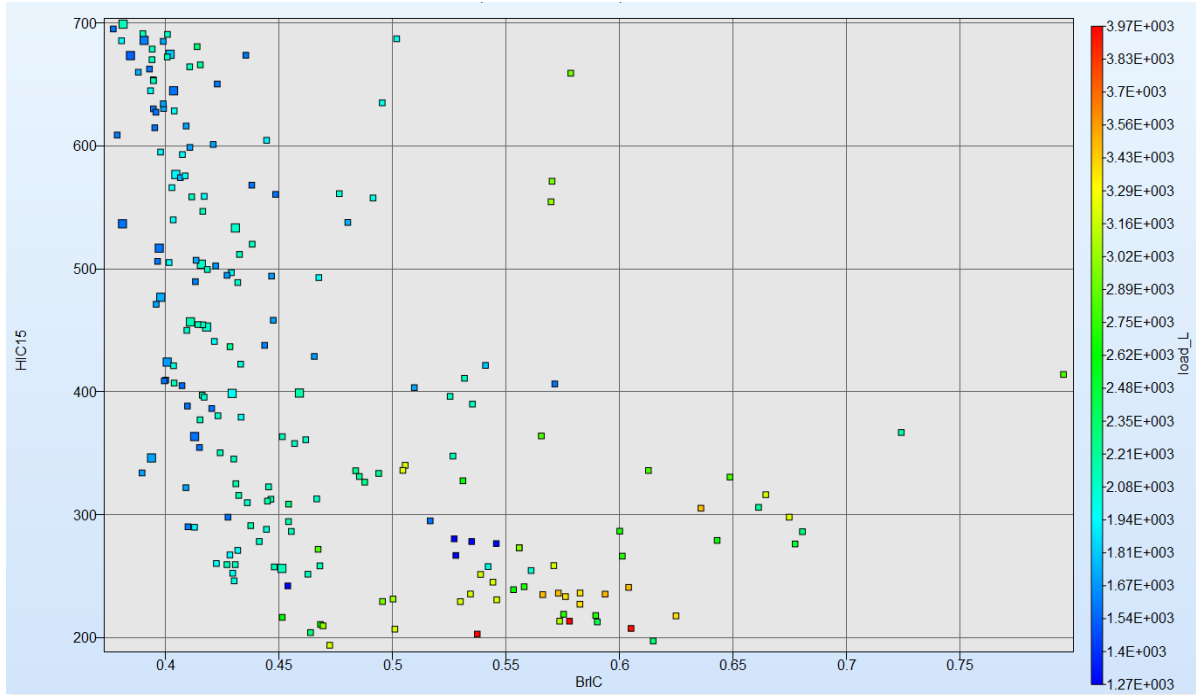


Figure C.21. Relationship between HIC₁₅, BrIC, and load limiter in frontal runs (only feasible designs are shown).

In Figure C.21 the relationship between HIC₁₅, BrIC and the load limiter is plotted indicating that low values of HIC₁₅ and BrIC can be achieved simultaneously when the load limiter is set to approximately 2.0 kN.

For the near side driver oblique runs, the plots corresponding to those of the frontal runs shown in Figure C.17 through Figure C.21, are given below in Figure C.22 through Figure C.26, while those for the far side oblique runs are shown in Figure C.27 through Figure C.31.

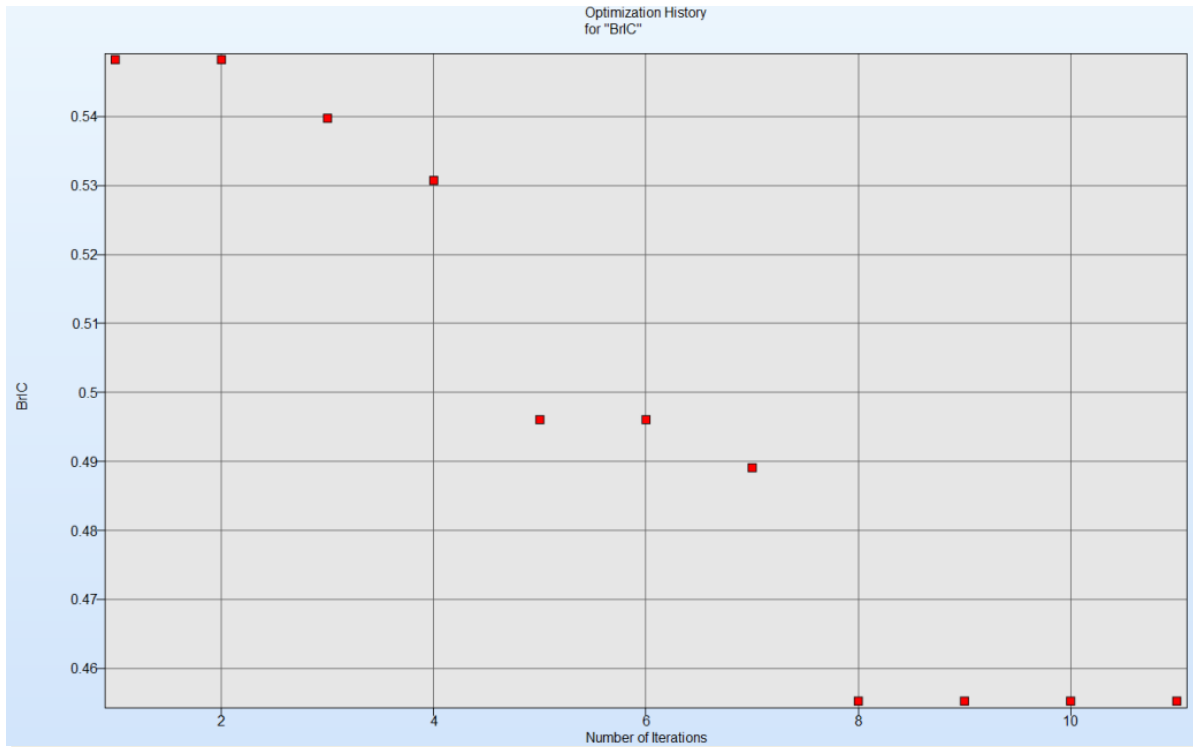


Figure C.22. Optimization history for BrIC in near side oblique runs.

The near side oblique runs converged (found global minimum for BrIC of 0.45) after 11 iterations (Figure C.22). The parallel coordinate chart for this mode (Figure C.23) shows significant increase in the right femur force compared to that in the frontal crash mode (Figure C.18), while the optimized (for BrIC) max sternal deflection reduced to 43 mm. The optimized frontal airbag firing time has reduced, and the frontal airbag mass flow rate along with the load limiter force slightly increased. The correlation matrix (Figure C.24) still demonstrates negative correlation between BrIC and max sternal deflection, while that between BrIC and HIC_{15} has become positive. Another important observation is that frontal airbag mass flow rate has become significant in this crash mode demonstrating that its increase in value will reduce the value of BrIC. Figure C.25 and Figure C.26 show that it is possible to select several parameters sets to obtain low values of both HIC_{15} and BrIC (lower left corner of the charts) while keeping max sternal deflection in low 30 mm range (Figure C.25) and the load limiter in the range of 2.0 – 2.5 kN (Figure C.26).

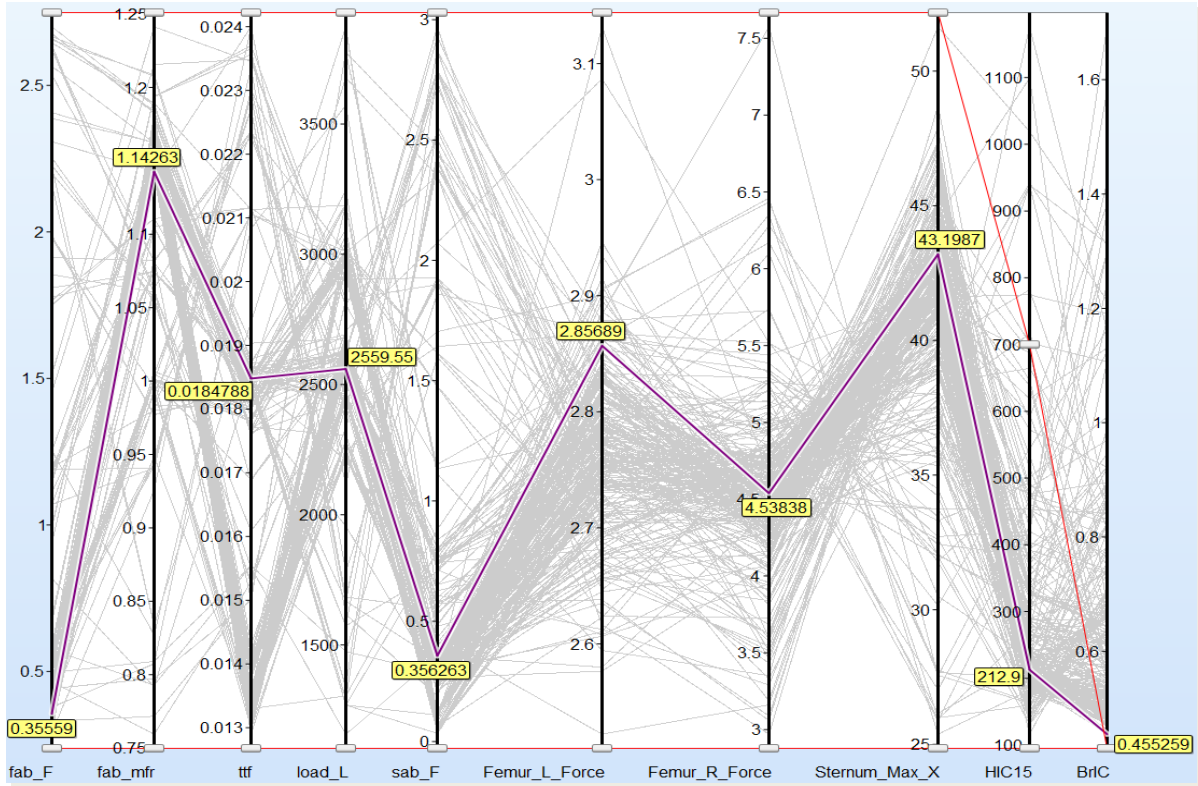


Figure C.23. Parallel coordinate chart for near side oblique runs.

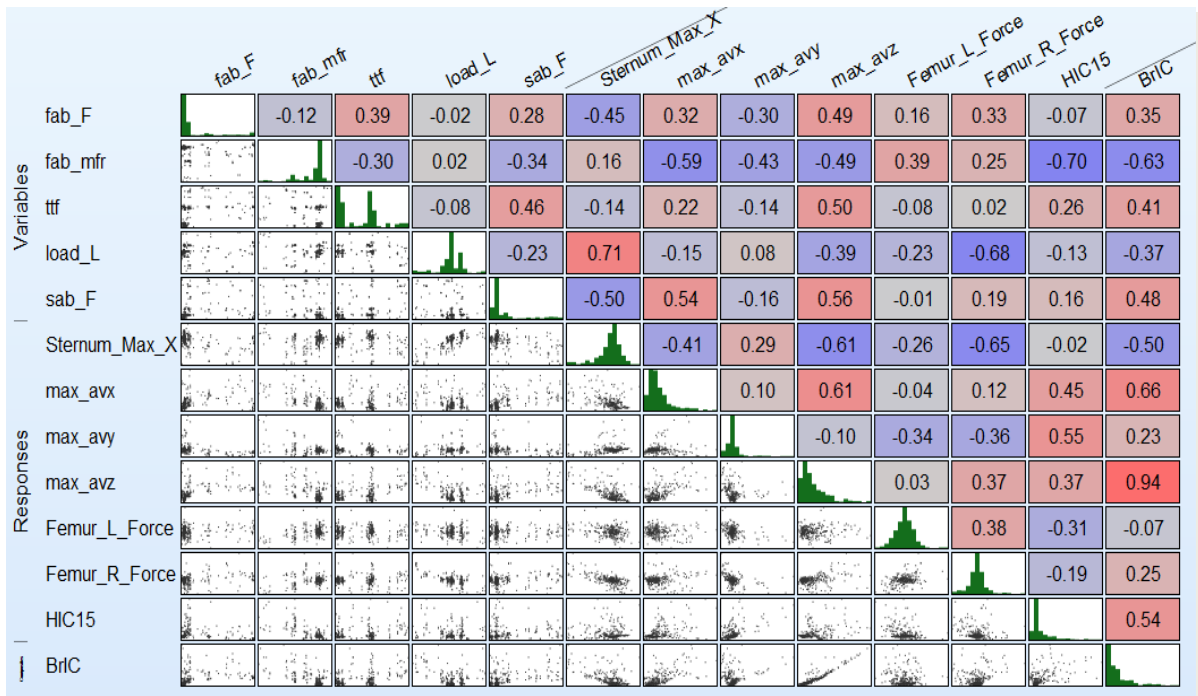


Figure C.24. Correlation matrix for near side oblique runs.

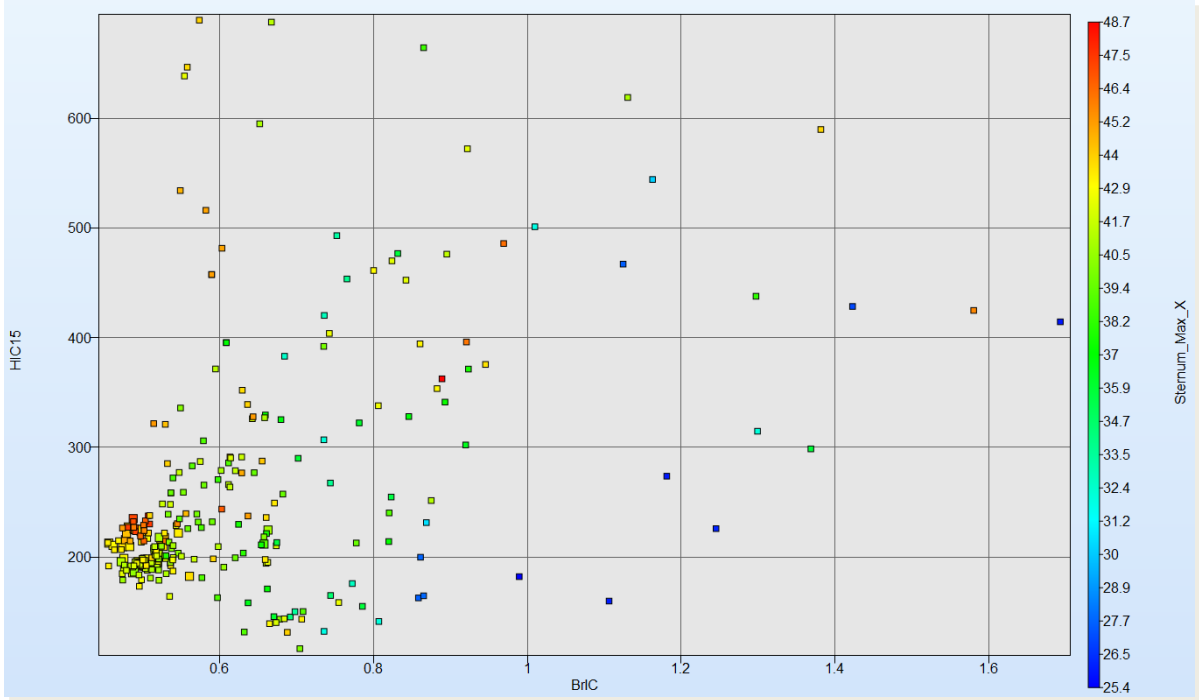


Figure C.25. Relationship between HIC₁₅, BrIC, and max sternal deflection in near side oblique runs (only feasible designs are shown).

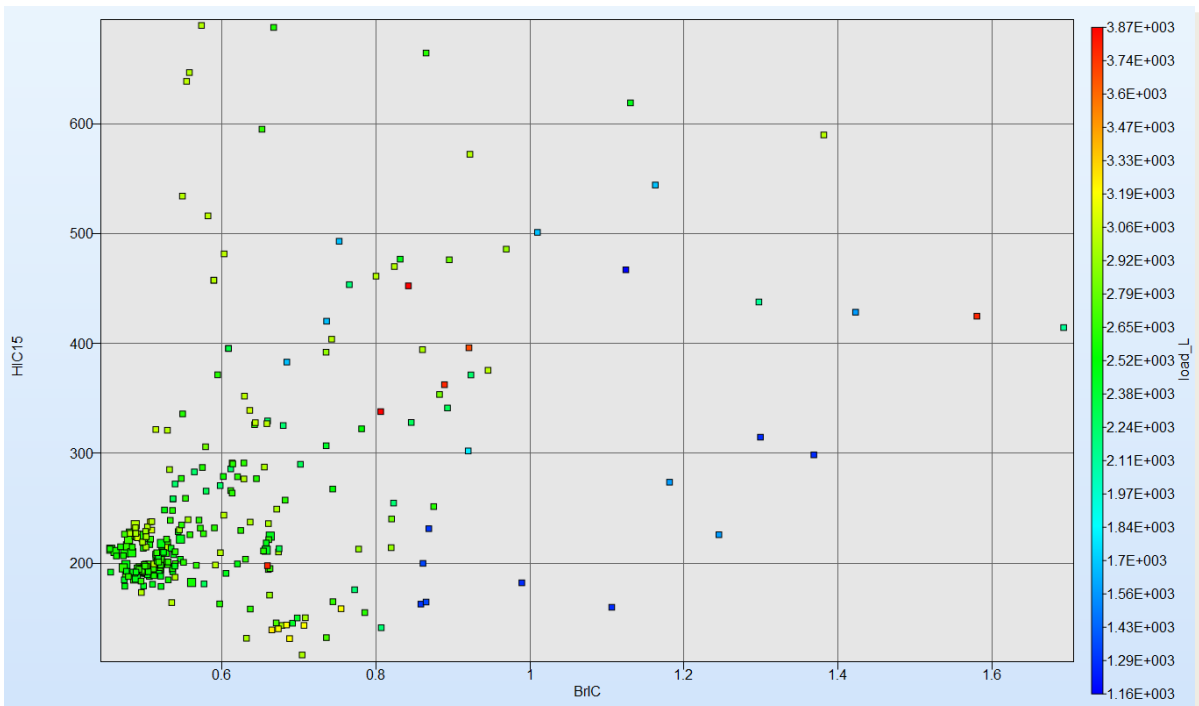


Figure C.26. Relationship between HIC₁₅, BrIC, and load limiter in near side oblique runs (only feasible designs are shown).

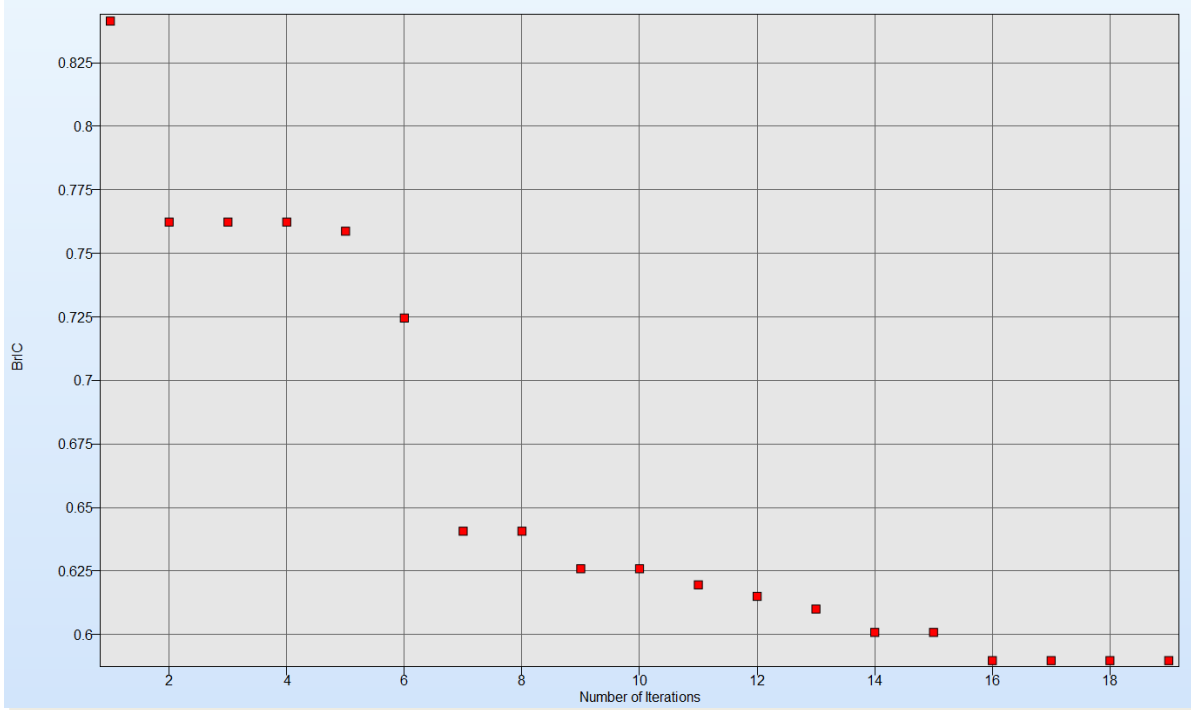


Figure C.27. Optimization history for BrIC in far side oblique runs.

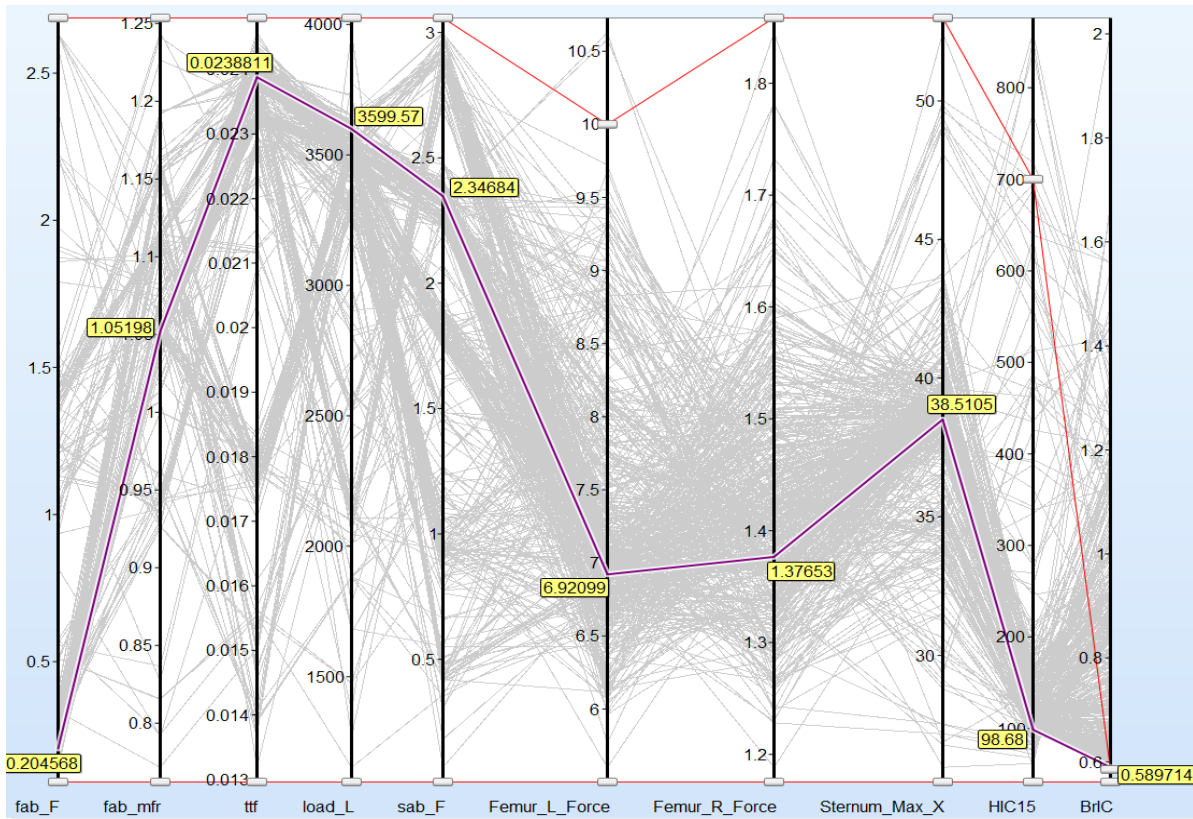


Figure C.28. Parallel coordinate chart for far side oblique runs.

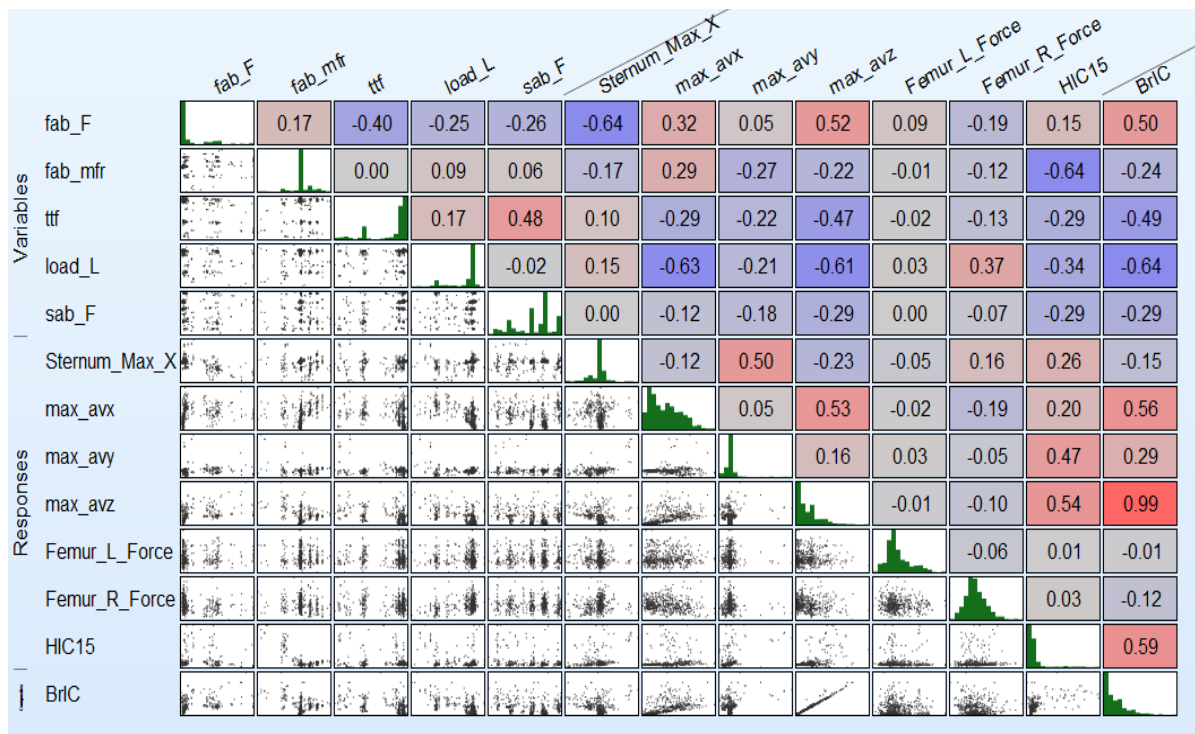


Figure C.29. Correlation matrix for far side oblique runs.

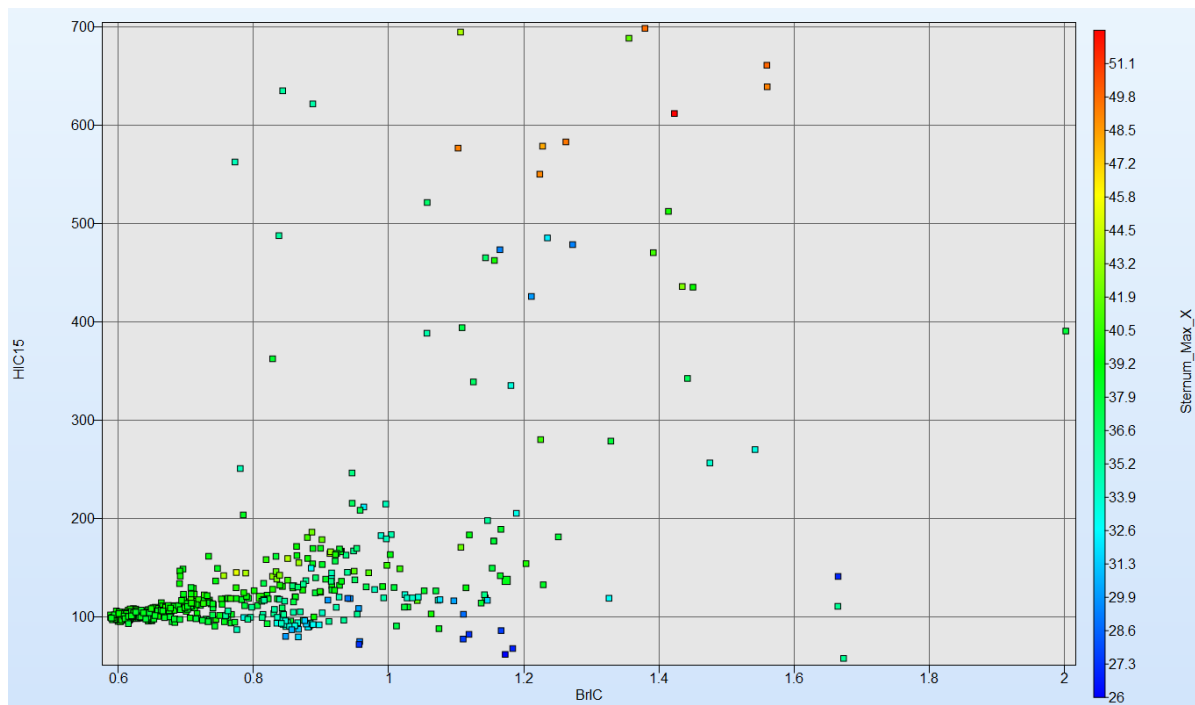


Figure C.30. Relationship between HIC₁₅, BrIC, and max sternal deflection in far side oblique runs (only feasible designs are shown).

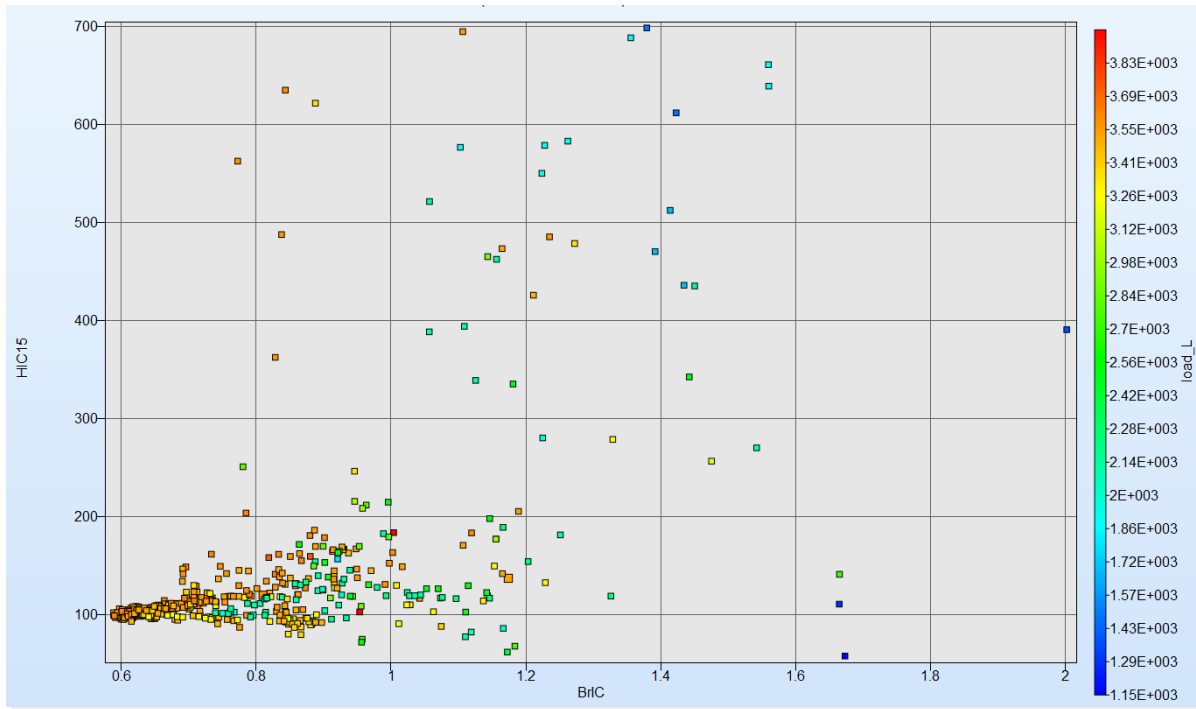


Figure C.31. Relationship between HIC₁₅, BrIC, and load limiter in far side oblique runs (only feasible designs are shown).

The optimization for BrIC in the far side oblique crash mode took the longest to converge – 19 iterations (Figure C.27) giving minimum BrIC value at just under 0.6. The parallel coordinate chart (Figure C.28) shows that for this crash mode, left femur force has significantly increased compared to that of the frontal or near side oblique crash modes. It also demonstrates that in order to keep the values of BrIC low, the load limiter force should increase to over 3.5 kN, which is the highest out the three crash modes considered in this study. Another observation from Figure C.30 is that both HIC₁₅ and max sternal deflection are the lowest here compared to those of frontal (Figure C.20) and near side driver oblique (Figure C.25) modes. This is, of course, at the expense of higher optimized value of BrIC. The simulation based correlation matrix (Figure C.29) still shows negative correlation between BrIC and max sternal deflection, albeit weaker than in the other two crash modes (correlation coefficient is -0.15). The load limiter has also a negative correlation coefficient here (compare with Figure C.21 for the frontal runs) along with the frontal airbag firing time, while correlation with HIC₁₅ is positive (note: there were no head impacts to the instrument panel the presence of which may change correlation between HIC₁₅ and BrIC). Figure C.30 and Figure C.31 show that there are plenty of parameter sets to choose from to obtain low values of both HIC₁₅ and BrIC, while keeping max sternal deflection in the mid 30-mm range (Figure C.30 lower left corner) and load limiter force in the range of 3.2 – 3.5 kN (Figure C.31 lower left corner).

Table C.10 lists, as an example, the values of variables for each crash mode that minimizes BrIC in this particular optimization study for this particular restraint (airbag size, etc.), vehicle (size, steering wheel assembly, etc.), and occupant (size, position, etc.) parameters.

Table C.10. Summary of the results from the optimization study #1.

Variables	Frontal (BrIC = 0.42)	Oblique - Near Side (BrIC = 0.46)	Oblique - Far Side (BrIC=0.59)
Frontal Airbag MFR	1.02	1.14	1.05
Load Limiter	1963	2559	3599
Frontal Airbag Firing Time	24	18.5	24
Frontal Airbag Friction	0.30	0.35	0.204
Side airbag Friction	N/A	0.36	N/A

In this study it was assumed that there exists an intelligent in-crash sensors system capable of detecting the PDOF of the crash within the first few milliseconds, which would give the restraint system enough time to select correct restraint system parameters (mass flow rate, load limiter, firing time, perhaps steering wheel stroke not considered in this study, etc.), examples of which are given in

Table C.10. In this example, rather low values of BrIC were obtained representing zero risk of brain injuries for the full frontal and near side driver oblique crash modes and about 2.3% risk of AIS4+ brain injury in the far side crash mode. However, if such an intelligent sensor system doesn't exist, the question then becomes: is there a unique set of parameters that works for all crash modes? The best way to find such a set is to construct the objective function of the optimization process such that it minimizes BrIC for all crash modes simultaneously. However, some information can be obtained from the data presented above, from which a set of fixed parameters is selected (Table C.11) for demonstration purposes and simulations were run again at various PDOFs, results of which are given in Table C.12.

Table C.11. Fixed restraint system parameters.

Crash Pulse	Fab_F	Fab_MFR	Load_L	Sab_F	ttf
35 mph	0.35	1.14	2560	0.35	18.5

Table C.12. Injury values at different PDOF for the parameters given in Table C.11 (negative PDOF angles are for the near side driver oblique runs).

PDOF	Sternal Deflection, mm	BrIC	HIC15
0 ⁰	53	0.50	362
-10 ⁰	48	0.63	304
-15 ⁰	47	0.66	248
-20 ⁰	43	0.46	212
-25 ⁰	41	0.62	201
-30 ⁰	38	0.93	257
+20 ⁰	40	0.82	149

Several observations can be made from Table C.12 for the fixed parameters:

1. The values of BrIC (not optimized) can be kept in a relatively low range for the near side driver oblique runs up until -25° PDOF; when the PDOF angle was furthered to -30° BrIC jumped up due to the head almost missing the frontal airbag
2. The value of BrIC for the far side driver oblique run at PDOF of $+20^{\circ}$ was relatively high compared to that when optimized for just this test condition (BrIC was equal to 0.59 – see last column of Table C.10)
4. HIC_{15} values were relatively low with the highest value of 362 in a full frontal run – this is the crash mode in which BrIC was the lowest
5. Similar to HIC_{15} , the highest value of the sternal deflection of 53 mm was in a full frontal run, while the lowest at -30° , the condition in which BrIC was the highest (0.93)

Here again, the reverse trend between BrIC and HIC_{15} (and sternal deflection) is evidenced. This means that if a restraint system is designed to minimize HIC_{15} and/or sternal deflection without the knowledge of BrIC, such design may lead to the increased risk of brain injuries. The reverse statement is true as well. However, currently restraint systems are designed without the knowledge of BrIC, which increases the risk of brain injuries as is also evidenced from the analysis of field data [See Chapter 9].

In the optimization study #1 a rather small airbag was used (50 liters) that provided limited coverage, and, as was demonstrated above, such limited coverage is insufficient to reduce BrIC values at the PDOF angles greater than -25° for the near side driver crash mode (and for the far side driver impact mode). To investigate how increased frontal airbag volume would affect the values of BrIC a second optimization study was conducted.

Optimization Study #2

To investigate how increased frontal airbag coverage affects BrIC, the optimization study was conducted for the near side driver oblique crash mode only with a simply scaled up frontal airbag so that its volume increased to approximately 98 liters. There are many different design solutions to increase the airbag coverage, including, but not limited to: increasing the frontal airbag size (was used in this study), deploying additional airbags installed at the A-pillar (for near side driver crash mode) and/or instrument panel (for the far side driver crash mode), redesigning the shape of the frontal and side airbags with the increased coverage, developing multi-chambered airbags, etc. The purpose here was not to suggest any particular design modification, but rather to demonstrate the concept of increased frontal airbag coverage regardless of how unfeasible it may be as a “real” design solution (such as simply increasing the frontal airbag volume). Many “real” design solutions were also considered, but are outside the scope of these particular optimization studies.

Reiterating the problem statement for the optimization study #2:

1. Minimize BrIC for the near side driver oblique crash mode (PDOF = -20°) by uniformly scaling up the volume of the frontal airbag to 98 liters
2. Keep other injury criteria to the same constraints as described in the optimization study #1
3. From all the feasible solutions of optimization (problem statement 1) find one set of parameters that would reduce the values of BrIC for any PDOF when compared to those given in Table C.12

The nominal values and the varied range of parameters are given in Table C.13. Note here that the range of friction coefficients was also reduced here, and the ranges for the frontal airbag mass flow rate and firing time were increased due to increased volume, when compared to those given in Table C.3.

Table C.13. Parameters varied in the optimization study #2 (crash pulse was kept the same as in all other studies and fixed at 35 mph).

<u>Parameters</u>	<u>Nominal</u>	<u>Range</u>
Frontal Airbag Friction, fab_F	0.5	0 – 1.0
Frontal Airbag Mass Flow Rate, fab_mfr	1	0.75 – 2.0
Load Limiter, load_L	3000 N	2000- 4000
Side Airbag Friction, sab_F	0.3	0 – 1.0
Frontal Airbag (firing) Time, ttf	18 ms	6- 30
Side Airbag Mass Flow Rate, sab_mfr	1	0.75 – 1.25

After the first iteration the solution converged to the BrIC value of under 0.38 (Figure C.32) and after just four iterations the optimization process stopped as the termination criterion was met. Several more iterations were kept to generate enough runs with various parameters ranges as is shown in the parallel coordinate chart (Figure C.33– gray lines). The simulation based correlation matrix and relationship between BrIC and HIC₁₅ (sternal deflection and load limiter) are shown in Figure C.34 through Figure C.36.

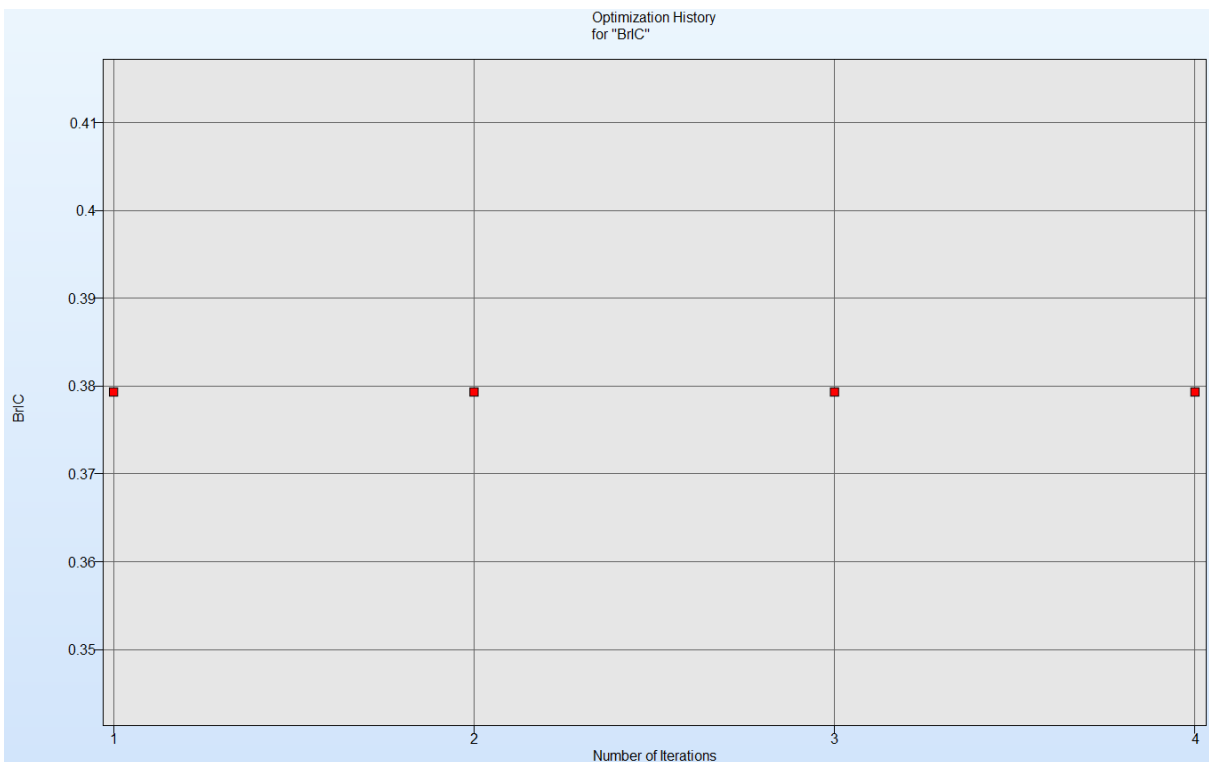


Figure C.32. Optimization history for BrIC in near side oblique runs with increased frontal airbag size.

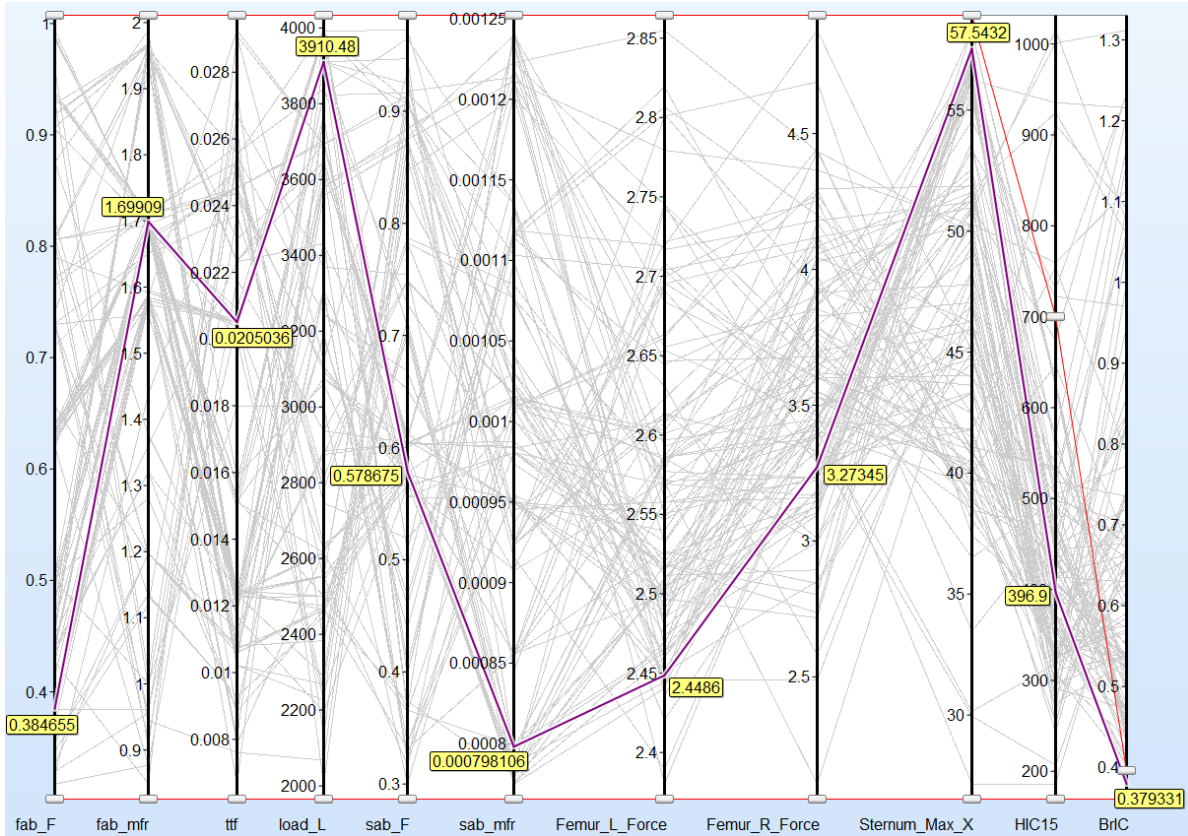


Figure C.33. Parallel coordinate chart for near side oblique runs with increased frontal airbag size.

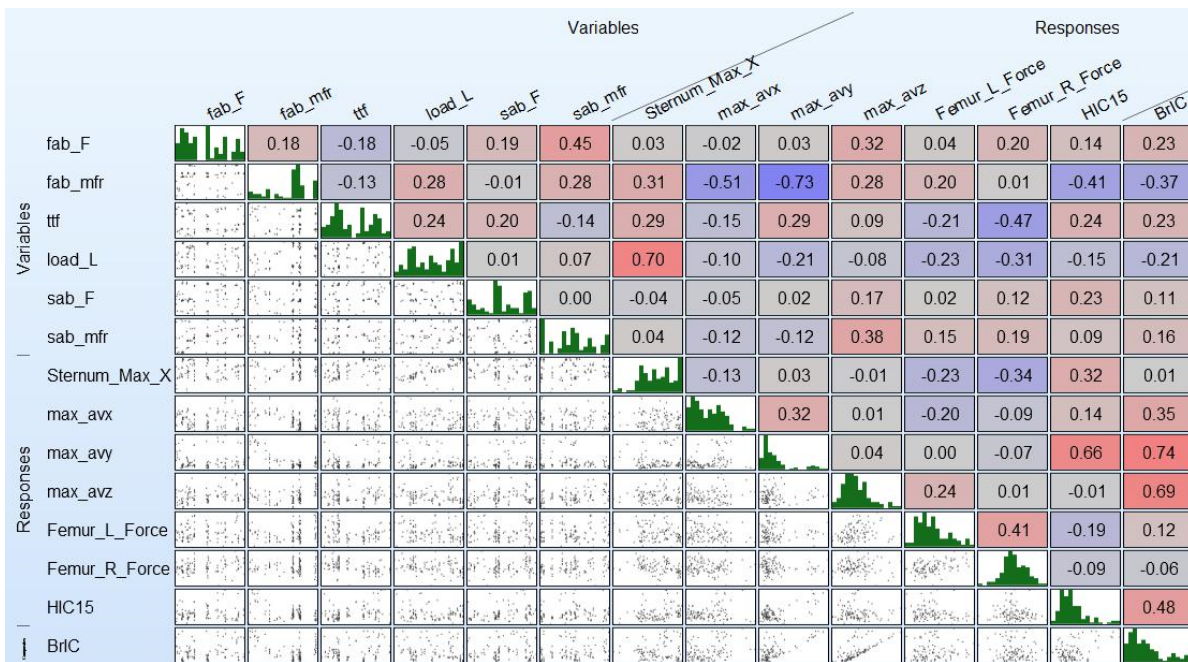


Figure C.34. Correlation matrix for near side oblique runs with increased frontal airbag size.

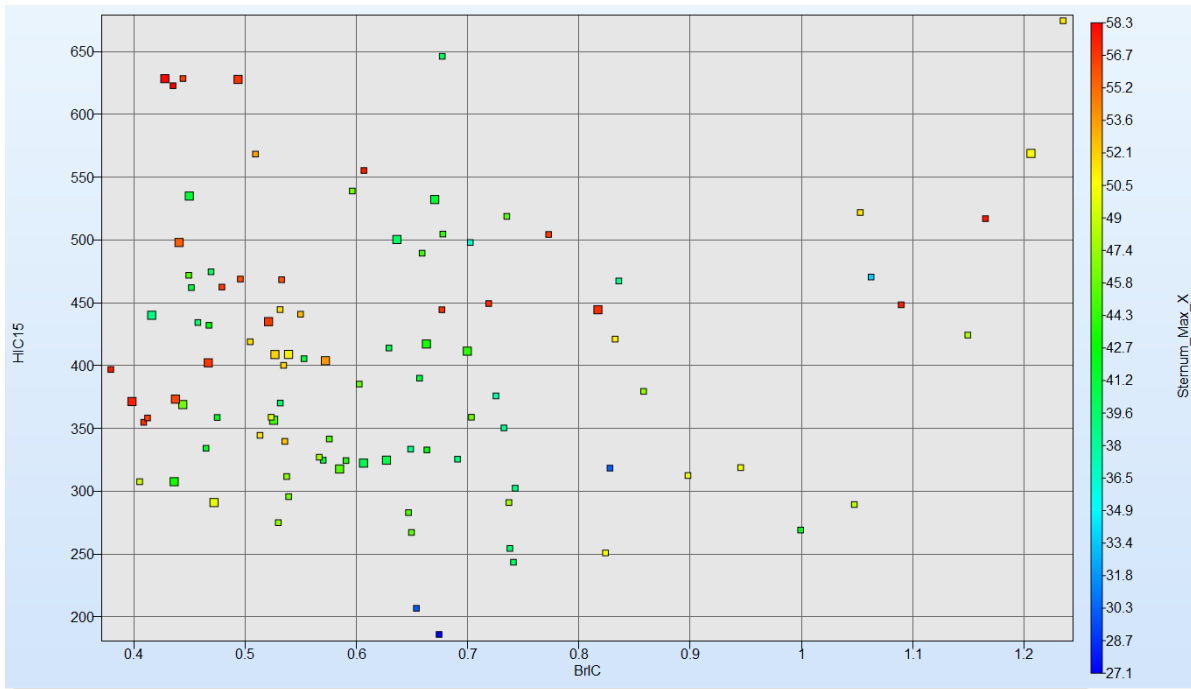


Figure C.35. Relationship between HIC₁₅, BrIC, and max sternal deflection in near side oblique runs with increased frontal airbag size (only feasible designs are shown).

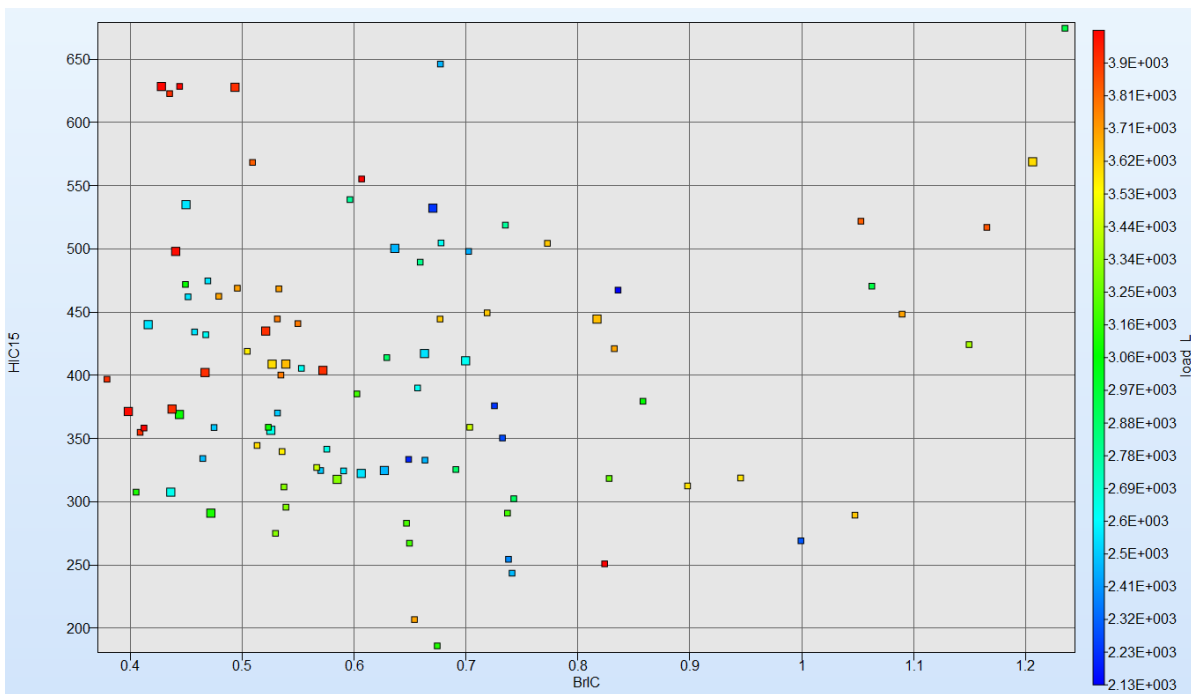


Figure C.36. Relationship between HIC₁₅, BrIC, and load limiter in near side oblique runs with increased frontal airbag size (only feasible designs are shown).

The results of the optimization are given in Table C.14 along with the parameters values. The value of BrIC now is lower than that in optimization study #1 with a 50-liter frontal airbag size. Not surprisingly, the value of HIC₁₅ has increased as well as the value of the sternal deflection (similar trend as in the studies with the smaller frontal airbag). The knowledge of these trends is vital in designing future restraint systems that would offer protection from both head/brain and chest injuries.

Table C.14. Results of the optimization near side driver oblique crash mode (PDOF = - 20⁰) with increased frontal airbag size.

Crash Pulse	Fab_F	Fab_MFR	Load_L	Sab_F	Sab_MFR	ttf	Sternal Deflection	BrIC	HIC 15
35 mph	0.38	1.69	3910	0.58	0.80	20.5	57.5	0.38	397

Next, a single set of parameters (Table C.15) was chosen from the feasible design space (not the optimal point) and the model was exercised again with these fixed parameters at various PDOFs. The results of these simulations are shown in Table C.16.

Table C.15. Fixed restraint system parameters with increased frontal airbag size.

Crash Pulse	Fab_F	Fab_MFR	Load_L	Sab_F	Sab_MFR	ttf
35 mph	0.94	1.71	3075	0.60	1.03	15

Table C.16. Injury values at different PDOF for the parameters given in Table C.15 (negative PDOF angles are for the near side driver oblique runs) with increased frontal airbag size.

PDOF	Sternal Deflection, mm	BrIC	HIC15
0 ⁰	45	0.38	500
-5 ⁰	48	0.37	341
-10 ⁰	48	0.38	426
-15 ⁰	46	0.47	392
-20 ⁰	46	0.44	368
-25 ⁰	43	0.55	356
-30 ⁰	41	0.66	450
+20 ⁰	40	0.66	189

Comparing the results given in Table C.16 with that in Table C.12 for a smaller frontal airbag, it can be observed that the sternal deflection didn't change much. However, the values of BrIC reduced substantially while the values of HIC₁₅ increased substantially (all are still far below the 700 limit). For all PDOFs from 0⁰ (full frontal crash mode) to -20⁰ (near side driver oblique) the values of BrIC indicate zero risk of any brain injury with a slightly increased risk at the increased PDOFs in near side driver oblique crash mode and the far side driver oblique crash mode. Again, this example is for demonstration purposes only and should be considered as such. However, it does demonstrate that increasing frontal airbag size/coverage decreases values of BrIC and increases values of HIC₁₅ (which are still under the limit of 700).

APPENDIX D. Fleet Data

	VehDB TSTNO	Model Year	Make	Model	THOR Locations	Test Weight [kg]
Frontal Rigid Barrier 0 degrees Full overlap 56 km/h	09964	2016	Toyota	Scion IA	Driver	1387
	09566	2016	Honda	Fit	Driver	1436
	09336	2015	Mazda	Mazda3	Driver	1599
	09965	2016	Toyota	Prius	Driver	1670
	09966	2016	Mazda	CX-5	Driver	1797
	09567	2016	Chevrolet	Malibu	Driver	1826
	09569	2016	Nissan	Rogue	Driver	1888
	09570	2015	Toyota	Sienna	Driver	2295
	09334	2015	Toyota	Highlander	Driver	2335
	09571	2016	Ford	F150 Super crew	Driver	2485
09568	2016	Chevrolet	Tahoe	Driver	2762	
Oblique Moving Deformable Barrier 15 degrees 35% overlap 90 km/h	09978	2016	Toyota	Scion IA	Driver, RFP	1333
	09572	2016	Honda	Fit	Driver, RFP	1403
	09804	2015	Nissan	Sentra	Driver, RFP	1573
	10133	2017	Toyota	Corolla	Driver, RFP	1574
	08787	2014	Mazda	Mazda3	Driver, RFP	1588
	09977	2016	Toyota	Prius	Driver, RFP	1622
	10154	2017	Nissan	Altima	Driver, RFP	1709
	08789	2014	Honda	Accord	Driver, RFP	1744
	09976	2016	Mazda	CX-5	Driver, RFP	1767
	08478	2014	Subaru	Forester	Driver, RFP	1803
	09573	2016	Chevrolet	Malibu	Driver, RFP	1808
	09574	2016	Nissan	Rogue	Driver, RFP	1860
	08488	2012	Volvo	S60	Driver, RFP	1936
	10099	2017	Honda	Ridgeline	Driver, RFP	2247
	09585	2015	Toyota	Sienna	Driver, RFP	2272
	09481	2015	Toyota	Highlander	Driver, RFP	2306
09587	2016	Ford	F150 Super crew	Driver, RFP	2434	
09586	2016	Chevrolet	Tahoe	Driver, RFP	2722	

APPENDIX E. Thoracic Injury Criteria Source Data

Occupant Position	Environment	Restraint	Delta-V (km/h)	Age	Sex	Mass (kg)	Height (cm)	AIS 3+	PMHS BioDB	THOR BioDB	THOR	THOR
											Peak Res	PCA
											Defl (mm)	
Front Driver	Gold Standard	3-point standard belt	10	59	F	80	167	No		11125	12.62	1.457
				69	M	84	178	No	11126			
				60	M	81	191	No				
Front Driver	Gold Standard	3-point standard belt	40	59	F	80	167	Yes		11123	49.40	6.243
				69	M	84	178	Yes	11124			
				60	M	81	191	Yes				
Front Passenger	1997 Ford Taurus	3-point force-limited belt plus airbag	48	57	M	70	174	No	8371	11129	51.30	6.972
				69	F	53	155	Yes	8372	11130		
				72	F	59	156	Yes	8373			
				57	M	57	177	No	8374			
Front Passenger	1997 Ford Taurus	Lap belt with airbag	48	40	M	47	150	Yes	8377	11131	30.08	3.326
				70	M	70	176	No	8378	11132		
				46	M	74	175	No	8379			
Front Passenger	1997 Ford Taurus	3-point standard belt with airbag	48	55	M	85	176	Yes	8382	11127	54.83	7.547
				69	M	84	176	Yes	8383	11128		
				59	F	79	161	Yes	8384			
Front Passenger	1997 Ford Taurus	3-point standard belt	29	49	M	58	178	No		11133	42.75	5.912
				44	M	77	172	No	11134			
				39	M	79	184	No				
Front Passenger	1997 Ford Taurus	3-point standard belt	38	44	M	77	172	No		11135	51.17	7.150
									11136			
Front Passenger	Gold Standard 1	3-point standard belt	40	76	M	70	178	Yes	9546	11117	47.73	6.857
				47	M	68	177	Yes	9547	11118		
				54	M	79	177	Yes		11119		
				49	M	76	184	Yes				
				57	M	64	175	Yes				
				72	M	81	184	Yes	11014			
				40	M	88	179	Yes	11015			
				37	M	78	180	No	11016			
Front Passenger	Gold Standard 2	3-point force-limited belt	30	59	M	68	178	No	11468	11120	26.78	3.788
				66	M	70	179	No	11469	11121		
				67	M	68	177	Yes	11509	11122		
				67	M	68	173	Yes	11510			
				74	M	70	183	No	11511			
Front Passenger	Gold Standard 3 (Near-side Oblique)	3-point force-limited belt	30	69	M	72	173	Yes	11518	11514	36	5.164
				66	M	76	172	Yes	11519	11515		
				67	M	65	177	No	11520	11516		
									11517			
Front Passenger	Far-side Oblique	3-point force-limited belt with airbag	59.5	73	M	69	180	Yes	11500	11503	53	6.475
				83	M	85	178	Yes	11501	11504		
				63	M	69	187	Yes	11502	11505		
									11506			
Rear Passenger	2004 Ford Taurus	3-point standard belt	48	51	M	55	175	Yes	9337	11143	57.96	7.999
				57	F	109	165	Yes	9338	11144		
				57	M	59	179	Yes	9339	11145		
Rear Passenger	2004 Ford Taurus	3-point force-limited belt with pretensioner	48	67	M	71	175	Yes		11140	46.66	6.520
				69	M	60	171	No		11141		
				72	M	73	175	Yes		11142		
Rear Passenger	2004 Ford Taurus	3-point inflatable force-limited belt with pretensioner	48	72	M	88	173	Yes		11137	29.66	3.790
				69	M	69	175	No		11138		
				40	M	83	186	No		11139		

APPENDIX F. Neck Injury Criteria Source Data

Table F.1. Experimental PMHS and volunteer data used in risk function development.

Specimen	Sex	Age (years)	Peak Extension (Nm)	Rate adjusted Extension	Peak Flexion (Nm)	Rate Adjusted Flexion	Peak Tension (N)	Rate Adjusted Tension	Peak Axial Compression (N)	Injury (AIS 3+)	Injury (AIS 2+)
Dibb et al. (2011)											
T22M FAOC	1	47	.	.	1.28	1.79	1993	2790	.	1	1
T23M FAOC	1	52	.	.	0.63	0.88	2147	3006	.	1	1
T24M FAOC	1	57	12.77	17.88	.	.	2145	3003	.	1	1
T25M FAOC	1	58	9.20	12.88	.	.	1726	2416	.	1	1
T26M FAOC	1	59	4.12	5.77	.	.	2357	3300	.	1	1
T27M FAOC	1	65	0.74	1.04	.	.	1756	2458	.	1	1
T28M FAOC	1	68	12.51	17.51	.	.	2319	3247	.	1	1
T29M FAOC	1	65	.	.	3.18	4.45	1811	2535	.	1	1
T31M FACG	1	61	18.92	26.49	.	.	2544	3562	.	1	1
T32M FACG	1	62	2.33	3.26	.	.	2761	3865	.	1	1
T33M FACG	1	57	17.95	25.13	.	.	2314	3240	.	1	1
T35M FACG	1	59	47.36	66.30	.	.	2239	3135	.	1	1
T36M FACG	1	58	23.93	33.50	.	.	2473	3462	.	1	1
T40M FACG	1	67	26.14	36.60	.	.	2112	2957	.	1	1
T41M FACG	1	53	24.67	26.49	.	.	2476	3466	.	1	1
Pintar et al. (2005)											
HPC22 03	0	46	12	6.6	.	.	1524	838	.	0	0
HPC32 03	1	72	44	24	.	.	1931	1062	.	0	1
HPC29 03	0	50	73	4	.	.	1984	1091	.	1	1
HPC33 04	1	54	33	18	.	.	2002	1101	.	1	1
HPC28 05	1	63	92	51	.	.	2037	1120	.	0	1
HPC20 02	0	64	35	19	.	.	2158	1187	.	0	1
HPC31 04	0	71	53	29	.	.	2254	1240	.	0	1
HPC14 04	1	63	43	24	.	.	2545	1400	.	0	1
HPC21 02	0	65	41	23	.	.	3583	1971	.	0	1
HPC30 04	1	73	69	38	.	.	3620	1991	.	1	1
Yliniemi et al. (2009)											
1	1	35	4060	4060	.	1	1
2	1	48	3860	3860	.	1	1
3	1	50	2810	2810	.	1	1
4	1	60	3150	3150	.	1	1
5	1	59	3230	3230	.	1	1
6	1	37	3220	3220	.	1	1
7	1	59	2440	2440	.	1	1
8	1	61	3230	3230	.	1	1
9	0	48	3560	3560	.	1	1
10	0	45	2250	2250	.	1	1
11	0	56	1910	1910	.	1	1
12	0	43	3490	3490	.	1	1
Nightingale et al. (2007)											
B19	1	69	.	.	46.2	60.1	.	.	.	0	0
B22	1	56	.	.	45.8	59.5	.	.	.	0	1
B24	1	71	.	.	33.6	43.7	.	.	.	0	0
B26	1	74	.	.	33.1	43.0	.	.	.	0	0
B28	1	69	.	.	35.0	45.5	.	.	.	0	0
B30	1	51	.	.	37.4	48.6	.	.	.	0	0
B32	1	57	.	.	36.2	47.1	.	.	.	1	1
B34	1	58	.	.	47.6	61.9	.	.	.	1	1
B23	1	65	44.8	53.78	1	1
B25	1	74	71.6	85.9	1	1
B27	1	72	56.4	67.7	1	1
B29	1	74	66.4	79.7	1	1
B31	1	64	60.8	73.0	1	1
Panjabi et al. (1991)											
1	1	61	3200	0	0
2	1	61	3100	1	1

Specimen	Sex	Age (years)	Peak Extension (Nm)	Rate adjusted Extension	Peak Flexion (Nm)	Rate Adjusted Flexion	Peak Tension (N)	Rate Adjusted Tension	Peak Axial Compression (N)	Injury (AIS 3+)	Injury (AIS 2+)
3	1	61	3300	1	1
4	1	61	3400	1	1
5	1	61	3500	0	1
6	1	61	2200	0	1
7	1	61	2600	0	1
8	1	61	3100	1	1
Carter et al. (2002)											
14	0	55	13.7	13.7	2632	.	1
29	1	88	80.9	80.9	5676	.	1
39	0	76	51.6	51.6	3094	.	1
41	1	91	45.6	45.6	3432	.	1
43	0	87	40.8	40.8	3036	.	1
45	0	88	34.3	34.3	2566	.	1
47	1	94	58.8	58.8	3540	.	1
49	0	86	56.9	56.9	3800	.	1
3	0	70	.	.	18.1	18.1	.	.	330	0	0
5	0	90	.	.	7	7	.	.	930	.	1
7	0	53	.	.	22.6	22.6	.	.	1073	0	0
8	0	34	.	.	23.9	23.9	.	.	542	.	1
15	1	50	.	.	32.2	32.2	.	.	459	0	0
17	1	61	.	.	37.4	37.4	.	.	486	.	1
27	0	77	.	.	13.8	13.8	.	.	1214	0	0
48	0	72	.	.	15.9	15.9	.	.	1091	.	1
2	0	78	23.5	23.5	3447	.	1
10	1	30	9.8	9.8	4110	.	1
12	1	80	8.2	8.2	2768	.	1
23	0	69	31.1	31.1	4180	.	1
28	0	84	12.7	12.7	2656	.	1
40	1	41	13.7	13.7	4755	.	1
44	0	67	7.2	7.2	1988	.	1
46	1	61	14.0	14.0	2153	.	1
Parr et al. (2013)											
	0	20	.	.	36.4	36.4	118.9	118.9	.	0	0
	0	29	.	.	46.6	46.6	152.7	152.7	.	0	0
	0	28	.	.	44.8	44.8	187.5	187.5	.	0	0
	0	19	.	.	38.2	38.2	66.7	66.7	.	0	0
	1	24	.	.	27.1	27.1	240.1	240.1	.	0	0
	0	27	.	.	40.6	40.6	15.4	15.4	.	0	0
	0	46	.	.	53.2	53.2	160.9	160.9	.	0	0
	0	23	.	.	42.4	42.4	49.6	49.6	.	0	0
	0	28	.	.	39.8	39.8	369.5	369.5	.	0	0
	1	35	.	.	18.1	18.1	3.0	3.0	.	0	0
	0	25	.	.	23.5	23.5	103.0	103.0	.	0	0
	1	30	.	.	30.3	30.3	2.5	2.5	.	0	0
	1	24	.	.	38.2	38.2	115.1	115.1	.	0	0
	1	27	.	.	31.6	31.6	44.4	44.4	.	0	0
	1	36	.	.	40.3	40.3	170.4	170.4	.	0	0
	1	30	.	.	34.1	34.1	134.4	134.4	.	0	0
	0	23	.	.	57.0	57.0	93.0	93.0	.	0	0
	0	29	.	.	41.8	41.8	89.4	89.4	.	0	0
	1	28	.	.	36.1	36.1	423.8	423.8	.	0	0
	1	31	.	.	37.6	37.6	168.1	168.1	.	0	0
	1	27	.	.	39.6	39.6	4.5	4.5	.	0	0
	1	22	.	.	30.9	30.9	2.7	2.7	.	0	0
	1	37	.	.	41.9	41.9	235.9	235.9	.	0	0
	1	36	.	.	39.9	39.9	9.1	9.1	.	0	0
	1	33	.	.	50.4	50.4	162.8	162.8	.	0	0
	1	36	.	.	42.3	42.3	0.1	0.1	.	0	0
	1	32	.	.	64.6	64.6	10.1	10.1	.	0	0

Table F.2. Sled test data matched with THOR-50M tests (unless otherwise noted, all tests have 0° PDOF). These include multiple PMHS test series conducted by the University of Virginia, as well as PMHS and volunteer tests conducted at Naval Biodynamics Research Laboratory (NBDL). THOR-50M values shown represent an average of between two and four tests (test numbers for individual THOR tests are tabulated in the THOR BioDB column).

Restraint condition / Study Reference	Subject Age	Subject Sex	Neck AIS	PMHS BioDB	THOR BioDB	THOR Peak Neck Tension (N)	THOR Peak Neck Compression (N)	THOR Peak Neck Flexion (Nm)	THOR Peak Neck Extension (Nm)	Max Nij
3-point standard belt (Lopez-Valdes et al., 2010)	59	F	0		11125	178.15	-230.99	7.87	-4.25	0.18
	69	M	0		11126					
	60	M	0							
3-point standard belt (Lopez-Valdes et al., 2010)	59	F	0		11123	2743.39	-476.67	22.00	-24.90	0.77
	69	M	2		11124					
	60	M	0							
3-point force-limited belt with airbag (Forman et al., 2006a)	57	M	0	8371	11129	1872.14	-1170.48	23.07	-20.53	0.57
	69	F	0	8372	11130					
	72	F	0	8373						
	57	M	0	8374						
Lap belt with airbag (Kent et al., 2001)	40	M	0	8377	11131	1062.33	-939.92	8.81	-18.39	0.37
	70	M	0	8378	11132					
	46	M	0	8379						
3-point force-limited belt and airbag (Forman et al., 2006a)	55	M	0	8382	11127	2370.62	-1668.57	12.87	-30.57	0.76
	69	M	0	8383	11128					
	59	F	0	8384						
3-point standard belt (Forman et al., 2006a)	49	M	0		11133	1388.98	-645.74	11.69	-11.12	0.38
	44	M	0		11134					
	39	M	0							
3-point standard belt (Forman et al., 2006b)	44	M	0		11135	2396.56	-677.22	16.77	-13.34	0.64
					11136					
3-point standard belt (Shaw et al., 2009)	76	M	0	9546		2134.18	-372.46	14.03	-17.90	0.61
	47	M	0	9547						
	54	M	0		11117					
	49	M	0		11118					
	57	M	0		11119					
	72	M	0	11014						
	40	M	0	11015						
37	M	0	11016							
3-point force-limited belt (Shaw et al., 2012)	59	M	0	11468	11120	969.16	-272.75	13.86	-10.67	0.29
	66	M	2	11469	11121					
	67	M	3	11509	11122					
	67	M	2	11510						
Near-side 30° oblique, 3-point force-limited belt	69	M	2	11518	11514	1101.28	-102.30	8.71	-10.45	0.34
	66	M	1	11519	11515					
					11516					
	67	M	0	11520	11517					
Far-side 30° oblique, 3-point force-limited belt and airbag	73	M	2	11500	11503	1636.40	-308.81	17.23	-13.00	0.60
	83	M	2	11501	11504					
	63	M	0	11502	11505 11506					
3-point standard belt (Forman et al., 2009)	51	M	2	9337	11143	3061.90	-55.88			0.70
	57	F	5	9338	11144					
	57	M	3	9339	11145					
3-point force-limited belt with pretensioner (Forman et al., 2009)	67	M	3		11140	2465.46	-697.68	23.82	-24.26	0.69
	69	M	0		11141					
	72	M	0		11142					
3-point inflatable belt with pretensioner (Kent et al., 2011)	72	M	0		11137	1671.19	-963.39	13.56	-21.29	0.50
	69	M	0		11138					
	40	M	0		11139					
15G sled test (NBDL condition) with volunteers (denoted by *, Thunnissen et al.,	50	M	0		10999	1083.19	-1265.96	32.77	-12.96	0.58
	51	M	0		11000					
	61	F	0		11001					
	51	F	2							

Restraint condition / Study Reference	Subject Age	Subject Sex	Neck AIS	PMHS BioDB	THOR BioDB	THOR Peak Neck Tension (N)	THOR Peak Neck Compression (N)	THOR Peak Neck Flexion (Nm)	THOR Peak Neck Extension (Nm)	Max Nij
1995) and PMHS (Wismans et al., 1987)	46	F	0							
	37	M	0							
	24	F	0							
	59	M	0							
	38	M	0							
	20*	M	0							
	20*	M	0							
	20*	M	0							
	20*	M	0							
	20*	M	0							

Table F.3. Fleet data from THOR-50M used in determination of tensile loading rate.

TSTNO	Vehicle Year	Make	Model	Impact Angle	Seat Location	Load Cell Peak Neck Compression [N]	Load Cell Peak Neck Tension [N]	Load Cell Peak Neck Flexion [Nm]	Load Cell Peak Neck Extension [Nm]	Tension Rate [N/s]
08787	2014	MAZDA	MAZDA3	345	01	-286	1890	8.9	-5.9	39785
08787	2014	MAZDA	MAZDA3	345	02	-780	1656	5.9	-12.3	23341
08789	2014	HONDA	ACCORD	345	01	-47	1544	11.1	-8.7	62527
08789	2014	HONDA	ACCORD	345	02	-224	2117	4.6	-12.1	32141
08788	2014	MAZDA	CX-5	345	01	-81	1968	11.2	-7.8	63800
08788	2014	MAZDA	CX-5	345	02	-35	1392	6.1	-13.7	16738
08478	2014	SUBARU	FORESTER	345	01	-204	2036	16.1	-9.6	25852
08478	2014	SUBARU	FORESTER	345	02	-119	1081	3.9	-9.1	118320
08488	2012	VOLVO	S60	345	01	-94	1820	9.7	-5.8	48100
08488	2012	VOLVO	S60	345	02	-434	1105	6.7	-7.7	27559
09481	2015	TOYOTA	HIGHLANDER	345	01	-99	1925	10.7	-7.9	86885
09481	2015	TOYOTA	HIGHLANDER	345	02	-368	1560	4.4	-6.0	80823
09573	2016	CHEVROLET	MALIBU	345	01	-250	1594	10.3	-10.8	53653
09573	2016	CHEVROLET	MALIBU	345	02	-533	1180	9.2	-9.3	35020
09574	2016	NISSAN	ROGUE	345	01	-179	1774	6.0	-21.4	73840
09574	2016	NISSAN	ROGUE	345	02	-155	1277	1.3	-9.0	93132
09572	2016	HONDA	FIT	345	01	-810	2088	22.5	-12.1	86662
09572	2016	HONDA	FIT	345	02	-686	2525	3.7	-12.4	47567
09585	2015	TOYOTA	SIENNA	345	01	-158	1959	6.0	-8.7	84339
09585	2015	TOYOTA	SIENNA	345	02	-599	1504	6.0	-8.4	59047
09586	2016	CHEVROLET	TAHOE	345	01	-183	1028	8.9	-11.0	21974
09586	2016	CHEVROLET	TAHOE	345	02	-1061	1039	1.7	-8.8	32870
09587	2016	FORD	F150	345	01	-280	1009	5.5	-12.4	25416
09587	2016	FORD	F150	345	02	-163	1029	4.2	-10.0	50006
09567	2016	CHEVROLET	MALIBU	0	01	-441	1239	17.5	-13.3	127300
09566	2016	HONDA	FIT	0	01	-207	1117	10.4	-9.5	28334
09571	2016	FORD	F150	0	01	-311	1083	13.8	-9.9	22670
09334	2015	TOYOTA	HIGHLANDER	0	01	-366	2481	15.3	-23.9	81092
09336	2015	MAZDA	MAZDA3	0	01	-272	1407	8.5	-8.6	26430
09568	2016	CHEVROLET	TAHOE	0	01	-898	1693	17.9	-19.2	41733
09569	2016	NISSAN	ROGUE	0	01	-339	1793	14.1	-11.8	49068
09570	2015	TOYOTA	SIENNA	0	01	-352	1539	10.3	-11.1	60549

APPENDIX G. Lower Extremity Injury Criteria Source Data

Table G.1. Upper tibia source data (Banglmeier et al., 1999).

Specimen	Age	Sex	Height (m)	Mass (kg)	Censor Interval	
					Lower	Upper
10-97-L	81	0	1.78	61.4	5.6 ²	6.8
10-97-R ¹	81	0	1.78	61.4	9.1	.
118-96-L	84	1	1.81	81.8	5.3 ²	6.4
118-96-R	84	1	1.81	81.8	5.8	.
11-97-L ¹	73	0	.	.	.	5.6
11-97-R	73	0	.	.	7.8 ²	8.2
145-96-L	83	0	1.72	59.1	.	3.8
145-96-R	83	0	1.72	59.1	3.7 ²	6
147-96-L	48	1	1.78	102.7	6 ²	8.1
147-96-R	48	1	1.78	102.7	4.3	.
153-94-L	71	0	1.86	90.9	6.6	.
153-94-R	71	0	1.86	90.9	9.4 ²	10.8
176-97-L	63	0	1.73	100.9	7.9 ²	11.5
176-97-R ¹	63	0	1.73	100.9	10.4	.
3-98-L	60	0	1.85	86.4	6.4 ²	9.7
3-98-R ¹	60	0	1.85	86.4	9.3	.
43-97-L ¹	72	0	1.75	69.5	.	6.9
43-97-R	72	0	1.75	69.5	6 ²	7.6
48-97-L	80	1	1.6	53.2	.	7
48-97-R	80	1	1.6	53.2	6.4 ²	7.5
51-95-L	82	1	1.6	65.9	3.8	.
51-95-R	82	1	1.6	65.9	4.7 ²	5.8
69-97-L	72	1	1.73	68.2	7.5 ²	7.9
69-97-R ¹	72	1	1.73	68.2	7.7	.

¹ Tests conducted at constant energy were excluded due to pressure films being placed in the joint prior to impact

² Lower interval represents independent uninjured observation in logistic regression analysis

Table G.2. Lower tibia source data.

Study	Height (cm)	Age	Sex	Mass (kg)	Censor Interval	
					Lower	Upper
Yoganandan et al. (1996)	175	27	1	66	2.669 ¹	.
Yoganandan et al. (1996)	175	27	1	66	10.159	.
Yoganandan et al. (1996)	183	46	1	102	2.718 ²	11.454
Yoganandan et al. (1996)	183	46	1	102	.	11.236
Yoganandan et al. (1996)	180	27	1	77	4.493 ²	9.75
Yoganandan et al. (1996)	175	55	1	82	6.227 ²	8.269
Yoganandan et al. (1996)	180	27	1	77	2.802 ²	9.265
Yoganandan et al. (1996)	175	55	1	82	.	7.815
Yoganandan et al. (1996)	178	60	1	75	.	6.685
Yoganandan et al. (1996)	178	60	1	75	.	5.934
Yoganandan et al. (1996)	166	64	1	70	.	10.204
Yoganandan et al. (1996)	166	64	1	70	2.749	.
Yoganandan et al. (1996)	185	50	1	93	4.154	.
Yoganandan et al. (1996)	185	50	1	93	7.281	.
Yoganandan et al. (1996)	178	67	1	82	.	6.654
Yoganandan et al. (1996)	178	67	1	82	.	5.529
Yoganandan et al. (1996)	175	27	1	66	6.203 ¹	.
Yoganandan et al. (1996)	175	27	1	66	7.51	.
Yoganandan et al. (1996)	185	74	1	104	0.508	.
Yoganandan et al. (1996)	183	58	1	73	1.162	.
Yoganandan et al. (1996)	163	67	0	57	.	4.559
Yoganandan et al. (1996)	163	67	0	57	.	4.328
Begeman et al. (1996)	.	70	1	49	6.11 ²	6.99
Begeman et al. (1996)	.	68	0	55	6.44 ²	6.88
Begeman et al. (1996)	.	43	0	69	7.44 ²	8.65
Begeman et al. (1996)	.	53	0	101	.	8.03

Study	Height (cm)	Age	Sex	Mass (kg)	Censor Interval Lower	Censor Interval Upper
Begeman et al. (1996)	.	53	0	101	8.315 ²	8.69
Begeman et al. (1996)	.	63	1	82	3.43	.
Begeman et al. (1996)	.	63	1	82	5.48	.
Begeman et al. (1996)	.	52	0	53	4	.
Begeman et al. (1996)	.	65	1	93	6.05	.
Begeman et al. (1996)	.	63	1	64	5.97	.
Begeman et al. (1996)	.	63	1	64	6.84	.
Begeman et al. (1996)	.	65	1	69	6.26	.
Begeman et al. (1996)	.	59	1	64	7.55	.
Kitagawa et al. (1998)	.	68	0	.	.	7.801
Kitagawa et al. (1998)	.	68	0	.	8.152	.
Kitagawa et al. (1998)	.	69	0	.	.	8.549
Kitagawa et al. (1998)	.	69	0	.	.	7.62
Kitagawa et al. (1998)	.	59	1	.	.	7.11
Kitagawa et al. (1998)	.	59	1	.	.	7.349
Kitagawa et al. (1998)	.	75	0	.	.	7.145
Kitagawa et al. (1998)	.	75	0	.	.	7.437
Kitagawa et al. (1998)	.	83	0	.	.	7.779
Kitagawa et al. (1998)	.	83	0	.	.	7.759
Kitagawa et al. (1998)	.	69	0	.	.	6.738
Kitagawa et al. (1998)	.	69	0	.	.	5.737
Kitagawa et al. (1998)	.	75	1	.	.	8.654
Kitagawa et al. (1998)	.	75	1	.	.	8.803
Kitagawa et al. (1998)	.	70	0	.	.	9.108
Kitagawa et al. (1998)	.	70	0	.	.	7.091
Funk et al. (2002)	163	67	0	63.6	.	4.106
Funk et al. (2002)	178	47	1	52.3	.	4.463
Funk et al. (2002)	160	74	0	60	.	2.574
Funk et al. (2002)	160	74	0	60	.	3.827
Funk et al. (2002)	163	67	0	63.6	.	4.685
Funk et al. (2002)	168	42	0	71.4	.	7.349
Funk et al. (2002)	170	59	1	47.7	.	6.854
Funk et al. (2002)	168	62	0	52.3	.	3.221
Funk et al. (2002)	170	59	1	47.7	.	4.801
Funk et al. (2002)	168	62	0	52.3	.	4.644
Funk et al. (2002)	191	67	1	80.5	.	6.334
Funk et al. (2002)	191	67	1	80.5	.	5.829
Funk et al. (2002)	188	65	1	84.1	.	5.506
Funk et al. (2002)	188	65	1	84.1	.	5.824
Funk et al. (2002)	175	67	1	70.5	.	5.185
Funk et al. (2002)	175	67	1	73.6	.	6.248
Funk et al. (2002)	173	57	1	74.5	.	9.312
Funk et al. (2002)	178	72	0	66.8	.	3.912
Funk et al. (2002)	173	62	1	75.9	.	8.606
Funk et al. (2002)	163	74	0	78.2	.	7.486
Funk et al. (2002)	160	41	0	89.5	.	5.577
Funk et al. (2002)	163	74	0	78.2	.	5.875
Funk et al. (2002)	173	62	1	75.9	.	8.87
Funk et al. (2002)	170	71	1	87.7	.	5.525
Funk et al. (2002)	157	65	0	46.8	.	2.846
Funk et al. (2002)	145	69	0	57.3	.	4.302
Funk et al. (2002)	178	51	1	84.1	.	10.837
Funk et al. (2002)	157	65	0	46.8	.	2.94
Funk et al. (2002)	145	69	0	57.3	.	3.835
Funk et al. (2002)	178	51	1	84.1	.	10.55
Funk et al. (2002)	163	67	0	63.6	2.205	.
Funk et al. (2002)	160	63	0	55.9	5.887	.
Funk et al. (2002)	175	67	1	70.5	5.263	.
Funk et al. (2002)	175	67	1	73.6	4.159	.

¹ Excluded due to multiple non-injury tests on a single specimen. Only highest non-injury force value was included

² Lower interval represents independent uninjured observation in logistic regression analysis

Table G.3. Bending moment source data.

Study	Test ID	Sex	Mass	Moment Total (Nm)	Moment Applied (Nm)	Axial Force Applied (kN)	Age	Load Direction
Nyquist et al. (1985)	116	M	57	176	176	0	59	AP
Nyquist et al. (1985)	117	M	68	326	326	0	54	AP
Nyquist et al. (1985)	118	M	68	395	395	0	54	LM
Nyquist et al. (1985)	124	M	82	287	287	0	64	LM
Nyquist et al. (1985)	125	M	73	182	182	0	58	AP
Nyquist et al. (1985)	126	M	73	224	224	0	58	LM
Nyquist et al. (1985)	127	M	79	237	237	0	56	LM
Nyquist et al. (1985)	128	M	99	312	312	0	57	AP
Nyquist et al. (1985)	129	M	99	349	349	0	57	LM
Nyquist et al. (1985)	132	M	45	264	264	0	57	LM
Nyquist et al. (1985)	133	M	45	402	402	0	57	AP
Nyquist et al. (1985)	134	M	57	287	287	0	59	AP
Nyquist et al. (1985)	135	M	84	324	324	0	57	AP
Nyquist et al. (1985)	145	M	79	424	424	0	56	AP
Nyquist et al. (1985)	146	F	75	315	315	0	57	AP
Nyquist et al. (1985)	147	M	84	431	431	0	57	LM
Nyquist et al. (1985)	148	F	75	254	254	0	57	LM
Nyquist et al. (1985)	152	F	68	274	274	0	51	LM
Nyquist et al. (1985)	153	F	68	246	246	0	51	AP
Schreiber et al. (1998)	1000-R	M	105	458	458	0	85	PA
Schreiber et al. (1998)	1002-R	F	57.9	259	259	0	70	PA
Schreiber et al. (1998)	1003-R	M	69.5	577	577	0	77	PA
Schreiber et al. (1998)	1004-R	F	59.9	535	535	0	59	PA
Schreiber et al. (1998)	1005-R	M	73.6	445	445	0	75	PA
Schreiber et al. (1998)	1006-R	F	80.4	372	372	0	70	PA
Schreiber et al. (1998)	1010-R	F	73.9	440	440	0	55	PA
Schreiber et al. (1998)	48-L	M	61.3	239	239	0	83	PA
Schreiber et al. (1998)	50-R	F	46.7	371	371	0	68	PA
Schreiber et al. (1998)	68-R	M	72.6	424	424	0	56	PA
Schreiber et al. (1998)	69-R	M	90.3	534	534	0	62	PA
Schreiber et al. (1998)	73-L	F	57.2	242	242	0	61	PA
Schreiber et al. (1998)	1000-L	M	104	453	388	4.448	85	PA
Schreiber et al. (1998)	1001-L	M	58.9	277	212	4.448	94	PA
Schreiber et al. (1998)	1003-L	M	69.5	547	482	4.448	77	PA
Schreiber et al. (1998)	1004-L	F	59.9	453	388	4.448	59	PA
Schreiber et al. (1998)	1006-L	F	80.4	394	329	4.448	70	PA
Schreiber et al. (1998)	48-R	M	61.3	270	205	4.448	83	PA
Schreiber et al. (1998)	50-L	F	46.7	384	319	4.448	68	PA
Schreiber et al. (1998)	73-R	F	57.2	278	213	4.448	61	PA
Schreiber et al. (1998)	74-L	F	50.3	331	266	4.448	55	PA
Ivarsson et al. (2006)	1.05*	M	81.8	.	0	11.317	76	C
Ivarsson et al. (2006)	1.06	M	81.8	.	0	10.394	76	C
Ivarsson et al. (2006)	1.08*	M	54.4	.	0	7.936	52	C
Ivarsson et al. (2006)	1.09*	M	54.4	.	0	8.386	52	C
Ivarsson et al. (2006)	2.21*	M	89.4	.	0	14.362	60	C
Ivarsson et al. (2006)	2.22	M	89.4	.	0	16.776	60	C
Ivarsson et al. (2006)	3.01*	F	94.8	.	0	8.62	38	C
Ivarsson et al. (2006)	3.02	M	105.2	.	0	10.945	70	C
Ivarsson et al. (2006)	3.03*	M	77.1	.	0	12.487	73	C
Ivarsson et al. (2006)	3.04*	M	90.7	.	0	6.549	56	C
Ivarsson et al. (2006)	3.13	F	60.8	.	0	4.83	57	C
Ivarsson et al. (2006)	2.23	M	90.7	250.23	250.23	0	49	AP
Ivarsson et al. (2006)	2.24	M	90.7	266.01	266.01	0	49	AP
Ivarsson et al. (2006)	3.06*	M	.	267.5	267.5	0	64	PA
Ivarsson et al. (2006)	3.07	M	72.6	220.92	220.92	0	55	AP
Ivarsson et al. (2006)	3.08	M	65.9	269.91	269.91	0	51	AP
Ivarsson et al. (2006)	2.01	M	87.1	319.9	228.37	3.465	53	AP
Ivarsson et al. (2006)	2.02*	M	87.1	333.0	240.7	3.428	53	AP
Ivarsson et al. (2006)	2.03	M	73.5	.	121.79	5.021	66	PA
Ivarsson et al. (2006)	2.04	M	73.5	.	137.51	4.512	66	PA
Ivarsson et al. (2006)	2.05*	M	59	.	101.99	2.473	70	PA

Study	Test ID	Sex	Mass	Moment Total (Nm)	Moment Applied (Nm)	Axial Force Applied (kN)	Age	Load Direction
Ivarsson et al. (2006)	2.06*	M	59	.	84.822	5.115	70	PA
Ivarsson et al. (2006)	2.07	M	68	243.0	200.52	1.742	48	AP
Ivarsson et al. (2006)	2.08*	M	68	276.4	174.73	3.834	48	AP
Ivarsson et al. (2006)	2.09*	M	53.1	212.5	143.16	3.323	66	AP
Ivarsson et al. (2006)	2.1*	M	53.1	.	160.58	2.07	66	PA
Ivarsson et al. (2006)	2.11*	M	74.8	.	108.69	6.725	58	PA
Ivarsson et al. (2006)	2.12	M	74.8	.	130.81	4.156	58	PA
Ivarsson et al. (2006)	2.13	M	59.9	321.2	205.71	4.874	65	AP
Ivarsson et al. (2006)	2.14	M	59.9	324.7	198.31	4.778	65	AP
Ivarsson et al. (2006)	2.17	F	79.8	.	119.5	4.36	43	PA
Ivarsson et al. (2006)	2.19*	M	45.4	.	121.1	2.168	69	PA
Ivarsson et al. (2006)	3.09	M	86.2	266.4	130.68	6.805	66	AP
Ivarsson et al. (2006)	3.1	F	54.4	192.9	74.598	6.538	42	AP
Ivarsson et al. (2006)	3.11	M	77.1	333.3	76.255	6.89	44	AP
Ivarsson et al. (2006)	3.12	M	65.9	320.9	123.75	6.915	51	AP
Ivarsson et al. (2006)	3.15*	M	58.1	.	54.511	7.218	49	PA
Ivarsson et al. (2006)	3.16	M	79.4	.	133.58	6.933	39	PA
Ivarsson et al. (2006)	3.17	F	60.8	171.6	130.91	2.014	57	AP
Ivarsson et al. (2006)	3.18*	M	76.7	238.4	97.625	5.00	67	AP
Ivarsson et al. (2006)	3.19	M	77.1	241.7	117.82	5.336	73	AP
Ivarsson et al. (2006)	3.2	M	77.1	273.8	147.69	4.95	61	AP
Ivarsson et al. (2006)	3.21	M	79.4	.	169.94	5.659	39	PA
Ivarsson et al. (2006)	3.22	M	68	.	171.09	4.462	51	PA
Ivarsson et al. (2006)	3.23*	M	72.6	.	81.419	5.296	55	PA
Ivarsson et al. (2006)	3.24	M	77.1	.	148.75	5.755	61	PA
Ivarsson et al. (2006)	3.25	F	94.8	197.1	98.258	5.362	38	AP
Ivarsson et al. (2006)	3.26	M	77.1	245.8	129.45	3.534	44	AP
Ivarsson et al. (2006)	3.27	M	68	285.7	205.29	3.493	51	AP
Ivarsson et al. (2006)	3.28	M	86.2	196.5	165.64	1.854	66	AP
Ivarsson et al. (2006)	3.3	M	105.2	.	173.25	3.634	70	PA
Ivarsson et al. (2006)	3.31	M	77.1	173.0	159.8	1.838	52	AP
Ivarsson et al. (2006)	3.32*	M	.	.	145.48	3.388	64	PA
Ivarsson et al. (2006)	3.33	M	90.7	.	165.66	1.909	56	PA

*Fractures were noted as being associated with the distal potting and were therefore excluded from risk function development

APPENDIX H. Field Data Charts

The following figures show the distribution of various crash and occupant factors associated with the field data analysis done in Chapter 9. Unless otherwise noted, the frontal crash filters used to produce these figures used the same filter or filters described in producing Table 9.3. As with Chapter 9, the NASS-CDS case years used were 2001 to 2015.

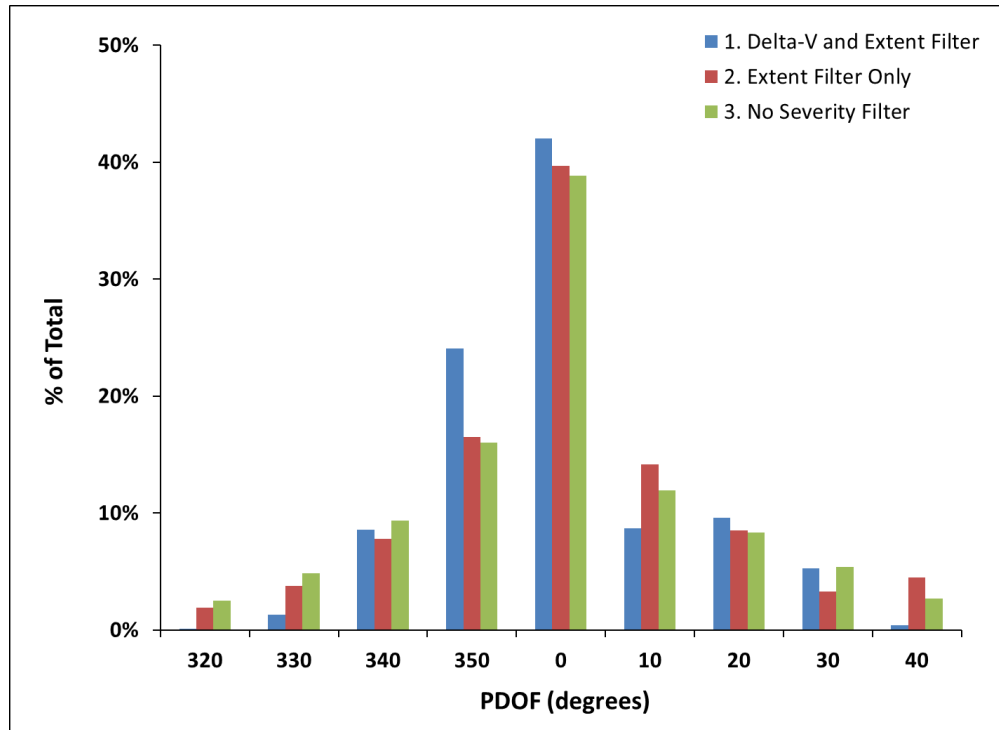


Figure H.1. PDOF for frontal crashes using same filters as used for Table 9.3.

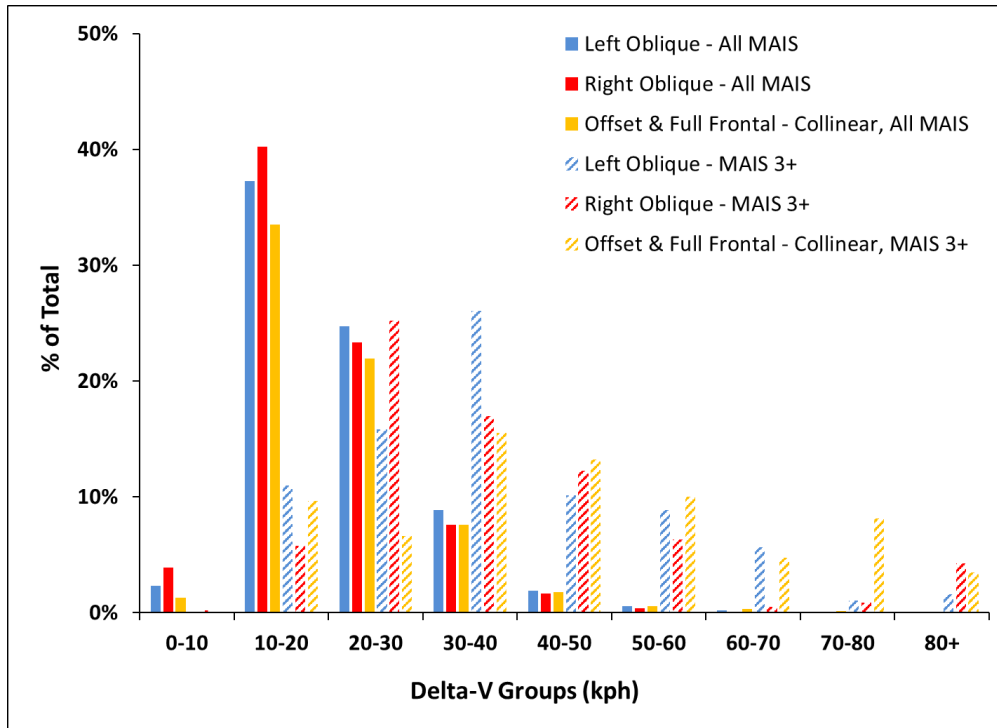


Figure H.2. Delta-V distribution for different frontal crash types (all MAIS and MAIS 3+). No delta-V, damage extent or airbag deployment restrictions.

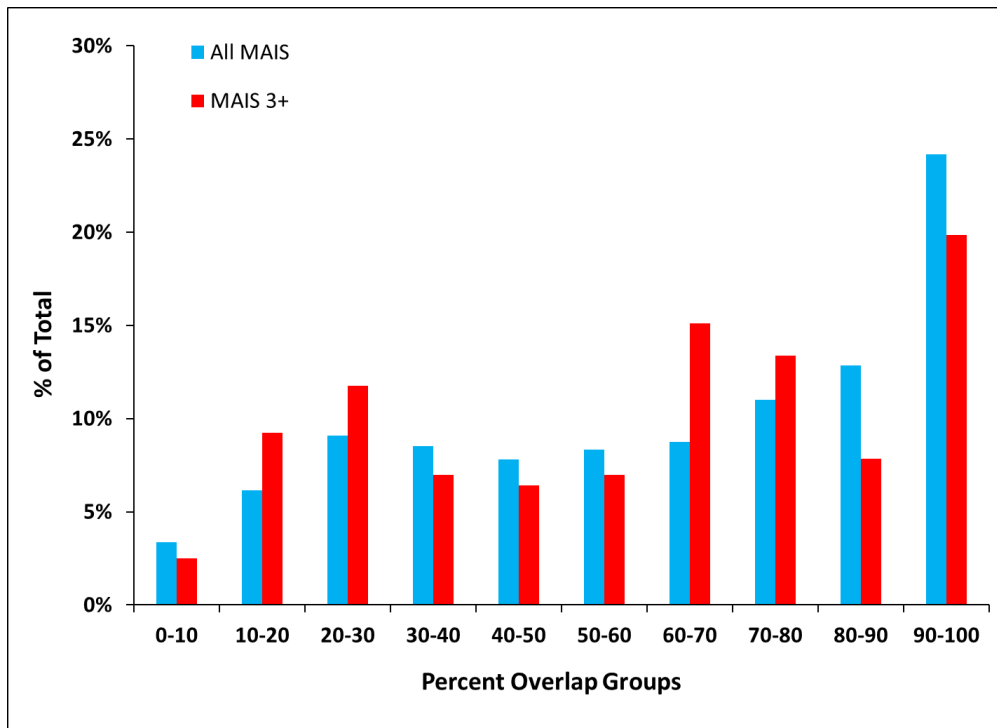


Figure H.3. Percent overlap for frontal crashes. No delta-V or damage extent restrictions.

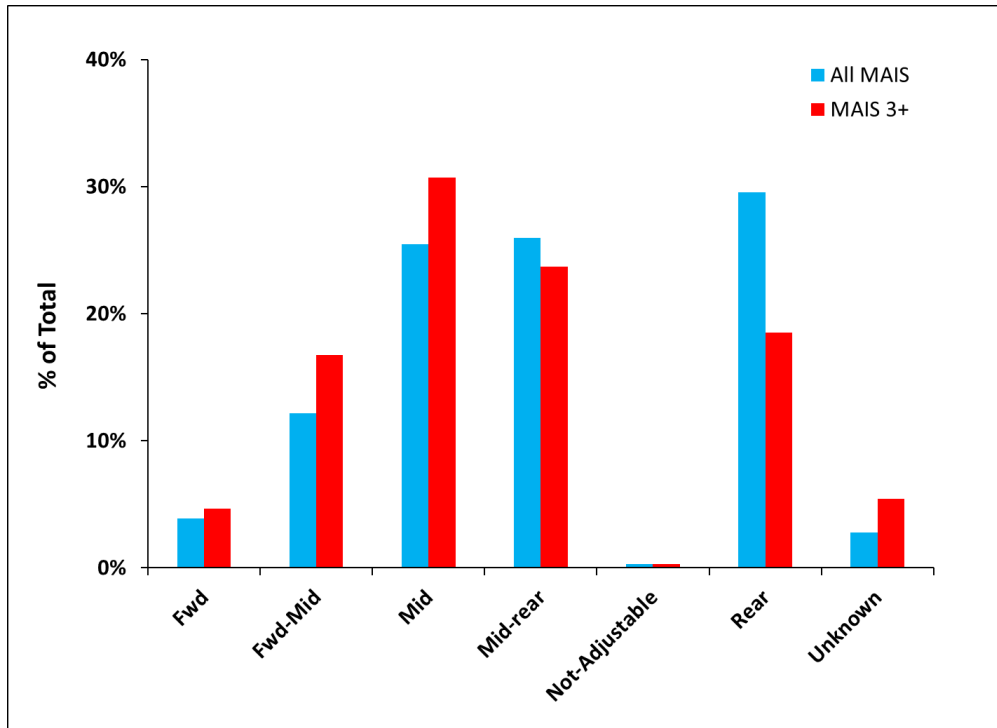


Figure H.4. Driver seat track position in frontal crashes. No delta-V or damage extent restrictions.

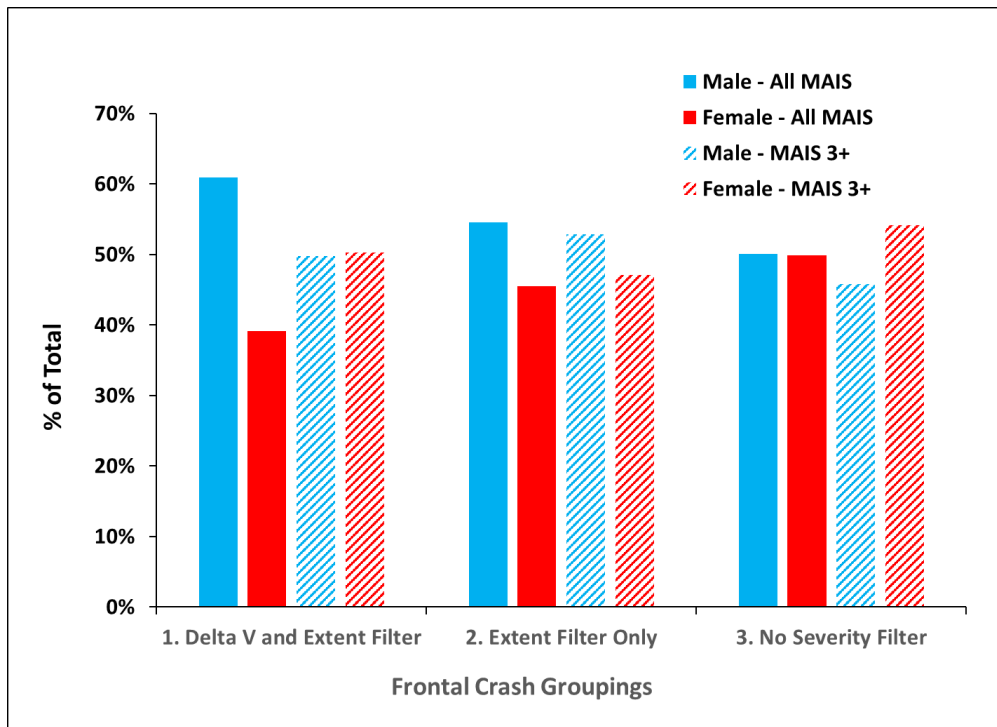


Figure H.5. Driver sex in frontal crashes using same filters as Figure 9.3.

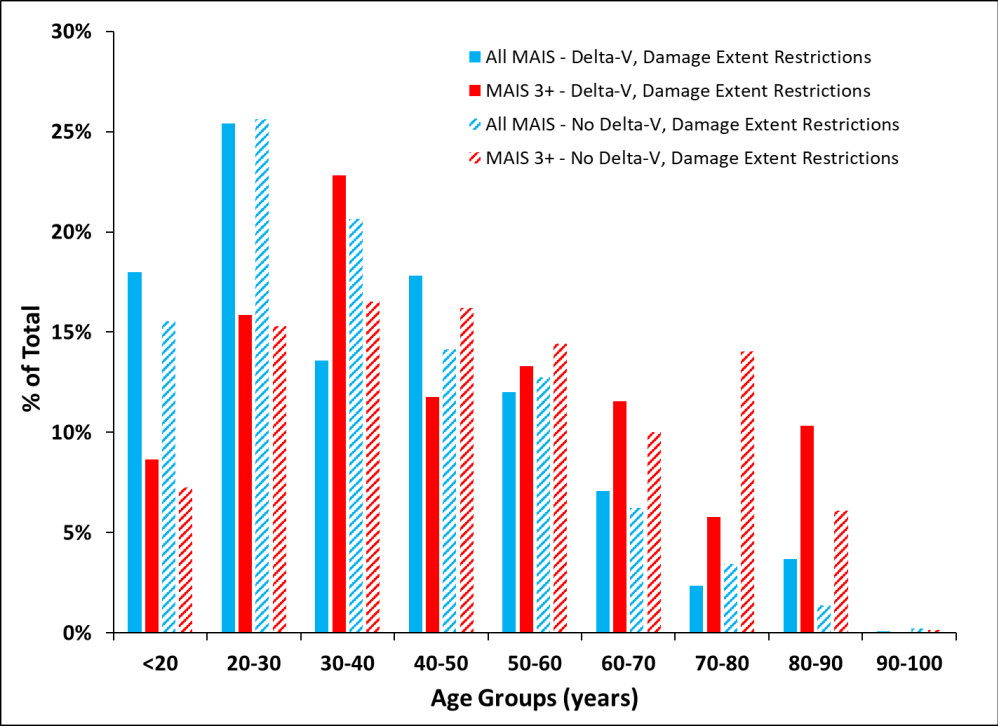


Figure H.6. Driver age in frontal crashes.

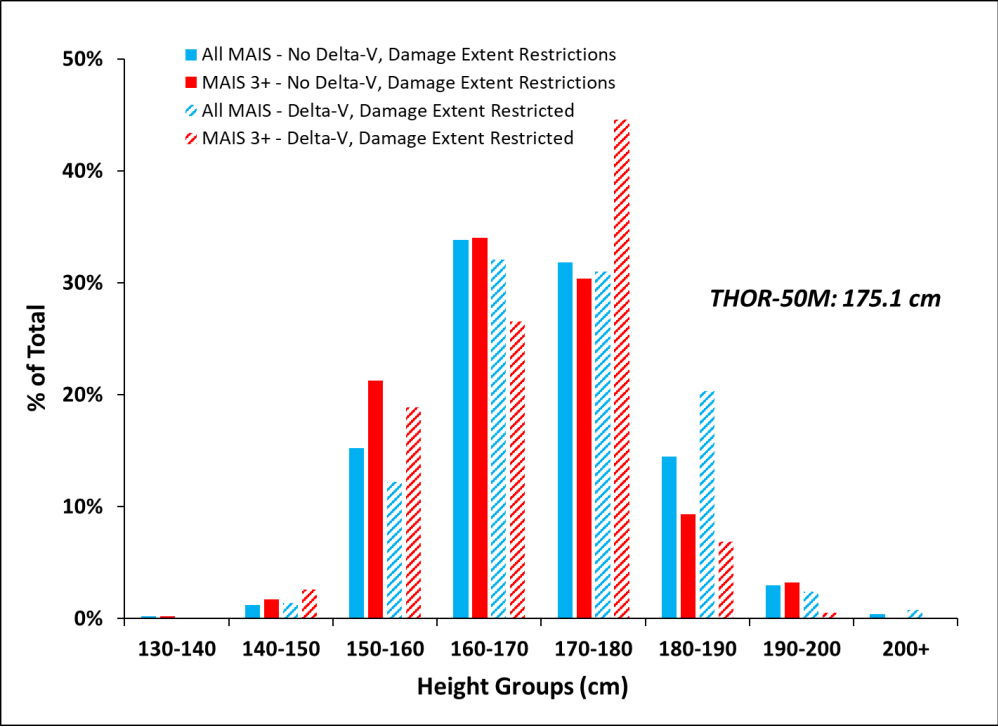


Figure H.7. Driver height in frontal crashes.

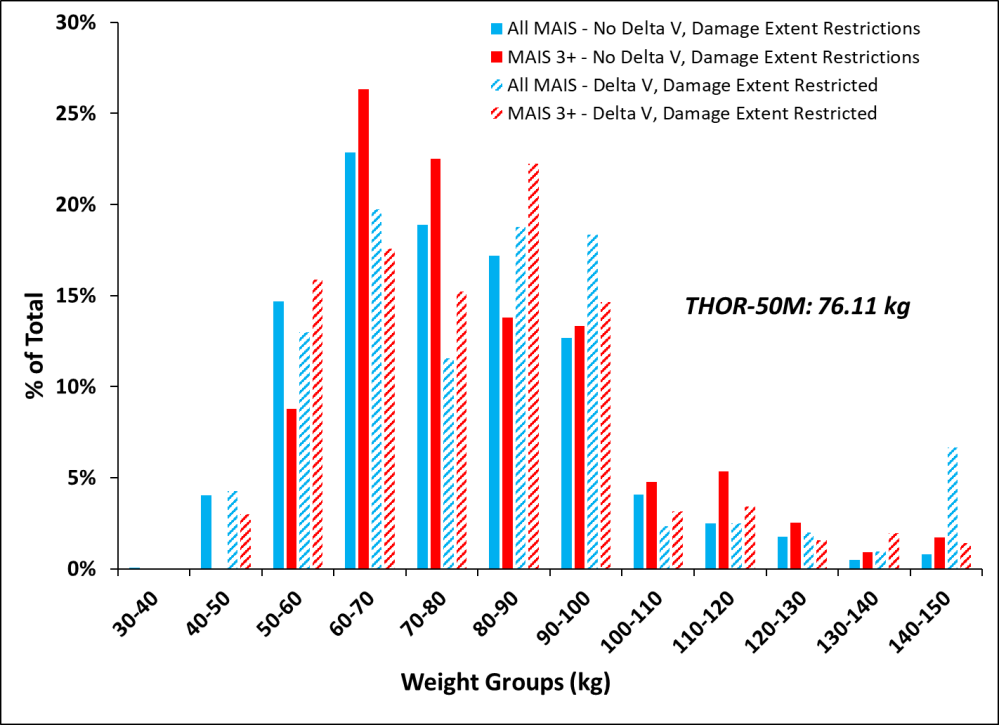


Figure H.8. Driver weight in frontal crashes.

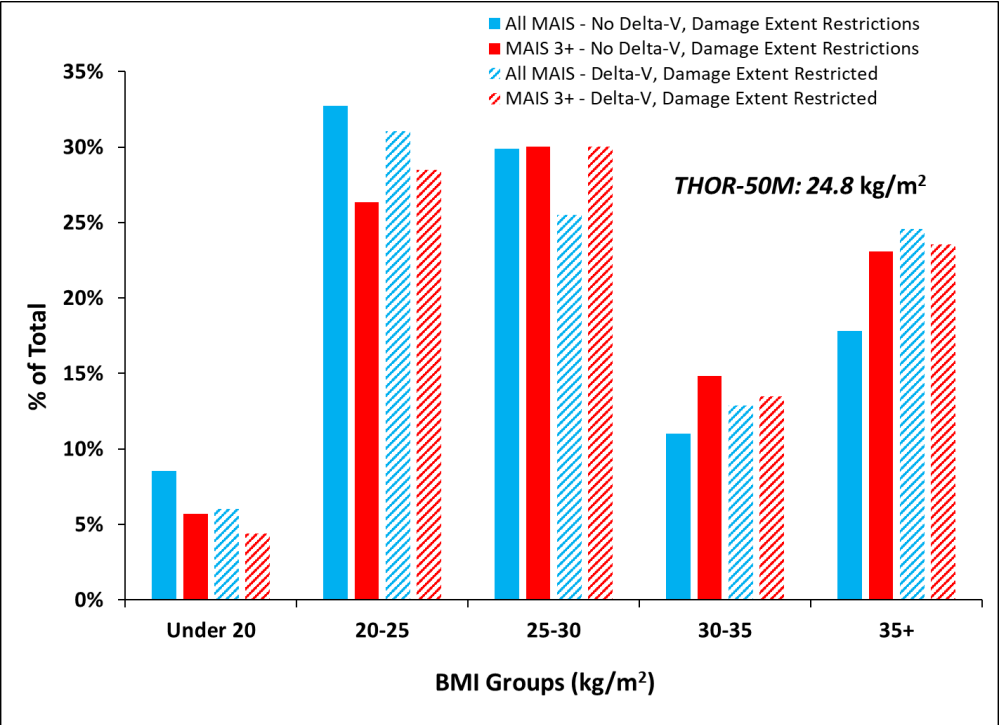


Figure H.9. Driver BMI in frontal crashes.

APPENDIX I. Knee/Femur Injury Criteria Source Data

NHTSA BioDB TSTNO	Subject Mass (kg)	Subject Stature (cm)	Subject Age (yr)	Sex	Peak Applied Force (kN)	MAIS	Censor Interval Lower	Censor Interval Upper	Reference
45	72.7	170.2	66	M	7.94	0	7.94	.	
45	72.7	170.2	66	M	8.68	0	8.68	.	
46	50	152.4	54	F	5.45	0	5.45	.	
46	50	152.4	54	F	4.25	0	4.25	.	
47	96.3	185.4	56	M	10.22	0	10.22	.	
47	96.3	185.4	56	M	10.4	0	10.4	.	
48	74	180.3	63	M	12.28	0	12.28	.	
48	74	180.3	63	M	11.67	0	11.67	.	
109	83.1	175.3	68	M	11	0	11	.	
109	83.1	175.3	68	M	10.37	0	10.37	.	
110	60	175.3	67	M	9.18	0	9.18	.	
110	60	175.3	67	M	8.18	0	8.18	.	
251	87.7	167.6	61	M	7.08	0	7.08	.	
251	87.7	167.6	61	M	6.86	0	6.86	.	
252	60.9	177.8	66	M	8.85	0	8.85	.	
252	60.9	177.8	66	M	7.63	0	7.63	.	
453	80.4	162.6	58	F	10.08	3	10.08	10.08	
453	80.4	162.6	58	F	9.27	3	9.27	9.27	Cheng et al. (1982)
249	60	170.2	21	M	9.35	0	9.35	.	
249	60	170.2	21	M	9.16	0	9.16	.	
250	56.3	167.6	65	M	6.31	0	6.31	.	
253	95.9	175.3	29	M	9.75	0	9.75	.	
253	95.9	175.3	29	M	10.97	0	10.97	.	
450	51.3	152.4	56	F	10.42	0	10.42	.	
450	51.3	152.4	56	F	5.94	0	5.94	.	
452	70.4	172.7	63	M	10.6	0	10.6	.	
452	70.4	172.7	63	M	7.86	0	7.86	.	
454	74.5	172.7	58	M	10.09	0	10.09	.	
454	74.5	172.7	58	M	12.25	0	12.25	.	
798	67.2	162.6	46	F	6.94	0	6.94	.	
799	80.9	175.3	60	M	9.08	0	9.08	.	
799	80.9	175.3	60	M	8.23	0	8.23	.	
800	52.2	175.3	63	M	8.21	0	8.21	.	
800	52.2	175.3	63	M	10.33	0	10.33	.	
1052	73.1	170.2	61	M	14.02	0	14.02	.	
1052	73.1	170.2	61	M	11.26	0	11.26	.	
875	57.2	165.1	60	F	8.55	3	8.55	8.55	
876	57.2	165.1	60	F	7.73	2	.	7.73	
879	59.5	170.2	70	F	9.4	3	9.4	9.4	
880	59.5	170.2	70	F	7.91	2	.	7.91	
883	68.1	175.3	69	M	11.39	3	11.39	.	
884	68.1	175.3	69	M	15.13	2	.	15.13	Donnelly and Roberts (1987)
887	72.7	175.3	61	M	17.18	2	17.18	.	
888	72.7	175.3	61	M	10.89	2	.	10.89	
902	68.6	170.2	71	M	9.33	0	9.33	9.33	
903	68.6	170.2	71	M	7.02	3	7.02	7.02	
906	84	175.3	66	M	18.66	2	.	18.66	
907	84	175.3	66	M	18.13	2	.	18.13	

NHTSA BioDB TSTNO	Subject Mass (kg)	Subject Stature (cm)	Subject Age (yr)	Sex	Peak Applied Force (kN)	MAIS	Censor Interval Lower	Censor Interval Upper	Reference
910	64	180.3	55	M	21.06	2	.	21.06	
911	64	180.3	55	M	19.68	3	19.68	19.68	
918	73.1	170.2	57	M	13.29	2	.	13.29	
919	73.1	170.2	57	M	14.06	2	.	14.06	
922	46.8	157.5	57	F	9.34	2	.	9.34	
923	46.8	157.5	57	F	8.99	3	8.99	8.99	
1055	79.5	182.9	62	M	10.01	3	10.01	10.01	
1056	79.5	182.9	62	M	14.19	3	14.19	14.19	
1099	86.3	172.7	66	M	11.6	3	11.6	11.6	
1100	86.3	172.7	66	M	11.88	3	11.88	11.88	
2284	40	160	34	M	1.26	0	1.26	.	
2284	40	160	34	M	2.97	0	2.97	.	
2285	60.9	165.1	60	M	2.41	0	2.41	.	
2285	60	165.1	60	M	6.09	0	6.09	.	
2286	49	162.6	57	M	3.3	0	3.3	.	
2286	49	162.6	57	M	7.15	0	7.15	.	
2288	51.8	162.6	63	M	6	0	6	.	
2288	51.8	162.6	63	M	6.91	0	6.91	.	
2289	55.9	165.1	68	M	7.28	0	7.28	.	
2289	55.9	165.1	68	M	8.09	0	8.09	.	
2290	51.8	154.9	42	F	2.28	0	2.28	.	
2290	51.8	154.9	42	F	3.16	0	3.16	.	
2291	64	165.1	42	M	5.68	0	5.68	.	
2291	64	165.1	42	M	7.45	0	7.45	.	Leung et al. 1983
2292	70.9	165.1	68	M	5.39	0	5.39	.	
2292	70.9	165.1	68	M	8.12	0	8.12	.	
2293	65.9	172.7	62	M	5.5	0	5.5	.	
2294	81.8	180.3	55	M	5.42	0	5.42	.	
2294	81.8	180.3	55	M	7.8	0	7.8	.	
2295	50	165.1	52	M	2.49	0	2.49	.	
2295	50	165.1	52	M	3.64	0	3.64	.	
2296	77.7	175.3	62	M	10.6	2	.	10.6	
2296	77.7	175.3	62	M	12.53	3	12.53	12.53	
2297	63.1	165.1	73	M	7.73	3	7.73	7.73	
2297	63.1	165.1	73	M	9.1	2	.	9.1	
2298	69	165.1	71	M	11.26	3	11.26	11.26	
2298	69	165.1	71	M	11.56	0	.	11.56	
2266	77.1	177.8	75	M	12.99	3	12.99	12.99	
2266	77.1	177.8	75	M	21.7	3	21.7	21.7	
2267	87	188	49	M	18.21	3	18.21	18.21	
2267	87	188	49	M	21.73	3	21.73	21.73	Melvin and Nusholtz 1980
2268	83	.	79	M	20.75	3	20.75	20.75	
2268	83	.	79	M	18.84	3	18.84	18.84	
2269	47.3	157.5	58	F	6.35	0	6.35	.	
2269	47.3	157.5	58	F	8.6	0	8.6	.	
1160	68.1	177.8	62	M	6.39	0	6.39	.	
1160	68.1	177.8	62	M	2.26	0	2.26	.	
1265	54.5	170.2	79	M	0.93	0	0.93	.	
1265	54.5	170.2	79	M	2.13	0	2.13	.	
1444	78.6	185.4	74	M	2.51	0	2.51	.	Morgan et al. (1987)
1444	78.6	185.4	74	M	2.7	0	2.70	.	
1445	77.2	172.7	68	M	3.25	0	3.25	.	
1445	77.2	172.7	68	M	2.69	0	2.69	.	
1789	70.4	177.8	75	M	3.22	0	3.22	.	

NHTSA BioDB TSTNO	Subject Mass (kg)	Subject Stature (cm)	Subject Age (yr)	Sex	Peak Applied Force (kN)	MAIS	Censor Interval Lower	Censor Interval Upper	Reference
1789	70.4	177.8	75	M	2.37	0	2.37	.	
1790	58.1	175.3	74	M	7.24	0	7.24	.	
1790	58.1	175.3	74	M	4.11	0	4.11	.	
1817	53.1	152.4	60	F	8.63	0	8.63	.	
1877	59	172.7	56	M	2.09	0	2.09	.	
1877	59	172.7	56	M	6.66	0	6.66	.	
1878	76.3	177.8	72	M	4.91	0	4.91	.	
1878	76.3	177.8	72	M	4.56	0	4.56	.	
1880	57.2	172.7	54	M	6.79	0	6.79	.	
1880	57.2	172.7	54	M	4.18	0	4.18	.	

APPENDIX J.THOR-50M Post-processing for Injury Criteria Calculation

Introduction

This appendix describes the step-by-step post-processing procedure for calculation of the injury assessment values and associated injury risk for the injury criteria described in this report.

At the end of the step-by-step post-processing procedure, two validation data sets are described – one for a frontal rigid barrier test and one for an oblique moving deformable barrier test. The raw data from these tests are available in the NHTSA Vehicle Crash Test Database. The intent of these validation data sets and published results is to confirm that consistent results can be achieved independent of post-processing software and/or data workflow.

THOR-50M Instrumentation List for Injury Criteria Calculation

The following channels represent a minimum set of measurement channels to calculate the injury criteria described in this document:

Channel Description	CFC	ISO-MME Code	NHTSA Database Codes				
			AXIS	DASTAT	SENATT	SENTYP	YUNITS
Head CG Accelerometer, X-axis (g)	1000	??HEAD0000THACXA	XL	AM	HDCG	AC	G'S
Head CG Accelerometer, Y-axis (g)	1000	??HEAD0000THACYA	YL	AM	HDCG	AC	G'S
Head CG Accelerometer, Z-axis (g)	1000	??HEAD0000THACZA	ZL	AM	HDCG	AC	G'S
Head CG Angular Velocity, X-axis (deg/s)	60	??HEAD0000THAVXD	XL	AM	HDCG	AV	DPS
Head CG Angular Velocity, Y-axis (deg/s)	60	??HEAD0000THAVYD	YL	AM	HDCG	AV	DPS
Head CG Angular Velocity, Z-axis (deg/s)	60	??HEAD0000THAVZD	ZL	AM	HDCG	AV	DPS
Upper Neck Force, Z-axis (N)	1000	??NECKUP000THFOZA	ZL	AM	NEKU	LC	NWT
Upper Neck Moment, Y-axis (Nm)	600	??NECKUP000THMOYB	YL	AM	NEKU	LC	NWM
Upper left IR-TRACC tube (V)	*	??CHSTLEUPTHVOOC	NA	AM	CHLU	DS	VOL
Upper left Y-axis rotational pot. (deg)	180	??CHSTLEUPTHANYC	YL	AM	CHLU	AD	DEG
Upper left Z-axis rotational pot. (deg)	180	??CHSTLEUPTHANZC	ZL	AM	CHLU	AD	DEG
Upper right IR-TRACC tube (V)	*	??CHSTRIUPTHVOOC	NA	AM	CHRU	DS	VOL
Upper right Y-axis rotational pot. (deg)	180	??CHSTRIUPTHANYC	YL	AM	CHRU	AD	DEG
Upper right Z-axis rotational pot. (deg)	180	??CHSTRIUPTHANZC	ZL	AM	CHRU	AD	DEG
Lower left IR-TRACC tube (V)	*	??CHSTLELOTHVOOC	NA	AM	CHLL	DS	VOL
Lower left Y-axis rotational pot. (deg)	180	??CHSTLELOTHANYC	YL	AM	CHLL	AD	DEG
Lower left Z-axis rotational pot. (deg)	180	??CHSTLELOTHANZC	ZL	AM	CHLL	AD	DEG
Lower right IR-TRACC tube (V)	*	??CHSTRILOTHVOOC	NA	AM	CHRL	DS	VOL
Lower right Y-axis rotational pot. (deg)	180	??CHSTRILOTHANYC	YL	AM	CHRL	AD	DEG
Lower right Z-axis rotational pot. (deg)	180	??CHSTRILOTHANZC	ZL	AM	CHRL	AD	DEG
Left abdomen IR-TRACC tube (V)	*	??ABDOLE000THVOOC	NA	AM	ABDL	DS	VOL
Left abdomen Y-axis rotational pot. (deg)	180	??ABDOLE000THANYC	YL	AM	ABDL	AD	DEG
Left abdomen Z-axis rotational pot. (deg)	180	??ABDOLE000THANZC	ZL	AM	ABDL	AD	DEG
Right abdomen IR-TRACC tube (V)	*	??ABDORIO00THVOOC	NA	AM	ABDR	DS	VOL
Right abdomen Y-axis rotational pot. (deg)	180	??ABDORIO00THANYC	YL	AM	ABDR	AD	DEG
Right abdomen Z-axis rotational pot. (deg)	180	??ABDORIO00THANZC	ZL	AM	ABDR	AD	DEG
Left Acetabulum Force, X-axis (N)	600	??ACTBLE000THFOX B	XL	AM	PVAL	LC	NWT
Left Acetabulum Force, Y-axis (N)	600	??ACTBLE000THFOY B	YL	AM	PVAL	LC	NWT
Left Acetabulum Force, Z-axis (N)	600	??ACTBLE000THFOZ B	ZL	AM	PVAL	LC	NWT
Right Acetabulum Force, X-axis (N)	600	??ACTBRI000THFOX B	XL	AM	PVAR	LC	NWT
Right Acetabulum Force, Y-axis (N)	600	??ACTBRI000THFOY B	YL	AM	PVAR	LC	NWT
Right Acetabulum Force, Z-axis (N)	600	??ACTBRI000THFOZ B	ZL	AM	PVAR	LC	NWT
Left Femur Axial Force, Z-axis	600	??FEMRLE000THFOZ B	ZL	AM	FMRL	LC	NWT
Right Femur Axial Force, Z-axis	600	??FEMRRI000THFOZ B	ZL	AM	FMRR	LC	NWT
Left Upper Tibia Axial Force, Z-axis (N)	600	??TIBILEUPHFOZ B	ZL	AM	TBLU	LC	NWT
Right Upper Tibia Axial Force, Z-axis (N)	600	??TIBIRIUPHFOZ B	ZL	AM	TBRU	LC	NWT
Left Lower Tibia Axial Force, Z-axis (N)	600	??TIBILELOTHFOZ B	ZL	AM	TBLL	LC	NWT
Right Lower Tibia Axial Force, Z-axis (N)	600	??TIBIRILOTHFOZ B	ZL	AM	TBRL	LC	NWT
Left Upper Tibia Moment, X-axis (Nm)	600	??TIBILEUPHMOX B	XL	AM	TBLU	LC	NWM
Left Upper Tibia Moment, Y-axis (Nm)	600	??TIBILEUPHMOY B	YL	AM	TBLU	LC	NWM
Right Upper Tibia Moment, X-axis (Nm)	600	??TIBIRIUPHMOX B	XL	AM	TBRU	LC	NWM
Right Upper Tibia Moment, Y-axis (Nm)	600	??TIBIRIUPHMOY B	YL	AM	TBRU	LC	NWM
Left Lower Tibia Moment, X-axis (Nm)	600	??TIBILELOTHMOX B	XL	AM	TBLL	LC	NWM
Left Lower Tibia Moment, Y-axis (Nm)	600	??TIBILELOTHMOY B	YL	AM	TBLL	LC	NWM
Right Lower Tibia Moment, X-axis (Nm)	600	??TIBIRILOTHMOX B	XL	AM	TBRL	LC	NWM
Right Lower Tibia Moment, Y-axis (Nm)	600	??TIBIRILOTHMOY B	YL	AM	TBRL	LC	NWM

THOR-50M Instrumentation List – Additional Channels

While not necessary for injury criteria calculation, the following channels may also be available:

Channel Description	CFC	ISO-MME Code	NHTSA Database Codes				
			AXIS	DASTAT	SENATT	SENTYP	YUNITS
Upper Neck Force, X-axis (N)	1000	??NECKUP00THFOXA	XL	AM	NEKU	LC	NWT
Upper Neck Force, Y-axis (N)	1000	??NECKUP00THFOYA	YL	AM	NEKU	LC	NWT
Upper Neck Moment, X-axis (Nm)	600	??NECKUP00THMOXB	XL	AM	NEKU	LC	NWM
Upper Neck Moment, Z-axis (Nm)	600	??NECKUP00THMOZB	ZL	AM	NEKU	LC	NWM
Neck Cable Force, Anterior (N)	1000	??NECKFR00THFOZA	ZL	AM	NKCA	LC	NWT
Neck Cable Force, Posterior (N)	1000	??NECKRE00THFOZA	ZL	AM	NKCP	LC	NWT
Head/Neck Angle, Y-axis (deg)	180	??NECKUP00THANYB	YL	AM	NKOC	AD	DEG
Lower Neck Force, X-axis (N)	1000	??NECKLO00THFOXA	XL	AM	NEKL	LC	NWT
Lower Neck Force, Y-axis (N)	1000	??NECKLO00THFOYA	YL	AM	NEKL	LC	NWT
Lower Neck Force, Z-axis (N)	1000	??NECKLO00THFOZA	ZL	AM	NEKL	LC	NWT
Lower Neck Moment, X-axis (Nm)	600	??NECKLO00THMOXA	XL	AM	NEKL	LC	NWM
Lower Neck Moment, Y-axis (Nm)	600	??NECKLO00THMOYA	YL	AM	NEKL	LC	NWM
Lower Neck Moment, Z-axis (Nm)	600	??NECKLO00THMOZA	ZL	AM	NEKL	LC	NWM
Upper Thoracic Spine Accel, X-axis (g)	180	??THSP0100THACXA	XL	AM	SPNU	AC	G'S
Upper Thoracic Spine Accel, Y-axis (g)	180	??THSP0100THACYA	YL	AM	SPNU	AC	G'S
Upper Thoracic Spine Accel, Z-axis (g)	180	??THSP0100THACZA	ZL	AM	SPNU	AC	G'S
Chest C.G. Accelerometer, X-axis (g)	180	??THSP0400THACXA	XL	AM	SPNM	AC	G'S
Chest C.G. Accelerometer, Y-axis (g)	180	??THSP0400THACYA	YL	AM	SPNM	AC	G'S
Chest C.G. Accelerometer, Z-axis (g)	180	??THSP0400THACZA	ZL	AM	SPNM	AC	G'S
Sternum Accelerometer, X-axis (g)	1000	??STRN0000THACXA	XL	AM	CHST	AC	G'S
Lower Thoracic Spine Accel, X-axis (g)	180	??THSP1200THACXA	XL	AM	SPNL	AC	G'S
Lower Thoracic Spine Accel, Y-axis (g)	180	??THSP1200THACYA	YL	AM	SPNL	AC	G'S
Lower Thoracic Spine Accel, Z-axis (g)	180	??THSP1200THACZA	ZL	AM	SPNL	AC	G'S
Lower Thoracic Spine Force, X-axis (N)	600	??THSP1200THFOXA	XL	AM	SPNL	LC	NWT
Lower Thoracic Spine Force, Y-axis (N)	600	??THSP1200THFOYA	YL	AM	SPNL	LC	NWT
Lower Thoracic Spine Force, Z-axis (N)	600	??THSP1200THFOZA	ZL	AM	SPNL	LC	NWT
Lower Thoracic Spine Moment, X-axis (Nm)	600	??THSP1200THMOXA	XL	AM	SPNL	LC	NWT
Lower Thoracic Spine Moment, Y-axis (Nm)	600	??THSP1200THMOYA	YL	AM	SPNL	LC	NWT
Left ASIS Force, X-axis (N)	600	??ILACLE00THFOXA	XL	AM	PILL	LC	NWT
Left ASIS Moment, Y-axis (Nm)	600	??ILACLE00THMOYA	YL	AM	PILL	LC	NWM
Right ASIS Force, X-axis (N)	600	??ILACRI00THFOXA	XL	AM	PILR	LC	NWT
Right ASIS Moment, Y-axis (Nm)	600	??ILACRI00THMOYA	YL	AM	PILR	LC	NWM
Pelvis Accelerometer, X-axis (g)	1000	??PELV0000THACXA	XL	AM	PVCN	AC	G'S
Pelvis Accelerometer, Y-axis (g)	1000	??PELV0000THACYA	YL	AM	PVCN	AC	G'S
Pelvis Accelerometer, Z-axis (g)	1000	??PELV0000THACZA	ZL	AM	PVCN	AC	G'S
Left Femur Force, X-axis (N)	600	??FEMRLE00THFOXB	XL	AM	FMRL	LC	NWT
Left Femur Force, Y-axis (N)	600	??FEMRLE00THFOYB	YL	AM	FMRL	LC	NWT
Left Femur Moment, X-axis (Nm)	600	??FEMRLE00THMOXB	XL	AM	FMRL	LC	NWM
Left Femur Moment, Y-axis (Nm)	600	??FEMRLE00THMOYB	YL	AM	FMRL	LC	NWM
Left Femur Moment, Z-axis (Nm)	600	??FEMRLE00THMOZB	ZL	AM	FMRL	LC	NWM
Right Femur Force, X-axis (N)	600	??FEMRRI00THFOXB	XL	AM	FMRR	LC	NWT
Right Femur Force, Y-axis (N)	600	??FEMRRI00THFOYB	YL	AM	FMRR	LC	NWT
Right Femur Moment, X-axis (Nm)	600	??FEMRRI00THMOXB	XL	AM	FMRR	LC	NWM
Right Femur Moment, Y-axis (Nm)	600	??FEMRRI00THMOYB	YL	AM	FMRR	LC	NWM
Right Femur Moment, Z-axis (Nm)	600	??FEMRRI00THMOZB	ZL	AM	FMRR	LC	NWM

Channel Description	CFC	ISO-MME Code	NHTSA Database Codes				
			AXIS	DASTAT	SENATT	SENTYP	YUNITS
Left Knee Slider, X-axis (mm)	180	??KNSLLE00THDSXB	XL	AM	KNEL	DS	MM
Right Knee Slider, X-axis (mm)	180	??KNSLRI00THDSXB	XL	AM	KNER	DS	MM
Left Upper Tibia Force, X-axis (N)	600	??TIBILEUPTHFOXB	XL	AM	TBLU	LC	NWT
Left Upper Tibia Force, Y-axis (N)	600	??TIBILEUPTHFOYB	YL	AM	TBLU	LC	NWT
Right Upper Tibia Force, X-axis (N)	600	??TIBIRIUPTHFOXB	XL	AM	TBRU	LC	NWT
Right Upper Tibia Force, Y-axis (N)	600	??TIBIRIUPTHFOYB	YL	AM	TBRU	LC	NWT
Left Lower Tibia Force, X-axis (N)	600	??TIBILELOTHFOXB	XL	AM	TBLL	LC	NWT
Left Lower Tibia Force, Y-axis (N)	600	??TIBILELOTHFOYB	YL	AM	TBLL	LC	NWT
Right Lower Tibia Force, X-axis (N)	600	??TIBIRILOTHFOXB	XL	AM	TBRL	LC	NWT
Right Lower Tibia Force, Y-axis (N)	600	??TIBIRILOTHFOYB	YL	AM	TBRL	LC	NWT
Left Tibia Accelerometer, X-axis (g)	1000	??TIBILE00THACXA	XL	AM	TIBL	AC	G'S
Left Tibia Accelerometer, Y-axis (g)	1000	??TIBILE00THACYA	YL	AM	TIBL	AC	G'S
Right Tibia Accelerometer, X-axis (g)	1000	??TIBIRI00THACXA	XL	AM	TIBR	AC	G'S
Right Tibia Accelerometer, Y-axis (g)	1000	??TIBIRI00THACYA	YL	AM	TIBR	AC	G'S
Left Achilles Force, Z-axis (N)	600	??ANKLLE00THFOZB	ZL	AM	ANKL	LC	NWT
Right Achilles Force, Z-axis (N)	600	??ANKLRI00THFOZB	ZL	AM	ANKR	LC	NWT
Left Ankle Rotation, X-axis (deg)	180	??ANKLLE00THANXB	XL	AM	ANKL	AD	DEG
Left Ankle Rotation, Y-axis (deg)	180	??ANKLLE00THANYB	YL	AM	ANKL	AD	DEG
Left Ankle Rotation, Z-axis (deg)	180	??ANKLLE00THANZB	ZL	AM	ANKL	AD	DEG
Right Ankle Rotation, X-axis (deg)	180	??ANKLRI00THANXB	XL	AM	ANKR	AD	DEG
Right Ankle Rotation, Y-axis (deg)	180	??ANKLRI00THANYB	YL	AM	ANKR	AD	DEG
Right Ankle Rotation, Z-axis (deg)	180	??ANKLRI00THANZB	ZL	AM	ANKR	AD	DEG
Left Foot Accelerometer, X-axis (g)	1000	??FOOTLE00THACXA	XL	AM	FOTL	AC	G'S
Left Foot Accelerometer, Y-axis (g)	1000	??FOOTLE00THACYA	YL	AM	FOTL	AC	G'S
Left Foot Accelerometer, Z-axis (g)	1000	??FOOTLE00THACZA	ZL	AM	FOTL	AC	G'S
Right Foot Accelerometer, X-axis (g)	1000	??FOOTRI00THACXA	XL	AM	FOTR	AC	G'S
Right Foot Accelerometer, Y-axis (g)	1000	??FOOTRI00THACYA	YL	AM	FOTR	AC	G'S
Right Foot Accelerometer, Z-axis (g)	1000	??FOOTRI00THACZA	ZL	AM	FOTR	AC	G'S

1. HEAD

1.1. HIC₁₅

Required channels:

Channel Description	var	CFC	ISO-MME Code	NHTSA Database Codes				
				AXIS	DASTAT	SENATT	SENTYP	YUNITS
Head CG Accelerometer, X-axis (g)	$a_x(t)$	1000	??HEAD0000THACXA	XL	AM	HDCG	AC	G'S
Head CG Accelerometer, Y-axis (g)	$a_y(t)$	1000	??HEAD0000THACYA	YL	AM	HDCG	AC	G'S
Head CG Accelerometer, Z-axis (g)	$a_z(t)$	1000	??HEAD0000THACZA	ZL	AM	HDCG	AC	G'S
Head CG Resultant Acceleration (g)	$a_r(t)$	N/A	??HEAD0000THACRA	RS	CM	HDCG	PP	G'S

- 1.1.1. Record the “as measured” (DASTAT = AM) channels in the table above during a crash test or impact event.
- 1.1.2. Remove data channel offset per SAE J211-1 Section 8.4.3¹
- 1.1.3. Filter channels based on the CFC filter classes in the “CFC” column above.
- 1.1.4. Calculate Head CG Resultant Acceleration and record time-history. For NHTSA database submissions, include this channel in Entrée data.

$$a_r(t) = \sqrt{a_x(t)^2 + a_y(t)^2 + a_z(t)^2}$$

- 1.1.5. Evaluate the expression below over the entire resultant acceleration time-history. Record the value of HIC_{15} as well as the beginning of the calculation window (t_1) and the end of the calculation window (t_2). This calculation can be carried out using NHTSA Signal Analysis Software² or equivalent.

$$HIC_{15} = \left| (t_2 - t_1) \left[\frac{1}{t_2 - t_1} \int_{t_1}^{t_2} a_r(t) dt \right] \right|_{max}^{2.5} ; \quad t_2 - t_1 \leq 15 \text{ ms}$$

- 1.1.6. Calculate the probability of AIS 2+ or AIS 3+ injury using the equations below, where Φ is the cumulative distribution function of the standard normal distribution:

¹ For the purposes of this calculation, data channel offset was removed by subtracting the average value of the individual channel data in the range between the first recorded data point and time = 0 milliseconds.

² <https://www.nhtsa.gov/databases-and-software/signal-analysis-software-windows>

$$p(\text{AIS } 2+) = \Phi \left[\frac{\ln HIC_{15} - 6.96362}{0.84687} \right]$$

$$p(\text{AIS } 3+) = \Phi \left[\frac{\ln HIC_{15} - 7.45231}{0.73998} \right]$$

1.2. BrIC

Required channels:

Channel Description	var	CFC	ISO-MME Code	NHTSA Database Codes				
				AXIS	DASTAT	SENATT	SENTYP	YUNITS
Head CG Angular Velocity, X-axis (deg/s)	$\omega_x(t)$	60	??HEAD0000THAVXD	XL	AM	HDCG	AV	DPS
Head CG Angular Velocity, Y-axis (deg/s)	$\omega_y(t)$	60	??HEAD0000THAVYD	YL	AM	HDCG	AV	DPS
Head CG Angular Velocity, Z-axis (deg/s)	$\omega_z(t)$	60	??HEAD0000THAVZD	ZL	AM	HDCG	AV	DPS

- 1.2.1. Record the “as measured” (DASTAT = AM) channels in the table above during a crash test or impact event.
- 1.2.2. Remove data channel offset per SAE J211-1 Section 8.4.3
- 1.2.3. Filter channels based on the CFC filter classes in the “CFC” column above.
- 1.2.4. Evaluate the expression below by calculating the maximum absolute value of each axis of angular velocity independently, dividing by the respective critical value, and calculating the square root of the sum of the squares:

$$BrIC = \sqrt{\left(\frac{\max(|\omega_x(t)|)}{\omega_{xC}}\right)^2 + \left(\frac{\max(|\omega_y(t)|)}{\omega_{yC}}\right)^2 + \left(\frac{\max(|\omega_z(t)|)}{\omega_{zC}}\right)^2}$$

where

$$\omega_{xC} = 3,796 \text{ deg/s (66.25 rad/s)}$$

$$\omega_{yC} = 3,234 \text{ deg/s (56.45 rad/s)}$$

$$\omega_{zC} = 2,456 \text{ deg/s (42.87 rad/s)}$$

- 1.2.5. Calculate the probability of AIS 3+ or AIS 4+ injury using the equations below:

$$p(\text{AIS } 3+) = 1 - e^{-\left(\frac{BrIC - 0.523}{0.531}\right)^{1.8}}$$

$$p(\text{AIS } 4+) = 1 - e^{-\left(\frac{BrIC - 0.523}{0.647}\right)^{1.8}}$$

2. NECK

2.1. Nij

Required channels:

Channel Description	var	CFC	ISO-MME Code	NHTSA Database Codes				
				AXIS	DASTAT	SENATT	SENTYP	YUNITS
Upper Neck Force, Z-axis (N)	$F_z(t)$	600	??NECKUP00THFOZA	ZL	AM	NEKU	LC	NWT
Upper Neck Moment, Y-axis (Nm)	$M_y(t)$	600	??NECKUP00THMOYB	YL	AM	NEKU	LC	NWM

- 2.1.1. Record the “as measured” (DASTAT = AM) channels in the table above during a crash test or impact event.
- 2.1.2. Remove data channel offset per SAE J211-1 Section 8.4.3
- 2.1.3. Filter channels based on the CFC filter classes in the “CFC” column above. Note that when used in calculation of N_{ij} , filter Upper Neck Z-axis force at CFC 600.
- 2.1.4. Calculate the four components of N_{ij} as described below.

Component	Description	Equation
TF	Tension and Flexion	$N_{TF}(t) = \begin{cases} \frac{F_z(t)}{4,200} + \frac{M_y(t)}{60} & \text{if } F_z(t) > 0 \text{ and } M_y(t) > 0 \\ 0 & \text{otherwise} \end{cases}$
TE	Tension and Extension	$N_{TE}(t) = \begin{cases} \frac{F_z(t)}{4,200} + \frac{M_y(t)}{-79.2} & \text{if } F_z(t) > 0 \text{ and } M_y(t) < 0 \\ 0 & \text{otherwise} \end{cases}$
CF	Compression and Flexion	$N_{CF}(t) = \begin{cases} \frac{F_z(t)}{-4,520} + \frac{M_y(t)}{60} & \text{if } F_z(t) < 0 \text{ and } M_y(t) > 0 \\ 0 & \text{otherwise} \end{cases}$
CE	Compression and Extension	$N_{CE}(t) = \begin{cases} \frac{F_z(t)}{-4,520} + \frac{M_y(t)}{-79.2} & \text{if } F_z(t) < 0 \text{ and } M_y(t) < 0 \\ 0 & \text{otherwise} \end{cases}$

- 2.1.5. Evaluate the expression below to determine the maximum value of N_{ij} :

$$N_{ij} = \max[N_{TF}(t) + N_{TE}(t) + N_{CF}(t) + N_{CE}(t)]$$

- 2.1.6. Calculate the probability of AIS 2+ or AIS 3+ injury using the equations below:

$$p(\text{AIS } 2+) = \frac{1}{1 + e^{(5.819 - 5.681N_{ij})}}$$

$$p(\text{AIS } 3+) = \frac{1}{1 + e^{(6.047 - 5.44N_{ij})}}$$

3. CHEST

3.1. Peak Resultant Chest Deflection

Required channels:

Channel Description	var	CFC	ISO-MME Code	NHTSA Database Codes				
				AXIS	DASTAT	SENATT	SENTYP	YUNITS
Upper left IR-TRACC tube (V)	$V_{IR}(t)$	180*	??CHSTLEUPHVO0C	NA	AM	CHLU	DS	VOL
Upper left Y-axis rotational pot. (deg)	$\theta_Y(t)$	180	??CHSTLEUPHANYC	YL	AM	CHLU	AD	DEG
Upper left Z-axis rotational pot. (deg)	$\theta_Z(t)$	180	??CHSTLEUPHANZC	ZL	AM	CHLU	AD	DEG
Upper right IR-TRACC tube (V)	$V_{IR}(t)$	180*	??CHSTRIUPHVO0C	NA	AM	CHRU	DS	VOL
Upper right Y-axis rotational pot. (deg)	$\theta_Y(t)$	180	??CHSTRIUPHANYC	YL	AM	CHRU	AD	DEG
Upper right Z-axis rotational pot. (deg)	$\theta_Z(t)$	180	??CHSTRIUPHANZC	ZL	AM	CHRU	AD	DEG
Lower left IR-TRACC tube (V)	$V_{IR}(t)$	180*	??CHSTLELOTHVO0C	NA	AM	CHLL	DS	VOL
Lower left Y-axis rotational pot. (deg)	$\theta_Y(t)$	180	??CHSTLELOTHANYC	YL	AM	CHLL	AD	DEG
Lower left Z-axis rotational pot. (deg)	$\theta_Z(t)$	180	??CHSTLELOTHANZC	ZL	AM	CHLL	AD	DEG
Lower right IR-TRACC tube (V)	$V_{IR}(t)$	180*	??CHSTRILOTHVO0C	NA	AM	CHRL	DS	VOL
Lower right Y-axis rotational pot. (deg)	$\theta_Y(t)$	180	??CHSTRILOTHANYC	YL	AM	CHRL	AD	DEG
Lower right Z-axis rotational pot. (deg)	$\theta_Z(t)$	180	??CHSTRILOTHANZC	ZL	AM	CHRL	AD	DEG
Upper left X-axis deflection (mm)	$X_{rel}(t)$	N/A	??CHSTLEUPHDSXC	XL	CM	CHLU	PP	MM
Upper left Y-axis deflection (mm)	$Y_{rel}(t)$	N/A	??CHSTLEUPHDSYC	YL	CM	CHLU	PP	MM
Upper left Z-axis deflection (mm)	$Z_{rel}(t)$	N/A	??CHSTLEUPHDSZC	ZL	CM	CHLU	PP	MM
Upper right X-axis deflection (mm)	$X_{rel}(t)$	N/A	??CHSTRIUPHDSXC	XL	CM	CHRU	PP	MM
Upper right Y-axis deflection (mm)	$Y_{rel}(t)$	N/A	??CHSTRIUPHDSYC	YL	CM	CHRU	PP	MM
Upper right Z-axis deflection (mm)	$Z_{rel}(t)$	N/A	??CHSTRIUPHDSZC	ZL	CM	CHRU	PP	MM
Lower left X-axis deflection (mm)	$X_{rel}(t)$	N/A	??CHSTLELOTHDSXC	XL	CM	CHLL	PP	MM
Lower left Y-axis deflection (mm)	$Y_{rel}(t)$	N/A	??CHSTLELOTHDSYC	YL	CM	CHLL	PP	MM
Lower left Z-axis deflection (mm)	$Z_{rel}(t)$	N/A	??CHSTLELOTHDSZC	ZL	CM	CHLL	PP	MM
Lower right X-axis deflection (mm)	$X_{rel}(t)$	N/A	??CHSTRILOTHDSXC	XL	CM	CHRL	PP	MM
Lower right Y-axis deflection (mm)	$Y_{rel}(t)$	N/A	??CHSTRILOTHDSYC	YL	CM	CHRL	PP	MM
Lower right Z-axis deflection (mm)	$Z_{rel}(t)$	N/A	??CHSTRILOTHDSZC	ZL	CM	CHRL	PP	MM

* Filter IR-TRACC data after linearization

- 3.1.1. Record the “as measured” (DASTAT = AM) channels in the table above during a crash test or impact event.
- 3.1.2. Confirm the polarity of the IR-TRACC and rotational potentiometer channels using the procedure described in the THOR-50M PADI, Section 15.5.1: IR-TRACC Polarity. *Note that as installed, the IR-TRACC polarity will not necessarily correspond to SAE J211 polarity.* Invert any channels that show opposite results from the expected output.
- 3.1.3. Remove data channel offset, but do not zero the IR-TRACC and rotational potentiometer channels; per SAE J211 Section 8.4.3, bring the normalized value of a stable pre-test section of data to the *proper initial value* for the transducer.

- 3.1.4. Filter channels based on the CFC filter classes in the “CFC” column above. Do not filter the raw IR-TRACC voltage, as this will be filtered after it is linearized and scaled in the next step.
- 3.1.5. For each of the four quadrants (upper left, upper right, lower left, lower right), linearize and scale the measured IR-TRACC voltage using the equations below and the variable values provided on the IR-TRACC Calibration Summary (see THOR-50M PADI, Section 16: IR-TRACC Calibration Overview for more details).

$$D_{abs}(t) = [V_{IR}(t)]^{LE} IR_{sens} + I_{abs}$$

where

- $D_{abs}(t)$ = Absolute position time-history of the anterior attachment point of the IR-TRACC tube relative to the attachment origin at the Z-axis rotational potentiometer [mm]
- $V_{IR}(t)$ = Measured voltage time-history of IR-TRACC tube [Volts]
- LE = *Linearization exponent
- IR_{sens} = *IR-TRACC sensitivity [mm/V]
- I_{abs} = *IR-TRACC intercept [mm]
- *obtain values from IR-TRACC Calibration Summary for each quadrant

- 3.1.6. Filter linearized IR-TRACC deflection at CFC 180.
- 3.1.7. Calculate the absolute position time-history of the anterior attachment point in the x, y, and z axes using the equations below:

Upper Left:

$$X_{abs}(t) = D_{abs}(t)\cos(\theta_Z(t) + I_Z)\cos(\theta_Y(t) + I_Y) + 15.5\sin(\theta_Y(t) + I_Y)$$

$$Y_{abs}(t) = -D_{abs}(t)\sin(\theta_Z(t) + I_Z)$$

$$Z_{abs}(t) = -D_{abs}(t)\cos(\theta_Z(t) + I_Z)\sin(\theta_Y(t) + I_Y) + 15.5\cos(\theta_Y(t) + I_Y)$$

Upper Right:

$$X_{abs}(t) = D_{abs}(t)\cos(\theta_Z(t) + I_Z)\cos(\theta_Y(t) + I_Y) - 15.5\sin(\theta_Y(t) + I_Y)$$

$$Y_{abs}(t) = -D_{abs}(t)\sin(\theta_Z(t) + I_Z)$$

$$Z_{abs}(t) = D_{abs}(t)\cos(\theta_Z(t) + I_Z)\sin(\theta_Y(t) + I_Y) + 15.5\cos(\theta_Y(t) + I_Y)$$

Lower Left:

$$X_{abs}(t) = D_{abs}(t)\cos(\theta_Z(t) + I_Z)\cos(\theta_Y(t) + I_Y) - 15.5\sin(\theta_Y(t) + I_Y)$$

$$Y_{abs}(t) = D_{abs}(t)\sin(\theta_Z(t) + I_Z)$$

$$Z_{abs}(t) = -D_{abs}(t)\cos(\theta_Z(t) + I_Z)\sin(\theta_Y(t) + I_Y) - 15.5\cos(\theta_Y(t) + I_Y)$$

Lower Right:

$$X_{abs}(t) = D_{abs}(t)\cos(\theta_Z(t) + I_Z)\cos(\theta_Y(t) + I_Y) + 15.5\sin(\theta_Y(t) + I_Y)$$

$$Y_{abs}(t) = D_{abs}(t)\sin(\theta_Z(t) + I_Z)$$

$$Z_{abs}(t) = D_{abs}(t)\cos(\theta_Z(t) + I_Z)\sin(\theta_Y(t) + I_Y) - 15.5\cos(\theta_Y(t) + I_Y)$$

where

- $D_{abs}(t)$ = See Step 3.1.5
- $[X|Y|Z]_{abs}(t)$ = X-, Y-, and Z-axis components of the absolute position time-history of the anterior attachment point of the IR-TRACC assemblies in the local spine coordinate system [mm]
- $\theta_Y(t)$ = Measured angle time-history of Y-axis rotational potentiometer [deg]
- $\theta_Z(t)$ = Measured angle time-history of Z-axis rotational potentiometer [deg]
- I_Y = *Y-axis rotational potentiometer intercept [deg]
- I_Z = *Z-axis rotational potentiometer intercept [deg]
- *obtain values from IR-TRACC Calibration Summary for each quadrant

- 3.1.8. Calculate the relative position time-history of the anterior attachment point of the IR-TRACC assemblies for all three axes of all four quadrants. For NHTSA database submissions, include these channels in Entrée data.

$$[X|Y|Z]_{rel}(t) = [X|Y|Z]_{abs}(t) - [X|Y|Z]_{abs}(0)$$

- 3.1.9. Calculate the peak resultant deflection for all four quadrants:

$$[UL|UR|LL|LR]_{max} = \max \left[\sqrt{X_{rel}(t)^2 + Y_{rel}(t)^2 + Z_{rel}(t)^2} \right]$$

- 3.1.10. Calculate the overall peak resultant deflection:

$$R_{max} = \max[UL_{max}, UR_{max}, LL_{max}, LR_{max}]$$

- 3.1.11. Calculate the probability of AIS 3+ injury, assuming an age of 40 years:

$$p(\text{AIS } 3+) = 1 - e^{-\left(\frac{R_{max}}{58.183}\right)^{2.977}}$$

4. ABDOMEN

4.1. Peak Abdomen Compression

Required channels:

Channel Description	var	CFC	ISO-MME Code	NHTSA Database Codes				
				AXIS	DASTAT	SENATT	SENTYP	YUNITS
Left abdomen IR-TRACC tube (V)	$V_{IR}(t)$	180*	??ABDOLE00THVOOC	NA	AM	ABDL	DS	VOL
Left abdomen Y-axis rotational pot. (deg)	$\theta_Y(t)$	180	??ABDOLE00THANYC	YL	AM	ABDL	AD	DEG
Left abdomen Z-axis rotational pot. (deg)	$\theta_Z(t)$	180	??ABDOLE00THANZC	ZL	AM	ABDL	AD	DEG
Right abdomen IR-TRACC tube (V)	$V_{IR}(t)$	180*	??ABDORIO0THVOOC	NA	AM	ABDR	DS	VOL
Right abdomen Y-axis rotational pot. (deg)	$\theta_Y(t)$	180	??ABDORIO0THANYC	YL	AM	ABDR	AD	DEG
Right abdomen Z-axis rotational pot. (deg)	$\theta_Z(t)$	180	??ABDORIO0THANZC	ZL	AM	ABDR	AD	DEG
Left abdomen X-axis deflection (mm)	$X_{rel}(t)$	N/A	??ABDOLE00THDSXC	XL	CM	ABDL	PP	MM
Right abdomen X-axis deflection (mm)	$X_{rel}(t)$	N/A	??ABDORIO0THDSXC	XL	CM	ABDR	PP	MM

* Filter IR-TRACC data after linearization

- 4.1.1. Record the “as measured” (DASTAT = AM) channels in the table above during a crash test or impact event.
- 4.1.2. Confirm the polarity of the IR-TRACC and rotational potentiometer channels using the procedure described in the THOR-50M PADI, Section 15.5.1: IR-TRACC Polarity. *Note that as installed, the IR-TRACC polarity will not correspond to SAE J211 polarity.* Invert any channels that show opposite results from the expected output.
- 4.1.3. Remove data channel offset, but do not zero the IR-TRACC and rotational potentiometer channels; per SAE J211 Section 8.4.3, bring the normalized value of a stable pre-test section of data to the *proper initial value* for the transducer.
- 4.1.4. Filter channels based on the CFC filter classes in the “CFC” column above. Do not filter the raw IR-TRACC voltage, as this will be filtered after it is linearized and scaled in the next step.
- 4.1.5. For each of the two sides (left, right), linearize and scale the measured IR-TRACC voltage using the equations below and the variable values provided on the IR-TRACC Calibration Summary (see THOR-50M PADI, Section 16: IR-TRACC Calibration Overview for more details).

$$D_{abs}(t) = [V_{IR}(t)]^{LE} IR_{sens} + I_{abs}$$

where

- $D_{abs}(t)$ = Absolute position time-history of the anterior attachment point of the IR-TRACC tube relative to the attachment origin at the Z-axis rotational potentiometer [mm]
 - $V_{IR}(t)$ = Measured voltage time-history of IR-TRACC tube [Volts]
 - LE = *Linearization exponent
 - IR_{sens} = *IR-TRACC sensitivity [mm/V]
 - I_{abs} = *IR-TRACC intercept [mm]
- *obtain values from IR-TRACC Calibration Summary for each quadrant

4.1.6. Filter linearized IR-TRACC deflection at CFC 180.

4.1.7. Calculate the absolute position time-history of the anterior attachment point in the X, Y, and Z axes using the equations below for both sides:

$$X_{abs}(t) = D_{abs}(t)\cos(\theta_z(t) + I_z)\cos(\theta_y(t) + I_y)$$

where

- $D_{abs}(t)$ = See Step 4.1.5
 - $X_{abs}(t)$ = X-axis component of the absolute position time-history of the anterior attachment point of the IR-TRACC assemblies in the local spine coordinate system [mm]
 - $\theta_y(t)$ = Measured angle time-history of Y-axis rotational potentiometer [deg]
 - $\theta_z(t)$ = Measured angle time-history of Z-axis rotational potentiometer [deg]
 - I_y = *Y-axis rotational potentiometer intercept [deg]
 - I_z = *Z-axis rotational potentiometer intercept [deg]
- *obtain values from IR-TRACC Calibration Summary for each quadrant

4.1.8. Calculate the relative position time-history of the anterior attachment point of the IR-TRACC assemblies for all three axes of both sides. For NHTSA database submissions, include these channels in Entrée data.

$$X_{rel}(t) = X_{abs}(t) - X_{abs}(0)$$

4.1.9. Calculate the overall peak abdomen compression by calculating the maximum of the absolute value of left and right abdomen X-axis relative deflection:

$$\delta_{max} = \max[|X_{rel,left}(t)|, |X_{rel,right}(t)|]$$

4.1.10. Calculate the probability of AIS 3+ injury:

$$p(\text{AIS } 3+) = 1 - e^{-\left(\frac{\delta_{max}}{106.222}\right)^{4.3127}}$$

5. KNEE, THIGH, AND HIP (KTH)

5.1. Peak Resultant Acetabulum Force

Required channels:

Channel Description	var	CFC	ISO-MME Code	NHTSA Database Codes				
				AXIS	DASTAT	SENATT	SENTYP	YUNITS
Left Femur Axial Force, Z-axis	$LF_{FemurZ}(t)$	600	??FEMRLE00THFOZB	ZL	AM	FMRL	LC	NWT
Left Acetabulum Force, X-axis (N)	$LF_x(t)$	600	??ACTBLE00THFOX B	XL	AM	PVAL	LC	NWT
Left Acetabulum Force, Y-axis (N)	$LF_y(t)$	600	??ACTBLE00THFOY B	YL	AM	PVAL	LC	NWT
Left Acetabulum Force, Z-axis (N)	$LF_z(t)$	600	??ACTBLE00THFOZ B	ZL	AM	PVAL	LC	NWT
Right Femur Axial Force, Z-axis	$RF_{FemurZ}(t)$	600	??FEMRRI00THFOZ B	ZL	AM	FMRR	LC	NWT
Right Acetabulum Force, X-axis (N)	$RF_x(t)$	600	??ACTBRI00THFOX B	XL	AM	PVAR	LC	NWT
Right Acetabulum Force, Y-axis (N)	$RF_y(t)$	600	??ACTBRI00THFOY B	YL	AM	PVAR	LC	NWT
Right Acetabulum Force, Z-axis (N)	$RF_z(t)$	600	??ACTBRI00THFOZ B	ZL	AM	PVAR	LC	NWT
Left Acetabulum Force, Resultant (N)	$LF_r(t)$	N/A	??ACTBLE00THFOR B	RS	CM	PVAL	PP	NWT
Right Acetabulum Force, Resultant (N)	$RF_r(t)$	N/A	??ACTBRI00THFOR B	RS	CM	PVAR	PP	NWT

- 5.1.1. Record the “as measured” (DASTAT = AM) channels in the table above during a crash test or impact event.
- 5.1.2. Remove data channel offset per SAE J211-1 Section 8.4.3
- 5.1.3. Filter channels based on the CFC filter classes in the “CFC” column above.
- 5.1.4. Calculate the resultant force for both the left and right acetabulum. For NHTSA database submissions, include these channels in Entrée data.

$$LF_r(t) = \sqrt{LF_x(t)^2 + LF_y(t)^2 + LF_z(t)^2}$$

$$RF_r(t) = \sqrt{RF_x(t)^2 + RF_y(t)^2 + RF_z(t)^2}$$

- 5.1.5. Set the left and right resultant acetabulum force time-history to zero when the respective femur axial force is in tension.

$$LF_r(t) = 0 \text{ for } LF_{FemurZ}(t) > 0$$

$$RF_r(t) = 0 \text{ for } RF_{FemurZ}(t) > 0$$

- 5.1.6. Calculate the peak resultant acetabulum force:

$$F_{AR} = \max[LF_r(t), RF_r(t)] \times \frac{1 \text{ kN}}{1000 \text{ N}}$$

- 5.1.7. Calculate the probability of hip fracture using the equation below, where Φ is the cumulative distribution function of the standard normal distribution:

$$p(\text{Hip Fracture}) = \Phi \left[\frac{\ln 1.429F_{AR} - 1.5751}{0.2339} \right]$$

5.2. Peak Axial Femur Force

Required channels:

Channel Description	var	CFC	ISO-MME Code	NHTSA Database Codes				
				AXIS	DASTAT	SENATT	SENTYP	YUNITS
Left Femur Axial Force, Z-axis	$LF_z(t)$	600	??FEMRLE00THFOZB	ZL	AM	FMRL	LC	NWT
Right Femur Axial Force, Z-axis	$RF_z(t)$	600	??FEMRRI00THFOZB	ZL	AM	FMRR	LC	NWT

- 5.2.1. Record the “as measured” (DASTAT = AM) channels in the table above during a crash test or impact event.
- 5.2.2. Remove data channel offset per SAE J211-1 Section 8.4.3
- 5.2.3. Filter channels based on the CFC filter classes in the “CFC” column above.
- 5.2.4. Evaluate the expressions below to calculate the maximum left and right femur compression force:

$$LF_z = \max(LF_{compression}(t)), \quad \text{where } LF_{compression}(t) = \begin{cases} |LF_z(t)| & \text{if } LF_z(t) < 0 \\ 0 & \text{if } LF_z(t) \geq 0 \end{cases}$$

$$RF_z = \max(RF_{compression}(t)), \quad \text{where } RF_{compression}(t) = \begin{cases} |RF_z(t)| & \text{if } RF_z(t) < 0 \\ 0 & \text{if } RF_z(t) \geq 0 \end{cases}$$

- 5.2.5. Calculate the peak femur compression force:

$$F_{LC} = \max[LF_z, RF_z] \times \frac{1 \text{ kN}}{1000 \text{ N}}$$

- 5.2.6. Calculate the probability of AIS 2+ injury using the equation below:

$$p(\text{AIS } 2+) = \Phi \left[\frac{\ln(1.299F_{LC}) - 2.62}{0.3014} \right]$$

6. LOWER EXTREMITY

6.1. Upper Tibia Axial Force

Required channels:

Channel Description	var	CFC	ISO-MME Code	NHTSA Database Codes				
				AXIS	DASTAT	SENATT	SENTYP	YUNITS
Left Upper Tibia Axial Force, Z-axis (N)	$LF_z(t)$	600	??TIBILEUPHFOZB	ZL	AM	TBLU	LC	NWT
Right Upper Tibia Axial Force, Z-axis (N)	$RF_z(t)$	600	??TIBIRIUPHFOZB	ZL	AM	TBRU	LC	NWT

- 6.1.1. Record the “as measured” (DASTAT = AM) channels in the table above during a crash test or impact event.
- 6.1.2. Remove data channel offset per SAE J211-1 Section 8.4.3
- 6.1.3. Filter channels based on the CFC filter classes in the “CFC” column above.
- 6.1.4. Evaluate the expressions below to calculate the maximum left and right upper tibia compression force:

$$LF_z = \max(LF_{compression}(t)), \quad \text{where } LF_{compression}(t) = \begin{cases} |LF_z(t)| & \text{if } LF_z(t) < 0 \\ 0 & \text{if } LF_z(t) \geq 0 \end{cases}$$

$$RF_z = \max(RF_{compression}(t)), \quad \text{where } RF_{compression}(t) = \begin{cases} |RF_z(t)| & \text{if } RF_z(t) < 0 \\ 0 & \text{if } RF_z(t) \geq 0 \end{cases}$$

- 6.1.5. Calculate the peak upper tibia compression force:

$$F = \max[LF_z, RF_z] \times \frac{1 \text{ kN}}{1000 \text{ N}}$$

- 6.1.6. Calculate the probability of AIS 2+ injury using the equation below:

$$p(\text{AIS } 2+) = \frac{1}{1 + e^{(5.7415 - 0.8189F)}}$$

6.2. Lower Tibia Axial Force

Required channels:

Channel Description	var	CFC	ISO-MME Code	NHTSA Database Codes				
				AXIS	DASTAT	SENATT	SENTYP	YUNITS
Left Lower Tibia Axial Force, Z-axis (N)	$LF_z(t)$	600	??TIBILELOTHFOZB	ZL	AM	TBLL	LC	NWT
Right Lower Tibia Axial Force, Z-axis (N)	$RF_z(t)$	600	??TIBIRILOTHFOZB	ZL	AM	TBRL	LC	NWT

- 6.2.1. Record the “as measured” (DASTAT = AM) channels in the table above during a crash test or impact event.
- 6.2.2. Remove data channel offset per SAE J211-1 Section 8.4.3
- 6.2.3. Filter channels based on the CFC filter classes in the “CFC” column above.
- 6.2.4. Evaluate the expressions below to calculate the maximum left and right lower tibia compression force:

$$LF_z = \max(LF_{compression}(t)), \quad \text{where } LF_{compression}(t) = \begin{cases} |LF_z(t)| & \text{if } LF_z(t) < 0 \\ 0 & \text{if } LF_z(t) \geq 0 \end{cases}$$

$$RF_z = \max(RF_{compression}(t)), \quad \text{where } RF_{compression}(t) = \begin{cases} |RF_z(t)| & \text{if } RF_z(t) < 0 \\ 0 & \text{if } RF_z(t) \geq 0 \end{cases}$$

- 6.2.5. Calculate the peak lower tibia compression force:

$$F = \max[LF_z, RF_z] \times \frac{1 \text{ kN}}{1000 \text{ N}}$$

- 6.2.6. Calculate the probability of AIS 2+ injury using the equation below:

$$p(\text{AIS } 2+) = \frac{1}{1 + e^{(3.7544 - 0.4683F)}}$$

6.3. Tibia Bending Moment

Required channels:

Channel Description	var	CFC	ISO-MME Code	NHTSA Database Codes				
				AXIS	DASTAT	SENATT	SENTYP	YUNITS
Left Upper Tibia Moment, X-axis (Nm)	$LUM_x(t)$	600	??TIBILEUPTHMOXB	XL	AM	TBLU	LC	NWM
Left Upper Tibia Moment, Y-axis (Nm)	$LUM_y(t)$	600	??TIBILEUPTHMOYB	YL	AM	TBLU	LC	NWM
Right Upper Tibia Moment, X-axis (Nm)	$RUM_x(t)$	600	??TIBIRIUPTHMOXB	XL	AM	TBRU	LC	NWM
Right Upper Tibia Moment, Y-axis (Nm)	$RUM_y(t)$	600	??TIBIRIUPTHMOYB	YL	AM	TBRU	LC	NWM
Left Lower Tibia Moment, X-axis (Nm)	$LLM_x(t)$	600	??TIBILELOTHMOXB	XL	AM	TBLL	LC	NWM
Left Lower Tibia Moment, Y-axis (Nm)	$LLM_y(t)$	600	??TIBILELOTHMOYB	YL	AM	TBLL	LC	NWM
Right Lower Tibia Moment, X-axis (Nm)	$RLM_x(t)$	600	??TIBIRILOTHMOXB	XL	AM	TBRL	LC	NWM
Right Lower Tibia Moment, Y-axis (Nm)	$RLM_y(t)$	600	??TIBIRILOTHMOYB	YL	AM	TBRL	LC	NWM
Left Upper Tibia Moment, Resultant (Nm)	$LUM_r(t)$	N/A	??TIBILEUPTHMORB	RS	CM	TBLU	PP	NWM
Right Upper Tibia Moment, Resultant (Nm)	$RUM_r(t)$	N/A	??TIBIRIUPTHMORB	RS	CM	TBRU	PP	NWM
Left Lower Tibia Moment, Resultant (Nm)	$LLM_r(t)$	N/A	??TIBILELOTHMORB	RS	CM	TBLL	PP	NWM
Right Lower Tibia Moment, Resultant (Nm)	$RLM_r(t)$	N/A	??TIBIRILOTHMORB	RS	CM	TBRL	PP	NWM

- 6.3.1. Record the “as measured” (DASTAT = AM) channels in the table above during a crash test or impact event.
- 6.3.2. Remove data channel offset per SAE J211-1 Section 8.4.3
- 6.3.3. Filter channels based on the CFC filter classes in the “CFC” column above.
- 6.3.4. Calculate the resultant moment for upper left, upper right, lower left, and lower right tibia. For NHTSA database submissions, include these channels in Entrée data:

$$LUM_r(t) = \sqrt{LUM_x(t)^2 + LUM_y(t)^2}$$

$$RUM_r(t) = \sqrt{RUM_x(t)^2 + RUM_y(t)^2}$$

$$LLM_r(t) = \sqrt{LLM_x(t)^2 + LLM_y(t)^2}$$

$$RLM_r(t) = \sqrt{RLM_x(t)^2 + RLM_y(t)^2}$$

- 6.3.5. Calculate the peak resultant tibia moment:

$$M_{res} = \max[LUM_r(t), RUM_r(t), LLM_r(t), RLM_r(t)]$$

- 6.3.6. Calculate the probability of AIS 2+ injury using the equation below:

$$p(\text{AIS } 2+) = 1 - e^{-e^{\left(\frac{\ln M_{res} - 5.8704}{0.2947}\right)}}$$

6.4. Revised Tibia Index

Required channels:

Channel Description	var	CFC	ISO-MME Code	NHTSA Database Codes				
				AXIS	DASTAT	SENATT	SENTYP	YUNITS
Left Upper Tibia Axial Force, Z-axis (N)	$LUF_z(t)$	600	??TIBILEUPTHFOZB	ZL	AM	TBLU	LC	NWT
Left Upper Tibia Moment, X-axis (Nm)	$LUM_x(t)$	600	??TIBILEUPTHMOXB	XL	AM	TBLU	LC	NWM
Left Upper Tibia Moment, Y-axis (Nm)	$LUM_y(t)$	600	??TIBILEUPTHMOYB	YL	AM	TBLU	LC	NWM
Right Upper Tibia Axial Force, Z-axis (N)	$RUF_z(t)$	600	??TIBIRIUPTHFOZB	ZL	AM	TBRU	LC	NWT
Right Upper Tibia Moment, X-axis (Nm)	$RUM_x(t)$	600	??TIBIRIUPTHMOXB	XL	AM	TBRU	LC	NWM
Right Upper Tibia Moment, Y-axis (Nm)	$RUM_y(t)$	600	??TIBIRIUPTHMOYB	YL	AM	TBRU	LC	NWM
Left Lower Tibia Axial Force, Z-axis (N)	$LLF_z(t)$	600	??TIBILELOTHFOZB	ZL	AM	TBLL	LC	NWT
Left Lower Tibia Moment, X-axis (Nm)	$LLM_x(t)$	600	??TIBILELOTHMOXB	XL	AM	TBLL	LC	NWM
Left Lower Tibia Moment, Y-axis (Nm)	$LLM_y(t)$	600	??TIBILELOTHMOYB	YL	AM	TBLL	LC	NWM
Right Lower Tibia Axial Force, Z-axis (N)	$RLF_z(t)$	600	??TIBIRILOTHFOZB	ZL	AM	TBRL	LC	NWT
Right Lower Tibia Moment, X-axis (Nm)	$RLM_x(t)$	600	??TIBIRILOTHMOXB	XL	AM	TBRL	LC	NWM
Right Lower Tibia Moment, Y-axis (Nm)	$RLM_y(t)$	600	??TIBIRILOTHMOYB	YL	AM	TBRL	LC	NWM
Left Upper Tibia Moment, Resultant (Nm)	$LUM_r(t)$	N/A	??TIBILEUPTHMORB	RS	CM	TBLU	PP	NWM
Right Upper Tibia Moment, Resultant (Nm)	$RUM_r(t)$	N/A	??TIBIRIUPTHMORB	RS	CM	TBRU	PP	NWM
Left Lower Tibia Moment, Resultant (Nm)	$LLM_r(t)$	N/A	??TIBILELOTHMORB	RS	CM	TBLL	PP	NWM
Right Lower Tibia Moment, Resultant (Nm)	$RLM_r(t)$	N/A	??TIBIRILOTHMORB	RS	CM	TBRL	PP	NWM

- 6.4.1. Record the “as measured” (DASTAT = AM) channels in the table above during a crash test or impact event.
- 6.4.2. Remove data channel offset per SAE J211-1 Section 8.4.3
- 6.4.3. Filter channels based on the CFC filter classes in the “CFC” column above.
- 6.4.4. Set the tibia Z-axis force time-history to zero when in tension.

$$[LU|RU|LL|RL]F_z(t) = 0 \text{ for } [LU|RU|LL|RL]F_z(t) > 0$$

- 6.4.5. Calculate the resultant moment for upper left, upper right, lower left, and lower right tibia.

$$[LU|RU|LL|RL]M_r(t) = \sqrt{[LU|RU|LL|RL]M_x(t)^2 + [LU|RU|LL|RL]M_y(t)^2}$$

- 6.4.6. Calculate the Revised Tibia Index:

$$RTI = \max \left[\frac{|F_z(t)|}{12000} + \frac{M_r(t)}{240} \right]$$

- 6.4.7. Calculate the probability of AIS 2+ injury using the equation below:

$$p(\text{AIS } 2+) = 1 - e^{-e^{\left(\frac{\ln RTI - 0.3376}{0.3213}\right)}}$$

7. VALIDATION DATA SET – FRONTAL RIGID BARRIER

To confirm proper execution of the calculations in this appendix and to assist in the implementation of these calculations in commercial software packages, an example data set and the expected results are presented in this section. This validation data set consists of measurements recorded from one THOR ATD during a frontal rigid barrier test. Raw data can be downloaded from the NHTSA Vehicle Crash Test Database³ in a variety of formats.

Vehicle/Test Information		
Test Number (TSTNO)	9966	
Model Year (YEAR)	2016	
Make (MAKED)	MAZDA	
Model (MODELID)	CX-5	
Closing Speed (CLSSPD)	56.29 km/h	
Impact Angle (IMPANG)	0 deg	
Occupant Information		
Occupant Location (OCCLOC)	01 LEFT FRONT SEAT (Driver)	
Dummy Description (DUMDSC)	THOR 50TH PERCENTILE MALE DUMMY	
Dummy Manufacturer (DUMMAN)	THOR MFG: HUMANETICS S/N: DO9798	
Data Download Instructions		
Entrée V5 (EV5)	http://www-nrd.nhtsa.dot.gov/database/VSR/Download.aspx? ... tstno=9966&curno=&database=v&name=&format=EV5	
DIAdem TDMS	http://www-nrd.nhtsa.dot.gov/database/VSR/Download.aspx? ... tstno=9966&curno=&database=v&name=&format=tdms	
ISO-MME	http://www-nrd.nhtsa.dot.gov/database/VSR/Download.aspx? ... tstno=9966&curno=&database=v&name=&format=iso	

³ <http://www-nrd.nhtsa.dot.gov/database/VSR/veh/QueryTest.aspx>

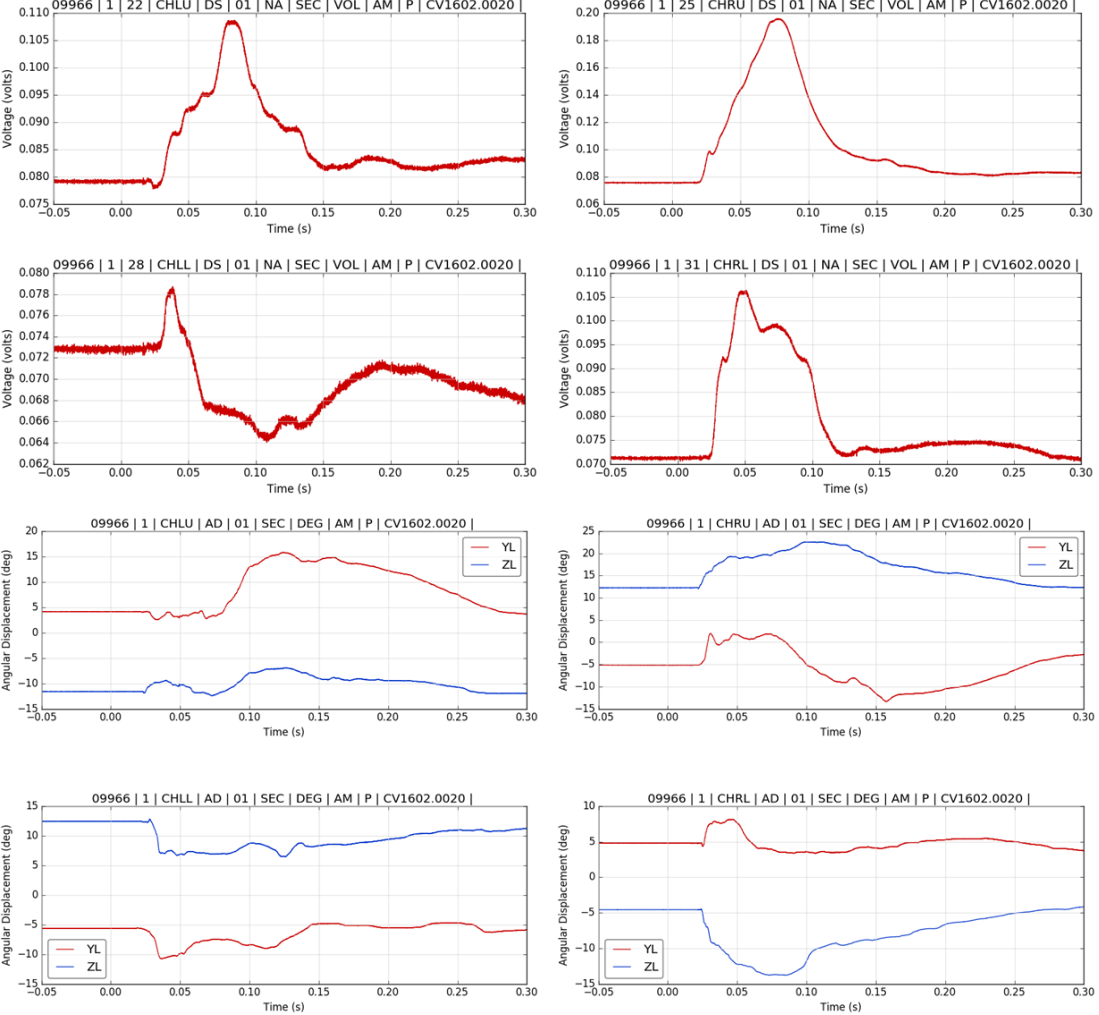
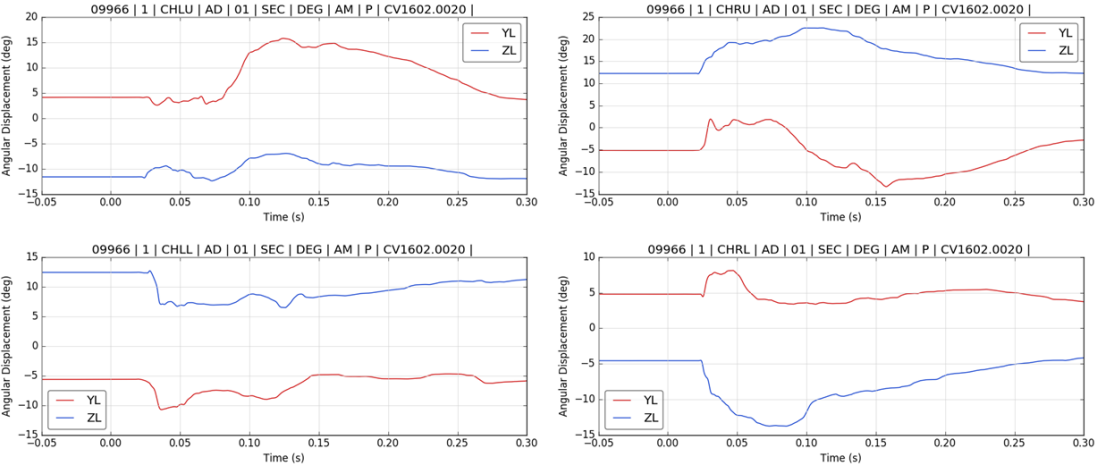
1.1 HIC15		Driver (OCCLOC = 01)
Step	Result (plot or value)	
1.1.1 1.1.2		
1.1.3		
1.1.4		
1.1.5	$HIC_{15} = 149.077$ $T_1 = 92.5 \text{ ms}$ $T_2 = 107.5 \text{ ms}$	
1.1.6	$p(\text{AIS } 2+) = 0.010350$ $p(\text{AIS } 3+) = 0.000470$	

1.2 BrIC		Driver (OCCLOC = 01)
Step	Result (plot or value)	
1.2.1 1.2.2		
1.2.3		
1.2.4	<p> $BrIC = 0.65251$ $\omega_x = 4.2971 \text{ rad/s}$ $\omega_y = 34.0655 \text{ rad/s}$ $\omega_z = 10.2709 \text{ rad/s}$ </p>	
1.2.5	<p> $p(AIS\ 3+) = 0.0759$ $p(AIS\ 4+) = 0.0538$ </p>	

2.1 N_{ij}	Driver (OCLOC = 01)	
Step	Result (plot or value)	
2.1.1 2.1.2		
2.1.3		
2.1.4		
2.1.5	$N_{ij} = 0.48364$	
2.1.6	$p(\text{AIS } 2+) = 0.04430$ $p(\text{AIS } 3+) = 0.03180$	

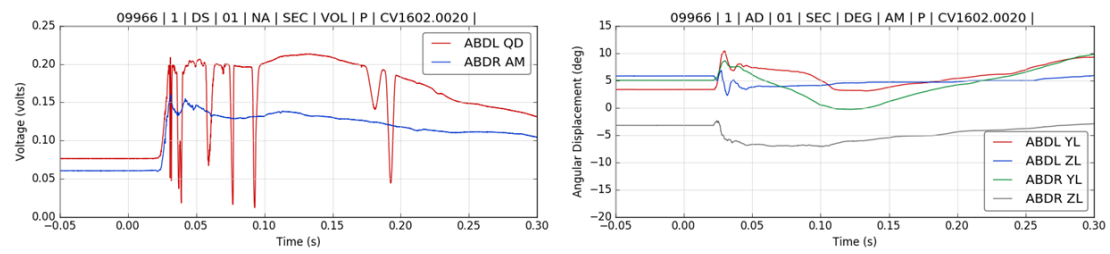
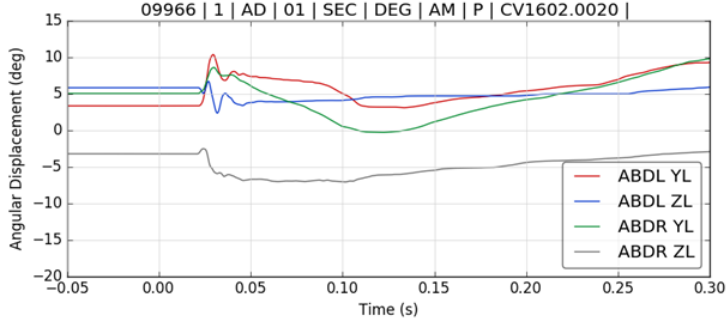
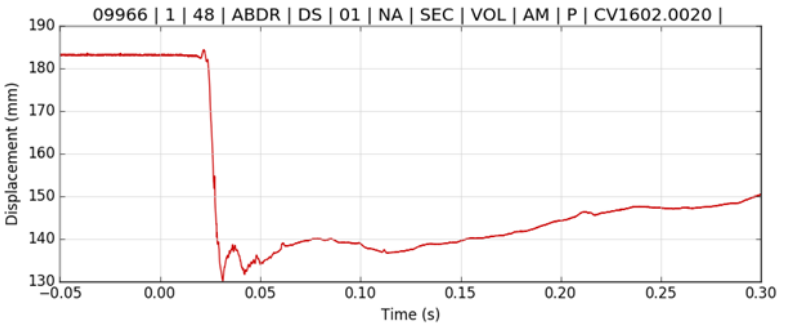
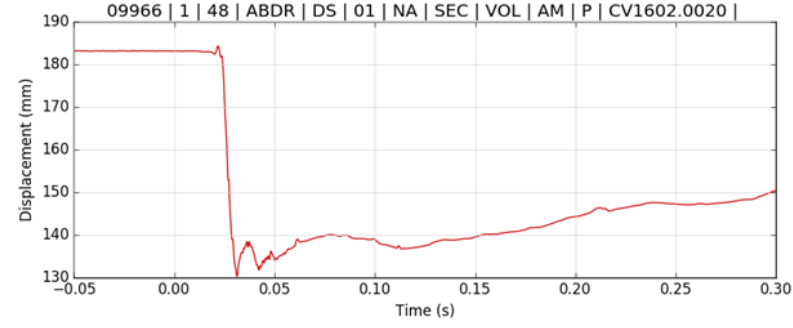
3.1 Peak Resultant Chest Deflection

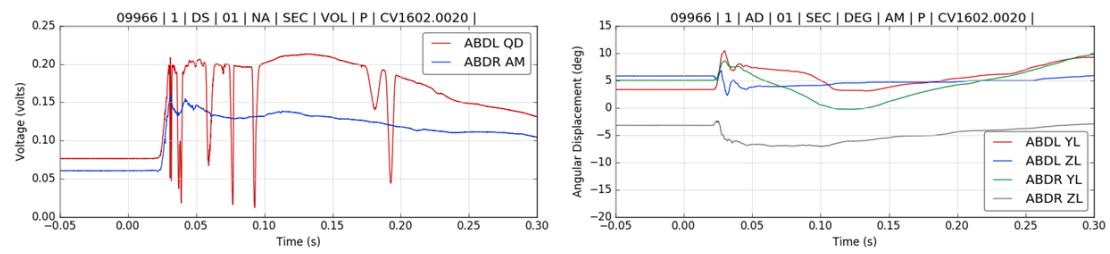
Driver (OCCLC = 01)

Step	Result (plot or value)	
3.1.1	 <p>The figure consists of eight subplots arranged in a 4x2 grid. The top four rows show Voltage (volts) vs Time (s) for different chest deflection tests. The bottom two rows show Angular Displacement (deg) vs Time (s) for YL (red) and ZL (blue) conditions. The subplots are titled as follows:</p> <ul style="list-style-type: none"> Row 1, Left: 09966 1 22 CHLU DS 01 NA SEC VOL AM P CV1602.0020 Row 1, Right: 09966 1 25 CHRU DS 01 NA SEC VOL AM P CV1602.0020 Row 2, Left: 09966 1 28 CHLL DS 01 NA SEC VOL AM P CV1602.0020 Row 2, Right: 09966 1 31 CHRL DS 01 NA SEC VOL AM P CV1602.0020 Row 3, Left: 09966 1 CHLU AD 01 SEC DEG AM P CV1602.0020 Row 3, Right: 09966 1 CHRU AD 01 SEC DEG AM P CV1602.0020 Row 4, Left: 09966 1 CHLL AD 01 SEC DEG AM P CV1602.0020 Row 4, Right: 09966 1 CHRL AD 01 SEC DEG AM P CV1602.0020 	
3.1.2	Polarity confirmed to match polarity checklist in THOR-50M PADI.	
3.1.3	N/A	
3.1.4	 <p>The figure consists of four subplots arranged in a 2x2 grid, showing Angular Displacement (deg) vs Time (s) for YL (red) and ZL (blue) conditions. The subplots are titled as follows:</p> <ul style="list-style-type: none"> Top Left: 09966 1 CHLU AD 01 SEC DEG AM P CV1602.0020 Top Right: 09966 1 CHRU AD 01 SEC DEG AM P CV1602.0020 Bottom Left: 09966 1 CHLL AD 01 SEC DEG AM P CV1602.0020 Bottom Right: 09966 1 CHRL AD 01 SEC DEG AM P CV1602.0020 	

<p>3.1.5</p> <p>Example: Upper Left (see IR-TRACC Calibration Summary)</p> <p>$LE = -0.4581$</p> <p>$IR_{sens} = 33.7101$</p> <p>$I_{abs} = 41.08$</p>	
<p>3.1.6</p>	
<p>3.1.7</p> <p>Example: Upper Left (see IR-TRACC Calibration Summary)</p> <p>$I_Y = 2.55$</p> <p>$I_Z = -2.01$</p>	
<p>3.1.8</p>	
<p>3.1.9</p> <p>$UL_{max} = 31.7661 \text{ mm}$</p> <p>$LL_{max} = 19.1603 \text{ mm}$</p>	<p>$UR_{max} = 47.4284 \text{ mm}$</p> <p>$LR_{max} = 27.6703 \text{ mm}$</p>
<p>3.1.10</p>	<p>$R_{max} = 47.4284 \text{ mm}$</p>
<p>3.1.11</p>	<p>$p(\text{AIS } 3+) = 0.41970$</p>

4.1 Peak Abdomen Compression **Driver (OCLOC = 01)**

Step	Result (plot or value)
4.1.1	 <p style="font-size: small;">* NOTE – The IR-TRACC recorded questionable data in this test (DASTAT = QD), thus is disregarded in the calculation of abdomen deflection.</p>
4.1.2	Polarity confirmed to match polarity checklist in THOR-50M PADI.
4.1.3	N/A
4.1.4	
4.1.5	<div style="display: flex; align-items: flex-start;"> <div style="flex: 1;"> <p>Example: Right Abdomen (see IR-TRACC Calibration Summary)</p> <p>$LE = -0.4837$</p> <p>$IR_{sens} = 36.27$</p> <p>$I_{abs} = 42.15$</p> </div> <div style="flex: 2;">  </div> </div>
4.1.6	

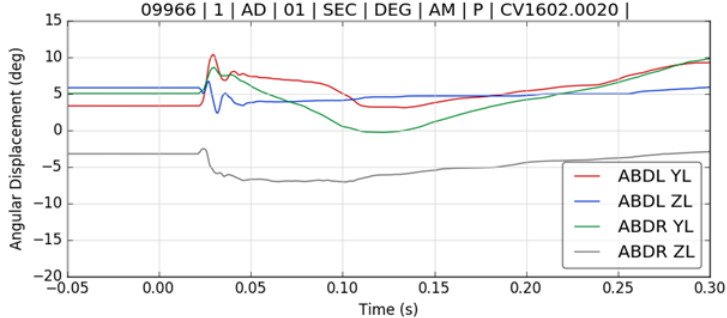


* NOTE – The IR-TRACC recorded questionable data in this test (DASTAT = QD), thus is disregarded in the calculation of abdomen deflection.

4.1.2 Polarity confirmed to match polarity checklist in THOR-50M PADI.

4.1.3 N/A

4.1.4



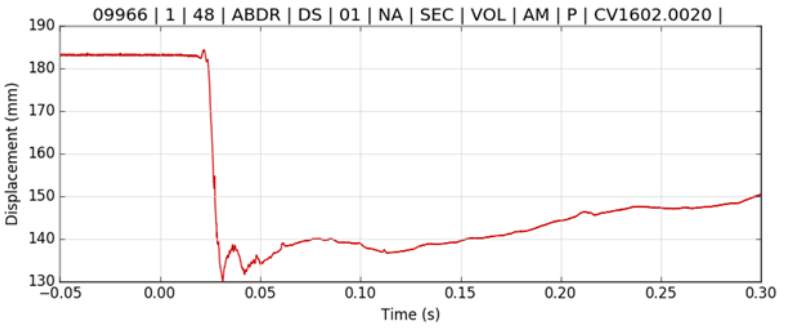
4.1.5

Example: Right Abdomen (see IR-TRACC Calibration Summary)

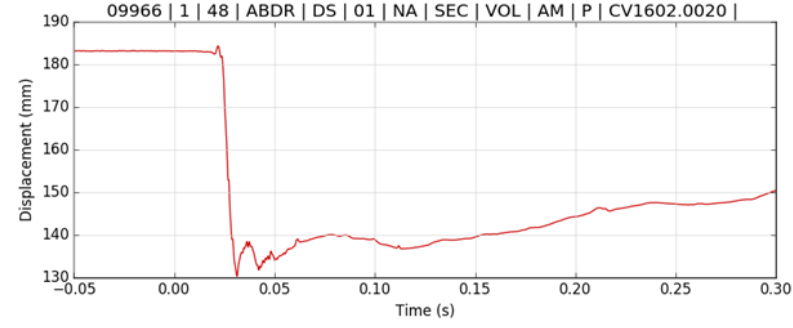
$LE = -0.4837$

$IR_{sens} = 36.27$

$I_{abs} = 42.15$



4.1.6



4.1.7	<p>Example: Right Abdomen (see IR-TRACC Calibration Summary)</p> <p>$I_Y = -1.09$</p> <p>$I_Z = 1.55$</p>	<p>09966 1 48 ABDR PP 01 XL SEC MM AM P CV1602.0020 </p>
4.1.8		<p>09966 1 48 ABDL PP 01 XL SEC MM AM P CV1602.0020 </p>
4.1.9	$\delta_{max} = 53.1915 \text{ mm}$	
4.1.10	$p(\text{AIS } 3+) = 0.049389$	

**5.1. Peak Resultant
Acetabulum Force**

Driver (OCCLC = 01)

Step	Result (plot or value)	
5.1.1 5.1.2		
5.1.3		
5.1.4	<p>$LF_{r,max} = 1687.7556\text{ N}$ $RF_{r,max} = 1165.7713\text{ N}$</p>	
5.1.5	<p>$LF_{r,max} = 1687.7556\text{ N}$ $RF_{r,max} = 1037.5709\text{ N}$</p>	
5.1.6	<p>$F_{AR} = 1687.7556\text{ N}$</p>	
5.1.7	<p>$p(\text{Hip Fracture}) = 0.001488$</p>	

5.2 Peak Axial Femur Force		Driver (OCCLOC = 01)
Step	Result (plot or value)	
5.2.1 5.2.2		
5.2.3		
5.2.4	<p style="text-align: center;"> $LF_{z,max} = 2898.2577 \text{ N}$ $RF_{z,max} = 2528.4346 \text{ N}$ $F_{LC} = 2898.2577 \text{ N}$ </p>	
5.2.5		
5.2.6	$p(\text{AIS } 2+) = 0.0000087$	

6.1 Upper Tibia Axial Force **Driver (OCCLOC = 01)**

Step	Result (plot or value)
6.1.1 6.1.2	
6.1.3	
6.1.4	<p style="text-align: center;"> $LF_{z,max} = 1752.5584 \text{ N}$ $RF_{z,max} = 2090.0684 \text{ N}$ $F = 2090.0684 \text{ N}$ </p>
6.1.5	<p style="text-align: center;">$F = 2090.0684 \text{ N}$</p>
6.1.6	<p style="text-align: center;">$p(\text{AIS } 2+) = 0.017465$</p>

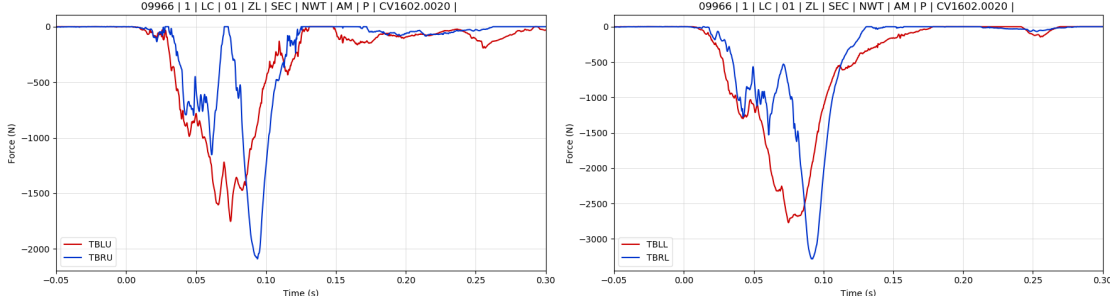
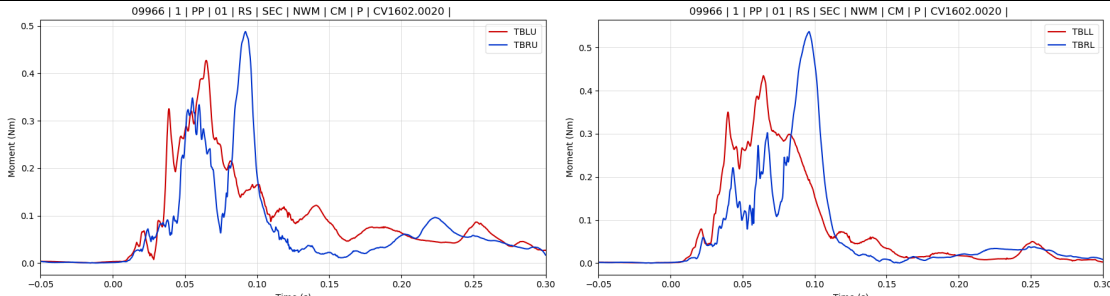
6.2 Lower Tibia Axial Force **Driver (OCCLOC = 01)**

Step	Result (plot or value)
6.2.1 6.2.2	
6.2.3	
6.2.4	<p style="text-align: center;"> $LF_{z,max} = 2770.9309 \text{ N}$ $RF_{z,max} = 3283.3442 \text{ N}$ $F = 3283.3442 \text{ N}$ </p>
6.2.5	<p style="text-align: center;">$F = 3283.3442 \text{ N}$</p>
6.2.6	<p style="text-align: center;">$p(\text{AIS } 2+) = 0.09825$</p>

6.3 Tibia Bending Moment

Driver (OCCLOC = 01)

Step	Result (plot or value)
6.3.1 6.3.2	
6.3.3	
6.3.4	
6.3.5	<p> $LUM_{r,max} = 70.7043 \text{ Nm}$ $RUM_{r,max} = 75.9898 \text{ Nm}$ $LLM_{r,max} = 59.9116 \text{ Nm}$ $RLM_{r,max} = 72.9968 \text{ Nm}$ </p>
6.3.6	<p>$p(\text{AIS } 2+) = 0.005366$</p>

6.4 Revised Tibia Index		Driver (OCCLC = 01)
Step	Result (plot or value)	
6.4.1	[LR]UF _z (t) – See Step 6.1.1-3	
6.4.2	[LR]LF _z (t) – See Step 6.2.1-3	
6.4.3	[LR][UL]M _y (t) – See Step 6.3.1-3	
6.4.4		
6.4.5	See 6.3.4	
6.4.6	 <p style="text-align: center;"> $RTI_{LU,max} = 0.42707$ $RTI_{RU,max} = 0.48792$ $RTI_{LL,max} = 0.43472$ $RTI_{RL,max} = \mathbf{0.53718}$ $p(AIS\ 2+) = 0.04929$ </p>	
6.4.7		

INJURY SUMMARY			
TSTNO	9966		
YEAR	2016		
MAKED	MAZDA		
MODEL	CX-5		
CLSSPD	56.29 km/h		
IMPANG	0 deg		
OCCLOC	01 LEFT FRONT SEAT (Driver)		
DUMDSC	THOR 50TH PERCENTILE MALE DUMMY		
DUMMAN	THOR MFG: HUMANETICS S/N: DO9798		
Injury Criterion	Value	Risk	
HIC15	149.08	p(AIS 2+) = 0.0104	p(AIS 3+) = 0.0005
BrIC	0.6525	p(AIS 3+) = 0.0759	p(AIS 4+) = 0.0538
Nij	0.4836	p(AIS 2+) = 0.0443	p(AIS 3+) = 0.0318
Resultant Chest Deflection	47.43	p(AIS 3+) = 0.4197	
Abdomen Compression	53.19	p(AIS 3+) = 0.0494	
Resultant Acetabulum Force	1687.8	p(hip fracture) = 0.0015	
Axial Femur Force	2898.3	p(AIS 2+) = 0.0000	
Upper Tibia Axial Force	2090.1	p(AIS 2+) = 0.0175	
Lower Tibia Axial Force	3283.3	p(AIS 2+) = 0.0983	
Tibia Bending Moment	75.99	p(AIS 2+) = 0.0054	
Revised Tibia Index	0.537	p(AIS 2+) = 0.0493	

8. VALIDATION DATA SET – OBLIQUE

To confirm proper execution of the calculations in this appendix and to assist in the implementation of these calculations in commercial software packages, an example data set and the expected results are presented in this section. This validation data set consists of measurements recorded from one THOR ATD during a frontal rigid barrier test. Raw data can be downloaded from the NHTSA Vehicle Crash Test Database⁴ in a variety of formats.

Vehicle/Test Information		
Test Number (TSTNO)	9976	
Model Year (YEAR)	2016	
Make (MAKED)	MAZDA	
Model (MODELD)	CX-5	
Closing Speed (CLSSPD)	90.39	
Impact Angle (IMPANG)	345	
Occupant Information		
Occupant Location (OCCLOC)	01 LEFT FRONT SEAT (Driver)	
Dummy Description (DUMDSC)	THOR 50TH PERCENTILE MALE DUMMY	
Dummy Manufacturer (DUMMAN)	THOR MFG: HUMANETICS S/N: DL9207	
Data Download Instructions		
Entrée V5 (EV5)	http://www-nrd.nhtsa.dot.gov/database/VSR/Download.aspx? ... tstno=9976&curno=&database=v&name=&format=EV5	
DIAdem TDMS	http://www-nrd.nhtsa.dot.gov/database/VSR/Download.aspx? ... tstno=9976&curno=&database=v&name=&format=tdms	
ISO-MME	http://www-nrd.nhtsa.dot.gov/database/VSR/Download.aspx? ... tstno=9976&curno=&database=v&name=&format=iso	

⁴ <http://www-nrd.nhtsa.dot.gov/database/VSR/veh/QueryTest.aspx>

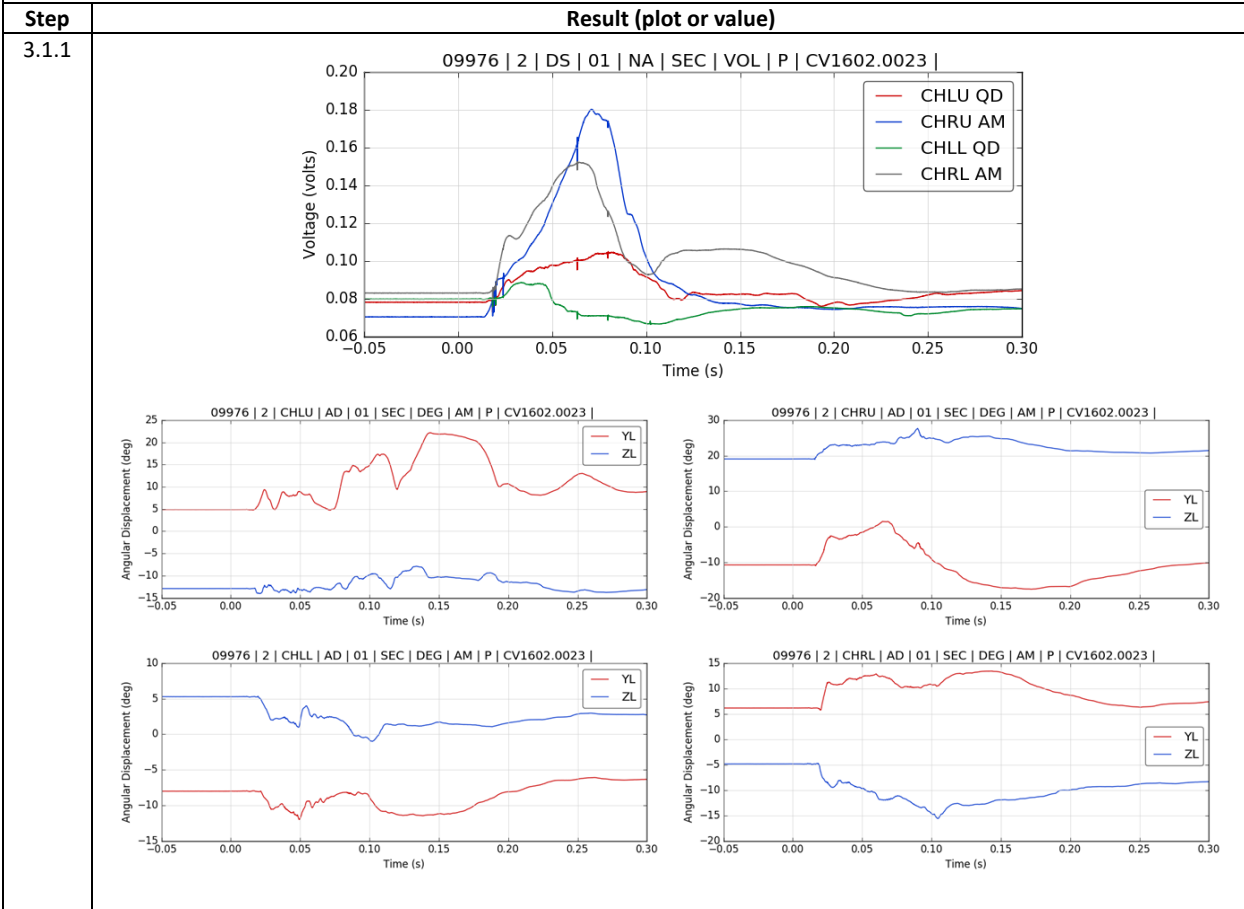
1.1 HIC15		Driver (OCCLOC = 01)
Step	Result (plot or value)	
1.1.1 1.1.2		
1.1.3		
1.1.4		
1.1.5	$HIC_{15} = 229.842$ $T_1 = 90.4 \text{ ms}$ $T_2 = 105.4 \text{ ms}$	
1.1.6	$p(\text{AIS } 2+) = 0.035757$ $p(\text{AIS } 3+) = 0.003235$	

1.2 BrIC		Driver (OCCLOC = 01)
Step	Result (plot or value)	
1.2.1 1.2.2	<p>09976 2 HDCG AV 01 SEC DPS AM P CV1602.0023 </p>	
1.2.3	<p>09976 2 HDCG AV 01 SEC DPS AM P CV1602.0023 </p>	
1.2.4	$BrIC = 0.986087$ $\omega_x = 30.4948 \text{ rad/s}$ $\omega_y = 27.4755 \text{ rad/s}$ $\omega_z = 31.0206 \text{ rad/s}$	
1.2.5	$p(AIS\ 3+) = 0.542358$ $p(AIS\ 4+) = 0.421738$	

2.1 Nij	Driver (OCCLC = 01)	
Step	Result (plot or value)	
2.1.1 2.1.2		
2.1.3		
2.1.4		
2.1.5	$N_{ij} = 0.49729$	
2.1.6	$p(\text{AIS } 2+) = 0.047702$ $p(\text{AIS } 3+) = 0.034167$	

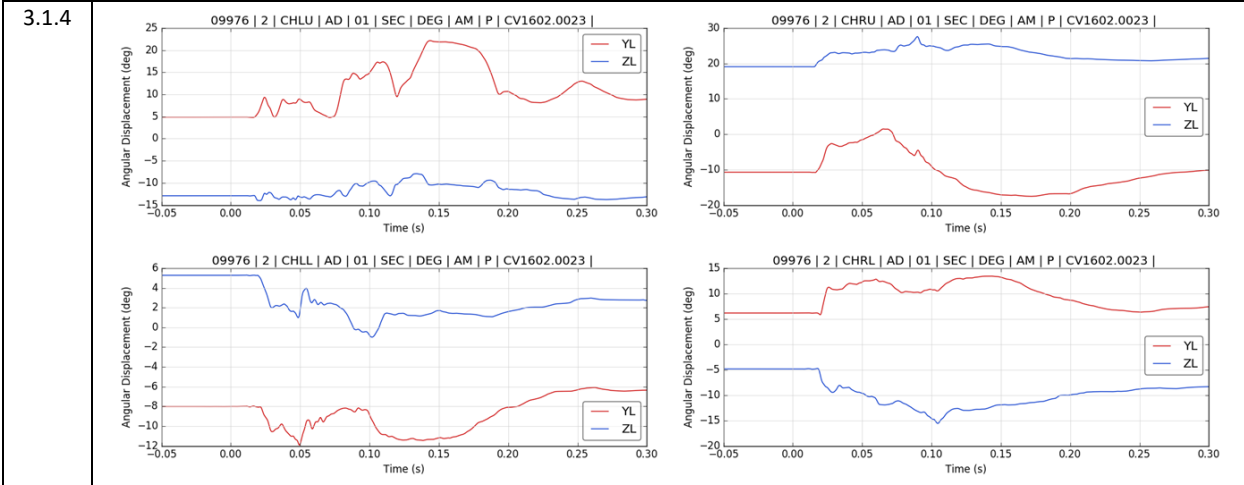
3.1 Peak Resultant Chest Deflection

Driver (OCCLOC = 01)



3.1.2 Polarity confirmed to match polarity checklist in THOR-50M PADI.

3.1.3 N/A

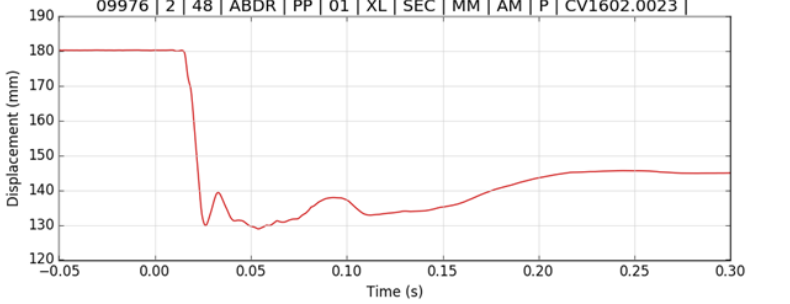
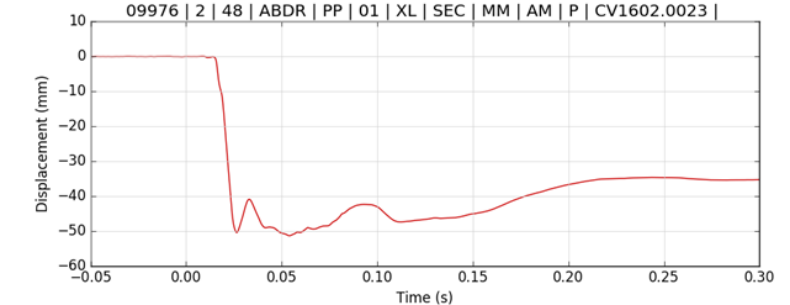


3.1.5	<p>Example: Upper Left (see IR-TRACC Calibration Summary)</p> $LE = -0.4948$ $IR_{sens} = 29.85$ $I_{abs} = 48.16$	
3.1.6		
3.1.7	<p>Example: Upper Left (see IR-TRACC Calibration Summary)</p> $I_Y = 0.00$ $I_Z = 2.57$	
3.1.8		
3.1.9	$UL_{max} = 45.8244 \text{ mm}$ $LL_{max} = 19.4249 \text{ mm}$	$UR_{max} = 50.5460 \text{ mm}$ $LR_{max} = 32.3471 \text{ mm}$
3.1.10	$R_{max} = 50.5460 \text{ mm}$	
3.1.11	$p(\text{AIS } 3+) = 0.481997$	

4.1 Peak Abdomen Compression

Driver (OCLOC = 01)

Step	Result (plot or value)
4.1.1	<div style="display: flex; justify-content: space-around;"> <div data-bbox="305 268 841 499"> </div> <div data-bbox="857 268 1393 499"> </div> </div> <p data-bbox="279 508 1325 562">* NOTE – The left IR-TRACC recorded questionable data in this test (DASTAT = QD), thus is disregarded in the calculation of abdomen deflection.</p>
4.1.2	Polarity confirmed to match polarity checklist in THOR-50M PADI.
4.1.3	N/A
4.1.4	
4.1.5	<p data-bbox="289 974 561 1050">Example: Right Abdomen (see IR-TRACC Calibration Summary)</p> <div style="margin-left: 40px;"> <p data-bbox="305 1066 571 1096">$LE = -0.4511$</p> <p data-bbox="292 1104 571 1134">$IR_{sens} = 39.5833$</p> <p data-bbox="305 1142 571 1171">$I_{abs} = 35.9456$</p> </div>
4.1.6	

4.1.7	<p>Example: Right Abdomen (see IR-TRACC Calibration Summary)</p> <p>$I_Y = -4.177$</p> <p>$I_Z = -0.429$</p>	
4.1.8		
4.1.9	$\delta_{max} = 50.93107 \text{ mm}$	
4.1.10	$p(\text{AIS } 3+) = 0.04113$	

**5.1. Peak Resultant
Acetabulum Force**

Driver (OCCLC = 01)

Step	Result (plot or value)	
5.1.1 5.1.2		
5.1.3		
5.1.4	$LF_{r,max} = 1797.8165\text{ N}$ $RF_{r,max} = 1861.8294\text{ N}$	
5.1.5	$LF_{r,max} = 1797.8165\text{ N}$ $RF_{r,max} = 1861.8294\text{ N}$	
5.1.6	$F_{AR} = 1861.8294\text{ N}$	
5.1.7	$p(\text{Hip Fracture}) = 0.005378$	

5.2 Peak Axial Femur Force		Driver (OCCLOC = 01)
Step	Result (plot or value)	
5.2.1 5.2.2		
5.2.3		
5.2.4	<p style="text-align: center;"> $LF_{z,max} = 3173.0535 \text{ N}$ $RF_{z,max} = 2277.3259 \text{ N}$ $F_{LC} = 3173.0535 \text{ N}$ </p>	
5.2.5		
5.2.6	$p(\text{AIS } 2+) = 0.0000324$	

6.1 Upper Tibia Axial Force **Driver (OCCLOC = 01)**

Step	Result (plot or value)
6.1.1 6.1.2	
6.1.3	
6.1.4	<p style="text-align: center;"> $LF_{z,max} = 1708.0185 \text{ N}$ $RF_{z,max} = 2103.2637 \text{ N}$ $F = 2103.2637 \text{ N}$ </p>
6.1.5	<p style="text-align: center;">$F = 2103.2637 \text{ N}$</p>
6.1.6	<p style="text-align: center;">$p(\text{AIS } 2+) = 0.017651$</p>

6.2 Lower Tibia Axial Force **Driver (OCCLOC = 01)**

Step	Result (plot or value)
6.2.1 6.2.2	
6.2.3	
6.2.4	<p style="text-align: center;"> $LF_{z,max} = 3295.8877 \text{ N}$ $RF_{z,max} = 3326.6180 \text{ N}$ $F = 3326.6180 \text{ N}$ </p>
6.2.5	<p style="text-align: center;">$F = 3326.6180 \text{ N}$</p>
6.2.6	<p style="text-align: center;">$p(\text{AIS } 2+) = 0.10006$</p>

6.3 Tibia Bending Moment

Driver (OCCLOC = 01)

Step	Result (plot or value)
6.3.1 6.3.2	
6.3.3	
6.3.4	
6.3.5	<p> $LUM_{r,max} = 92.8805 \text{ Nm}$ $RUM_{r,max} = 168.6428 \text{ Nm}$ $LLM_{r,max} = 71.7720 \text{ Nm}$ $RLM_{r,max} = 133.1874 \text{ Nm}$ </p>
6.3.6	<p>$p(\text{AIS } 2+) = 0.077315$</p>

6.4 Revised Tibia Index		Driver (OCCLC = 01)
Step	Result (plot or value)	
6.4.1	[LR]UF _z (t) – See Step 6.1.1-3	
6.4.2	[LR]LF _z (t) – See Step 6.2.1-3	
6.4.3	[LR][UL]M _y (t) – See Step 6.3.1-3	
6.4.4		
6.4.5	See 6.3.4	
6.4.6	<p style="text-align: center;"> $RTI_{LU,max} = 0.45107$ $RTI_{RU,max} = \mathbf{0.76716}$ $RTI_{LL,max} = 0.42569$ $RTI_{RL,max} = 0.68782$ </p>	
6.4.7	$p(\text{AIS } 2+) = 0.14209$	

INJURY SUMMARY			
TSTNO	9976		
YEAR	2016		
MAKED	MAZDA		
MODEL	CX-5		
CLSSPD	90.39 km/h		
IMPANG	345 deg		
OCCLOC	01 LEFT FRONT SEAT (Driver)		
DUMDSC	THOR 50TH PERCENTILE MALE DUMMY		
DUMMAN	THOR MFG: HUMANETICS S/N: DL9207		
Injury Criterion	Value	Risk	
HIC15	229.84	p(AIS 2+) = 0.0358	p(AIS 3+) = 0.0032
BrIC	0.9861	p(AIS 3+) = 0.5424	p(AIS 4+) = 0.4217
Nij	0.4973	p(AIS 2+) = 0.0477	p(AIS 3+) = 0.0342
Resultant Chest Deflection	50.55	p(AIS 3+) = 0.4828	
Abdomen Compression	50.93	p(AIS 3+) = 0.0411	
Resultant Acetabulum Force	1861.8	p(hip fracture) = 0.0054	
Axial Femur Force	3173.1	p(AIS 2+) = 0.0000	
Upper Tibia Axial Force	2103.3	p(AIS 2+) = 0.0177	
Lower Tibia Axial Force	3326.6	p(AIS 2+) = 0.1001	
Tibia Bending Moment	168.643	p(AIS 2+) = 0.0773	
Revised Tibia Index	0.767	p(AIS 2+) = 0.1421	

INJURY SUMMARY			
TSTNO	9976		
YEAR	2016		
MAKED	MAZDA		
MODEL	CX-5		
CLSSPD	90.39 km/h		
IMPANG	345 deg		
OCCLOC	02 RIGHT FRONT SEAT (Passenger)		
DUMDSC	THOR 50TH PERCENTILE MALE DUMMY		
DUMMAN	THOR MFG: HUMANETICS S/N: DO9798		
Injury Criterion	Value	Risk	
HIC15	197.88	p(AIS 2+) = 0.0239	p(AIS 3+) = 0.0017
BrIC	0.5733	p(AIS 3+) = 0.0143	p(AIS 4+) = 0.0100
Nij	0.41554	p(AIS 2+) = 0.0305	p(AIS 3+) = 0.0222
Resultant Chest Deflection	39.35	p(AIS 3+) = 0.2686	
Abdomen Compression	55.16	p(AIS 3+) = 0.0575	
Resultant Acetabulum Force	2515.9	p(hip fracture) = 0.1032	
Axial Femur Force	2926.3	p(AIS 2+) = 0.0000	
Upper Tibia Axial Force	2583.2	p(AIS 2+) = 0.0259	
Lower Tibia Axial Force	3342.4	p(AIS 2+) = 0.1007	
Tibia Bending Moment	168.725	p(AIS 2+) = 0.0774	
Revised Tibia Index	0.846	p(AIS 2+) = 0.1877	